Department of Civil Engineering

University of Strathclyde

Behaviour of a collapsible, structured, unsaturated fill material

A Thesis presented for the Degree of Doctor of Philosophy

by

Gráinne El Mountassir (née McCloskey)

2011

To Othmane

This thesis is the result of the author's original research. It has been composed by the author and has not been previously submitted for examination which has led to the award of a degree.

Signed:

Date:

Abstract

Many geotechnical engineering problems are related to the behaviour of unsaturated soils. Despite this many studies on unsaturated soils have used artificially created soil mixtures investigated primarily to validate constitutive models, or expansive clays researched for their proposed use in geological disposal applications. This thesis investigates a fill material from a typical engineering application: flood embankments located along the Bengawan Solo River in East Java, Indonesia.

Conventional load and soak oedometer tests carried out on this fill, highlighted the collapsible nature of this material under as-constructed conditions. A microstructural study conducted to investigate the fabric changes occurring due to loading and wetting, indicated that the undisturbed material may already have undergone the process of volumetric collapse in-situ. This research argues that volumetric collapse upon wetting may contribute to flood embankment instabilities, although the mechanism is often overlooked in favour of more spectacular failure modes.

The isotropic compression and shearing behaviour of the Bengawan Solo fill was also investigated under saturated, suction controlled and constant water content conditions. Isotropic compression results indicated that both yield stress and post-yield compressibility increased with increasing suction. The angle of friction and cohesion determined from triaxial tests were both found to increase with increasing suction.

An irregular compaction curve was found to exist at low compactive energy levels. The nature of the soil aggregates (created on mixing with water) was found to be responsible for the compacted structure created at low dry densities. This research isolated the influence of compacted fabric on volumetric behaviour by conducting suction controlled oedometer tests on specimens with different soil structures but similar conditions of moisture content and dry density. Results from suction controlled tests suggest that the influence of compacted fabric alone (separate from initial state conditions of moisture content, dry density, mean net stress and suction) is small, and therefore in terms of constitutive modelling it is sufficient to assume one set of model parameters for a given soil (of specific particle size distribution and mineralogy) regardless of compaction conditions.

Publications

McCloskey, G., Sánchez, M., Dyer, M. & Kenny, M. (2008a). Behaviour of a silt used in flood embankment construction in Indonesia, Unsaturated Soils: Advances in Geo-Engineering, *Proc 1st European Conf on Unsaturated Soils*, Durham, UK (ed. Toll, D.G., Augarde, C.E., Gallipoli, D. & Wheeler, S.J.), Taylor and Francis Group, 465-470.

McCloskey, G., Sánchez, M., Dyer, M. and Soemitro R.A.A. (2008b). Experimental behaviour of a compacted silt used in a flood defence embankment in Indonesia. *International Conference on Geotechnical and Highway Engineering, Geotropika 2008*, Kuala Lumpar. Proceedings on CD-ROM, ISBN 978-983-42613-4-4.

McCloskey, G., Sánchez, M., Dyer, M. and Soemitro R.A.A. (2008c). Collapse behaviour of a silt used in flood embankment construction in Indonesia. *Proc 3rd International Workshop on Unsaturated Soils "Between Theory and Practice in Unsaturated Soil Mechanics",* Trento, Italy.

McCloskey, G., Sánchez, M. and Romero, E. (2009). Characterisation, mechanical and microstructural behaviour of an unsaturated silt. Unsaturated soils: Experimental studies in unsaturated soils and expansive soils, *Proc 4th Asia-Pacific Conf on Unsaturated Soils*, Newcastle, Australia, (ed. Sheng, D., Buzzi, O. & Fityus, S.), CRC Press, 51-56.

El Mountassir, G., Sánchez, M., Romero, E. and Soemitro, R. A. A. (2011). Behaviour of compacted silt used to construct flood embankments, In: Compacted fills: assessment, behaviour, design and construction, *Proc Inst Civ Eng Geotech Eng* (Paper accepted).

Tarantino, A., Gallipoli, D., Augarde, C., De Gennaro, V., El Mountassir, G., Gomez, R., Laloui, L., Mancuso, C., Munoz, J., Pereira, J.-M., Peron, H., Pisoni, G., Romero, E., Raveendiraraj, A., Rojas, J.C., Toll, D., Tombolato, S. and Wheeler, S. (2011). Benchmark of experimental techniques for measuring and controlling suction, In: Partial saturation in compacted soils, *Géotechnique* (Paper accepted).

Acknowledgements

First of all, I would like to thank my supervisor Dr Marcelo Sánchez for encouraging me to study in the field of unsaturated soil mechanics, and moreover for his continued interest and support throughout my PhD. I would like to acknowledge the support of Dr Rebecca Lunn who took on a supervisory role after Marcelo's move to Texas and helped in the final completion stages. I am also grateful to Prof Mark Dyer for his involvement in the initial stages of this research project.

Most of the experimental work presented in this thesis was carried out in the Department of Civil Engineering at the University of Strathclyde. I would like to thank Mr Alex Brown and the rest of the technical staff in the Department for their help. In particular, special thanks are offered to Mr Gerry Carr for the technical assistance provided during the set-up of the geotechnical post-graduate research laboratory.

I am also indebted to Dr Ria Soemitro of Institut Teknologi Sepuluh Nopember (ITS), Surabaya, Indonesia who introduced me to the Bengawan Solo River and its flood embankments, the fill material studied in this thesis. I would also like to thank the technical staff and students at ITS who made me feel very welcome during my visit to Indonesia and who provided valuable assistance during the site investigation.

The microstructural studies presented in this research was carried out at Universitat Politècnica de Catalunya (UPC), Barcelona. I am very grateful to the staff and students in the Department of Geotechnical Engineering and Geosciences who helped me during my visit to UPC. In particular, I would like to thank Dr Enrique Romero for his interest in my research, and for the many useful discussions on the testing of unsaturated soils, while at UPC and during his visits to Strathclyde.

I am grateful to Dr Ana María Fernández Díaz who carried out the X-ray diffraction tests at CIEMAT in Madrid and also to Dr José María Manero Planella who kindly provided assistance in the use of the ESEM equipment, which was located within the Department of Material Sciences and Metallurgy at UPC, Barcelona.

A special mention must go to the past and present PhD students at the University of Strathclyde who have shared this journey with me: Marti, Marcín, Caroline, Alvis, Antoine, Daniela, Heather, Marco, Araceli, Nick and Harald. You all provided a listening ear, or a helping hand in the laboratory when I needed it, thank-you. I am particularly grateful to Marti for the many discussions we had on unsaturated soils and to Marcín for his practical experimental advice and for preparing the AutoCAD drawings presented in Chapter 6. I also appreciate the efforts of the following undergraduate and exchange students who carried out some of the characterisation tests and routine oedometer tests on the Bengawan Solo fill under my supervision in the laboratory: Andrew, Pierre, Graeme and Daniele.

I am very grateful to the Faculty of Engineering and the Department of Civil Engineering at the University of Strathclyde, for providing me with a scholarship throughout my PhD studies. I would also like to thank the Department of Civil Engineering for all the support and opportunities it has given me over the years, both as an undergraduate and as a postgraduate student. I would like to acknowledge the financial assistance provided by the Carnegie Trust in the form of a research grant, which allowed me to travel to Indonesia and which funded the site visits to the Bengawan Solo River. I am also grateful to the Bellahouston Bequest Fund for awarding me a travel scholarship in order to carry out the microstructural studies at UPC. Furthermore, I acknowledge the support of the EC via 'Marie-Curie IIF', contract number MIF1-CT-2006-040375 which supported collaboration between the University of Strathclyde and UPC.

I would like to thank my parents, John and Mary, my brothers Pádraig and Lorcán, and my sisters Ciara and Sorcha for their continual support and understanding during my PhD studies. Finally, I wish to thank my husband Othmane for his endless support, encouragement and patience, particularly in the later stages of my PhD.

Contents

List of Figures

List of Tables

Chapter 1

Introduction

1.1 Background

Interest in the performance of flood embankments has increased in recent years due to two main factors: (i) catastrophic failure events and (ii) climate change predictions. In particular the failure of flood defences in New Orleans during hurricanes Katrina and Rita in 2005 contributed to the loss of life of over 1,800 people and economic damages greater than 200 billion dollars (Basham et al., 2009). This experience highlighted the important role of flood embankments in providing public safety during storm events. In the UK, the widespread flooding in the summer of 2007 resulted in damages estimated at £3.1 billion (Defra, 2008). As a direct result of the impact of these flood events, investment in managing the risks of coastal and river flooding was increased to £2.15 billion for the period 2008 - 2011 (Defra, 2008).

Across the world climate change predictions indicate that sea levels are likely to rise, putting pressure on coastal defences, particularly in archipelagic nations such as Indonesia (Cruz et al., 2007). Furthermore, in other regions high extremes of precipitation are very likely to increase in magnitude and frequency, for example in northern and central Europe (Christensen et al., 2007) putting increased pressure on fluvial embankments. It is likely that many countries will have to upgrade existing defences or construct additional flood protection measures, in order to protect populations and settlements against higher intensity, more frequent storm and flood events. Considering these current & future challenges, it is important that all potential failure modes in such structures are revisited (Seed et al., 2008).

This thesis investigates fill material sampled from earth flood embankments along the Bengawan Solo River in East Java, Indonesia. These embankments were selected for investigation due to the recurrent history of geotechnical failures along the defences, which are detailed in Chapter 2. Earth flood embankments are typically constructed from compacted fill but in contrast with embankments associated with highway and dam projects, flood embankments are often constructed using traditional low cost techniques as opposed to modern construction methods (Morris et al., 2007; Jommi and Della Vecchia, 2010). The type of construction method used generally depends on the local sources of fill material available (Morris et al., 2007) and these less rigorous methods can subsequently result in poorly controlled compaction during construction. This may also be a consequence in poorer countries where the budget afforded to embankment construction does not perhaps reflect the importance of the protection that it provides. Hence, a good knowledge of the compaction behaviour of fill material used in such low cost flood embankments may be useful for understanding their structural performance. There has long been interest in the topic of soil structure created during compaction (e.g. Lambe, 1958b; Juang and Holtz, 1986a). Considering that poorly controlled compaction of low cost flood embankments may result in significant variations in moisture content and dry density, it is proposed here that different soil structures may be created, which may evolve further due to drying or wetting. Different soil structures created during compaction, their evolution and subsequent influence on soil behaviour is investigated in detail in Chapter 7.

Compacted earth flood embankments are structures which are subject to significant changes in moisture content, depending on changes in the river level, water table, infiltration and also evapo-transpiration processes. Such changes in moisture content and correspondingly suction affect both the shear strength of soils and the seepage through embankments (Nam et al., 2009). There are many different failure mechanisms associated with flood embankments which are related to the response of the fill material (presented in Chapter 2) and these may occur under saturated or unsaturated conditions, or as a result of the transition between different states of saturation. For this reason the Bengawan Solo fill material was studied from an unsaturated soils perspective, enabling the unsaturated conditions present immediately after construction to be considered but also the changes in the saturation conditions due to drying and wetting depending on local environmental conditions, thus affording a better understanding of the soil behaviour and performance of the embankments. Research in the field of unsaturated soil mechanics has

increased rapidly over the last twenty years (Tarantino et al., 2008), creating a wealth of knowledge on the behaviour of unsaturated soils. It is thus, topical to review traditional geotechnical problems such as those associated with flood embankments in light of these advances. Indeed Jommi and Della Vecchia (2010) express surprise that unsaturated geomechanics has rarely been used in the design or maintenance of flood embankments, considering their construction conditions and the fact that if they are to fulfil their function of protecting neighbouring land from inundation, sections of the embankments should remain in an unsaturated state for most of their lifetime.

The experimental testing of unsaturated soils has made significant advances since the 1960s largely due to (i) the formulation of independent stress state variables (e.g. Fredlund and Morgenstern, 1977) and (ii) technical developments facilitating the control or measurement of soil suction in the laboratory (e.g. Hilf, 1956; Bishop and Donald, 1961; Ridley and Burland, 1993). The testing campaigns which have been carried out to date on unsaturated soils can loosely be classified as being aligned with one of the following three aims:

1. To identify the mechanisms and processes occurring in porous materials when subjected to changes in load, fluid pressure and temperature (*porous materials*)
2. To understand the behaviour of soil which has been designed for use in a specific engineering application (*man-made soils*)
3. To characterise and understand the behaviour of soils sampled from soil deposits or compacted fills (*natural soils*).

In order to address the first aim it has been important that reproducible specimens which are well understood and relatively homogeneous be tested. Typically this type of experimental testing has been carried out on commercially available clay samples (e.g. speswhite kaolin studied by Wheeler and Sivakumar, 1995; Thom et al., 2007; Raveendiraraj, 2009; Tarantino, 2009; Sivakumar et al., 2010). Other studies have investigated sand, silt and clay mixtures, which are often selected in order to create specimens which will exhibit a specific behaviour. For example, Cunningham et al. (2003) investigated a reconstituted artificial mixture of kaolin, silica silt and London clay, the mixture was selected such that the air-entry value of the soil was

well within the range of the suction probe used (0-1500kPa). Jotisankasa et al. (2009) studied the behaviour of this same mixture but prepared specimens by compaction in order to create collapsible specimens. Experimental testing on such materials has been key to the development of concepts and frameworks for understanding unsaturated soils. Advantages of this type of material is that work can be reproduced and continued by different research groups. In these tests it is the porous nature and the corresponding processes and mechanisms which are of particular interest rather than the inherent behaviour of the particular soil, thus these materials are referred to here as *porous materials.*

A major focus of the second aim has been the investigation of the use of expansive soils in clay barriers for deep geological repositories. Much research has been carried out on studying the response of these soils to the highly complex nature of such an environment taking into account thermo-hydro-mechanical-chemical couplings (e.g. Romero, 1999; Lloret et al., 2003; Romero et al., 2003). These testing campaigns select a material suitable for the application under consideration (e.g. bentonite pellets or sand-bentonite mixtures) and attempt to replicate the highly complex in-situ conditions that the material may experience. This may include for example studying the behaviour of these *man-made soils* under drying and wetting paths in order to simulate different stages of the design life of expansive buffers (e.g. Alonso et al., 2005). Investigation has also been carried out regarding the evolution of the microstructure of compacted expansive clays over time (e.g. Delage et al., 2006). Such studies suggest that time-dependent changes in the microstructure may influence the engineering properties of the material, for example permeability and swelling behaviour, and should be considered when designing expansive material for use in engineered barriers (Delage et al., 2006). Another example of an engineering application for which soil mixtures may be specifically designed includes landfill liners (e.g. Dineen et al., 1999; Agus et al., 2010).

Experimental testing has also been carried out to characterise and understand the behaviour of unsaturated *natural soils* in the laboratory either under undisturbed or disturbed conditions. Futai and Almeida (2005) presented one of the few studies into the mechanical behaviour of undisturbed *natural soils* under suction controlled conditions, investigating the behaviour of undisturbed gneiss residual soil from Brazil. Experimental campaigns which have been carried out on unsaturated disturbed *natural soils* which have been compacted in the laboratory have

been presented for example by Cui and Delage (1996) using Jossigny silt, an aeolian deposit and by Toll and Ong (2003) on residual sandy clay from Singapore. Such materials, where no attempt has been made to design the testing mixture are referred to here as *natural soils*.

This is a very general classification of the different types of research which has been carried out within the field of unsaturated soils testing. It is clear from the above discussion that the aim of the research has often dictated the type of material studied. There are very valid reasons for the different types of materials discussed to be studied, and for the continued investigation of well known materials. Nevertheless, it is also necessary to continually widen the scope of experimental data available by testing *natural soils* to ensure that the behaviour of unsaturated materials and their studied response to loading and environmental conditions is well understood. This is also necessary to ensure that the existing frameworks for unsaturated soils can be applied for problems of practical interest which are associated with *natural soils*, particularly as many of the existing frameworks have been developed based on experimental observations of *porous materials* and *man-made soils*. As such the experimental campaigns presented in this thesis were designed to provide an additional set of experimental data for a *natural soil* (compacted fill) under different saturation conditions.

1.2 Research objectives

The underlying aim of this thesis was to characterise and to investigate the mechanical behaviour of the Bengawan Solo fill material in order to understand how its response to changes in load and variations in moisture content may be influencing its performance as a construction material as used in the flood defence embankments. To account for changes in soil behaviour due to moisture content variations it was considered beneficial to study this material as an unsaturated soil. Advanced testing techniques enabling the control of suction and measurement of suction were used in this research. However, relatively simple conventional tests were also used to illustrate how they could provide useful information to a practising engineer. In this thesis additional tests less commonly used in routine geotechnical testing such as X-ray diffraction, Environmental Scanning Electron Microscopy (ESEM) and Mercury Intrusion Porosimetry (MIP) were used to provide additional information to assist in the interpretation of macroscopic mechanical tests.

The specific objectives of this research were to:

1. Undertake a site and laboratory characterisation of the Bengawan Solo fill material, including detailed investigation of the soil mineralogy, compaction and water retention behaviour
2. Investigate the potential for volumetric collapse behaviour in this material, and to investigate the changes in soil fabric occurring due to loading and wetting
3. Investigate the isotropic compression and shearing behaviour of this material under different levels of suction
4. Investigate the soil structure of the Bengawan Solo fill created by compaction at different moisture contents and attempt to isolate the effect of compacted fabric on soil compressibility.

1.3 Outline of thesis

In order to address each of the research objectives outlined above the thesis has been organised into eight chapters as detailed below.

Chapter 2 Flood embankments: Case study and review introduces the site investigated along the Bengawan Solo River in East Java, Indonesia. The scale of flooding in this area and associated consequences are presented. Geotechnical failures which have been observed along the embankments are described. A brief review of typical failure mechanisms occurring in flood embankments is presented at the end of this chapter.

Chapter 3 Experimental testing, behaviour and constitutive modelling of unsaturated soils presents a general overview of the field of unsaturated soil mechanics. The concepts and experimental techniques used in the testing of unsaturated soils are introduced followed by the typical features of the water retention and mechanical behaviour observed in these soils. An overview of the different elasto-plastic models which have been developed to model the behaviour of unsaturated soils is also presented.

Chapter 4 Characterisation of Bengawan Solo fill presents the in-situ data obtained during the site investigation alongside the laboratory characterisation of the Bengawan Solo fill including information on the soil properties, particle size distribution, soil mineralogy, compaction behaviour and water retention behaviour.

Chapter 5 Volumetric collapse behaviour presents a short summary regarding the volumetric collapse phenomenon commonly observed in unsaturated soils. An investigation into this phenomenon in the Bengawan Solo fill using simple conventional load and soak oedometer tests is then presented. A microstructural study investigating changes in fabric due to loading and wetting is also presented.

Chapter 6 Isotropic compression and shearing behaviour begins with a brief discussion on the influence of suction on soil compressibility and on shear strength. Isotropic and triaxial tests carried out under saturated, suction controlled and constant water content conditions are presented. Details of the equipment and procedures used are outlined and the results for the Bengawan Solo fill material are presented.

Chapter 7 Influence of compacted fabric on volumetric behaviour presents a review on the current understanding of the influence of structure on soil behaviour. Conventional oedometer and suction controlled oedometer tests investigating the influence of initial compacted conditions and soil structure are presented. In particular specimens with different soil fabrics but similar initial conditions are tested under suction controlled conditions in an attempt to isolate the influence of compacted fabric on soil stiffness. These results are supported by a microstructural study conducted using Mercury Intrusion Porosimetry.

Chapter 8 Conclusions outlines the main conclusions and contributions of the research presented in this thesis and suggests recommendations for further study.

Appendix A contains detailed information on the calibration of the various equipment and instrumentation used in the experimental campaigns presented in this thesis.

Chapter 2

Flood embankments: Case study and review

2.1 Introduction

The research presented within this thesis investigates the behaviour of a soil sampled from a flood embankment, located along the Bengawan Solo River in East Java, Indonesia. This chapter presents first a general introduction into flood defence embankments, including logistical issues concerning their management and typical construction methods used. A detailed description of the Bengawan Solo River embankments is then presented along with information regarding the scale of the flooding problem in the region and the associated consequences. The different types of geotechnical failures observed along these embankments are then discussed. This chapter concludes by reviewing the different mechanisms typically attributed to failures in flood embankments. The failure mechanisms are considered in terms of those which relate to the founding layers and those related to the fill material.

The term flood embankments as used within this thesis refers to earth fill structures constructed to direct the passage of flowing water and to protect surrounding areas from flooding. This term is synonymous with the following: levees, dikes and fluvial or coastal embankments as used in the US, the Netherlands and the UK respectively.

2.2 National infrastructure

One of the main challenges in the provision of flood embankments is the immense length of protection required. In England and Wales there is an estimated 25,400 miles of coastal and river embankments with an annual budget of over £570 million spent on construction and maintenance (EA, 2009). However, it is anticipated that this figure will need to increase to £1 billion per year by 2035, if current levels of protection are to be maintained (EA, 2009). In the US there is estimated to be around 100,000 miles of flood embankments (14,000 miles of federal levee systems), and estimates suggest that nationwide financial losses of $5-10 billions per year are associated with flood embankments (Basham et al., 2009). Flood embankments have historically been regarded as low cost, simple to build structures; however the consequences of poorly designed, constructed or maintained systems can have catastrophic consequences as experienced in New Orleans both in terms of loss of life and economic damages. Even disregarding such extreme events the figures suggest that breaches occur on a regular basis, indicating that these low cost structures can become very costly indeed. This chapter deals with geotechnical failures of flood embankments; however it is also noted here that perhaps a revision in the level of protection designed for flood embankments should be considered in light of the local conditions and expected risk rather than all embankments being designed for the same level of protection, typically for a 1 in 100 year flood (Basham et al., 2009).

Considering the immense lengths of flood embankments provided on a national scale, it is not surprising that there has often been a lack of centrally held information regarding the defences provided. However recently there have been attempts to address this issue, for example in the US, the National Levee Safety Act (2007) (which was passed in response to the storm events in New Orleans, 2005) seeks to develop basic information on federal levees including the development of a database, inventory, inspection and assessment of levees (Basham et al., 2009). Elsewhere other countries are also developing central databases with basic information on their flood defence infrastructure. In England, The National Flood and Coastal Defence Database project was set up in 2001 by the Department for environment, food and rural affairs (Defra) to form a core repository of information on flood defences, watercourses, assets and flood frequency in England and Wales (Linford et al., 2002). Catering specifically for defences the database aims to provide information on location, composition, standards and condition of fluvial, tidal and

coastal defences (Linford et al., 2002). The aim of this project is to highlight where some form of defence is required, where existing defences need to be improved and where further information must be sought regarding existing defences. A similar database (Scottish flood defence asset and database) has also been developed in Scotland (Bassett et al., 2007).

2.3 Construction

Due to the large volumes of fill material required in constructing long sections of flood embankments, locally available material is generally sourced. As a result, embankments are constructed in a variety of different ways, depending on the type of material which is locally available (Morris et al., 2007). Figure 2.1 presents nevertheless the typical form of a flood embankment which consists of the embankment body constructed on top of the existing founding material. The outward slope faces the river or sea and usually has surface protection in the form of vegetation but may also benefit from additional revetment. It is important to note that many flood embankments in the UK are relatively old structures that have been upgraded over decades or even centuries from original constructions (Morris et al., 2007). As such these have been constructed using traditional methods including the excavation of soil from a ditch running along the landward side of the embankment, see Figure 2.1 (Dyer, 2004). Warping silt traps have also be used in the construction of flood embankments; constructed on the outward side of the embankment, these traps form berm-like structures, which increase both toe and global stability of the existing embankment. Another traditional method of construction is by river dredging, this was typically used in the Fens, East Anglia as a source of fill material (Dyer, 2004; Morris et al., 2007). The fill material generated from these types of construction methods would thus be fluvial deposits composed of fine silt and clay sized particles. Depending on the height of the embankment required and the importance given to its construction, fill material is often placed on top of existing material and lightly compacted without necessarily complying with engineering specifications (Dyer, 2004; Morris et al., 2007).

Modern methods of flood embankment construction involve the placing of fill in layers and the use of standard compaction techniques as used for highway construction (BS6031, 1981; Pilarczyk, 1998). The design of flood embankments does however vary from country to country

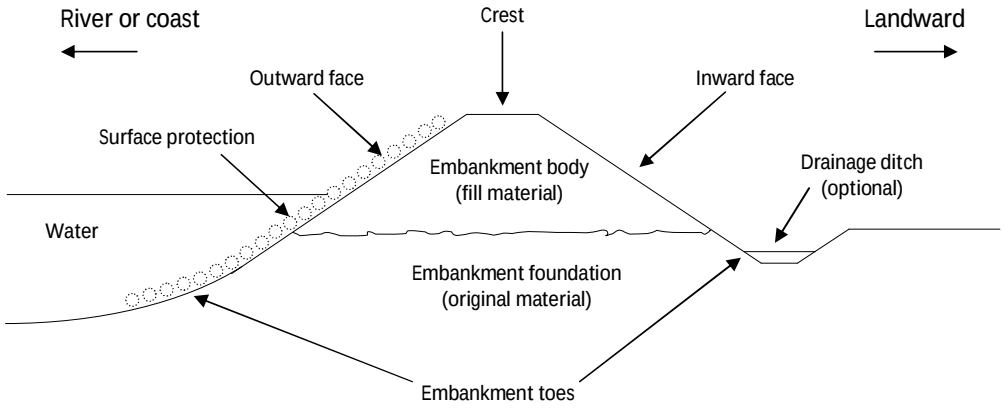

Figure 2.1: Typical cross-section of a flood embankment (after Dyer, 2004)

and the compaction of fill material is not always rigorously controlled during construction. Flood embankments in the UK should be constructed with an impervious (clay) core to prevent unacceptable internal seepage, although this is often not used in practice (Morris et al., 2007). However in the Netherlands typically clay liners are used as the upper surface layer of the slopes and crest, and protect an inner sand core (Kruse, 1998).

Additional challenges are faced when constructing flood embankments in tropical regions. Perhaps the greatest of these is the extreme weather experienced in such regions, typified by the dry and wet monsoon seasons. Such climatic conditions mean that the embankments must be able to withstand high hydraulic gradients due to rapidly rising water levels during storm events. Another consequence is that construction of the embankments can only be carried out during the dry season when river levels are low (Brown, 1999). In areas where population density is high, settlements can restrict realignment or relocation of embankments during upgrades (Brown, 1999). The lack of available land in densely populated urban areas or poor access routes in remote rural areas can prevent large construction equipment from reaching sites, resulting in smaller compaction plant often being used (Brown, 1999). The issue of securing suitable local material is perhaps of greater importance in tropical regions, where it is simply not economically feasible to transport material, even for short distances (Brown, 1999). Further limitations associated with construction costs can result in the use of an unskilled local workforce. However

projects do benefit from local knowledge regarding site specific flood issues and if properly conducted knowledge transfer can ensure continued maintenance of defences by local communities (FAO/RAP, 1999). The difficulties associated with obtaining good quality fill material, available funds and poor access to site can all lead to traditional, less rigorous construction methods being used. Brown (1999) experienced many of the difficulties listed above during construction of flood embankments along the Mekong River, Thailand.

2.4 Bengawan Solo Embankments

2.4.1 Site Description

The material investigated in this research was sampled from flood embankments located along the Bengawan Solo River in East Java, Indonesia (Figure 2.2). Indonesia is the largest archipelago in the world consisting of over 17,000 islands (UN, 2004). Lying over the equator, Indonesia (Figure 2.2) has a predominantly tropical climate. Temperature varies little from season to season with average temperatures in the coastal regions of 28°C, 26°C in inland and mountainous areas and 23°C in higher mountainous areas (UN, 2004). The main variation in weather in Indonesia is in terms of rainfall, as there are primarily two seasons, a wet season and a dry season. Generally speaking the dry season is between May and October and the wet season between November and April (UN, 2004). Indonesia has an average relative humidity between 70% and 90%, with a minimum of 73% and a maximum of 87% (UN, 2004). Climate change predictions for Indonesia (Susandi, 2007 as cited by Hidayat et al., 2008) suggest that rainfall will increase by 2 to 3% each year. The island of Java is the most populous island in the world, with a population of 130 million (BPS, 2006).

The Bengawan Solo River is the longest river on the Island of Java at approximately 600km. The source of the river lies in the Sewu Mountain Range in Central Java and it enters the sea, north of Surabaya in East Java (Figure 2.3). The Bengawan Solo River drains a catchment area of almost 20,000 km^2; the population within this basin was estimated at over 16 million in 2005 (Hidayat et al., 2008). Both the natural and man-made embankments along the Bengawan Solo River have a history of failure and overtopping along the length of the river. The high

Figure 2.2: Location of Indonesia and East Java in South East Asia

population density in the river basin (811 people/km^2, Hidayat et al., 2008), means that often villages are located directly behind the flood embankments and as such flooding can result in the relocation of entire villages and even fatalities. Furthermore flooding has negative impacts on local agriculture, due to the loss of crops as a result of inundation. The following example indicates to some extent the scale of the problem.

Between late December 2007 and early January 2008, Java was subjected to persistent heavy rains with an average rainfall of 136mm/day in the upper parts of the Bengawan Solo Basin, resulting in widespread flooding and landslides (Hidayat et al., 2008). Hidayat et al. (2008) report in detail the damages and impact of the flooding in the Bengawan Solo Basin: over one hundred people died as a result of the floods and landslides. In the Municipality of Bojonegoro alone almost 300,000 people were affected by the floods with almost 200,000 people being evacuated from their homes (Hidayat et al., 2008). Total costs associated with damage to infrastructure (roads, dams, bridges, irrigation facilities) and agricultural losses due to this flooding event in the Bengawan Solo Basin were estimated by the State Ministry of National Planning and Development to be in the region of 2,000 billion Indonesian Rupiahs (approx. £145 million) (Hidayat et al., 2008). Damage to embankments and flood gates were estimated at 85 billion Indonesian Rupiahs (approx. £6.2 million) and agricultural losses due to crop inundation were estimated to be around 93.3 billion Indonesian Rupiahs (approx. £6.8 million) (Hidayat et al., 2008). Alongside the heavy rains, Hidayat et al. (2008) suggest that deforestation in the catchment

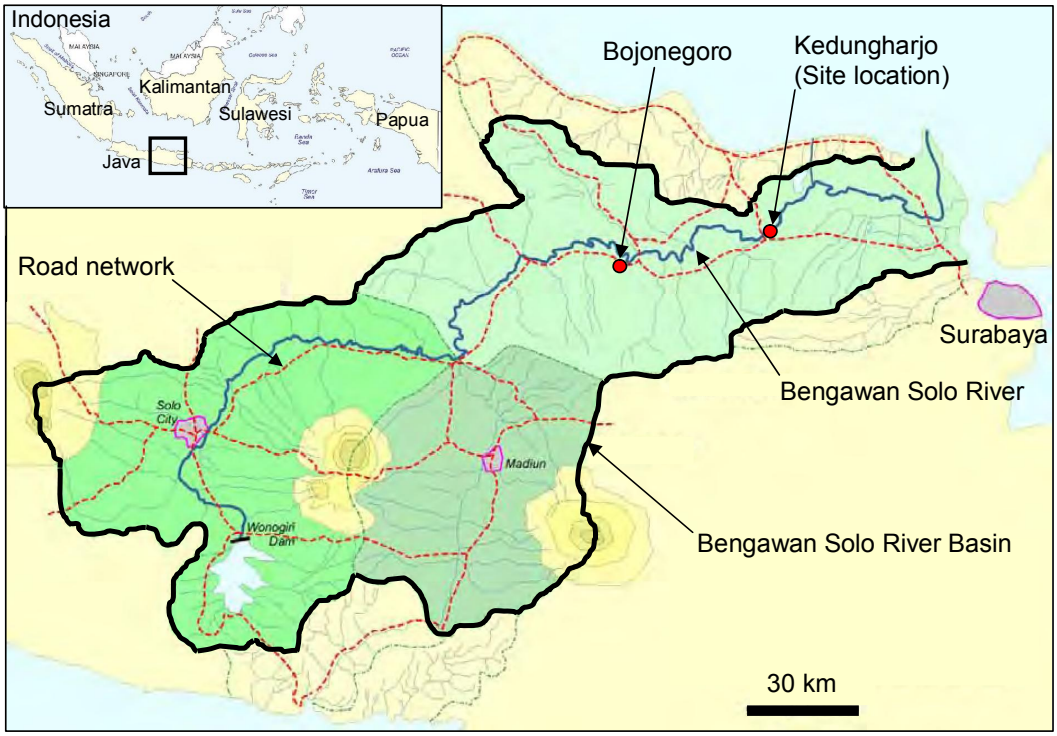

Figure 2.3: Site location within the Bengawan Solo River Basin (After Sudarsono, 2009)

area and a lack of flood control structures and drainage systems, along with incomplete river engineering works, were also responsible for the resulting widespread flooding in the Bengawan Solo Basin.

Flooding along the Bengawan Solo River is not an uncommon event and in February 2009, the overtopping of embankments led to the inundation of over 10,000 homes across 12 districts in the Bengawan Solo Basin and the failure of a 10m stretch of embankment in the Kanor district resulted in the evacuation of a further 11,000 families (The Jakarta Post, 2009) .

2.4.2 Construction of embankments

Figure 2.4 presents a typical cross-section of the Bengawan Solo embankments in the Bojonegoro Municipality. Typically the river is bounded by natural embankments but where significant population settlements are located in close proximity to the river, sections of man-made embankments have been constructed. The natural embankments along the Bengawan Solo River are in a continual state of erosion, as shown in Figure 2.4b, the mechanical action of the river

erodes the outward face, until a steep face remains. This eroded material enters the river. When man-made embankments are to be constructed along the Bengawan Solo, material is removed from the riverbed and placed on existing embankments. Considering the immense length of the river (~600km) it is uneconomical to use anything other than locally available material. Construction or repair of the embankments can only take place during the dry season due to the high river level during the wet season. Figure 2.4a, c and d illustrates the high variation in river level between the dry and wet seasons, which can vary as much as 10m. During the wet season these embankments are frequently overtopped, whereas during the dry season only a smaller deeper river channel remains filled with water.

The section of flood defence embankment investigated within this research is located in the village of Kedungharjo, in the city region of Bojonegoro. At this location the embankments were frequently overtopped or breached resulting in the evacuation of Kedungharjo village. The height of the existing embankments were raised and surface protection in the form of stone filled gabions were installed. The gabion reinforced section of embankment (Figure 2.4d) was constructed during the dry season of 2005 and was completed in November 2005. The embankment was constructed as is traditional for these embankments using material from the river bed (i.e. eroded material) and placed on top of the existing embankments. The material was compacted dry of optimum to 80-85% of the maximum Proctor dry density (Soemitro, private communication, 2006).

2.4.3 Evidence of geotechnical failures

The site was visited in May 2006 during a month long visit to Institut Teknologi Surabaya (ITS) working in collaboration with Dr. Ria Soemitro. The travel to Indonesia was supported by a Carnegie Trust Research Grant. During visits to the site a number of different types of processes were evident which could play a role in triggering instabilities in the Bengawan Solo embankments. The different processes and or failure mechanisms observed along the embankments are described below.

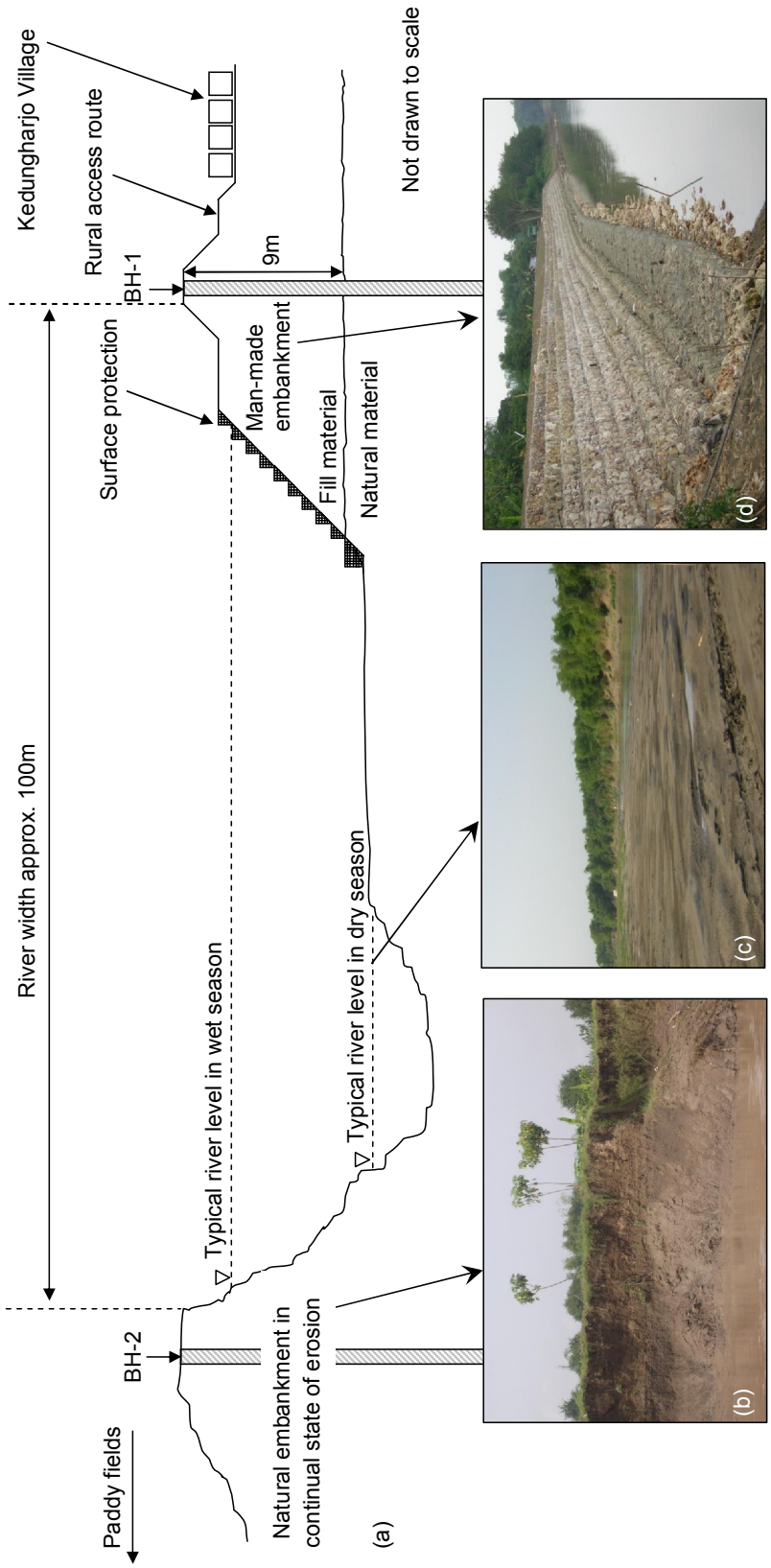

Figure 2.4: Typical cross-section of Bengawan Solo embankment at site where soil was sampled, Kedungharjo, Bojonegoro

Figure 2.5: Erosion due to river meandering

2.4.3.1 Erosion of embankments

Alongside the progressive erosion of the natural embankments (Figure 2.4b), erosion of man-made embankments due to river meandering was also evident (Figure 2.5a) at a section of embankment located close to the village of Kanor. Erosion of the outward face can lead to undercutting of the embankments. To prevent further migration of the river into the village of Kanor a concrete retaining wall was constructed in 2005 (Figure 2.5b). Warnana (2008) used Ground Penetrating Radar to identify possible regions of scouring along the Bengawan Solo River and suggested that scouring may be responsible for triggering failures along the embankments.

In much of the catchment area of the Bengawan Solo River, deforestation is ongoing. The removal of vegetation increases the risk that top soil will be removed during heavy rain, this leads to an increased amount of sediment entering the river. This has two effects: (i) raises the level of the riverbed which increases the likelihood of overtopping and (ii) increases the unit weight of the water in the river, increasing the risk of erosion due to the impact of the river flow. At this section the river is approximately 100m wide, thus contributing to the very high discharge. Flow control measures (such as small gates) have been installed in several location to reduce the discharge in the river, however many of these measures have been damaged by the river flow, for example see Figure 2.6.

In order to prevent erosion of the outward slope, surface protection has been installed at different sections along the embankment, in the form of concrete slabs (Figure 2.7) or in the form of gabions (Figure 2.4d). However it appears from Figure 2.7 that slippage of the concrete slabs

Figure 2.6: Damage of flow control structures

Figure 2.7: Differential settlements due to concrete slab protection

has occurred at some locations and even differential settlements have been observed.

2.4.3.2 Desiccation cracks

During visual inspection of the embankments, evidence of desiccation cracking of the fill material was found. Figure 2.8a illustrates the crack patterns which form on the outward slope during drying. At these high moisture contents the material is very soft and the crack formation enables the material from the embankment slope surface to be eroded away in blocks. Desiccation was also observed in the form of cracks extending vertically into the embankment up to a depth of 35cm (2.8b). However it must be noted that one week prior to this site visit the embankment had been completely overtopped and the soil had retained a high degree of saturation. Therefore it would be expected that during a drier period desiccation would extend to perhaps greater depths and be more widespread throughout the embankment. The problem of desiccation cracking in this material forms part of an ongoing doctoral research programme by Alvis Atique, a research student within the Department of Civil Engineering at the University of Strathclyde.

Figure 2.8: Evidence of desiccation cracks (a) on embankment face and (b) extending into embankment

Figure 2.9: (a) Babat barrage and (b) rapid drawdown failure at Plangwot village

2.4.3.3 Rapid drawdown failures

Further upstream the Babat Barrage is located at Lamongan (Figure 2.9a), the function of which is to supply water for irrigation, domestic and industrial use to the surrounding areas, and also to act as a means of storing water for the dry season, when the river level decreases considerably. However the use of this 140m wide barrage has in itself contributed to geotechnical failures of the embankments. For example, in May 2006 closure of the barrage resulted in the collapse of 98 houses and damage to 57 additional houses in the village of Plangwot, which lies downstream of the Babat Barrage (R. Soemitro, personal communication, May 2006). This failure was attributed to rapid drawdown as the river level under which the embankments were submerged decreased considerably in a short period of time due to the closure of the barrage upstream. Figure 2.9b illustrates the type of failure caused by rapid drawdown at Plangwot village. Here all the land in front of the gates fell away into the river, taking with it houses.

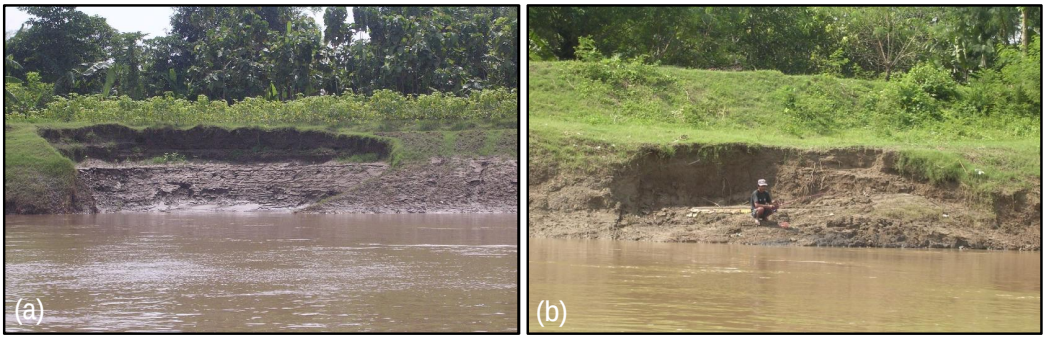

Figure 2.10: Shallow slip failures (a) close to Kanor village and (b) close to Kedungharjo village

Figure 2.11: Global failure of gabion reinforced embankment (a) front view, (b) side view

2.4.3.4 Shallow slip failures

Shallow slip failures were also evident along the outward slopes of the embankments. Figure 2.10a shows a shallow slip failure close to Kanor village near where the concrete retaining wall (Figure 2.5b) was constructed. Figure 2.10b shows a shallow slip failure close to the village of Kedungharjo. Slips of this type were evident along the length of these embankments.

2.4.3.5 Global slip failure

A large global slip was also in evidence along the gabion reinforced embankment located next to the village of Kedungharjo. This embankment was constructed during the dry season of 2005, and was completed in November 2005. The global slip failure presented in Figure 2.11 occurred in December 2005, during the first wet season.

Figure 2.12: Secondary uses of the river and embankments (a) removal of river sediment for use as a construction material and (b) location of shop and animal grazing on crest of embankment

2.4.4 Secondary uses

It should be noted that there are various third parties interested in the Bengawan Solo River. Villagers living along the embankments view the river as a resource; using the river sediment as one of the primary construction materials in the building of local roads and homes. As such material is often removed from the river (Figure 2.12a), which destabilises the riverbed. The Ministry for Public works in East Java has primary responsibility for the construction, monitoring and repair of the Bengawan Solo embankments. As a measure to stabilise the riverbed, heavy revetment is placed onto the riverbed on an annual basis.

Embankments can have secondary uses aside from their primary function of retaining and directing the passage of water. The embankments along the Bengawan Solo River are often used as areas for grazing, transportation routes for light motor vehicles and even have shops or houses located on top of them (Figure 2.12b).

It is evident from the above the description that there are many different types of instabilities arising along the Bengawan Solo embankments as a result of the interaction and combination of a number of different natural and human factors.

2.5 Review of typical failure mechanisms

A brief review of the main widely accepted failure mechanisms associated with flood embankments is presented here, it is categorised into two main groups, mechanisms related to the

problematic response of the (i) founding strata and (ii) fill material.

2.5.1 Founding layers

The type of failure mechanisms which can occur as a result of the underlying or foundation layers can result in physically larger, global failures than the smaller local failures typically observed as a result of the problematic response of the fill material. Schematic representations of the failure mechanisms related to the founding material are presented in Figure 2.13. Deep seated rotational failure of the embankment may occur during or shortly after the construction of an embankment on soft founding strata of low shear strength (Leroueil et al., 1990). Another mechanism which may also result in a deep rotational failure is the build up of excessive uplift pressures in underlying gravel or sand layers which are in continuity with the river or sea. However more typically it can result in heave at the toe of the embankment rather than a complete rotational failure. Failure due to excessive uplift pressures is a mechanism which received a lot of attention after being identified as being responsible for some of the embankments failures during the North Sea floods (Cooling and Marsland, 1954; Marsland, 1957, 1961; Marsland and Randolph, 1978; Hird et al., 1978; Padfield and Schofield, 1983) and is a mechanism which still continues to be investigated (Baudin et al., 1989; Van et al., 2005; van Baars, 2005). Another global failure mechanism is translational failures due to underlying organic strata. Embankment failures due to underlying peat layers have been recorded both in the UK and in the Netherlands (e.g. Ward et al., 1955). For example, van Baars (2005) details the horizontal failure mechanism observed at the Wilnis peat dyke in the Netherlands as a result of desiccation of the peat layer during a particularly dry summer.

The final mechanism related to the underlying layers is that of settlements due to consolidation or creep. This occurs typically if the founding layers are highly compressible clays or organic soils (Morris et al., 2007). The effect of settlements is to reduce the crest level of the embankment. This may in turn increase the likelihood of overtopping occurring which could in turn lead to erosion of the landward face and as such compromise embankment stability.

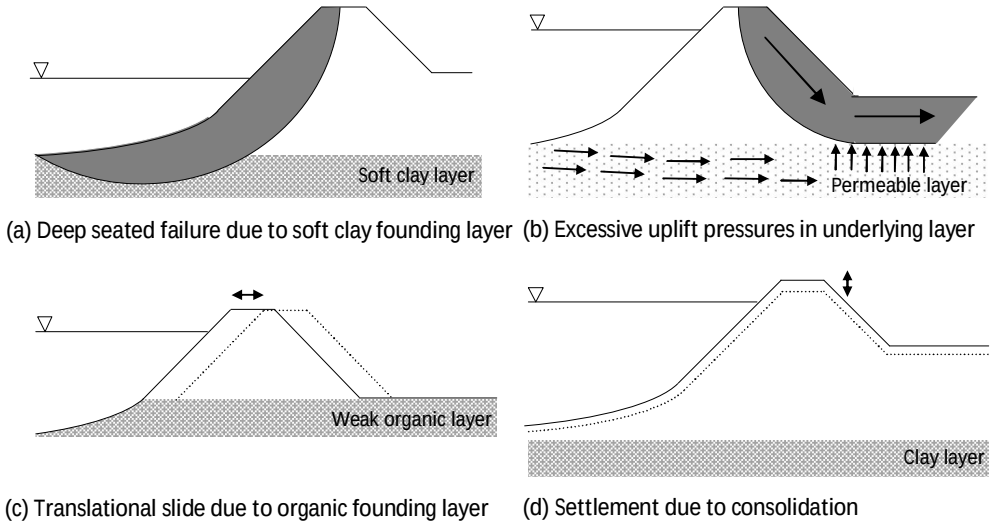

Figure 2.13: Failure mechanisms related to the founding layers

2.5.2 Fill material

Many failure mechanisms found in flood embankments are due to the problematic response of the fill material under hydraulic loading, external loading or environmental loading. Figure 2.14 presents a schematic representation of all the failure mechanisms described here related to the fill material. The first four diagrams in Figure 2.14 illustrate different forms of erosion processes occurring within the fill material. It should be noted here that all earthwork structures undergo some form of erosion due to their interaction with the environment, however the erosion described here refers to that which significantly reduces the embankment's ability to retain and direct water. Several types of erosion are described here, depending on both the location of where the erosion takes place within the embankment and also the cause of the erosion.

After the North Sea floods in the UK in 1953, important research began into the identification of possible failure mechanisms (Cooling and Marsland, 1954; Marsland, 1957; Marsland and Cooling, 1958; Marsland, 1961, 1968; Marsland and Randolph, 1978). Both erosion of the outward and landward faces were cited as possible failure mechanisms in some of the failed embankments (Cooling and Marsland, 1954; Marsland, 1957). The erosion of an outward face

may occur either due to the result of wave action (Cooling and Marsland, 1954) or as a result of the meandering of a river (Morris et al., 2007). For example large shingle deposits on the outward face of a flood defence at Scrapsgate on the Isle of Sheppey were completely removed during the North Sea Floods (Cooling and Marsland, 1954). Erosion of the landward slope on the other hand, occurs mainly due to overtopping of the structure during flooding conditions and is a result of the mechanical action of the flowing water (Cooling and Marsland, 1954). Furthermore the slopes and crest of an embankment may be subject to erosion due to rainfall infiltration (Perry, 1998).

Erosion of the outward face, landward face and crest can all be classified as external erosion and while these examples have focused mainly on the action of hydraulic loading on the embankment it should be noted that the crest and faces of an embankment are often subject to erosion from other sources. This may include erosion due to animal grazing on the slopes, erosion as a result of walking or cycle paths, which may or may not have been provided for. In fact embankments often have secondary uses (Dyer, 2004), which attracts animals and pedestrians. However, it is important that they should be maintained in such a way that their secondary use (access route, environmental habitat, recreational area, Morris et al. 2007) does not cause such significant erosion so as to compromise their primary function. A final type of erosion occurring with respect to the fill material is that of the internal transportation of particles (internal erosion). Lindenberg and de Groot (1998) describe different types of internal erosion, the most commonly referred to with regard to flood embankments is piping. Piping occurs where there is strong through-seepage, following a particular channel through the embankment. This flow is then responsible for transporting soil particles through the embankment. Piping may occur within the fill material itself (through-seepage) or within the underlying layers (under-seepage), and is likely to occur within a granular layer (e.g. sand) which is located just below a cohesive clay layer of low permeability. Other types of internal erosion include: the washing out of finer soil particles of the fill material through coarser pores of the same layer, the transport of base layer particles into coarser upper layers (suffosion) and micro-instability on the slope due to the direction of groundwater flow (Lindenberg and de Groot, 1998).

The erosion mechanisms described above may be responsible for triggering further failure mechanisms within an embankment. For example sufficient toe erosion may result in shallow slippage

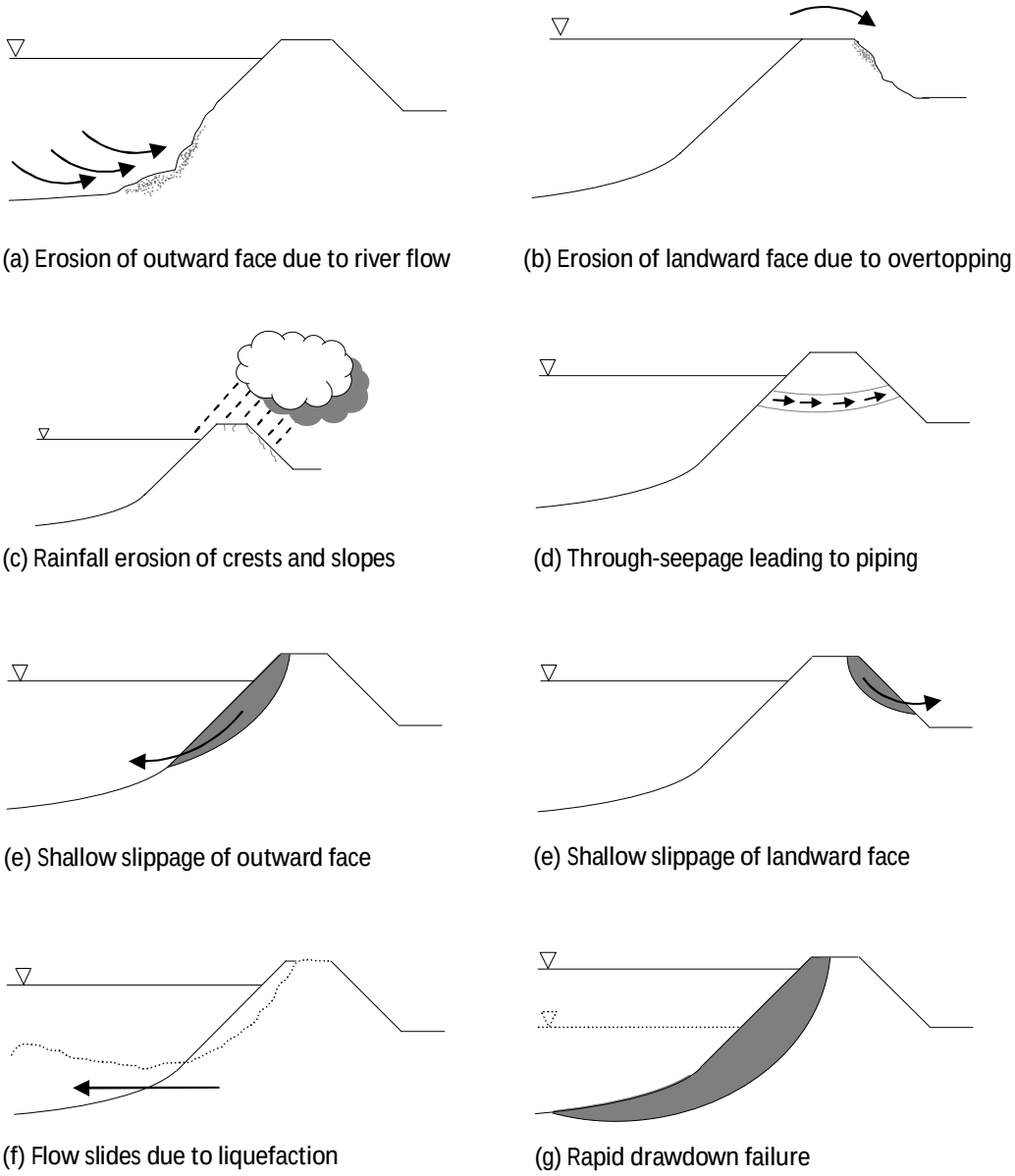

Figure 2.14: Failure mechanisms related to the fill material

of the outward face (Cooling and Marsland, 1954). Erosion at the toe may occur as a result of a scour pool developing, resulting in an over steepening of the outward slope, triggering either an immediate instability or a gradual regression of the slope face depending on the severity of scouring (Dunbar et al., 1999). Furthermore shallow slippage of the landward face may occur in embankments due to through-seepage. However in clayey embankments a different mechanism may also take place due to fine fissuring. Soft highly shrinkable clays tend to have fissures extending to up to approximately 1m depth into the embankment due to desiccation of the embankments and their loss of moisture to surrounding vegetation (Cooling and Marsland, 1954; Marsland and Cooling, 1958; Marsland, 1968). Subsequently a shallow slip may occur when the river level reaches the crest of the embankment, due to strong seepage through the fissured material. This is an area of research which has seen continued interest in the UK (Dyer et al., 2009; Sentenac and Zielinski, 2009). On the other hand, in loose sand embankments, flow slides or slumping of the fill material would be observed rather than defined shallow slips. If sufficient toe erosion or cyclic loading of a sand embankment occurred, liquefaction may in fact take place resulting in the large displacement of the fill material (Lindenberg and de Groot, 1998).

Another distinct type of failure mechanism related to the response of the fill material is rapid drawdown failure. This failure mechanism occurs when a submerged slope is subjected to a rapid reduction in water level. This may be due to natural changes in the water level of the river but more commonly occurs due to the managed release of water in the river through control structures. Instability may arise if the water level (external confining pressure) is reduced at a rate which does not allow for drainage of excess pore water pressures from the embankment (Simon et al., 2003). Typically this may occur in clayey soils of low permeability and may result in a deep rotational failure.

Due to the wide range of materials which may be used in the construction of flood embankments (depending on locally available material), their performance is highly variable and there are a large number of different types of failure mechanisms (Dyer, 2004). In some cases the type of failure mechanism observed is a direct result of the fill material used during construction. Dyer (2004) reported use of slate waste in the Mawddach estuary, Wales which resulted in high seepage rates causing piping failure. Sand and shingle used in embankments in Western Wales also resulted in high seepage rates and embankments constructed in East Anglia using

highly plastic clays failed due to fine fissuring as a result of seasonal wetting and drying (Dyer, 2004). In New Orleans in 2005, failures occurred in sections of embankment constructed of lightweight shell-sand fill, due to its low resistance to erosion (Seed et al., 2008). Furthermore Seed et al. (2008) highlighted a second material which played a role in the catastrophic failures of sections of embankments in New Orleans: dredged material from adjacent shipping channels. However the interesting point to note here is that the problem resulted not just from the inherent characteristics of the material itself but the fact that it was placed at high moisture contents with little or no compaction, therefore making it prone to erosion (Seed et al., 2008). Seed et al. (2008) suggests steps which should have been taken to process the fill material in order to achieve better compaction properties. Design can fail not only in the selection of an appropriate fill material but also in the selection and execution of appropriate compaction conditions.

At this point it is important to note that any of the described failure mechanisms can occur in combination and in any one flood embankment there will often be several different mechanisms occurring although to varying degrees. These combinations can make it more difficult to detect the mechanism which is primarily responsible for triggering the failure of an embankment. It is often the mechanism which leaves behind the most (visual) clues for the engineer, to which the failure is credited.

In Table 2.1 further references regarding studies and observations of each type of failure mechanism discussed here are provided, although this is by no means meant to be an exhaustive list. In general most of the mechanisms related to founding layers are generally investigated by assuming saturated conditions. The mechanisms related to the fill material on the other hand may occur:

1. under saturated conditions: e.g. erosion of toe or outward face, (Cooling and Marsland, 1954)
2. under unsaturated conditions: e.g. erosion of faces and crest due to rainfall, (Perry, 1998) or erosion of landward face due to overtopping, (Möller et al., 2002)
3. due to the transition from saturated to unsaturated conditions: e.g. rapid drawdown failure, (Pinyol et al., 2008)

Table 2.1: Failure mechanisms occurring in flood embankments

	Failure mechanisms occurring in flood embankments	References
Founding layers	Deep seated slope instability due to soft clay founding layers	Leroueil et al. (1990); Dyer (2004)
	Excessive uplift pressures in underlying layers	Cooling and Marsland (1954); Marsland (1957, 1961); Marsland and Randolph (1978); Hird et al. (1978); Padfield and Schofield (1983); Baudin et al. (1989); Dyer (2004)
	Translational sliding due to organic founding layers	Ward (1948); Ward et al. (1955); Dyer (2004); Bezuijen et al. (2005); Van et al. (2005)
	Internal erosion (e.g. piping)	Perry (1998); Dunbar et al. (1999); Morris et al. (2007)
	Settlements due to consolidation or creep	Cooling and Marsland (1954); Leroueil et al. (1990); Lindenberg and de Groot (1998)
Fill material	Erosion of outward face due to river current or wave attack	Cooling and Marsland (1954); Marsland (1957); Lindenberg and de Groot (1998); Perry (1998); Dunbar et al. (1999); Dyer (2004)
	Erosion of landward face due to overtopping	Cooling and Marsland (1954); Marsland (1957); Miller (1990); Perry (1998); Möller et al. (2002); Dyer (2004)
	Rainfall erosion of slopes and crest	Perry (1998)
	Internal erosion (e.g. piping, suffosion)	Lindenberg and de Groot (1998); Perry (1998); Dunbar et al. (1999); Ghataora et al. (2007); Morris et al. (2007)
	Shallow slippage of outward face due to erosion	Simon et al. (2003); Dyer (2004)
	Shallow slippage of landward face due to through-seepage	Cooling and Marsland (1954); Marsland (1957, 1968); Perry (1998); Dyer et al. (2009); Sentenac and Zielinski (2009)
	Flow slides due to liquefaction	Lindenberg and de Groot (1998); Dunbar et al. (1999)
	Rapid drawdown failure	Simon et al. (2002); Pinyol et al. (2008)

4. due to transition between unsaturated to saturated conditions: e.g. reduction of shear strength due to wetting, (Krahn et al., 1989 investigated a railway embankment).

Thus, it is clear that the response of fill material in flood embankments may be affected significantly by changes in moisture content and suction. However, despite this, few laboratory experimental campaigns investigating the unsaturated mechanical behaviour of fill material from flood embankments are available in the literature (e.g. Hoffmann and Tarantino, 2008) and fewer still have been carried out under suction controlled conditions. In this thesis the mechanical behaviour of the Bengawan Solo fill material is investigated under saturated, suction controlled and constant water content conditions.

Lindenberg and de Groot (1998) state that there are two functional requirements of a flood embankment: (i) it must be sufficiently high to protect against flooding (and remain so) and (ii) it should be stable. However it is evident from Table 2.1 that it is the failure mechanisms related to the stability of embankments which have attracted the most interest from practising engineers and researchers over the years. All but one of the failure mechanisms listed in Table 2.1 are concerned primarily with the stability of embankments. Only the mechanism of settlements due to consolidation or creep is directly concerned with the reduction in height of the embankment, reducing the ability of the embankment to retain water. Considering that flood embankments may be compacted at low dry density due to poor compaction control during construction, and that additional loading of embankments are commonly introduced in the form of surface protection, alongside the readily available access to water, it is proposed here that it may also be relevant to investigate the potential for volumetric collapse in fill materials of flood embankments.

2.6 Conclusions

The Bengawan Solo embankments investigated in this thesis have been introduced in this chapter and the different types of processes and mechanisms which may be contributing to failure have been discussed. A brief review of the typical failure mechanisms associated with flood embankments has been outlined. Considering that failure mechanisms related to the fill material

may occur under different saturation conditions, it is clear that it can be useful to investigate embankment fill material under unsaturated conditions. For this reason the Bengawan Solo fill has been studied under saturated and unsaturated conditions within this research. Chapter 3 presents a general overview of the field of unsaturated soil mechanics. The volumetric collapse potential of the Bengawan Solo fill is investigated in Chapter 5, and therein it is also proposed how such a reduction in height may trigger further instabilities in a flood embankment. The unsaturated mechanical behaviour of the fill material is investigated in Chapter 6 in isotropic compression and shearing tests. Information determined experimentally is also used in a routine slope stability analysis to investigate the effect of the reduction of shear strength due to wetting on the stability of the Bengawan Solo embankments.

Chapter 3

Experimental testing, behaviour and constitutive modelling of unsaturated soils

3.1 Introduction

The void spaces in saturated soils are completely filled with liquid which is typically water, whereas the porous phase of unsaturated soils is partially filled with liquid (water) and partially filled with gas, a combination of air and water vapour but generally referred to as air. This additional presence of air creates a multi-phase porous material which results in additional complexities regarding (i) the fundamental behaviour of the soil, (ii) experimental testing and (iii) numerical aspects. This brief review of the field of unsaturated soil mechanics begins with a short discussion on where unsaturated soils are found and why it is considered important to study them. The concept of soil suction is discussed and the types of ways water may be present within unsaturated soils is briefly presented. Some of the methods which have been developed to control

or measure suction in the laboratory are then discussed followed by experimental techniques for measuring volume changes in unsaturated soils. The water retention and hydraulic behaviour of unsaturated soils is presented. This is followed by a discussion on the influence of suction on the mechanical behaviour of unsaturated soils. This chapter concludes by discussing the elasto-plastic constitutive models which may be used to model the behaviour of unsaturated soils.

3.2 Prevalence and importance of unsaturated soils

Despite the fact that the study of soil mechanics has developed with a bias towards saturated soils (Fredlund and Rahardjo, 1993), unsaturated soils are prevalent in the environment. In particular, the surface layer of natural soil deposits are typically unsaturated. The depth of this unsaturated zone varies depending on local climatic conditions. In arid regions an unsaturated zone may be several metres in depth whereas in a temperate climate this zone may only be a few centimetres. Below the water table, (saturated zone), pore water is present in the soil under compression; resulting pore water pressures are assigned a positive value, whereas in the unsaturated zone pore water is held in the soil under tension, these pressures are assigned negative values, between these two zones exists a capillary fringe zone in which the soil may be saturated but pore water pressures remain negative. Soils in the unsaturated zone, close to the ground surface are often considered to be problematic (Fredlund, 2006). In natural soil deposits, damage to structures such as roads or buildings has often been reported due to the swelling or shrinkage of expansive soils (Fredlund and Rahardjo, 1993), or due to collapse settlements in natural soils with an open structure (Houston et al., 2001). These problems result from the moisture sensitive nature of these soils, which undergo important volume changes when subjected to drying or wetting.

Alongside natural surface deposits it can also be beneficial to consider compacted soils from an unsaturated perspective. Compaction reduces the volume of air voids present in soils in order to increase their dry density and ultimately improve their engineering behaviour (Head, 1992). However the process does not allow for total removal of all the air voids present and as such compacted materials contain voids partially filled with water and partially filled with

air. Compacted materials are commonly used in civil engineering works as fill material in the construction of embankments and dams, backfill material behind retaining walls or underneath foundations. However it has been reported that loosely compacted fills may exhibit volumetric collapse when wetted under load (e.g. Booth, 1977; Lawton et al., 1992; Pereira and Fredlund, 2000). Similarly densely compacted fills may exhibit swelling when subjected to wetting (e.g. Kassif and Ben Shalom, 1971; Alonso et al., 2005). Significant deformations in such soils may cause damage to overlying pavements or structures, failure of earth dams or the disruption of underground utilities ((Lawton et al., 1992; Houston et al., 2001).

Gassy soils may also be considered as unsaturated soils. Gassy soils may develop due to biological activity which involves the release of natural gases or where gas flows into a deposit from a deeper hydrocarbon reservoir. These soils may be found in deep offshore environments and organic deposits where anaerobic activity may prevail. In these cases gases tend to be discrete bubbles and it is the size of the gas bubbles relative to the average solid particle which dictates how the material should be considered. If the gas bubbles are small an effective stress approach may still be suitable if the increased compressibility of the pore fluid is also taken into account (Wheeler, 1986). However if the gas bubbles are large such that a single bubble is surrounded by many particles, the gas and water phases should be considered independently (Wheeler, 1988b). Such large bubbles can have a significant influence on the mechanical behaviour of these soils (Wheeler, 1988a; Karstunen and Pande, 1994).

As described many geotechnical engineering problems encountered are related to the behaviour of unsaturated soils in the form of both surface soil deposits or compacted materials. The research presented in this thesis has been carried out within the context of unsaturated soil mechanics due to its investigation of a compacted material used in the construction of a flood embankment.

3.3 Retention of water and soil suction in unsaturated soils

3.3.1 Capillary effects

The forces acting on a water molecule located at gas-liquid interfaces are different to those acting on molecules completely surrounded by other liquid molecules (Figure 3.1) (Fredlund and Rahardjo, 1993). When located within (bulk) liquid a molecule experiences equal forces in all directions. However a liquid molecule located at the gas-liquid interface experiences an unbalanced resultant force towards the liquid. In order for the gas-liquid interface to be in equilibrium, a tensile stress is generated, commonly referred to as surface tension (T_s) which causes the interface to act like a membrane under tension (Fredlund and Morgenstern, 1977; Fredlund and Rahardjo, 1993).

When gas-liquid interfaces come into contact with a solid body, the interface curves near the solid surface, forming a meniscus. The contact angle which the liquid makes with the solid surface varies depending on the type of liquid, nature of the solid and fluid pressures. For wetting liquids such as water, contact angles (θ) of less than 90° are typically formed when in contact with solid soil particles (Figure 3.2a), the liquid has a greater attraction for the solid surface than for other liquid particles (adhesion > cohesion). Whereas non-wetting liquids such as mercury tend to form contact angles greater than 90°, mercury particles have greater attraction for each other than for the solid surface (cohesion > adhesion) (Tarantino, 2010a).

If we consider the simple example of an air-water interface within a capillary tube (Figure 3.3), the pore water pressure (u_w) and the pore air pressure (u_a) on each side of the meniscus can be

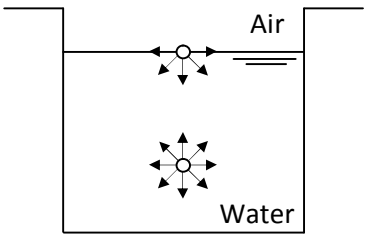

Figure 3.1: Forces acting on molecules located (a) at an air-water interface and (b) within water (After Fredlund and Rahardjo, 1993)

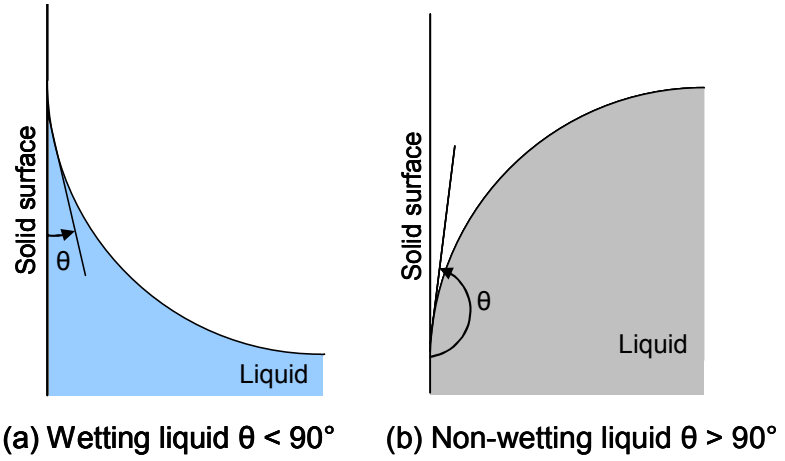

Figure 3.2: Gas-liquid interfaces in contact with solid surface (a) for wetting liquid and (b) non-wetting liquid (After Tarantino 2010a)

related to surface tension (T_s), the radius of the capillary tube (r) and the radius of curvature of the meniscus (R) by considering equilibrium across the air-water interface:

$$u_a \pi r^2 = u_w \pi r^2 + 2\pi r T_s \cos\theta \tag{3.1}$$

Thus:

$$u_w - u_a = -\frac{2T_s \cos\theta}{r} = -\frac{2T_s}{R} \tag{3.2}$$

Equation 3.2 is known as Kelvin's capillary model equation and illustrates that for contact angles less than 90°, the gauge pressure ($u_w - u_a$) will be negative, i.e. a concave meniscus is formed where pore air pressure is greater than pore water pressure. It can be useful to consider soils as being made up of many inter-connected capillaries of varying diameter. Sands typically have a grain size in the range of several mm, whereas clays are typically in the range of several µm, as pore space is also highly dependent on grain size it follows that in sands pore diameters would also be much greater than the pore diameters found in clays (~ 1000 times greater). Using Equation 3.2 with representative values for pore space found in soils, ($u_w - u_a$) becomes increasingly negative as pore diameter decreases, (i.e. moving from sands to clays). Given that in the field pore air pressure is usually atmospheric (0kPa gauge pressure, 101.325 kPa absolute pressure) and that ($u_w - u_a$) found in silts and clays can be much lower than -100kPa, this

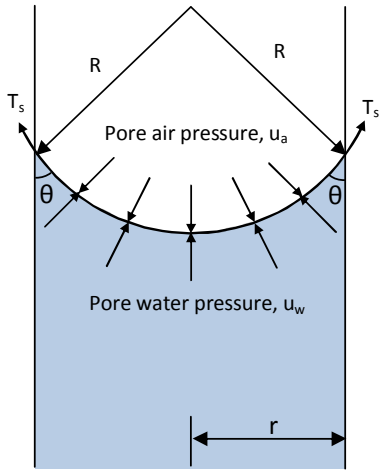

Figure 3.3: Forces acting across air-water interface in capillary tube

indicates that the pore water is being held in tension within such soils (Tarantino, 2010a).

3.3.2 Evaporation of water from soils

Given that most unsaturated soils are found in soil deposits close to the ground surface or in compacted earthworks, the main processes by which water is removed from soil pores are evaporation and lowering of the soil water table. If we still consider that the pore space in soils can be represented in a simplified manner by a series of inter-connected capillary tubes, water can be assumed to be removed from the pore space during evaporation in steps similar to those illustrated in Figure 3.4. Initially in Stage 1, it is assumed that gauge pore water pressure is zero and thus the air-water interface is flat (contact angle = 90^o). As evaporation occurs, water is first removed without moving the location of the meniscus with respect to the solid surface, but rather the curvature of the meniscus increases, the contact angle reduces and the water pressure behind the meniscus falls below atmospheric pressure (Stage 2) until a limiting value of the contact angle, termed the receding contact angle (θ_r). Since water pressure must be equal behind each of the three menisci present in tubes A, B and C, the contact angle will be lowest in the largest tube, tube A and thus the receding contact angle limit will be reached in tube A first. Therefore tube A will empty of water first (Stage 3) while at constant water pressure, the minimum that the tube can withstand. Continued evaporation will cause the curvature of the menisci in tubes B and C to increase, until the limit receding angle for tube B is reached

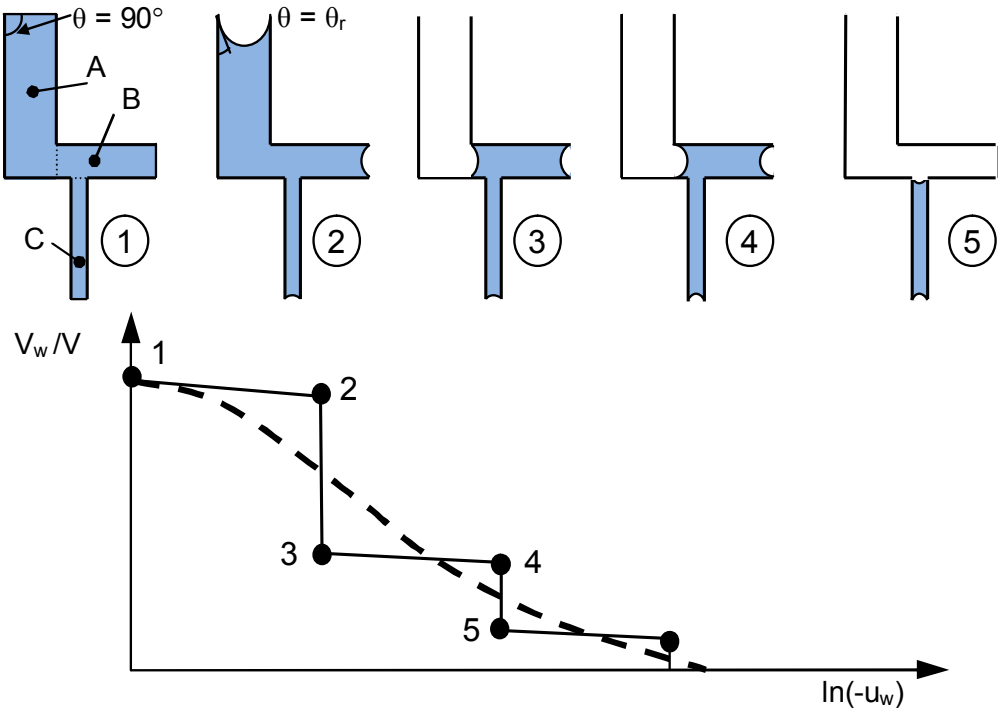

Figure 3.4: Evaporation from a capillary system (Tarantino, 2010a)

(Stage 4), which will empty at constant water pressure (Stage 5). Further evaporation would ultimately lead to the removal of water from tube C, of smallest diameter. In Figure 3.4 the degree of saturation (volume of water per total volume of capillary system) is plotted against water pressure following the stages described above. For an infinite number of capillary tubes of varying diameter, a relationship between degree of saturation of the system and water pressure may be expected to be similar to the dashed line shown in Figure 3.4, closer to representing the pore network present within soils. This description of the evaporation of water in soils is summarised from the clear explanation provided by Tarantino (2010a).

3.3.3 Retention of water

The relationship between degree of saturation and negative water pressure found experimentally by subjecting soils to subsequent drying stages is essentially the same as that presented in Figure 3.4. Within the field of unsaturated soils, this relationship is commonly referred to as the soil water retention curve, and may be plotted in terms of gravimetric moisture content (w),

volumetric moisture content (θ_w) or degree of saturation (S_r) against negative water pressure ($-u_w$) or the excess of pore air pressure over pore water pressure ($u_a - u_w$). Figure 3.5 illustrates the main features of a typical water retention curve for a fine grained soil (Vanapalli et al., 1996, 1999; Tarantino, 2010a). As a soil is dried from a fully saturated condition, initially only water is removed as the curvature of the menisci increase, but the soil remains in a *saturated state*, albeit at water pressures below atmospheric. On continued drying some of the larger pores will empty of water, but the air phase will remain discontinuous (*quasi-saturated state*). Further drying will cause the menisci to recede and air to enter into the soil. Both the air and water phases are continuous in the *partially saturated state*. Finally continued drying will result in only meniscus water remains at inter-particle contacts, the water phase is no longer continuous (*residual state*).

The air-entry value (AEV) denoted in Figure 3.5a identifies the value of negative pressure at which drainage of the largest soil pores begins, beyond this value, soils exhibit a rapid decrease in moisture content (Vanapalli et al., 1996). This value is typically determined by intersecting the horizontal line drawn at $S_r = 1$ with the tangent to the inflection point of the drying curve (Vanapalli et al., 1996). The residual degree of saturation (s_{rR}) is the saturation level at which increasing negative water pressure no longer significantly causes moisture content loss and where further moisture loss must be transferred through vapour transfer (Figure 3.5a).

A number of soil water retention curves are illustrated in Figure 3.5b. The main drying curve is that which refers to the changes occurring within a soil which has been dried continuously from a fully saturated sample. If a fully dry sample is wetted continuously, it will follow along the main wetting curve. It is evident that there is significant hydraulic hysteresis between the paths followed by drying and wetting curves. This means that for a given negative water pressure the soil may have a different degree of saturation depending on what curve the sample is on. This hysteresis is due to a number of different phenomenon including the ink bottle effect, the raindrop effect and the entrapment of air bubbles (Haines, 1930; Bear, 1972; Romero, 1999). The ink bottle effect stems from the fact that soil pores are not perfectly cylindrical and in fact are highly irregular with varying cross-sectional area along their length. This effect is explained in Figure 3.6. Along a drying curve it is the small entrance radius r_1 which dictates whether water will drain out of the pore whereas along a wetting curve it is the maximum radius r_2 of

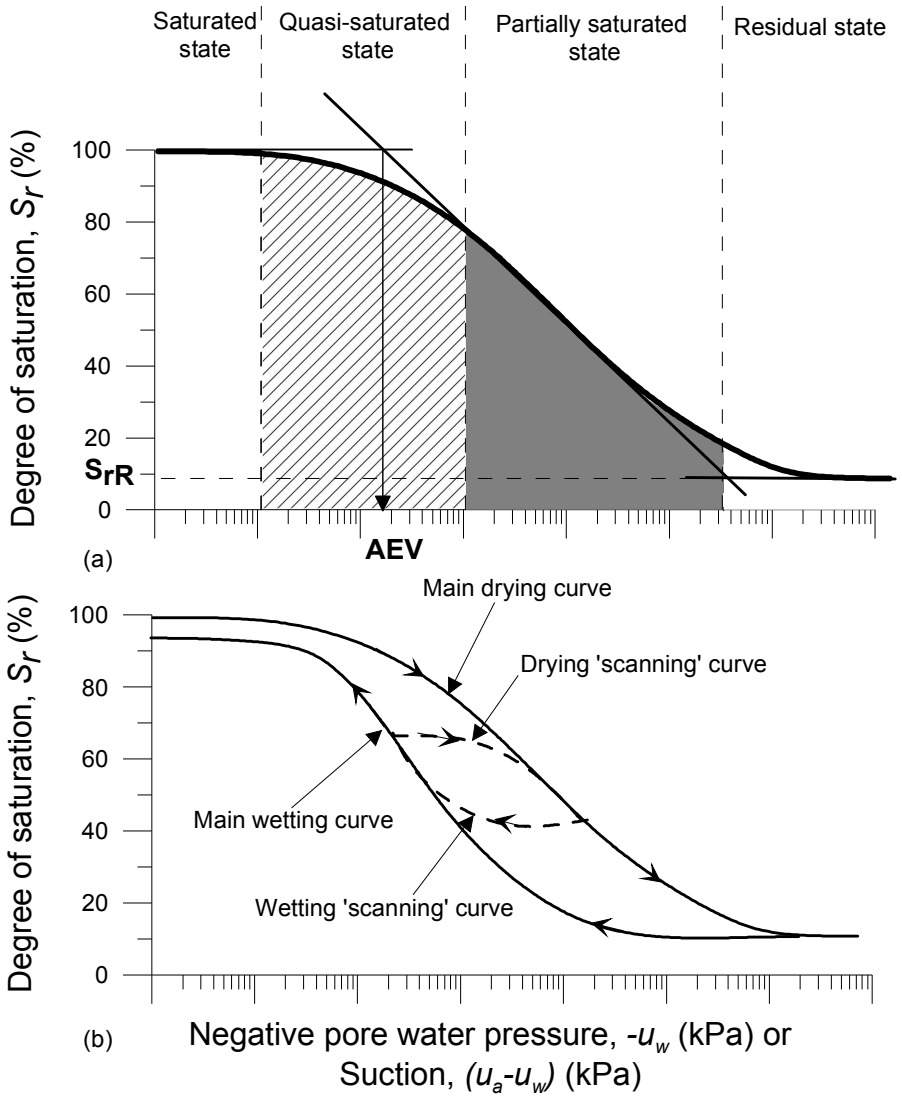

Figure 3.5: Typical features of a water retention curve (a) saturation states along a main drying curve and (b) hysteresis between drying and wetting curves (After Tarantino, 2010a)

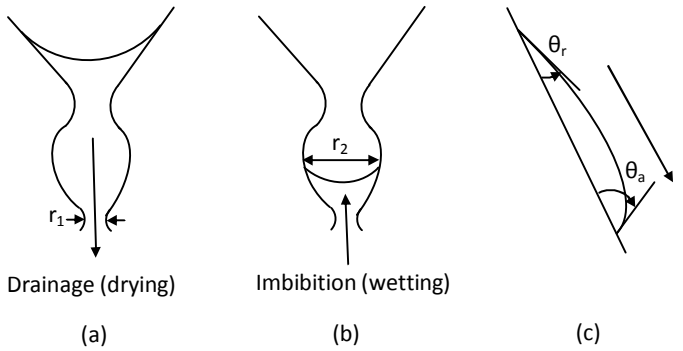

Figure 3.6: Hysteresis phenomenon: the ink bottle effect during (a) drying, (b) wetting and (c) the raindrop effect

the large pores which dictates the negative water pressure required for the pore space to fill with water (Haines, 1930). Therefore for the same water pressure level, different volumes of the same pore space may be filled (different degree of saturation). The so called raindrop effect refers to the variation in contact angle which is dependent on the direction of movement of the fluid. The contact angle between the pore fluid and soil surface is different depending on whether the pore fluid is receding (drying) or advancing (wetting) (see Figure 3.6c). Variations in the contact angle may further depend on the roughness of the surface, the presence of impurities and also whether or not the surface has previously been wetted (Bear, 1972). Furthermore hysteresis between the drying and wetting curves also occurs due to the difficulty of achieving full saturation along the wetting curve when starting from a dry sample. In reality some air bubbles remain in the pore fluid and thus full saturation is not achieved (see Figure 3.5). Finally hysteresis occurs between the main drying and wetting curves because many soils are deformable materials which may undergo volume changes during drying and wetting, particularly if active clay minerals are present. Such changes may significantly alter the soil structure during drying or wetting and contribute to the hysteresis observed between the different water retention paths (Romero and Vaunat, 2000; Nuth and Laloui, 2008a).

Between the two main drying and wetting curves, any number of scanning curves may be observed (Figure 3.5b). Increasingly the hydraulic history of the soil is being considered for soil water retention behaviour, in a manner similar to the way in which stress history is considered in mechanical behaviour. That is to say the behaviour within the scanning region may be assumed

to be reversible, whereas changes in degree of saturation and negative water pressure along the main drying or wetting curves may be considered to be irreversible (Nuth and Laloui, 2008a; Tarantino, 2010a).

3.3.4 Soil suction

Considering the negative water pressures found within unsaturated soils, if such soils are placed in contact with free water (under atmospheric pressure) they would have an affinity for this water (water would be drawn towards the soil), this affinity is commonly referred to as soil suction. Thus far, the discussion has focused on the capillary effects occurring within unsaturated soils and the corresponding negative water pressures typically present. However capillary effects are not the only phenomenon controlling soil suction and the transfer of water within unsaturated soils, nor does water transfer only occur via the liquid phase (Tarantino, 2010a).

3.3.4.1 Matric suction

Matric suction is the affinity of the soil for water, which arises from water retention mechanisms which are related to the solid phase. Capillary effects are indeed the dominant contribution of matric suction for granular materials where no chemical interactions exist between the solids and pore water (e.g. sands). Even in clayey soils, capillary forces play a role in the lower suction range (Tuller et al., 1999; Tuller and Or, 2005), however at much higher suctions, surface adsorptive forces dominate. At low degrees of saturation (high suction range), water is held as films of liquid covering the soil particles, the thickness of the water films are dependent on surface adsorptive forces (Tuller and Or, 2005), (Figure 3.7).

Surface adsorption of pore water onto soil particles is controlled by a number of physico-chemical effects, including (i) van der Waal's forces, (ii) electrostatic forces and (iii) hydration forces (Tuller et al., 1999; Tuller and Or, 2005; Tarantino, 2010a). Van der Waal's forces are the weak inter-molecular bonds formed between the positive anions present in inter-layer water and the negative cations of the clay particles. Due to the negatively charged clay particles, there is a difference in concentration in the pore water found within the inter-layer space and the concentration of the pore water solution. Thus water molecules tend towards the inter-layer space

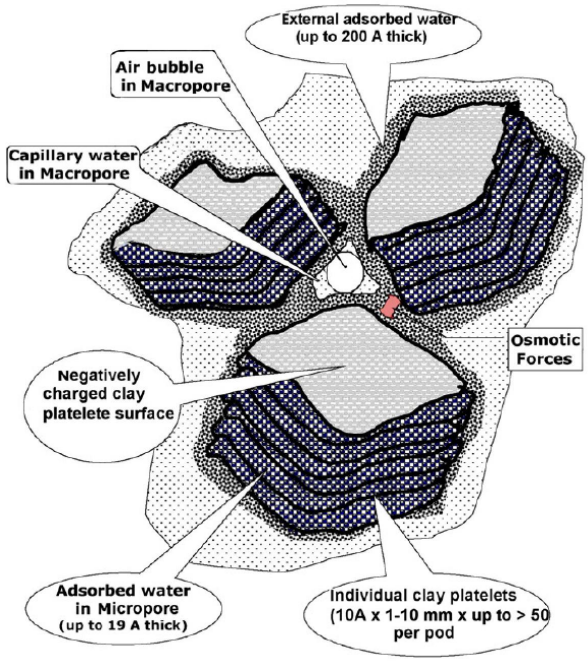

Figure 3.7: Simplified schematic of water present as liquid films covering soil particles due to surface adsorptive forces (Baker and Frydman, 2009)

in order to equalise the charge concentration. Electrostatic forces arise from water molecules forming hydrogen bonds with hydroxyl molecules found in the tetrahedral and octahedral silica sheets of which clay particles are formed. Hydration forces are important in active clays, where hydration of inter-layer cations results in repulsive forces, increasing the inter-layer space, i.e. expansion of clay layers. All of the physio-chemical effects giving rise to adsorbed water films depend on the minerals present and surface properties of the soil particles (Tuller et al., 1999; Tuller and Or, 2005).

Increasingly discussions have argued that more consideration should be afforded to the contribution of surface adsorption to matric suction alongside that of capillarity (Nitao and Bear, 1996; Baker and Frydman, 2009; Frydman and Baker, 2009), as often in geotechnical engineering only capillary effects are considered to contribute to matric suction (Baker and Frydman, 2009). It is important to note however that regardless of whether pore water is present in capillary form or as adsorbed surface water, it is still held under tension in unsaturated soils. The influence of this suction on the overall macroscopic behaviour appears to be similar, for example collapse behaviour has been observed in sandy soils (Leonards and Narain, 1963; Lawton et al., 1992)

and equally in clayey soils (Peterson and Iverson, 1953; Lawton et al., 1992).

Both capillary and adsorptive forces are thus responsible for contributions to matric (or matrix) suction and the transfer of water within the liquid phase of unsaturated soils. Matric suction is commonly defined as the excess of pore air pressure (u_a) over pore water pressure (u_w) (Fredlund and Rahardjo, 1993):

$$s = u_a - u_w \tag{3.3}$$

although this is derived only from capillary effects. However it is more appropriate to consider matric suction as a variable which quantitatively reflects the degree of attachment of the liquid phase to the solid phase, arising from solid-liquid-air interfaces (Gens, 2010). Considering matric suction as a measure of the potential of the liquid located close to the solid surface should minimise confusion surrounding the physical meaning of very high suctions of hundred of MPa observed in some clays; matric suctions should not be considered as pressures in the typical (bulk thermo-dynamic) sense (Gens, 2010).

3.3.4.2 Total suction

Water can also be transferred to or from soils via the vapour phase. This transfer is made possible by the fact that the partial water vapour pressure in equilibrium with pore water (P) is lower than the water vapour pressure in equilibrium with pure free water (Tarantino, 2010a). This reduced vapour pressure in equilibrium with pore water (P_0) is due to two main mechanisms: (i) negative pore water pressure and (ii) the concentration of pore water (Tarantino, 2010a). The Poynting effect means that the pressure of vapour in equilibrium with its own liquid decreases as liquid pressure decreases where the liquid pressure decrease is generated by the solid phase (matric suction) (Tarantino, 2010a). Secondly Raoult's law states that the vapour pressure in equilibrium with an aqueous solution will decrease as the solute concentration increases (Tarantino, 2010a). The suction generated due to changes in solute concentration is commonly referred to as osmotic suction.

The concept of soil suction was developed by soil physicists in the early 1900s (e.g. Buckingham, 1907). The importance of soil suction in terms of the mechanical behaviour of unsaturated soils was first recognised by Croney and Coleman (1948). Aitchison (1965) defined the soil-water

(total) potential (ψ), which corresponds to the free energy state of the soil per unit mass (J/kg) as being the sum of four components:

$$\psi = \psi_g + \psi_p + \psi_m + \psi_o \tag{3.4}$$

where ψ_g is the gravitational potential, ψ_p is the gas pressure potential, ψ_m is the matric potential and ψ_o is the osmotic potential. Neither the gravitational nor gas pressure potential influence the mechanical behaviour of unsaturated soils in a significant way and are thus not generally considered in geotechnical engineering (Gens, 2010). Considering the soil-water potential energy in terms of per unit volume of soil (instead of per unit mass), the term is called suction, and is expressed in terms of pressure (kPa). Thus total suction (s_t) may be written as the sum of matric suction (s) and osmotic suction (s_o), $s_t = s + s_o$. Total suction (s_t), the free energy state of the soil water per unit volume, may be related to relative humidity using Kelvin's law:

$$s_t = -\frac{RT}{M_w} ln \left(\frac{P}{P_0} \right) \tag{3.5}$$

where R is the universal gas constant (8.314 J/Kmol), T is the absolute temperature (K), M_w is the molecular mass of water (kg/mol), $(\frac{P}{P_o})$ is the relative humidity of air in equilibrium with the pore water. In non-active soils, osmotic effects are likely to be negligible (Gens, 2010) and as such attention is generally focused on matric suction. For non-active soils measurements of total suction should also give a good indication of the changes in matric suction occurring. Furthermore osmotic suction tends to be a much smaller component of the total suction than matric suction. For these reasons it is generally the total suction or matric suction which is controlled or measured in the laboratory. The different techniques which have been developed for controlling or measuring suction in the laboratory are discussed in the next section.

3.4 Experimental techniques for unsaturated soils

The presence of pore air in the porous phase of unsaturated soils and the subsequent suction present in the soil present additional complexities in terms of experimental techniques: (i) the ability to control or measure suction in the laboratory (and in-situ) and (ii) the determination

of volume changes in unsaturated soils, which can be difficult to determine considering that air is compressible. Six different methods which can be used used to control or measure suction in the laboratory are briefly discussed in this section. Considering that the growing interest in the field of unsaturated soil mechanics has led to more experimental research being carried out and increasing numbers of conferences in this field (Delage, 2002), there is now a wealth of information available on experimental techniques for unsaturated soils in keynote papers and state of the art reviews. In particular a recent issue of the Journal of Geotechnical and Geological Engineering was dedicated to the topic: Special Issue on Laboratory and Field Testing of Unsaturated Soils (Tarantino et al., 2008). Please refer to the following papers for a more in-depth discussion of the techniques outlined below: Ridley and Wray (1996); Delage (2002); Blatz et al. (2008); Delage et al. (2008); Marinho et al. (2008); Vanapalli et al. (2008).

The different types of techniques which can be used to measure volume changes in unsaturated soils are also briefly outlined in this section.

3.4.1 Methods of suction control

Three methods which can be used to control suction in the laboratory are presented here: (i) axis translation technique, (ii) osmotic method for control of matric suction and (iii) vapour equilibrium technique. The general principles of these methods are presented, followed by advantages and limitations or concerns related to each method. Alternative methods of suction control (at very low suctions) include the hanging column and centrifuge techniques.

3.4.1.1 Axis translation technique

Typically in unsaturated soils pore air pressure is atmospheric (u_a= 0 kPa) and pore water pressures are negative with respect to atmospheric pressure. The axis translation technique originally proposed by Hilf (1956) translates the origin of reference for the pore water pressure from standard atmospheric conditions to the air pressure applied in the chamber. This translation of the pore water pressures relative to the pore air pressure applied avoids the problem of cavitation which typically occurs when a body of water is brought towards a suction level of -100kPa (relative to atmospheric conditions).

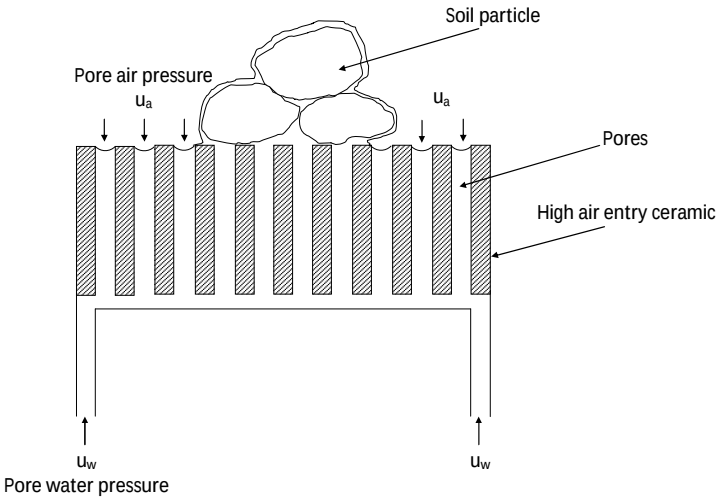

Figure 3.8: Principles of axis-translation technique

Matric suction is controlled by liquid transfer through a saturated interface in contact with a soil specimen; typically a saturated high air entry (HAE) ceramic is commonly used to separate the pore water and pore air phases in the axis-translation technique. The high air entry value is the value at which air will enter the ceramic; this is dependent on the size of the pores within the ceramic. A fully saturated HAE ceramic will allow water to flow down through its pores while acting as a barrier to pore air flow. Ceramic stones with air entry values of 100kPa, 500kPa and 1500kPa are commercially available (Soil Moisture Equipment Corp.). Thus the maximum suction which can be applied using this technique is 1500kPa; the highest air entry value ceramic currently available. Furthermore the range of its application depends on the maximum air pressure source available within a laboratory and the availability of high capacity pressure cells if high suctions are to be tested.

The axis translation technique was first incorporated into geotechnical testing systems by Bishop and Donald (1961) where it was implemented in the triaxial apparatus. Since then the axis translation technique has become the most widely used method of suction control in the investigation of unsaturated soils and has been incorporated into a number of different types of experimental apparatus. This technique is routinely used by researchers as a method of determining the water retention curve in the pressure plate apparatus (e.g. Krahn and Fredlund, 1972; Navaneethan et al., 2005). It has also been incorporated into direct shear boxes (Escario, 1980) and one-

dimensional consolidation testing apparatus, in both Rowe cells (Barden and Sides, 1970) and oedometers (e.g. Alonso et al., 1995; Hoffman et al., 2005) and continues to be used within triaxial testing systems (e.g. Wheeler and Sivakumar, 1995; Futai and Almeida, 2005). For the most part it has been the experimental results obtained using the axis translation technique which have been used to validate the constitutive models developed for unsaturated soils.

Although widely used there are a number of criticisms and limitations regarding the axis translation technique: (i) the raised pore water pressure is not representative of field conditions as it prevents cavitation from occurring, (ii) there is concern over how the pressurisation affects water held by adsorption and (iii) the technique is not applicable at high degrees of saturation where pore air may be present in the form of occluded bubbles (Delage et al., 2008). Due to its possible influence on desaturation processes Baker and Frydman (2009) questioned the relevance of results obtained using the axis translation technique in the laboratory for field conditions.

Experimental issues related to the axis translation technique include (i) diffusion of air through the ceramic stone which may occur due to the pressure difference applied across the ceramic, (ii) evaporation of the specimen due to suctions imposed by the relative humidity of the air applied and (iii) time to reach suction equalisation (Delage et al., 2008). Pore air dissolved in the pore water present above the ceramic (at a higher pressure) may come out of solution after passing through the ceramic and reaching a lower pressure. This may result in the formation of air bubbles underneath the ceramic stone. To minimise the effects of this a flushing system should be used (e.g. Sivakumar, 1993). Furthermore to minimise the amount of diffusion which will occur, elevated pore water pressures should be used (Delage et al., 2008). Further information on the limitations and experimental concerns related to the axis translation technique can be found in Delage et al. (2008); Marinho et al. (2008); Vanapalli et al. (2008).

In this thesis the axis translation technique has been used as the principle form of suction control, in both oedometer and triaxial testing. Pressure plate testing was also carried out as part of this research as a means of investigating the soil water retention behaviour.

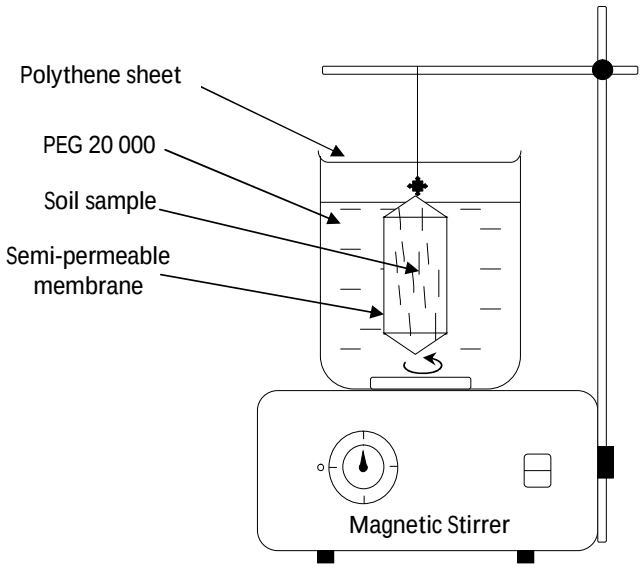

Figure 3.9: Osmotic technique for determination of water retention behaviour (After Cui and Delage, 1996)

3.4.1.2 Osmotic control of matric suction

In this technique the transfer of water occurs by the process of osmosis, where the sample is placed on a semi-permeable membrane, (permeable to water) which is in contact with a circulating polyethylene glycol (PEG) solution (see Figure 3.9). The solution must be continuously circulated to avoid the solution becoming diluted at the membrane boundary. A PEG solution is made up of large sized molecules which cannot pass through the semi-permeable membrane thus applying an osmotic potential to the sample across the membrane. A number of different PEG solutions exist which are defined in terms of their molecular weight, commonly PEG solutions of 20,000 or 6,000 molecular weight are used in geotechnical testing (Delage et al., 1998). Delage et al. (1998) were however able to obtain suctions as high as 12.6MPa using a low molecular weight solution of 1,500. The semi-permeable membrane to be used must be selected in terms of its molecular weight cut off (MWCO), i.e. for a PEG solution of 20,000 a membrane with a MWCO of 14,000 should be selected, so that the molecules cannot pass through the membrane.

The osmotic technique was first developed by biologists and soil scientists (e.g. Zur, 1966) and was introduced into geotechnical engineering testing by Kassif and Ben Shalom (1971), where this method was used to study the behaviour of expansive soils in an oedometer. This technique

was further refined by Cui and Delage (1996) who incorporated a peristaltic pump to ensure continuous circulation of the PEG solution and applied it to triaxial testing. This technique has also been investigated at Imperial College, London (e.g. Dineen, 1997; Cunningham, 2000; Monroy, 2006).

Osmotic control of the matric suction does allow cavitation to occur and thus conditions similar to the field may be replicated (Delage et al., 2008). Furthermore it enables suctions $>$ 10MPa to be reached without the need to raise cell pressures, as in the axis translation technique. A disadvantage of the osmotic technique is that matric suction cannot be continuously varied as different PEG concentrations are required in order to achieve different suction levels. Furthermore as pore water is removed from a specimen, the concentration of the PEG solution will vary, affecting the suction being applied. The main area of concern with regard to the osmotic technique is the degradation of the semi-permeable membrane with time, which is due to bacteria attacks on the cellulose acetate membranes which are generally used, this can be improved by adding penicillin to the PEG solution (Blatz et al., 2008; Delage et al., 2008). Alternatively polyether sulfonated semi-permeable membranes have also been used in tests up to 146 days, greatly improving the durations which can be achieved by the osmotic method (Monroy et al., 2007; Delage et al., 2008). Another limitation of the technique is the time required for equilibrium to be reached. For the set-up shown in Figure 3.9, it took around one week for suction equilibration to be reached. Further information regarding the osmotic technique can be found in Delage et al. (1998); Blatz et al. (2008); Delage et al. (2008).

3.4.1.3 Vapour equilibrium technique

The vapour equilibrium technique is based on the psychrometric law (Equation 3.5) where the relative humidity of the surrounding air is controlled. For a soil sample placed in a desiccator with an aqueous solution (Figure 3.10), water exchanges will occur by vapour transfer between the pore water in the soil and the aqueous solution until a vapour equilibrium is reached, thus applying a given suction to the soil sample. This technique can be used to apply very high total suctions to a soil sample, and can be used within the range of 3-1000MPa (Pintado et al., 2009). The relative humidity may be varied by using different aqueous solutions or by using different concentrations of the same solution. The use of of saturated saline solutions is now preferred

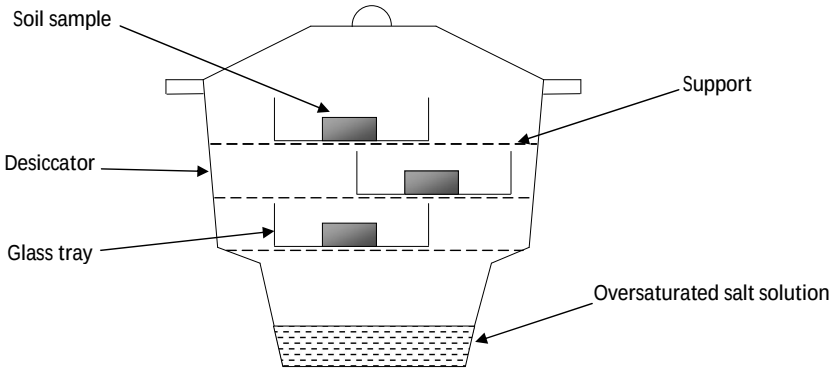

Figure 3.10: Vapour equilibrium technique (After Tang and Cui, 2005)

over the use of acidic solutions (e.g. sulphuric acid) for both experimental and safety reasons (Delage et al., 1998; Pintado et al., 2009). Experimentally it is easier to control the saturation condition of a solution than it is to control its salt or acid concentration (Pintado et al., 2009).

The vapour equilibrium technique was initially developed by soil scientists and was first introduced into geotechnical testing by Esteban and Saez (1988). This technique has been incorporated into oedometer testing for the investigation of highly swelling clays or evaporitic rocks, which require testing under high suctions (e.g. Esteban, 1990; Cusinier and Masrouri, 2005; Pintado et al., 2009). Furthermore it has also been incorporated into triaxial testing (e.g. Blatz and Graham, 2000).

The main limitation of this technique is the particularly long time for equilibrium to be reached after suction changes, due to the fact that moisture content changes occur by vapour transfer. For heavily compacted clay samples with low permeability, the time to reach equilibrium after a suction change may reach several weeks. In order to reduce the time taken for equilibrium to be reached, humid air may be circulated through a sample or at its extremities using a pump (e.g. Blatz and Graham, 2000; Lloret et al., 2003). Pintado et al. (2009) found that circulating humid air through a sample can reduce equilibrium times from weeks to days. However the applied flow of the humid air must be carefully controlled to avoid a different suction being applied than desired, at high velocities it may be the flow of humid air controlling the suction rather than the relative humidity of the solution (Pintado et al., 2009).

Additional information regarding the vapour equilibrium technique can be found in Blatz et al. (2008); Delage et al. (2008).

3.4.2 Methods of suction measurement

The following three methods of measuring suction are described here: (i) high capacity tensiometers, (ii) the filter paper method and (iii) chilled-mirror dew-point technique. The general principle of each of these methods is presented alongside advantages and drawbacks associated. Alternative methods of measuring suction include the use of thermocouple psychrometers, transistor psychrometers, electrical conductivity sensors and thermal conductivity sensors. Further information on these alternative methods can be found in Bulut and Leong (2008).

3.4.2.1 High capacity tensiometers

Tensiometers are devices which measure the matric suction of soil directly by measuring the negative pore water pressure while pore air pressure is atmospheric, i.e. under conditions similar to the field. Ridley and Burland (1993) presented the first instrument of this kind which was capable of measuring matric suctions greater than 100kPa (high capacity tensiometer). This device is often referred to as the Imperial College tensiometer. Prior to this development, tensiometers were only capable of reaching matric suctions between 60-100kPa due to the problem of cavitation. Figure 3.11 shows an updated version of the Imperial College tensiometer presented by Ridley et al. (2003), based on the same principles. The instrument consists of three main components: (i) a high air entry value ceramic, (ii) a water reservoir and (iii) a pressure or strain gauge. The high air entry value ceramic is typically 15bar (1500kPa) in these tensiometers and separates the water and air phases as in the axis translation technique. The water reservoir must be very small in magnitude to reduce the risk of bubble formation in the reservoir. If the ceramic is in good contact with the pore water of the soil sample, water will flow between the soil and the reservoir until equilibrium is reached. An electronic transducer, typically a strain gauge attached to the water reservoir will be able to detect changes in movement due to flow of water into or out of the reservoir. This enables a direct measurement of the matric suction of a soil to be measured. The device presented in Figure 3.11 was able to sustain matric suctions of up to 1500kPa, corresponding to the air entry value of the ceramic.

The main disadvantage of these instruments is water cavitation which may occur before pressure equalisation has occurred, thus interrupting the test and requiring resaturation. The issue of

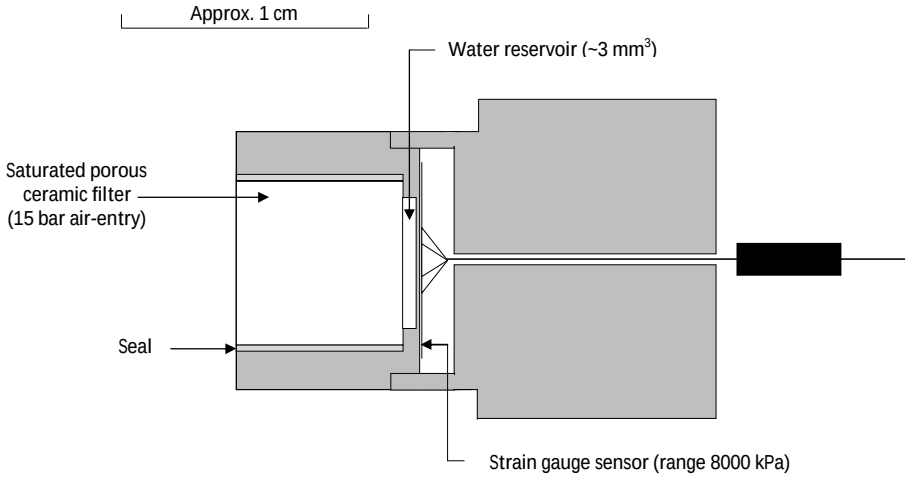

Figure 3.11: Imperial College tensiometer (After Ridley et al., 2003)

cavitation has had an important role in the design of these instruments (i.e. use of a very small water reservoir, smooth surfaces free from roughness etc.) but also it is responsible for the development of methodical procedures which must be followed in order to achieve reliable suction measurements. Important procedures include the initial removal of air by vacuum, initial saturation of the water reservoir and ceramic disc, saturation prior to each measurement, etc. Detailed procedures can be found in Ridley and Burland (1999); Tarantino and Mongovì (2001). Furthermore the calibration of this instrument has typically been carried out in the positive range and then calibrated to the negative range. Tarantino and Mongovì (2003) verified experimentally using a new tensiometer (Trento tensiometer) that this is a justified approach by developing a system to allow direct calibration in the negative range.

Despite their limitations, the use of tensiometers in geotechnical testing campaigns has been successful, but has been largely restricted to those research groups with the most knowledge and experience in the design, construction and experimental functioning of these devices (i.e. Imperial College and Università degli Studi di Trento). However, more recently work on high capacity tensiometers has also been carried out at Durham University in conjunction with Wykeham Farrance (Lourenço, 2008). Equipment has been developed to allow the incorporation of tensiometers in oedometer testing (e.g. Jotisankasa, 2005), direct shear testing (Tarantino and Tombolato, 2005), triaxial testing (e.g. Jotisankasa, 2005) and to allow suction measurements during static compaction (Tarantino and De Col, 2008). The main advantage of tensiometers is

their very quick response time, allowing for suction measurements to be taken within minutes or hours (depending on the soil type, degree of saturation etc.), as opposed to the equilibrium time periods of days and weeks as is required by all of the suction control methods.

Further information on the use of high capacity tensiometers can be found in the following keynote and state of the art papers: Ridley and Wray (1996); Tarantino (2004); Delage et al. (2008); Marinho et al. (2008).

3.4.2.2 Filter paper method

The filter paper method relies on the principle that the water content of a filter paper in contact or closely located to a soil sample will come to equilibrium with the moisture content in the soil, corresponding to the soil suction of the sample. This method is an indirect method of suction measurement; the moisture content of the filter paper is measured at equilibrium and related to suction by means of a calibration relationship. Water transfer may be either by liquid or vapour exchange depending on whether or not the soil is in direct contact with the filter paper. If in direct contact, matric suction may be measured, under non-contact conditions total suction can be measured. Filter papers can measure soil suction over a wide range of values up to as high as 30MP. Equilibrium times are typically in the region of 7 days for matric suction measurements and 14 days for total suction measurements (e.g. Ridley et al., 2003). However, this may vary depending on soil type, distance of filter paper from sample, etc. The filter paper method must be carried out with great care as it is highly user dependent: good technique is of the utmost importance in obtaining accurate results (Bulut et al., 2001; Bulut and Leong, 2008). In general two types of filter papers have been used for suction measurements in unsaturated soils: Schleicher & Schuell No. 589 and Whatman's No. 42 filter papers.

This technique was first used by soil scientists but has been routinely used for suction measurements in geotechnical research for more than twenty years. As such for the two filter papers mentioned, extensive work has been carried out in determining calibration relationships and in refining procedural techniques, (e.g. Chandler and Gutierrez, 1986; Chandler et al., 1992; Bulut et al., 2001; Ridley et al., 2003. Bulut et al. (2001) gives a comprehensive description of the theory behind the filter paper method, details methods for determining a calibration relationship and presents a definitive procedure for carrying out these tests.

Filter paper methods can be used to determine the soil water retention curve or to make independent suction measurements of a sample before or after carrying out other experimental tests, however the use of this method is limited in that it cannot be incorporated into existing hydro-mechanical testing systems, i.e. it can only be used in the determination of the water retention behaviour. The filter paper method was used in this research in the identification of the soil water retention curve.

3.4.2.3 Chilled-mirror dew-point technique

The principle of the chilled-mirror dew-point psychrometer is based on measuring the relative humidity of a volume of air surrounding a soil sample in a sealed chamber (Cardoso et al., 2007). At equilibrium the relative humidity of the surrounding air is equal to the relative humidity of the soil sample. By measuring the relative humidity, the total suction can be derived from the psychrometric law (Equation 3.5). Thus, this is an indirect method of measuring total suction. Figure 3.12 presents a schematic drawing of the chilled-mirror dew-point psychrometer. In this device the chamber in which the soil specimen is placed also contains a mirror, a fan and a temperature sensor. The temperature of the mirror is precisely controlled by a thermoelectric cooler. Detection of the exact point at which condensation first appears on the mirror is observed with a photoelectric cell. A beam of light is directed onto the mirror and reflected into a photodetector cell. The photodetector senses the change in reflectance when condensation occurs on the mirror. A thermocouple attached to the mirror then records the temperature at which condensation occurs. Additionally, the chilled-mirror dew-point psychrometer uses an internal fan that circulates the air within the sample chamber to reduce the time taken to reach equilibrium. Since both dew-point and sample surface temperatures are simultaneously measured, the need for complete thermal equilibrium is eliminated, which reduces measurement times to less than five minutes (Decagon Devices, 2003).

Although the concept of using psychrometers to measure the relative humidity in a soil has been in use for many years (e.g. Richards and Ogata, 1958), the chilled-mirror dew-point device has been a more recent development. Devices similar to that shown in Figure 3.12 have been used by a number of different authors (e.g. Leong et al., 2003; Tang and Cui, 2005; Cardoso et al.,

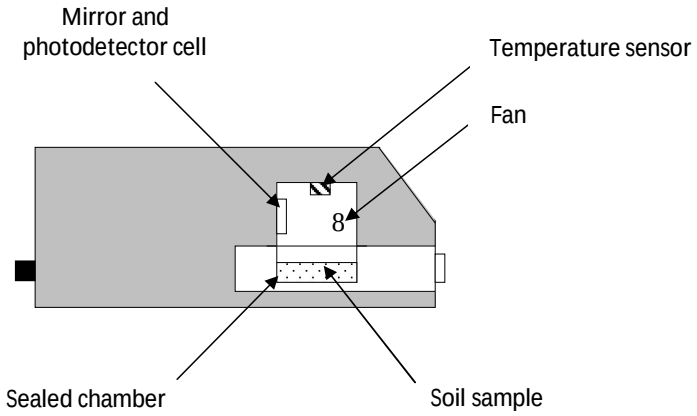

Figure 3.12: Chilled-mirror dew-point psychrometer (After Cardoso et al., 2007)

2007; Leong et al., 2007). This technique has been found to be reliable from 1 to 60MPa of suction (Cardoso et al., 2007).

Similar to the filter paper method the chilled-mirror dew-point psychrometer can not be incorporated into hydro-mechanical testing systems and thus can only be used in the investigation of the soil water retention behaviour. In this research the WP4 chilled-mirror dew-point psychrometer was used to measure total suction measurements of samples at high suction to complete the water retention curve.

All of the methods described herein for the control or measurement of suction are summarised and compared in Table 3.1. It is important to note here that it is generally necessary to use a number of different methods in order to determine the water retention behaviour of a single soil over its full suction range. As such the researcher must select methods suitable for the type of soil and consider the equilibrium times and limitations of the different techniques.

3.4.3 Volume change measurements

Aside from the additional control or measurement of suction in the experimental investigation of unsaturated soils, testing also increases in complexity in terms of volume change measurements. Accurate measurement of volume changes in unsaturated soils is much more difficult than in saturated soils (Ng et al., 2002). In saturated soils testing it is assumed that the total change in volume of a sample is equal to the change in the volume of water in the sample (Head, 1998). In

Table 3.1: Summary of laboratory techniques used for measuring and controlling suction (Ridley and Wray, 1996; D6386-02, 2003; Blatz et al., 2008; Bulut and Leong, 2008; Masrouri et al., 2008; Vanapalli et al., 2008)

SC/SM*	Method	Suction Component	Suction range (MPa)	Approx. equilibrium time	Limitations/Concerns
SC	Axis-translation	Matric	0 - 1.5	days - weeks	Translation of pressures to positive range High air pressures required Saturation of and air diffusion through ceramic disc Evaporation of moisture from specimen
SC	Osmotic	Matric	0 - 10	days - weeks	Weakness of semi-permeable membrane
SC	Vapour Equilibrium	Total	3 - 1000	weeks - months	Long equilibrium times if air flow is not circulated High sensitivity to temperature changes Safety issues when using concentrated acids
SC	Hanging water column	Matric	0 - 0.08	days	Very narrow suction range Point measurements only
SC	Centrifuge	Matric	0- 0.12	2 hrs	Very narrow suction range Point measurements only
SM	Tensiometer	Matric	0 - 1.5	minutes - hours	Rigorous saturation and preconditioning procedures
SM	Filter Paper	Total/Matric	0.05 - 30	7 - 14 days	Strict laboratory protocol required Point measurements only
SM	Chilled-mirror psychrometer	Total	1 - 60	~ 10 mins	Point measurements only
SM	Thermocouple psychrometer	Total	0.3 - 7	~ 1 hr	Sensitive to ambient temperature changes
SM	Transistor psychrometer	Total	1 - 70	~ 1 hr	Only very small soil specimens can be tested Point measurements only
SM	Thermal conductivity sensor	Matric	0.001- 1.5	hours - days	Sensors show hysteresis on drying and wetting Contact between soil and sensor affects response
SM	Electrical conductivity sensor	Matric	0.05 - 1.5	6 - 50hrs	Sensors show hysteresis on drying and wetting

*SC - Suction Control, SM - Suction Measurement

unsaturated soils testing, this assumption is no longer valid as the volume change of a sample depends on changes in volume of both the pore water and pore air phases. Geiser et al. (2000) summarised and evaluated existing methods of measuring volume changes in unsaturated soils and classified these techniques into three main groups: (i) measurement of the cell fluid, (ii) measurement of changes in water and air volumes separately and (iii) direct measurement of the soil specimen.

Global measurement refers to measuring the changes in the volume of cell fluid surrounding the soil sample. Bishop and Donald (1961) developed a modified triaxial cell with an inner cell. The lower part of the inner cell was filled with mercury, the upper and outer part of the inner cell were filled with water. Volume changes were monitored by monitoring the vertical movement of a stainless steel ball floating in the mercury. In order to avoid volume changes due to expansion-compression of the inner cell, the pressure in the inner and outer cells was maintained at equal pressures via a direct connection at the top of the inner cell. Cui and Delage (1996) replaced the mercury with water and used air as the confining fluid. A layer of silicon oil was used to prevent evaporation of the water, and this level was optically monitored. Ng et al. (2002) again used an inner open cell, and measured the difference in water level between the inner cell and a reference water level in the outer cell using a differential pressure transducer enabling automatic recording of volume measurements.

Wheeler (1986) developed a fully sealed inner wall, referred to as the double-walled cell, and used water as the cell fluid in both the inner cell and between the outer and inner walls. Similar types of double-walled cell are now available commercially (e.g. Wykeham Farrance). The design by Wheeler (1986) improved the ability to determine volume changes by requiring only the volume change of the fluid entering or leaving the inner cell to be measured. Despite the double-walled cell arrangement though it was still found necessary to calibrate the cell against pressure to take into account effects such as absorption of water by the cell walls and flexure of the top and bottom plates (Wheeler, 1986). The tendency to absorb water was due to the fact that the cell walls were made of an acrylic material (perspex); this effect can be minimised by using a suitable material such as aluminium (Ng et al., 2002) or glass for the inner cell wall.

Measurement of the cell fluid may also be carried out without the benefit of the double-walled arrangement, using a single walled cell. However a number of problems are associated with

this method, including expansion and compression of the cell, creep under constant pressure, absorption of water by cell walls and connecting tubes and possible leakage (Head, 1998; Geiser et al., 2000; Ng et al., 2002). Despite these drawbacks it may be possible to use this simpler system if suitably thick rigid materials are selected as cell walls and if the cell is carefully calibrated, as used for example by Raveendiraraj (2009). A disadvantage of using materials such as stainless steel or aluminium in the cell wall is that there can be no visual inspection of the sample during testing.

The second method described of measuring separately changes in the volume of pore air and pore water is rarely used in triaxial testing of unsaturated soils. There are many difficulties associated with measuring changes in pore air volume including sensitivity to temperature changes, inability to detect small air leakages, diffusion through membranes and tubing (Geiser et al., 2000; Ng et al., 2002).

An alternative approach is to directly measure volume changes of the soil specimen using local measurements. This may include the use of Hall Effect transducers (e.g. Ng and Chiu, 2001; Maâtouk et al., 1995). However these only involve measurements between two fixed points and thus assumption needs to be made regarding the shape of the sample during loading and shearing. Although accurate over the small strain range, at large strains this method may give unrepresentative volume changes overall due to non-uniform deformations of the sample. Ng and Chiu (2001, 2003) used a combination of techniques: using Hall-effect local transducers at small strains and measuring volume changes in the cell fluid at larger strains. Alternative local measuring techniques which have also been developed include the use of lasers to scan the overall profile of the soil specimen (Romero et al., 1997; Romero, 1999) and image processing techniques in triaxial testing were introduced by Macari et al. (1997).

3.5 Water retention behaviour

The soil water retention curve defines the relationship between the water retained within the pores of a soil over a range of suctions and can be determined experimentally using a combination of the different techniques presented in Section 3.4.

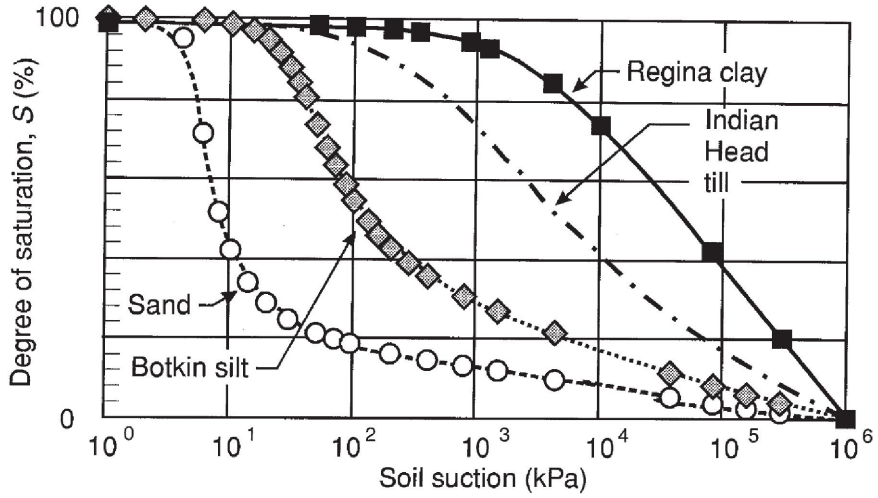

Figure 3.13: Influence of soil type on water retention behaviour (Barbour, 1998; Vanapalli et al., 1999)

3.5.1 Influence of soil type

Figure 3.13 presents the water retention curves determined experimentally for four different soils including a sand, silt and clay (Barbour, 1998; Vanapalli et al., 1999). It is evident that in the Regina clay, water is retained within the soil up to suctions of hundreds of MPa, whereas the sand sample is largely desaturated at around 100kPa. Part of this difference in retention behaviour presented in Figure 3.13 can indeed be attributed to the difference in pore sizes present in sands, silt and clays. Section 3.3 described how based on capillary effects alone, different pore sizes could relate to varying negative water pressures (matric suction) (Equation 3.2). Furthermore considering that adsorptive forces dominate at suctions higher than 10MPa (Tuller and Or, 2005), it can be deduced that essentially these forces are not present in sands, but do have a significant influence on the retention behaviour of clays. Given then that the different mechanisms by which water is held in soils (capillary or adsorbed) occurs to varying degrees within different types of soils, it is not surprising that different types of soils exhibit significant differences in their ability to retain water.

3.5.2 Influence of void ratio and soil structure

Even for the same soil, the effect of pore size distribution has an influence on water retention behaviour. Figure 3.14 presents the water retention behaviour for three specimens of compacted Boom clay following drying paths each at a different initial void ratio (Romero, 1999; Nuth and Laloui, 2008a). Void ratio e is defined as the ratio of the volume of voids V_v to the volume of solids V_s present in a volume of soil:

$$e = \frac{V_v}{V_s} \tag{3.6}$$

and can be related to the porosity n of a soil as:

$$n = \frac{e}{1+e} \tag{3.7}$$

where n is the ratio of the volume of voids V_v to the total soil volume V:

$$n = \frac{V_v}{V} \tag{3.8}$$

In Figure 3.14 as the initial void ratio of the specimens decrease, the main drying curve is shifted such that higher suctions are required to drain water from the pores in order to achieve a given degree of saturation. This shift of the retention curve can be explained by considering that a reduction in void ratio corresponds to an increase in dry density of the soil, which has been found only to affect inter-aggregate porosity (macropores) (e.g. Delage et al., 1996; Lloret et al., 2003; Romero and Simms, 2008). By considering capillary effects higher suctions are required to drain water from smaller pores (Equation 3.2). However aside from the shift of the curves, another difference is evident, the shape of the curve for the specimen with the highest initial void ratio (more open initial structure) is markedly different from the other two curves presented. It is proposed that this change in shape of the curve occurs because this is a deformable soil, and thus during drying significant changes in volume occur which alter soil structure and subsequently the shape of the retention curve (Romero and Vaunat, 2000; Nuth and Laloui, 2008a). The changes in volume due to drying of the specimen with the lowest initial void ratio in this case appears to be greater than for the other two specimens (Nuth and Laloui, 2008a). This can be related to the fact that the specimen has an initially more open structure, characterised by

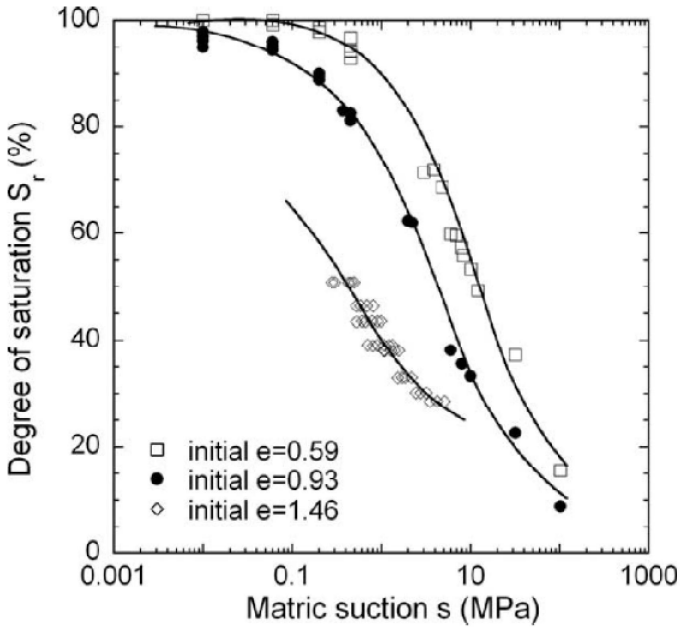

Figure 3.14: Influence of void ratio and structure on water retention behaviour of Boom clay (Romero, 1999; Nuth and Laloui, 2008a))

a higher proportion of inter-aggregate (macro) pores, which subsequently undergo significant changes in volume in response to drying.

Independent of the influence of void ratio, soil structure has also been found to influence the water retention behaviour (Vanapalli et al., 1999). Vanapalli et al. (1999) investigated the retention behaviour of a sandy clay till with different soil structures corresponding to specimens (i) compacted under dry-of-optimum, (ii) at optimum and (iii) under wet-of optimum conditions (Figure 3.15). Individual specimens were compacted at different initial moisture contents (corresponding to dry, wet or optimum) at approximately the same dry density and then brought to equilibrium with the desired level of suction either in the pressure plate or desiccator. In Figure 3.15 it is evident that despite having similar void ratios for the same soil (identical particle size distribution and mineralogy) a difference in the air-entry value is exhibited for the retention behaviour of specimens compacted dry of optimum compared to those compacted wet of optimum. This may be explained by considering the soil structure which is created during compaction at different moisture contents. It is now widely accepted that clayey soils compacted dry of optimum tend to exhibit bi-modal pore size distributions, characterised by inter-aggregate pores (macropores between clay aggregates) and intra-aggregate pores (micropores within clay

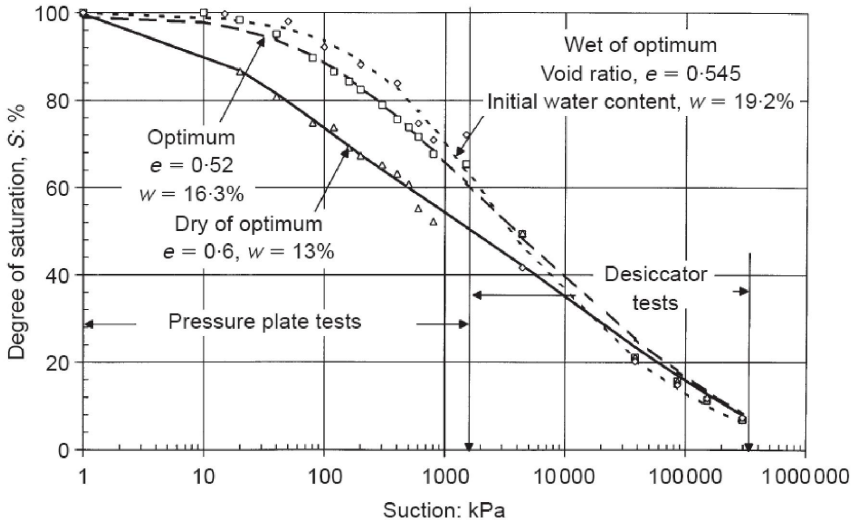

Figure 3.15: Influence of compacted structure on water retention behaviour (Barbour, 1998; Vanapalli et al., 1999)

aggregates). Whereas clays compacted wet of optimum tend to exhibit mono-modal pore size distributions characterised by intra-aggregate pores, see Figure 3.16. Experimentally this has been confirmed by Ahmed et al. (1974); Delage et al. (1996); Prapaharan et al. (1991), among others.

Vanapalli et al. (1999) proposes that the differences in water retention behaviour observed between the different compacted specimens can be directly related to the different structures created during compaction at different moisture contents. The specimen compacted under dry of optimum conditions has a more open soil structure with a dominant inter-aggregate pore mode. On drying it is these large inter-aggregate pores which will empty first (Equation 3.2) and thus it is the macrostructure which governs the drainage of water for dry of optimum specimens at low suctions. Whereas in the fused fabric created at wet of optimum conditions and characterised by intra-aggregate porosity (micropores), it is the microstructure which governs the emptying of water from soil pores during drying. Consequently at a given suction level the wet of optimum specimens can retain more water than the dry of optimum specimens.

The experimental evidence discussed here indicates the complex nature of water retention behaviour in unsaturated soils, which depends on grain size distribution, pore size distribution, soil mineralogy and activity of clay minerals present. This discussion also highlights the coupled

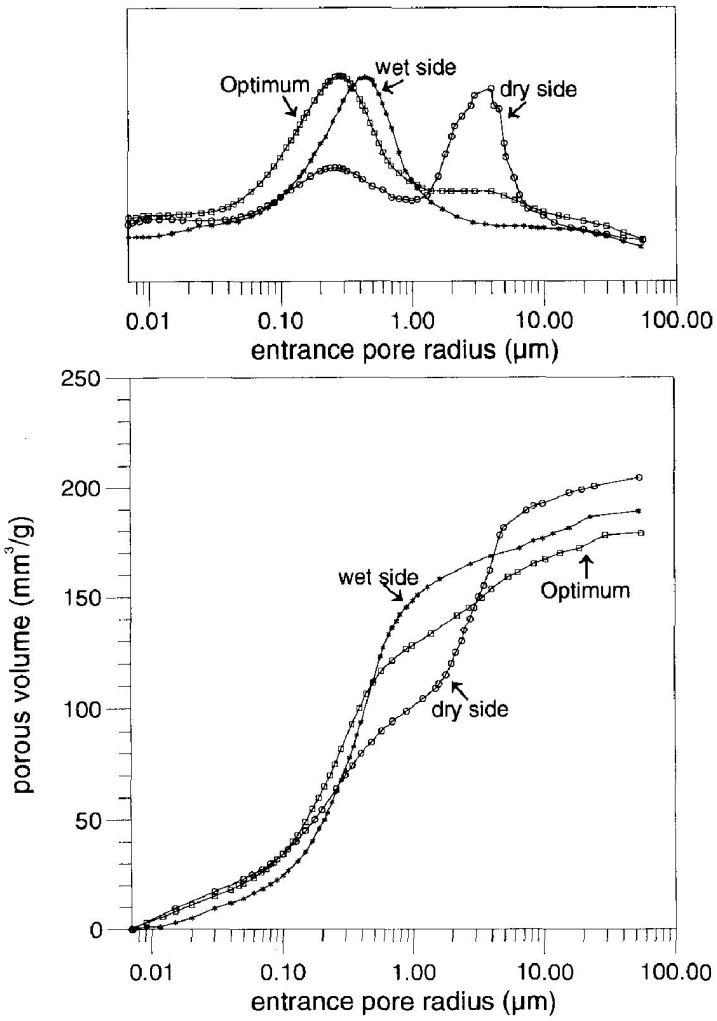

Figure 3.16: Influence of compaction moisture content on pore size distribution for Jossigny silt (Delage et al., 1996)

nature of water retention and mechanical behaviour in soils and the importance of considering soil structure in order to understand the (micro-scale) interactions which influence (macro-scale) water retention and mechanical behaviour.

3.5.3 Modelling water retention behaviour

Several different models have been proposed since the late 1950s in order to capture the water retention behaviour of a soil, most of them have been empirical methods based on experimental data (e.g. Gardner, 1956; Brooks and Corey, 1964). The equations proposed by van Genuchten (1980) and Fredlund and Xing (1994) are presented here as they are two of the most widely used equations. Both of these models have been derived by considering a pore size distribution function in combination with capillary theory.

The following relationship between volumetric water content θ and suction s was proposed by van Genuchten (1980):

$$\theta = \theta_r + (\theta_s - \theta_r)\left[\frac{1}{1+(as)^n}\right]^m \tag{3.9}$$

where θ_r is the residual water content, θ_s is the saturated water content and a, n, m are parameters relating to the water retention curve where a relates to the air entry value, n to the rate of change of the slope of the curve and m to the asymmetric shape of the curve. This equation provided more flexibility than equations previously proposed. In order to obtain a closed form equation, van Genuchten (1980) proposed that m and n were related:

$$m = 1 - (\frac{1}{n}) \tag{3.10}$$

Fredlund and Xing (1994) proposed a similar equation to van Genuchten (1980) as given below:

$$\theta = \theta_s\left[\frac{1}{\ln\left[e+s/a\right]^n}\right]^m \tag{3.11}$$

where a is a parameter closely related to the air-entry value, n is a parameter which controls the slope of the retention curve, m the asymmetric shape of the curve and e is the base of natural logarithms. Sillers et al. (2001) state that equations which require three parameters, such as

those presented, are in fact easier to use than two parameter equations due to their being more flexible in terms of fitting experimental data.

More recently other equations have been developed which account for the influence of void ratio on water retention behaviour Romero and Vaunat (2000); Gallipoli et al. (2003). Furthermore Wheeler et al. (2003) proposed a water retention model which includes both hydraulic hysteresis and the influence of void ratio.

It has long been recognised that soil water retention behaviour can be useful for determining soil properties of unsaturated soils (Childs and Collis-George, 1948). In particular information obtained from the retention behaviour may be used to predict the shear strength (e.g. Vanapalli, 1994; Fredlund et al., 1996; Vanapalli et al., 1996), hydraulic conductivity (e.g. Mualem, 1986; Huang, 1994; Huang et al., 1998) and diffusion and adsorption coefficients (e.g. Lim, 1995; Lim et al., 1998) in unsaturated soils. An overview of the different methods used to predict unsaturated soil properties from the water retention behaviour is provided in Barbour (1998).

3.6 Mechanical behaviour of unsaturated soils

3.6.1 Influence of suction on inter-particle contacts

As a soil is progressively dried, water is removed from the voids, initially from those pores which have the largest entry diameter, however small amounts of pore water remain at the inter-particle contacts of voids which have become filled with air. The pore water present in soils can thus be classified as two types: bulk water or meniscus water (see Figure 3.17). Bulk water is the pore water which is present within voids which are filled with water, whereas meniscus water is the pore water which surrounds inter-particle contacts in air-filled voids (Wheeler et al., 2003). Adsorbed water, discussed in Section 3.3.4.1, is so tightly bound to the soil surface, that for this discussion it can be considered to act as part of the soil skeleton. The negative pore water pressures acting within the bulk water have a different effect on the soil skeleton compared to the negative pore water pressures acting within the meniscus water. In a similar manner to saturated soils changes in pore water pressure within bulk water influences both the tangential and normal

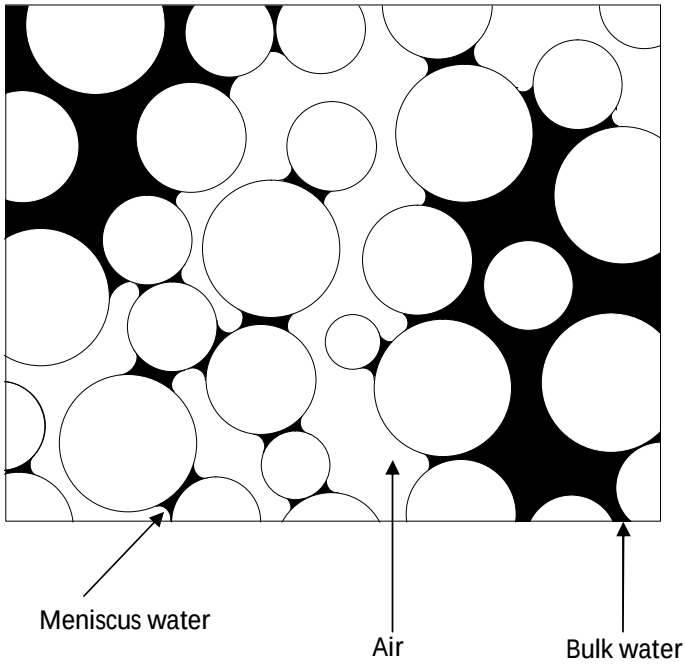

Figure 3.17: Bulk and meniscus water present in soil capillaries (After Wheeler et al., 2003)

forces transmitted at inter-particle contacts (Fisher, 1926; Wheeler et al., 2003). However the presence of meniscus water at the particle contacts provides an additional component of inter-particle force which is approximately normal to the contact, with no addition to the tangential force (Fisher, 1926; Wheeler et al., 2003). This additional normal force at the inter-particle contacts has a stabilising effect on the soil skeleton (Gens, 2010; Tarantino, 2010a).

Figure 3.18 illustrates two idealised spherical soil particles where meniscus water is present at the inter-particle contact. N_{net} is the contact force transmitted through the soil particles constituting the soil skeleton upon loading. The additional normal force (ΔN) is a result of the surface tension between the water and air phases across the meniscus at the inter-particle contact. Fisher (1926) derived an equation for the additional inter-particle contact force (ΔN) generated by meniscus water, between two particles of equal radius (R):

$$\Delta N = \pi T_s R(2 - \frac{r_2}{R}) \tag{3.12}$$

where r_2 is the radius of curvature of the air-water interface measured on the water side (see

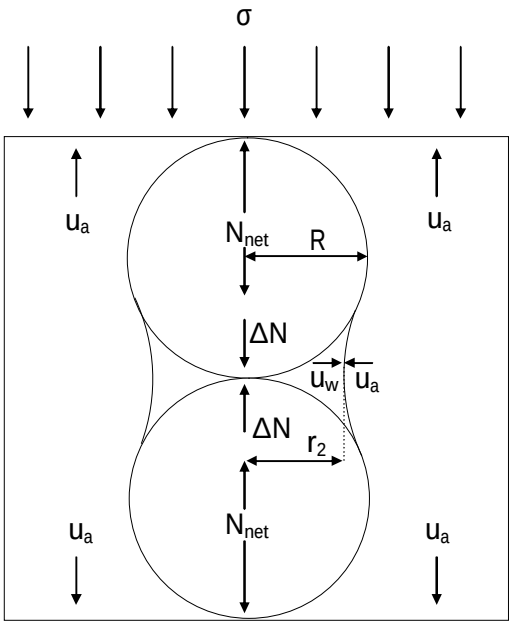

Figure 3.18: Idealised unsaturated soil inter-particle contact (After Karube and Kawai, 2001)

Figure 3.18), using the Young-Laplace equation for the pressure difference across the air-water interface:

$$u_a - u_w = T_s(\frac{1}{r_1} - \frac{1}{r_2}) \tag{3.13}$$

where r_1 and r_2 are the principal radii of curvature of the air-water interface. Fisher (1926) also assumed that the cross-section of the meniscus water has a circular profile, though it is thought that this is unlikely to be responsible for large errors.

Using Equation 3.12, Wheeler et al. (2003) showed that ΔN due to a single meniscus lens increases with increasing suction up to some limiting value as suction tends to infinity (see Figure 3.19). Considering that the limiting value of ΔN as suction tends to infinity is only 50% greater than the value of ΔN at zero suction, suggests that changes in suction within a single water lens has little effect on the stability of that contact (Wheeler et al., 2003) . Rather what is important in terms of stability is the overall number of inter-particle contacts within a soil sample which have meniscus water present (Wheeler et al., 2003). The stabilising effect of meniscus water can be said to be an on-off effect, where meniscus water is present at inter-

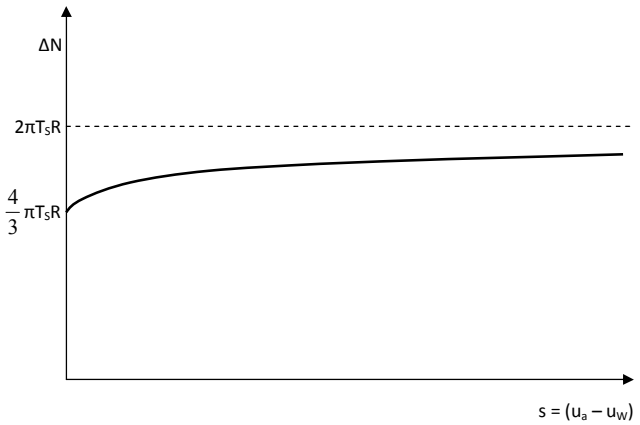

Figure 3.19: Additional inter-particle force due to presence of meniscus water (After Wheeler et al., 2003)

particle contacts, the menisci act to bonds particles together, as the voids fill with water, this bonding effect is removed (Tarantino, 2010a).

In summary, changes in suction may influence the mechanical behaviour of an unsaturated soil in two different ways (Wheeler and Karube, 1996): (a) changes to the stress acting on the soil skeleton by modifying the pore water (and or pore air) pressure acting within the voids and (b) by providing an additional stabilising force which may be attributed to the presence of meniscus water at inter-particle contacts.

3.6.2 Features of unsaturated soils behaviour

Often, it is the volumetric response of unsaturated soils to changes in water content which can be the most problematic feature of their use as materials in engineering works. The main features of the volume change behaviour and shear strength behaviour of unsaturated soils are described below alongside experimental evidence related to each feature. Additional information and experimental evidence regarding each of these features of unsaturated soil behaviour is presented in Alonso et al. (1987).

- *Influence of suction on preconsolidation stress*: Much experimental evidence is available that suggests that an increase in soil suction increases the yield stress p_o (apparent preconsolidation stress) exhibited upon increased externally applied stresses. This effect has

commonly been observed in constant water content oedometer tests (e.g. Dudley, 1970), in suction controlled oedometer tests (e.g. Vicol, 1990) and more recently in suction controlled isotropic compression tests (e.g. (Maâtouk et al., 1995; Wheeler and Sivakumar, 1995; Cui and Delage, 1996; Futai and Almeida, 2005)), see Figure 3.20. This behaviour can be explained by considering the soil skeleton at a microscopic level. An increase in suction would lead to the emptying of voids of bulk water, leading to an increased number of inter-particle contacts being surrounded by meniscus water. Such meniscus water contribute an additional normal component to the inter-particle forces at these contacts, leading to increased stability which would inhibit yielding or slippage at the contacts. Similar to constitutive models for saturated soils, the apparent preconsolidation stress in unsaturated soils is considered to be the stress which denotes the transition between recoverable (elastic) and irrecoverable (plastic) volume changes.

- *Variation in soil compressibility with suction*: With regard to this aspect of unsaturated soil behaviour, the experimental evidence has been less conclusive. Some researchers have reported a reduction in post-yield compressibility with increasing suction, i.e. a reduction in the slope of the normal compression line (stiffening effect) (e.g. Vicol, 1990), however others have reported an increase in compressibility with increasing suction (e.g. Futai and Almeida, 2005). Yet other experimental campaigns have indicated an initial increase in compressibility on moving from saturated to an unsaturated state, but further increases in suction resulted in little variation or slight reductions in compressibility (e.g. Wheeler and Sivakumar, 1995; Maâtouk et al., 1995; Ng and Chiu, 2001). The isotropic compression results from Wheeler et al. (2003) and Futai and Almeida (2005) are compared in Figure 3.20. This is an area where further experimental evidence is required to inform the development of future constitutive models.

- *Wetting induced collapse:* It has commonly been observed that natural and compacted soils with an open structure (low density) may undergo volumetric collapse compression when wetted under load (e.g. Jennings and Knight, 1957; Booth, 1975; Lawton et al., 1989; Pereira and Fredlund, 2000 among many others). The amount of volumetric collapse which occurs is dependent on the magnitude of the externally applied load. In fact swelling is often observed on wetting under a low confining stress and the same soil wetted under

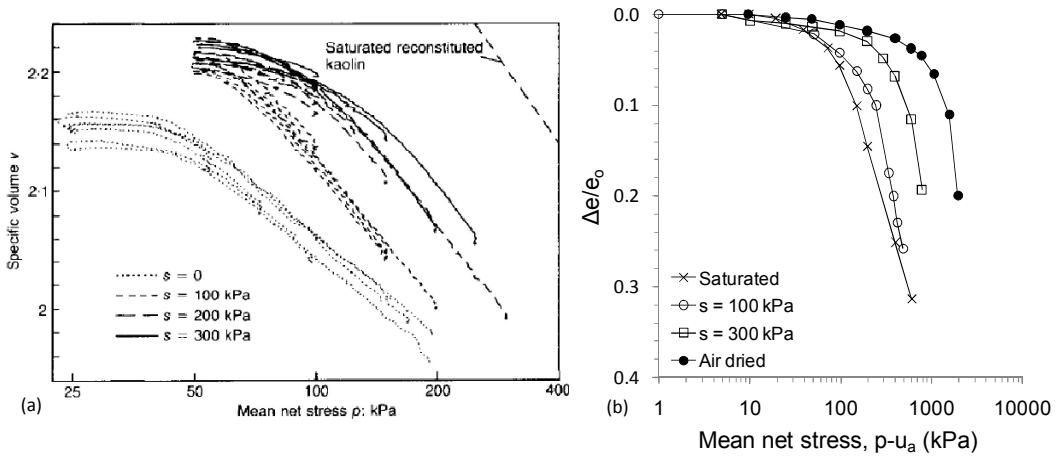

Figure 3.20: Experimental evidence for (i) increase in preconsolidation stress with increasing suction and (ii) variation in post-yield compressibility with suction: (a) initial increase and subsequent reduction in soil compressibility with suction (Wheeler et al., 2003) and (b) increase in compressibility with increasing suction (after Futai and Almeida, 2005)

a higher confining may exhibit collapse compression, (see Series 1 in Figure 3.21). For a certain range of stresses the amount of collapse will increase with increasing confining stress (e.g. Jennings and Knight, 1957; Booth, 1975), after which a maximum amount of collapse may be reached at some intermediate value of confining stress, thereafter decreasing (e.g. Balmaceda, 1991; Rao and Revanasiddappa, 2006), (see Series 2 in Figure 3.21). Experimental evidence has also indicated that it is possible for a soil specimen to undergo first expansive (swelling) and then compressive (collapse) behaviour along a single wetting path (e.g. Josa et al., 1987; Sivakumar, 1993). This reversal in volumetric behaviour is illustrated in Figure 3.22 during wetting paths for compacted kaolin (Wheeler and Sivakumar, 1995). The swelling which occurs on wetting at low stresses in non-expansive soils is due to the relaxation of the stresses on the soil skeleton as the suction reduces, this behaviour is considered to be elastic in constitutive models. The phenomenon of volumetric compression on wetting may also be explained by considering the soil skeleton at a microscopic level. As a soil is wetted under load, there is a progressive loss of meniscus water, as voids become filled with bulk water, and correspondingly there is an associated loss of the additional normal forces at inter-particle contacts. If the applied external stress is high enough to generate high tangential forces at the inter-particle contacts, on wetting these tangential forces may overcome the normal forces causing slippage of the particles

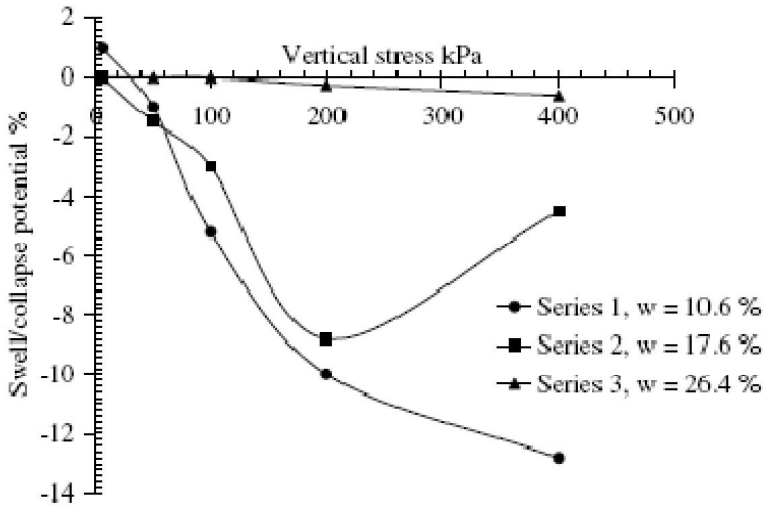

Figure 3.21: Volumetric collapse observed in compacted clayey sand specimens prepared from residual soil: Specimen 1 exhibiting swelling at low vertical stress, Specimen 2 exhibiting a maximum collapse at an intermediate stress level (Rao and Revanasiddappa, 2006)

at these contacts (Tarantino, 2010a). The phenomenon of volumetric collapse due to wetting, results in an irrecoverable compression, due to the slippage of the particles and is considered as plastic behaviour in constitutive models.

- *Irrecoverable volumetric deformations due to changes in suction:* Aside from the irrecoverable collapse compression due to wetting described above, unsaturated soils may also undergo irreversible volumetric deformations due to (a) a reduction in suction, i.e. wetting, such irreversible deformations are typically observed in expansive clays or (b) due to the accumulation of irreversible deformations during drying-wetting cycles. Chu and Mou (1973) subjected expansive Texan clays to wetting - drying cycles under suction controlled conditions and both of the listed types of irreversible volumetric deformations were observed: irreversible swelling during the first wetting cycle and a small accumulation of swelling strains due to wetting-drying cycles (see Figure 3.23). Similar results exhibiting both of these types of deformations have also been presented by Escario and Sáez (1986) for Madrid grey clay. Additionally the accumulation of irreversible deformations due to drying-wetting cycles has been widely reported for low to moderately active clays (e.g. Yong et al., 1971; Josa et al., 1987).

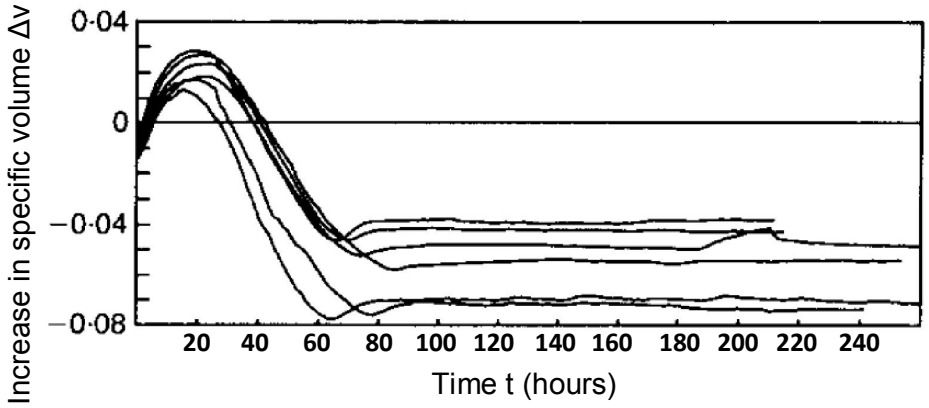

Figure 3.22: Reversal in volumetric behaviour observed during wetting tests on compacted kaolin (Wheeler and Sivakumar, 1995)

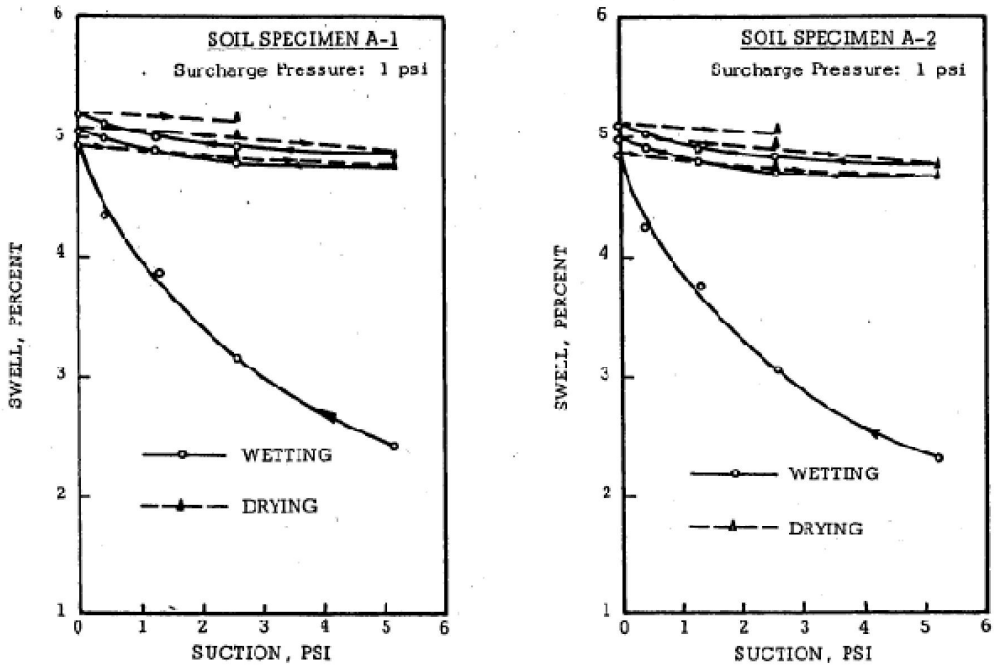

Figure 3.23: Irreversible volumetric deformations induced by changes in suction for expansive Texan clays tested under suction controlled conditions (Chu and Mou, 1973) (NB: 1psi = 6.9kPa)

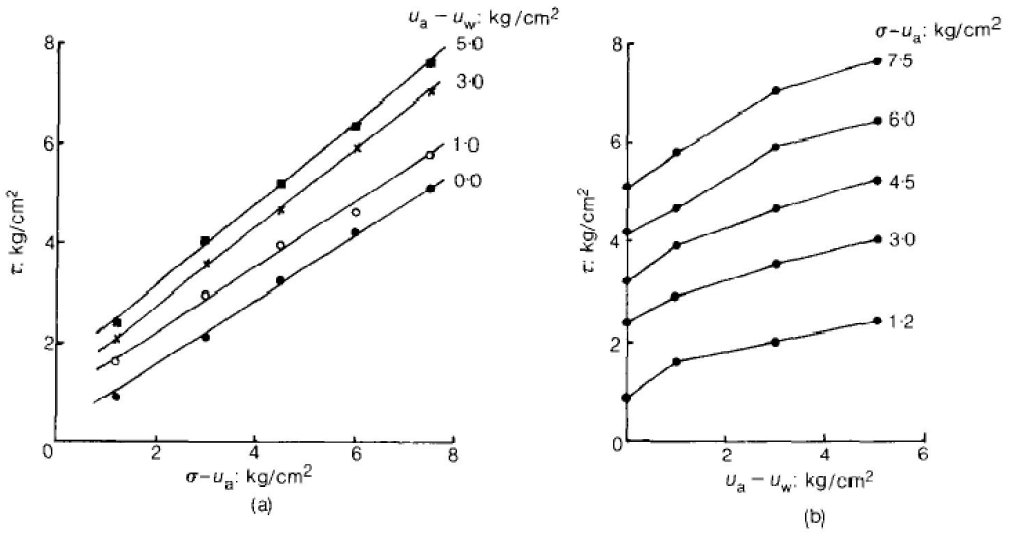

Figure 3.24: Shear strength data obtained for tests on Guadalix de la Sierra red clay in suction controlled direct shear tests. Data presented in terms of (a) shear stress versus normal stress and (b) shear stress versus suction (Escario and Sáez, 1986) (NB: 1kg/cm^2 = 98.1kPa)

- *Influence of suction on shear strength*: Experimentally it has commonly been observed that the shear strength of soils increases as suction increases (e.g. Fredlund et al., 1978; Escario and Sáez, 1986, 1987), see Figure 3.24. Again this influence of suction on unsaturated soil behaviour can be explained by considering the influence of meniscus water at inter-particle contacts. As soil desaturates increasing numbers of the inter-particle contacts are surrounded by meniscus water. As such these contacts have an additional normal component of inter-particle force, with no additional tangential component, and therefore provide additional frictional resistance to applied shear stresses. A number of different failure envelopes have been proposed to describe the increase of shear strength with suction in unsaturated soils (e.g. Fredlund et al., 1978), these are discussed in more detail in Section 3.7.2.

In this thesis, experimental campaigns have been designed to contribute to the existing knowledge of unsaturated soil behaviour for a (*natural*) compacted fill material. In particular, the influence of suction on the preconsolidation and soil compressibility of the Bengawan Solo fill material is investigated under one-dimensional constant water content conditions in Chapter 5 and under isotropic suction controlled conditions in Chapter 6. The potential for collapse of the Bengawan Solo fill material for a wide range of different initial specimen conditions is explored

in Chapter 5. Additionally the influence of suction on shear strength is investigated in a number of suction controlled triaxial tests presented in Chapter 6.

Attempts have been made to represent the main features of unsaturated soil behaviour, which have been listed above, using constitutive models. A number of different types of approaches, models and their associated limitations are outlined in the following section.

3.7 Constitutive modelling of unsaturated soils

Constitutive modelling of the behaviour of unsaturated soils has progressively developed to represent more and more of the features of unsaturated soil behaviour listed in Section 3.6.2 and in an increasingly integrated manner. In this section the different types of stress states variables which have been selected for the basis of model formulations are introduced. This is followed by a brief discussion of the different types of approaches which have been developed for the constitutive modelling of unsaturated soils: (i) Failure envelopes, (ii) State surface approach (iii) Elasto-plastic models. One of the first elasto-plastic frameworks proposed for describing the mechanical behaviour of unsaturated soil behaviour is then presented in some detail (Alonso et al., 1987, 1990). Following this, more recent advanced elasto-plastic models which are able to incorporate (i) the behaviour of expansive clays, (ii) temperature and chemical effects and (iii) hydro-mechanical coupling are discussed.

3.7.1 Stress state variables

Terzaghi (1936) described the stress state variable for saturated soils as the difference between the total principle stresses and the pore water pressure acting on a soil plane. This stress state variable for saturated soil is commonly known as the effective stress (σ'_{ij}) and the average acting over a volume of soil may be expressed as:

$$\sigma'_{ij} = \sigma_{ij} - u_w \delta_{ij} \tag{3.14}$$

where σ_{ij} is the total normal stress and δ_{ij} is the Kronecker's delta: where $\delta_{i=j}$=1 and $\delta_{i\neq j}$=0. Terzaghi (1936) proposed that all measurable effects of a change in stress in saturated soil, in-

cluding compression, distortion and changes in shearing resistance are exclusively due to changes in effective stress. The effective stress concept has been fundamental in the development of soil mechanics, given its ability to relate changes in soil behaviour to changes in stress conditions. Equation 3.14 is valid for soils with incompressible grains where the pore space is filled completely (saturated) with incompressible fluid. However Skempton (1960) determined that the compressibility of grains in soils is generally negligible with respect to the overall compressibility of the soil skeleton.

3.7.1.1 Single effective stress for unsaturated soils

Given the wide success of the effective stress approach for describing the behaviour of saturated soils, attempts were made to find a similar single stress state variable applicable to the behaviour of unsaturated soils (e.g. Croney et al. 1958; Bishop 1959). One of the most well known of these is the single effective stress equation proposed by Bishop (1959):

$$\sigma'_{ij} = (\sigma_{ij} - u_a\delta_{ij}) + \chi(u_a - u_w)\delta_{ij} \tag{3.15}$$

where χ is a parameter related to the degree of saturation of the soil which varies between 0 (for a dry soil) and 1 (for a saturated soil). χ varies non-linearly and is highly dependent upon the degree of saturation of the soil and the type of soil. Jennings and Burland (1962) were among the first to criticise Bishop's effective stress equation as it was capable of predicting swelling on wetting, but could not explain the phenomenon of volumetric collapse which is commonly observed in unsaturated soils following wetting under load (e.g. Jennings and Burland, 1962; Booth, 1975). Considering that on wetting, matric suction reduces down to zero upon reaching saturation, according to Equation 3.15, this would lead to a reduction in effective stress. In line with the behaviour of saturated soils, a slight increase in void ratio (swelling) would be expected for a reduction in effective stress. However as outlined in Section 3.6.2, although swelling may be observed as a result of on wetting at low confining stresses, at higher confining stresses collapse compressions are often exhibited for soils with open structures.

The single effective stress approach, although suitable for explaining elastic behaviour exhibited by unsaturated soils (e.g. swelling on wetting) is not capable of representing behaviour result-

ing from the stabilising effect of meniscus water at the inter-particle contacts and associated volumetric effects (Gens et al., 2006).

3.7.1.2 Independent stress variables

After the limitations of a single effective stress approach were realised, experimental research provided support for the use of two separate stress state variables (e.g. Matyas and Radhakrishna, 1968; Fredlund and Morgenstern, 1977). Fredlund and Morgenstern (1977) proposed that the mechanical behaviour of unsaturated soils could be adequately described by using a combination of two of the following three stress state variables $(\sigma - u_a)$, $(\sigma - u_w)$ and $(u_a - u_w)$, which was validated by a series of null tests (Fredlund and Morgenstern, 1977). In null tests each quantity of the combined stresses is increased by the same amount and overall sample volume and degree of saturation are monitored to ensure there are no changes as a result of the changes in the stresses. $(\sigma - u_a)$ and $(u_a - u_w)$ have been by far the most widely used stress state variables in the experimental investigation and development of constitutive models for unsaturated soils (e.g. Fredlund et al., 1978; Alonso et al., 1990; Maâtouk et al., 1995; Cui and Delage, 1996). This combination enables the effects of total stress to be separated from the effects of pore water pressure. Furthermore in practical problems pore air pressure is usually atmospheric; therefore it appears appropriate that the stress state variables used should be those that are both referenced to pore air pressure.

3.7.1.3 Alternative stress variables

More recently other stress state variables have been proposed which see a return to the use of a Bishop-like effective stress alongside another stress variable to represent the stabilising effect of suction. The variable based on that of Bishop's effective stress has been referred to as the constitutive stress (σ_c) in order to indicate that it is not the only stress variable required to describe fully unsaturated soil behaviour (Gens et al., 2006). Gens et al. (2006) and Nuth and Laloui (2008b) further classify these more recent stress variables into two groups. In Group 1 suction is explicitly included in the definition of constitutive stress:

$$(\sigma_{ij})_c = (\sigma_{ij} - u_a\delta_{ij}) + \mu_1(s)\delta_{ij} \tag{3.16}$$

where μ_1 is a function of suction. The use of a Group 1 type of constitutive stress as proposed by Geiser et al. (2000) and Loret and Khalili (2002) among others, implies an increase in strength with suction, and therefore an additional relationship is not required as is the case for independent stress state variables. However similar to the independent stress variables hydraulic hysteresis cannot easily be represented by Group 1 variables. In Group 2 the constitutive stress explicitly includes suction and degree of saturation:

$$(\sigma_{ij})_c = (\sigma_{ij} - u_a\delta_{ij}) + \mu_2(s,\, S_r)\delta_{ij} \tag{3.17}$$

where μ_2 is a function of suction and degree of saturation. As such hydraulic hysteresis effects are incorporated through the inclusion of degree of saturation and the increase in strength with suction is also represented by the definition of the constitutive stress in Group 2. Such a constitutive stress has been proposed by Gallipoli et al. (2003); Wheeler et al. (2003) and Sheng et al. (2004) among others. Increasingly the selection of such modified stress state variables have been based on thermodynamic considerations, primarily on the work by Houlsby (1997). Considering that the constitutive stress in constitutive modelling is assumed to be work conjugate with strains, Houlsby (1997) attempted to identify the strain-like quantity which is work conjugate with suction by considering the rate of work input (dW) per unit volume of unsaturated soil:

$$dW = [\sigma_{ij} - (S_r u_w + (1 - S_r)u_a)\delta_{ij}]d\varepsilon_{ij} - n(u_a - u_w)dS_r \tag{3.18}$$

where $d\varepsilon_{ij}$ is the strain increment tensor, n is the porosity and dS_r is the increment of degree of saturation. Equation 3.18 neglects the work input required to compress the air phase and the work dissipated by the flow of fluids. Equation 3.18 indicates that the average skeleton stress is work conjugate with the strain of the soil skeleton and that suction is work conjugate with the strain-like variable $-nS_r$. Wheeler et al. (2003) made direct use of the work input considerations in the selection of their choice of stress variables termed Bishop's stress (σ^*_{ij}) and modified suction (s^*):

$$\sigma^*_{ij} = \sigma_{ij} - [S_r u_w + (1 - S_r)u_a]\, \delta_{ij} \tag{3.19}$$

$$s^* = ns = n(u_a - u_w) \tag{3.20}$$

The use of alternative stress variables is an area of increasing research in the constitutive modelling of unsaturated soils. Some of the different models proposed using these alternative stress variables are described further in the review of advanced elasto-plastic models for unsaturated soils (Section 3.7.5). Further information on the different types of stress variables selected for use in the constitutive modelling of unsaturated soils and their associated limitations are presented in detail by Gens et al. (2006); Nuth and Laloui (2008b) and summarised in Gens (2010).

3.7.2 Failure envelopes

The independent stress variable approach has been used to represent the variation in shear strength (τ) observed with suction. One of the most widely known of these expressions is that proposed by Fredlund et al. (1978):

$$\tau = c' + (\sigma - u_a)tan\phi' + (u_a - u_w)tan\phi^b \tag{3.21}$$

where c' is the cohesion intercept, ϕ' is the angle of friction related to changes in net normal stress and ϕ^b is the internal angle of friction related to changes in suction. Equation 3.21 is an extension of the Mohr-Coulomb failure envelope for saturated soils, incorporating the two independent stress state variables $(\sigma - u_a)$ and $(u_a - u_w)$ discussed in Section 3.7.1. This extended Mohr-Coulomb failure envelope corresponds to a three-dimensional planar surface as illustrated in Figure 3.25. At zero matric suction, the extended Mohr-Coulomb diagram reverts to the saturated condition. This is a desirable feature and one which is incorporated in most of the constitutive models which have been developed for unsaturated soils.

Two main trends exist in the shear strength behaviour of unsaturated soils, both of which are evident in the experimental data by Escario and Sáez (1986) which was presented in Figure 3.24. Firstly as with saturated soils, shear strength increases with increasing net normal stress. Secondly shear strength increases with increasing matric suction. Fredlund et al. (1978) assumed ϕ^b to be constant for a particular soil, which is clearly indicated in Figure 3.25, where ϕ^b illustrates the rate of increase in shear strength due to matric suction. However experimental evidence over larger suction ranges presented by Escario and Sáez (1986, 1987); Gan et al. (1988) among others, showed that shear strength varied non-linearly with suction, (see Figure 3.24). In fact

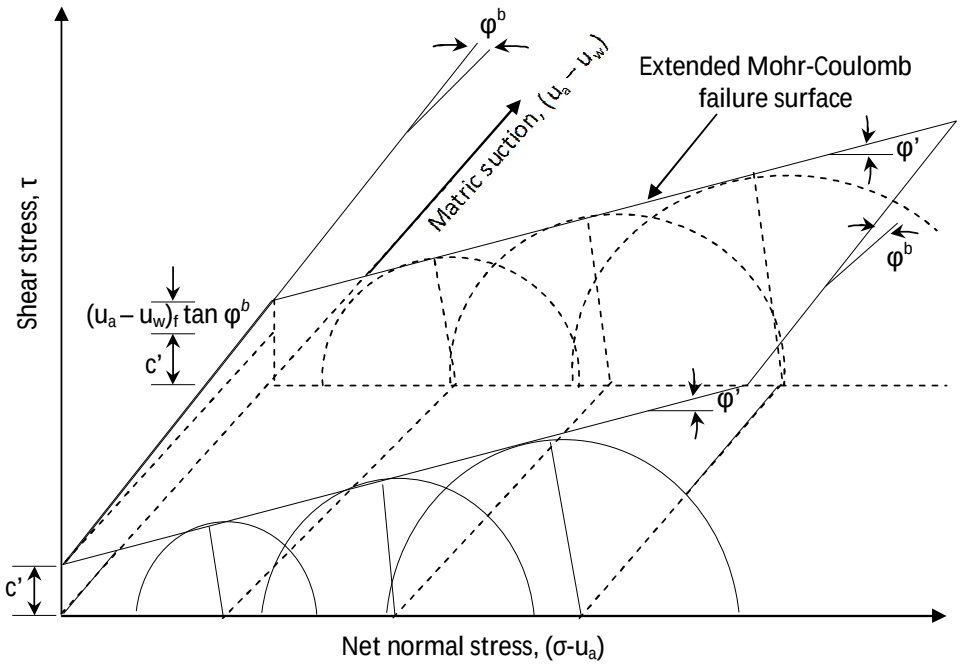

Figure 3.25: Extended Mohr-Coulomb failure envelope and surface for an unsaturated soil (Fredlund and Rahardjo, 1993)

at low matric suctions near the saturated condition, ϕ^b may be close to or equal to ϕ' until the air entry value of the soil is reached (saturated state). As matric suction increases ϕ^b decreases to values as low as zero or even negative values on approaching residual shear strength (Escario and Juca, 1989). Furthermore from a physical perspective, as illustrated in Figure 3.19, the additional inter-particle force at contacts where meniscus water is present tends towards a limiting value with increasing suction. Thus, once most of the inter-particle contacts are surrounded by meniscus water (i.e. most of the bulk water has been removed) there will be no further significant increase in shear strength with suction.

The shear strength criterion proposed in Equation 3.21 also assumes that ϕ' does not vary with suction, which is supported by experimental evidence presented by Fredlund et al. (1978) and Escario and Sáez (1986). However experimental evidence which suggests that ϕ' may increase with increasing suction has also been reported (e.g. Toll, 1990 for a lateritic gravel and Toll and Ong, 2003 for a residual sandy clay). Others have also reported a decrease in ϕ' with increasing suction (e.g. Delage et al., 1987; Maâtouk et al., 1995 for silty soils). Delage et al. (1996) and Delage (2002) collated various experimental shear strength data sets and although evidence for

both increasing and decreasing angles of friction with increasing suction were observed, cohesion was typically found to increase with increasing suction. Additional experimental evidence is required for a wide range of soils in order to further investigate the influence of suction on ϕ'.

Some researchers have proposed non-linear relationships between shear strength and suction based on knowledge of the soil water retention curve (e.g. Vanapalli et al., 1996). Alternative shear strength criteria for unsaturated soils have also been proposed by Khalili and Khabbaz (1998), who use a single effective stress approach and Vaunat et al. (2002) who attempt to incorporate the influence of hydraulic hysteresis on shear strength, among others.

3.7.3 State surface approach

One of the first attempts to describe volume change behaviour in unsaturated soils using two independent stress variables (net stress and suction) was carried out by Bishop and Blight (1963) using three-dimensional plots with axes of net stress ($\sigma - u_a$), void ratio (e) and suction ($u_a - u_w$). Matyas and Radhakrishna (1968) later proposed that such a representation be considered as a constitutive relationship for the volumetric behaviour of unsaturated soils, and that such a "unique" representation be termed the state surface of the soil. Figure 3.26 illustrates the state surface relating void ratio to net stress and suction. The state surface approach was capable of representing the different volume change behaviour resulting from wetting at different net stress, i.e. swelling at low net stresses and collapse at higher net stresses, (compare paths $A - A_S$ and $B - B''$ in Figure 3.26). An additional state surface was also proposed for changes in the degree of saturation - net stress - suction space. Later analytical expressions for the different state surfaces (e, w or S_r) were proposed by Fredlund (1979) and Lloret and Alonso (1985).

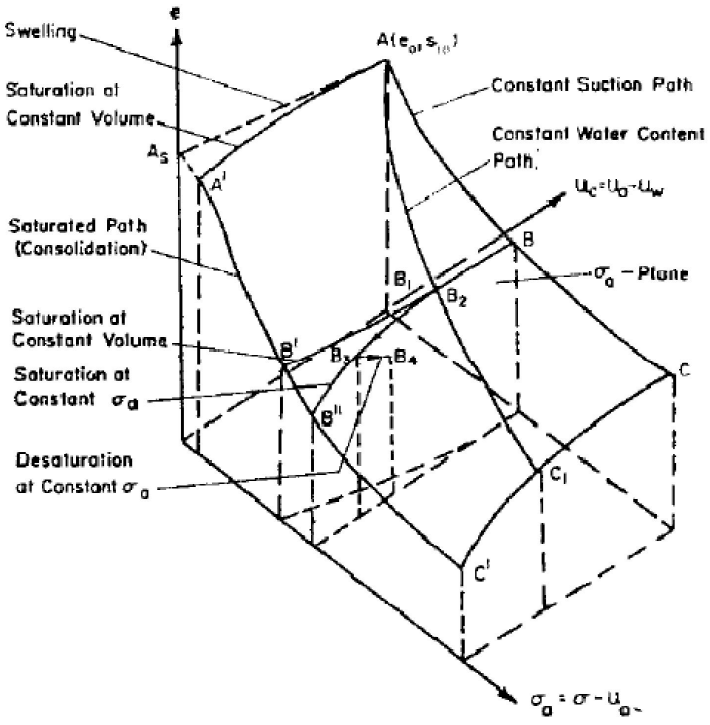

Figure 3.26: State surface approach: volume changes under equal all-round pressure plotted in void ratio-net stress-suction space (Matyas and Radhakrishna, 1968)

Although the state surface approach was able to represent the swelling-collapse behaviour of unsaturated soils on wetting at different net stresses, a number of significant limitations of the approach have been outlined by a number of authors including Fredlund (1979) and Lloret and Alonso (1985):

1. The state surface approach assumes that volume changes in unsaturated soils are not stress path dependent. Matyas and Radhakrishna (1968) among other authors found that state surfaces were unique, for a non-expansive silty clay, if the paths followed involved only decreases in suction (wetting path) or increases in applied load. However the state surfaces were not found to be unique if stress paths involved suction increases (drying) or decreases in external load (Lloret and Alonso, 1985).

2. The state surfaces would have to be determined empirically for each given material and for particular stress state conditions. Matyas and Radhakrishna (1968) presented different state surfaces for the same soil (80% flint powder - 20% kaolin) under (a) isotropic

conditions and (b) K_o compression.

The state surface approach may provide a good method of presenting results from experimental tests investigating volumetric behaviour of unsaturated soils, but considering the limitations regarding stress path dependency and material specificity, this approach did not appear to be a good basis on which to form a more general framework of unsaturated soil behaviour.

3.7.4 An elasto-plastic framework for unsaturated soils

Following the development of the state surface approach to represent volumetric behaviour and failure envelopes to describe the shear strength behaviour of unsaturated soils, there was motivation to develop a general consistent framework for unsaturated soil behaviour which could (a) adequately represent the volume change behaviour of unsaturated soils (overcoming the limitations of the state surface approach) and (b) provide an integrated approach to understanding the volumetric and shear strength behaviour of unsaturated soils. Considering the relative success of representing the volumetric and shear strength behaviour of saturated soils through elasto-plastic models, such as the Modified Cam Clay (MCC) model (Roscoe and Burland, 1968), elasto-plasticity was also considered for the development of a constitutive model for unsaturated soil behaviour. This path also ensured that developments in unsaturated soil mechanics remained closely related to the field of saturated soil mechanics (Gens, 2010).

Alonso et al. (1987) presented the concepts of an elasto-plastic framework for unsaturated soil behaviour. Following this the mathematical formulation of an elasto-plastic critical state model for unsaturated soils was presented in Alonso et al. (1990). This model is now commonly referred to as the Barcelona Basic Model (BBM). The BBM was formulated using the independent stress variables of net stress $(\sigma_m - u_a)$ and suction $(u_a - u_w)$ and uses the MCC model as the reference model, such that when suction is equal to zero (soil is saturated) the BBM reverts to the classic MCC model. For isotropic conditions (σ_1=σ_2= σ_3), the soil behaviour is described in the mean net stress and suction (p, s) stress space, where:

$$Mean\,net\,stress\;\; p = \sigma_m - u_a = (\sigma_3 - u_a) \tag{3.22}$$

$$Suction \;\; s = u_a - u_w \tag{3.23}$$

and for triaxial conditions ($\sigma_2 = \sigma_3$) in the deviator stress - mean net stress - suction (q, p, s) stress space where:

$$Mean\,net\,stress \;\; p = \sigma_m - u_a = \frac{1}{3}(\sigma_1 + 2\sigma_3) - u_a \tag{3.24}$$

$$Deviator\,stress \;\; q = (\sigma_1 - u_a) - (\sigma_3 - u_a) = \sigma_1 - \sigma_3 \tag{3.25}$$

The BBM was intended to be a simple framework which would be able to represent many of the fundamental features observed in unsaturated soils which are slightly or moderately expansive. The success of this model ensures that it continues to be one of the most widely used constitutive model for unsaturated soil behaviour. Some of the main elements of this model are outlined here.

3.7.4.1 Loading-collapse yield surface

The framework presented by Alonso et al. (1987) introduced a yield surface termed the Loading-Collapse (LC) curve (Figure 3.27) which could explain the volumetric behaviour associated with soils following (external) loading and wetting paths. The framework predicts that any changes in suction or load such that a specimen follows a path within the LC curve, will result in reversible deformations (elastic behaviour), whether it be shrinkage/swelling due to changes in suction or compression/expansion due to changes in load. Whereas any path which reaches the LC yield surface whether due to an increase in load or a reduction in suction, will cause the yield surface to shift to another position (A_1B_1 to A_2B_2) inducing irreversible volumetric deformations. Movement of the LC yield surface will expand the elastic zone and will be controlled by a single hardening parameter p_o^*, the saturated preconsolidation pressure. The irreversible strain induced by following the loading path in Figure 3.27, will be equal to the irreversible strain induced by following the collapse path and therefore the irreversible compression will be equal to that which occurs along the Normal Compression Line at zero suction (saturated) between p_{o1}^* to p_{o2}^*. The LC yield curve therefore links together the compressive strains related to loading and compressive strains induced by wetting.

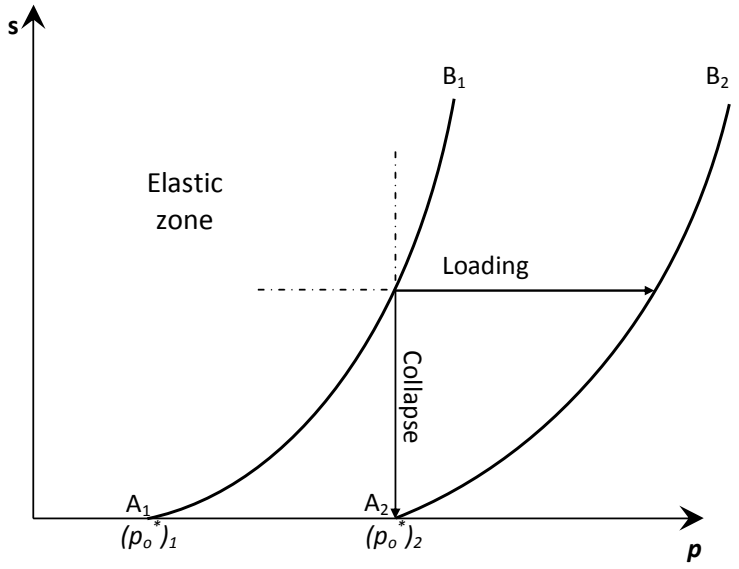

Figure 3.27: LC yield curve in (p, s) stress space, used in BBM to describe loading and collapse behaviour of an unsaturated soil (AfterAlonso et al., 1987)

Figure 3.28 presents the volumetric behaviour predicted by the BBM model for different loading and wetting paths. Paths L1, L2 and L3 represent loading paths at constant suction, these are plotted in terms of specific volume ($v = 1 + e$) and load (mean net stress, p) in Figure 3.28b. The LC curve predicts that as suction increases, the yield stress (preconsolidation stress) in the v-p space increases. A stiffening of the compression behaviour with increasing suction has also been assumed, thus the post-yield compression curves diverge. In Figure 3.28a C1, C2 and C3 represent wetting paths at constant load, and are plotted in the v-p space in Figure 3.28c. C1 follows a wetting path (reducing suction) under low constant stress, which lies within the LC curve (elastic region) and thus reversible swelling is predicted. C2 initially follows a path within the elastic region, but as suction is reduced further, it reaches the LC curve and irreversible volumetric compression occurs. If this is greater than the initial swelling or expansion, then net collapse may result (Figure3.28c). The wetting path C3 at a higher stress level reaches the LC curve almost immediately and thus is predicted to undergo the largest amount of collapse.

In the BBM model, isotropic normal compression lines are assumed to have different gradients and intercepts depending on the level of suction, (i.e. stiffness dependence on suction). Thus

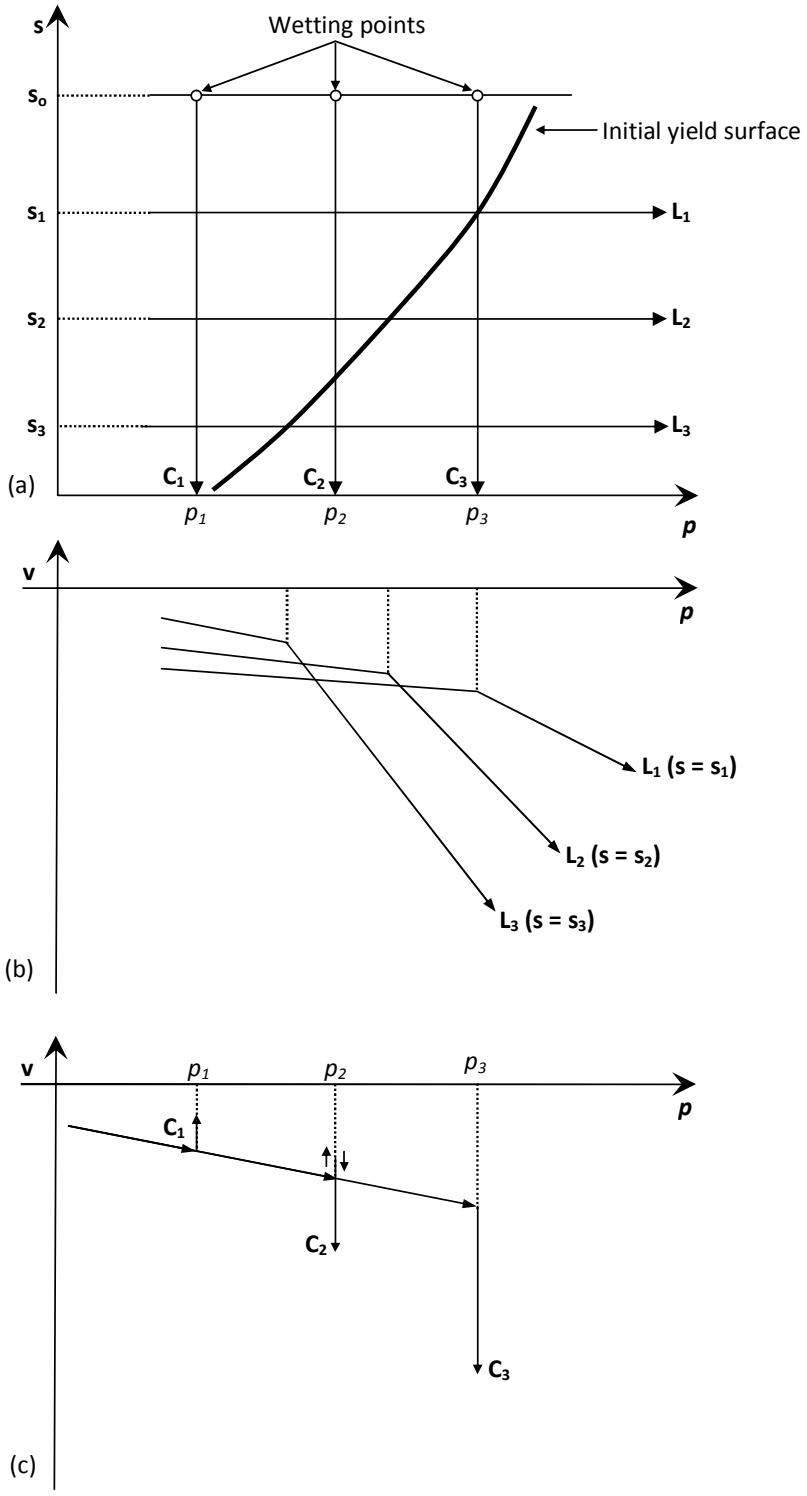

Figure 3.28: Volumetric deformations following different loading and wetting paths: (a) Loading and wetting paths in the p-s space, (b) Compression behaviour in v-p space and (c) Swelling-collapse behaviour in v-p space (After Alonso et al., 1987)

following saturated soil behaviour the variation of specific volume v with suction s is given by:

$$v = N(s) - \lambda(s) \ln \frac{p}{p^c} \tag{3.26}$$

where $\lambda(s)$ is the gradient of the normal compression line and p^c is a reference stress state at which $v = N(s)$. In this formulation it is assumed that $\lambda(s)$ decreases with increasing suction and its variation with suction is given by:

$$\lambda(s) = \lambda(0) \left[(1 - r) \exp(-\beta s) + r \right] \tag{3.27}$$

where $\lambda(0)$ is the gradient of the normal compression under saturated conditions, r is a constant related to the maximum stiffness of the soil, which lies between 0 and 1 and β is a parameter which controls the rate of increase of soil stiffness with suction.

It is assumed that on unloading and reloading at constant suction that the soil behaves elastically (e.g. reversible swelling on unloading as for saturated soils). The BBM also incorporates elastic volume changes due to suction unloading, i.e. reversible swelling due to wetting at low confining stresses. Thus the elastic changes in specific volume are given by:

$$dv^e = -\kappa \frac{dp}{p} - \kappa_s \frac{ds}{(s + p_{atm})} \tag{3.28}$$

where κ is the elastic stiffness parameter for changes in net mean stress and κ_s is the elastic stiffness parameter for changes in suction and p_{atm} is atmospheric pressure. The model assumes that κ_s is a soil constant, although Alonso et al. (1990) do suggest that it is likely to vary with suction, but in the interest of developing a simple model and due to the lack of conclusive experimental evidence, a constant value was adopted.

In the BBM model the expression of the LC yield surface is derived from the gradient of the post-yield compression curve at different suctions and is given by:

$$\left(\frac{p_o}{p^c} \right) = \left(\frac{p_o^*}{p^c} \right)^{[\lambda(0) - \kappa] / [\lambda(s) - \kappa]} \tag{3.29}$$

where p_o is the preconsolidation stress and p_o^* is the preconsolidation stress at saturated conditions. The LC curve is a fundamental element of the model allowing some of the main features

associated with the volumetric behaviour of unsaturated soils to be predicted, including an increase in the preconsolidation stress with increasing suction and volume changes due to wetting at constant stress. In particular the LC curve can predict that a soil may exhibit (i) swelling at a low confining stress (inside the elastic zone), (ii) collapse at a high confining stress (initial condition is on the LC curve) and (iii) swelling and then collapse at an intermediate value of confining stress (initial position inside the elastic zone and then reaches the LC curve).

3.7.4.2 Suction-increase yield surface

The BBM formulation also includes a suction-increase (SI) yield surface which can be seen in Figure 3.29b. The suction-increase yield surface enables irreversible volumetric deformations due to drying to be predicted. It is proposed that irreversible strains will begin to develop once the soil has reached a value of suction corresponding to its past maximum value, (similar to the concept of preconsolidation stress being the yield point for plastic volumetric strains due to loading). With little experimental evidence regarding this behaviour, the suction-increase yield surface is assumed to be a constant equal to s_0 which represents the maximum past suction experienced by the soil.

3.7.4.3 Extension to q-p-s space

The LC and SI yield surfaces explained above were extended into the triaxial stress space as illustrated in Figure 3.29. In Figure 3.29a, in the $q-p$ space the curve labelled $s=0$ represents the yield surface for saturated conditions. Considering that one of the desirable features of a general framework for unsaturated soils was that it be compatible with saturated models, the ellipse yield surface of the MCC model (Roscoe and Burland, 1968) was adopted. The ellipse yield surface in the $q-p$ plane is given by the equation:

$$q^2 - M^2(p+ks)(p_o - p) = 0 \tag{3.30}$$

where M is the slope of the critical state line, k is a constant describing the increase in cohesion with suction. In the BBM model the increase in shear strength with suction is represented by

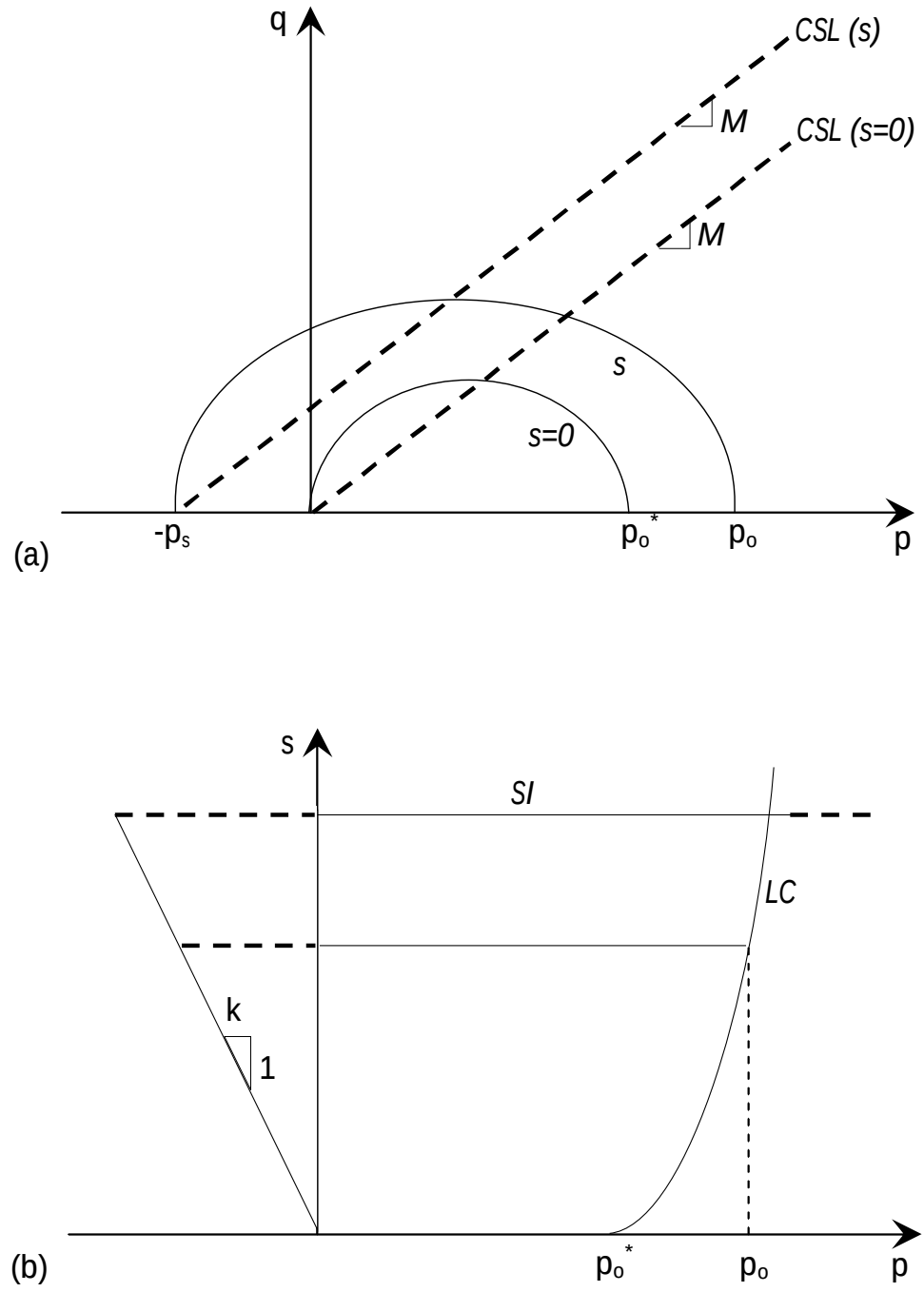

Figure 3.29: BBM yield surfaces (a) Yield surface in (q, p) stress space for saturated ($s = 0$) and unsaturated conditions (s) and (b) yield surface in (p, s) isotropic plane (Alonso et al., 1990)

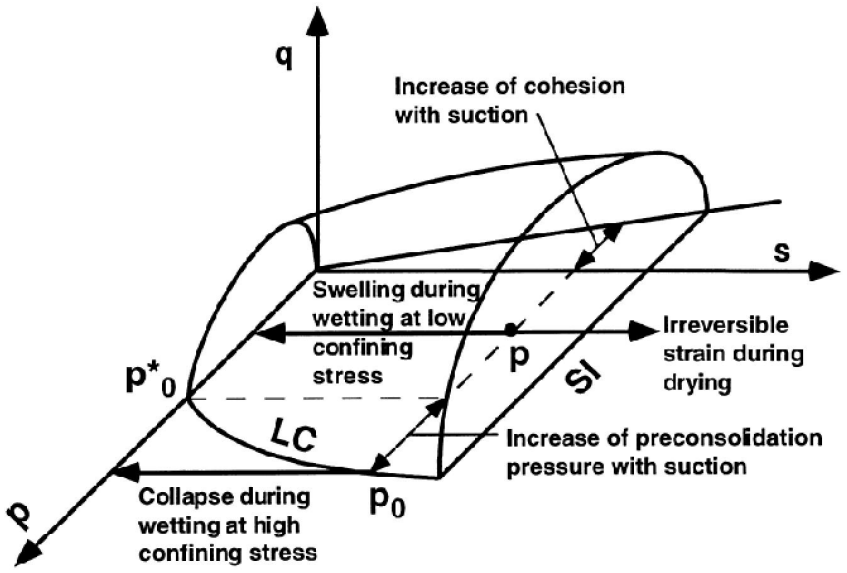

Figure 3.30: Three-dimensional view of the yield surfaces of the BBM model in (p, q, s) stress space (Alonso et al., 1990, 1999)

a critical state line (CSL) which is parallel to the CSL for saturated conditions (Figure 3.29a). The slope of the CSL M is assumed to remain constant and can be expressed as:

$$q = Mp + ks \tag{3.31}$$

ks is equal to p_s and is responsible for the linear shift of the critical state line in the (p, q) plane (Figure 3.29). The model thus assumes that the increase in shear strength due to suction is due only to an increase in apparent cohesion (M constant similar to constant ϕ') and also assumes that apparent cohesion increases linearly with suction. These simplistic assumptions are in line with the failure envelope for unsaturated soils proposed by Fredlund et al. (1978), despite experimental evidence suggesting that shear strength varies non-linearly with suction (Escario and Sáez, 1986; Escario and Juca, 1989), and that ϕ' may not always be constant (Delage et al., 1987; Futai and Almeida, 2005). The BBM model is summarised in Figure 3.30, where all the yield surfaces are plotted in the three-dimensional $q - p - s$ stress space.

3.7.4.4 BBM assumptions and limitations

As a first attempt at developing an elasto-plastic model integrating the volumetric and shearing behaviour of unsaturated soils, a number of simplifying assumptions were made, including (i) the use of straight lines for the $v - \ln p$ relationships, (which predict that collapse strains will continually increase with increased net stress), (ii) a linear increase of apparent cohesion with suction, which experimental evidence has suggested otherwise, (iii) that the elastic stiffness parameter k_s is a constant and not dependent on suction, (iv) that the suction-increase yield surface is a straight line corresponding to the maximum past suction and (v) the use of linear $v - \ln s$ relationships, suggesting a linear reduction in specific volume with increasing suction, however as the degree of saturation approaches the residual state the specific volume will converge to a value corresponding to the air dried state (e.g. Cunningham, 2000).

Yet despite these simplifying assumptions the BBM model can describe many of the main features associated with the mechanical behaviour of unsaturated soils including (see Figure 3.30):

- an increase in preconsolidation stress with increasing suction
- the occurrence of reversible swelling strains due to a reduction in suction at low confining stresses
- the occurrence of irreversible collapse strains when suction decreases at high confining stresses
- reversal of volumetric strains during wetting induced collapse
- the occurrence of irreversible shrinkage strains when suction increases above a threshold value
- an increase in shear strength with increasing suction.

With respect to the variation in soil compressibility with suction, the BBM model initially assumed that increases in suction stiffens the soil response to external load post-yielding, i.e. diverging normal compression lines in $v - \ln p$ space. However, experimental evidence has equally been found for opposing behaviour, increasing post-yield compressibility with increasing suction,

as discussed in Section 3.6.2 (e.g. Wheeler and Sivakumar, 1995; Futai and Almeida, 2005), where λ increases with increasing suction. Wheeler et al. (2002) proposed that the BBM model could however be used to predict converging normal compression lines at different suctions by selecting suitable values of the model parameters r and p^c. Therefore using the BBM model, depending on the values of parameters r and p^c, the collapse strains predicted will either monotonically increase or monotonically decrease with increasing applied stress.

The BBM model however cannot predict collapse strains which initially increase and then decrease with increasing applied stress which correspond to the occurrence of a maximum collapse strain, which has commonly been reported in the literature (e.g. Balmaceda, 1991; Rao and Revanasiddappa, 2006). This reduction in collapse compression observed at high stress levels can be explained by considering that sufficiently high loads will act to destroy the initially open (collapsible) soil structure, such that soil behaviour will tend towards a unique compression curve which is independent of suction (Alonso et al., 1987). Based on the BBM model, Josa et al. (1992) developed a model where non-linear relationships between void ratio and $\ln p$ enabled collapse strains to be predicted which increased initially and then decreased at higher stresses.

Subsequent refinements of the BBM model were made by a number of different authors. For example, Wheeler and Sivakumar (1995) proposed model functions derived more directly from experimental results, including a non-linear increase of shear strength with suction and Cui and Delage (1996) introduced an inclined ellipse yield surface in the $q - p$ space, which is typical of soils exhibiting anisotropy.

Despite the success of the BBM model and the associated refinements which have been made to the model, there remain other additional features of unsaturated soil behaviour which the BBM model was never intended to predict, including:

1. irreversible strains exhibited by highly expansive clays
2. hydraulic hysteresis exhibited during wetting & drying cycles
3. coupling between water retention and mechanical behaviour.

3.7.5 Advanced elasto-plastic models for unsaturated soils

Advanced elasto-plastic models have been developed in order to incorporate the mechanical behaviour exhibited by expansive clays and to incorporate the effects of hydraulic hysteresis on mechanical behaviour and the influence of the mechanical behaviour on the water retention behaviour (i.e. influence of void ratio on water retention behaviour). These models introduce additional complexity by considering additional yield surfaces and additional or alternative stress variables. A number of these models are briefly described here.

3.7.5.1 Model for expansive clays

Gens and Alonso (1992) presented a conceptual framework based on the BBM model that was extended in order to incorporate the features of mechanical behaviour typically exhibited by expansive clays: (i) irreversible stress path dependent behaviour on wetting and (ii) the accumulation of irreversible strains during drying-wetting cycles (e.g. Chu and Mou, 1973, see Figure 3.23). Due to the fact that the behaviour of expansive clays largely arises from the physico-chemical phenomena interactions occurring at the clay particle level, it was considered beneficial to incorporate a microstructural level into the elasto-plastic model (Gens and Alonso, 1992). Thus the model considers two levels of structure the microstructure, the clay particle level and the macrostructural level which relates to the overall fabric and arrangement consisting of clay aggregates and macropores. At the microstructural level, the clay particle arrangements are assumed to be fully saturated and strains to be largely reversible. At the macrostructural level the mechanical behaviour is characterised by the LC yield surface, as presented for the BBM. It is assumed that changes in the macrostructure do not influence the microstructure, but that deformations at the microstructural level may induce irreversible strains at the macrostructural level. This model is summarised in Figure 3.31. The suction-increase (SI) and suction-decrease (SD) yield surfaces introduced represent the onset of macrostructural irreversible (plastic) strains. A mathematical formulation for the expansive model was presented by Alonso et al. (1994) and refined by Alonso et al. (1999) in the Barcelona Expansive Model (BExM) to include the features related to behaviour exhibited during drying-wetting cycles. The expansive model has more recently been developed using generalised plasticity concepts (Sánchez and Gens, 2005).

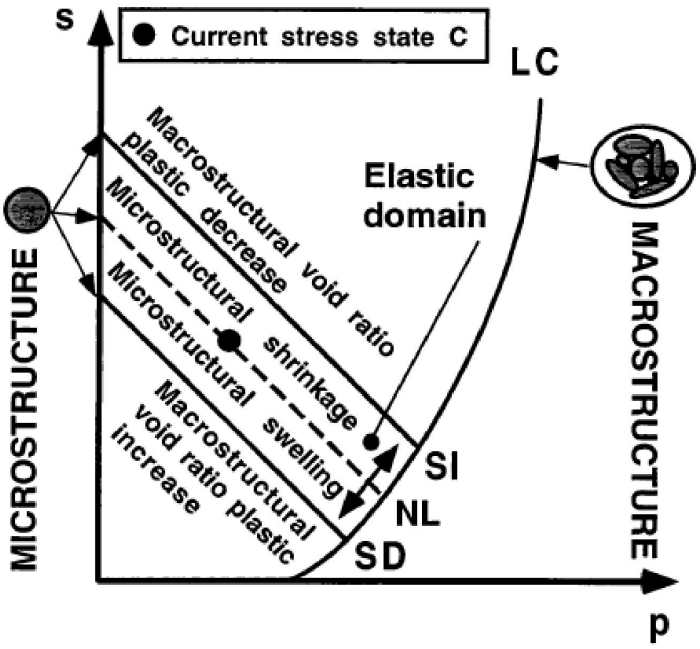

Figure 3.31: Yield surfaces in $(p-q)$ stress space in BExM including (i) loading-collapse (LC) (ii) suction-increase (SI) and (iii) suction-decrease (SD) yield surfaces (Alonso et al., 1999)

Motivation for models surrounding the behaviour of expansive clays has largely been due to their use in the design of high level radioactive waste storage schemes. Considering that high level radioactive waste is strongly heat emitting, the influence of temperature on mechanical behaviour is a significant issue. In particular, Sánchez et al. (2007) presented experimental and modelling data which suggests that swelling pressures decrease with increasing temperature. The BExM was extended to incorporate temperature effects occurring in the microstructural level (Sánchez et al., 2007) and has been successfully used to predict the thermo-hydro-mechanical behaviour observed in full-scale tests (Gens et al., 2009).

The mechanical behaviour of expansive clays due to their active clay content may also be susceptible to changes in the chemical environment. There are a wide number of different chemical processes which may influence the mechanical behaviour, for example precipitation or dissolution phenomena, oxidation or reduction processes, cation exchanges (Mitchell and Soga, 2005) to name but a few. A number of different chemo-mechanical models have been proposed which address the effect of a specific chemical process, for example: the chemical degradation of bonded geomaterials (Nova et al., 2003). The effects of cation exchanges in swelling clays has received

particular attention due to its relevance to the use of expansive clays in nuclear waste repositories (Gens et al., 2002, 2008; Gens, 2010).

3.7.5.2 Coupled water retention-mechanical models

The BBM does not directly take into account the influence of degree of saturation on the mechanical behaviour, (this influence is solely expressed through matric suction). An additional separate water retention model is required to relate matric suction to the degree of saturation, which generally does not take into account hydraulic hysteresis. Furthermore the BBM also does not directly take into account the influence of the void ratio on water retention behaviour. If hydraulic parameters such as the degree of saturation are incorporated into the stress variables of the constitutive model it is possible for water retention and mechanical behaviour to be coupled.

Vaunat et al. (2000) presented perhaps the first complete attempt at coupling water retention and mechanical behaviour for unsaturated soils by coupling the water retention model proposed by Romero and Vaunat (2000) with the BBM mechanical model. The model based on net stress and suction variables incorporates an LC yield surface and two additional yield surfaces related to hydraulic hysteresis: the suction-increase (SI) yield surface which defines irreversible (plastic) behaviour due to drying and the suction-decrease (SD) yield surface defining plastic changes due to wetting. The SI and SD yield surfaces are coupled with each other but not with the LC curve.

Wheeler et al. (2003) also presented an elasto-plastic model which fully coupled hydraulic hysteresis with mechanical behaviour (Figure 3.32). Wheeler et al. (2003) used the alternative stress variables of Bishop's stress and modified suction ($s* = ns$) as presented in Section 3.7.1.3, based on the thermodynamic considerations and work input equation proposed by Houlsby (1997), selecting the work-conjugate variables of strains and degree of saturation. Using these variables Wheeler et al. (2003) proposed that the LC yield surface could be approximated to be a vertical straight line and the SI and SD yield surfaces could be horizontal straight lines in the $(s - p)$ plane (see Figure 3.32) and that these three yield surfaces are fully coupled with each other.

In addition to the features of unsaturated soils captured by Alonso et al. (1990), the coupled water retention-mechanical model proposed by Wheeler et al. (2003) is also capable of capturing (i) irreversible compression during wetting-drying cycles, (ii) influence of wetting-drying cycles

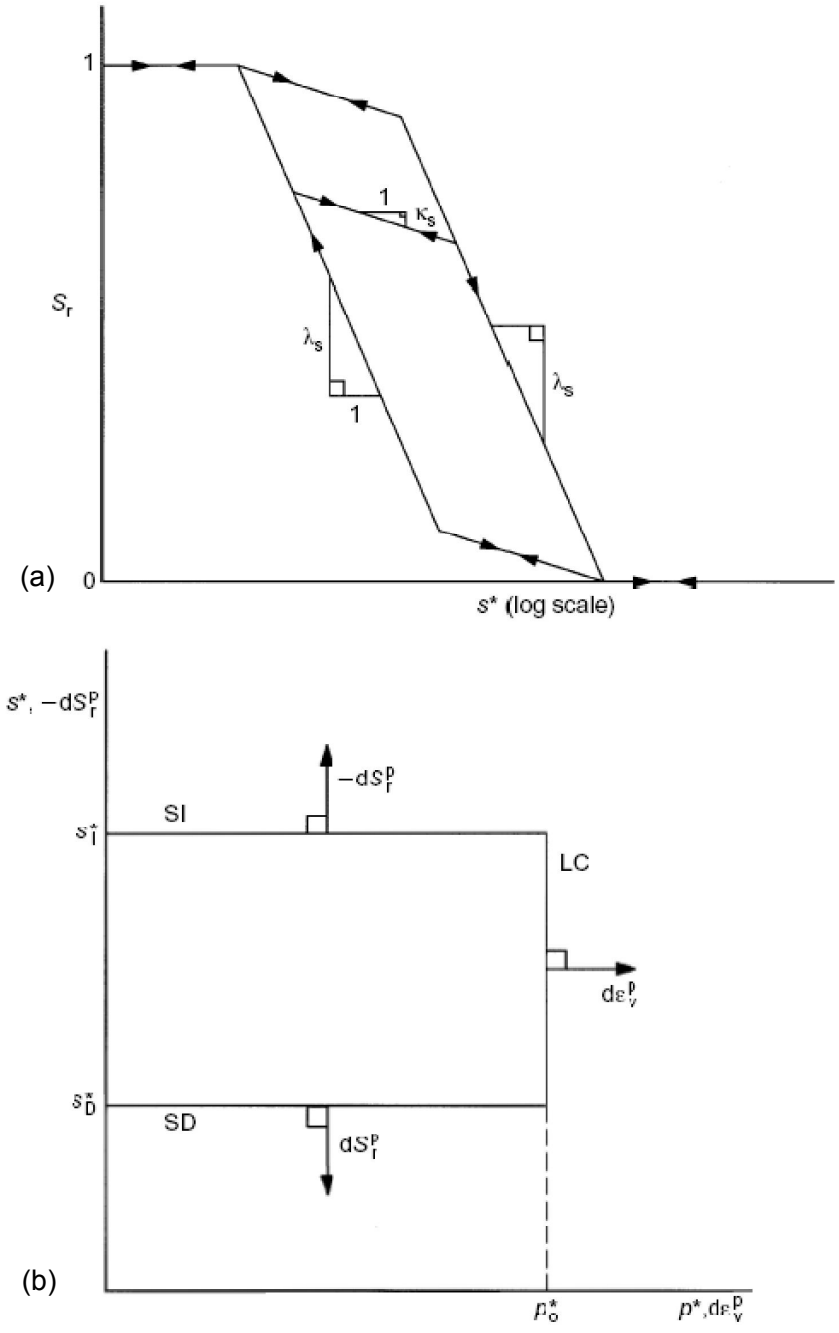

Figure 3.32: Coupled water retention and mechanical behaviour model proposed by Wheeler et al. (2003): (a) hydraulic hysteresis incorporated in water retention model and (b) loading-collapse (LC), suction-increase (SI) and suction-decrease (SD) yield surfaces in modified suction $s*$- Bishop's stress $p*$ plane

on subsequent isotropic loading behaviour and (iii) a smooth transition between saturated and unsaturated responses. A similar coupled water retention-mechanical behaviour model was proposed by Sheng et al. (2004) using stress variables of Bishop's stress and suction.

In light of this shift towards the development of coupled water retention-mechanical behaviour models, a number of works have been dedicated to improving water retention models for deformable soils, where changes in the degree of saturation are related to not only hydraulic paths (wetting or drying) but also due to changes in void ratio (mechanical paths), for example Gallipoli et al. (2003); Nuth and Laloui (2008a) and Tarantino (2009). Considering the significant developments in constitutive models of unsaturated soils in recent years, a wealth of information is provided in review and key note papers dedicated to the topic (e.g. Gens et al., 2006, 2008; Nuth and Laloui, 2008b). It is important to note here that as the level of complexity of these elasto-plastic models increases, including the selection of alternative stress variables, the following of particular stress paths in an experimental setting becomes increasingly more difficult (e.g. controlling Bishop's stress). Furthermore if degree of saturation is included in the definition of the constitutive stress variables then information regarding changes in water content is required, and often such data is either not available or is unreliable (Gens, 2010).

It is evident from reviewing the literature on the development of these constitutive models that one of the limiting factors to the development of such models is the availability of good quality experimental data sets for a wide range of suctions, stress paths and soil types. Many of the constitutive models have been validated using typically homogeneous materials such as compacted Speswhite kaolin (Sivakumar, 1993) or artificial mixtures of bentonite and kaolin (Sharma, 1998) or material which has been very widely studied for a particular engineering purpose (e.g. Boom clay, Romero, 1999). One of the aims of this research is to provide an experimental data set for an unsaturated *natural* soil sampled from an engineering application exhibiting problematic response. It is in this way that the database of experimental results for unsaturated soils can expand to include different soil types and can be related to the importance of understanding the role of unsaturated soil behaviour in practical engineering applications.

3.8 Conclusion

The Bengawan Solo material has been investigated in this research from an unsaturated soils perspective due to its role as a fill material in the construction of flood embankments. Considering the significant advances which have been made in the field of unsaturated soils in recent decades, this chapter attempted to present an overview of this increasingly widening and rapidly developing research area. Some of the basic physical mechanisms surrounding the retention of water in soils under unsaturated conditions have been discussed alongside the concept of soil suction. A number of the experimental techniques which have been developed in order to control or measure suction were then reviewed. The important features of unsaturated soil behaviour, both with respect to volume change and shear strength have been outlined in this chapter. However, it remains clear that there is still a need for additional experimental results in order to further explore certain aspects of their behaviour. This thesis investigates further some important features through experimental testing of the Bengawan Solo fill material, including: (i) the phenomenon of volumetric collapse (Chapter 5), (ii) the influence of suction on soil compressibility (Chapter 6), (iii) the influence of suction on shearing behaviour (Chapter 6). Furthermore this thesis investigates the role of compacted fabric in the behaviour of unsaturated soils. This is explored in detail in Chapter 7, investigating in particular the influence of fabric on preconsolidation stress and on soil compressibility. As highlighted in the review of constitutive models, there is a need for high quality data sets to assist in furthering the understanding of unsaturated soil behaviour. The experimental work presented in this thesis is intended to provide such a data set.

Chapter 4

Characterisation of Bengawan Solo fill

4.1 Introduction

This chapter presents a detailed characterisation of the Bengawan Solo fill material. This includes a description of the site investigation including details of the in-situ tests and soil sampling carried out. The laboratory characterisation carried out is then presented including information regarding the soil properties, particle size distribution, soil mineralogy, compaction and soil water retention behaviour of this material.

4.2 Background site information

4.2.1 Seasonal weather variations

Takeuchi et al. (1995) present hydrological data recorded at the Bojonegoro observation station (Table 4.1), which is located at a distance of approximately 40km from the site (see Figure 4.1). Temperatures in the area remain fairly constant throughout the year, ranging from 26-28°C.

However levels of precipitation and evaporation vary greatly depending on the season (wet or dry), with evaporation greatly exceeding precipitation for six months of the year (May to October, dry season). During the dry season, the lowered river level and higher levels of evaporation both contribute to reduce the moisture content of the fill material within the embankment body. Inversely, higher river levels and levels of precipitation during the wet season contribute to higher moisture contents within the fill material of the embankment.

4.2.2 Geology and founding layers

The research presented in this thesis is focused on the unsaturated mechanical behaviour of the Bengawan Solo fill, material sampled from within the embankment body, however for the sake of completeness, a brief description of the geology and materials found at depth below the embankments are presented here. The geology of the Bengawan Solo River Basin is presented in Figure 4.1, which indicates that the site is predominantly characterised by alluvial deposits. Information on the founding soils present below the man-made and natural embankments at the Kedungharjo site are summarised in Figure 4.2. This data was obtained from two boreholes drilled by ITS in September and October 2005 (Soemitro, 2005). The borehole data for both embankments indicates subsurface layers of varying fractions of sand, silt and clay (typical of alluvial soils). Below the man-made embankment (Figure 4.2a) N-values are are within the range of 6-8 blows per 30cm of soil penetration. The founding soils below the natural embankment Figure 4.2b) on the other hand show greater variation, ranging from 2-23 blows required per 30cm penetration. Assuming a correlation between undrained shear strength (Cu) and SPT N-values of Cu = 5N (Stroud and Butler, 1975) and according to BS 8004 (BSI, 1986) the founding material below the man-made embankment is mainly soft soil, whereas below the natural embankment (Figure 4.2) the material ranges from very soft to stiff.

4.3 Site investigation of embankment fill material

The site selected for further investigation of the embankment fill material was the section of embankment located next to the village of Kedungharjo, in particular the stretch of embankment

Table 4.1: Monthly weather data recorded at Bojonegoro observation station (Takeuchi et al., 1995)

Observation item	Jan	Feb	March	April	May	June	July	Aug	Sept	Oct	Nov	Dec	Annual
Temperature (°C)	27.3	27.8	28.1	28.1	27.8	27.2	26.7	27.0	27.5	27.8	28.4	28.1	27.7
Precipitation (mm)	263	247	233	151	86	47	42	21	22	70	183	256	1628
Evaporation* (mm)	81.1	78.5	99.5	101.7	117.1	118.8	124.6	142.9	156.8	164.6	127.5	103.0	1180
Solar radiation ($MJ/m^2/d$)	5.1	5.4	5.9	5.5	5.8	5.7	5.9	6.3	6.7	7.1	6.3	5.6	5.93
Duration of sunshine (hr)	223	209	198	328	380	456	670	539	540	242	351	251	4387

*Average Evaporation using Class A Pan

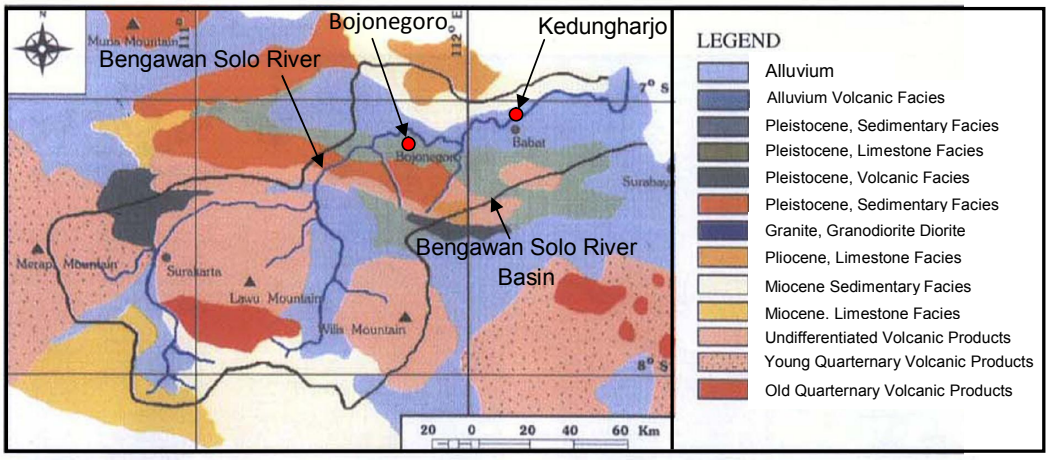

Figure 4.1: Geological map of Bengawan Solo River Basin, East Java, Indonesia (After Takeuchi et al., 1995)

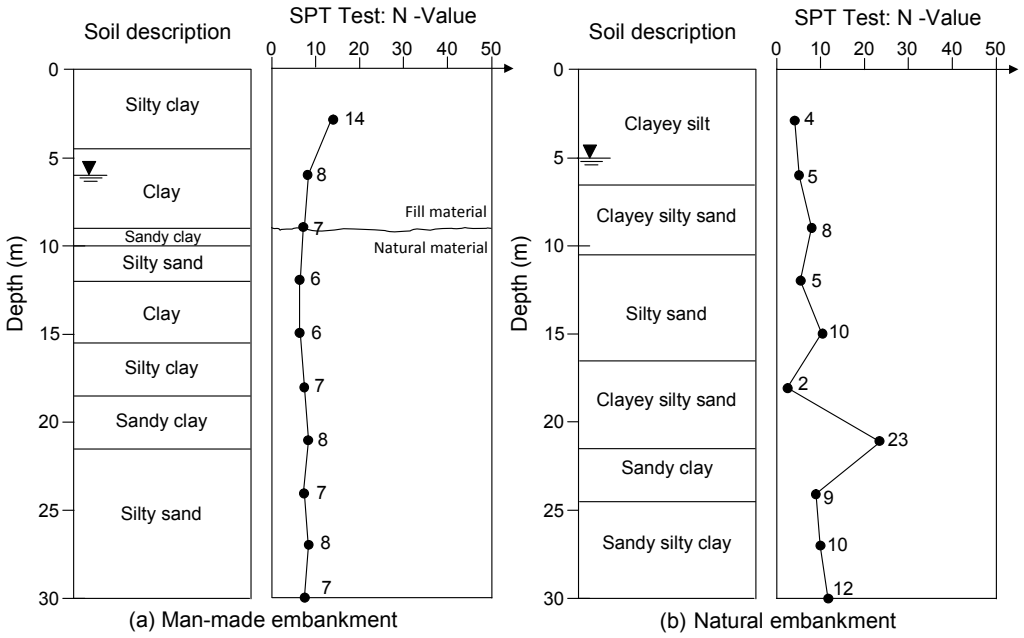

Figure 4.2: Soil profile up to a depth of 30m at Kedungharjo (a) BH-1 Man-made embankment (b) BH-2 Natural embankment (Borehole data after Soemitro, 2005)

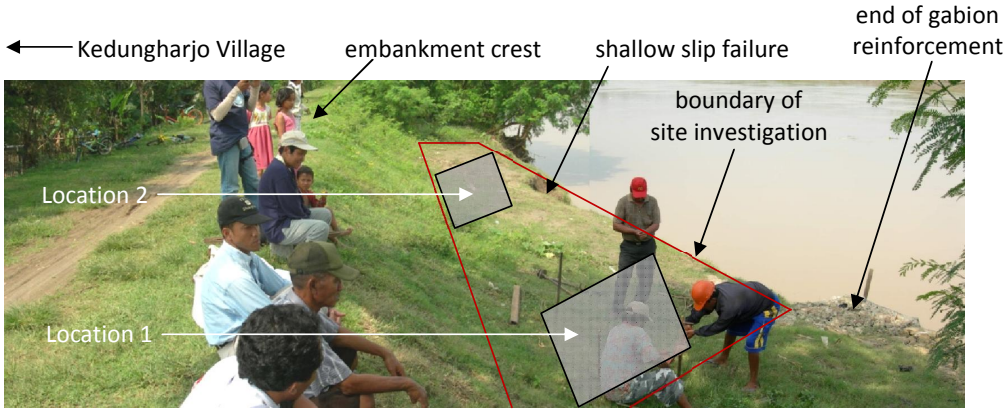

Figure 4.3: Area of site investigation located along Bengawan Solo River next to the village of Kedungharjo, East Java, Indonesia

located between the global failure of the gabion reinforced embankment shown in Figure 2.11 and the shallow slip failure shown in Figure 2.10b. The boundary of the site investigation area is highlighted in Figure 4.3.

The site investigation described herein took place in early May 2006. The site visit took place at the end of the wet season (Table 4.1) and one week prior to the visit the embankments investigated herein had been overtopped. As evident in the site investigation results presented below the soil had retained a high moisture content. Due to this high moisture content, and subsequent soft nature of the soil and the high level of the river, it was not possible to investigate the soil on the outward face of the embankment. As such the investigation and sampling was carried out on the step of the embankment as shown in Figure 4.3.

During the site investigation the soil was characterised as a soft brown clayey silt (EMBANKMENT FILL) according to descriptions given in BS5930:1999. In the upper layer (0 - 0.5m depth) there was evidence of desiccation cracks and there was significant small root content. With increasing depth the root content decreased although fewer larger tap roots were observed at 1.0 - 1.5m depth.

4.3.1 In-situ tests

In order to determine the in-situ density (or field density) the small pouring cylinder sand replacement method was used in accordance with BS1377-9:1990. A hole was excavated in the field and filled with (clean, air-dried and specifically graded) sand of which the bulk density had been previously determined in the laboratory using a calibrated mould. At the field, the mass of sand required to fill the excavated hole was determined, and from this the volume of the excavated hole was calculated. All of the soil from the excavated hole was removed and weighed on site and thus the bulk density was determined. Representative samples of the excavated material were stored in airtight containers for moisture content determination in the laboratory. The moisture content, w refers to the mass of water removed by oven drying at 105°C m_w, expressed as a percentage of the dry mass of solids (oven dried soil mass), m_s. The oven dry soil mass refers to the constant soil mass achieved by drying, typically in a period of 12 - 24hrs. The moisture content, w is thus given as:

$$w\,(\%) = \frac{m_w}{m_s} \times 100 \tag{4.1}$$

From the bulk density ρ and the moisture content, the dry density, ρ_d can be determined:

$$\rho_d = \frac{100\rho}{100 + w} \tag{4.2}$$

Table 4.2 presents the range of bulk densities, dry densities and moisture contents found during the site investigation using the sand replacement method. In particular, it should be noted that in-situ dry densities as low as 1.18Mg/m^3 were found. The high moisture contents found reflected the recent overtopping of the embankments (up to 43%). Furthermore the moisture contents and in-situ dry densities varied significantly along the short stretch of the embankment investigated (20m) (Figure 4.3), indicating heterogeneity within the fill material. This is perhaps not surprising to find in embankments which are constructed at relatively low cost and which are therefore not strictly controlled in terms of compaction during construction.

In-situ undrained shear strength measurements were carried out using the vane shear test according to BS1377-9:1990. A vane of cruciform cross-section, 150mm long and 75mm wide was

Table 4.2: In-situ density measurements determined using sand replacement method

Property	Range
In-situ bulk density (Mg/m^3)	1.69 - 1.80
In-situ dry density (Mg/m^3)	1.18 - 1.36
Moisture Content (%)	32 - 43
Degree of saturation (%)	88 - 90

used in the tests. A calibrated torque measurement device was clamped to the extension rods of the vane. The torque head was rotated at a rate of between 0.1°/s and 0.2°/s until the maximum deflection was observed on the gauge. This maximum deflection was recorded indicating the torque required to shear the soil. At failure a cylindrical failure surface develops. The vane shear strength (τ_f) in kPa can be calculated as (BS1377-9:1990):

$$\tau_f = \frac{M}{K} \tag{4.3}$$

where M is the torque required to shear the soil (Nm) and K is a constant depending on the dimensions and shape of the vane used which can be calculated as:

$$K = \pi \frac{D^2 H}{2}(1 + \frac{D}{3H})10^{-6} \tag{4.4}$$

where D is the width of the vane (mm) and H the height of the vane (mm). This calculation assumes that the distribution of the shear strength is uniform across the ends of a cylinder and around its perimeter.

Table 4.4 presents the undrained shear strength measurements recorded along the embankment. Measurements were taken at two different locations at two different depths, 0.3m and 0.8m respectively. At each location, four measurements were made in close proximity, but at a distance so as not to be disturbed by the other tests. The Bengawan Solo fill can thus be classified as a soft soil according to BS8004:1986 as it has undrained shear strength values between 20 - 40kPa.

Table 4.4: In-situ undrained shear strength measurements determined using shear vane test

Location	Depth (m)	Undrained shear strength (kPa)
1	0.3	25
	0.3	30
	0.3	31
	0.3	22
2	0.8	38
	0.8	30
	0.8	24
	0.8	37

4.3.2 Soil sampling

During the site investigation both disturbed and undisturbed material was sampled for further laboratory investigation at the University of Strathclyde. Disturbed material was sampled from two different depths 0.5m - 1.0m and 1.0 - 1.5m depth, herein referred to as D1 and D2 respectively. In total approximately 75kg of disturbed material was sampled. Undisturbed samples were taken using both open-drive tube sampling and block sampling. For the open-drive sampling thin walled tubes were driven into the embankment using a manually rotated jack incorporated within a loading frame. Supposedly undisturbed tube samples were taken using ten, 100mm diameter tubes (U_{100s}) made of galvanised steel with a sharpened cutting edge. Immediately after sampling both ends of the sample were covered in wax to inhibit water loss and were additionally capped with PVC ends. Undisturbed block samples were retrieved as described in the Report on Tropical Residual Soils by the Geological Society Engineering Group Working Party (Fookes, 1990). See Figure 4.4 for details on the block sampling method. Two wooden boxes were used, which were internally lined a priori with aluminium sheets and further sealed externally with wax around all edges and corners to inhibit water loss. The boxes were approximately 50cm x 50cm x 50cm. Due to the difficulty in sampling undisturbed block samples of this size, samples were only taken between depths of 0 - 0.5m and 0.5 - 1.0m. Generally the amount of soil sampled in a single block sample is larger than for a tube sample. The increase in mass makes it much more difficult to remove easily from the ground and also increases transportation costs. Block samples also require a larger trench to be excavated, disturbing more of the site under investigation. The trenches at the Bengawan Solo embankments were refilled with neighbouring material after sampling in order to minimise the negative impact of

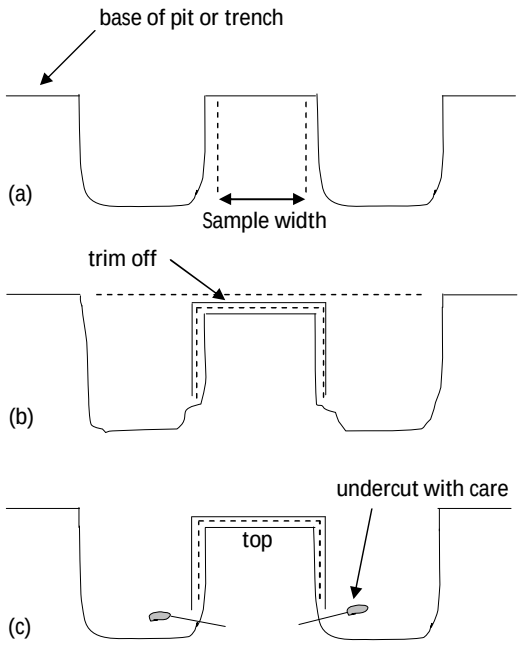

Figure 4.4: Procedure for retrieving undisturbed block samples (after Fookes, 1990)

this sampling on the embankments.

Most of the testing campaigns presented in this research used the disturbed material sampled in order to control initial moisture contents and dry densities. However a number of tests presented in Chapter 5 were carried out using the undisturbed material, taken from the block samples. The block samples were preferred for testing over the tube samples due to the reduced disturbance of soil retrieved by block sampling (Chandler et al., 1992). In fact samples from the cylindrical tubes were not used in any of the tests presented in this thesis.

4.3.3 Importing soil material

The disturbed and undisturbed samples were shipped back to the University of Strathclyde for further investigation in the laboratory. The soil samples took over a month to be delivered to Glasgow. In order to import non-European soil into the UK it was necessary to obtain a soil licence from Science and Advice for Scottish Agriculture (SASA), a division of the Scottish Government. The main concern with importing foreign material of this kind is the risk to native

plants by the introduction of foreign pests. A soil licence was granted on an annual basis in order for this material to remain stored in the UK. A SASA representative visited the research laboratory where the material was to be stored and tested in order to assess that the facilities were suitable. Conditions of the licence include that the material must not be used as a growth medium and that the material must be sterilised in an Autoclave before disposal.

4.4 Basic Soil Properties

On return to the University of Strathclyde, initially a basic characterisation of the Bengawan Solo fill material was carried out. This characterisation included the determination of the particle density, the particle size distribution, the Atterberg limits and organic content. These tests were carried out in accordance with BS1377-2:1990, following the detailed procedures presented in Head (1992).

Particle densities of 2.73Mg/m^3 and 2.72Mg/m^3 were determined for depths 0.5-1.0m (D1) and 1.0 - 1.5m (D2) respectively using the small pyknometer method. The particle size distribution curve was determined for material sampled from both depths using wet sieving (1mm - 63µm) and hygrometer sedimentation (<63µm). The soil samples were first pretreated with hydrogen peroxide and hydrochloric acid to remove any organic or calcareous material. After filtration the samples were then dispersed using a solution of sodium hexametaphosphate and sodium carbonate to ensure separation of particles within the silt and clay range (Head, 1992). Figure 4.5 presents the combined particle size distribution curves for the two depths investigated. The two depths presented very similar particle size distributions. D1 is made up of 30% sand, 57% silt and 13% clay and D2 consists of 29% sand, 55% silt and 16% clay. These particle fractions are plotted on the US Department of Agriculture textural classification chart in Figure 4.6. Using this chart, the material can be classified as a silty loam using the USDA terminology or clayey silt in British Standard terminology. The uniformity coefficient, U can give an indication of the grading of the material and is the ratio of the 60% particle size to the 10% particle size. For D1, $U = 29$ and for D2, $U = 27$, indicating that the Bengawan Solo fill is a well graded material in the clay, silt and sand range.

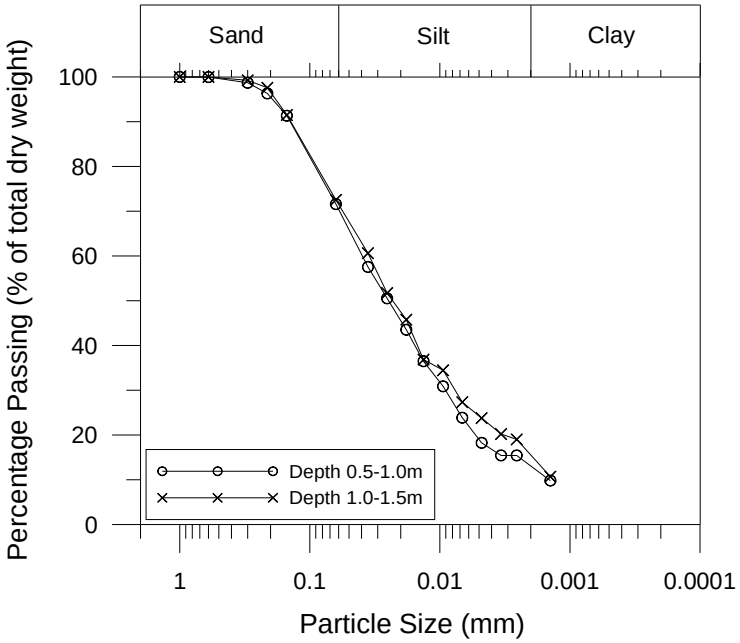

Figure 4.5: Particle Size Distribution, D1: 30% sand, 57% silt, 13% clay; D2: 29% sand, 55% silt, 16% clay

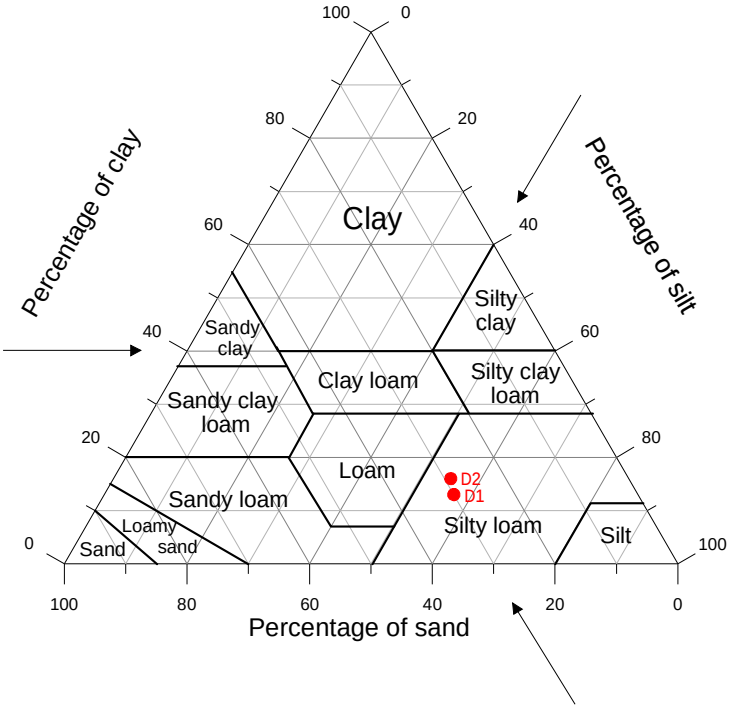

Figure 4.6: USDA textural classification chart, classification: silty loam

The Liquid Limit was determined using the Cone Penetrometer Method according to BS1377-2:1990. The plastic limit was determined by the traditional method of rolling threads on a glass plate until the thread crumbles when rolled to a diameter of 3mm (BS1377-2:1990). Both the liquid limit and plastic limit tests were carried out using two methods: (i) Dry preparation and (ii) Natural preparation to investigate the influence of drying on the plasticity behaviour. For the dry preparation, the soil was allowed to air dry, aggregations were broke down using a mortar and pestle and was then sieved on the 425μm sieve. Water was then added to the sample and mixed thoroughly and left overnight to homogenise. For the natural preparation, undisturbed samples were used from cylindrical sampling tubes. The samples were chopped up into small pieces and coarse materials removed where possible by hand. The sample was then mixed with water and stored as before. The shrinkage limit tests were determined by Alvis Atique as part of the investigation on the desiccation behaviour of this material. Shrinkage limits were determined again for two different methods: (i) air dried and (ii) oven dried samples. The plasticity limits determined by the different methods are presented in Table 4.5. There appears to be little variation in the limits determined by both methods except for the liquid limit of D2, which showed a difference of 13% between the dry method and the natural preparation method. This may be due to coarser particles, perhaps organic matter remaining in the sample during the natural preparation method.

Both depths had liquid limits greater than 50% indicating a soil of high plasticity as classified in the British Soil Classification System (BSCS) as presented in BS5930:1999. Fookes (1990) discusses the effects of air drying and oven drying on the behaviour of tropical residual soils. Although it appeared that air drying of this material had little effect on the plasticity behaviour, it was decided at this stage that no oven drying of the material should take place prior to its being used in any of the tests presented in this research, due to it being a tropical soil (albeit a transported soil). From a practical point of view, that meant that no soil which had been oven dried was reused as testing material at any stage throughout this experimental investigation, only material which had been air dried was reused.

The plasticity index (I_P) is the difference between the liquid limit and the plasticity limit. Using the plasticity indices determined from the dry preparation method, gives I_P values of 18% and 16% for D1 and D2 respectively. The plasticity chart used in the BSCS classification of fine soils

Table 4.5: Atterberg limits determined under dry and natural preparation methods

Index	D1: 0.5 - 1.0m	D2: 1.0 - 1.5m
Air dried prep. w_L	54	53
Natural prep. w_L	52	40
Air dried prep. w_P	36	37
Natural prep. w_P	39	35
Air dried prep. w_s	14	15
Oven dried prep. w_s	15	15

is based on the plasticity index and liquid limit. Typically clays plot above the A-line and silts below the A-line. As shown in Figure 4.7, the material plots below the A-line confirming that this material is indeed a silt of high plasticity (MH).

A linear relationship exists between the plasticity index of a soil and its clay fraction, this relationship is referred to as the soil activity, as defined by Skempton (1953):

$$Activity = \frac{I_P}{(\%\, of\, clay\, size\, fraction)} \tag{4.5}$$

The activity of D1 and D2 is 1.4 and 1.0 respectively. Activity is used as an index to indicate the swelling potential of a clay soil as it can indicate which type of clay minerals are present. Mitchell (1993) presents the activity of some clay minerals, most generally have activities lower than 1.0, with the exception of smectites, which can have activities ranging between 1-7. These high activity values found for this material, suggest that smectites are present in the clay fraction. Further investigation of the clay minerals was carried out using X-ray diffraction, as presented in Section 4.5.

The organic content was determined using the loss on ignition method according to BS1377-3:1990. Samples of soil from both depths were dried for 24hrs in a furnace at 440°C. During the ignition test, the carbon (constituting the organic matter) combines with the oxygen in the furnace to form carbon dioxide gas, thus there is a change in mass of the specimens as the organic content is removed. An organic content of 8% was found for D1 and 6% for D2. It is also important to note that after heating in the furnace, both samples had turned red in colour, most likely due to the oxidation of iron minerals in the soil. Details of the soil mineralogy are

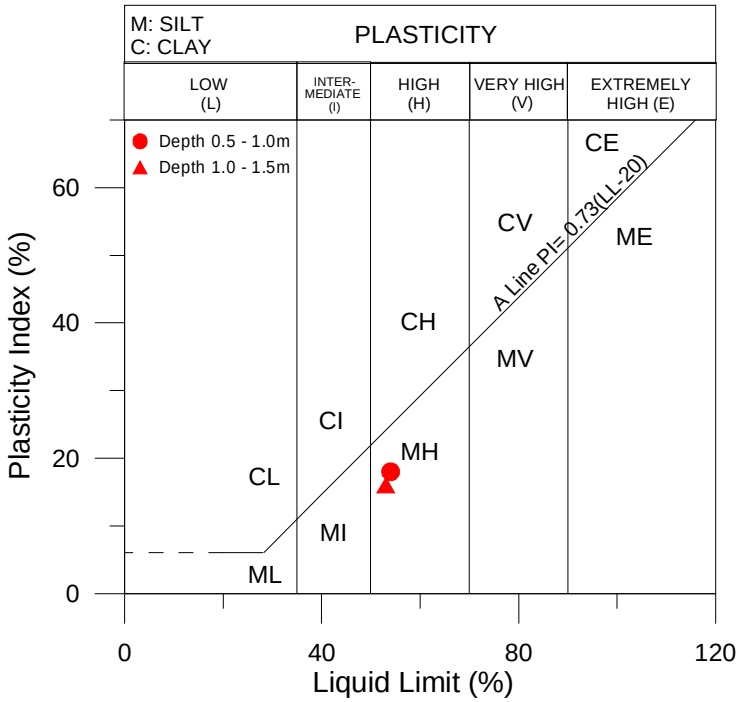

Figure 4.7: Plasticity chart, classification: silt of high plasticity (MH)

discussed in detail in Section 4.5. It is not surprising that the soil closer to the ground surface had a slightly higher organic content, corresponding to the large number of roots observed in the upper layers during the site investigation. Although these percentages are low, such percentages of organic content can have a significant effect on engineering behaviour. For example, Franklin et al. (1973) found that when the organic content exceeds 8 to 10% the maximum dry density of compaction decreased rapidly. Furthermore Croney and Croney (1998) state that the organic content of soils immediately below road structures should not exceed 4 percent. According to BS5930:1999, soils with an organic content between 5 - 10% may be referred to as organic silts or clays. As such referring back to Figure 4.7, this material can be classified as an organic silt of high plasticity (MHO) according to the British Soils Classification System (BS5930:1999).

Table 4.6 presents a summary of all the soil properties determined for the Bengawan Solo fill.

Table 4.6: Summary of Bengawan Solo fill properties at depths of 0.5 - 1m and 1 - 1.5m

Properties	D1: 0.5 - 1.0m	D2: 1.0 - 1.5m
Particle density (Mg/m^3)	2.73	2.72
Sand content (%)	30	29
Silt content (%)	57	55
Clay content (%)	13	16
Uniformity Coefficient	29	27
Liquid Limit (%)	54	53
Plastic Limit (%)	36	37
Shrinkage Limit (%)	14	15
Plasticity Index (%)	18	16
Activity	1.4	1
Organic Content (%)	8	6
BSCS Classification	MHO	MHO

4.5 Soil mineralogy

Information regarding the minerals present in a soil can be beneficial in the understanding of macro-scale testing results. In particular clay minerals have an important influence on soil behaviour, even when they are present in small quantities (e.g. Grim, 1953; Mitchell, 1993). Clay minerals also termed phyllosilicates are hydrous aluminium silicates with layered structures, made up of silica sheets (Si-O), gibbsite sheets (Al-O) and brucite sheets (Mg/Fe-O) (Mitchell, 1993). The different types of clay minerals differ in the arrangement and composition of the silica, gibbsite and brucite sheets. For example kaolinite is a 1:1 type mineral, composed of one silica sheet and one gibbsite sheet, whereas montmorillonite is a 2:1 mineral where one gibbsite sheet is sandwiched between two silica sheets (Mitchell, 1993). In montmorillonite polar molecules including water and other organic minerals can enter between the unit cells in montmorillonite commonly causing expansion of the minerals or even complete separation of individual layers (Grim, 1953). This phenomenon at the unit cell level is responsible for the significant volume changes exhibited on wetting in expansive clays.

The soil mineralogy of the Bengawan Solo fill was investigated in a series of X-ray diffraction tests, which were kindly carried out at CIEMAT in Madrid, Spain under the direction of Dr. Ana María Fernández Díaz. Powdered X-ray diffraction tests were undertaken to determine the clay and non-clay minerals present in the soil. Figure 4.8 presents the X-ray diffractograms of random powder samples using the total soil fraction. The samples were prepared by drying

to 60°C and then grinding the sample down to a particle size $< 63\mu m$. Figure 4.8 indicates the different minerals present in the soil. Non-clay minerals present include quartz, calcite and feldspar (plagioclases). To the left of Figure 4.8 some of the smaller peaks indicate the presence of Montmorillonite and Kaolinite clay minerals. Table 4.7 presents the mineralogical quantification of the total fraction. The largest percentage (60%) found was that of total phyllosilicates indicating clay minerals followed by quartz and then calcite for both depths. The large percentage of clay minerals found in the total fraction can be explained by the preparation which required particles of $< 63\mu m$ to be selected, thus showing a bias to those particles readily found in that fraction. The change in colour which was observed during the organic content test can be explained by the presence of magnesium hornblend (Table 4.7) which is an iron magnesium silicate. The ignition test resulted in the oxidation of the iron ions present within this compound.

The type and quantity of clay minerals present were further investigated by carrying out X-ray diffraction tests on oriented aggregates. Oriented aggregate mounts force the clay minerals (plate-shaped phyllosilicates) to lie flat, which allows the operator to direct the incident X-ray beam down the z axis of the minerals, enabling changes in the d-spacing of the mineral to be detected (i.e. expansion or contraction) during subsequent treatments (Poppe et al., 2001). Figure 4.9 presents the X-ray diffractograms of oriented samples in the $< 2\mu m$ fraction for D1 (0.5 - 1.0m), after three different treatments: (i) sample obtained at room temperature (AO), (ii) after saturating with ethylene glycol (EG) and (iii) after heating to 550°C (550°C). Figure 4.10 similarly presented the oriented X-ray diffractograms for D2 (1.0 - 1.5m). These oriented diffractograms highlight that montmorillonite and kaolinite are the main clay minerals present in this soil. Table 4.8 presents the quantification of the clay minerals present by (% mass) and indicates that the clay fraction is made up of 88% montmorillonite for both depths. The high percentage of montmorillonite present in the clay fraction (88%) explains the high activity values found (D1 = 1.4 and D2 = 1.0). As we will see in later chapters the presence of montmorillonite plays an important role in the behaviour of the Bengawan Solo fill, despite the fact that the clay fraction is relatively small (~15%). In particular the strong attraction that montmorillonite has for water influences the types of aggregates created at different moisture contents and its attraction for water, this is discussed in detail in Chapter 7.

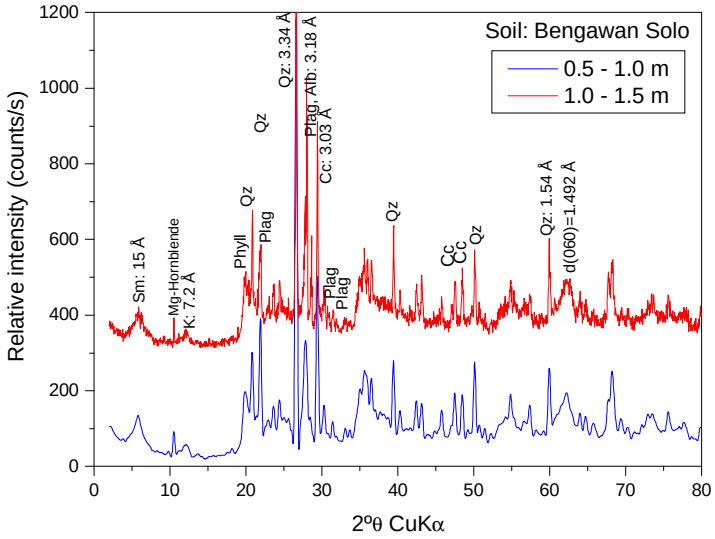

Figure 4.8: X-ray diffraction patterns of random powder samples (total fraction) (Sm: montmorillonite, K: kaolinite; Phyll: total phyllosilicates; Qz: quartz; Plag: plagioclases; Cc: Calcite) for samples D1: 0.5 - 1.0m and D2: 1.0 - 1.5m

Table 4.7: Total fraction mineralogical semi-quantification by means of X-ray diffraction (% mass)

Minerals*	D1: 0.5 - 1.0m	D2: 1.0 - 1.5m
Total Phyllosilicates	60	60
Quartz	18	14
Calcite	12	11
Plagioclases	9	14
Mg-hornblende	1	0.5

*Sample <63µm prepared

Table 4.8: Clay fraction (< 2µm fraction) mineralogical semi-quantification by means of X-ray diffraction (% mass)

Minerals	D1: 0.5 - 1.0m	D2: 1.0 - 1.5m
Smectite	88	88
Kaolinite	12	12

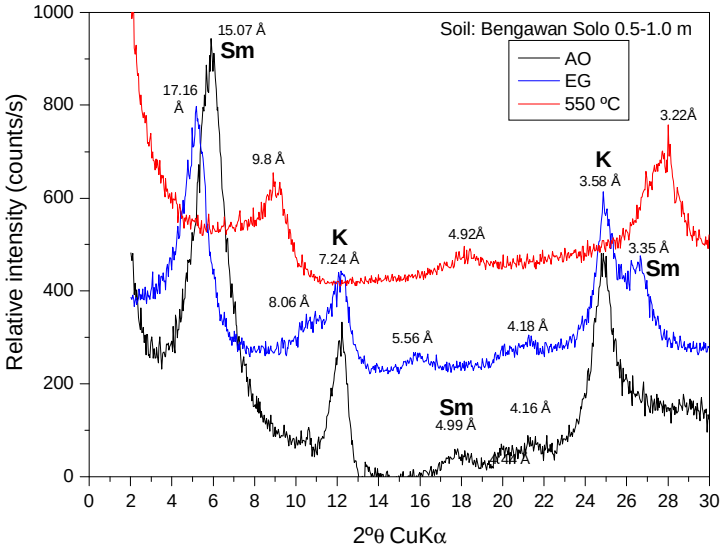

Figure 4.9: X-ray diffractograms of oriented samples (< 2μm fraction) for D1: 0.5 - 1.0m(Sm: montmorillonite, K: kaolinite)

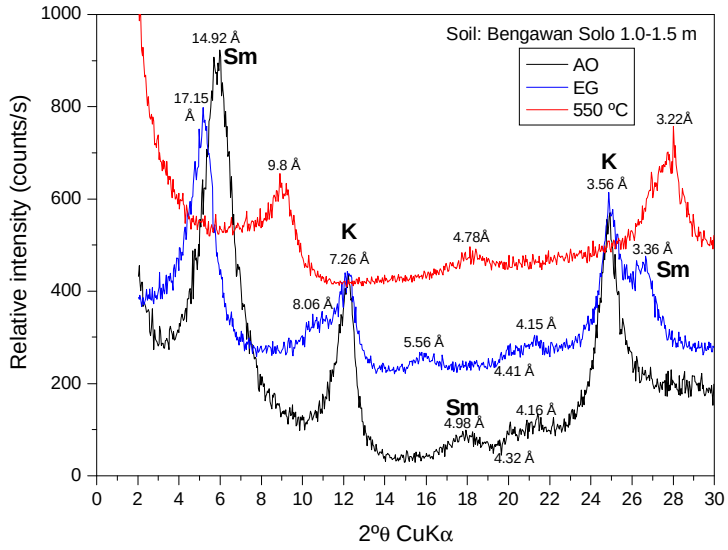

Figure 4.10: X-ray diffractograms of oriented samples (< 2μm fraction) for D2: 1.0 - 1.5m(Sm: montmorillonite, K: kaolinite)

4.6 Compaction behaviour

Compaction is the process by which solid soil particles are packed more closely together by mechanical means. This is achieved by reducing the volume of air voids present in the soil and thus increasing the dry density. Compaction is the most common method used to improve the engineering properties of fill material prior to construction. The increase in dry density due to compaction can result in higher shear strength, lower compressibility and lower permeability of the fill material, properties generally desired in engineering works. In compaction tests the bulk density, ρ is determined by measuring the mass of soil which fills a mould of specific volume under a given compactive effort and subsequent determination of the moisture content of the soil (Equation 4.2).

Considering that flood embankments are structures in which compaction specifications may not be carefully adhered to, it was deemed important that the compaction behaviour of the Bengawan Solo fill be investigated for a wide range of moisture contents and dry densities. As such tests were carried out at several different compactive efforts: (i) Extreme Light, (ii) BS Light and (iii) BS Heavy. The compactive effort applied is dependent on a number of different factors and can be calculated as:

$$Compactive\,effort = \frac{mass\,of\,rammer \times drop \times no.\,of\,blows \times no.\,of\,layers \times g}{mould\,volume} \tag{4.6}$$

Table 4.9 presents the different procedures used to apply the corresponding compactive efforts. All of the tests were carried out using a British Standard compaction mould (volume = 1 litre). BS Light and BS Heavy are the standard compaction tests as described in BS1377-4:1990. The BS Heavy test (2682kJ/m^3) uses a compactive effort 4.5 times greater than that of the BS Light test (596kJ/m^3). In order to obtain the relationship between moisture content and lower dry densities, similar to those found in the field, the Extreme Light test (132kJm/m^3) was carried out with a compactive effort 4.5 times less than the BS Light test. The Extreme Light test used the light rammer (2.5kg) with a drop of 300mm, but only 9 blows were applied over 2 layers (see Table 4.9).

Figure 4.11 presents the compaction curves at the three different compactive efforts described.

Table 4.9: Procedures used to achieve different compactive efforts

Test Name	Rammer		No.	Blows	Compactive Effort
	Mass (kg)	Drop (mm)	of layers	per layer	(kJ/m³)
Extreme Light	2.5	300	2	9	132
BS Light	2.5	300	3	27	596
BS Heavy	4.5	450	5	27	2682

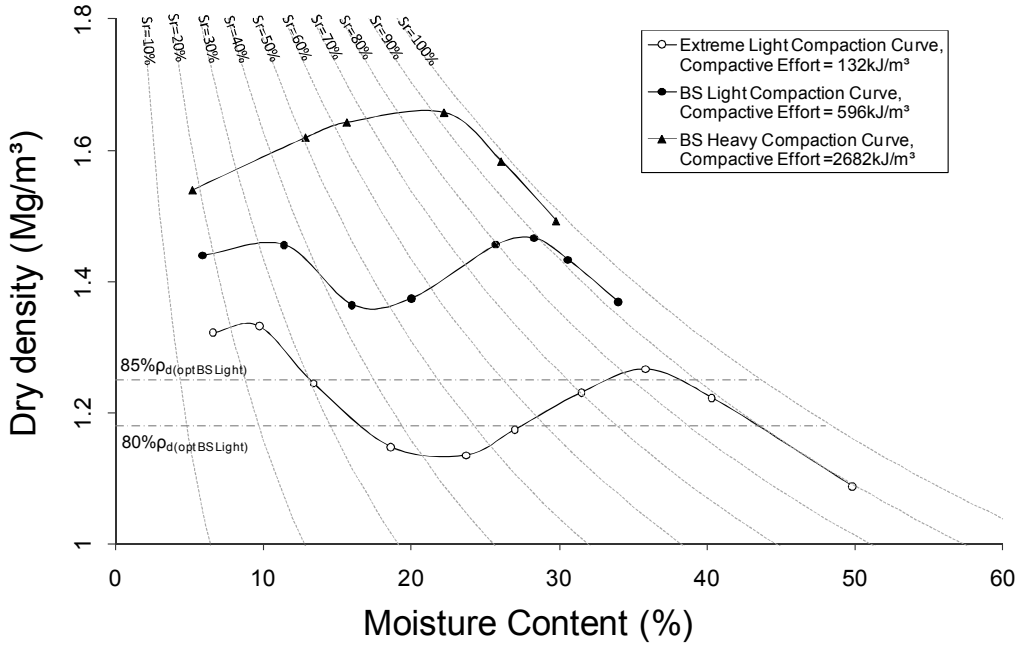

Figure 4.11: Compaction curves at three different compactive efforts: (i) Extreme Light, 132kJ/m³, (ii) BS Light, 596kJ/m³ and (iii) BS Heavy, 2682kJ/m³

For each of these tests, soil was prepared by sieving air dried crushed material through a 2mm sieve. Each batch of soil was prepared at a different moisture content separately and after mixing with water was sealed for at least 48hrs to ensure that a homogeneous moisture content was achieved, prior to testing.

It is interesting to note that an irregular double-peak compaction curve exists for this material at low compactive efforts. This double-peak is removed during compaction at a higher energy level (BS Heavy) where the compaction curve returns to a typical single-peak curve. Table 4.10 presents details of the peaks and corresponding moisture contents obtained for the different compactive efforts. As expected with increasing compactive effort the second peak occurred at higher dry densities and lower moisture contents, (peak shifted upwards and to the left). The

Table 4.10: Peak dry densities and moisture contents determined from compaction curves

Test	Peak 1		Peak 2	
	ρ_d (Mg/m^3)	w (%)	ρ_d (Mg/m^3)	w (%)
Extreme Light	1.34	9	1.27	36
BS Light	1.46	10	1.47	28
BS Heavy	-	-	1.66	21

first peak present also occurs at a higher dry density with increasing compactive effort. It is also important to note that in the Extreme Light curve, the first peak at low moisture content occurs at a dry density of 1.34Mg/m^3 which is higher than that found at peak 2 (1.27Mg/m^3). In the case of the BS Light test the two peaks occur at a similar density. Specifications for engineering works are often given as a percentage of the optimum value of dry density. In this thesis where the term optimum dry density or optimum moisture content is used it refers to the conditions found at the second peak of the compaction curves, the peak occurring at higher moisture contents.

The embankments along the Bengawan Solo river were compacted to 80-85% of the optimum dry density of the standard Proctor test. The standard Proctor test (593kJ/m^3) is equivalent to the BS Light test (596kJ/m^3). 80-85% of the optimum dry density of the BS Light test lies within the range of densities covered by the Extreme Light tests (see Figure 4.10). It is evident that compacting at these densities would require a low compactive effort similar to that applied in the Extreme Light test. Specified design dry densities may not be achieved in low cost projects, either due to difficulties in accurately controlling the mechanical energy applied or due to difficulties in controlling the moisture content of the fill, which is often subject to drying or wetting, (depending on weather conditions) before compaction. In particular, in poorer countries where basic compaction methods are used instead of more expensive compaction machinery, it can be difficult to achieve the desired dry density. From Figure 4.11 it can be seen how small variations in moisture content may result in very different dry densities achieved for a specific compactive effort. For example, assuming the moisture content was specified to be 30% in order to give a design dry density of 1.21Mg/m^3, an increase in moisture content of only 5% would result in a dry density of 1.26Mg/m^3, however more importantly a reduction in moisture content of only 5% would result in a dry density of only 1.14Mg/m^3. This is important for explaining the heterogeneous nature of the fill material found on site.

Irregular compaction curves have been presented in the literature (e.g. Olson, 1963; Lee, 1976; Ellis, 1980; Nawari and Schetelig, 1991), and are normally classified as one and one-half peak, double-peak or odd shaped curves. Irregular curves have been used as the justification for the use of dry compaction in arid areas, where water for compaction is an expensive resource (e.g. Ellis, 1980). Olson (1963) proposed that the double-peak compaction curve that he found for illitic clay was due to the formation of water menisci. Olson (1963) attributed the increasing dry density at low moisture contents to a lubrication effect and suggested that the first peak at low moisture content occurred due to a balance being reached between lubrication and the formation of water menisci. Olson (1963) suggested that as the moisture content increases more menisci forms and the dry density decreases, due to the increased resistance of the inter-particle contacts, until all possible menisci have formed, at which the valley between the two peaks is reached. Lee (1976) carried out tests on soils treated with an aerosol, a surface tension reducing agent, this had the effect of reducing the amount of meniscus water formed. On these aerosol treated soils the depression of the double-peak curve was removed, indicating that meniscus water and thus matric suction plays a role in the formation of double-peak compaction curves.

Olson (1963) proposed that the double-peak curve would only occur in soils with a dominating percentage of plate shaped particles. The Bengawan Solo fill material however, has only a small fraction of clay particles (~15%), albeit largely montmorillonite, which is made up of plate shaped particles. Lee and Suedkamp (1972) researched the characteristics of irregularly shaped compaction curves by investigating 34 different soils. They found that typically soils with a liquid limit of between 30 and 70% yielded single peak compaction curves, whereas soils with a liquid limit lower than 30% or greater than 70% usually produced irregularly shaped curves. There were a few exceptions to this rule caused by the mineralogy of the soils. The liquid limit of the Bengawan Solo fill material is 53-54% which suggests again that it is perhaps the mineralogy of this material which has an influence on its compaction behaviour.

Lee (1976) also highlighted the importance of specimen preparation when dealing with soils with irregularly shaped compaction curves. In particular Lee (1976) compared curves for reused samples and new samples. Irregular curves were found for reused samples even after they had been air dried and pulverised. This was found to be true for highly cohesive soils consisting of a large clay fraction (75% and 100%) and was attributed to the creation of very dense clay

packets created by pulverising. In this research, there was no opportunity to have new samples for each compaction test as a limited amount of soil was brought from Indonesia to the UK for testing. However the smaller amount of clay fraction present in the Bengawan Solo fill suggests that although this may have an influence it is not the only factor responsible in creating the double-peak compaction curve.

This study proposes that it is the different types of aggregates which are created at different moisture contents which is responsible for the irregular double-peak compaction curve observed. With increasing moisture content, the aggregates (i) increase in size and (ii) become softer. For example, in the case of the Extreme Light compaction curve, the first peak at w = 9% can be explained by a dense packing of very fine dry aggregates. The second peak of this curve occurs at w = 36% and can be explained by its large soft aggregates, which easily fuse together under this compactive effort. The trough (or valley) of the Extreme Light compaction curve occurs at 22% and is a result of the medium sized relatively firm aggregates which retain their aggregate form under this compactive effort, resulting in an open macrostructure being created. Evidence of the effect of increasing moisture content on aggregate size and softness is presented in Chapter 7.

The compaction behaviour is fundamental to this research and testing throughout the thesis has been based on the compaction curves presented and related back to the low dry densities found in-situ. In Chapter 5 testing is carried out on samples at a number of different compacted states, in order to investigate the influence of initial moisture content and dry density on collapse potential. In Chapter 6 isotropic and triaxial tests are carried out on specimens with an initial compacted dry density of 1.18Mg/m^3 and moisture content, 24%. This compacted state was selected for a number of different reasons: (i) in order to be of similar magnitude to the in-situ dry density, (ii) as this dry density corresponds to 80%$\rho_{d(opt)}$ and (iii) as it represents a dry-of-optimum condition, which is the condition in which the embankments were constructed in the field. Chapter 7 investigates in detail, the different fabrics created by low-energy compaction at a number of different moisture contents for the same initial level of dry density (1.18Mg/m^3) and their influence on subsequent soil behaviour.

4.7 Soil water retention behaviour

Alongside information on the compaction behaviour, it is also beneficial to have information regarding the the soil water retention behaviour when investigating unsaturated soils. In this research three different methods were used in the determination of the soil water retention behaviour of the Bengawan Solo fill: (i) Pressure plate method, (ii) Filter paper method and (iii) Chilled mirror dew-point technique. The principles, advantages and disadvantages of each of these methods were described in Chapter 3 (Section 3.4). The methodologies used for each test is described here and the results obtained presented. Attempts were also made to use a commercial (Wykeham Farrance) high capacity tensiometer for determination of the soil water retention behaviour, although without success. Despite efforts to follow the required saturation procedures (Tarantino and Mongovì 2001), including the manufacturing of a custom saturation chamber, after a few months the tensiometer stopped working due to internal leakages.

The initial conditions of the specimens used in the determination of the soil water retention behaviour are presented in Table 4.11. w_o is the initial moisture content, ρ_{d_o} is the initial dry density, e_o is the initial void ratio and $S_{r_o}$is the initial degree of saturation of the specimens tested. The different conditions tested here are relevant for the tests carried out in the following chapters. Specimens compacted under dry-of-optimum conditions at low dry density (CM01, CM02) are investigated further in terms of volumetric collapse behaviour in Chapter 5. The potential for volumetric collapse in undisturbed specimens (CM04) is also investigated in Chapter 5. The compacted conditions of w_o = 24 %, ρ_{d_o} = 1.18 Mg/m^3 as tested in FP04, FP05 and CM03 is the main reference condition used throughout this thesis, results corresponding to these conditions are presented in Chapters 5, 6 and 7. Also further investigated in Chapter 7 is the wet-of-optimum low dry density conditions at w_o = 36 %, ρ_{d_o} = 1.18 Mg/m^3 (PP02, FP06).

4.7.1 Low suction range: 0 - 1500kPa

The pressure plate method was used to determine the soil water retention curve in the low suction range up to 1500kPa. The pressure plate method uses the axis translation technique as discussed previously in Section 3.6. Testing was carried out using a 15bar ELE pressure plate extractor (Model No. ELE 532-132) and a 15bar Soil Moisture Corp. high air entry ceramic

Table 4.11: Initial conditions of specimens used in investigation of water retention behaviour

Experimental method	Test Reference	Dimensions of samples prepared Ø mm x H mm	w_o (%)	ρ_{d_o} (Mg/m^3)	e_o	S_{r_o} (%)	Comments
Pressure plate (PP) (0-1500kPa)	PP01	50 x 10	30.7	1.21	1.245	67.2	Compacted → Saturated → Drying
	PP02	50 x 10	36.6	1.18	1.304	76.4	Compacted → Saturated → Drying
Filter paper (FP) ($<$ 15MPa)	FP01	105 x115.5	-	1.20	-	-	Compacted at $\rho_d = 1.2$Mg/m^3
	FP02	105 x115.5	-	-	-	-	Compacted on BS Light curve
	FP03	105 x115.5	-	-	-	-	Compacted on Extreme Light curve
	FP04	60 x 20	23.6	1.18	1.315	48.8	Compacted → Drying
	FP05	60 x 20	24.8	1.18	1.307	49.6	Compacted → Drying
	FP06	60 x 20	35.7	1.18	1.315	73.9	Compacted → Drying
Chilled mirror dew-point (CM) (1-100MPa)	CM01	60 x 20	18.2	1.15	1.366	36.3	Compacted → Drying
	CM02	60 x 20	18.2	1.15	1.366	36.3	Compacted → Wetting
	CM03	60 x 20	23.6	1.17	1.326	48.4	Compacted → Drying
	CM04	60 x 20	34.6	1.36	1.001	94.1	Undisturbed → Drying

plate. The pore water pressure was open to atmospheric pressure allowing a matric suction of 1500kPa to be reached. Prior to starting a pressure plate test, it was important to ensure that the high air entry ceramic was fully saturated. This was achieved by half filling the pressure chamber in Figure 4.12a, with water and applying a pressure higher than the air entry value of the stone (1600kPa) to ensure that water entered all the pores of the ceramic plate. This high pressure was applied for several hours and the permeability of the stone was checked to ensure full saturation was achieved.

Specimens were compacted in PVC retaining rings of 50mm diameter and 10mm height. Muslin cloth was attached to the retaining rings using rubber bands. This was included to improve contact between the soil specimen and the surface of the ceramic plate to ensure capillary action took place between the two materials. The samples were compacted into PVC retaining rings in two layers and the initial moisture content and dry density (immediately after compaction) were determined (see Table 4.11).

Prior to placing the specimens in the chamber excess water due to saturation of the high air entry ceramic was removed. However, a fine mist of water was sprayed onto the surface of the ceramic in order to further ensure that a good contact was achieved. Alongside the specimens, a further two empty rings filled only with water were placed on the ceramic (Figure 4.12b). This was to create a more humid environment in the chamber and prevent evaporation occurring at the top of the samples and to minimise loss of water from the ceramic plate. This is an important issue in the use of the axis-translation technique, as often the air applied is dry air, in this case coming from a compressor, which typically has low values of relative humidity (5%, Jotisankasa et al., 2007), which in itself can impose a suction much higher than the suction imposed by the axis translation technique via the psychrometric law. It is important to ensure that the main physical phenomenon occurring in the pressure cell are due to the axis translation technique and not other processes. This water was topped up during the test when the chamber was opened to weigh the specimens.

After placing the specimens onto the ceramic plate, de-aired water was carefully applied to the surface of the ceramic plate in order to allow saturation of the compacted specimens via capillary rise. The initial samples were allowed to saturate over a period of 5 days and it was assumed that full saturation had been reached when a film of water was observed on the upper surface of

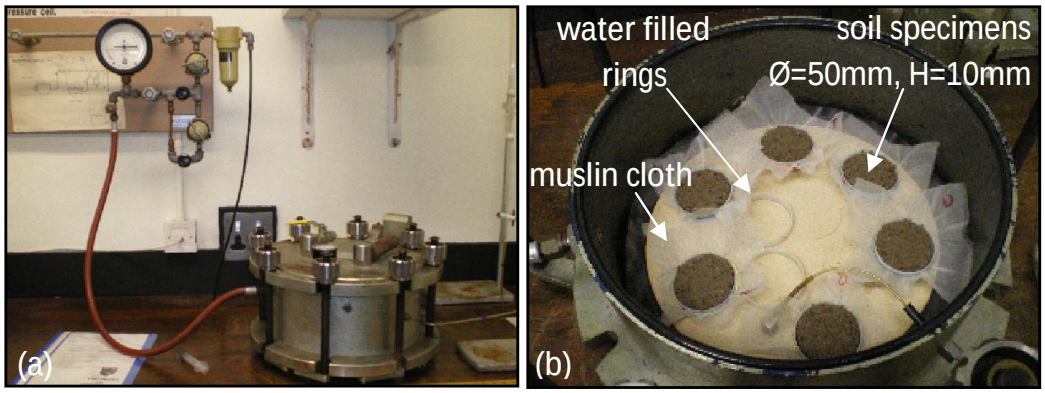

Figure 4.12: Pressure plate method: (a) 15bar ELE pressure chamber, (b) samples placed on ceramic plate

each specimen. After the saturation stage each sample was weighed and one sample was used to determine the initial moisture content of the specimens. As such these tests were used to determine the main drying curve of the soil water retention curve, starting from a fully saturated state. Matric suction was applied by increasing the air pressure inside the chamber in stages, at each stage the specimen was allowed to equalise and then the moisture content of one sample was determined for each matric suction applied. In order to determine if equilibration had occurred the samples were weighed on a daily basis after an initial 4 days equilibrium time after each new pressure was applied (to avoid unnecessary loss of soil material). The muslin cloth also aided in minimising soil loss during weighing. Each specimen was deemed to be in equilibrium if the change in mass (equivalent to change in water volume) was less than 0.025g/day. The weighing method was preferred over the volumetric method which is dependent on observing the change of volume of water in the pore water pressure line, typically in a graduated burette when open to atmospheric pressure. It can be difficult to determine accurately if equilibrium has been reached using the burette due to air diffusion through the ceramic stone. Air which may be dissolved in the water above the ceramic plate may come out of solution below the ceramic plate as it reaches a lower water pressure (atmospheric). Matric suctions up to 1200kPa were applied in this method.

Figure 4.13 presents results obtained using the pressure plate method. Series PP01 were compacted at an initial moisture content of 30.7% to an initial dry density of 1.21Mg/m^3 (see Table 4.11). In this series the moisture content achieved after equalisation at a given suction level was determined by carrying out a moisture content check on a single specimen. Series PP02 were

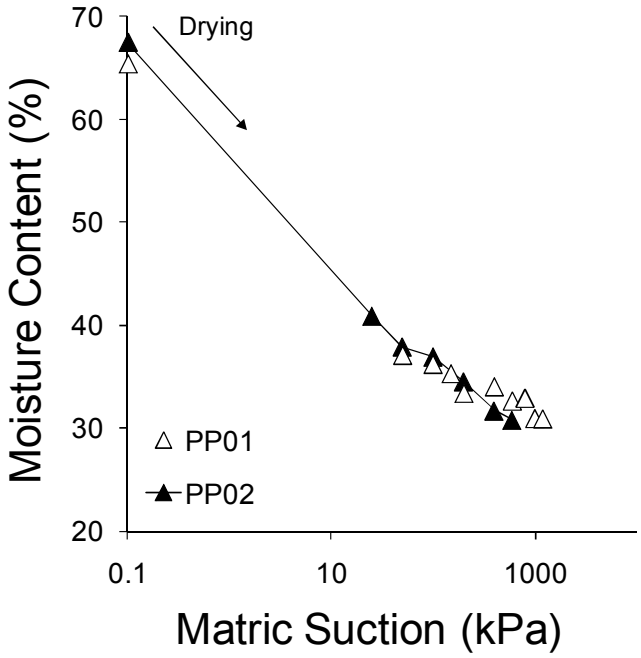

Figure 4.13: Pressure plate results, PP01: w_o = 30.7 %, ρ_{d_o} = 1.21 Mg/m^3; PP02: w_o = 36.6 %, ρ_{d_o} = 1.18 Mg/m^3

compacted at a higher moisture content (36.6%) and slightly lower dry density (1.18Mg/m^3). In PP02, the moisture content at each stage was determined by the change in mass recorded after equalisation at each stage and an average was calculated for the different specimens tested. As all of these samples were brought to an initial saturated state before the application of air pressure, this represents the main drying curve within the range 0-1500kPa. It is difficult to measure accurately changes in the volume of specimens due to suction in the pressure plate and this was not attempted in these tests. It is noted however that that the method outlined by Péron et al. (2007) involving immersion of the soil specimens in kerdane oil, is a good technique for enabling additional volumetric information to be obtained from pressure plate tests.

4.7.2 Intermediate suction range: $<$ 5MPa

The filter paper method was carried out according to the procedure detailed in Bulut et al. (2001) to determine the relationship between moisture content and matric suction up to 5MPa. Air dried, crushed soil passing the 2mm sieve was used in these tests. Samples were mixed at a specified moisture content, and sealed in plastic bags to homogenise for at least 24hrs prior

to testing. A Whatman No. 42 filter paper was sandwiched between two Whatman No. 1 filter papers. Tweezers were used at all times when handling filter papers. The soil slices were taped together using insulating tape and wrapped in two layers of cling film and place in a labelled container. All containers were placed in a temperature controlled environment (cool box filled with polystyrene) and left in a temperature controlled room.

In order to determine the matric suction, the samples were left for 7 days to reach equilibrium. Prior to removing the filter paper, the cool mass of the moisture content tins was recorded (T_c). The sample was then taken out of the plastic container, unwrapped and the Whatman No. 42 filter paper placed inside the weighing tin and weighed (M_1). This stage was initially carried out with two people in order to achieve as short a time as possible (typically 5s) (see Figure 4.14b). However with practice, it was possible to achieve this short exposure time, working alone. After weighing the moisture content tins containing the filter papers, they were placed in an oven at 105°C for at least 24hrs with their lids half open. Prior to weighing the now dry filter papers the moisture content tin lids were closed for approximately 15 mins (in the oven) in order for the hot mass to equalise before weighing. On removal from the oven the tins were placed on an aluminium block for 10s to expedite the cooling process and then immediately weighed (M_2). The hot mass of the empty tin was then also recorded (T_h). All measurements taken, were recorded to four decimal places. The moisture content of the filter papers (w_f) was then determined:

$$w_f = \frac{(M_1 - T_c) - (M_2 - T_h)}{(M_2 - T_h)} \tag{4.7}$$

This moisture content was then used to determine the corresponding suction using the calibration equations given in Ridley et al. (2003) for Whatman No. 42 filter papers. For moisture contents $<47\%$, suction (kPa) can be calculated as:

$$log_{10}(suction) = 4.842 - 0.0622 w_f \tag{4.8}$$

For moisture contents $> 47\%$, suction (kPa) can be calculated as:

$$log_{10}(suction) = 6.050 - 2.48 log w_f \tag{4.9}$$

Figure 4.14: Filter paper method: (a) specimen in 3 slices, (b) removal of filter people by two people

Figure 4.15 presents results of several different series of tests carried out using the filter paper method. Series FP01, FP02 and FP03 correspond to single point measurements carried out on compacted specimens. In series FP01 specimens at different moisture contents were compacted to a dry density of 1.2Mg/m^3. In series FP02 and FP03, measurements were made on samples with initial as-compacted states corresponding to different positions on the BS Light and Extreme Light compaction curves, respectively. Specimens in series FP01, FP02 and FP03 (see table 4.11) were compacted in the BS compaction mould, at a desired moisture content and dry density, these samples (105mm in diameter) were then extruded from this mould and sliced into 3 layers of approximately 30cm (see Figure 4.14a). In this way two different moisture contents of the filter paper could be determined for one sample and an average obtained. These independent measurements all tend to follow along the same curve, regardless of compacted dry density.

Measurements in Series FP04, FP05 and FP06 were carried out on compacted specimens following a drying path, in which subsequent measurements were taken after periods of drying (2 hrs) followed by equalisation. In Figure 4.15 these series are represented with symbols connected with lines. It is also important to note that specimens in FP04, FP05 and FP06 were all compacted within a much smaller mould, (retaining ring of 60mm diameter, 20mm high) to the same initial dry density of 1.18Mg/m^3. For each specimen two slices were compacted, between which a Whatman No. 42 was sandwiched. Interestingly on drying, Series FP04, FP05 and FP06 all indicate a change in water retention behaviour as they approach the results of Series FP01 and FP02. This appears to suggest that these may be scanning curves tending towards a main drying curve. Nuth and Laloui (2008a) drew an analogy between this type of soil water

retention behaviour and the normal compression line determined during consolidation. During mechanical consolidation, where reversible and irreversible changes due to loading are generally indicated by a change in slope at a yielding position (preconsolidation stress), similar "yielding" may also occur when scanning curves approach main drying curves. In Figure 4.15 FP04, FP05 and FP06 a clear change in slope is evident as they approach what appears to be the main drying curve. The scanning portions of these curves appear to be relatively parallel. Furthermore, FP06 compacted at a higher moisture content of ~ 36% rejoined the main drying curve at a suction of 75kPa whereas specimens FP04 and FP05 compacted at lower moisture contents exhibited somewhat "stiffer" behaviour "yielding" at higher suctions. Even the small shift of the retention behaviour between FP04 and FP05 appears to be due to the slightly higher (1%) initial moisture content of FP05.

In Figure 4.15 there appears to be an important difference in the retention behaviour of those specimens compacted in the BS mould (FP01, FP02, FP03) and those prepared by compacting in smaller retaining rings (FP04, FP05, FP06). It appears that the different sizes of these specimens and ultimately preparation method resulted in different retention behaviour of the fill material.

Throughout this thesis the specimen conditions of particular interest are those at low dry density close to the as-constructed conditions (1.18 - 1.25 Mg/m^3). This range is covered by the Extreme Light compaction curve. In Figure 4.16 the variation of suction across the Extreme Light compaction curve is plotted. From the valley to wet-of-optimum the suction ranges from close to 1000 kPa to as little as several kPa. Suction increases rapidly on the dry side with small reductions in moisture content (even at constant dry density) resulting in significantly higher suction values.

4.7.3 High suction range: 1-100MPa

The chilled mirror dew-point technique was used to determine water retention behaviour at higher suctions in the range of 1-100MPa. Tests were carried out using the WP4 potentiameter (Decagon Devices, 2003) (Figure 4.17) in the Department of Geotechnical Engineering and

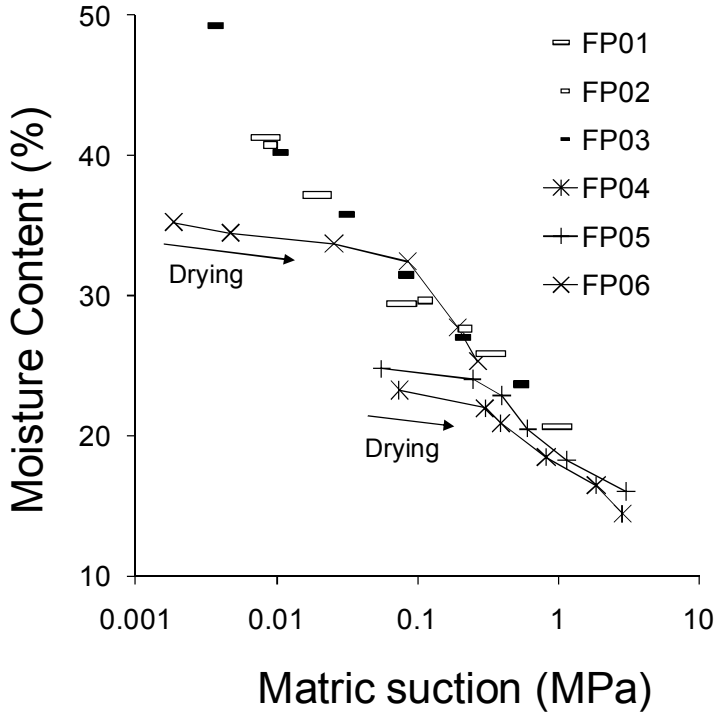

Figure 4.15: Filter paper results, FP01 specimens compacted to 1.2Mg/m^3, FP02 and FP03 specimens compacted to positions along BS Light and Extreme Light compaction curves respectively, FP04: w_o = 23.6 %, ρ_{d_o} = 1.18 Mg/m^3, FP05: w_o = 24.8 %, ρ_{d_o} = 1.18 Mg/m^3, FP06: w_o = 35.7 %, ρ_{d_o} = 1.18 Mg/m^3. In FP04, FP05 & FP06 compacted specimens were subjected to subsequent drying stages (lines connecting symbols)

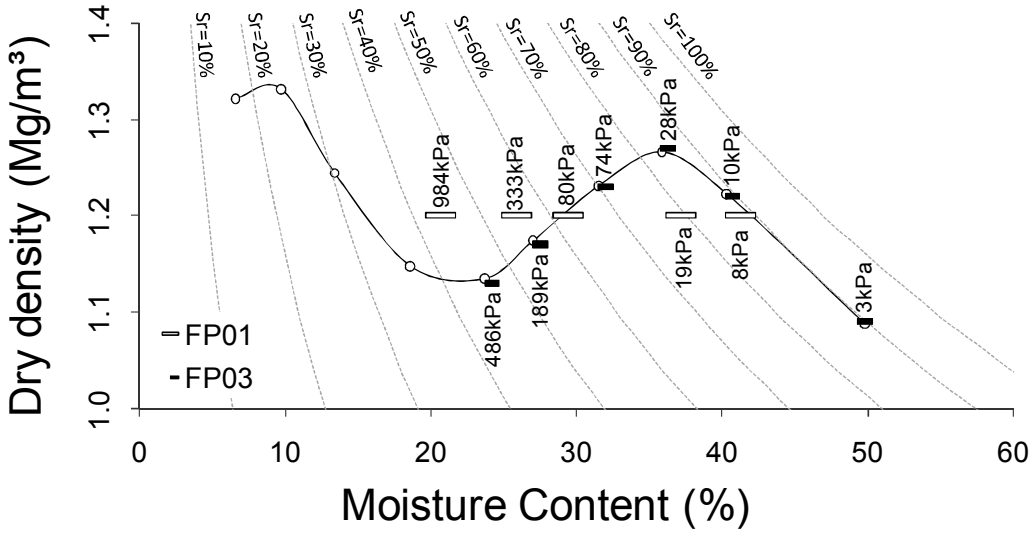

Figure 4.16: Suction variation plotted on Extreme Light compaction curve, FP01: specimens compacted to 1.2Mg/m^{3}and FP03:specimens compacted at positions along the Extreme Light compaction curve

Geosciences at the Universitat Politècnica de Catalunya (UPC), Barcelona. The principle behind this test was explained in Section 3.6. The methodology used is briefly explained here.

Specimens were trimmed from larger compacted or undisturbed samples to fit the testing cups used ($15mm^3$), making sure that the height of the sample was not greater than the cup height as this could result in contamination of the sensors within the dew-point chamber (Decagon Devices, 2003). The initial mass of the cup was recorded, followed by the mass of the cup plus the specimen. It was also important to check the initial moisture content of each specimen, using the trimmings of the prepared sample, as the moisture content values for the retention curve were determined based on the change in mass from the initial conditions. All mass measurements were taken using a high precision balance with readings to 4 decimal places. Suction readings were taken by placing the specimen into the drawer of the potentiameter as shown in Figure 4.17b. First of all the temperature of the soil specimen was recorded, if it was lower than the chamber temperature, a cooler was activated to lower the temperature in the chamber, if the temperature of the soil was too high, the drawer was opened and the specimen allowed to cool in the laboratory. Once the temperature reading equalised, a suction reading was obtained. Two suction measurements were recorded and the second reading used, and corresponding temperature recorded. Before and after each measurement the mass of the specimen plus cup was recorded as the mass of the specimen may vary during the reading time. The average mass was used to calculate the moisture content for the corresponding suction reading.

Depending on the retention path to be followed the specimens were wetted or dried. To follow a drying path, specimens were left open to the laboratory atmosphere for a period of approximately 1hr, after which time they were sealed using the cup lid and insulating tape, and allowed to equalise for a minimum period of 2hrs. To follow a wetting path, very small water drops were applied using a hypodermic needle. Care was taken to ensure that water was not applied to the same area in subsequent wetting stages. After this the samples were again sealed and allowed to equalise for a minimum period of 2hrs. These short equalisation times were deemed sufficient due to the small volume of soil being investigated.

The chilled mirror dew-point psychrometer measures total suction, the values recorded were then adjusted using a calibration for this specific device as presented in Cardoso et al. (2007), which was carried out by comparing the total suction measured recorded for a wide range of

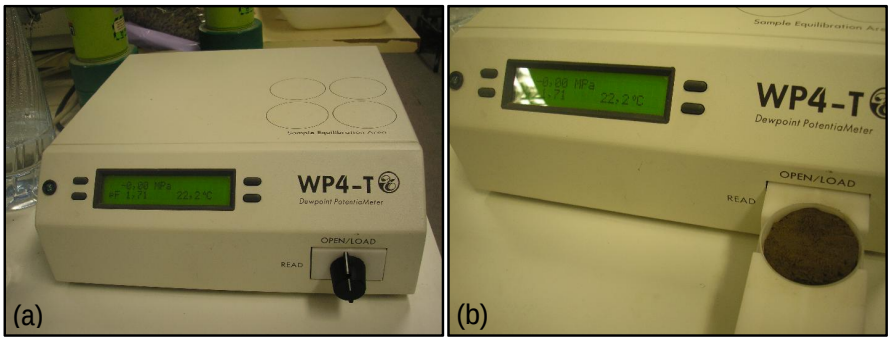

Figure 4.17: Chilled mirror dew-point technique (a) WP4 psychrometer and (b) mounting a specimen

NaCl standard salt solutions of varying molality.

Figure 4.18 presents the soil water retention behaviour up to 100MPa for both compacted and undisturbed specimens. A number of tests were carried out on samples compacted under dry-of-optimum conditions to low dry densities and subjected to drying paths (CM01 AND CM03). The wetting path followed by CM02 appears to have a distinctly different slope to the path of the same specimen subjected to drying (CM01), suggesting that it may be a scanning curve bounded by the main drying curve. In series CM04, it was evident that the initial higher dry density (1.36Mg/m^3) of the undisturbed specimen was responsible for the shift in the retention curve. Despite the differences between the various specimens, all of the curves converged at a suction close to 100MPa. This very high suction was achieved by letting the specimens dry in the laboratory until a constant moisture content had been achieved (~6%). During the investigation of the isotropic and shearing behaviour (Chapter 6), specimens were prepared by air drying until the residual moisture content had been reached, in order to determine the behaviour of the Bengawan Solo fill under this high suction of 100MPa.

4.7.4 Combined soil water retention behaviour

In Figure 4.19 the results obtained using the filter paper method and chilled mirror dew-point psychrometer are plotted alongside the van Genuchten model with parameters: a = 7kPa, n = 1.17, m = 0.145. It is interesting to note that the results from CM02 (specimen followed wetting path) lie approximately parallel to the curves obtained at low suctions in the filter

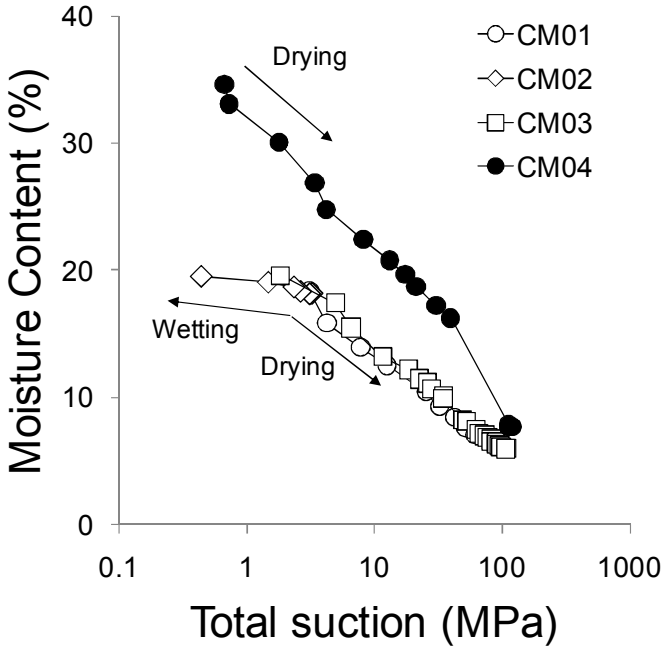

Figure 4.18: Chilled mirror dew-point results, CM01: $w_o = 18.2$ %, $\rho_{d_o} = 1.15$ Mg/m^3 (drying), CM02: $w_o = 18.2$ %, $\rho_{d_o} = 1.15$ Mg/m^3 (wetting), CM03: $w_o = 23.6$ %, $\rho_{d_o} = 1.17$ Mg/m^3 (drying), CM04: $w_o = 34.6$ %, $\rho_{d_o} = 1.36$ Mg/m^3 (undisturbed - drying)

paper experiments due to drying (FP04, FP05, FP06). This confirms that these portions of the curves with distinctly different slopes are indeed scanning curves. It appears that the independent measurements carried out using the filter paper method (FP01, FP02, FP03) may also lie along individual scanning paths. For all of these results (for low density compacted specimens), at suctions greater than 1MPa the curves all converge along one main drying path. It appears however though that the initial (compacted) moisture content has an important influence on the retention behaviour at suctions lower than 1.5MPa with specimens compacted at higher moisture contents (FP06: 36%) rejoining the main drying curve at much lower suctions (~75kPa) compared to 1.5MPa for a specimen compacted at a lower moisture content (CM02: 18%).

Figure 4.19 indicates that there is a lack of retention data at very low suctions ($<$ 10kPa). This should be further investigated for samples starting from initially saturated conditions and could be carried out for example using a Delta-T T5 tensiometer which operates from 0-85kPa. Neither the undisturbed results nor those obtained using the pressure plate method were plotted in Figure 4.19 as the results obtained appear to differ from the other results presented.

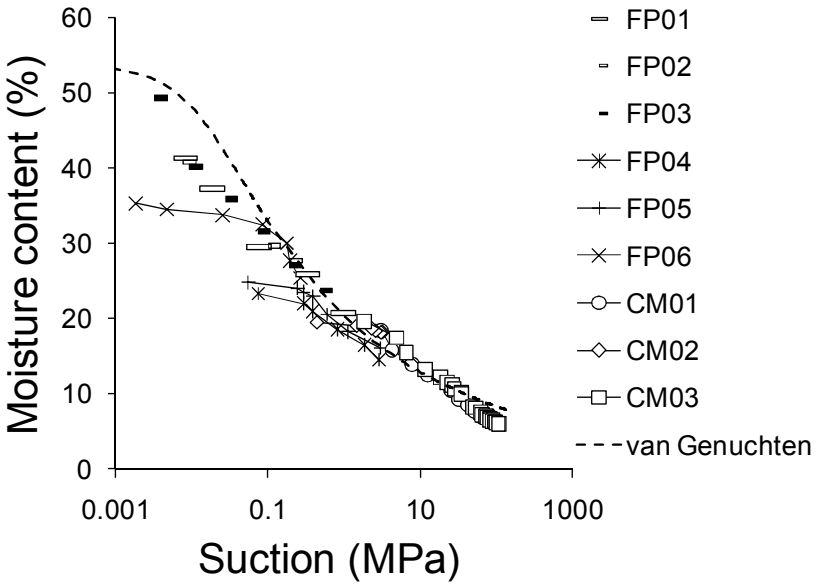

Figure 4.19: Combined soil water retention behaviour: experimental results from different testing methods and van Genuchten (1980) model where $a = 7$kPa, $n = 1.17$, $m = 0.145$

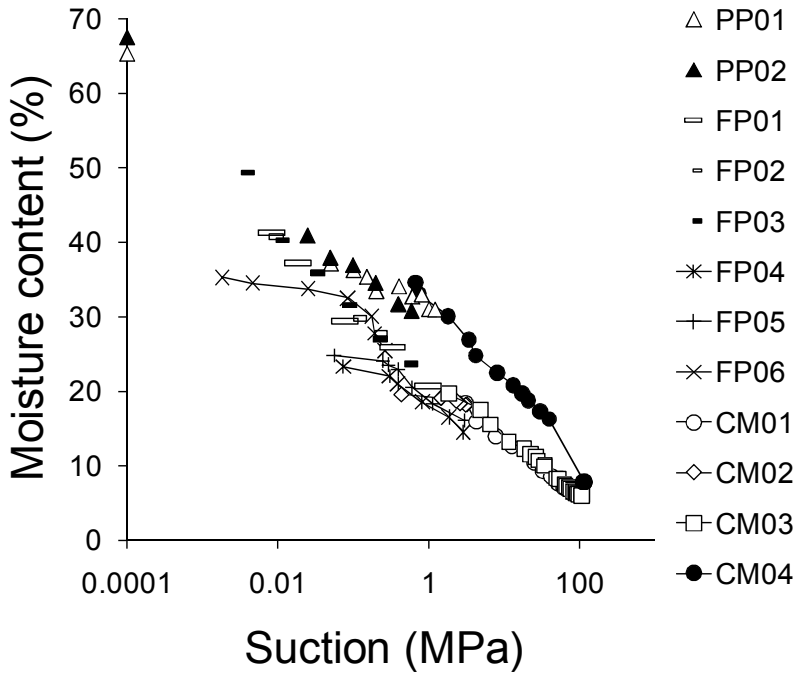

Figure 4.20: All soil water retention results determined using different experimental methods: (i) Pressure plate, (ii) filter paper and (iii) chilled mirror dew-point techniques

All the experimental results determined using the different methods are presented in Figure 4.20. It is evident that the curve for the undisturbed specimen (CM04) lies above that of the other curves presented. This can be explained by considering that as the dry density of a sample increases, the pore sizes decrease and considering capillary phenomenon (Kelvin's capillary model equation) higher suctions are required to drain water from the soil.

The results of the pressure plate method also appear to overestimate suction when compared with the filter paper measurements (Figure 4.20) for specimens of the same initial dry density and within the same low suction range. These difference may be explained by: (i) considering that the pressure plate specimens were all initially saturated prior to drying (unlike in the other methods) and (ii) during drying in the pressure plate, specimens undergo shrinkage, perhaps more shrinkage than occurs when drying in the laboratory due to the dry air applied, even with the extra free water inside the chamber. This shrinkage, results in higher dry densities during drying and may explain the shift upwards in the retention curve towards the measurements of the undisturbed samples. Suction measurements carried out by the MUSE network (Marie Curie Research Training Network) as part of a benchmark exercise found pressure plate measurements overestimated suction, when compared to measurements obtained using high capacity tensiometers and the osmotic technique (Tarantino et al., 2011). Furthermore the pressure plate results also overestimated suction when compared to results of the suction controlled oedometer, although both techniques made use of the axis translation technique (Tarantino et al., 2011). Tests carried out by the author also presented in Tarantino et al. (2011) appear to suggest that the contact load applied to specimens within the pressure chamber controls the nature of the contact between the specimen and the high air entry ceramic plate. As the vertical stress applied to the specimen increased, the moisture content of the specimens at the end of equalisation under a given suction, reduced significantly. These results appear to suggest that a higher contact load improves the hydraulic connectivity between the ceramic plate and the soil specimen.

4.8 Conclusion

This chapter has presented an overview of the Bengawan Solo fill material which is investigated throughout this thesis. This material can be classified as an organic silt of high plasticity

(MHO). Investigation of the mineralogy identified that montmorillonite was the main clay mineral present, which may have an important influence on the behaviour of this material. An important finding during the characterisation of this material was the irregular double-peak compaction curve which was found to exist at low dry densities. The irregular compaction curve is investigated further in Chapter 7, where the double peak curve is explained based on the nature of the soil aggregates created at different moisture contents. The experimental campaigns presented in the following chapters were carried out with specific reference to the compaction and retention behaviour presented here.

Chapter 5

Volumetric collapse behaviour

5.1 Introduction

This chapter focuses on one of the important features commonly observed in the behaviour of unsaturated soils: volumetric collapse compression. Relatively simple, load and soak tests were carried out using conventional oedometer apparatus to investigate the collapse potential of the Bengawan Solo fill under different initial compaction conditions (w_o, ρ_{d_o}). Such tests can be easily carried out in engineering practice and provide useful information to engineers particularly where earthworks are to be constructed using compacted fill. In order to assist the interpretation of these relatively simple tests, a fabric study using Environmental Scanning Electron Microscopy and Mercury Intrusion Porosimetry was carried out and the evolution of the soil fabric due to loading and soaking was investigated. Within this chapter, three failure pathways are presented which propose that volumetric collapse behaviour may play a role in triggering flood embankment instabilities.

A major part of this PhD programme was dedicated to the development of the geotechnical research laboratory in the Department of Civil Engineering at the University of Strathclyde. As such, all the testing equipment used at the University of Strathclyde presented within this thesis was purchased, acquired, adapted, designed, manufactured, set-up and calibrated (as required) by or on behalf of the author, for the purposes of carrying out this research. The one exception to

this was the pressure plate chamber, which was already in the laboratory prior to the beginning of this research. Thus, the initial stages of this PhD research focused on carrying out relatively simple load and soak tests using conventional oedometer apparatus as presented in this chapter.

5.2 Load and soak oedometer tests

5.2.1 Background

Many unsaturated soils may undergo significant volume changes when wetted under load (Fredlund and Rahardjo, 1993). At low stress levels, wetting may induce swelling, whereas irreversible volumetric collapse compression may result from wetting under higher stress levels (Alonso, 1993). This settlement may occur rapidly if water is readily available. Lawton et al. (1992) defined wetting-induced collapse as the densification of a soil caused by the addition of water at a constant total stress. Figure 5.1 presents a simplified schematic of the rearrangement of soil aggregates within a low density specimen subjected to wetting under a constant vertical stress (oedometer conditions). It is evident that the rearrangement due to soaking results in an irrecoverable settlement (ΔH) and ultimately a denser specimen. The term 'volumetric collapse' is used in the rest of this thesis to identify this irreversible hydro-mechanical phenomenon as opposed to the term "collapse" which can be ambiguous, as it is more generally used to indicate a failure along a slip surface. There are four main conditions required for volumetric collapse to occur (Barden et al., 1973; Mitchell, 1993): (i) an open partly unstable, partly saturated fabric; (ii) high enough total stress that causes the structure to be metastable; (iii) soil suction or cementing agent which stabilises the structure when unsaturated and (iv) the addition of water. Each of these must be present to produce volumetric collapse, the degree to which each is present influences the resulting settlement observed.

A common observation during load and soak tests is that samples collapse from their initial water content loading curve to the saturated compression line (Holtz and Hilf, 1961). It is generally accepted that the amount of volumetric collapse which occurs is dependent on (i) dry density, (ii) moisture content and (iii) the applied stress level. Lawton et al. (1989) found that collapse potential generally increases as the as-compacted dry density decreases and as the compaction

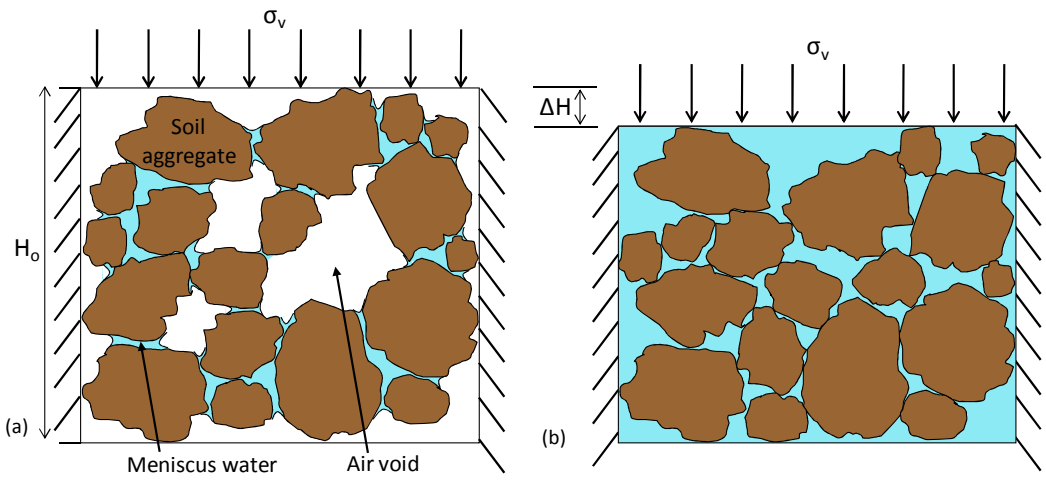

Figure 5.1: Simplified schematic of the rearrangement of soil aggregates due to volumetric collapse (a) specimen compacted to low dry density under dry of optimum conditions and (b) saturated specimen after wetting at constant stress under one-dimensional loading

moisture content decreases. Studies have also observed that above a certain dry density no volumetric collapse will occur regardless of moisture content (e.g. Booth, 1975, 1977; Lawton et al., 1989). However for expansive soils, although a higher density may eliminate volumetric collapse it may induce unacceptable swelling potentials (Lawton et al., 1989). Some researchers suggested that samples compacted at a moisture content above the Proctor optimum do not collapse (e.g. Barden et al., 1973). However, data from Booth (1975) illustrated how specimens compacted at moisture contents wet of optimum and then conditioned to drier moisture contents may exhibit significant volumetric collapse. Furthermore data from Lawton (1986) (as cited in Lawton et al., 1992) indicated that depending on stress level, significant volumetric collapse can also occur in specimens compacted at moisture contents wet of optimum and then subsequently tested at the as-compacted condition. This led to the suggestion that some critical pre-wetting degree of saturation exists above which negligible volumetric collapse will occur, taking into account both dry density and the stress level applied (e.g. Booth, 1977; Lawton et al., 1989, 1992).

The studies mentioned above have been very useful in terms of understanding the likelihood for volumetric collapse in compacted soils, particularly for application to practical problems. However, these studies were largely carried out before an elasto-plastic framework for the behaviour of unsaturated soils was developed. The BBM model presented in Section 3.7.4 illustrates how

the use of the Loading-Collapse yield surface can be used to predict both elastic and plastic deformations occurring along wetting and loading paths. Elastic behaviour corresponding to paths followed within the yield surface, e.g. wetting at low confining stresses resulting in elastic swelling, and plastic behaviour occurring on reaching the yield surface, e.g. wetting at higher confining stresses resulting in plastic volumetric compression. The benefit of considering volumetric collapse in light of the elasto-plastic models developed for unsaturated soils is that the phenomenon can be explained in an integrated manner, considering jointly volumetric deformations due to loading and wetting in the form of the LC curve. Furthermore it reduces the reliance on empirical relationships related to soil specific characteristics (e.g. compaction conditions, pre-wetting conditions). Within the BBM model (Alonso et al., 1990) the response of any soil to wetting can be predicted by considering its initial state in terms of suction, initial applied stress, and the wetting path to be followed. This requires the determination of the LC curve, which generally should be carried out using suction controlled or suction monitored apparatus. The tests presented in this chapter were however conducted using conventional apparatus without the benefit of suction control.

Often it is the addition of water which is reported as the trigger for volumetric collapse occurring in-situ. Booth (1977) reported slip failures in highway embankments attributed to collapse failures due to infiltration of water. Miranda (1988) reported crack failures in earth dams in Brazil due to volumetric collapse settlements occurring after the first filling of the reservoirs after heavy periods of rainfall. In naturally occurring arid soils, urbanisation may give rise to a number of potential water sources e.g. landscape irrigation sources, broken pipelines or poor surface drainage resulting in irrecoverable volumetric settlements (Houston et al., 2001).

It was considered important to investigate the potential for volumetric collapse occurring within the Bengawan Solo fill material as all four of the requirements for collapse could be identified as occurring in-situ:

1. The gabion reinforced embankment was constructed dry-of-optimum at 80-85% of Proctor peak dry density (R. Soemitro, personal communication, March 2007) creating a low density open, partly unstable structure.

2. At conditions dry of optimum and at low dry density, the Bengawan Solo fill exhibited

suctions up to 1MPa (Figure 4.14), indicating that suction plays an important stabilising role in unsaturated conditions for this material.

3. Clearly due to its use in the construction of a flood defence embankment, the Bengawan Solo fill has a readily available access to water at the site.

4. The engineering works constructed at the site to protect the outward face of the embankments from erosion, (as presented in Chapter 2) have provided a source of additional loading.

This chapter suggests that the remediation works introduced (gabions or concrete slabs) have provided the additional loading required alongside the low dry densities, dry of optimum moisture contents and readily available access to water to produce conditions favouring in-situ volumetric collapse.

5.2.2 Objectives & experimental campaign

Conventional oedometer apparatus was used for the load and soak tests presented in this chapter in order to illustrate how simple tests on unsaturated material can be useful to engineers in practice. A series of conventional load and soak oedometer tests were carried out with the aim of identifying the potential for collapse within the Bengawan Solo fill material under a number of different initial conditions. Of particular interest was the potential for collapse in specimens close to the as-constructed conditions, dry of optimum and at low dry densities, Series COA and Series COB in Table 5.1. As illustrated in Figure 5.2 the initial conditions for Series COA and COB lie within the valley of the Extreme Light compaction curve. In order to investigate the influence of initial dry density on the collapse potential a number of tests were carried out at the valley of the BS Light compaction curve (Series COC, see Figure 5.2). For comparison tests were also conducted close to the peaks of the BS Light (Series COD) and Extreme Light (Series COE) compaction curves. In order to further investigate the influence of initial moisture content on the collapse behaviour, tests were conducted at the optimum moisture content of the Extreme Light curve (Series COF) but at the same low initial dry density of Series COB. Series COG investigated the potential for collapse in specimens which are compacted wet of optimum

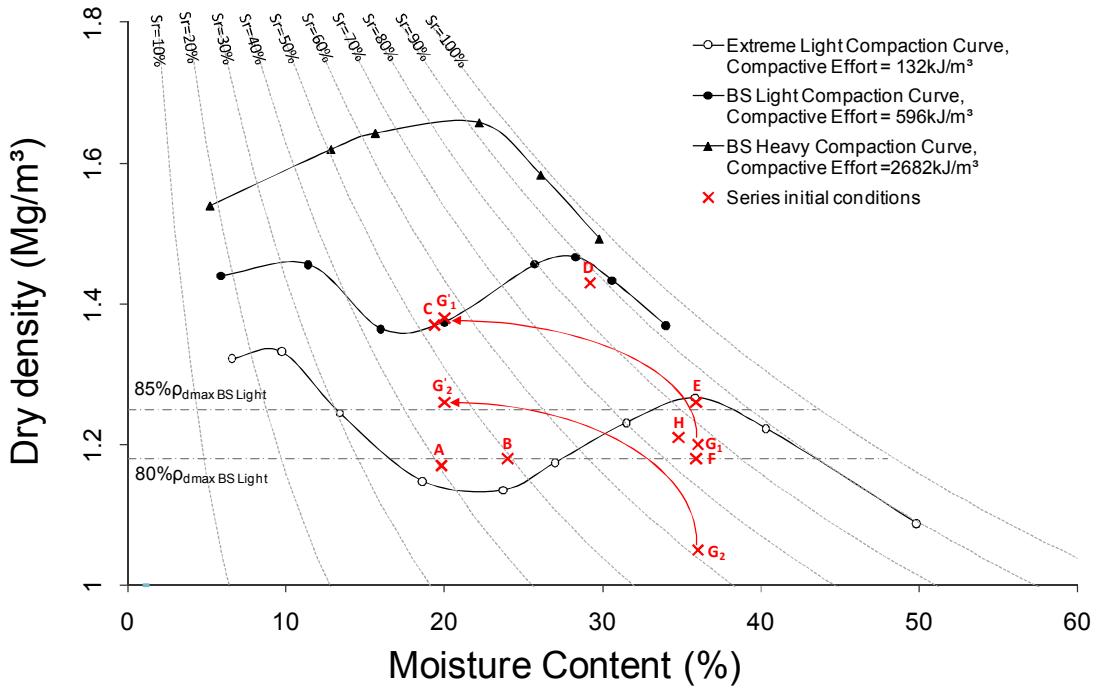

Figure 5.2: Load and soak average series initial conditions with reference to compaction curves

and allowed to dry (compacted at 36% dried to 20%). Finally, load and soak tests were carried out on undisturbed specimens (Series COH), whose average initial conditions are also presented in Figure 5.2.

The description of each series and the average series initial moisture content (w_o) and initial dry density (ρ_{d_o}) are presented in Table 5.1. Please note that as mentioned in Chapter 4, where the term "peak" or "optimum" is used, this refers to the second peak observed at higher moisture contents for the Extreme Light and BS Light compaction curves. The test reference assigned to each individual specimen tested is presented in Table 5.2, where for example COA1, refers to Conventional Oedometer, Series A, Test 1. Table 5.2 also presents the individual initial conditions (w_o, ρ_{d_o}, e_o, S_{r_o}) along with the vertical stress at which the specimen was soaked, if relevant.

Table 5.1: Load and soak testing campaign series

Series	Series Description	Average series w_o (%)	Average series ρ_{d_o}(Mg/m^3)
COA	Valley of Extreme Light compaction curve	19.8	1.17
COB	Dry of optimum of Extreme Light compaction curve at low dry density	24.0	1.18
COC	Valley of BS Light compaction curve	19.4	1.37
COD	Peak of BS Light compaction curve	29.2	1.43
COE	Peak of Extreme Light compaction curve	35.9	1.26
COF	Optimum w% of Extreme Light compaction curve at low dry density	35.9	1.18
COG	Prepared at optimum w% of Extreme Light compaction curve then dried	20.0	1.26, 1.38
COH	Undisturbed	34.8	1.21

Table 5.2: Initial conditions of specimens used in load and soak testing campaign

Test reference	w_o (%)	ρ_{d_o} (Mg/m^3)	e_o	S_{r_o} (%)	Vertical stress on soaking (kPa)
COA1	20.8	1.17	1.336	42.3	SAT (3)
COA2	19.1	1.19	1.289	40.3	CW
COA3	20.8	1.17	1.331	42.5	32
COA4	18.2	1.16	1.339	37.0	63
COA5	18.8	1.15	1.358	37.7	125
COA6	20.5	1.16	1.337	41.7	253
COA7	20.5	1.19	1.284	43.4	538
COB1	24.0	1.18	1.298	50.3	SAT (3)
COB2	24.0	1.18	1.301	50.2	CW
COB3	24.0	1.18	1.305	50.0	125
COC1	19.4	1.37	0.982	53.6	SAT (3)
COC2	19.4	1.37	0.986	53.4	CW
COC3	19.4	1.37	0.982	53.6	125
COD1	29.2	1.44	0.882	89.7	SAT (3)
COD2	29.2	1.43	0.896	88.4	CW
COD3	29.2	1.43	0.896	88.4	125
COE1	35.9	1.22	1.239	78.8	SAT (3)
COE2	35.9	1.29	1.108	88.2	CW
COE3	35.9	1.28	1.129	86.6	125
COF1	36.2	1.16	1.356	72.7	SAT (3)
COF2	35.4	1.20	1.277	75.4	CW
COF3	36.2	1.18	1.297	76.0	63
COG1	20.1	1.26	1.153	47.4	125
COG2	19.8	1.38	0.969	55.4	125
COH1	33.6	1.23	1.206	75.8	SAT (3)
COH2	34.1	1.27	1.145	81.2	CW
COH3	35.6	1.23	1.212	80.0	63
COH4	35.7	1.12	1.437	67.6	125

5.2.3 Specimen Preparation

The samples for the load and soak tests were prepared using air dried crushed material passing the 4mm sieve. The air dried material was then mixed with water to give the desired moisture content. Due to the fact that some water remains within the particles when air dried it was important to carry out a moisture content check of this material prior to mixing. The amount of water to be added (Δm_w) was then calculated as:

$$\Delta m_w = \frac{(w_d - w_a)}{(100 + w_a)} \times m_a \tag{5.1}$$

where w_d is the desired moisture content, w_a is the air dried moisture content and m_a is the mass of the air dried soil to be mixed with water. De-aired water was added to the air dried soil in small amounts by using a fine nozzle spray and was hand mixed at regular intervals. The mixing process was carried out in zip-lock sealable plastic bags to minimise both soil and moisture losses during this process. Water continued to be added until the total mass of the sample had increased by the amount calculated above, i.e. equal to the additional mass of water required. After mixing, the samples were sealed in their plastic bags, after removal of most of the air, and sealed in plastic containers. Sample were left for at least 24hrs in order for the distribution of moisture to homogenise before preparing the specimens.

At the beginning of this research, samples were initially prepared separately for each specimen to be tested. As is evident in the specimens of Series COA, this led to some variation in the initial conditions. With practise and by changing some small procedures such as preparing all specimens for one series together in a single batch, the preparation of nominally identical samples was improved, for example in Series COB and COC.

Series COA-G were all carried out on compacted specimens. With the exception of Series COD and COE, all of these specimens were prepared in the following manner. The mass of soil (m) to be added in order to reach a required dry density (ρ_d) was calculated as follows:

$$m = \frac{\rho_d(100 + w)}{(100)} \times V \tag{5.2}$$

where V is the volume of the retaining ring. The mass of soil required was added to the

retaining rings in three stages. The retaining rings used in this oedometer apparatus were 60mm in diameter and 18mm high. The specimens were compacted in three layers using a tamping rod, and a small light hammer; the number of blows varied depending on the target dry density. After the addition of each layer the soil was scarified to ensure good contact was made with the above layer. An oedometer cell and the accessories used for specimen preparation are presented in Figure 5.3.

In Series COD and COE samples were compacted at the BS Light and Extreme Light peak conditions in the BS compaction mould in order to recreate as closely as possible the peak conditions. These samples were then extruded and retaining rings with a sharp cutting edge were used to sample the specimens in these series (Figure 5.3). The specimens tested in Series COG were first prepared in a larger ring (75mm diameter) at a moisture content of 36% and were dried until a moisture content of 20% had been reached. The new moisture content determined was first estimated using the change in mass due to drying, at this stage the specimens were sampled from the dried samples using retaining rings with sharp cutting edges. After sampling the new moisture content was verified using the soil trimmings.

In Series COH undisturbed specimens were tested. These were sampled from one of the undisturbed block samples, again using the retaining rings with a sharp cutting edge. Typical of the heterogeneous nature of this fill material, the undisturbed samples showed variation in moisture content (33.6-35.6%) and dry density (1.12-1.27Mg/m^3) within the same block sample.

All of the specimens which were sampled using retaining rings with a sharp cutting edge were tested within these same rings to minimise soil disturbance.

5.2.4 Experimental Methodology

The load and soak tests were carried out in front loading oedometer apparatus. Loading frames and 10mm vertical displacement transducers (Wykeham Farrance) were used in the test set-up (Figure 5.4). Details of the calibration of the loading frames and the transducers used are presented in Appendix A. Existing oedometer cells of the fixed ring type, previously manufactured in the Department of Civil Engineering at the University of Strathclyde were used. The dis-

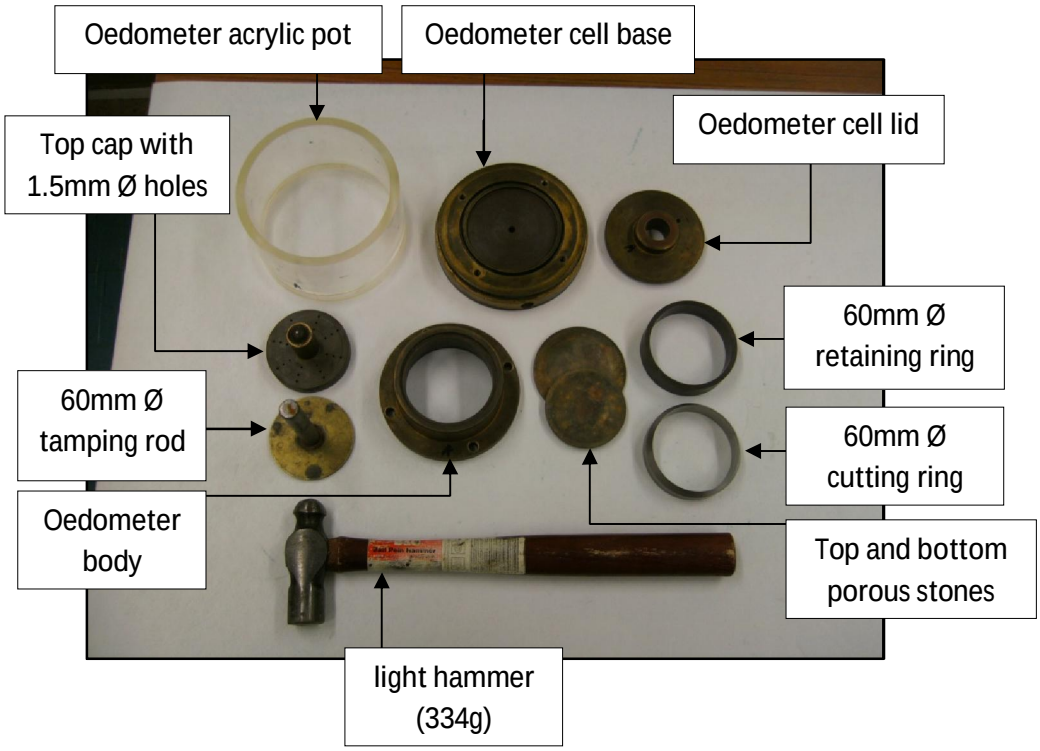

Figure 5.3: Photograph of oedometer cell and accessories

placement transducers were connected to National Instruments hardware (SCXI chassis) and controlled using LabVIEW, enabling measurements to be recorded automatically.

In most of the series, at least one saturated test, one unsaturated test and one collapse test was carried out. A fully saturated test, as referred to here, is one in which after applying a contact load of 3kPa (100g mass), water was added to the oedometer pot, and any swelling taking place recorded. In these tests, the porous discs placed above and below the soil specimen were kept in de-aired water prior to testing. Furthermore in the saturated tests, drainage was allowed to take place both at the bottom and at the top of the specimen.

In the unsaturated tests, no water was added to the specimen at any stage during the test. The porous discs used in these tests were oven dried before use. Essentially these were constant water content tests. As such no drainage was allowed at the bottom of the sample (bottom drainage outlet closed) and the top of the sample was open to atmospheric pressure. In order to minimise moisture losses due to evaporation at the upper drainage outlet, a small tube was connected to the outlet and placed in a beaker of water. Typically moisture content losses of

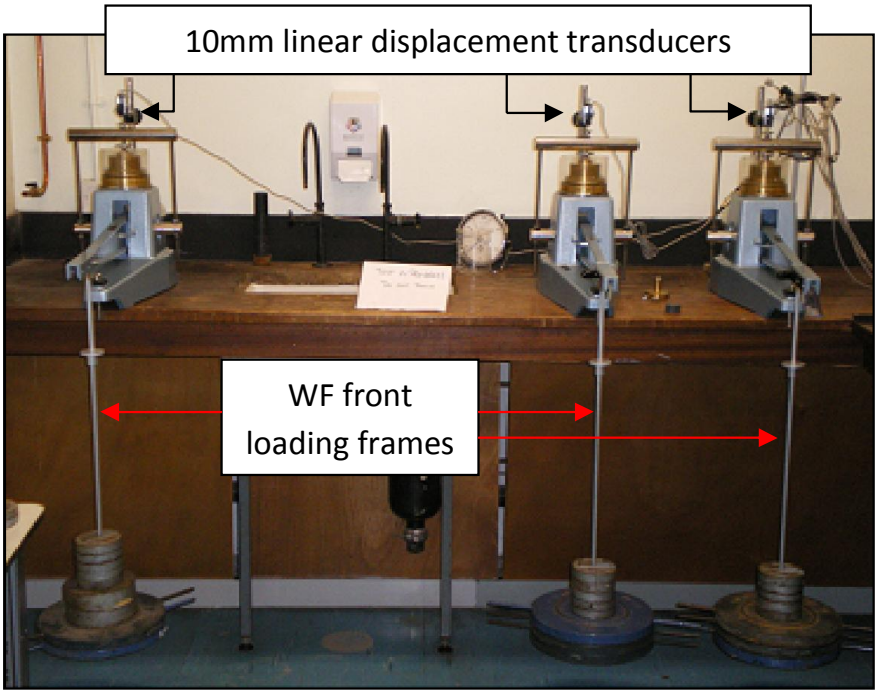

Figure 5.4: Photograph of oedometer apparatus used in load and soak tests

around 1% were observed at the end of the two week testing period. It is thought that this small loss in moisture content may have been due to water being pushed into the dry porous stones during loading.

When investigating the collapse potential, the samples followed first the conditions of the unsaturated tests under constant water content conditions. After loading to the specified stress level, the specimen was soaked by adding de-aired water to the oedometer cell. Water entered the specimen via small holes in the top cap (Figure 5.3). At this stage the bottom drainage outlet was also opened. Any immediate displacement due to the addition of water was recorded for a period of 60mins, after which the next loading increment was applied. This period of 60mins was deemed sufficient by recording the change in settlement over time after soaking. Figure 5.5 presents the evolution of collapse settlement for tests COA3 and COA5. For each specimen after 20mins, 89% and 98% of the total collapse settlement had occurred for COA3 and COA5 respectively.

The oedometer apparatus was set-up and the specimens were mounted as described in detail by Head (1982). Load increments were applied every 24hrs in the following increments: 3, 6, 12,

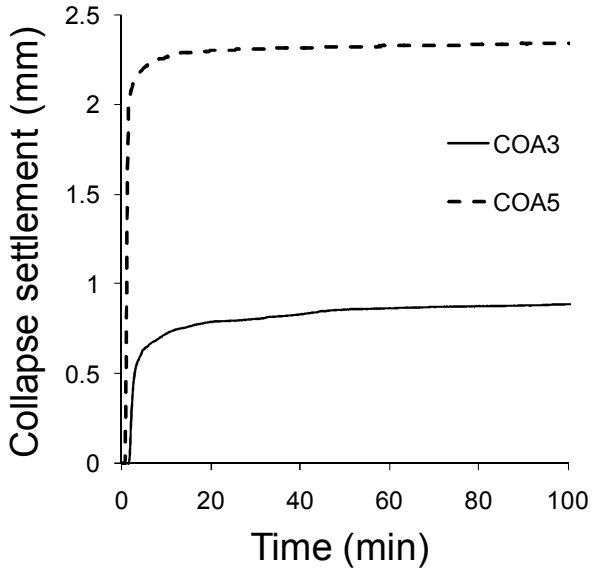

Figure 5.5: Collapse settlement over time for COA3 (water added at 32kPa) and COA5 (water added at 125kPa)

28, 60, 125, 185, 253, 538, 1100kPa. A total of 16 measurements were recorded over the 24hr period. However immediately after the addition of water (during swelling or collapse) readings were recorded every 15s.

5.2.5 Calculations

Of interest in oedometer tests is the volume change of the soil specimen due to loading and or wetting, which corresponds to a change in volume of the voids. The void ratio e is equal to:

$$e = \frac{V_v}{V_s} = \frac{\rho_s}{\rho_d} - 1 \tag{5.3}$$

where V_v is the volume of voids, V_s is the volume of solids, ρ_s is the particle density of the soil and ρ_d is the dry density. As the specimen is laterally restrained within a retaining ring in an oedometer test only changes in the height of the specimen are permitted. Thus the change in height ΔH with respect to the initial height H_o is proportional to the change in the void ratio Δe with respect to the initial void ratio e_o:

$$\frac{\Delta H}{H_o} = \frac{\Delta e}{1 + e_o} \tag{5.4}$$

thus Δe can be determined as:

$$\Delta e = \frac{1 + e_o}{H_o} \Delta H \quad = F \Delta H \tag{5.5}$$

where F is a coefficient which relates the change in void ratio to the change in height, and is dependent only on the initial specimen conditions. In this way the void ratio of the specimen at any stage of the test can be determined from the initial void ratio and the cumulative settlement recorded. In this chapter results from the oedometer tests are plotted in terms of specific volume against vertical stress, where specific volume, v is defined as:

$$v = e + 1 \tag{5.6}$$

In Series COA and COH where there were significant discrepancies in the initial dry density of the specimens, the results are plotted in terms of normalised specific volume, (v/v_o) against vertical stress.

Where collapse was observed the specimens were evaluated in terms of their collapse potential. The collapse potential was calculated as (Jennings and Knight, 1957):

$$Collapse\,potential = \frac{\Delta e}{1 + e_u} \times 100\% \tag{5.7}$$

where Δe is the change in void ratio of the specimen on wetting under the desired pressure, e_u is the unsoaked void ratio of the specimen prior to wetting. Where swelling was observed they were calculated as in equation 5.7, but with Δe equal to the increase in void ratio of the specimen on wetting (positive values).

5.2.6 Results & discussion

For each series typically specimens have been tested under saturated and constant water content conditions. Furthermore at least one specimen has followed a path of loading under CW conditions followed by saturation. Under saturated conditions dissipation of the pore water pressure occurs such that at the end of a loading step, the vertical stress applied is equivalent to the effective stress $(\sigma_v - u_w)$ or σ'. Under CW conditions the vertical stress applied is equal to the

net vertical stress $(\sigma_v - u_a)$ or $\overline{\sigma}_v$, as u_a is equal to atmospheric pressure. Due to the different conditions tested in each series, the results are plotted as vertical stress against specific volume v or normalised specific volume (v/v_o).

Figure 5.6a presents the load and soak curves of Series COA, where specimens were compacted at low dry density and dry of optimum, within the valley of the Extreme Light compaction curve. Some swelling (swelling potential of 2.0%) occurred when water was added at a contact load of 3kPa (COA1). The swelling observed in the Bengawan Solo fill is associated with the active clay minerals, i.e. smectites which were present in high proportion within the clay fraction, as identified using X-ray diffraction (Section 4.5). Volumetric collapse of specimens occurred over a wide range of stress levels from 32kPa to 538kPa. In all of the specimens which underwent volumetric collapse (COA3-COA7), the paths first followed the compression curve of the unsaturated specimen (COA2) and after soaking followed that of the saturated specimen (COA1). The amount of volumetric collapse which occurred increased with vertical stress at low stress levels and reduced with stress at higher stress levels. Figure 5.6b presents the collapse potential determined for each stress level in Series COA and indicates that a maximum collapse potential of 13.6% was determined for test COA5, in which the specimen was soaked at a vertical stress of 125kPa. The results of Series COA are important because they indicate that close to the as-constructed conditions of the embankment the Bengawan Solo fill is collapsible and that applying a vertical stress up to 125kPa increases the collapse potential and loads above 125kPa act to reduce the collapse potential.

In Series COB specimens were again tested at low dry density, (ρ_{d_o} = 1.18Mg/m^3) which is equivalent to the lower limit of the range used to construct the embankments (80% of Proctor dry density), and at an initial moisture content dry of optimum (w_o = 24%). The initial conditions used in Series COB are the initial conditions selected for further investigation in Chapters 6 and 7. Swelling was again observed when wetting under a small contact load of 3kPa (swelling potential of 1.8%) (Figure 5.7). Soaking at a vertical stress of 125kPa again induced volumetric collapse (Figure 5.7), with a collapse potential of 11.6%, still a significant amount of volumetric collapse (Figure 5.7). This collapse potential is slightly lower than that found at the same stress level for Series COA and may be explained by considering the increase in initial moisture content and slight increase in initial dry density. (Figure 5.7).

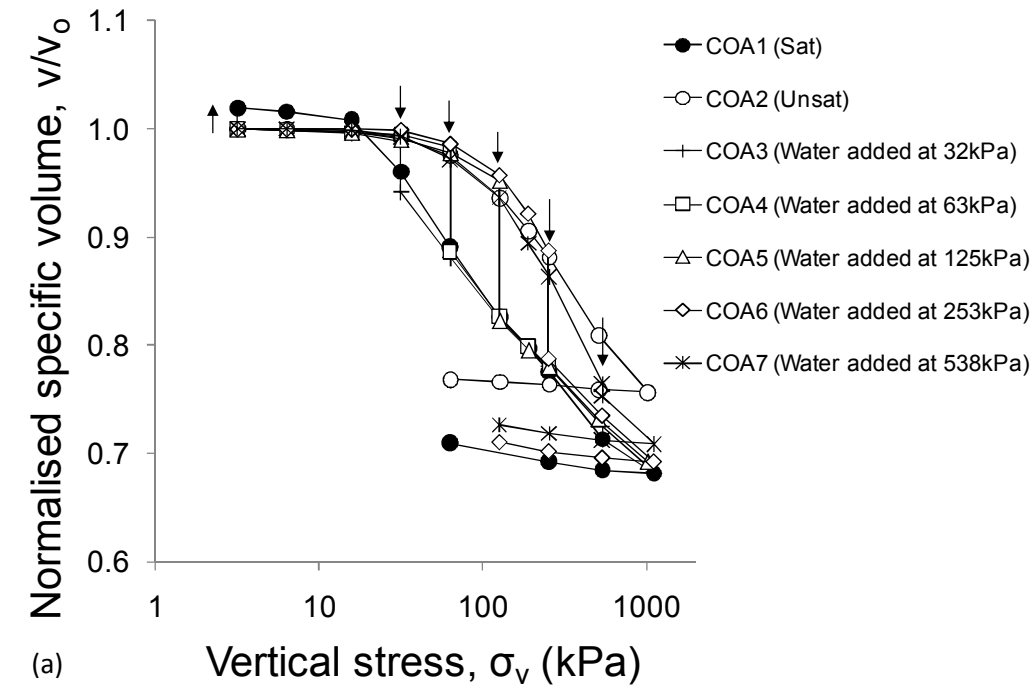

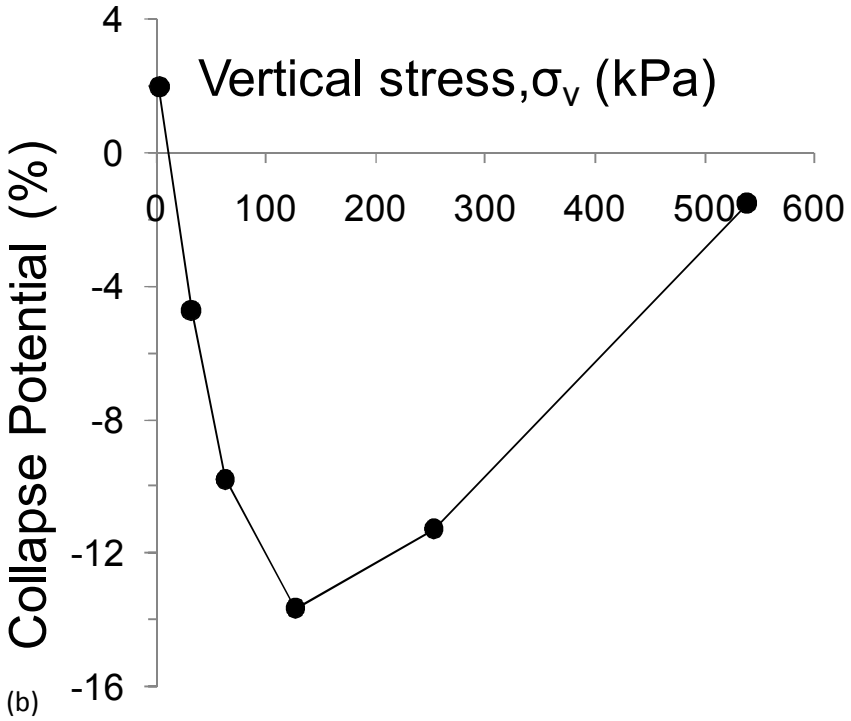

Figure 5.6: Load and soak results for Series COA: Valley of Extreme Light compaction curve (average series initial conditions: w_o= 19.8%, ρ_{d_o} = 1.17Mg/m^3) (a) load and soak curves and (b) collapse potentials at different vertical stresses, maximum collapse potential of 13.6% observed at a vertical stress of 125kPa

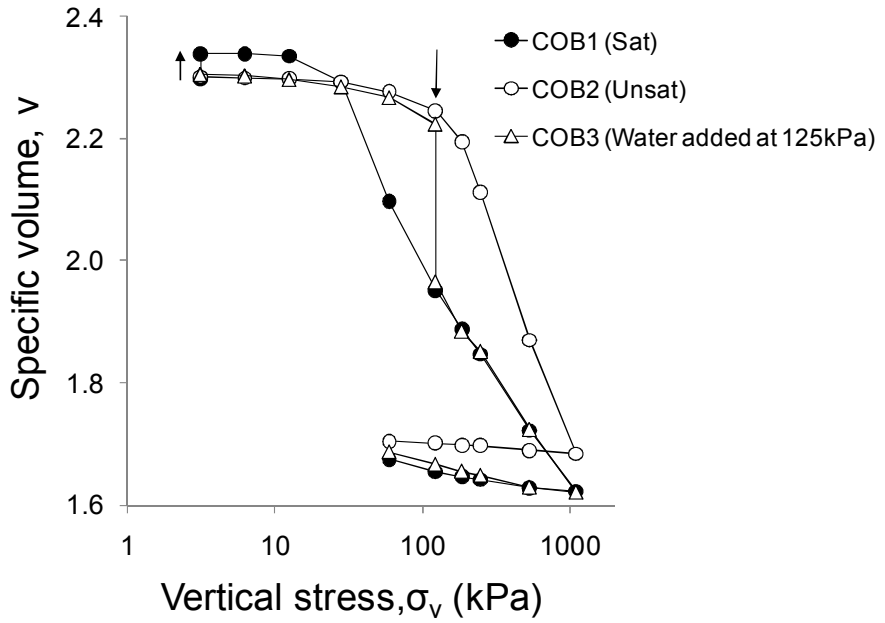

Figure 5.7: Load and soak results for Series COB: Dry of optimum of Extreme Light compaction curve (average series initial conditions: w_o= 24.0%, ρ_{d_o} = 1.18Mg/m^3)

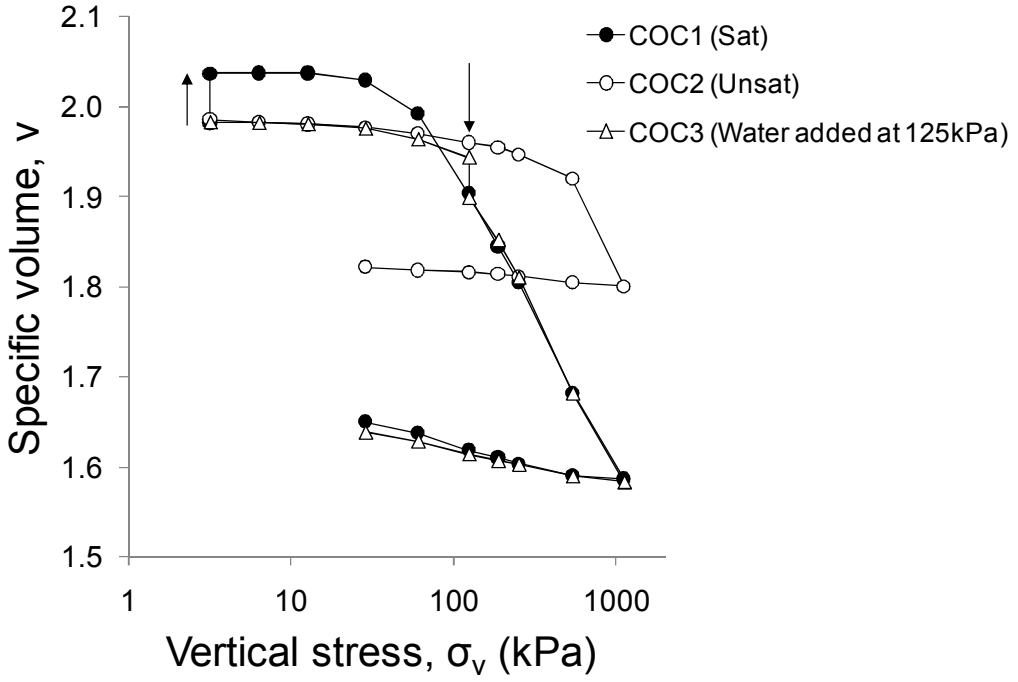

Figure 5.8: Load and soak results for Series COC: Valley of BS Light compaction curve (average series initial conditions: w_o= 19.4%, ρ_{d_o} = 1.37Mg/m^3)

In order to investigate the influence of initial compacted dry density on volumetric collapse behaviour, specimens in Series COC were compacted at approximately the same initial moisture content as Series COA but were compacted to a higher initial dry density (1.37Mg/m^3), representing the valley of the BS Light compaction curve. A higher amount of swelling was observed (COC1) when soaked at a vertical stress of 3kPa (swelling potential of 2.8%) compared to Series COA and COB, which can be explained by the higher initial dry density of this specimen (Figure 5.8). Even under this higher compactive effort volumetric collapse was still observed (COC3). However due to the higher initial dry density of the specimen, soaking at a vertical stress of 125kPa resulted in a smaller amount of collapse (collapse potential of 2.3%) than was observed in Series COA and COB. Series COC illustrates how increasing the initial dry density of the soil can reduce collapse potentials considerably. If we consider that the rearrangement of soil aggregates into a denser structure (Figure 5.1) on wetting is dependent on the porosity available and the distribution of the size of these available pore spaces, it follows that a specimen compacted at higher dry density and loaded, will have a lower available porosity into which aggregates can deform (causing overall volumetric changes) than a specimen compacted at a lower dry density. By comparing Series COA and COC, we can see that increasing the dry density from 1.15Mg/m^3 to 1.37Mg/m^3 (a 20% increase) reduced the collapse potential due to soaking at 125kPa from 13.6% to 2.3%, a reduction of over 80%. Specification of appropriate compaction conditions for collapsible fill material is one method of minimising unwanted settlements in construction projects where such settlements may lead to further damage or reduce the functional performance of an earth structure.

In Series COD and COE where specimens were compacted at the peak conditions of the BS Light and Extreme Light compaction curves respectively, little swelling was observed on wetting at 3kPa and little to no collapse was observed on wetting at 125kPa (Figures 5.9 and 5.10). ^{3}). These results indicate that for the Bengawan Solo fill material no collapse is likely to occur close to the optimum compaction conditions (Peak 2) of the Extreme Light or BS Light compaction curves. COE1 was prepared at an initially slightly lower dry density, which explains the difference in specific volume at low stress levels as seen in Figure 5.10.

Series F investigated specimens prepared at the optimum moisture content of the Extreme Light curve (36%) but at low dry density (1.18Mg/m^3) in order to investigate the influence of

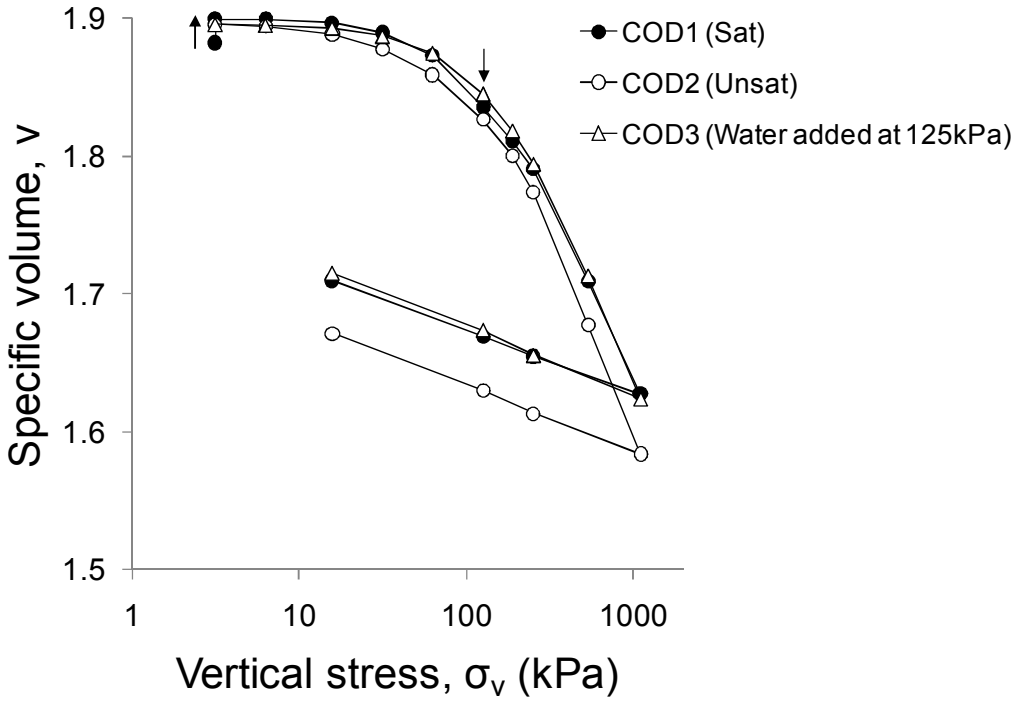

Figure 5.9: Load and soak results for Series COD: Peak of BS Light compaction curve (average series initial conditions: w_o= 29.2%, ρ_{d_o} = 1.43Mg/m^3)

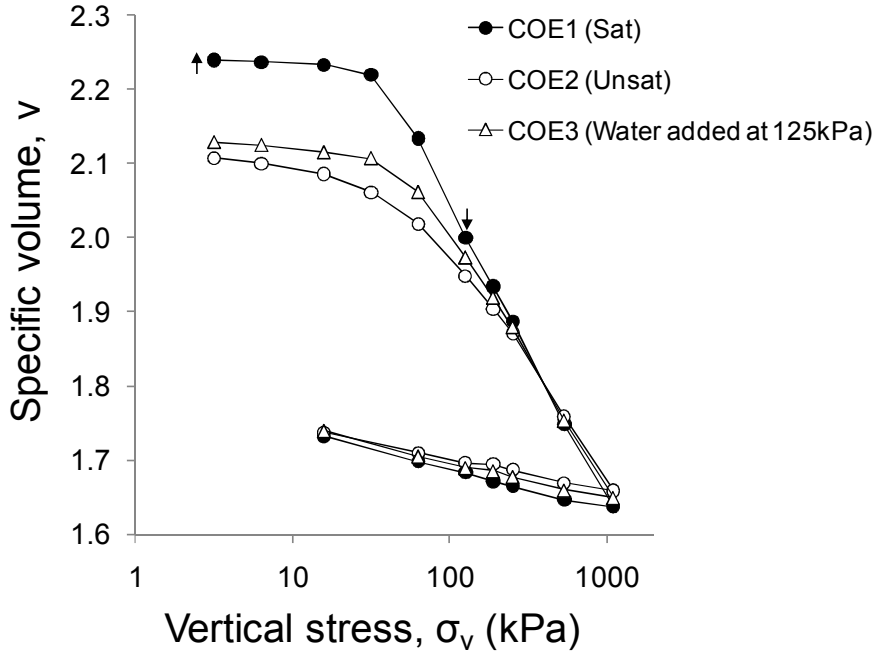

Figure 5.10: Load and soak results for Series COE: Peak of Extreme Light compaction curve (average series initial conditions: w_o= 35.9%, ρ_{d_o} = 1.26Mg/m^3)

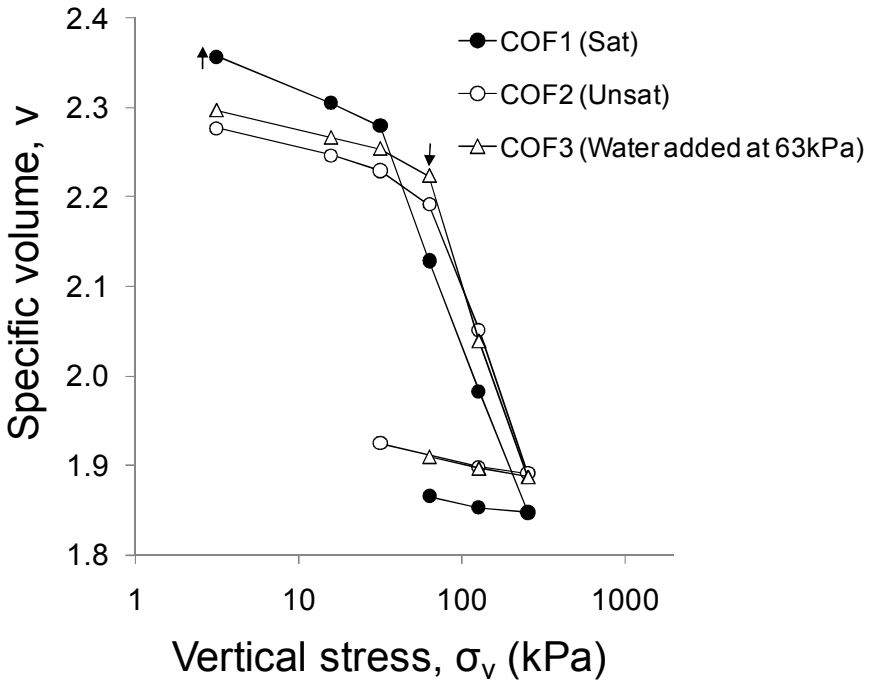

Figure 5.11: Load and soak results for Series COF: Optimum w% of Extreme Light compaction curve at low dry density (average series initial conditions: w_o= 35.9%, ρ_{d_o} = 1.18Mg/m^3)

moisture content. Little to no swelling or collapse was observed in these specimens (Figure 5.11). Comparing these results to those of Series COB, prepared at 24% and an initial dry density of 1.18Mg/m^3, it appears that increasing moisture content appears to minimise the potential for collapse for the Bengawan Solo fill. However unfortunately a load and soak test was not carried out at a vertical stress of 125kPa in Series COF which would enable a better comparison. At the higher moisture contents tested (Series COE and COF), minimal volume changes have been observed on wetting under load, even at relatively low dry densities. This can be explained by considering that at this moisture contents (~36%), the soil aggregates are of a softer nature than those compared at lower moisture contents, thus loading of the material deforms these soft aggregates, forcing them to move into the available pore space. Therefore, when water is added after loading, the potential for collapse has already reduced such that no significant volume changes will occur.

In an attempt to explore what could happen when compacted material dries, specimens in Series G were compacted initially at w = 36% and ρ_d = 1.05Mg/m^3 and ρ_d = 1.20 Mg/m^3 moisture content and allowed to dry to w = 20% and ρ_d = 1.26Mg/m^3 and 1.38Mg/m^3. Clearly

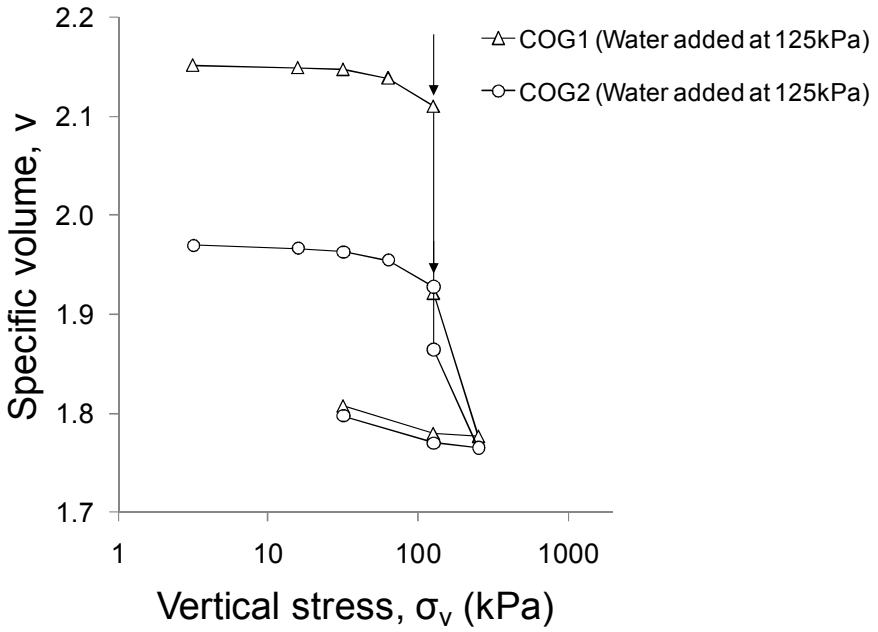

Figure 5.12: Load and soak results for Series COG: Prepared at optimum w% of Extreme Light compaction curve then dried to 20% (COG1: w= 20.1%, ρ_d = 1.26Mg/m^3, COG2: w= 19.8%, ρ_d = 1.38Mg/m^3),

specimen COG1 in Figure 5.12, dried to the lower dry density of 1.26Mg/m^3 exhibited more collapse (8.9% collapse potential) than COG2, which was dried to 1.38Mg/m^3 (3.3% collapse potential) on soaking at a vertical stress of 125kPa. This indicates the strong role of initial dry density on the amount of volumetric collapse occurring. A reduction in dry density of approx. 9% increased the collapse potential by almost threefold.

It is important to note here that volumetric collapse was observed in samples after drying, despite the fact that drying induced overall shrinkage of the specimens and thus an increase in dry density. However it is necessary to remember here that the Bengawan Solo fill contains expansive clay (montmorillonite) and it is very well known that expansive clays may undergo important volume changes under wetting and or drying paths and that changes in the microstructure can be responsible for overall macro-mechanical behaviour, e.g. Alonso et al. (1999). Here it is proposed that on drying although the overall porosity of the specimen reduces, it is possible that the portion of the pore space related to inter-aggregate pores (macro-porosity) has increased, and the pore volume related to intra-aggregate porosity has greatly reduced. This may create a more open macrostructure (although in an overall denser specimen) making it susceptible to

volumetric collapse under the appropriate conditions.

In terms of practical relevance it appears that the results of Series COG are also important, in that it is not sufficient for an engineer to specify compaction conditions wet of optimum in order to minimise volumetric collapse. It may also be important to consider the response of the soil to drying, if this is likely to occur in-situ and the potential for collapse any dried material may have. Series COG illustrated that samples compacted wet and then dried can still have significant collapse potentials on wetting under load. By comparing COG2 (w= 19.8%, ρ_d = 1.38Mg/m^3) with a similar compacted specimen COC3 (w= 19.4%, ρ_{d_o} = 1.37Mg/m^3) (both soaked at a vertical stress of 125kPa), it is apparent that the collapse potential remains of similar magnitude (and is even slightly higher) at 3.3% for COG2 compared with 2.3% determined for COC3, despite being compacted at a higher moisture content of 36% and then allowed to dry. Engineers must specify compaction conditions with relatively high dry densities even at high moisture contents (optimum or wet of optimum), so that even upon drying the collapse potential for the material will remain low. This issue of drying may not be important in every case, but in the case of the Bengawan Solo fill where embankments are generally constructed during the dry season, and as such material may undergo further drying before the beginning of the wet season, it should be taken into consideration.

The potential for collapse in undisturbed samples was investigated in Series COH. It should be noted however that when the sampling took place in-situ the embankments had been recently overtopped, which explains their high moisture content (approx. 35%). Due to the variability in the undisturbed samples, these results were plotted in terms of normalised specific volume. Little to no swelling or collapse was observed in these samples, most likely due to their high initial moisture contents, or because the specimens have already undergone volumetric collapse in-situ.

Table 5.3 presents a qualitative guide to understanding collapse potentials; this guide is primarily for use in relation to tropical residual soils (Fookes, 1990), but nevertheless this gives a useful indication of the severity of the problem of collapse according to the determined collapse potential.

Table 5.4 presents a summary of all of the load and soak tests carried out, including their initial conditions, conditions prior to soaking and indicates the collapse or swelling potential

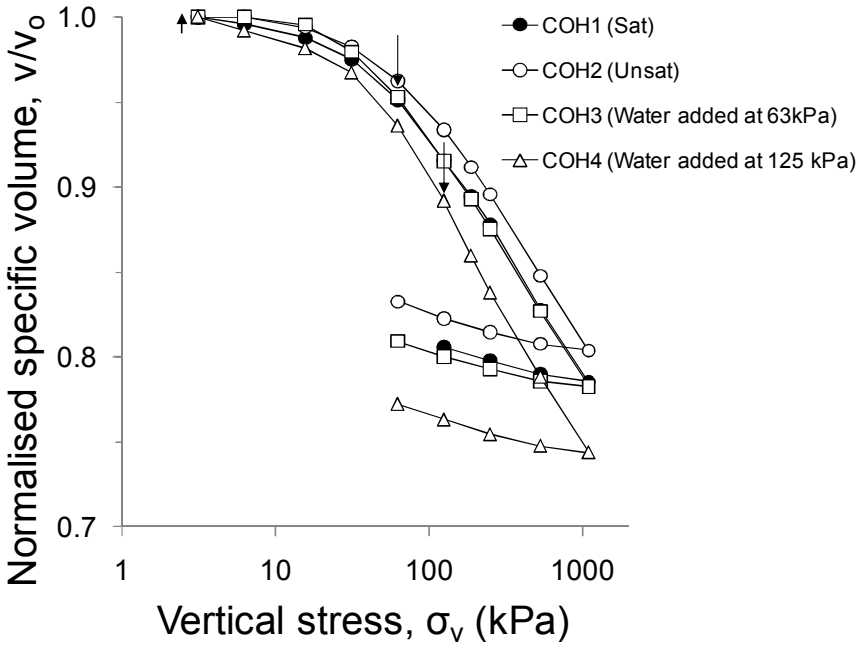

Figure 5.13: Load and soak results for Series COH: Undisturbed specimens (average series initial conditions: w_o= 34.8%, ρ_{d_o} = 1.21Mg/m^3)

Table 5.3: Guidance on collapse potential (Fookes, 1990, p.63)

Collapse Potential (%)	Likely severity of problem
< 1	No problem
1 - 5	Moderate trouble
5 - 10	Trouble
10 - 20	Severe trouble
> 20	Very severe trouble

determined. It may be inferred from these results that for the Bengawan Solo fill material, specimens with a degree of saturation above 80% prior to soaking are unlikely to exhibit significant volumetric collapse on wetting.

With a different objective, the results of the oedometer tests carried out, were analysed in terms of their yielding and compression behaviour. The yield stress (σ_{vc}) for both the saturated (σ'_{vc}) and unsaturated ($\overline{\sigma}_{vc}$), conditions was determined using Casagrande's graphical construction method (Casagrande, 1936). The term yield stress is used here to define the transition between low compressibility behaviour and a higher compressibility behaviour. The yield stresses discussed here are related to stress history, suction and structural effects (which is investigated in detail in Chapter 7). Casagrande's method was used because it is perhaps the most widely used method of determining the yield stress and is readily understood by the engineering community. It is acknowledged here that there are many other alternative methods for defining the yield stress including Janbu (1969), Pacheco Silva (1970), Becker et al. (1987), Burland (1990), Jacobsen (1992) and Onitsuka et al. (1995) among others. Grozic et al. (2003) presents a detailed study of the use of different methods for glaciomarine clays and gives an interesting overview of how these methods compare with each other. Despite the shortcomings of the Casagrande method, namely (i) that the position of maximum curvature of the compression curve can be difficult to locate precisely in soils that exhibit a more rounded transition and (ii) that the position of maximum curvature is subject to scale effects, it tended to give results neither higher nor lower than those obtained by five of the alternative methods listed above (Grozic et al., 2003).

Furthermore the compression index C_c and swell index C_s was determined from the saturated and constant water content oedometer tests, where C_c is the slope of the post-yield compression curve and C_s is the slope of the unloading portion of the curve in the $e - \log \sigma_v$ plot. Table 1.4 presents the σ_{vc}, C_c and C_s for the saturated and unsaturated condition of each series tested. As expected, in all the series, the saturated conditions had a lower σ_{vc} than the corresponding constant water content test. This indicates one of the ways in which matric suction can act to stiffen soil behaviour by increasing the region in which soil deformations are recoverable (elastic changes). The difference between the σ_{vc} for the saturated and constant water content tests for each series ranged from as little as 1kPa (Series COD) to as much as 467kPa (Series COC). The much higher σ_{vc} found in COC2 (compared to COC1) can be explained by the fact that

Table 5.4: Collapse potentials and severity of collapse for each load and soak test

Test Reference	w_o (%)	ρ_{d_o} (Mg/m^3)	S_r (%) prior to soaking	ρ_d (Mg/m^3) prior to soaking	σ_v (kPa) on soaking	Potentials (%) Swelling (+) Collapse (-)	Severity (Fookes, 1990)
COA1	20.8	1.17	42.3	1.17	3	+2.0	Moderate swelling
COA3	20.8	1.17	43.4	1.18	32	-4.7	Moderate trouble
COA4	18.2	1.16	46.2	1.18	63	-9.8	Trouble
COA5	18.8	1.15	41.1	1.21	125	-13.6	Severe trouble
COA6	20.5	1.16	51.9	1.31	253	-11.3	Severe trouble
COA7	20.5	1.17	74.8	1.56	538	-1.5	Moderate trouble
COB1	24.0	1.18	50.3	1.18	3	+1.8	Moderate swelling
COB3	24.0	1.18	53.4	1.22	125	-11.6	Severe trouble
COC1	19.4	1.37	53.6	1.37	3	+2.8	Moderate swelling
COC3	19.4	1.37	55.8	1.40	125	-2.3	Moderate trouble
COD1	29.2	1.44	89.7	1.44	3	+0.9	Slight swelling
COD3	29.2	1.43	93.6	1.47	125	-0.02	No problem
COE1	35.9	1.22	78.8	1.22	3	+0.04	Minimal swelling
COE3	35.9	1.28	100	1.38	125	+0.002	No problem
COF1	36.2	1.16	72.7	1.16	3	+0.03	Minimal swelling
COF3	36.2	1.18	80.5	1.22	63	+0.004	No problem
COG1	20.1	1.26	49.2	1.29	125	-8.9	Trouble
COG2	19.8	1.38	57.9	1.41	125	-3.3	Moderate trouble
COH1	33.6	1.23	75.7	1.23	3	+0.04	Minimal swelling
COH3	35.6	1.23	87.5	1.29	63	-0.01	No problem
COH4	35.7	1.12	82.7	1.25	125	-0.02	No problem

Table 5.5: Yield stress σ_{vc}, compression index C_c and swell index C_s of saturated and unsaturated specimens tested

Test Reference	Condition	w_o (%)	ρ_{d_o} (Mg/m^3)	σ_{vc} (kPa)	C_c	C_s
COA1	SAT	20.8	1.17	18	0.47	0.06
COA2	CW	19.1	1.19	95	0.46	0.02
COB1	SAT	24.0	1.18	27	0.60	0.05
COB2	CW	24.0	1.18	170	0.66	0.02
COC1	SAT	19.4	1.37	70	0.33	0.05
COC2	CW	19.4	1.37	537	0.38	0.01
COD1	SAT	29.2	1.44	126	0.25	0.05
COD2	CW	29.2	1.43	127	0.30	0.05
COE1	SAT	35.9	1.22	40	0.39	0.06
COE2	CW	35.9	1.29	61	0.33	0.04
COF1	SAT	36.2	1.16	32	0.47	0.03
COF2	CW	35.4	1.20	63	0.50	0.04
COH1	SAT	33.6	1.23	51	0.31	0.06
COH2	CW	34.1	1.27	68	0.30	0.06

it was a specimen of relatively high dry density, dry of optimum at 20% moisture content, and therefore correspondingly would presumably have a relatively high matric suction.

In terms of the post-yield compression behaviour the trend was less clear, in some cases, the compression index C_c was similar for both conditions in the same series (Series COA, COH), in others C_c was higher for the constant water content condition (Series COB, COC, COD, COF) and in others C_c was higher for the saturated condition (Series COE). The swell index appeared to be influence by the initial moisture content of the specimens tested, in each series where specimens were compacted dry of optimum of Extreme Light and BS Light compaction curves ($w_o <$ 28%), a higher swell index was determined for the saturated tests than the corresponding constant water content test (Series COA, COB, COC). This means that the saturated specimens exhibited more swelling on unloading than the unsaturated specimens. For specimens compacted at $w_o >$ 28% (Series COD, COE, COF) swell index was similar for both the saturated and unsaturated specimens. The influence of suction on the post-yield compression behaviour of the Bengawan Solo fill is further investigated in Chapter 6 in experiments equipped with suction control, in which specimens were subjected to isotropic loading.

5.2.7 Possible failure pathways

The mechanical study presented in this chapter has identified that the Bengawan Solo fill material is indeed collapsible under dry of optimum, low density conditions. In particular specimens prepared close to the as-constructed conditions of the gabion reinforced embankment exhibited significant collapse (as high as 13.6%). Considering that all the conditions required for volumetric collapse were identified as occurring along the Bengawan Solo embankments, it is proposed here that such irrecoverable deformations exhibited by collapsible fill on wetting could play a role in triggering instabilities in flood embankments, particularly where protection measures have been installed which have introduced additional loading.

Figure 5.14 presents three different failure pathways, which may be triggered by volumetric collapse behaviour. Pathway A illustrates how protection measures, resulting in additional loading may induce localised collapse failures in an embankment with one or more collapsible fill layers. This may simply be several layers of soil with a lower dry density due to variation in the compactive effort applied during construction. The localised collapse failures may be sufficient to trigger global failure of the embankment. It is possible that this pathway may have played a role in the large global failure observed in the gabion-reinforced section of the Bengawan Solo embankments, which occurred during the first wet season after its construction.

In Figure 5.14, Pathway B indicates how an embankment with a collapsible fill layer may undergo volumetric collapse under its own self-weight. The volumetric collapse would lead to a reduction of the height of the embankment, and perhaps a functional failure of the embankment, i.e. the design crest height is not maintained. The reduction in the crest height would also increase the risk of overtopping and once overtopped, erosion of the landward face could occur, seriously damaging the integrity of the embankment.

Due to the heterogeneity of fill material used and the poor control of compaction in flood embankment construction of extensive length, it is likely that volumetric collapse could occur to differing degrees along a susceptible embankment. This could result in differential settlements (Pathway C) along the length of an embankment where either Pathway A or Pathway B has occurred. These may induce transversal cracks along the crest and slopes of the embankment, creating preferential flow paths for seepage through the embankment, possibly resulting in piping

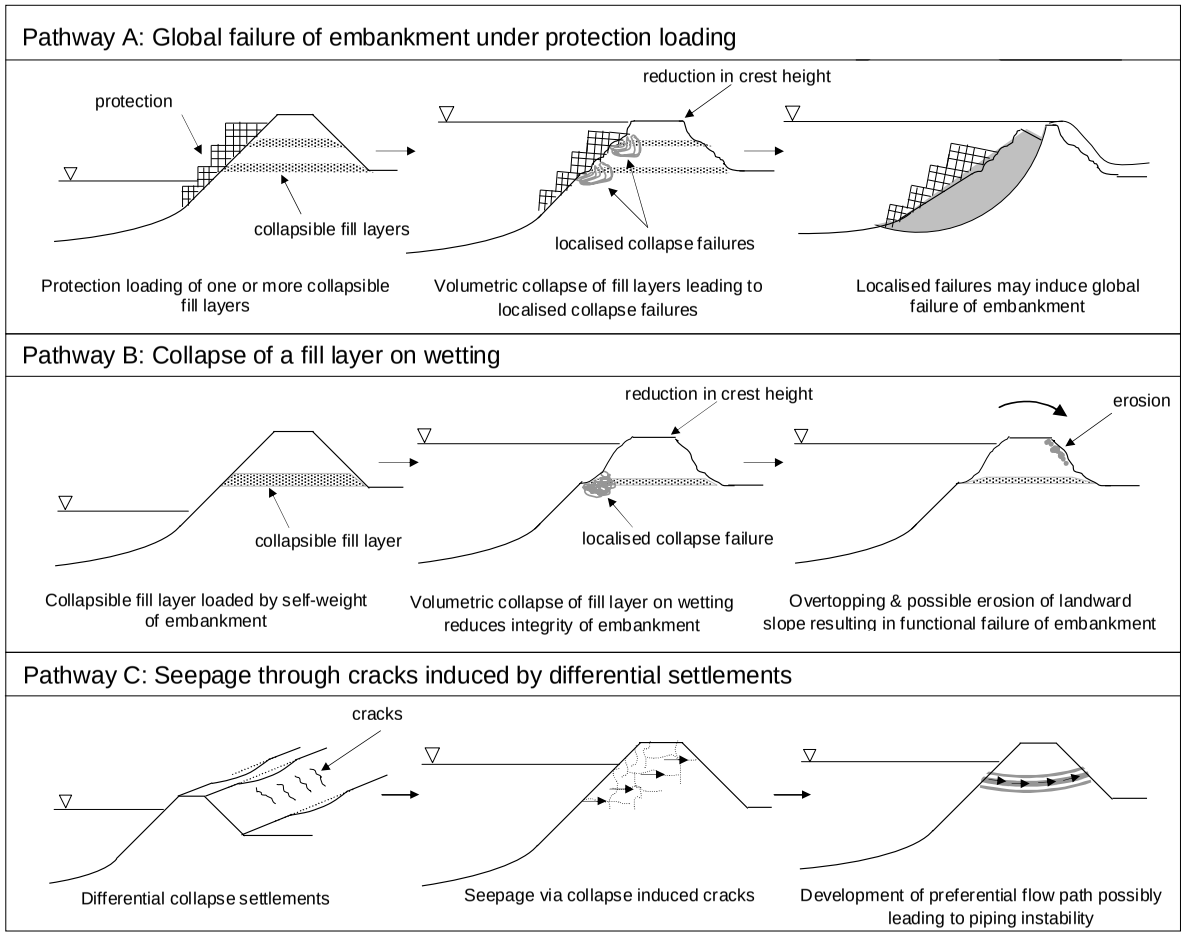

Figure 5.14: Possible failure pathways related to the presence of collapsible fill material in flood embankments, Pathway A: Global failure of embankment under protection loading, Pathway B: Volumetric collapse of a fill layer within embankment and Pathway C: Seepage through cracks induced by differential settlements

instability.

Assuming then that the occurrence of volumetric collapse within flood embankments may trigger a number of different failure modes, this may explain why this phenomenon has been overlooked. It is possible that after the failure of a flood embankment the mode of failure recorded has been attributed to the resulting macro-mechanism observed, where in fact volumetric collapse has possibly played a role in initiating the mechanism.

The three failure pathways proposed here are based on the records of types of failures occurring due to volumetric collapse in other types of engineered embankments. The role of collapsible soils in earth dam structures has been well documented, in particular in the so called "Alka-Seltzer" dams of North East Brazil (e.g.Miranda, 1988; Pereira and Fredlund, 2000; Pereira et al., 2005). In these earth dams piping failures due to cracks resulting from collapse settlements have been reported (Miranda, 1988; Lawton et al., 1992). Booth (1977) investigating highway failures in South Africa, reported large vertical deformations up to 0.5m due to collapse settlements and also indicated how a highway failure initially thought to be a shear slip failure was later attributed to volumetric collapse. Despite the recognition of this mechanism in the failure of earth dams, highway embankments and in compacted soils under foundations (e.g. Lawton et al., 1992), there remain few studies on the volumetric collapse of fill material in flood embankments. Given their close proximity to water and the large scale in which the construction of flood embankments is often carried out, (which may lead to poor compaction control), it is proposed that the volumetric collapse phenomenon should be routinely considered particularly if an embankment is to be constructed under dry of optimum conditions or where protection or remediation measures (involving additional loading) are to be introduced.

5.2.8 Mechanical Behaviour Summary

Relatively simple conventional load and soak oedometer tests presented herein have provided important information regarding the collapsible nature of this material. In particular, under low density, dry of optimum conditions (close to as-compacted conditions) this material may exhibit significant volumetric collapse (Series COA, COB). Increasing the compactive effort (Series COC) or compacted moisture content (Series COF) tended to reduce the amount of collapse

observed. Specimens compacted at optimum conditions of the BS Light or Extreme Light compaction curves (Series COD, COE), did not exhibit volumetric collapse behaviour. Interestingly specimens compacted at high moisture content and then dried (Series COG) exhibited significant volumetric collapse after drying, despite an overall increase in dry density. These tests indicate that for the Bengawan Solo fill important structural changes occur due to wetting and drying, which are responsible for overall macro-scale behaviour. Furthermore the results of Series COG indicate the importance of not only specifying wet of optimum moisture contents but also appropriate initial dry densities. Considering that the conditions for volumetric collapse may be present in flood embankments, three different failure pathways were presented here, which illustrate how the role of collapsible fill layers may trigger instabilities.

5.3 Fabric Study

5.3.1 Objective

A microstructural investigation was carried out in order to (i) investigate the fabric of the Bengawan Solo fill and (ii) to investigate the evolution of this fabric due to loading and wetting changes. The fabric study was carried out at UPC Barcelona, in collaboration with Dr Enrique Romero.

5.3.2 Background

The study of the fabric of compacted soils has long been a topic of interest, since the early works by Lambe (1958b), (1958a). The development and use of experimental techniques such as Scanning Electron Microscopy (SEM), Environmental Scanning Electron Microscopy (ESEM) and Mercury Intrusion Porosimetry (MIP) in the study of soils has enabled further revision and discussion on the arrangement of soil particles (e.g. Collins and McGown, 1974; Barden and Sides, 1970; Barden et al., 1973; Juang and Holtz, 1986a; Delage and Lefebvre, 1984; Romero, 1999). The importance of understanding soil fabric has been further highlighted by the links which have been made between fabric and mechanical response (Alonso et al., 1987) and the

development of the Barcelona Expansive Model (BExM) for expansive soils, where soil response is directly related to two distinct levels of structure: (i) microstructure and (ii) macrostructure (Gens and Alonso, 1992; Alonso et al., 1999).

The study presented in this chapter was carried out using both ESEM and MIP to investigate the evolution of soil fabric during volumetric collapse to assist the interpretation of the macroscopic mechanical tests. The ESEM technique enables a direct, qualitative observation of the soil fabric arrangement whereas the MIP technique provides quantitative data on the soil porosity, in particular enabling the pore size distribution of a soil specimen to be obtained. The pore size distribution is an essential element of soil fabric (Romero, 1999), and with all other things being equal (particle sizes and distribution, void ratio, dry density) pore size distribution may be responsible for differences in permeability, compressibility and strength (Juang and Holtz, 1986a). For example, a soil with many small pores is likely to have a lower saturated permeability than one with a fewer number of larger pores (Juang and Holtz, 1986a).

SEM and MIP have often been used independently or together in the investigation of microstructural features of soils (e.g. Barden et al., 1973; Collins and McGown, 1974; Delage and Lefebvre, 1984; Griffiths and Joshi, 1989; Prapaharan et al., 1991; Jommi and Sciotti, 2003). Barden et al. (1973) used SEM to investigate the arrangements existing within collapsible soils and concluded that the collapse mechanism of clayey soils was due to an effective aggregated macrostructure rather than the rearrangement of flocculated clay particles on wetting. Several studies have compared laboratory and field compacted material using SEM and MIP (Prapaharan et al., 1991; Jommi and Sciotti, 2003) raising questions over whether soil compacted in the laboratory should be used as a reliable reference material for field compaction given the resulting differences in microstructure.

With the shift towards the use of ESEM, in which the sample can be imaged in its natural wet condition, researchers are again turning their attention to the fabric changes which occur along hydraulic paths. Villar and Lloret (2001) observed the swelling behaviour of compacted FEBEX bentonite under constant volume, in which macropores became filled with the swelling bentonite particles. Zhang et al. (2005) investigated changes in the fabric of a double porosity tropical soil along drying and wetting paths.

Although primarily for the determination of pore size distribution MIP data has also been used

to determine saturated permeability (e.g. Garcia-Bengochea et al., 1979; Juang and Holtz, 1986a,b) to derive the water retention curve (e.g. Romero, 1999; Simms and Yanful, 2002, 2005) and more recently in the determination of unsaturated permeability (Simms and Yanful, 2005). Water retention behaviour determined using MIP may differ from experimental values for a number of reasons: (i) only the retention of water due to capillary effects is considered, any water held by adsorptive forces will not be accounted for and (ii) the MIP derived curve assumes that the material is non-deformable under drying paths, which is not the case for many soils, particularly those with expansive clays which undergo important volumetric changes on drying. A recent state of the art review of microstructure investigation with special attention to MIP and ESEM has been presented in Romero and Simms (2008).

5.3.3 Soil fabric classification

Based on SEM investigations for a wide range of natural soils, Collins and McGown (1974) developed a classification for soil fabric based on the main structural features observed: (i) elementary particle arrangements, (ii) particle assemblages and (iii) pore spaces. Elementary particle arrangements consist of individual clay platelet interactions or individual silt or sand grain interactions. The particle assemblages are made up of groupings of the elementary particle arrangements. Different types of particle assemblages are illustrated in Figure 5.15, and include connectors, aggregations, interweaving bunches and matrix fabrics (Collins and McGown, 1974). Collins and McGown (1974) identify four groups of pore space (see Figure 5.16): (i) Intra-element pores which are located within the elementary particle arrangements, (ii) Intra-assemblage pores, pores occurring within particle assemblages, (iii) Inter-assemblage pores occurring between assemblages and (iv) Trans-assemblage pores pores which traverse the soil fabric.

Alonso et al. (1987) presented an interpretation of these microfabric features which is illustrated in Figure 5.17. It is common to refer to the intra-assemblage pores with specific reference to the nature of the particle assemblage, for example pores within a matrix assemblage are termed intra-matrix pores and pores within an aggregate assemblage are termed intra-aggregate pores (Alonso et al., 1987). The inter-assemblage pores are also more commonly referred to as inter-aggregate pores for an aggregated fabric (e.g. Romero, 1999; Lloret et al., 2003). Similarly, Delage et al. (2006) presented a description of the pores found at different microstructural levels

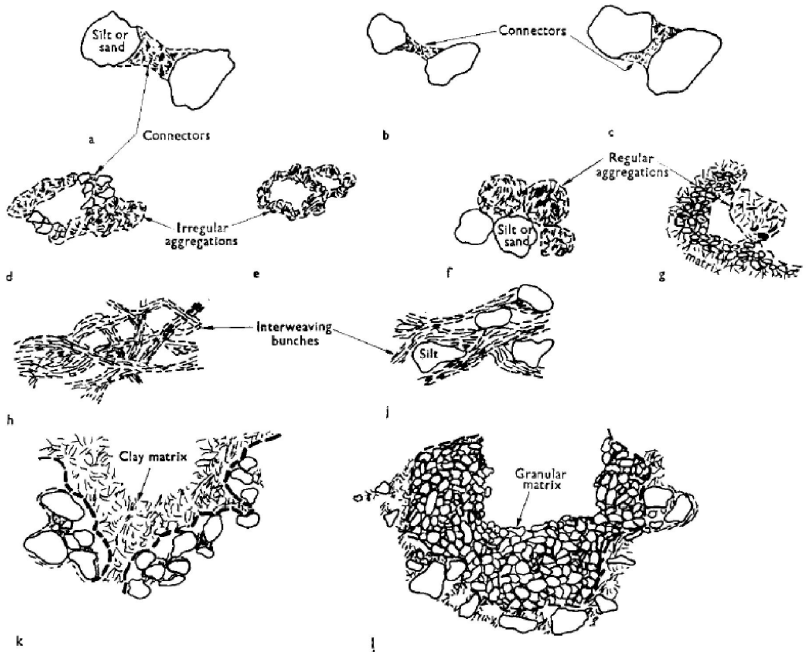

Figure 5.15: Schematic representations of particle assemblages; (a) (b) (c) connectors; (d) irregular aggregations linked by connector assemblages; (e) irregular aggregations forming a honeycomb arrangement; (f) regular aggregations interacting with silt or sand grains; (g) regular aggregation interacting with particle matrix; (h) interweaving bunches of clay; (j) interweaving bunches of clay with silt inclusions; (k) clay particle matrix: (I) granular particle matrix (Collins and McGown, 1974)

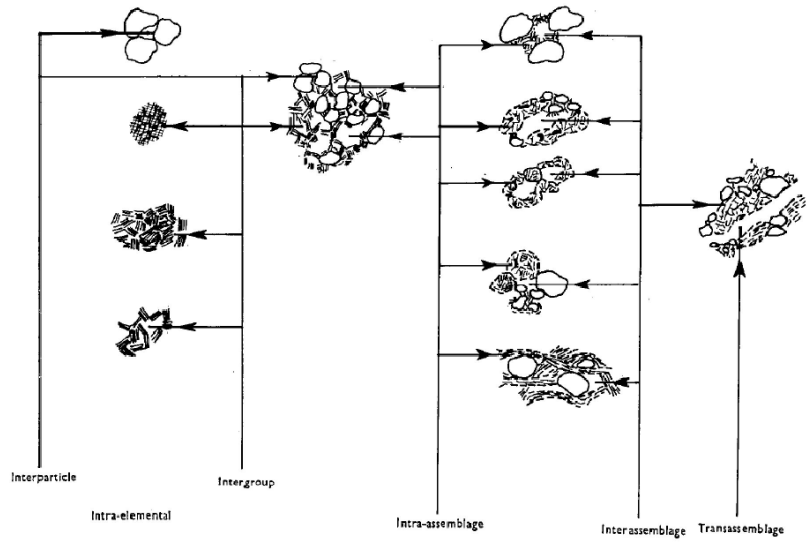

Figure 5.16: Schematic representation of pore space types (Collins and McGown, 1974)

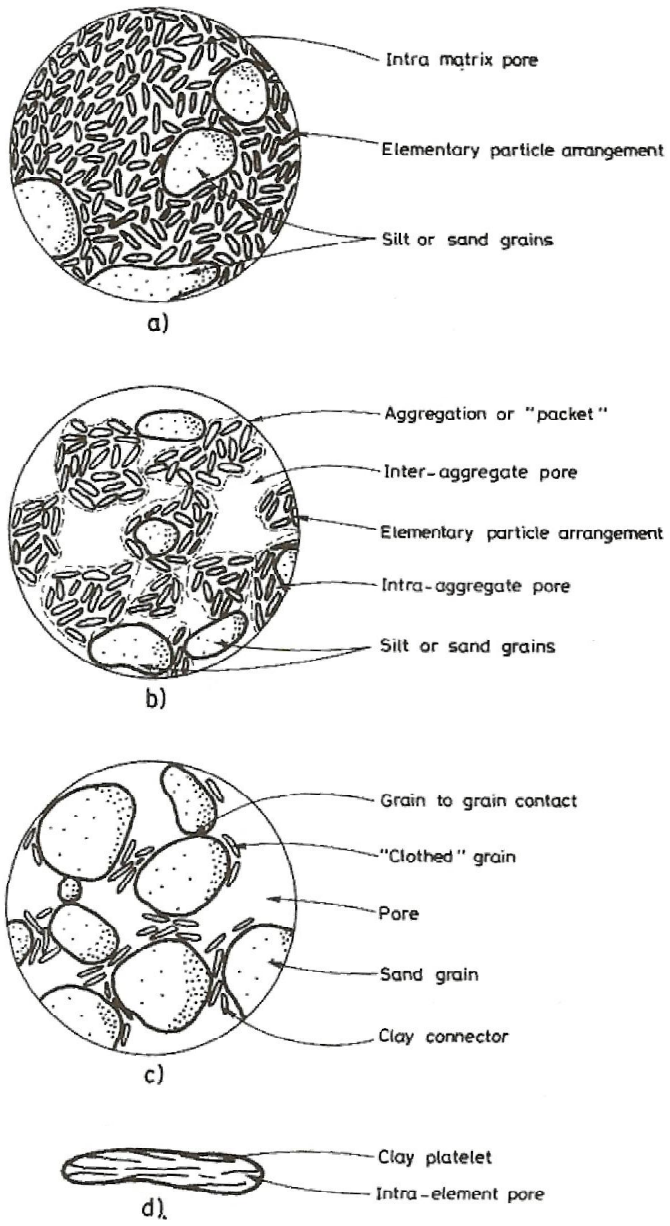

Figure 5.17: Types of microfabric (a) Clay matrix predominantly integrated by elementary particles of clay platelets and a few grains of silt or sand, (b) Microfabric of a clay predominantly integrated by aggregations of elementary particle arrangements, (c) Sand or silt matrix with clay connectors between individual grains and (d) Elementary particle arrangement in a parallel configuration (Alonso et al., 1987)

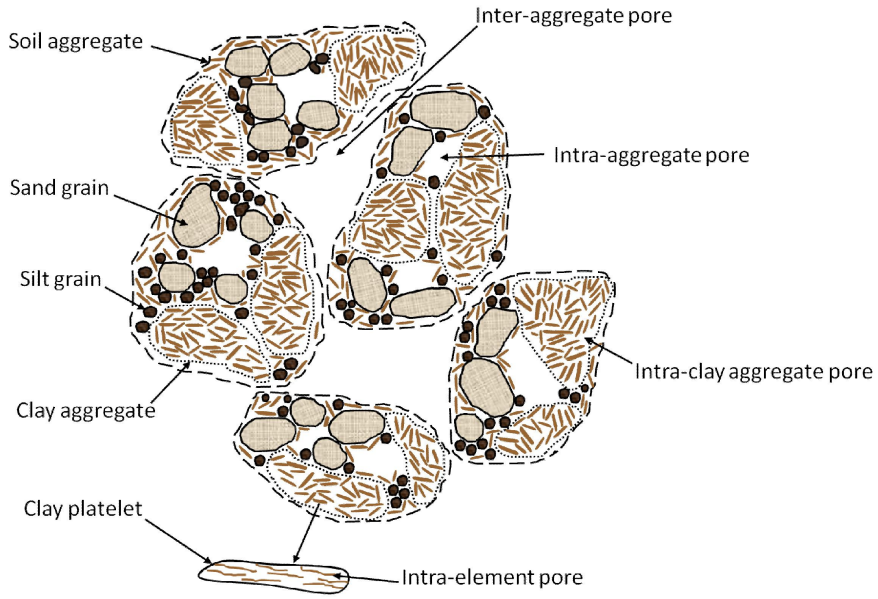

Figure 5.18: Schematic of soil fabric with pore space definitions as used in this research

in clays: (i) inter-layer spaces, pores inside clay particles (intra-element), (ii) inter-particle voids inside clay aggregates (intra-aggregate) and (iii) pores between clay aggregates (inter-aggregate).

Figure 5.18 presents a simplified schematic of the arrangement of soil particles for a material containing significant quantities of sand, silt along with an important clay fraction. The four different levels of pore spaces indicated are those used referred to within this thesis, based on the classifications outlined above:

1. Inter-aggregate pore: pore space between aggregations, where aggregations consist of sand and silt particles clothed in clay matrix and clay aggregates.

2. Intra-aggregate pore (or intra-matrix): pore space within aggregations (or within a matrix), between arrangements of sand and silt particles and clay aggregates.

3. Intra-clay aggregate pore (or intra-clay matrix): pore space between elementary clay particle arrangements whether in a clay aggregate or present in a clay matrix. A number of microstructural studies on compacted clays containing smectites have reported an intra-(clay) aggregate pore size of 0.008-0.02µm (e.g. Lloret et al., 2003; Delage et al., 2006).

4. Intra-element pore: pore space within the elementary clay particle arrangement and corre-

sponds to the planar inter-layer spaces (Delage et al., 2006). For soils containing montmorillonite the intra-element pore size has reported to be between 10Å - 21.6Å, corresponding to between 0 and 4 adsorbed water layers (Saiyouri et al., 2000).

5.3.4 Fabric study specimens

The compaction conditions of Series COA, tested in the load and soak oedometer (dry of optimum at low dry density), were selected for further investigation in the fabric study. The specimens investigated corresponded to the path followed when loading and soaking under a vertical stress of 125kPa, the maximum collapse observed for Series COA. As such three different specimens were prepared: (i) Compacted, (ii) Compacted loaded and (iii) Compacted loaded & soaked (Figure 5.19). The compacted specimen was prepared in the oedometer retaining ring. The compacted loaded specimen was prepared by loading the compacted specimen to 125kPa for 24hrs in the oedometer apparatus and then removing for testing. The compacted loaded and soaked specimen was loaded to 125kPa for 24hrs and then inundated with water in the oedometer apparatus. The specimen conditions are illustrated in Figure 5.19 and detailed in Table 5.6. Furthermore a specimen sampled from the undisturbed block sample was also investigated for comparison purposes.

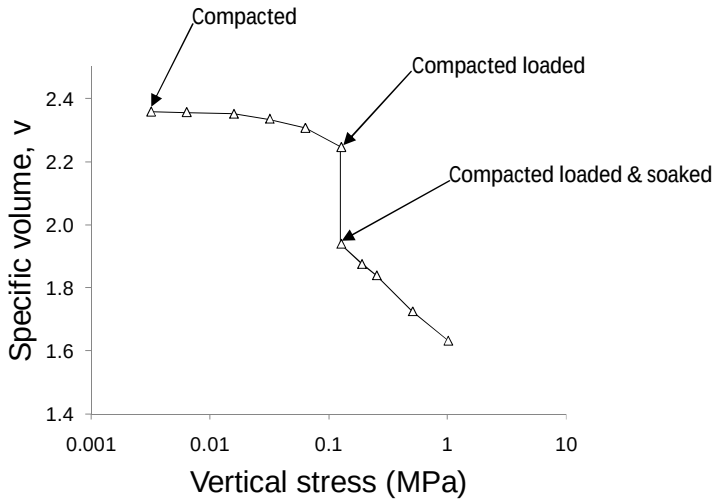

Figure 5.19: Specimens selected for investigated in fabric study according to load and soak tests: (i) Compacted, (ii) Compacted loaded and (iii) Compacted loaded & soaked

Table 5.6: Specimen conditions investigated in fabric study

Specimen Name	Reference	w (%)	ρ_d (Mg/m^3)	e	S_r (%)
Compacted	C	19.5	1.15	1.38	38.6
Compacted, loaded	CL	19.0	1.19	1.29	40.2
Compacted, loaded & soaked	CLS	27.7	1.39	0.95	79.2
Undisturbed	U	34.7	1.36	1.00	94.4

5.3.5 Environmental Scanning Electron Microscopy tests

5.3.5.1 Experimental Equipment

The Electroscan 2020 ESEM located within the Department of Material Sciences and Metallurgy at UPC, Barcelona was used in this study. Dr. José María Manero Planella kindly provided assistance in the imaging process.

Figure 5.20 presents a cross-section of a typical ESEM machine (Danilatos, 1993). Romero and Simms (2008) describe the processes operating within the ESEM equipment; the following is a brief summary of this explanation. Inside the ESEM there are regions of increasing vacuum; the specimen chamber has a low vacuum, which can have an absolute pressure up to 3kPa, whereas the electron gun chamber can maintain a very good vacuum (10^{-5}Pa). The application of the vacuum is important for ensuring the movement of electrons within the chambers. A beam of primary electrons is emitted from the electron gun in the direction of the specimen. These electrons, hit the surface of the specimen causing it to emit secondary electrons, which then accelerate towards the Gaseous Secondary Electron Detector (GSED), due to its positive charge. Moving through the gaseous environment these secondary electrons collide with gas particles resulting in additional secondary electrons being emitted, creating further positive gaseous ions. The positively charged gaseous ions are then attracted to the surface of the specimen, which has become negatively charged, due to the bombardment of the primary electrons, thus cancelling out charge effects. It is in this way that non-conductive samples can be imaged. The GSED forms an image based on the signal intensity of the secondary electrons received from different locations across the surface of the specimen.

Generally water vapour is the gas used in the sample chamber because it allows maximum signal amplification and has a high charge neutralisation capacity (Romero and Simms, 2008).

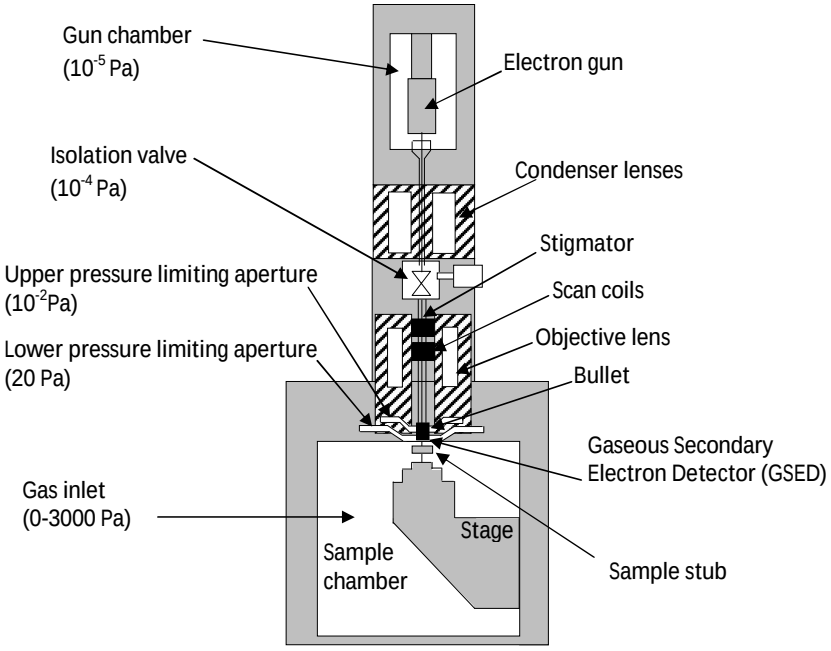

Figure 5.20: Schematic of ESEM equipment (After Danilatos, 1993)

In ESEM the vapour pressure can be controlled along with the chamber temperature allowing specimens to be observed under different relative humidity and hence under wetting and drying stages. Further information on the ESEM technique and its applications can be found in Danilatos (1993) and Romero and Simms (2008) among others.

5.3.5.2 Specimen Preparation

One of the main advantages of the ESEM over conventional SEM equipment is that it allows samples to be imaged in their natural (wet) condition, eliminating the need for freeze drying. Furthermore samples do not have to be covered in a conductive coating when imaging in the ESEM. This greatly reduces specimen preparation time.

Despite these advantages, care must still be taken during specimen preparation particularly as only very small specimens can be imaged (several mm^3). The specimen should be separated from the original sample not by cutting but by fragmenting or fracturing the sample in as natural a way as possible in order to maintain the natural structure of the soil. If the specimen were to be cut using a cutting tool, a completely flat unnatural surface would be observed under the

ESEM. Care must be taken so that the very small specimen selected is representative of the larger sample. After fracturing from the larger sample, the small specimen was placed on a black adhesive non-conducting material on a small mounting block.

5.3.5.3 Chamber conditions

In the observation of these specimens the sample chamber conditions were maintained at a constant vapour pressure of 5Torr and a temperature of 10°C (1Torr = 760mmHg = 0.133kPa). It should be noted that these were the conditions of the chamber and not the temperature or pressure of the sample. Saturated water vapour pressure in equilibrium with free water at a temperature of 10°C is equal to 9.21Torr (calculated using the Antoine equation). As such the relative humidity of the chamber at a constant vapour pressure of 5Torr is approximately 54%. The total suction imposed within the chamber can be calculated using the pyschrometric law (Equation 1.1) and is equivalent to 80MPa, however this is the imposed suction in the chamber and not the actual suction within the soil sample. Under such conditions, samples tend to dry and therefore specimens were imaged immediately after mounting in the chamber to avoid unnecessary drying.

5.3.5.4 ESEM Results

Figures 5.21 to 5.24 present the ESEM micrographs of the different specimens investigated. Figure 5.21 presents two images of the compacted specimen. The compacted specimen has an open structure characterised by large inter-aggregate pores, surrounded by defined soil aggregates which are linked via bridging material. In the ESEM images it is difficult to discern individual sand and silt grain particles, instead it appears that all the particles are clothed with clay particles forming aggregations.

Moving to the compacted, loaded specimen in Figure 5.22, inter-aggregate pores and defined soil aggregations are still present along with bridging connections. However, it appears perhaps that the loading process is responsible for breaking some bridging connections.

Figure 5.23 shows the compacted, loaded & soaked specimen (i.e. after collapse). In this specimen, there is a marked absence of inter-aggregate pores. It is though, still possible to

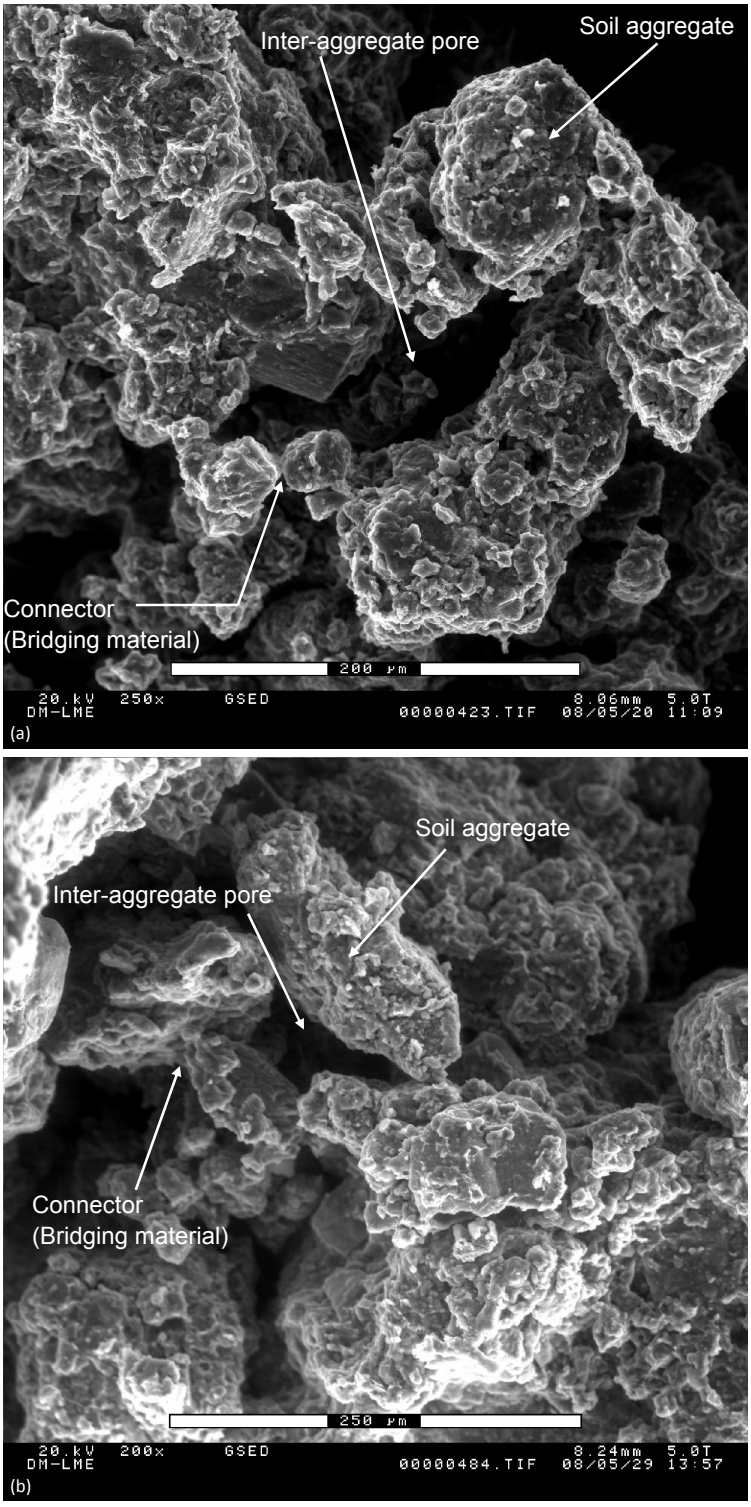

Figure 5.21: ESEM micrograph of Compacted specimen at (a) 250x magnification, and (b) 200x magnification

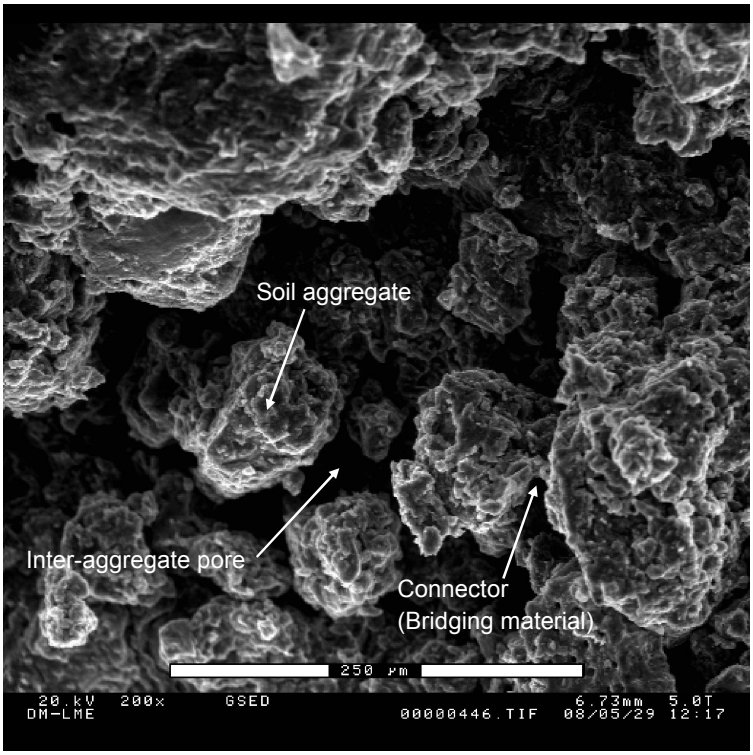

Figure 5.22: ESEM micrograph of Compacted loaded specimen (200x magnification)

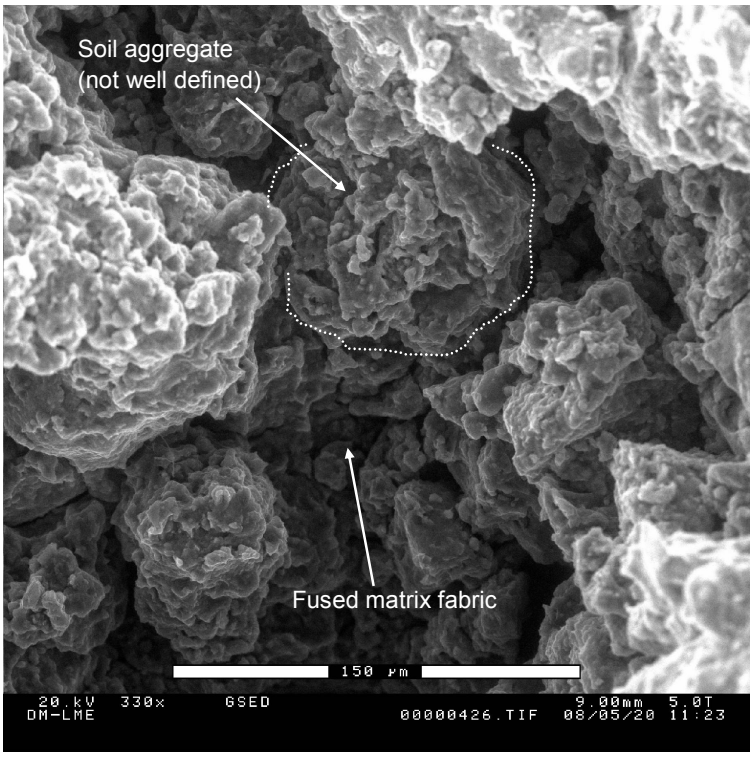

Figure 5.23: ESEM micrograph of Compacted loaded & soaked specimen (330x magnification)

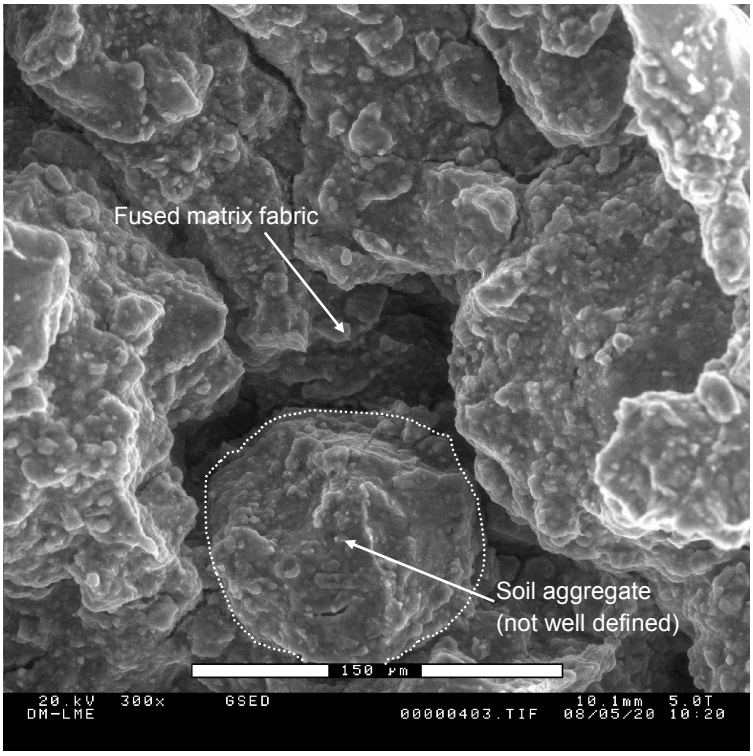

Figure 5.24: ESEM micrograph of Undisturbed specimen (300x magnification)

determine where soil aggregations existed prior to wetting, though these are not well defined. However as a result of the soaking, the fabric has become fused due to a softening of the aggregations and the fabric as a whole has become more uniform. Similar changes in fabric due to loading and wetting were observed in the ESEM by Monroy (2006). The overall change in fabric associated with a decrease in suction (wetting), as viewed in Figure 5.23 can be attributed to (i) the loss of rigidity of soil aggregations (softening), (ii) the loss of strength on wetting of bridging material and (iii) the loss of the stabilising effect arising from suction. These changes all result in the loss of inter-aggregate pores which are absent in Figure 5.23. It is the loss of these inter-aggregate pores on wetting which appears to be responsible for the collapse induced volume changes observed in the oedometer tests presented in this chapter.

Finally the microstructure of an undisturbed sample was also investigated using ESEM. There are distinct similarities between the Undisturbed specimen (Figure 5.24) and the Compacted, loaded & soaked specimen (Figure 5.23), namely both show fused soil aggregations within a uniform fabric, with a marked absence of inter-aggregate pores. The outer covering of the fabric

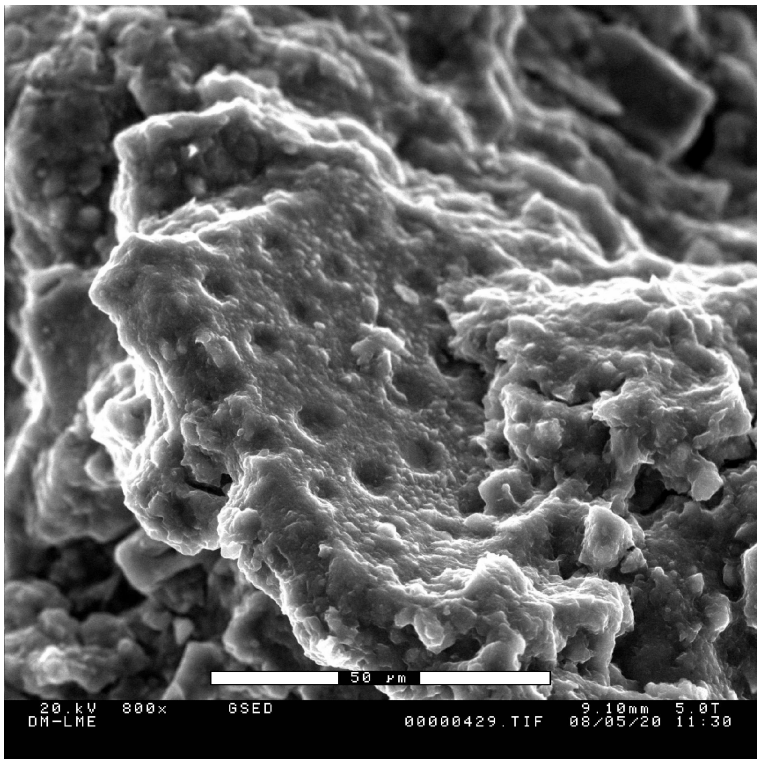

Figure 5.25: ESEM micrograph of diatom (phytoplankton) found in Bengawan Solo fill

in the undisturbed specimen appears to be more rounded than that of the Compacted, loaded and soaked specimen; this may attributed to the higher moisture content of the undisturbed sample (34.7% compared to 27.7%). The comparison of Figures 5.23 and 5.24 suggests that the microstructure of the undisturbed sample is very similar to that of the Compacted, loaded and soaked specimen (collapsed) created in the laboratory with initial conditions, dry of optimum at low dry density.

On a side note during the ESEM investigation evidence of plant fibres and the presence of diatoms were observed (Figure 5.25). Diatoms are single celled phytoplankton; this indicates the alluvial origin of the Bengawan Solo fill.

5.3.6 Mercury Intrusion Porosimetry tests

5.3.6.1 Principle

MIP is based on the principle that a non-wetting fluid (see Figure 3.2, Chapter 3) will enter the pores of a soil progressively under an applied pressure. Washburn (1921) related the pore entrance diameter d to the absolute pressure applied P:

$$P = \frac{-4\sigma_{Hg}\cos\theta_{nw}}{d} \tag{5.8}$$

where θ_{nw} is the non-wetting contact angle between mercury and the solid particle and σ_{Hg} is the surface tension of mercury. Diamond (1970) determined a contact angle of 139° for montmorillonite and 147° for other clay minerals. Romero (1999) suggested a contact angle of 140° for use with Boom clay. Due to the high proportion of montmorillonite in the clay fraction of the Bengawan Solo fill a contact angle of 140° was selected. A value of 0.484N/m for surface tension was used in these tests as has been repeatedly reported elsewhere (e.g. Delage and Lefebvre, 1984; Griffiths and Joshi, 1989; Romero and Simms, 2008).

The Washburn equation (5.8) is valid for pores of cylindrical shape which are infinitely parallel in form, this is an over simplification of the pore network found within soils. Similar to the hysteresis found in the soil water retention curve, hysteresis also exists in the use of the MIP technique: (i) rain drop effect, i.e. the contact angle may vary depending on whether the non-wetting fluid is advancing or receding, (ii) ink-bottle effect, where pores with larger diameters are not detected until their entrances of smaller diameter are penetrated (see Figure 3.16). Due to the effect of the constricted pores, the diameters determined in the MIP tests are referred to here as entrance pore size diameters. There are also a number of other limitations in the ability of the MIP technique to detect all pores within a soil. Isolated pores are pores which are entirely surrounded by solid particles and thus cannot be intruded. This enclosed porosity is thought not to be significant in soils (Romero and Simms, 2008). The smallest pores of a sample however, may also not be intruded due to the pressure capacity of the MIP equipment, this is referred to as the non-intruded porosity. Furthermore the minimum practical pressure of the apparatus limits the maximum pore diameter which can be detected, this is referred to

as the non-detected porosity (Romero and Simms, 2008). For these reasons the intruded void ratio determined using the MIP technique may not be similar to the actual void ratio of the soil specimen tested.

Another concern regarding the use of the MIP technique is the question over whether the high pressures applied during mercury intrusion damages or changes the very structure the technique is intended to investigate. Lawrence (1978), however presented data to suggest that virtually no sample damage occurred upon mercury intrusion. Three different soil types were intruded with mercury which was subsequently removed by heating to 200°C, a second intrusion with mercury showed an almost identical pore size distribution to the first intrusion indicating no sample damage. Delage and Lefebvre (1984) presented strong agreement between pore size diameters measured using SEM and from MIP analyses, again suggesting that the mercury intrusion is not detrimental to the soil structure. Two main factors have been proposed to support this evidence: (i) at high pressures the pore network is largely filled with mercury already which is nearly incompressible and (ii) although the pressures may be very high, the forces acting to cause volume changes are very low due to the very small diameters being investigated (Reed et al., 1980; Griffiths and Joshi, 1989). Despite its associated limitations and simplified assumptions the MIP technique enables a very useful quantification of soil microstructure to be determined (Romero and Simms, 2008).

5.3.6.2 Experimental Equipment

The MIP tests presented here were carried out in the Department of Geotechnical Engineering and Geosciences at UPC using a Micromeritics Autopore IV 9500 porosimeter (Figure 5.26a). The porosimeter used has a low pressure system (Figure 5.26b) for pressures from approximately 3kPa to 345kPa corresponding to a detection of entrance pore diameters in the range of 0.48mm to 4.4μm. The high pressure system (Figure 5.26c) reaches pressures up to 223MPa corresponding to an entrance pore diameter of 7nm, the smallest pore which can be intruded using this apparatus. Considering the classification of soil pores, intra-element pores cannot be detected using MIP. Due to the presence of montmorillonite in the clays fraction, it is expected that the inter-layer pores in the Bengawan Solo fill would be in the range of 1 - 2nm (Saiyouri et al., 2000).

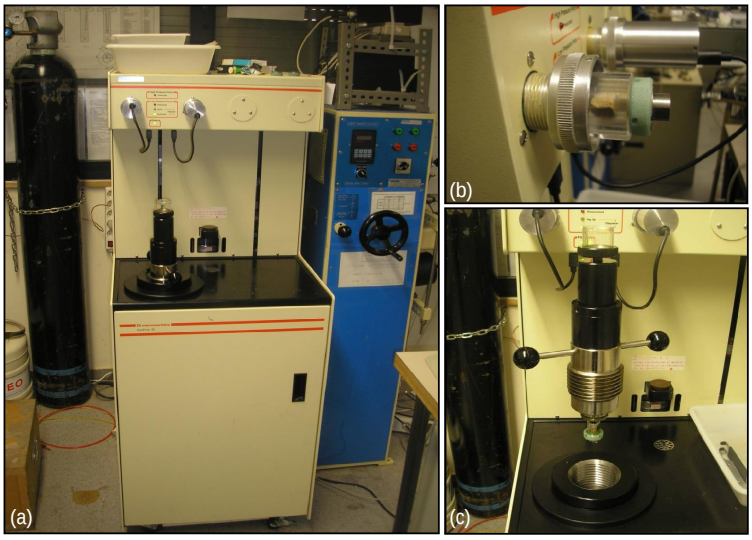

Figure 5.26: MIP Equipment: (a) Micromeritics Autopore IV 9500, (b) low pressure unit and (c) high pressure unit

5.3.6.3 Specimen Preparation

In order to accurately determine the pore size distribution of a soil sample, its pores must be free from water. Oven drying or air drying can cause significant alteration (shrinkage) to the soil structure of samples with clay particles (Ahmed et al., 1974). As such the freeze-drying technique (Delage et al., 1982) has become the standard method of specimen preparation for MIP tests. The samples to be investigated (Table 5.6) were carefully trimmed into cubes measuring approximately 10mm on each side (1cm^3) and were subsequently freeze dried. Freeze drying involves rapid freezing of the specimens to cryogenic temperatures ($<$ -130°C) usually by the direct immersion in liquid nitrogen. This was followed by true vacuum drying to remove water by sublimation at a temperature of between -60°C and -80°C, in order to prevent the formation of water menisci lenses which are responsible for the shrinkage which occurs on drying. After freeze drying the samples were kept in a desiccator until testing.

5.3.6.4 Experimental Methodology

The freeze dried specimen was weighed immediately prior to testing and then placed inside the cup penetrometer (Figure 5.27a). Penetrometer 950-61711-00 was used for all these tests with a bulb volume of 50cm^3. A little grease was smeared around the outer rim of the cup to ensure

a good contact with the penetrometer lid. The lid was then fixed to the cup using the fixing collar and tightening tool. The lid was tightly sealed in order to ensure a vacuum can be created inside the cup. The penetrometer shaft was then placed into the low pressure unit (Figure 5.26b) and the outer metal ring secured tightly. On starting the test, a vacuum is applied to the cup, this is because the mercury pressure applied is in terms of absolute pressure. This vacuum is applied in three steps: first the pressure inside the cup is reduced to 3psi (20.7kPa), then to 900µmHg, (0.1kPa) and finally the pressure is reduced to 50µmHg (effectively 0kPa). The vacuum application stage takes only a few minutes after which mercury is allowed to flow into the penetrometer. The low pressure intrusion stage which involves increasing mercury pressure up to 345kPa lasted approximately 2hours. Once complete the penetrometer was removed from the low pressure unit and the assembly weight of the penetrometer weighed to 4 decimal places before inserting into the high pressure unit (Figure 5.26c). In the high pressure intrusion stage, mercury pressure was increased continuously to 223MPa, lasting typically 12hrs, after which an extrusion cycle followed.

Figure 5.27 presents a specimen (a) before and (b) after mercury intrusion. The specimen taken after testing was cut open to illustrate how the mercury intrudes into the inner pores of the sample. After extrusion some mercury remains trapped in constricted pores. Delage and Lefebvre (1984) proposed that the entrapped or constricted porosity corresponds to the inter-aggregate pore space whereas the free porosity (that which can be extruded) corresponds to the intra-aggregate pore space.

Particular care was taken when dismantling the tests and during the cleaning of equipment to ensure that all of the used mercury was carefully collected and stored for disposal following safety procedures used routinely at UPC.

5.3.6.5 Calculations

The output of the MIP tests are given in terms of pressure p and cumulative intrusion volume $\overline{v}$ (ml/g), which is normalised by the specimen mass M_s. The pore entrance diameter can thus be determined by rearranging Equation 5.8. As the void ratio e in general, refers to the volume of voids V_v expressed in terms of the volume of solids V_s, the intruded void ratio e_{INTR} (void ratio

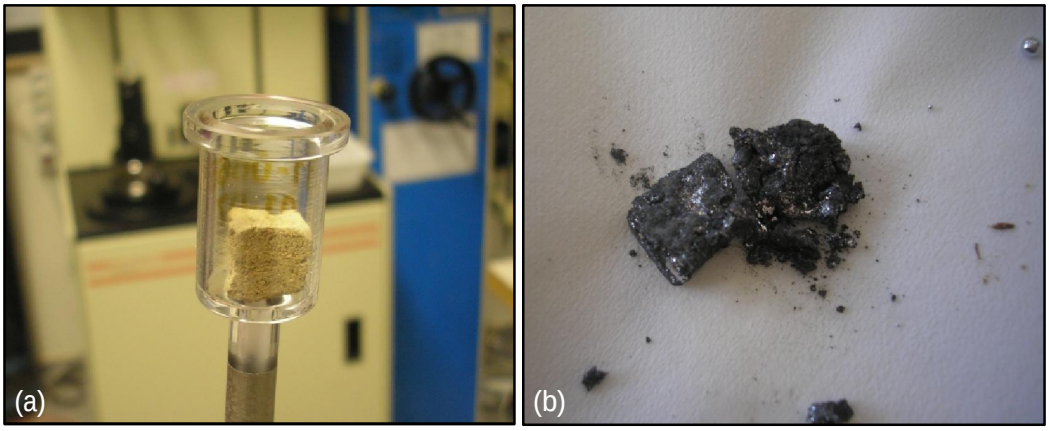

Figure 5.27: MIP samples (a) prior to testing and (b) after testing

of specimen intruded with mercury) can be determined as the product of the particle density ρ_s and the cumulative intrusion volume $\overline{v}$:

$$e_{INTR} = \frac{V_{v(intr)}}{V_s} = \rho_s \overline{v} = \frac{M_s}{V_s} \times \frac{V_{v(intr)}}{M_s} \tag{5.9}$$

As such the intruded porosity n_{INTR} can be determined as:

$$n_{INTR} = \frac{V_{v(intr)}}{V} = \frac{e_{INTR}}{1 + e_{INTR}} \tag{5.10}$$

The degree of saturation of mercury Sr_{nw} is thus equal to:

$$Sr_{nw} = \frac{V_{v(intr)}}{V_{v(total)}} = \frac{n_{INTR}}{(n_{INTR})_{max}} \tag{5.11}$$

Plotting the MIP results against a pore size density function PSD is a useful tool for identifying the dominant pore sizes found within soil specimens. Here the pore size density function was determined as the difference in the intruded void ratio divided by the logarithm of the entrance pore diameter. Calculating the pore size density function in terms of $log\triangle d$ helps to overcome distortions due to the wide range of pore sizes found in specimens, which typically range over several magnitudes (Romero, 1999).

$$PSD = \frac{-\triangle e_{INTR}}{log\triangle d} = \frac{-(e_{i+1} - e_i)}{log(\frac{d_{i+1}}{d_i})} \tag{5.12}$$

5.3.6.6 Results

As discussed above, the void ratio of a specimen intruded during a MIP test may not be similar to its estimated void ratio. In fact the void ratio e of a specimen may be equal to the sum of the maximum intruded void ratio e_{INTR}, the non-intruded void ratio e_{ni} and the non-detected void ratio e_{nd}:

$$e = e_{INTR(max)} + e_{ni} + e_{nd} \tag{5.13}$$

where the non-intruded void ratio is that which cannot be intruded due to the specimen having pores less than 7nm in size (minimum pore size which can be intruded according to pressure capacity of porosimeter, 223MPa), or due to the presence of totally isolated pores and the non-detected void ratio e_{nd}, is the void ratio which cannot be detected due to the presence of very large macropores in the specimen (>450µm). In order to account for this non-detected void ratio, it was thus necessary to first determine the non-intruded void ratio e_{ni}. The non-intruded void ratio was estimated by carrying out an MIP test on a desiccated slurry specimen. This specimen was prepared by first creating a slurry at a moisture content of 70%, and then allowing it to shrink freely until air dried. No cracks appeared during the shrinkage stage, due to the small initial geometry of the slurry sample (7cm x 7cm x 3cm). In this way a very high density sample was prepared with the following initial conditions: $w = 9.2\%$, ρ_d= 2.00Mg/m^3, $e = 0.361$, Sr =6.9%. Subsequently this specimen was freeze-dried. This high density specimen displayed no visible macropores (>450µm) and thus the void ratio of this specimen was considered to be equal to the maximum void ratio intruded $e_{INTR(max)}$ plus the non-intruded void ratio e_{ni}:

$$e = e_{INTR(max)} + e_{ni} \tag{5.14}$$

Figure 5.28 presents (a) the cumulative void ratio intruded and extruded and (b) the pore size density function for the desiccated slurry specimen. The maximum void ratio intruded is highlighted in Figure 5.28a: $e_{INTR(max)}$ = 0.283, thus e_{ni}= 0.078. It is assumed here that the non-intruded void ratio is the same for all specimens of the same material which have been tested using the same MIP equipment. Given that the non-intruded void ratio relates to micropores <7nm, and isolated pores, this void ratio is more dependent on the inherent nature

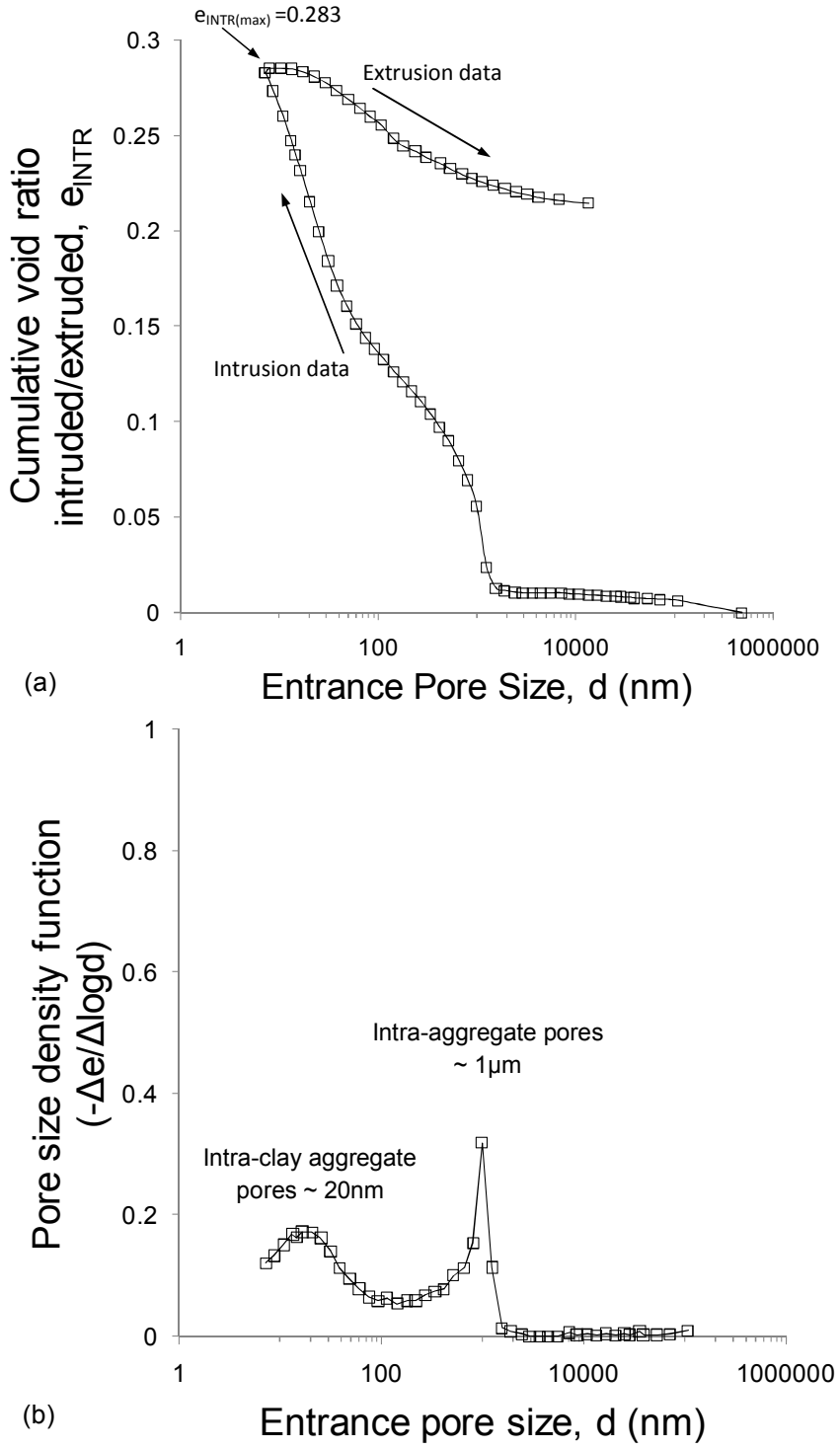

Figure 5.28: MIP results of high density dried slurry specimen (a) Cumulative void ratio intruded and (b) Pore size density function

of the particles rather than their rearrangement, and thus is unlikely to vary greatly for different specimens of the same soil material.

Figure 5.29 presents the cumulative void ratio intrusion and pore density function plots for the three specimens following the process of volumetric collapse: (i) Compacted, (ii) Compacted loaded and (iii) Compacted loaded & soaked. It is interesting to note that for all three samples a pore mode corresponding to 20nm was found. Lloret et al. (2003) and Delage et al. (2006) found similar pore modes for specimens of compacted bentonite from 8-20nm. This pore mode found in all the specimens of Bengawan Solo fill tested, including the dried slurry specimen (Figure 5.28) can be considered to correspond to the intra-clay aggregate porosity, i.e. the pore spaces between clay particles.

From Figure 5.29b it can be inferred that it is likely that the Compacted sample has a bi-modal pore size distribution, but one of the pore modes, corresponding to very large inter-aggregate pores, could not be detected in the MIP, as they occurred at a size $>$ 450μm. An example of a large inter-aggregate pore observed in the compacted sample is presented in Figure 5.30, however macropores as large as 450μm could also not be detected in the ESEM due to the very small specimen size imaged. The presence of these very large inter-aggregate pores indicates the very open structure created during compaction at low density and dry of optimum moisture content. Loading the compacted specimen to 125kPa resulted in a shift in the inter-aggregate pore size to 170μm, into the range detectable using MIP. Moving from the Compacted loaded to the Compacted loaded & soaked specimen resulted in a reduction in the dominant pore size observed from 170μm to 2.1μm. Evidence of these pore sizes found in the corresponding specimens are presented in Figures 5.31 and 5.33. In light of the ESEM images presented, it is evident that there is a shift from an aggregated fabric to a matrix dominated fabric. The shift in pore size can be interpreted as the significant reduction of the inter-aggregate pores as the aggregates become fused and are thus called here intra-matrix pores, the pores present within the matrix of soil particles. Figure 5.23 for the Compacted loaded & soaked specimen shows a distinct absence of inter-aggregate pores. Monroy (2006), similarly found the a reduction in the inter-aggregate porosity and the creation of an intra-aggregate porosity (or inter-arrangement porosity) after wetting loaded specimens. This can be explained by considering that soaking softens the bridging material present at aggregate contacts, causing rearrangement of aggregates

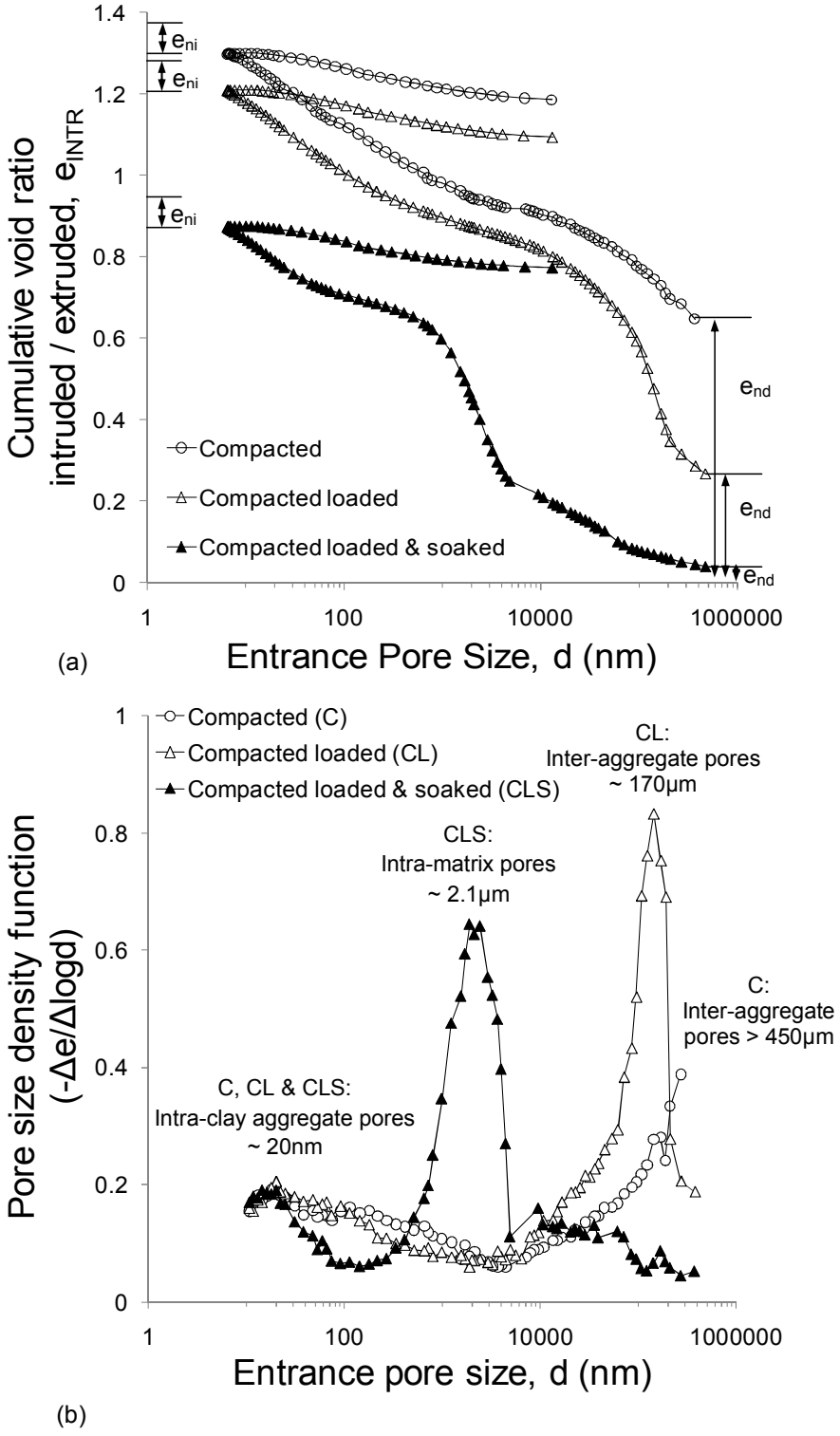

Figure 5.29: MIP results for (i) Compacted, (ii) Compacted loaded, (iii) Compacted loaded & soaked specimens (a) Cumulative void ratio intruded and (b) Pore size density function. Void ratio non-intruded e_{ni}= 0.078 for all specimens. Void ratio non-detected, C: e_{nd}= 0.568, CL: e_{nd}= 0.269, CLS: e_{nd}= 0.050.

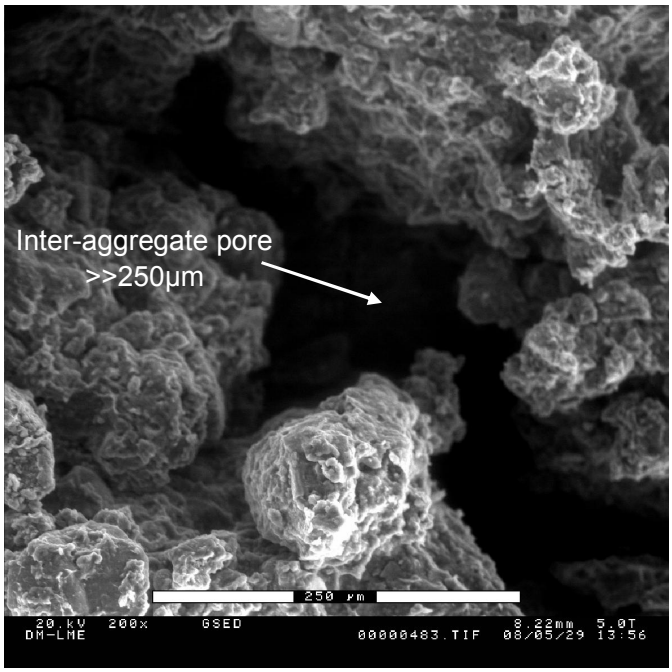

Figure 5.30: ESEM micrograph of an inter-aggregate pore present in the compacted specimen (>> 250µm)

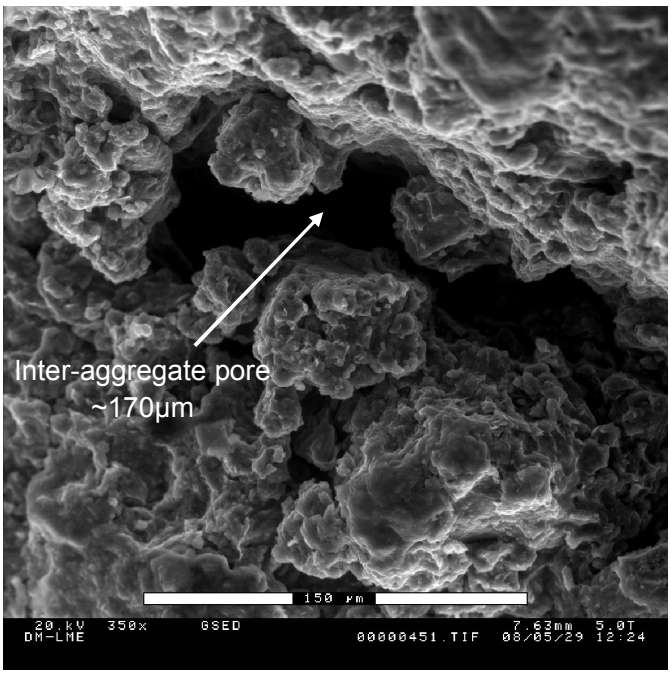

Figure 5.31: ESEM micrograph of inter-aggregate pore present in compacted loaded specimen (~170µm)

to fill inter-aggregate pores. This inter-aggregate porosity is further reduced as the aggregates themselves soften on wetting, and fuse together to form an overall matrix type fabric.

Figure 5.32 presents the cumulative void ratio intrusion and pore size density function plots for (i) the Compacted loaded & soaked specimen and (ii) the undisturbed specimen. It is evident that these specimens show striking similarities, in particular the pore size density function plot indicates that both samples have a dominant pore mode at 2.1μm. Evidence of pores of this size found in these specimens is presented in Figures 5.33 and 5.34. The similarity in the pore sizes found between these specimens further supports the observations made using the ESEM which presented similar fused fabrics for both the Compacted loaded & soaked specimen, and the undisturbed specimen (Figures 5.23 and 5.24).

5.3.7 Summary

The fabric investigation presented here highlights the changes which occur during the process of collapse. A summary of the results are presented in Figures 5.35 and 5.36. The MIP results confirmed the loss of inter-aggregate pores on wetting by indicating that it was responsible for a shift in pore mode from 170μm to 2.1μm. The sample which underwent volumetric collapse on loading and soaking in the laboratory showed a very similar fabric to the undisturbed sample in the ESEM images. The similarity of the microstructure was confirmed by the MIP results which indicated that both samples have the same dominant pore size (2.1μm). It appears from this investigation that it is possible that the undisturbed material sampled at the end of the wet season has already undergone the process of volumetric collapse in-situ under its own self weight.

5.4 Conclusions

In this chapter a series of simple load and soak laboratory tests were carried out on the Bengawan Solo fill material under a number of different initial compaction conditions. These tests highlighted the collapsible nature of this fill material under dry of optimum conditions (Series COA, COB and COC) and in particular when compacted to low dry density (Series COA) at

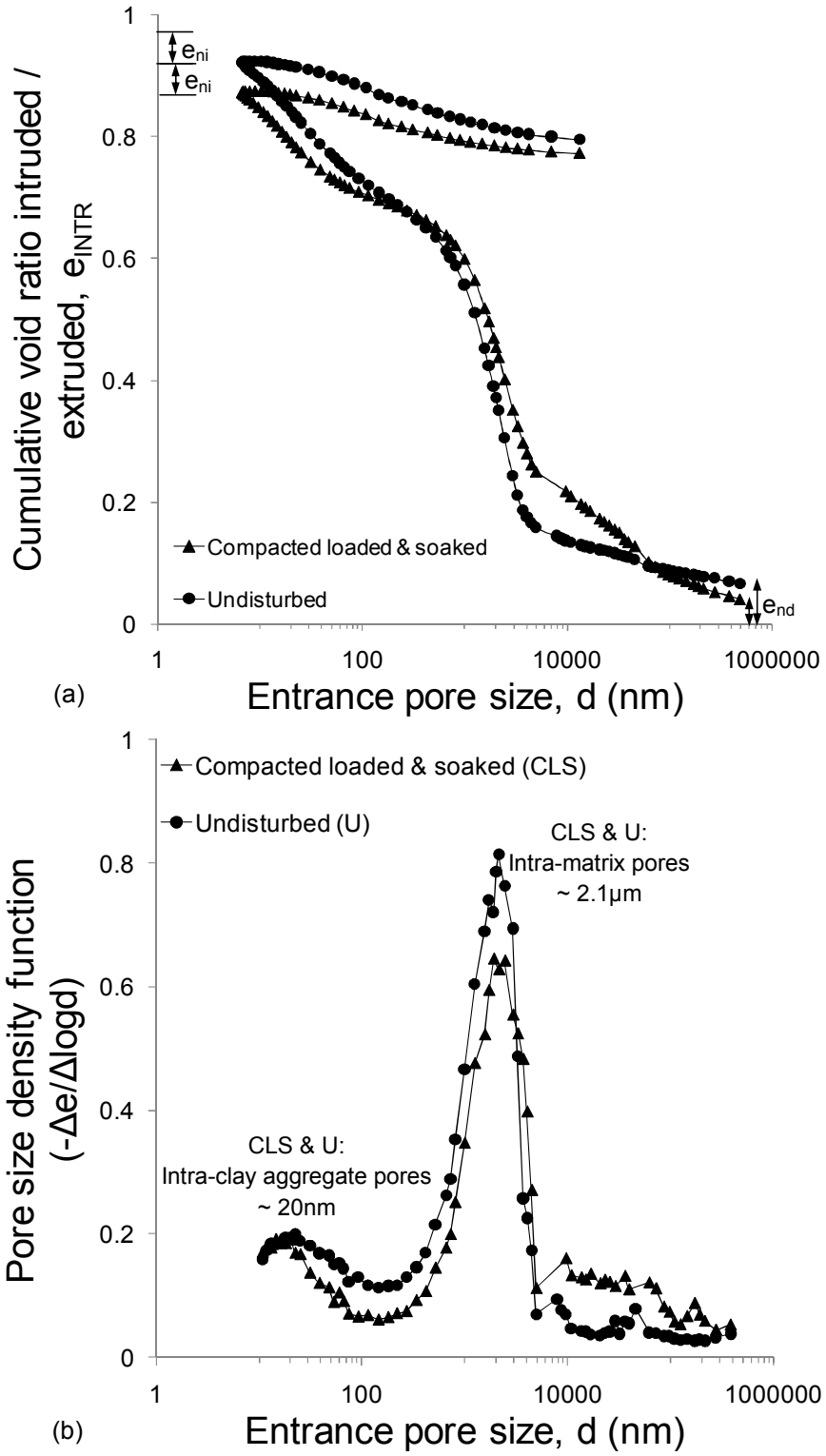

Figure 5.32: MIP results for (i) Compacted loaded & soaked and (ii) Undisturbed specimens (a) Cumulative void ratio intruded and (b) Pore size density function. Void ratio non-intruded e_{ni}= 0.078 for all specimens. Void ratio non-detected, CLS: e_{nd}= 0.040, U: e_{nd}= 0.066

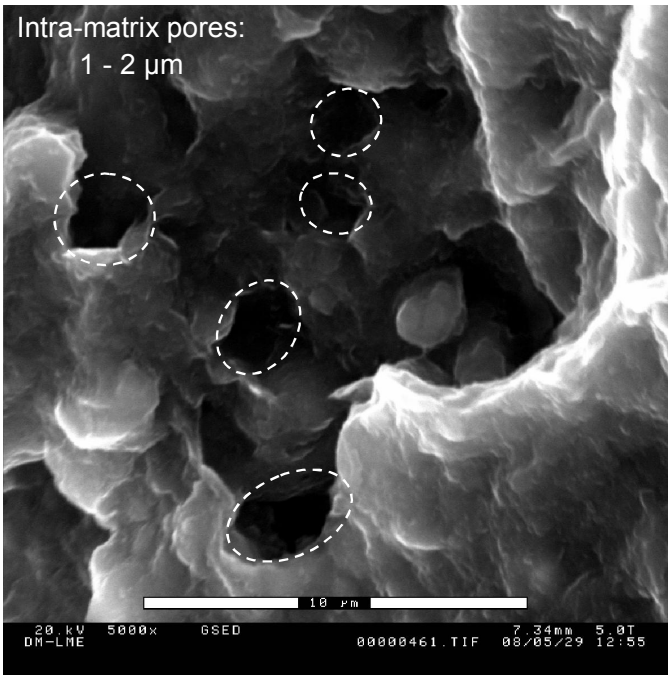

Figure 5.33: ESEM micrograph of dominant intra-matrix pores present in compacted loaded & soaked specimen (~2µm)

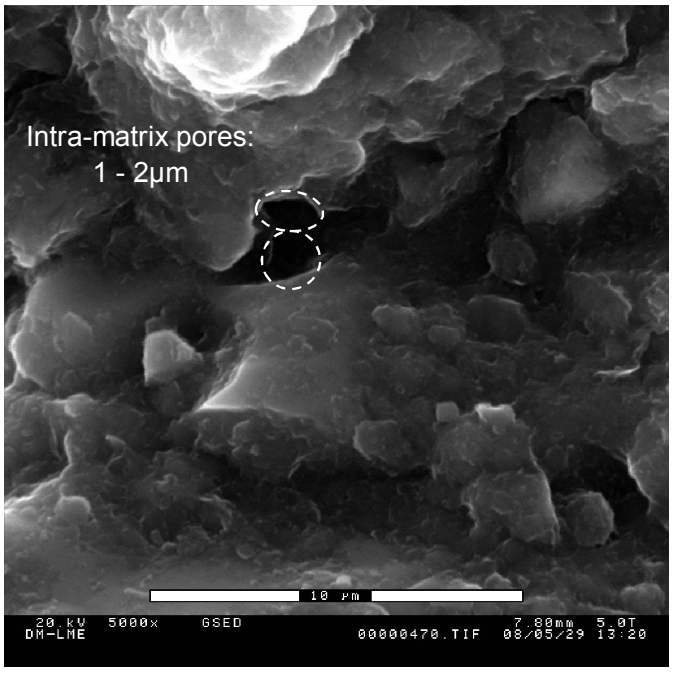

Figure 5.34: ESEM micrograph of dominant intra-matrix pore size present in undisturbed specimen (~2µm)

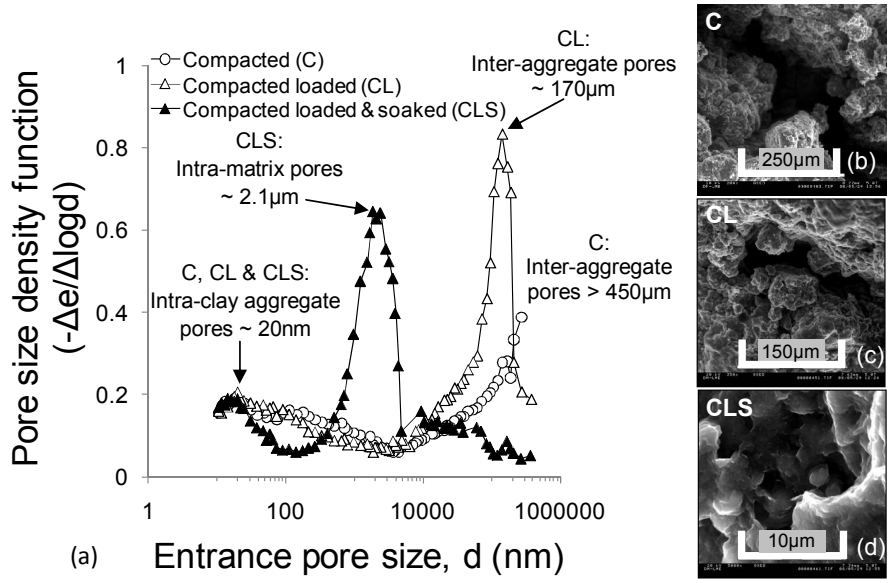

Figure 5.35: Summary of MIP and ESEM information obtained for (i) Compacted, (ii) Compacted loaded and (iii) Compacted loaded & soaked specimens

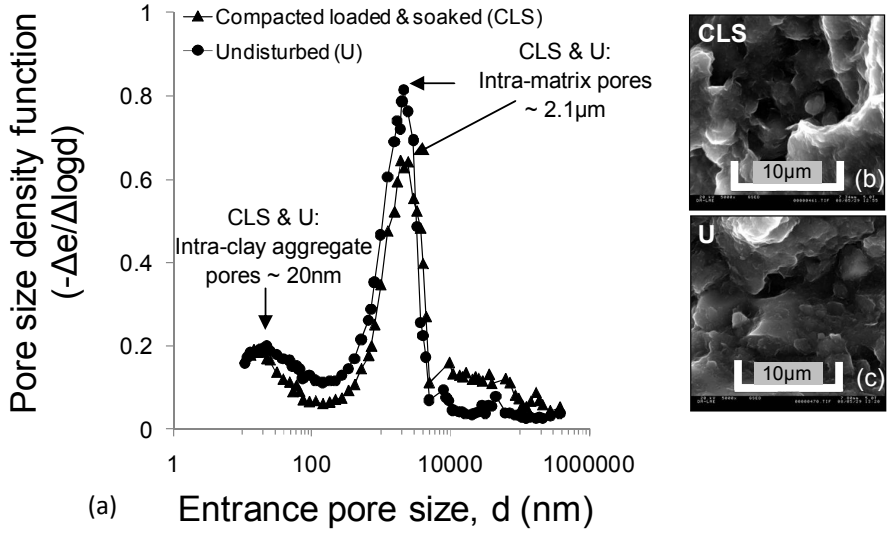

Figure 5.36: Summary of MIP and ESEM information obtained for (i) Compacted loaded & soaked and (ii) Undisturbed specimens

conditions similar to the as-constructed conditions of the Bengawan Solo embankment. Under these conditions collapse behaviour was exhibited under a number of different vertical stresses (32kPa to 538kPa), with maximum collapse occurring at 125kPa. Interestingly significant volumetric collapse was observed in specimens which had been compacted wet and then dried (Series COG), despite an overall reduction in dry density. This suggests that the presence of montmorillonite in this clay induces important structural changes during drying which may be responsible for macroscopic volumetric behaviour.

The oedometer tests were complemented with a fabric study which was carried out in order to identify the changes in soil fabric occurring due to loading and wetting. The ESEM micrographs indicated a reduction in inter-aggregate porosity due to soaking, which was confirmed by the MIP study which indicated that soaking alone was responsible for a shift in pore mode from 170µm to 2.1µm. It is proposed that the soaking process resulted in the softening of aggregations, the loss of strength of bridging material and the loss of the stabilisation due to suction all of which contributed to the formation of a fused uniform matrix type fabric with few inter-aggregate pores. Furthermore results of the fabric study suggest that the undisturbed sample tested may have already undergone the process of volumetric collapse in-situ.

This chapter also presented three possible different failure pathways which propose that volumetric collapse on wetting could play a role in the local or global failure of a flood embankment. In particular this may occur when flood embankments are additionally loaded by the installation of protection measures. These failure pathways have been presented here because although the mechanism is widely known and reported in the geotechnical engineering community, it is not often cited in the literature as a possible failure mode of flood embankments. Furthermore this chapter has demonstrated here how simple conventional load and soak oedometer tests can give an important indication of the collapsible behaviour of fill material under planned construction conditions (or conditions present in the field). It is recommended that these simple tests should be carried out as standard practice before selecting compaction conditions for new flood embankments or particularly as a check in cases where additional loading is to be introduced.

Chapter 6

Isotropic compression and shearing behaviour

6.1 Introduction

One of the main objectives of this research was to investigate the mechanical behaviour of the Bengawan Solo fill material under unsaturated conditions. In this chapter the influence of suction on the volumetric and shearing behaviour of this fill material is explored. Isotropic compression and triaxial (compression) tests were carried out under saturated, suction controlled and constant water content conditions. The experimental equipment used and the experimental procedures followed are described herein. Results of the isotropic compression tests and shearing tests carried out on the Bengawan Solo fill material at different suction levels are then discussed. Some of the experimental data obtained was subsequently used in a routine stability analysis carried out in order to investigate the effect of shear strength reduction upon wetting on the stability of the Bengawan Solo embankments.

6.2 Background

6.2.1 Influence of suction on volumetric behaviour

As briefly described in Chapter 3, Section 3.6.2, suction influences both the preconsolidation stress exhibited by an unsaturated specimen subjected to increasing external load, and also the compressibility of the material post-yielding. Many experimental investigations have confirmed that specimens with a higher suction will exhibit a higher yield stress upon external loading than a similar specimen at a lower suction (e.g. Dudley, 1970; Vicol, 1990; Maâtouk et al., 1995; Wheeler and Sivakumar, 1995).

Initially the influence of suction on preconsolidation stress was typically investigated by carrying out oedometer compression tests on samples compacted at the same initial dry density but at different initial moisture contents (representing varying suction) (e.g. Dudley, 1970). However this type of test does not account for the changes in structure resulting from compacting at different initial moisture contents. Studies have therefore also been carried out with the aim of minimising structural effects in order to better understand the effect of suction (e.g. Vicol, 1990). Vicol (1990) investigated the volumetric behaviour of reconstituted specimens which were brought to different suctions in a suction controlled oedometer, which were maintained constant during loading. The specimens tested therefore had an initial common microstructure but were tested under different suction levels (s=1500kPa, s = 0kPa). With the effects of structure minimised, the results of these tests (Vicol, 1990) did indeed illustrate an increase in preconsolidation stress with increasing suction.

Subsequently increasing experimental evidence to support this influence of suction on preconsolidation stress has been presented by different authors, who have prepared nominally "identical" compacted specimens and then allowed them to equalise under different suction levels before loading isotropically (e.g. Maâtouk et al., 1995; Wheeler and Sivakumar, 1995; Cui and Delage, 1996). Evidence that increasing suction increases the preconsolidation stress has also been presented for undisturbed specimens (e.g. Futai and Almeida, 2005) although it is more difficult to ensure specimens are identical when testing undisturbed material, perhaps due to structural effects. This influence of suction on preconsolidation stress has been incorporated into constitu-

tive models for unsaturated soils in the form of the loading-collapse curve (Alonso et al., 1987, 1990).

The influence of suction on the post-yield compression behaviour of soils is however less clear cut. The one-dimensional compression of the reconstituted samples by Vicol (1990) indicated that the specimen with a higher suction was markedly stiffer than the corresponding saturated specimen, i.e. the slope of the compression line decreased as suction increased. It is this influence of suction which was incorporated into the initial formulation of the BBM (Alonso et al., 1990). However experimental evidence has also been presented which indicates that soil stiffness may reduce with increasing suction, and that this is perhaps more noticeable when comparing the behaviour of saturated specimens and unsaturated specimens at low suction (e.g. Maâtouk et al., 1995; Wheeler and Sivakumar, 1995; Ng and Chiu, 2001). For example the isotropic compression results of compacted speswhite kaolin presented in Wheeler and Sivakumar (1995) indicate an increase in the slope of the normal compression line $\lambda(s)$ with increasing suction up to a suction of 200kPa, after which $\lambda(s)$ decreases. Similarly Ng and Chiu (2001) present results which indicate that $\lambda(s)$ increases (reduction in stiffness) up to a suction of 80kPa, and then decreases for a loosely compacted volcanic fill. Futai and Almeida (2005) observed a continued increase in soil compressibility from saturated conditions to air dried conditions for an undisturbed gneiss residual soil (Figure 3.20).

It is clear that experimental evidence is still required in order to further our understanding of the influence of suction on the stiffness of unsaturated soils. It is anticipated that the results obtained from the isotopic compression tests presented in this chapter can contribute to the existing body of work on the influence of suction on the volumetric behaviour of compacted *natural* soils.

6.2.2 Influence of suction on shearing behaviour

As discussed in Section 3.6.2, it has commonly been observed that an unsaturated soil exhibits a higher shear strength than the same soil under saturated conditions (e.g. Escario, 1980; Escario and Sáez, 1987). This phenomenon has been attributed to the effect of meniscus water at inter-particle contacts which provides an additional normal force and consequently acts to increase

the resistance of the soil to shearing (Figure 3.18). Much of the early research on the shear strength of unsaturated soils primarily focused on the determination of the angle of friction (ϕ') and cohesion (c') at failure. Many of these experiments were carried out using modified direct shear tests (e.g. Escario, 1980). Notably Bishop and Donald (1961) performed suction controlled triaxial tests at an early stage in the development of the field of unsaturated soil mechanics. Also of interest was the variation of cohesion and the angle of friction with suction; in particular shear strength was found to increase non-linearly with suction towards a limiting value of strength (Escario and Sáez, 1987).

The development of the Barcelona Basic Model (Alonso et al., 1990) provided one of the first constitutive models for unsaturated soils which integrated both volume change and shearing behaviour within a framework of elasto-plasticity. Subsequently experimental results were presented which monitored volume changes during shearing, among the first to present such results were Toll (1990); Maâtouk et al. (1995); Wheeler and Sivakumar (1995); Cui and Delage (1996). More recently frameworks, such as those presented by Gallipoli et al. (2003) and Wheeler et al. (2003) have helped to focus attention on the importance of the degree of saturation and its influence on critical state parameters. Among others, Toll and Ong (2003); Jotisankasa et al. (2009); Raveendiraraj (2009) have presented experimental evidence in terms of the degree of saturation. However, despite this progress there still remains a need for more triaxial testing which monitor specimen volume changes and changes in water content during shearing under suction controlled conditions for a wide range of different soils.

6.3 Objectives & experimental campaign

The aim of this experimental campaign was to investigate the isotropic compression behaviour and shearing behaviour of the Bengawan Solo fill material under saturated and unsaturated conditions. The specific objectives were to investigate the influence of suction on (i) yield stress, (ii) post-yield compressibility and (iii) shear strength. In order to span the full range of suction possible, four different levels of suction were investigated: (i) s = 0kPa (saturated conditions), (ii) s = 50kPa (suction controlled conditions), (iii) s = 400kPa (suction controlled conditions) and (iv) initial s ~ 100 MPa (constant water content conditions). The suction controlled tests were

carried out using the axis-translation technique, its implementation in these tests is described in Section 6.5.2.

In the isotropic compression tests, specimens were loaded to 1000kPa (effective or) net stress under constant loading rates (see Section 6.5.5). Triaxial tests were performed at each suction level under three different (effective or) net confining stresses of 25kPa, 100kPa and 300kPa respectively. These stresses were selected to represent confining stresses found close to the crest of the embankment, at the base of the embankment and within the founding layers, respectively.

6.4 Experimental Equipment

6.4.1 Isotropic compression testing equipment

Existing cells available in the civil engineering department were adapted for testing unsaturated soils. Primarily this involved replacing the standard acrylic cell body with an aluminium cell body in order to enable global measurements of the specimen volume change, by reducing expansion of the cell due to the application of cell pressures and avoiding cell volume losses due to absorption, typically found in acrylic cells (e.g. Wheeler, 1986). The aluminium cell body used had an internal diameter of 75mm and a wall thickness of 10mm. The aluminium cell body was fitted between the existing cell base and cell cover with two large flat membranes, and securely tightened with three tie rods, in order to seal the cell at the top and bottom. The main disadvantages of using the aluminium body was that the specimen could not be viewed during testing, and air bubbles which may have become entrained during filling of the cell could not be observed. To minimise the air bubbles entrained, the cell was filled very slowly, taking approximately 15mins to fill the cell. In suction controlled tests, a base pedestal with a high air entry ceramic (15bar) was used, to enable suction control via the axis translation technique (see Section 6.5.2).

The isotropic cell had four connections to the base: (i) Cell pressure line connected to the cell base, (ii) Pore water pressure line connected to the base pedestal, (iii) a second connection to the base pedestal, for flushing underneath the ceramic stone and (iv) Connection to the top

cap, for applying pore air pressure during suction controlled tests, or for applying back pressure during saturated tests. There was a second connection to the top cap available, which was not used in this experimental campaign.

In the isotropic tests the change in volume of the soil specimen under a constant rate of loading was of most interest. Due to the presence of air in unsaturated soil specimens, the volume change cannot be determined solely by the volume changes in the back pressure line. Thus, the volume change in the cell pressure line was recorded (global measurement). However measurements on the cell pressure line require several corrections and are less accurate than those on the back pressure line (Head, 1998). Head (1998) provides a detailed list of the different factors which should be taken into account when making independent volume measurements on the cell pressure line. These include: (i) irregularities on the specimen surface, (ii) air trapped between the specimen and the rubber membrane, (iii) air trapped at top of cell, (iv) expansion of cell walls due to pressure increase, (v) continued expansion of cell walls over time, at constant pressure (creep), (vi) absorption of water into, and migration through, cell body, (vii) leakage of water through piston bushing, through membrane, or from lines and valves, (viii) movement of piston during shearing. The actual volume change of the specimen which is the desired measured quantity, can be attributed to (i) the change in volume of the air voids and (ii) the change in volume due to the movement of water into or out of the specimen. Details of the calibration of the isotropic cell carried out to account for these different effects can be found in Appendix A, Section A.2.1.

Figure 6.1 presents the testing set-up used in the isotropic compression tests. Data from the pore pressure transducer was recorded using the data acquisition pad which was connected to a computer, along with the two pressure-volume controllers via an RS232 multiplexer. Pore air pressure was applied to the top cap of the specimen and was controlled manually by means of a pressure gauge. The system also included a humidity chamber and a flushing system, both of which are explained in further detail in Section 6.5.2. Calibration of the pore water pressure transducer used during the saturated tests and calibration of the air pressure gauge used during suction controlled tests are presented in Appendix A, Section A.2.3. Further information is also given regarding the range and accuracy of the pressure-volume controllers used in the isotropic testing set-up.

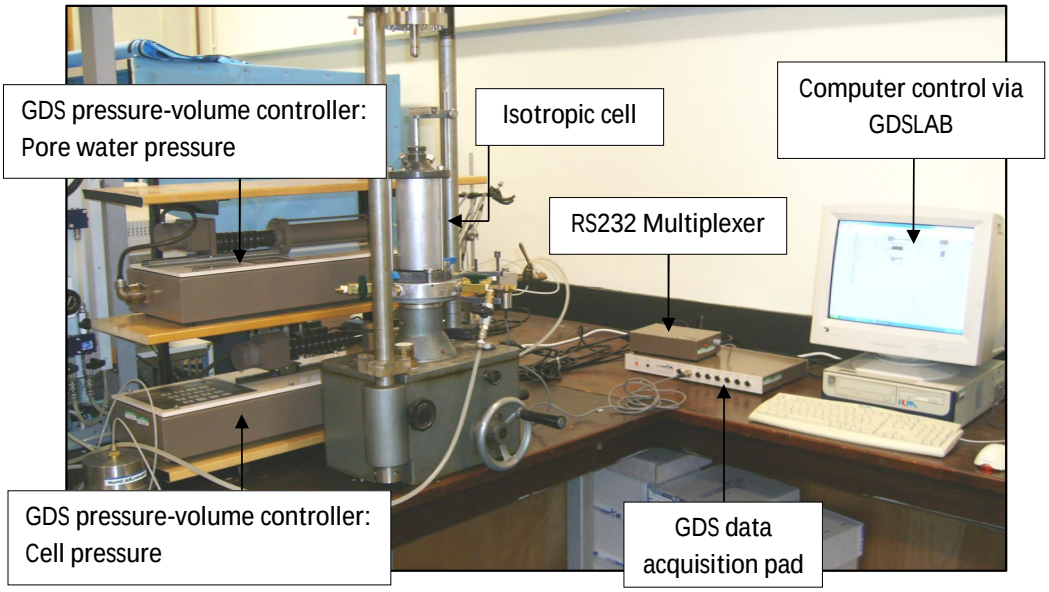

Figure 6.1: Isotropic testing set-up

6.4.2 Triaxial testing equipment

Similar to the isotropic equipment, the triaxial cell was adapted from an existing cell by introducing an aluminium body (10mm thickness) with an internal diameter of 75mm. The aluminium body was secured to the existing cell base and cover using three tie rods and sealed with flat rubber membranes at each end.

The triaxial cell had four connections to the base: (i) Cell pressure line connected to the cell base, (ii) Pore water pressure line connected to the base pedestal, (iii) a second connection to the base pedestal, for flushing underneath the ceramic stone during suction controlled tests (iv) Connection to the top cap, for applying pore air pressure during suction controlled tests, or for applying back pressure during saturated tests. During suction controlled tests a base pedestal with a 15 bar ceramic disc was used in order to control suction using the axis-translation technique.

Preliminary shearing tests indicated that the traditional top cap design was unsuitable for testing the Bengawan Solo fill material, as at the end of the tests the top cap and porous stones lay at a significant angle to the horizontal. This was attributed to the soft nature of this soil, which permitted localised failure to occur directly underneath the top cap. In order to avoid this type

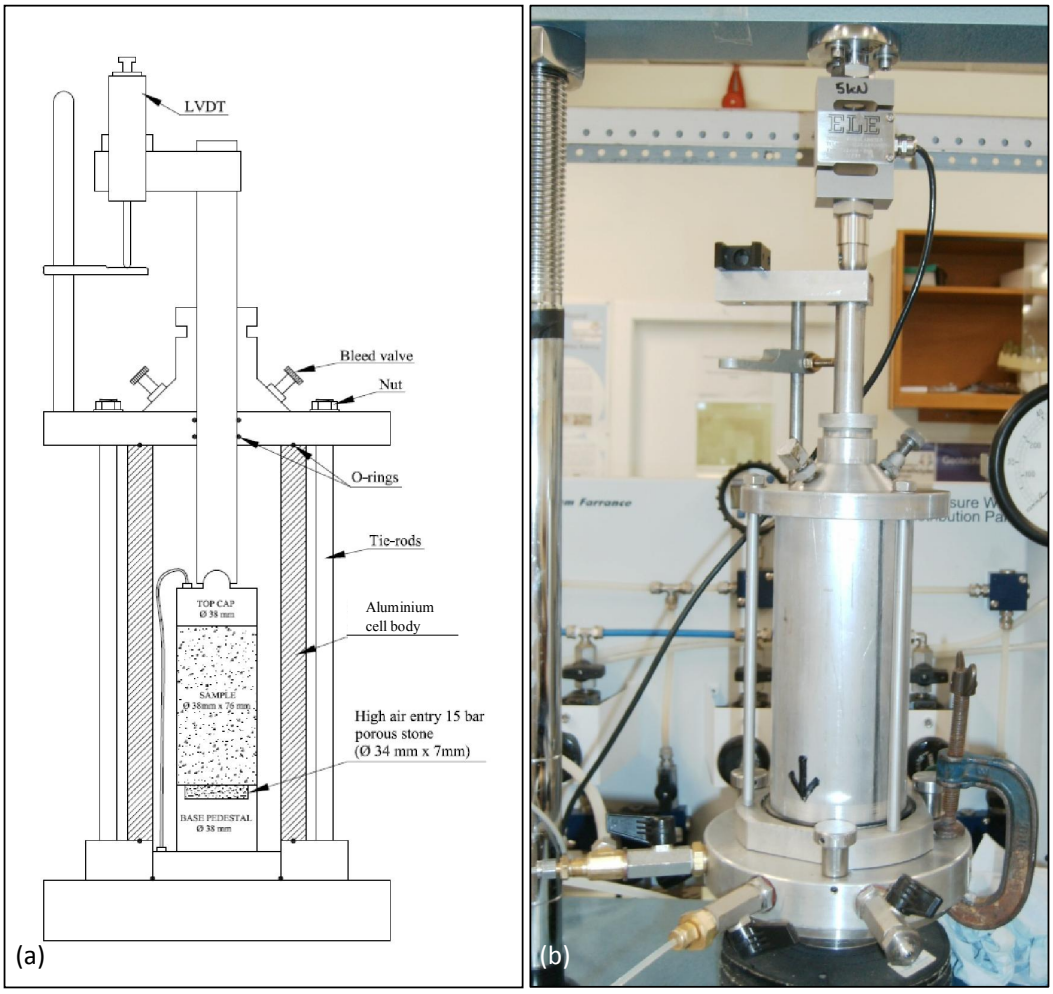

Figure 6.2: (a) Schematic and (b) Photograph of triaxial cell

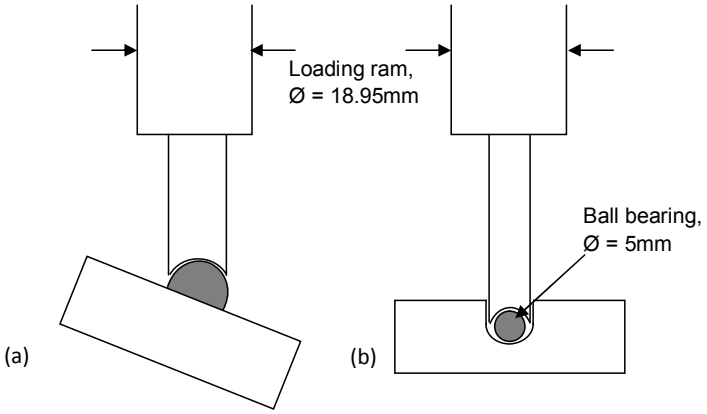

Figure 6.3: Top cap arrangement in triaxial cell (a) existing arrangement, (b) modified arrangement

of failure occurring the top cap design was altered as illustrated in Figure 6.3. In the modified design, a recess was manufactured into the top cap, into which a stainless steel ball bearing was placed. By forcing the loading ram to be inserted into the recess for the transmission of load, the amount of possible rotation of the top cap was greatly reduced (Figure 6.3). This modified design was successful as can be observed in Figure 6.21, all of the specimens appeared to have a fairly horizontal top surface at the end of testing.

Figures 6.4 and 6.5 present the overall triaxial system lay-out. A Wykeham Farrance 50kN Tritech load frame was used to set a constant shearing rate in these tests. Cell pressure was controlled and cell volume monitored using a GDS pressure-volume controller, with a maximum pressure limit of 2MPa. Pore water pressure was also controlled and changes in the water volume entering or leaving the specimen were monitored using a second GDS pressure-volume controller. The volume change of the specimen was determined by monitoring the global changes in the cell volume. The small internal diameter (~75mm) of the triaxial cell, meant that it was unfortunately not possible to introduce internal instrumentation. Pore air pressure was introduced via a port in the top cap during suction controlled tests. The pore air pressure was manually regulated using an air pressure gauge (see Figure 6.5). The pore air pressure was the only variable not monitored or controlled by the computer.

An external ELE s-type load cell, with an upper limit of 5kN was used to measure the axial force acting on the soil specimen. A WF 25mm external linear displacement transducer was used to measure the axial strain of the specimen. During saturated tests, a WF pore water pressure transducer was connected underneath the base pedestal to monitor changes in pore pressure through the specimen. The instrumentation was connected to a GDS 8 channel data acquisition pad, which was connected to the computer via a RS232 serial port. The two pressure-volume controllers used a GPIB bus connection, the load frame was connected to the PC using a RS232 to USB converter connection. All equipment was controlled using GDSLab software, a screen shot of the triaxial set-up can be seen in Figure 6.6.

Details of the calibration of the load cell, linear displacement transducer, pore water pressure transducer and air pressure gauge used in the triaxial testing system are presented in Appendix A, A.3.2. Additionally calibrations was also carried out to account for the effects of uplift pressure when using an s-type load cell.

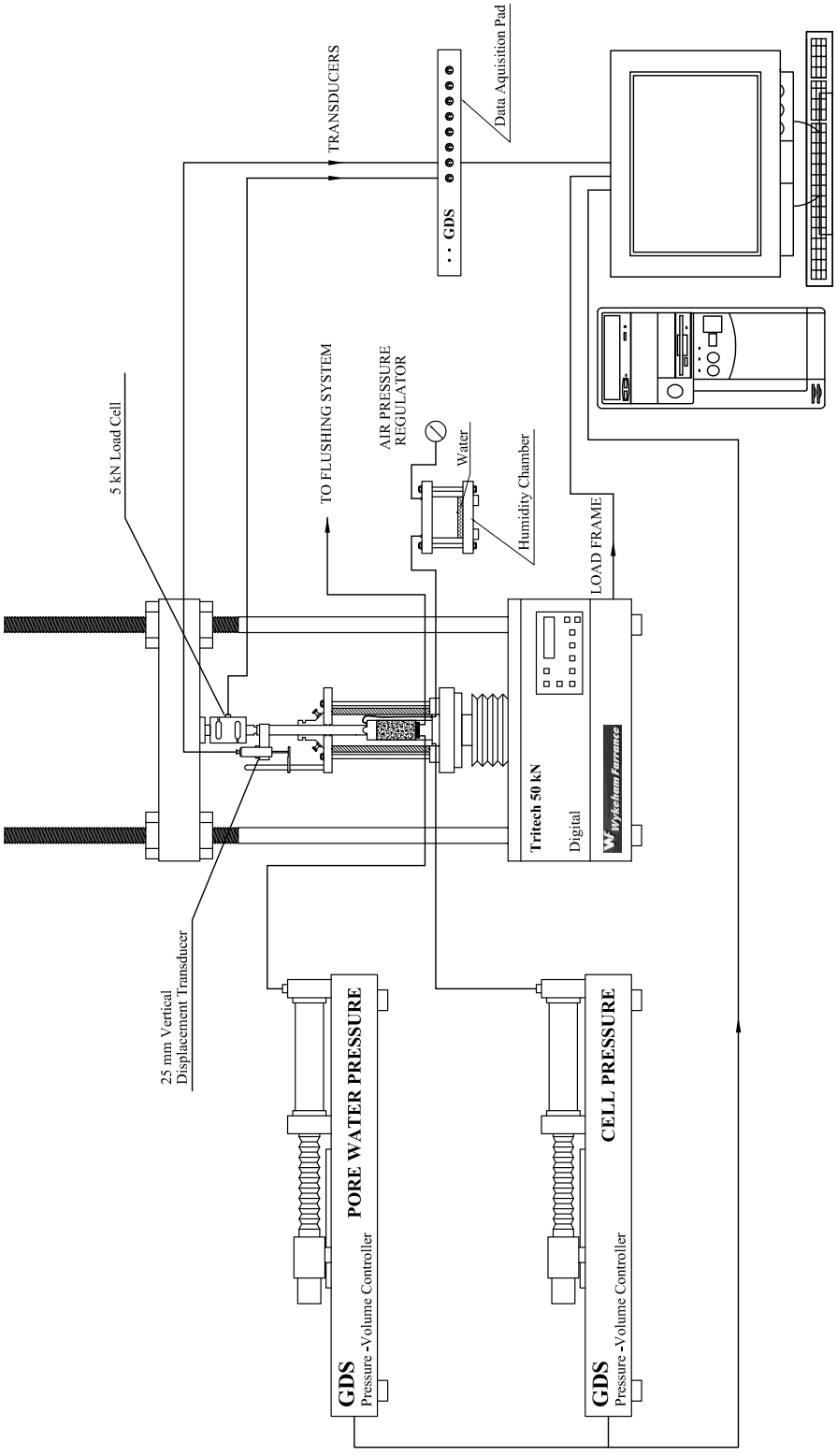

Figure 6.4: Triaxial tests system set-up

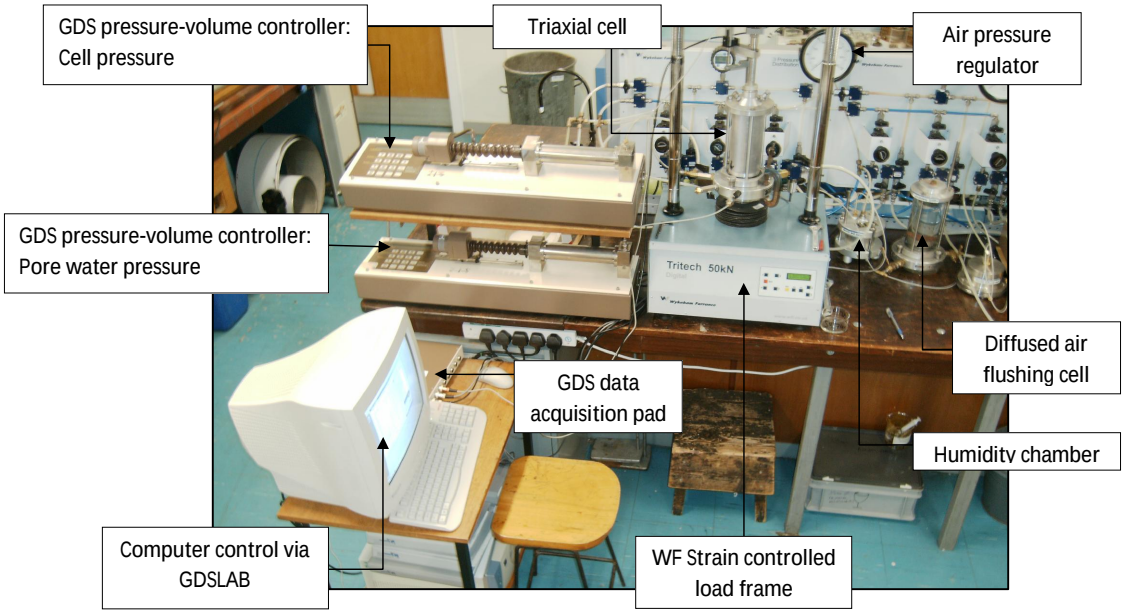

Figure 6.5: Photograph of triaxial system

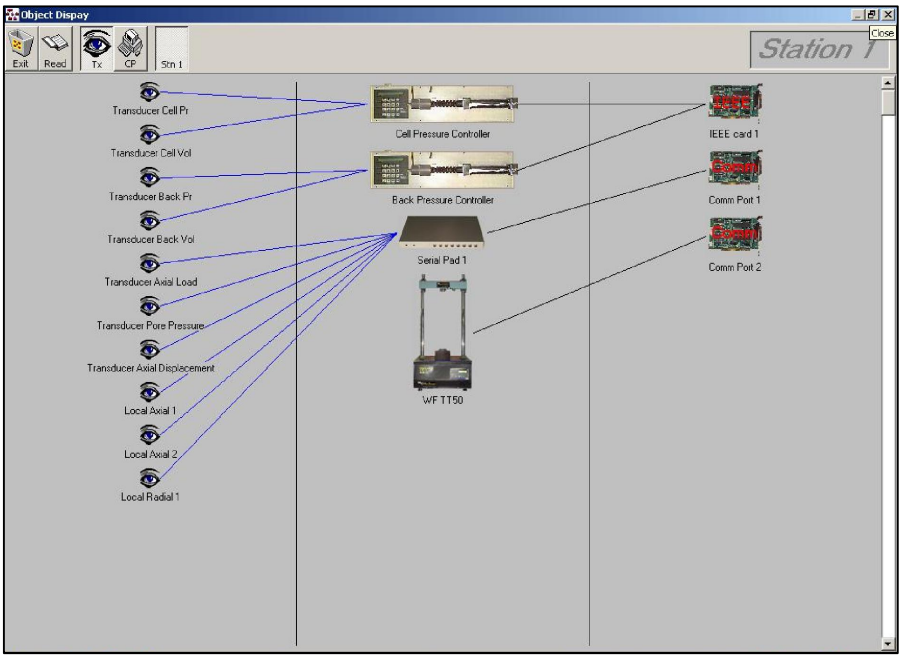

Figure 6.6: GDS Lab software screen

6.5 Experimental Methodology

6.5.1 Specimen preparation

The specimen initial conditions of $w_o = 24\%$ and $\rho_{d_o} = 1.18\text{Mg/m}^3$ ($\rho = 1.46\text{Mg/m}^3$, $Sr = 50.0\%$, $e = 1.31$) were the target initial conditions for all of the tests presented in this chapter. This dry density of 1.18Mg/m^3 was selected as it is similar to the low dry densities found in-situ and also it represents 80% of the BS Light peak density; the embankments were to be constructed at 80% of Proctor density, (Soemitro, private communication, 2006). A moisture content of 24% (4% less than optimum) was selected in order to represent the conditions under which the embankments were constructed, where material removed from the river bed was spread out and left to dry on top of the existing embankments prior to compaction.

Samples were prepared from air dried crushed material which passed the 2mm sieve. This material was then hand mixed with de-aired water in sealable plastic bags (to minimise water losses) to achieve the desired moisture content. Samples were left within the sealed plastic bags, and stored inside sealable plastic containers for at least 24hrs before compaction to ensure the mixed water had distributed evenly throughout the sample.

All specimens were compacted dynamically in a 3 part split mould, with an internal diameter of 38mm to achieve the initial desired conditions. The isotropic specimens were half height specimens with an initial height of 38mm, whereas the triaxial specimens had an initial height of 76mm. The isotropic specimens were compacted in 3 layers using 22g per layer and 8 blows of a small light hammer of mass 334g. The triaxial specimens were compacted in 5 layers using 26.5g per layer and 10 blows of the light hammer. The top of each layer was scarified before adding a new layer in order to ensure there was a good contact between layers. Figure 6.7 presents the equipment used to compact the specimens and illustrates a compacted triaxial specimen. After compaction, three measurements of the initial height and three measurements of the initial diameter were made using vernier callipers (measurement to 0.01mm) and the initial mass of each specimen was recorded to 3 decimal places.

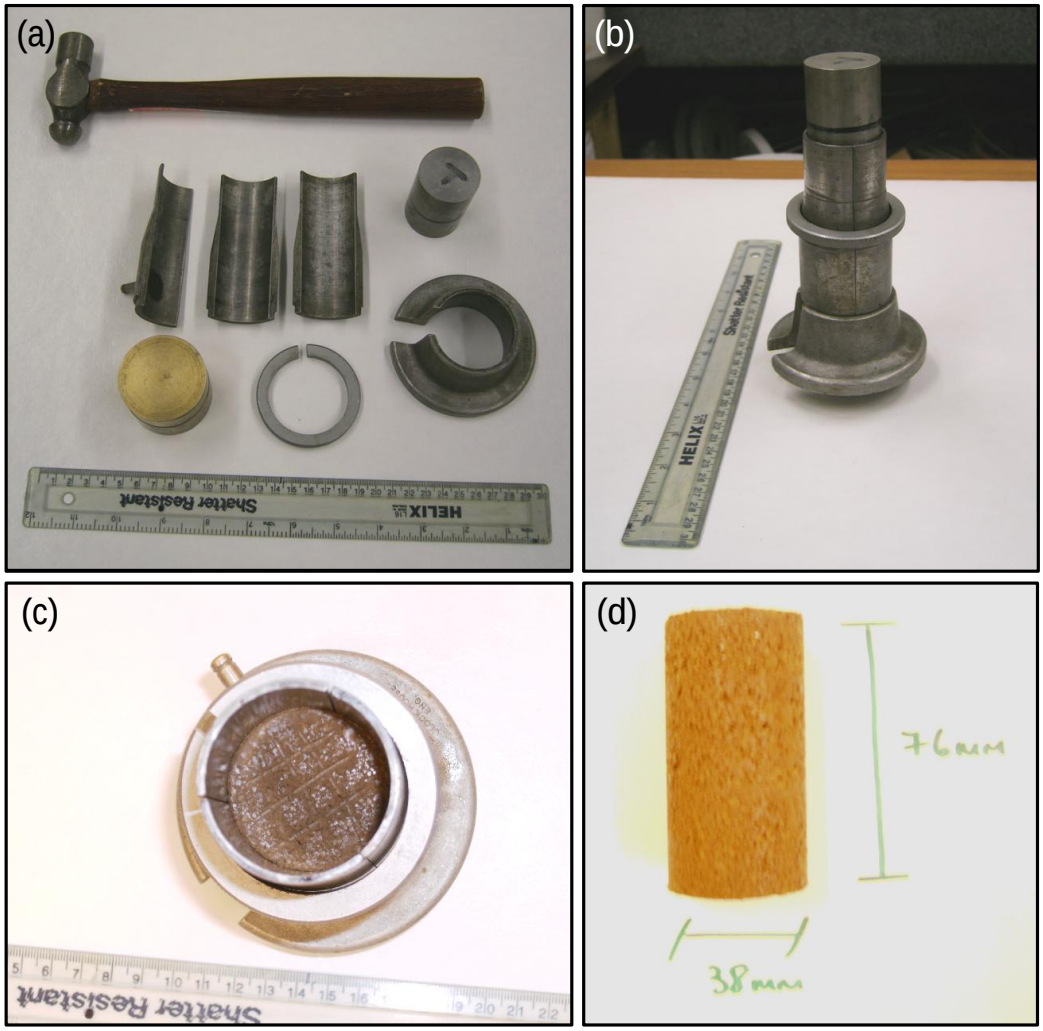

Figure 6.7: Compaction of triaxial specimen (a) Compaction equipment, (b) 3 part split mould, (c) scarification of layers and (d) compacted specimen

6.5.2 Axis translation technique

The axis translation technique was used as the method of controlling suction in both the isotropic and triaxial tests. This method was selected primarily due to the ease of adapting existing equipment in order to implement the technique. This including fitting a standard base pedestal with a 15bar high air entry value ceramic stone (34mm diameter, 7.14mm thickness), with a circular groove machined underneath the stone to aid the flushing of water. A fully saturated ceramic stone provides the necessary barrier to gas flow required to control suction using the axis translation technique (Hilf, 1956). Pore water pressure was applied underneath the ceramic stone using a GDS pressure-volume controller and pore air pressure was applied to the top of the specimen, via the top cap, from a manually controlled air pressure line.

Prior to each suction controlled test the ceramic disc was saturated and the permeability checked in order to ensure no cracking of the stone had occurred. Saturation of the ceramic disc was achieved by applying a water pressure of 1600kPa above the stone while the back pressure underneath the stone was controlled at 0kPa using the pressure-volume controllers. Full saturation was deemed to have been reached once a steady flow through the disc was achieved, and the permeability calculated was equal to the saturated permeability of the stone. The 1500kPa ceramic stone used in the triaxial tests has a saturated water permeability of 5.8×10^{-11} m/s and that used in the isotropic tests has a saturated water permeability of 3.79×10^{-11} m/s (see Figure 6.8), as determined in numerous tests in the laboratory. It should be noted however that these values differ from the saturated permeability of 2.6×10^{-11} m/s proposed by Soil Moisture Corporation for the 15bar ceramic stone (Soil Moisture 2008).

The saturated permeability (k) of the ceramic disc was calculated using Darcy's Law:

$$q = Aki \tag{6.1}$$

where q is the rate of flow (m^3/s), A is the cross-sectional area of the ceramic disc (m^2) (disc diameter is 50mm), and i is the hydraulic gradient (dimensionless) where i is determined as:

$$i = \frac{h_1 - h_2}{L} \tag{6.2}$$

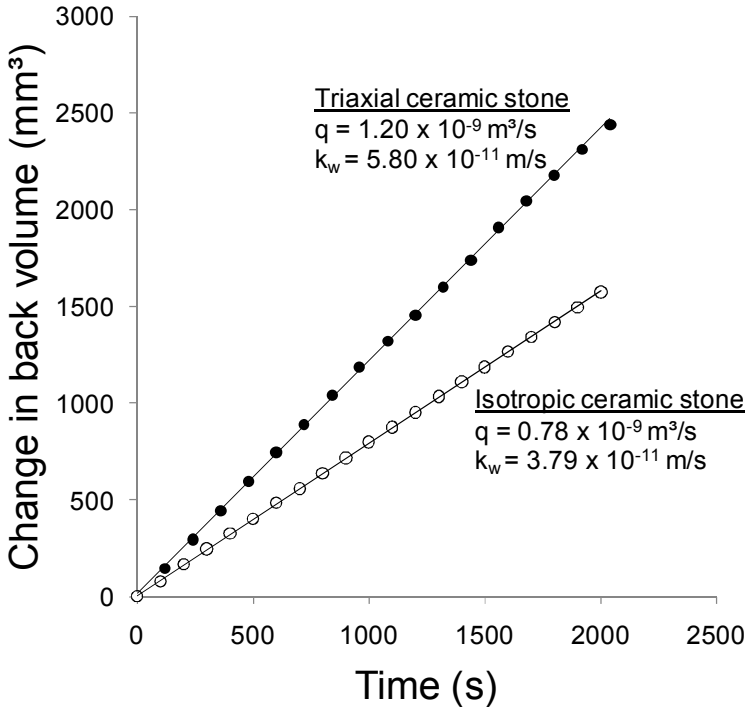

Figure 6.8: Permeability of ceramic stones used in isotropic and triaxial set-ups

where h_1 is the pressure above the disc in terms of water head, h_2 is the water head below the disc and L is the thickness of the ceramic disc (7.14mm).

This disc is a high air entry value ceramic, thus when fully saturated air should not pass through the disc unless an air pressure greater than 1500kPa is applied to its surface. However air may still pass through the disc, even when fully saturated due to the process of air diffusion. Air may dissolve into the pore fluid above the ceramic when under a high pressure and pass through the ceramic. As the pressure below the ceramic is generally lower than that above (in order to apply a matric suction) the air may come out of solution underneath the ceramic. The accumulation of diffused air under the ceramic stone may result in a loss of continuity between the pore water in the soil specimen and the water in the control system, furthermore it may lead to errors in pore water volume measurements during drained tests. The rate at which air may accumulate under the ceramic disc may be described by the following relationship (Fredlund and Rahardjo, 1993; Romero, 1999; Airò Farulla and Ferrari, 2005):

$$\frac{dV_d}{dt} = \frac{nADh(u_a - u_w)}{(u_w + u_{atm})t_c} \tag{6.3}$$

where V_d is the volume of diffused air accumulating under the disc in time t, n is the porosity, A the cross-sectional area and t_c is the thickness of the disc. h is the volumetric coefficient of solubility of dissolved air in water, from Henry's law $h = 0.018$ at 22°C (Henry's law states that the amount of gas which dissolves in a given type and volume of liquid is directly proportional to the partial pressure of that gas in equilibrium with that liquid). u_{atm} is the absolute atmospheric pressure and D is the air diffusion coefficient. Results presented by Airò Farulla and Ferrari (2005) indicate that values of D lie between 3×10^{-11} and 2×10^{-10}m²/s for suctions less than 700kPa. Above 700kPa D increases with increasing suction. For this reason, in these tests, the axis translation technique was not used in the application of suctions higher than 700kPa.

As can be deduced from Equation 6.3, increasing u_w is an effective means of reducing the accumulation of diffused air underneath the ceramic disc. This is the technique recommended by Delage et al. (2008) for minimising air diffusion. Accordingly, the pore water pressure underneath the stone was maintained at a minimum of 200kPa during suction controlled tests. In order to remove any air bubbles which accumulate underneath the ceramic stone, a flushing system was set-up, which was connected to the second port of the reservoir under the porous stone. A separate pressure system involving an air-water cylinder was used for this purpose, which enabled a slightly lower pressure (180kPa) to be applied, for 30s every 2-3 days during testing under suction controlled conditions. This resulted in a flow of water from the pore water pressure source (set at 200kPa) with the aim of flushing out any air bubbles present.

Another factor which should be considered when using the axis translation technique is the influence of the relative humidity of the imposed air. If the relative humidity is low, as is typically the case for air coming from air compressors, alongside the liquid flow through the ceramic disc, (which imposes matric suction), evaporation of the top surface of the soil specimen may also occur (Delage et al., 2008). Jotisankasa et al. (2007) reported a relative humidity value of 5% for dry air coming from a compressor. In order to minimise the effect of this dry air, it was passed through a humidity chamber (Figure 6.5) before entering the isotropic or triaxial cells. Essentially the humidity chamber consisted of a sealed stainless steel cell with an inlet and outlet, within which a height of water of several centimetres was maintained. The dry air coming from the compressor was thus forced to flow across the surface of the water, increasing its relative humidity.

6.5.3 General setting-up procedures

6.5.3.1 Flushing of drainage lines

An ELE de-airing tank was used to de-air tap water under vacuum. All water was de-aired for at least 30 minutes before use in the experimental set-up. Tap water was preferred over distilled water for these experiments due to the potential corrosive nature of de-aired distilled water on membranes and o-rings (Head, 1998). Only de-aired water was used to fill the cells, for flushing drainage lines and pressure transducers prior to testing and for the filling of pressure-volume controllers. The cell pressure and pore water pressure lines were primed before use. Considering that saturation of the high air entry ceramic discs occurred prior to the test set-up it was important to ensure no water remained in the line to the top cap for the suction controlled and constant water content tests, air at a pressure of 200kPa was forced to flow through these connections for 15min to remove any residual water. In the saturated tests the pore pressure transducer was flushed of any air bubbles using the de-airing block in which it was mounted. During this initial set-up, a layer of water was maintained at all times on top of the ceramic disc.

6.5.3.2 Setting a zero datum

Prior to each test, the pressure-volume controllers and pore water pressure (p.w.p.) transducer (saturated tests only) were checked against a zero datum and zeroed if necessary. The air vents at the top of the isotropic and triaxial cells were used as the datum points. The cells were filled with water and the controller responsible for the cell pressure and that for the pore water pressure would be zeroed at the point at which water emerged from the air vent. This was similarly carried out for the p.w.p. transducer (saturated tests only). For the suction controlled tests, this was carried out immediately prior to saturation of the high air entry ceramic disc.

6.5.3.3 Mounting a specimen

In the saturated tests a saturated porous stone was placed onto a conventional base pedestal (2 drainage ports), followed by a filter paper (Whatman No.1) onto which the specimen was

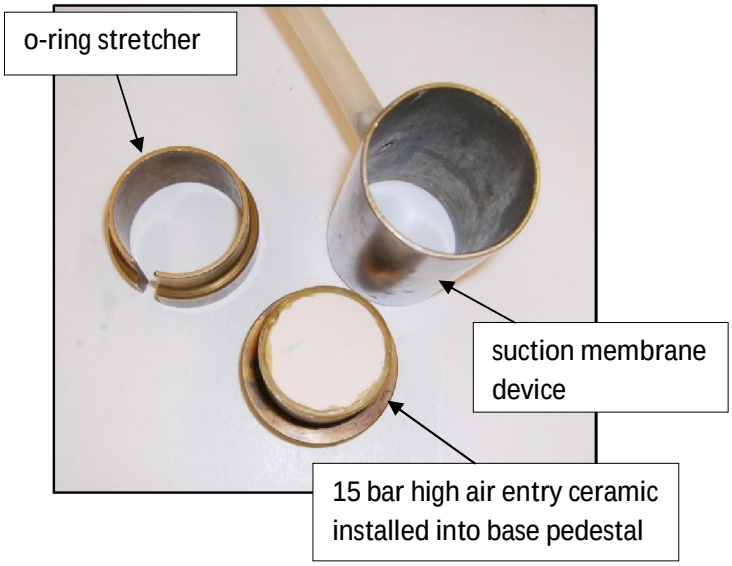

Figure 6.9: Triaxial mounting accessories

placed. In the suction controlled tests specimens were placed directly onto the saturated ceramic surface to ensure a good contact was achieved. The ceramic was lightly sprayed with water before placing the specimen to further ensure a good hydraulic connectivity between the specimen and the ceramic and to prevent drying out of the ceramic surface prior to the start of the test. In the constant water content tests, the high air entry ceramic was left to air dry for several days in the laboratory, to create a barrier to liquid flow.

After mounting the specimen on the base pedestal, latex membranes were placed around the specimens using a suction membrane device, Figure 6.9. Two latex membranes were used for each specimen and new membranes were used in each test to minimise risks due to leaking membranes. For the saturated tests, all membranes, o-rings and porous stones were stored in water overnight before the test. For the suction controlled tests and constant water content tests, dry membranes and porous stones were used. Silicon grease was smeared onto the outside of the inner membrane, before placing the second membrane in order to act as a barrier to water and air flow through the membranes, see Figure 6.10. A filter paper and porous stone was placed on the top of each specimen before attaching the top cap. O-rings were used to seal the soil specimen, two o-rings were placed at the bottom of both the inner and outer membrane to secure the membrane to the base pedestal and one o-ring secured the top of each membrane to the top cap. The o-rings at the top of the specimen were placed using the o-ring stretcher tool

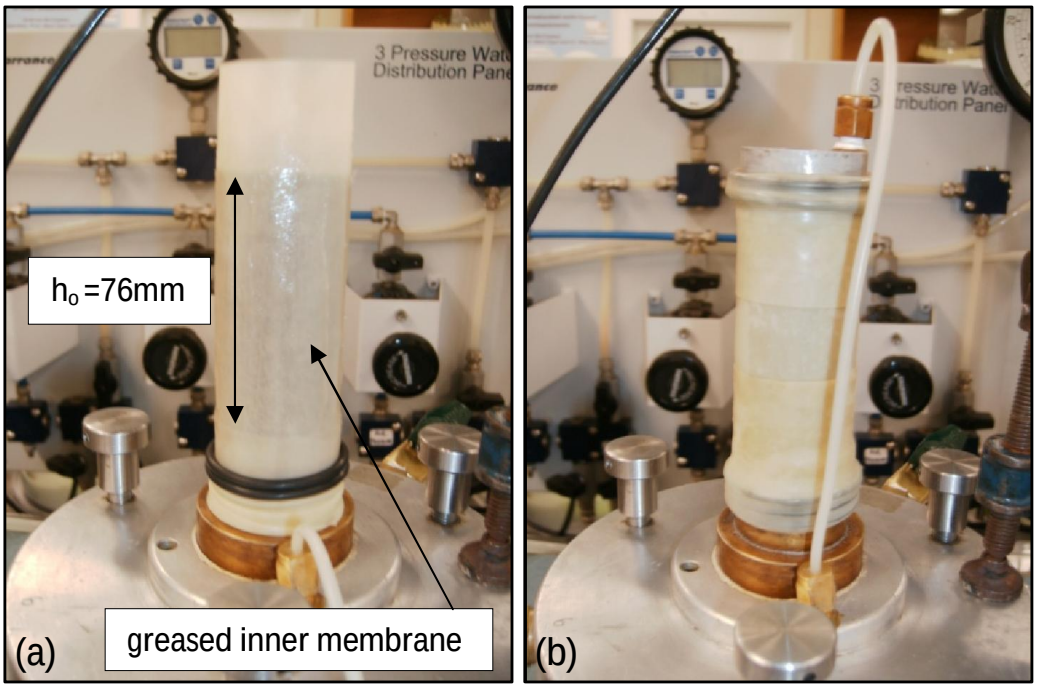

Figure 6.10: Mounting of triaxial specimen

(Figure 6.9). After each test porous stones were cleaned in an ultrasonic water bath to displace any soil particles which may have become clogged. After mounting the specimen, silicon grease was smeared into the groove of the base o-ring before placing the cell body, to ensure a good seal was made and to minimise the trapping of air bubbles. For the triaxial cell, silicon grease was also smeared around the loading ram to prevent any leakages during the shearing stage. With the air vent open the cell was then filled very slowly with de-aired water to minimise the risk of entrapping air bubbles during filling, typically taking 15mins to fill the cell.

6.5.3.4 Loading ram and specimen contact (triaxial tests)

An external s-type load cell was used in the triaxial set-up. As such the uplift force acting on the ram due to cell pressure had to be accounted for. Furthermore it was necessary to apply a nominal contact load of 0.015kN exceeding the uplift force to ensure that contact was maintained between the specimen and the loading ram. Once the specimen was mounted and the cell body in place (air vent still open), the base platen was raised such that an axial force of 0.015kN was measured (q = 13kPa). At this stage the linear displacement transducer mounted on the

crossbar connected to the loading ram, was fixed in place and the zero reading set.

The cell pressure increments which could be applied to the specimen at the beginning of the test also had to be considered in terms of the uplift force acting on the loading ram. Considering the large area of the loading ram (A_r= 282mm^2) and the contact load necessary to maintain contact 0.015kN, cell pressure had to be applied in increments less than 53kPa at the start of the test in order to ensure contact between the loading ram and the specimen was maintained.

6.5.4 Application of suction

6.5.4.1 Saturated tests

In the saturated tests (zero suction), specimens were wetted from their initially unsaturated compacted state in the isotropic or triaxial cell by circulating water from under the (conventional) base pedestal to the top of the specimen. During circulation the pore water pressure applied was maintained at 8kPa, the cell pressure at 15kPa and the top of the specimen was open to atmospheric pressure. Water was circulated until the rate of volume of water exiting the specimen via the top cap (measured by mass) was approximately equal to the rate of water entering the specimen under the base pedestal (determined from the pressure-volume controller). This was generally achieved in 15-20mins. Following this stage, pore water pressure was introduced via the top cap and the valve to the pore water pressure transducer (connected to the second port of the base pedestal) was opened. The cell pressure and pore water pressure were then ramped simultaneously to pressures of 210kPa and 200kPa over a period of 30mins. After these two saturation stages, B values $>$ 0.97 were typically achieved, where B is equal to the change in pore water pressure (measured by the p.w.p. transducer) over the change in cell pressure (Skempton, 1954).

6.5.4.2 Suction controlled tests

The limitation regarding the application of initial pressure increments ($<$53kPa) to ensure contact is maintained between the loading ram and specimen, became particularly significant in

the suction controlled tests, with elevated pore air and pore water pressures. Cell pressure was increased in increments of 15kPa controlled by the GDS Lab software. For each step, the axial force required to overcome the uplift force and maintain contact with the specimen was determined experimentally a priori and fed into the GDS Lab software. After each cell pressure increment the pore air pressure applied to the specimen was increased manually via the air pressure regulator, also in increments of 15kPa, with never more than a mean net stress of 20kPa applied between steps. This could correspond to up to as many as 40 steps to achieve the required initial stresses. Once the desired cell pressure and pore air pressures had been reached, then the pore water pressure under the base pedestal was raised. The pore water pressure was the last pressure to be applied and the first to be removed at the end of the test in order to ensure no high pressure differential existed across the ceramic disc from bottom to top which could cause it to crack.

Preliminary tests on the use of the axis-translation technique for suction control within the Bengawan Solo fill material highlighted difficulties related to wetting the specimens. Due to the open (low density) structure prepared by compaction, the material could not draw water up from the ceramic stone easily. After a few days of applying suction to the specimen, rates of water uptake had dropped to 0.0004mm^3/s. In order to wet the specimen sufficiently to reach a suction of 50kPa, (an addition of approx. 4.5cm^3 to the initial compacted specimen), would take 126 days to achieve (almost 4.5 months). To minimise this time an initial wetting stage was applied where $u_a - u_w$= -15kPa, i.e. a positive pore water pressure was applied underneath the ceramic stone (rate of water transfer to specimen equal to approx. 0.0144mm^3/s. Once the specimen had been wetted sufficiently, (up to 7 days for s= 50kPa) the pore water pressure was reduced to give the desired suction levels ($u_a - u_w$= 50kPa or 400kPa) and the suction allowed to equalise throughout the specimen. In summary for the suction controlled tests, suction was applied by subjecting the specimens to an initial wetting stage followed by a subsequent drying stage, to achieve an overall net wetting of the specimen.

6.5.4.3 Constant water content tests

Constant water content tests were carried out on air dried specimens in order to investigate the soil behaviour under the maximum suction considered in this study. The compacted specimens

prepared at w_o= 24% and ρ_{d_o}= 1.18Mg/m^3 were left to dry in the laboratory for a minimum of five days until a constant water content was obtained (w ~ 6%). Referring back to the soil water retention curves presented in Chapter 4, Figure 4.18 obtained using the chilled-mirror psychrometer, a moisture content of 6% (achieved by air drying in the laboratory) for a specimen with similar initial compacted conditions (Series CM03), corresponds to a suction of 100MPa.

6.5.5 Isotropic loading

In the isotropic compression tests, the radial stress (cell pressure) was continuously increased at constant suction (for s=0, 50 and 400kPa) and at constant water content for the air dried specimens. It may be preferable to carry out all the tests at the same constant rate of loading but for unsaturated soils this can result in inefficient testing campaigns. Mainly this is due to the fact that excess pore air pressure can dissipate at a rate up to fifty times faster than excess pore water pressure (Romero, 1999). Thus it is important in the selection of loading rates to consider if water or air drainage will be the dominant process; this is largely dependent on the degree of saturation of the specimens to be compressed. For this material it was considered that for specimens with $S_r > 85\%$, water drainage dominates, whereas for $S_r < 85\%$ air removal dominates. In suction controlled tests the presence of the ceramic disc directly below the specimen increases the drainage length and also has an impedance effect on water drainage. Different constant rates of loading were thus selected according to the degree of saturation of the specimen to be loaded. The different rates of loading selected are listed in Table 6.3.

In the triaxial tests the desired effective or net radial stress was applied in a single step loading and thereafter allowed to consolidate. For the saturated tests, this loading step was applied after saturation of the specimen (s = 0kPa). Similarly for the constant water content specimens, this was conducted after the specimens were air dried (initial s ~ 100,000kPa). However for the suction controlled tests, the cell pressure required to give the desired net radial stress was applied immediately prior to the suction application stage and thereafter allowed to equilibrate. Thus for these tests the volume changes due to suction application and equalisation and those due to consolidation processes cannot be distinguished. Results from the load and soak oedometer tests presented in Chapter 5 (Figures 5.6, 5.7 and 5.8) verify that the net volume change experienced by the Bengawan Solo fill material is the same irrespective of whether the material is wetted

Table 6.1: Rates of shearing used by various authors in controlled suction triaxial tests where drainage length was equal to H (After Delage, 2002)

Author	Soil	Shearing rate (μm/min)
Bishop and Donald (1961)	Braehead silt	2.13
Gulhati and Satija (1981)	Dhanauri clay	6
Ho and Fredlund (1982)	Silty sand	1.43
Wheeler and Sivakumar (1995)	Speswhite kaolin	1.4
Rampino et al. (1999)	Silty sand	1.27
Futai and Almeida (2005)	Residual gneiss	5

and then loaded or loaded first and then wetted, suggesting stress path independency. It is for this reason that it was decided in these tests to set the required net radial stress first and then immediately after to follow the initial wetting path to apply suction, in an attempt to reduce test durations. Although it is recognised that this involved sacrificing additional information which could have been obtained from these tests. This additional information was however obtained in the isotropic compression tests which were carried out at the same suction levels.

6.5.6 Shearing stage (triaxial tests)

Without the benefit of suction measurement, it is not possible to know if the imposed suction is the actual suction within the soil specimen during shearing. It is thus difficult to estimate an appropriate strain rate. In all of the triaxial tests presented herein, shearing of the Bengawan Solo fill was carried out at a constant shearing rate of 5μm/min (0.007%/min). This shearing rate was selected based on rates used by various authors for suction controlled tests, where the drainage length was equal to the length of the specimen, as used in this experimental campaign, see Table 6.1.

Table 6.2 presents the drainage conditions during suction equalisation, consolidation and shearing for the different tests conducted. In the saturated and suction controlled tests the pore water or pore air and pore water was permitted to drain. However in the constant water content tests, no drainage of the pore water was permitted, only pore air drainage was permitted. Fully undrained tests (no drainage of pore air or pore water) were not carried out due to the difficulty of ensuring there is no pore air drainage through the latex membrane. For all of the triaxial tests presented herein cell pressure was maintained constant during shearing.

Table 6.2: Drainage conditions during suction equalisation, consolidation and shearing stages

	Drainage	
	Pore air pressure	Pore water pressure
Saturated tests	N/A	Yes
Suction Controlled tests	Yes	Yes
Constant water content tests	Yes	No

6.6 Calculations

In a triaxial test with a cylindrical specimen it is generally implicitly assumed that the axial stress σ_a is equal to the major principal stress σ_1, and that the radial stress σ_r, the all-round pressure applied to the specimen by the cell pressure, is equal to the intermediate principal stress σ_2 and equal to the minor principal stress σ_3, such that the mean total principal stress p is equal to:

$$p = \frac{\sigma_a + 2\sigma_r}{3} \tag{6.4}$$

For saturated tests, the mean effective stress p' is equal to $p - u_w$. For unsaturated tests, the mean net stress $\overline{p}$ is equal to $p - u_a$. The deviator stress q is equal to the axial stress applied in excess of the radial stress and because it is defined as the difference between two stresses its value is the same irrespective of whether total or effective stresses are considered:

$$q = \sigma'_a - \sigma'_r = \sigma_a - \sigma_r \tag{6.5}$$

In the tests presented in this chapter, the GDS data acquisition system was used to record automatically the following readings and measurements every 2 minutes: Time from start of tests, time from start of stage, cell pressure, pore water pressure, flow of water into cell, flow of water into specimen, load cell reading and axial displacement. Only pore air pressure was required to be recorded manually. From these raw data values, deviator stress q, mean effective stress p', mean net stress $\overline{p}$ (unsaturated tests), specific volume v and degree of saturation can be calculated as outlined below.

In order to calculate the axial force F applied to the specimen, it is necessary to also consider the force applied to the specimen by the cell pressure applied within the cell and the uplift force

acting on the load cell due to the use of a non-submersible load cell :

$$F = LC + \sigma_r(A_s - A_{ram}) \tag{6.6}$$

where LC is the load cell measurement, A_s is the cross-sectional area of the soil specimen and A_{ram} is the cross-sectional area of the loading ram. The axial stress σ_a acting on the specimen is equal to:

$$\sigma_a = \frac{F}{A_s} = \frac{F}{(V_o - \Delta V)}(H_o - \Delta H) \tag{6.7}$$

where H_o is the height of the specimen at the beginning of the test stage, $\triangle H$ is the axial displacement since the beginning of the test stage, V_o is the volume of the specimen at the beginning of the test stage and $\triangle V$ is the change in volume of the specimen since the beginning of the test stage. In this way the change in cross-sectional area due to barrelling during shearing is accounted for by considering the progressive changes in height and volume of the specimen.

The measured deviator stress (q_m) can then be determined from the difference of the calculated axial stress and radial stress applied to the specimen (Equation 6.5). This value however should be corrected for the effects of the rubber membranes surrounding the specimen. In these tests two rubber membranes, each 0.2mm thick were used, thus the membrane correction (q_{mem}) given in BS1377-8:1990 was adjusted accordingly by the multiplication factor given by Head (1998):

$$\frac{38}{D} \times \frac{t}{0.2} \tag{6.8}$$

where D is the diameter of the specimen and t is the total thickness of the membranes used to enclose the specimen. Thus a value of q_{mem} equal to 0.3kPa at 1% axial strain was used for the membrane correction and the corrected deviator stress was determined as follows:

$$q = q_m - 100\frac{\triangle H}{H_o}q_{mem} \tag{6.9}$$

The mean effective and mean net stresses were calculated as follows:

$$p' = (\sigma_r - u_w) + \frac{q}{3} \tag{6.10}$$

$$\bar{p} = (\sigma_r - u_a) + \frac{q}{3} \tag{6.11}$$

and suction determined as the excess of pore air pressure over pore water pressure applied to the specimen:

$$s = u_a - u_w \tag{6.12}$$

The specific volume v and degree of saturation S_r of the specimens during testing was determined as:

$$v = \frac{\rho_s(V_o - \triangle V)}{M_s} \tag{6.13}$$

$$S_r = \frac{V_w}{V_v} = \frac{\frac{M_w}{\rho_w}}{V - V_s} = \frac{\frac{1}{\rho_w}(M_o - M_s) - \triangle V_w}{(V_o - \triangle V) - \left(\frac{M_s}{\rho_s}\right)} \tag{6.14}$$

where ρ_s is the particle density of the Bengawan Solo fill (2.72 Mg/m^3), M_o is the mass of the specimen at the beginning of the test, M_s is the mass of solids within the specimen as measured by oven drying at the end of the test, ρ_w is the density of water at 20°C (0.99 Mg/m^3), $\triangle V_w$ is the change in pore water volume since the start of the test.

6.7 Results & discussion

6.7.1 Specimen conditions

Table 6.3 presents the conditions of all the specimens tested measured immediately after compaction and at the end of testing.

Despite using dynamic compaction to prepare the isotropic and triaxial specimens, relatively similar initial conditions were achieved in all the test specimens. The average initial moisture content and dry density of all the specimens immediately after compaction was 23.9% ±1.2, 1.19Mg/m^3 ±0.02 respectively. The average initial specific volume and degree of saturation of the specimens immediately after compaction was 2.288 ±0.044 and 50.5% ±1.8 respectively. The ranges achieved are similar to those reported by Raveendiraraj (2009) who used static compaction to prepare specimens of speswhite kaolin. Figure 6.11 presents the variation in

Table 6.3: Conditions of isotropic and triaxial specimens measured after compaction and at the end of testing

Test Ref.	Testing Condition	Suction (kPa)	σ_3' or $\sigma_3 - u_a$ (kPa)	CRL (kPa/hr)	Conditions after compaction				Conditions at end of test			
					w (%)	ρ_d (Mg/m^3)	v	S_r (%)	w (%)	ρ_d (Mg/m^3)	v	S_r (%)
I1	SAT	0	-	2	23.6	1.18	2.297	49.6	27.3	1.56	1.746	99.5
I2	SC	50	-	2.2	24.1	1.20	2.267	51.7	23.9	1.53	1.784	83.8
I3	SC	400	-	10	23.5	1.18	2.311	48.7	22.5	1.50	1.810	75.6
T1	SAT	0	25	-	23.1	1.21	2.244	50.4	35.5	1.40	1.940	99.7
T2	SAT	0	100	-	24.0	1.19	2.290	50.6	30.9	1.51	1.799	99.8
T3	SAT	0	300	-	23.0	1.21	2.257	49.9	27.5	1.55	1.750	99.1
T4	SC	50	25	-	24.6	1.18	2.296	51.6	27.8	1.38	1.979	74.8
T5	SC	50	100	-	25.1	1.17	2.315	51.9	27.0	1.49	1.830	88.3
T6	SC	50	300	-	23.9	1.18	2.298	50.2	25.0	1.56	1.739	91.9
T7	SC	400	25	-	23.1	1.21	2.244	50.4	23.3	1.28	2.127	56.1
T8	SC	400	100	-	23.9	1.19	2.281	50.7	23.4	1.41	1.932	69.6
T9	SC	400	300	-	23.9	1.20	2.274	51.0	22.4	1.58	1.719	84.8
T10	CW	100,000‡	25	-	24.4	1.17	2.327	49.9	7.5	*	*	*
T11	CW	100,000‡	100	-	24.2	1.18	2.309	50.3	6.9	*	*	*
T12	CW	100,000‡	300	-	24.2	1.18	2.310	50.2	8.0	1.35	2.011	20.2

SAT - Saturated, SC - Suction controlled, CW - Constant water content
CRL - Constant rate of loading employed in isotropic compression tests
‡Approximate initial suction
*Not possible to determine as large portion of the specimens crumbled during shearing

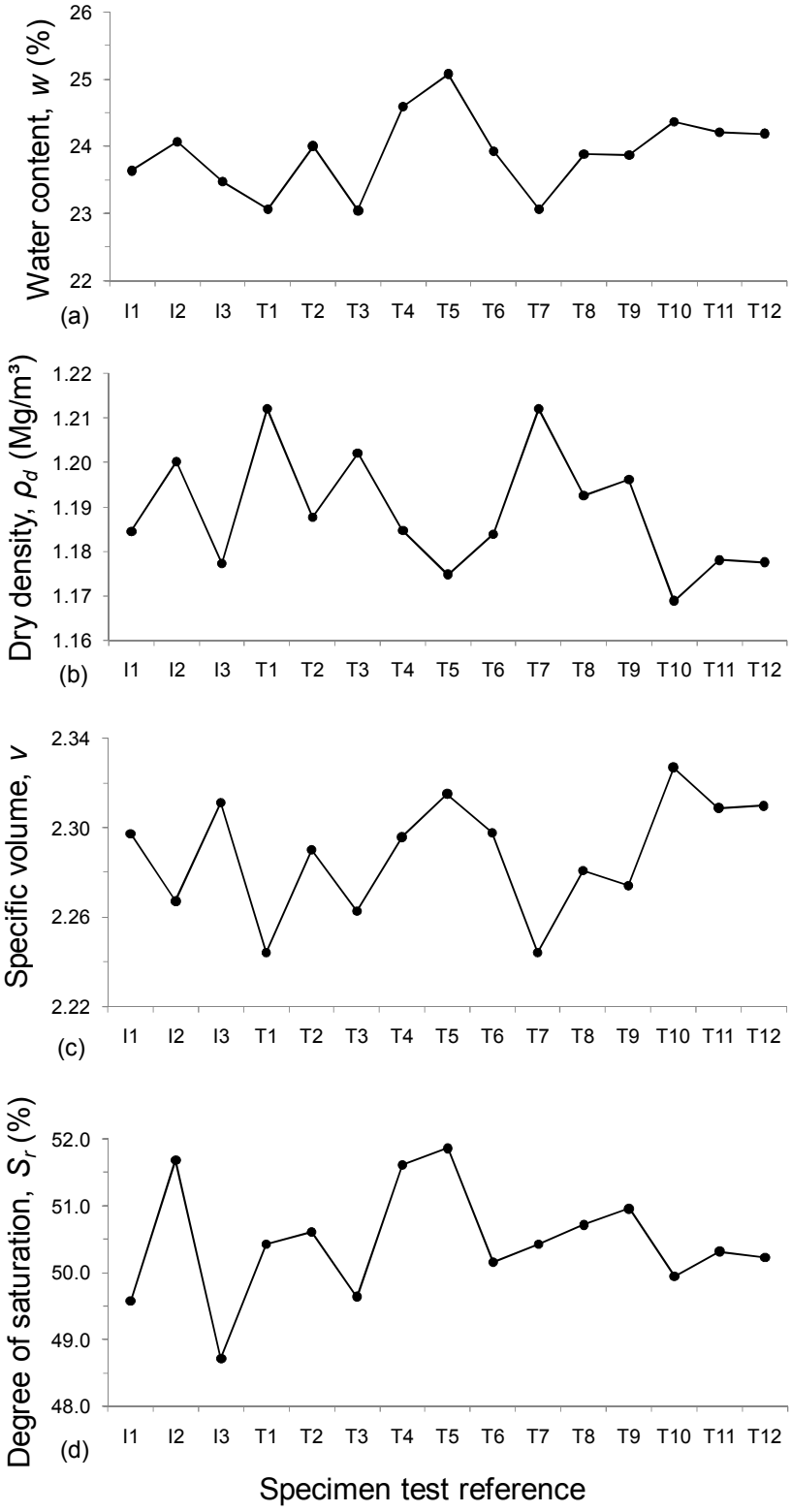

Figure 6.11: Variation of initial conditions (a) moisture content, (b) dry density, (c) specific volume and (d) degree of saturation of triaxial specimens after compaction

initial water content, dry density, specific volume and degree of saturation of all specimens immediately after compaction. Initial moisture content was relatively well controlled as all specimens were within ±1.2 of 23.9%, typically lower moisture contents were due to evaporation during mixing and during storage, whereas higher moisture contents were due to the addition of too much water during sample mixing.

6.7.2 Isotropic compression behaviour

The stress paths followed by the isotropic compression tests in the suction - mean net stress plane are shown in Figure 6.12. For specimens I1, I2 and I3 the specimens were wetted from their initial compacted state with an approximate suction of 470kPa (determined from the water retention curve) to the desired level of suction. Once suction had equalised the specimens were then loaded to 1 MPa (800kPa for I1) mean net stress and then unloaded.

The isotropic compression behaviour exhibited at different suction levels is presented in Figure 6.13 in terms of specific volume versus mean net stress. It is evident in Figure 6.13 that as suction increases the yield stress (p_0) increases from 15kPa to 155kPa. Furthermore the slope of the normal compression line (λ) increases with increasing suction, with the compression curves appearing to converge at higher stress levels. The slope of the swelling line (κ) appears to vary much less, suggesting that the swelling behaviour due to unloading is independent of suction as was proposed by Alonso et al. (1990). It is also evident in Figure 6.13 that the normal compression curves at different suctions appear to converge towards that of the saturated behaviour at higher stresses.

In Figure 6.14 the variation of λ and κ with suction for the Bengawan Solo fill are compared with values reported in the literature for other soils. For the six data sets presented it appears that there is significant increase in λ between saturated conditions and low suction levels ($<$100kPa). Thereafter there is a slower rate of increase in λ with increasing suction (Bengawan Solo fill, Futai and Almeida, 2005) or a decrease in λ with further increases in suction (Maâtouk et al., 1995; Wheeler and Sivakumar, 1995; Ng and Chiu, 2001). In terms of the swelling behaviour due to unloading, only one of the data sets presented shows a strong trend: κ reducing with

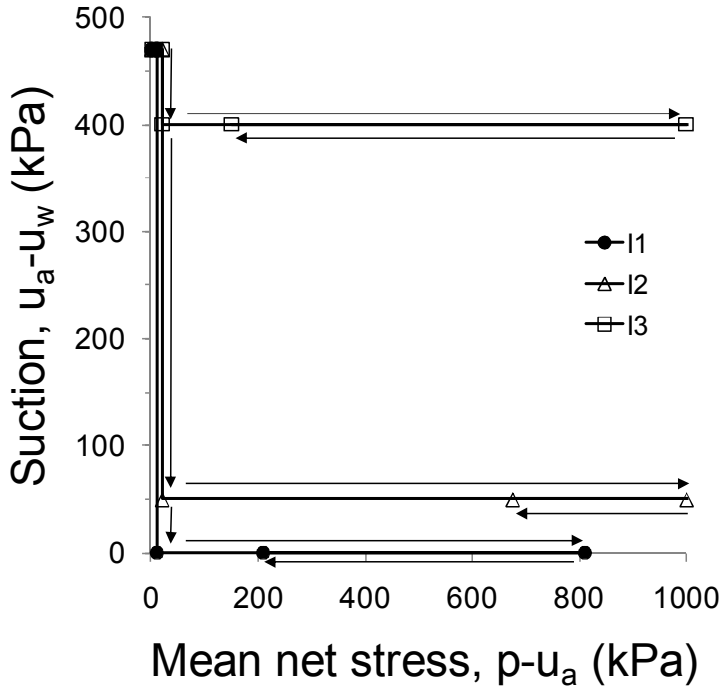

Figure 6.12: Plot of stress paths followed in isotropic compression tests in s - p space for saturated and suction controlled tests

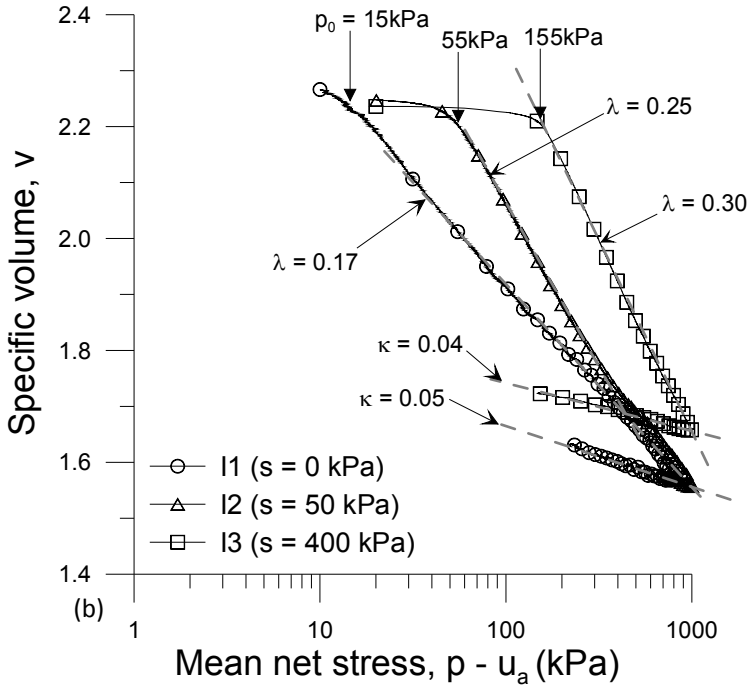

Figure 6.13: Isotropic compression behaviour at different levels of suction: specific volume against mean net stress

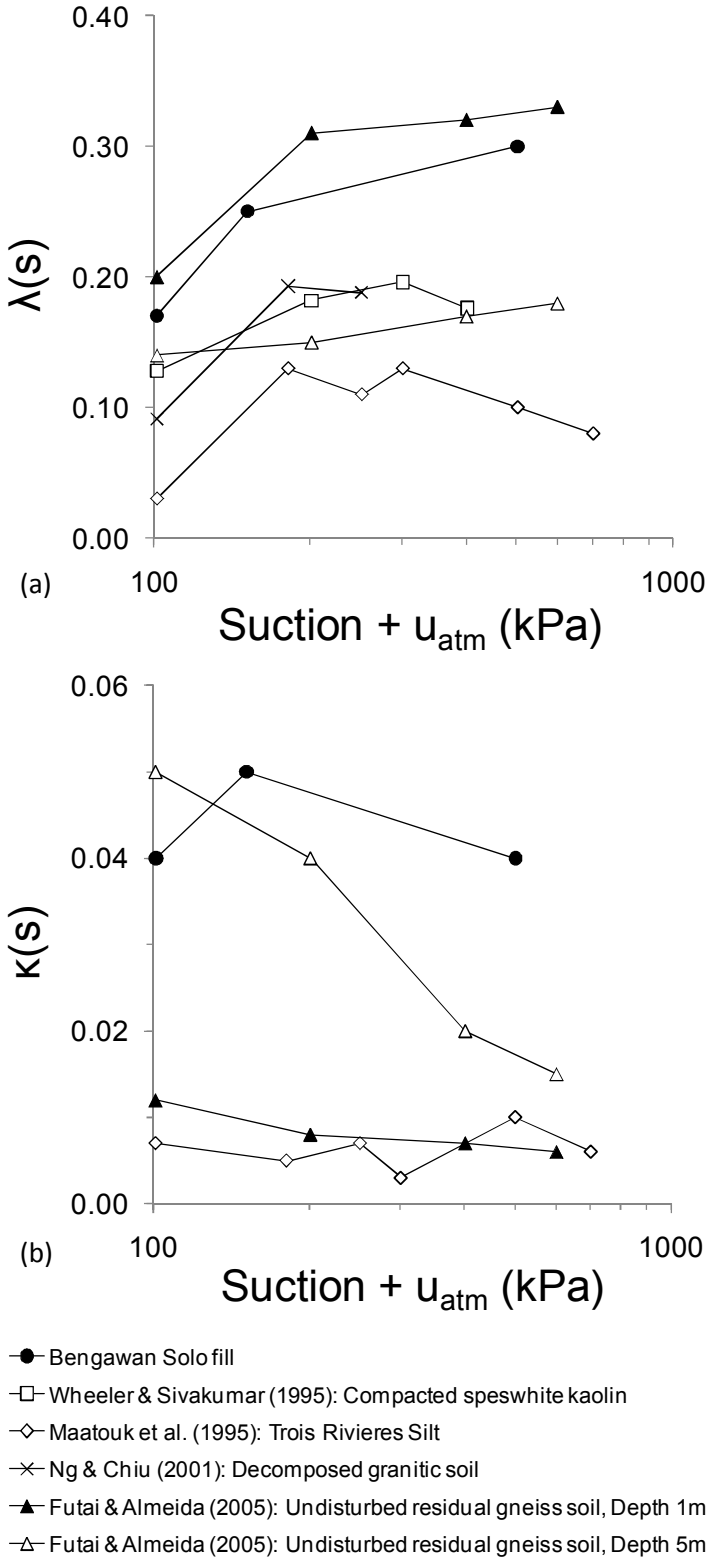

Figure 6.14: Variation of (a) λ and (b) κ with suction for Bengawan Solo fill compared with values reported by other authors

Table 6.4: Isotropic compression parameters

Test Reference	Suction	p_0	$\lambda(s)$	$\kappa(s)$
I1	0	15	0.17	0.05
I2	50	55	0.25	0.05
I3	400	155	0.30	0.04

‡Approximate initial suction

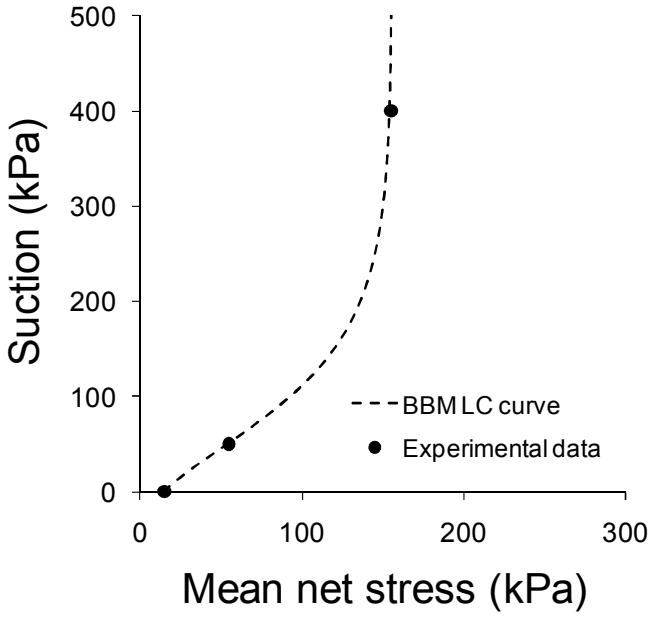

Figure 6.15: Yield stresses p_0 against suction: Experimental data and BBM loading collapse curve

increasing suction (Futai and Almeida, 2005), for the other soils, the Bengawan Solo fill included it appears that κ varies around a fairly constant value for a particular soil, regardless of suction.

The yield stresses exhibited upon isotropic loading for each suction levels are plotted in Figure 6.15 alongside the BBM loading collapse curve (LC). In the original BBM formulation (Alonso et al., 1990), it was anticipated that λ would decrease with increasing suction, this was not found to be the case for the Bengawan Solo fill material. Thus, the selection of parameters for determining the LC curve followed the recommendations given by Wheeler et al. (2002) such that an r value greater than 1 was selected ($r = 1.25$) and a sufficiently high value of p^c (reference stress) was selected ($p^c = 200{,}000$kPa). Additionally the following parameter values were selected:$\beta = 0.013\text{kPa}^{-1}$, p_0^*= 15kPa, $\lambda(0) = 0.17$ and $\kappa = 0.04$.

6.7.3 Shearing behaviour

6.7.3.1 Suction application

For the saturated tests, the initial compacted specimen (w_o=24%, ρ_{d_o}= 1.18Mg/m^3) was wetted by circulating water from the bottom of the specimen to the top, in a second stage the cell pressure and back pressure were ramped to pressures of 210kPa and 200kPa respectively, during this stage the B value (Skempton, 1954) was monitored to ensure close to full saturation had occurred. Figure 6.16 presents the variation of B during the saturation ramp applied to specimens T1, T2 and T3.

In the suction controlled tests, the variation in the pore water volume was monitored in order to determine when suction equalisation had occurred. The amount of water to be added to the specimens during the wetting stage was determined from the water retention curve for unconfined specimens, considering that the confining stress was applied simultaneously to the wetting stages, this explains the subsequent reduction in pore water volume observed during all the tests during the suction equalisation stage (Figures 6.17 and 6.18). As a general rule, the time required for equalisation of the suction throughout the specimen was equal to twice the duration of the wetting stage.

Figure 6.19 illustrates the variation in moisture content of the specimens air dried in the laboratory. A more or less constant moisture content of 6-7% was achieved after 5 days, this is considered to correspond to a total suction of approximately 100MPa, based on data obtained using the chilled mirror dew point psychrometer tests, presented in Section 4.7.3. Due to the high suction present, suction was not controlled during these tests, rather they were sheared under constant water content conditions.

6.7.3.2 Triaxial results

In Figure 6.20 the deviator stress q versus axial strain ε_a is plotted for each of the different suction levels tested (a) saturated conditions, (b) suction = 50kPa, (c) suction = 400kPa and (d) constant water content tests with an initial suction of approximately 100MPa. As expected

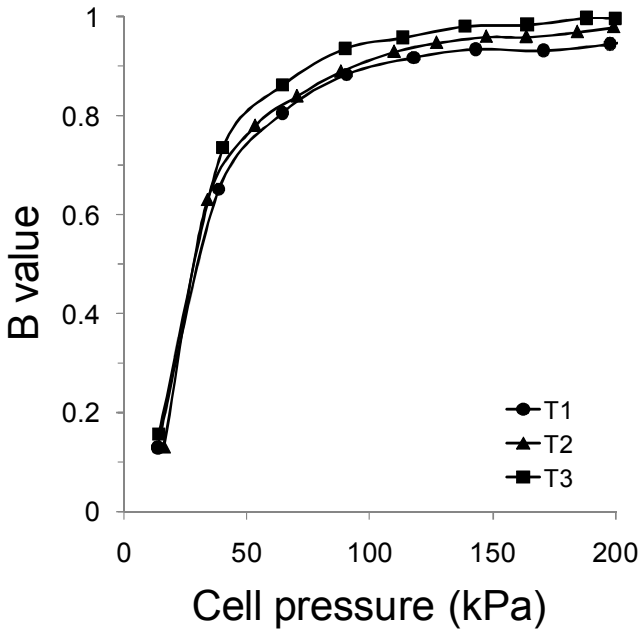

Figure 6.16: Variation of B value during saturation ramp applied to specimens T1, T2 and T3

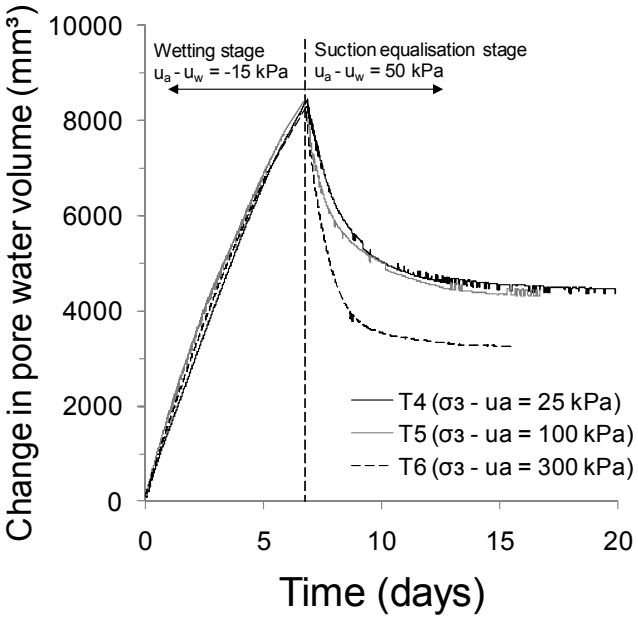

Figure 6.17: Variation of pore water volume during suction application for tests carried out at s = 50kPa (T4, T5 and T6)

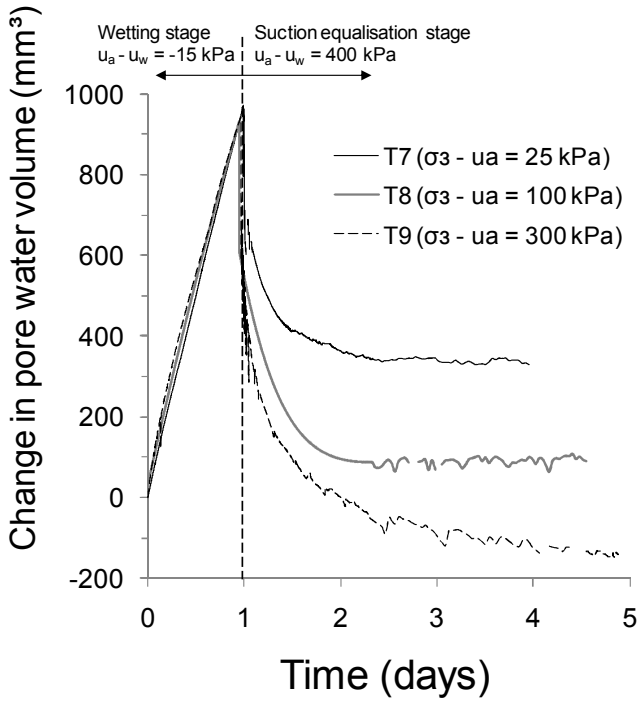

Figure 6.18: Variation of pore water volume during suction application for tests carried out at s = 400kPa (T7, T8 and T9)

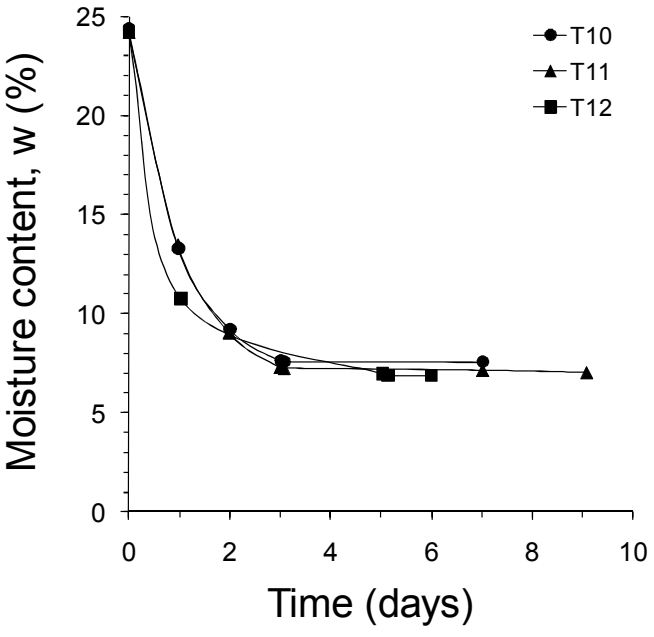

Figure 6.19: Air drying of specimens in laboratory (T10, T11 and T12)

the shear strength of the soil increases with increasing effective or net confining stress. There is a clear distinction between the behaviour of the soil under saturated and suction controlled conditions (Figure 6.20a, b and c) and the behaviour of the soil at the maximum suction level (Figure 6.20d). In the former (Figure 6.20a, b and c) deviator stress monotonically increases with increasing axial strain, with only some of the tests (T1, T2, T7) reaching a fairly constant q by the end of the tests (axial strain = 20%). In tests T3, T4, T5, T6, T8 and T9, q is still continuing to increase at the end of the test, suggesting that these tests have not reached a critical state. The critical state of a soil specimen is defined as having been reached when shearing produces no further changes of stress (q or p) or volume, typically at large axial strains (Roscoe et al., 1958). For tests T1 - T9 initial shearing produces a steep increase in deviator stress at very small axial strains. Figure 6.21 illustrates that these specimens (T1-T9) tended to undergo barrelling during shearing.

The air dried specimens (T10 - T12) on the other hand all exhibited a peak shear strength between 0.5 and 1.1% axial strain, followed by rapid softening behaviour, reaching fairly constant values of q by axial strains of around 10%. Such behaviour is typical of dense sands and overconsolidated clays. It should be noted here that the air drying of the compacted Bengawan Solo fill essentially created aggregates of low moisture content, strongly bonded together at this high suction level (100MPa). At this low level of moisture content (6-7%) the material behaves as a bonded granular material. In fact specimens T10 and T11 (at 25kPa and 100kPa net confining stress) crumbled entirely during shearing, although it was still possible to distinguish shear planes, see Figure 6.21. T12 exhibited barrelling deformation, with shear planes also evident.

In Figure 6.22, deviator stress versus axial strain are plotted for each level of net confining stress applied (25, 100 and 300kPa). In these plots it is evident that increasing suction increases the shear strength of the Bengawan Solo fill. It is clear that at all the stress levels the air dried specimens exhibit a much higher shear strength and markedly different behaviour characterised by peak failures.

Despite best efforts to calibrate the triaxial cell used in this testing campaign in order to determine specimen volume changes from changes in the global cell volume, (see Appendix A, A.3.1), the specimen volume change results during shearing were found to be unreliable and for this

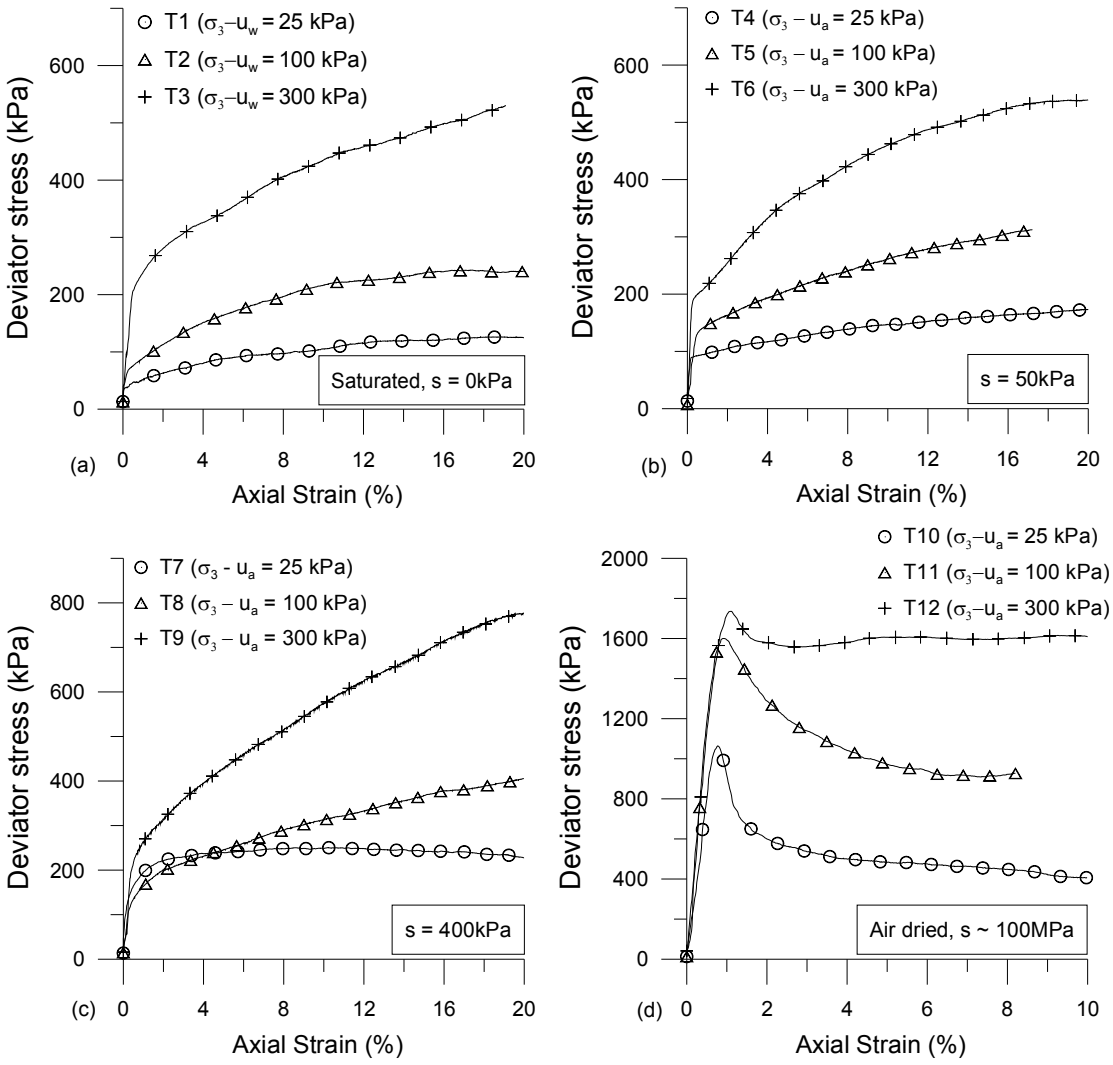

Figure 6.20: Deviator stress vs axial strain for different levels of suction (a) Saturated tests (s = 0kPa), (b) Suction controlled (s =50kPa), (c) Suction controlled (s = 400kPa) and (d) Constant water content tests (initial s ~ 100MPa)

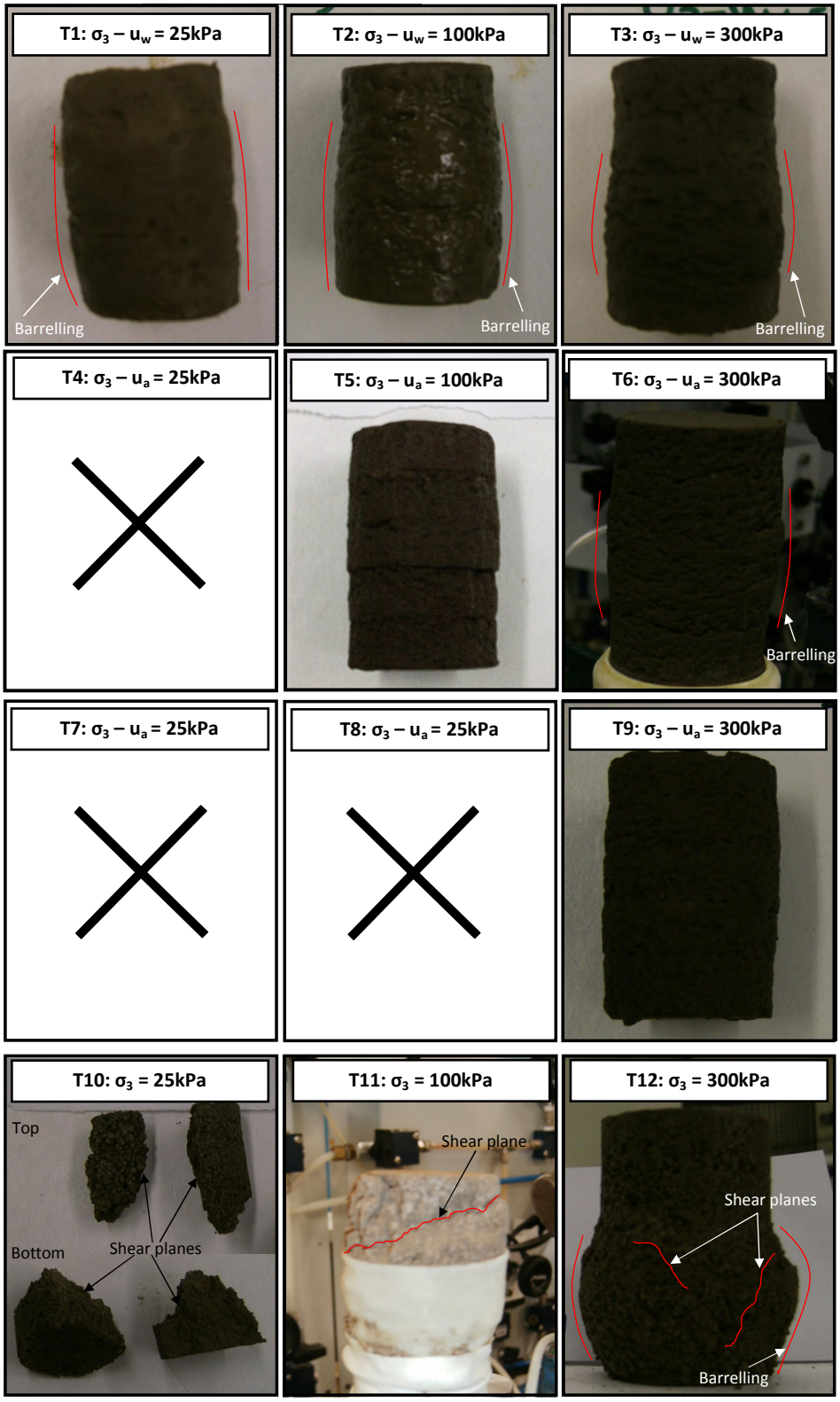

Figure 6.21: Photos of triaxial specimens at end of triaxial tests (Xs indicate where no photo of the corresponding specimen is available)

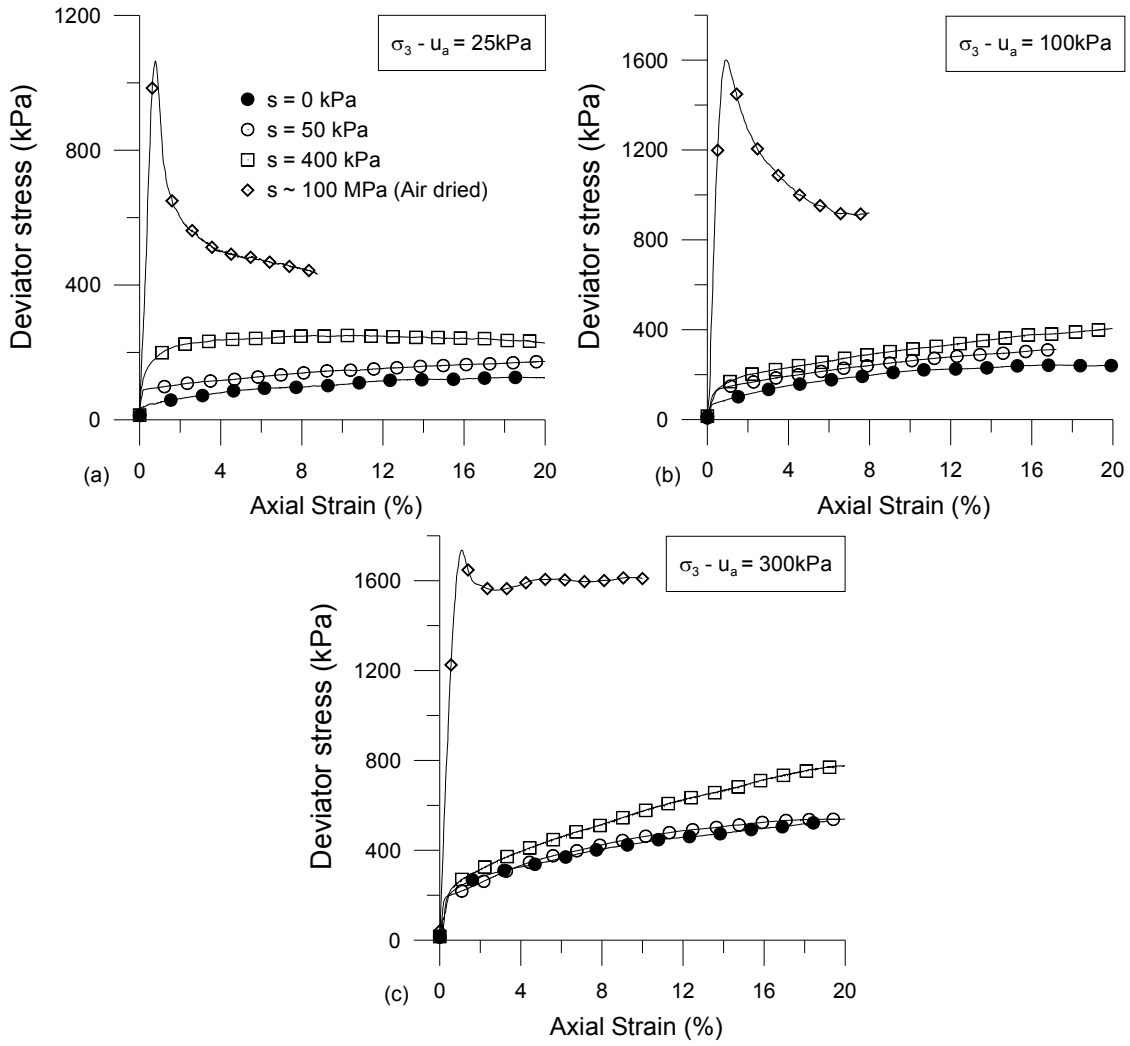

Figure 6.22: Deviator stress vs axial strain at different values of net confining stress (a) $\sigma_3 - u_a$= 25kPa, (b) $\sigma_3 - u_a$= 100kPa and (c) $\sigma_3 - u_a$= 300kPa

reason have not been presented here. One of the main drawbacks of the cell used was the fact that the loading ram had a relatively large cross-sectional area (A_{ram} = 282mm^2) compared to the initial cross-sectional area of the specimen (A_s = 1134mm^2). During shearing as the piston moves into the cell, a volume of water equal to $A_{ram}\Delta H$ is forced to move out of the cell. Considering the large area of the loading ram, the volume displaced during shearing could be as much as 7200mm^3, corresponding to more than 8% of the initial specimen volume. Although this effect was accounted for during data analysis, the specimen volume change determined remained unsatisfactory and it is thought that this effect contributed to masking the true specimen volume change during shearing. Furthermore the cell volume measuring line remained open to a large bore diameter pipe (1/4 inch NPT) (used for filling the cell) during volume measurement. It is thought that any air bubbles or fluctuations in volume in this large diameter pipe due to temperature effects also contributed to errors in determining changes in the specimen volume. In the isotropic cell, the cell pressure line was isolated during testing and connected only to the test cell and the position of the loading ram remained fixed throughout the isotropic tests.

It is recognised here that the lack of reliable volumetric data is a significant shortcoming of the experimental data presented herein and its potential for use as a data set in future works. Furthermore the adaptation of existing triaxial equipment for the testing of unsaturated soils is thus not as straightforward as it may seem, it appears that the cell used was not fit for purpose in terms of its suitability for measuring specimen volume changes.

Given the lack of volumetric data and the fact that half of the specimens tested had not reached a constant level of stress by the end of the test, it was not considered a worthwhile exercise to consider the data in terms of an unsaturated critical state framework. Rather the data are considered here in terms of shear strength parameters. It is hoped that the information presented can contribute to existing knowledge on the influence of suction on shear strength.

6.7.3.3 Shear strength parameters

The peak deviator stress (either at failure or at an axial strain of 20%) and the stress path followed during the triaxial tests are presented in Figure 6.23a. The peak deviator stress obtained for each confining stress level is then plotted against suction (suction + atmospheric pressure)

in Figure 6.23b. The much higher shear stress exhibited by the air dried specimens is a function not only of the suction level but also the soil fabric, which in this state is markedly different to that of the specimens tested at lower suction levels, which contributes to a much higher apparent cohesion. The very high apparent cohesion determined for the air dried specimens (e.g. 260 kPa in T12) may be explained by the bonded aggregated specimen created by air drying.

In order to investigate the influence of suction on the shear strength behaviour of the Bengawan Solo fill, the parameters, ϕ' (effective angle of friction) and c' (apparent cohesion) were determined from Mohr's circles plotted for each of the suction levels tested (see Figure 6.24). It should be noted that the drained cohesion determined under saturated conditions (30kPa) is particularly high. With increasing suction, it appears that both ϕ' and c' increase for the Bengawan Solo fill material, although at low suctions (0 - 400kPa) cohesion appears to be less influenced by changes in suction than the angle of friction. Similar evidence for increasing ϕ' with suction has also been reported by a number of authors (e.g. Toll and Ong, 2003; Futai and Almeida, 2005). Delage and Graham (1996) collated various experimental data sets and found evidence of increasing and decreasing angles of friction with increasing suction. In Figure 6.25 the variation of shear strength parameters with suction determined for the Bengawan Solo fill are compared with values reported in the literature. For all the data sets presented in Figure 6.25 ϕ' and c' increase to varying degrees with increasing suction. Despite this one of the most commonly used shear strength criterion (that proposed by Fredlund et al., 1978) assumes that ϕ' does not vary with suction. Similarly within a critical state framework, the BBM (Alonso et al., 1990) assumes that M (slope of the critical state line in $q - p$ space) is constant and that cohesion increases with increasing suction, whereas data by Wheeler and Sivakumar (1995) and Cui and Delage (1996) found both M and cohesion to increase with increasing suction. An increase in M with suction may be explained by the inclined yield curves found for such soils ($q - p$ space), due to anisotropy, either as a result of compaction (Cui and Delage, 1996; Wheeler and Sivakumar, 1995) or anisotropy present in undisturbed soils (Futai and Almeida, 2005). Alternatively, Toll (2000) argues that the increase in the angle of friction with suction is due to the aggregated fabric of compacted clayey soils which may vary significantly with suction. Furthermore Toll (2000) argues that the symbol ϕ' should be reserved for the angle of friction in saturated conditions and that ϕ^a should be used to represent the strength component due to net stress and ϕ^b the strength component due to suction.

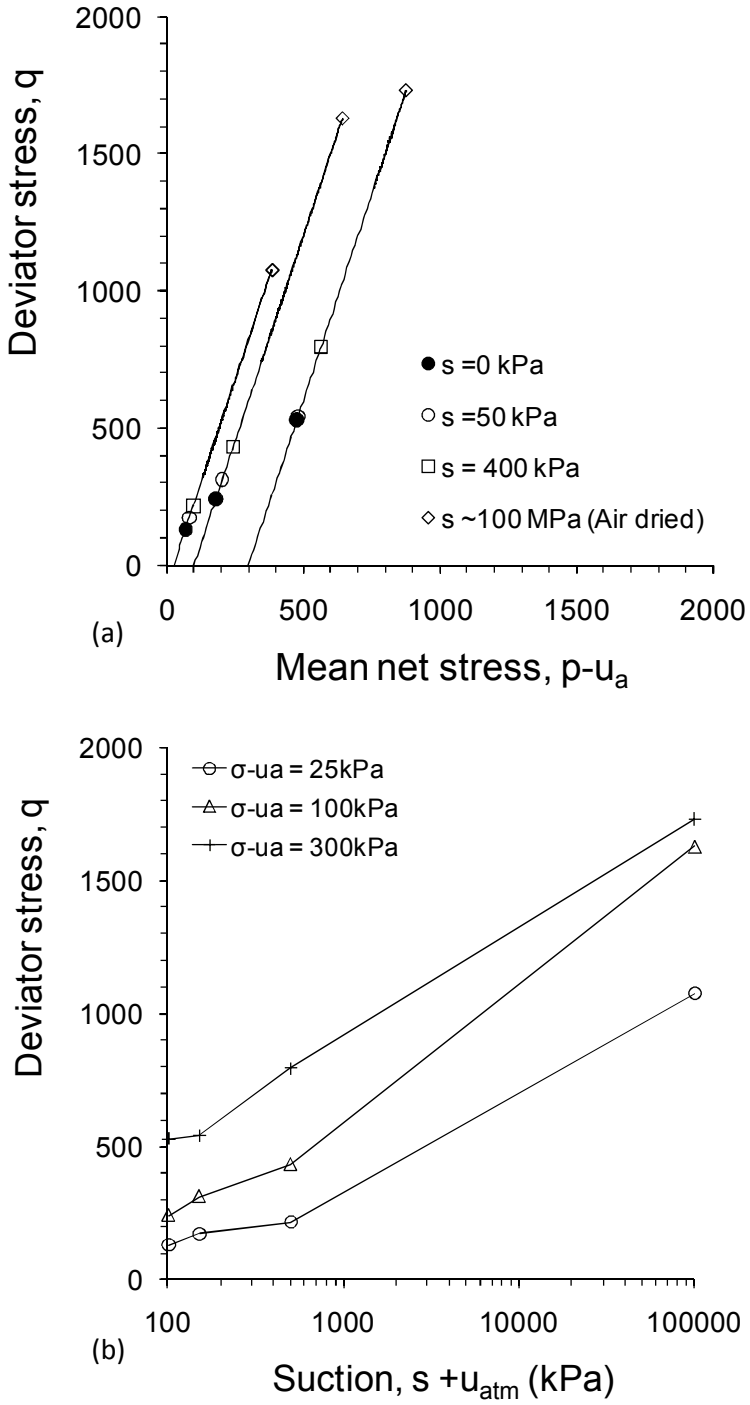

Figure 6.23: Failure envelopes: (a) deviator stress vs normal stress for different values of suction and (b) peak deviator stress vs suction (suction + atmospheric pressure)

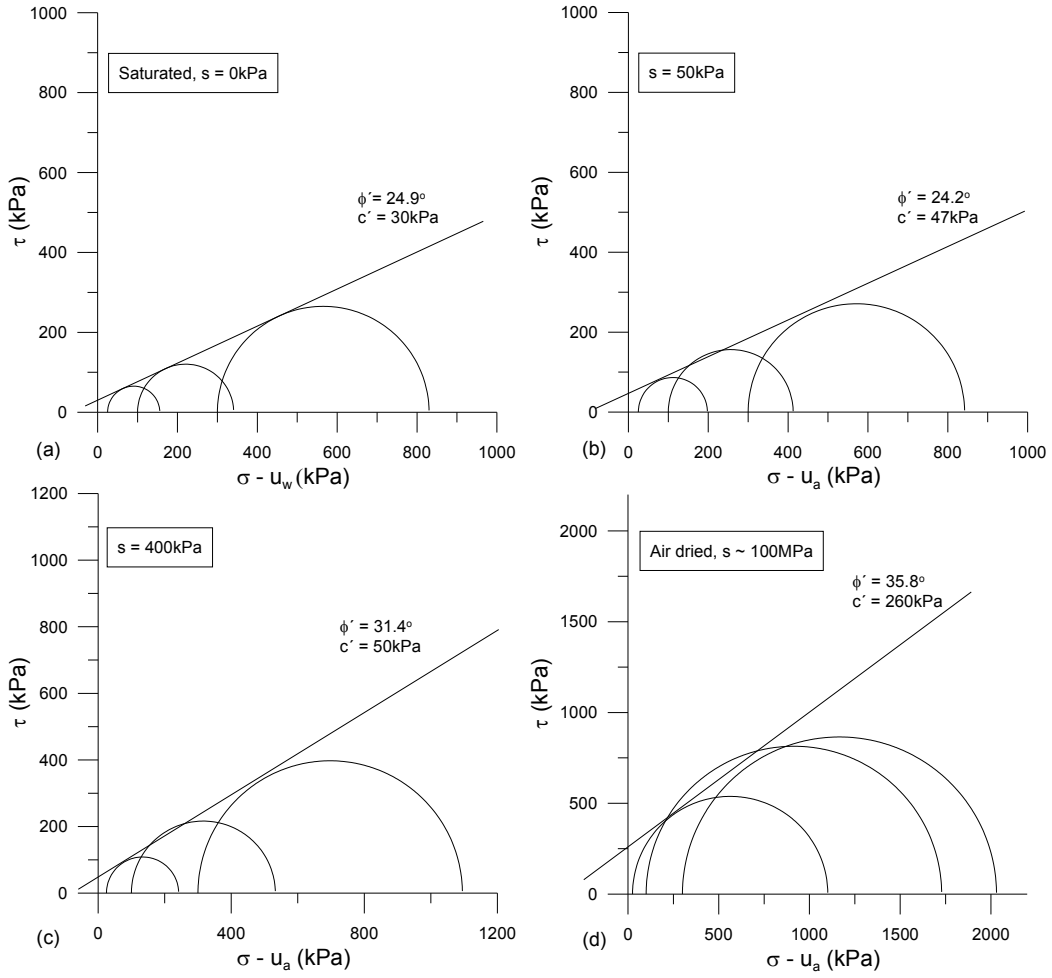

Figure 6.24: Mohr circle failure envelopes (a) Saturated, (b) s = 50kPa, (c) s = 400kPa and (d) Air dried tests (peak failure)

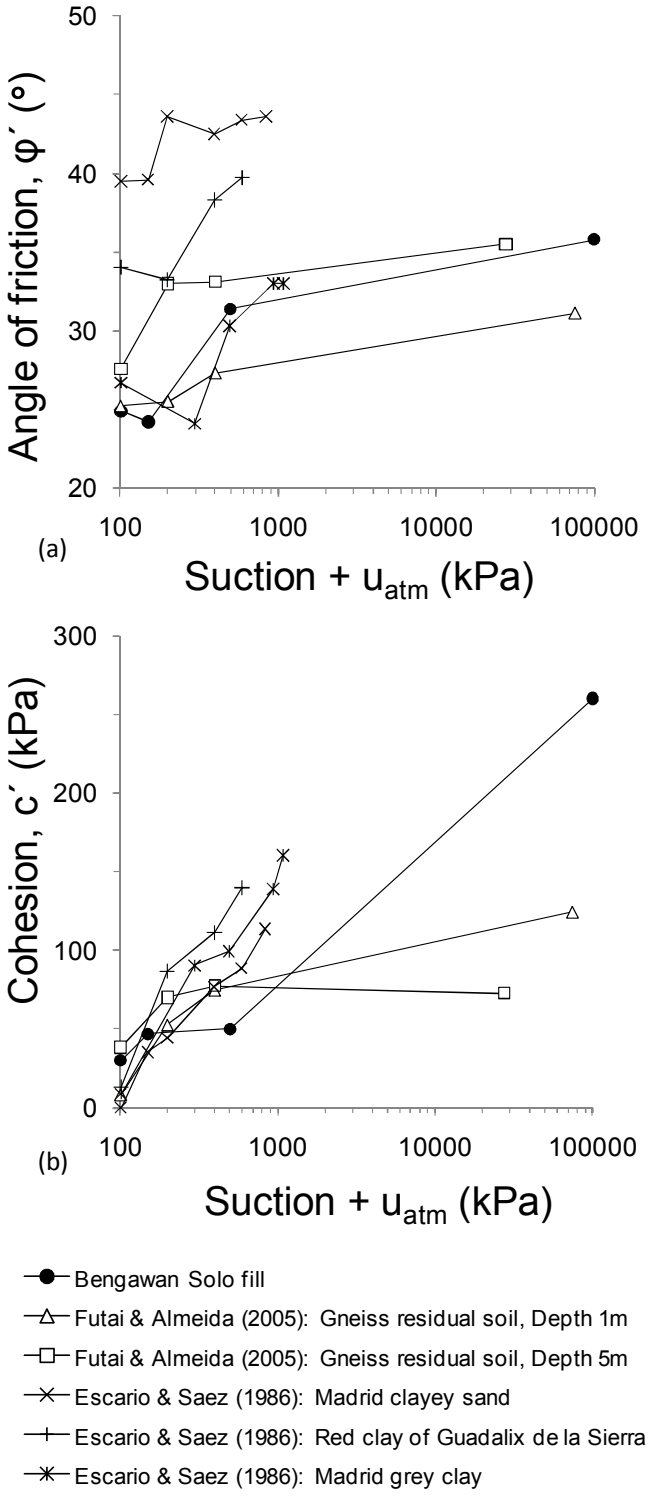

Figure 6.25: Variation of shear strength parameters with suction: (a) angle of friction and (b) cohesion compared with values reported by other authors

6.8 Slope stability analysis

A well known phenomenon reported in the literature for the failure of slopes and embankments is the reduction of shear strength due to wetting (e.g. Krahn et al., 1989; Rahardjo et al., 1995; Kim et al., 2004). In an attempt to investigate how the variation in shear strength of the fill material with changes in suction may influence the stability of the Bengawan Solo flood embankments, a routine stability analysis was carried out using the limit equilibrium method, using Slope/w (Geoslope International Ltd.). The Factor of Safety was computed using the Morgenstern-Price Method (Morgenstern and Price, 1965) and a half sine inter-slice function.

The borehole data presented in Figure 4.2 (Chapter 4) was used in the selection of the geotechnical properties for the founding layers. The different layers were converted to values of undrained shear strength, assuming the relationship proposed by Stroud and Butler (1975) which considers that the undrained shear strength (C_u) is equal to 5 times the SPT N-value. The founding layers were assumed to be fully saturated at all times and were considered to be undrained. This may not strictly be the case but the assumptions are considered suitable for investigating the influence of suction on the embankment stability.

Two scenarios were investigated representing: (i) the condition of the embankment immediately after construction in which the embankment fill is unsaturated and the Bengawan Solo River level is low, as construction was carried out during the dry season and (ii) the condition of the embankment typical of the wet season, when most of the embankment body has become saturated and the river level is high. In the scenario representing conditions immediately after construction, the river level was assumed to be 1 m high; in the wet season scenario the river level was set to be 7 m high.

Values of angle of friction and apparent cohesion determined in the triaxial testing campaign were used in the selection of the geotechnical properties of the fill material. The fill material below the water table was assigned as saturated and that above the water table was deemed to be unsaturated. For the saturated fill material, the saturated parameters determined were used, $\phi' = 24.9$ ° and $c' = 30$ kPa. Although the failure criterion proposed by Fredlund et al. (1978) can be used in conjunction with Slope/w, it was preferred not to use it in this case considering that the founding assumption that ϕ' is independent of suction, is not valid for the Bengawan

Solo fill material. Rather the unsaturated material was assumed to be at a moisture content of approx. 22-23 % at a suction of 400 kPa, corresponding to dry of optimum compaction conditions and values of $\phi' = 30.4$ ° and $c' = 55$ kPa determined for this suction level in the triaxial tests were used. Considering that during the long dry season from May to October, evaporation considerably exceeds precipitation in the Bojonegoro area (Takeuchi et al., 1995), it is not unreasonable to assume that such moisture contents may also be typical of the fill material during the dry season (especially in the absence of additional in-situ data). Additionally the influence of loading due to the gabions present along this section of embankment was also introduced into the stability analysis. The gabion fill was assumed to have a density of 1.6 tonnes per m^3 (MGS, 2004).

Considering only the increase in water level between the dry and wet season and thus changes in the bulk unit weight and shear strength of the fill material due to saturation, the Factor of Safety determined was higher in the wet season (2.19) than in the dry season (1.52), (see Figure 6.26). The higher Factor of Safety determined for the wet season scenario may be explained by considering that the higher river level applies a greater hydrostatic pressure which acts to stabilise the embankment. This simple analysis indicates that the variation of the shear strength of the fill material due to changes in suction is not the mechanism responsible for the global failure of the gabion reinforced embankment illustrated in Figure 2.11 (Chapter 2). This result is essentially an artifact of the high drained cohesion determined for the Bengawan Solo fill under saturated conditions.

A simple analysis was carried out to investigate the effect of rapid drawdown on stability assuming that the whole of the embankment body remains fully saturated and undrained immediately after drawdown (see Figure 6.27). A low Factor of Safety of 1.12 was obtained which illustrates that embankments constructed with the Bengawan Solo fill may be susceptible to instability due to rapid drawdown as has been observed along these embankments (Soemitro, private communication, 2006). However the global failure of the gabion reinforced embankment was not linked with any closure of the Babat barrage upstream. It is likely then that the global failure of the gabion reinforced embankment was due to a combination of different factors, including seepage, overtopping erosion and the volumetric collapse of the poorly compacted layers. Investigation of the influence of such factors would require coupled seepage analyses and unsaturated finite

element modelling of the embankments, work which is outside the scope of this thesis, though is recommended for further research.

6.9 Conclusions

The isotropic compression tests presented herein indicate that for the Bengawan Solo fill material the yield stress (p_o) exhibited upon external loading increases with increasing suction. Furthermore the results presented indicate an increase in soil compressibility (an increase in λ) with increasing suction. As is evident from the literature the influence of suction on post-yield compressibility is not yet well understood, with increasing suction leading to a reduction in the compressibility of some soils (e.g. Matyas and Radhakrishna, 1968; Cui and Delage, 1996), an increase in others (e.g. Futai and Almeida, 2005), or only a distinct difference between saturated and unsaturated states with little variation thereafter (e.g. Wheeler and Sivakumar, 1995; Ng and Chiu, 2001). Some authors have suggested that such variation in the influence of suction on compressibility may be related to soil fabric (e.g. Toll, 1990; Toll and Ong, 2003). Chapter 7 investigates the role of compacted fabric on soil compressibility under different saturation conditions.

The shear strength behaviour of the Bengawan Solo fill has been investigated at a number of different suction levels, it is evident that shear strength increases with increasing suction. In particular angle of friction and cohesion have been found to increase with increasing suction. A routine slope stability analysis indicated that the reduction in shear strength due to saturation did not negatively influence the stability of the Bengawan Solo embankment. It is likely that a combination of other mechanisms have been responsible for the global failure of the gabion reinforced embankment. It is anticipated that erosion and volumetric collapse may have played a role in this failure. Further experimental information is required on the variation in the permeability of this material in order to investigate in more detail mechanisms contributing to the poor performance of these flood embankments.

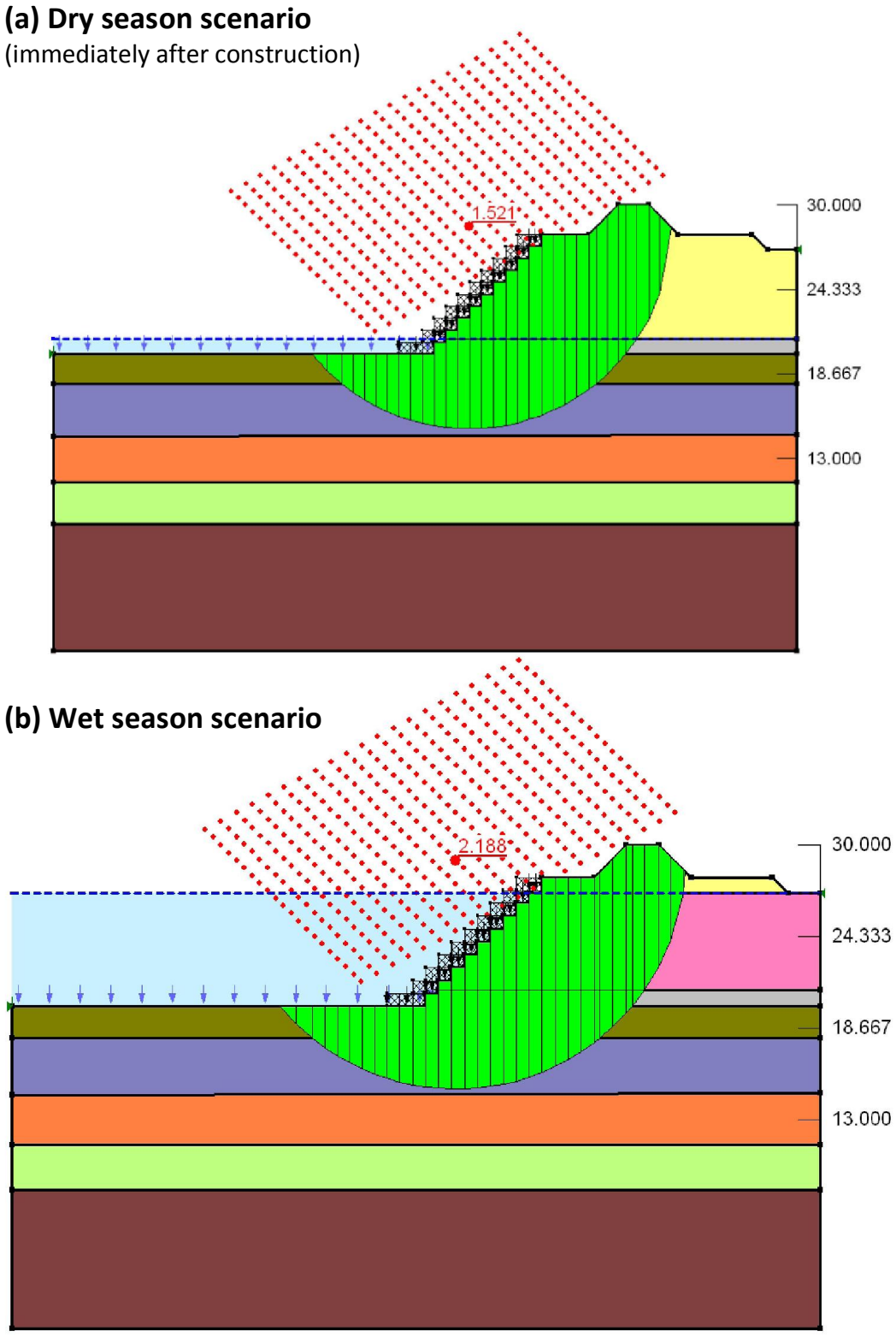

Figure 6.26: Variation in factor of safety of Bengawan Solo embankments (a) immediately after construction in the dry season (river level = 1m) and (b) during the wet season (river level = 7m)

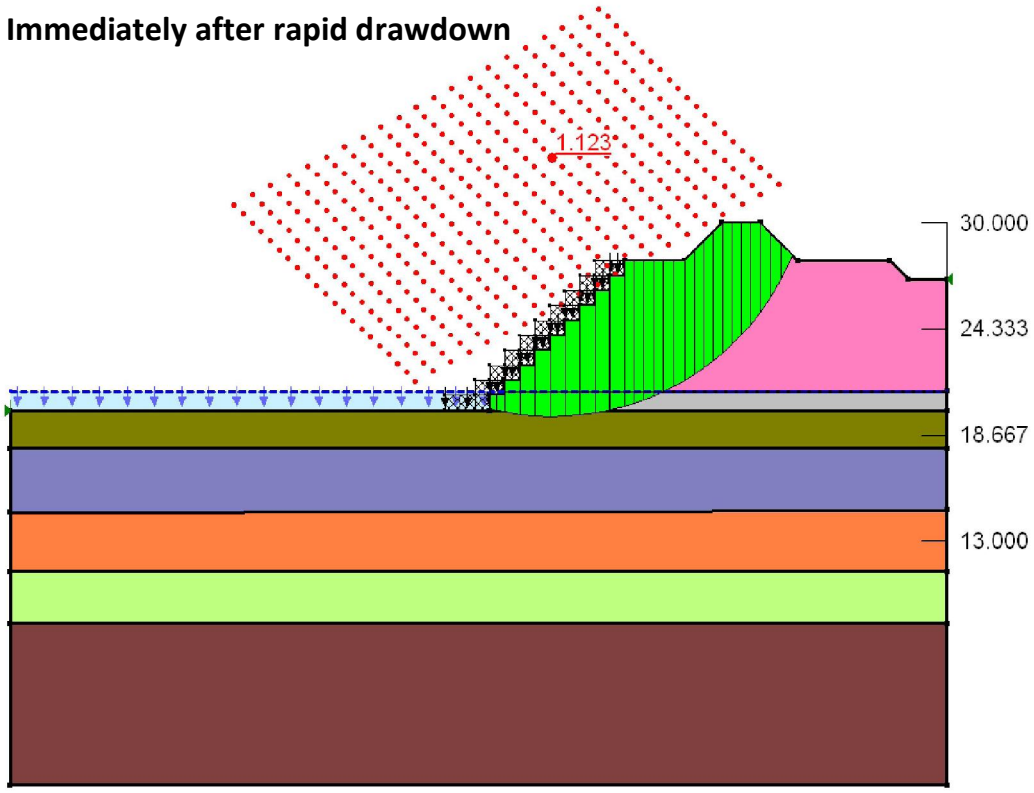

Figure 6.27: Critical slip surface and Factor of Safety obtained immediately after rapid drawdown

Chapter 7

Influence of compacted fabric on volumetric behaviour

7.1 Introduction

In this chapter, the soil fabric created during compaction of the Bengawan Solo fill material is investigated, with particular emphasis given to its influence on compression behaviour. As a first attempt to investigate the influence of soil structure on volumetric behaviour, tests were conducted at different initial compaction conditions (w_o, ρ_{d_o}) using the conventional oedometer apparatus under constant water content and saturated conditions. During mixing of the soil with water the formation of soil aggregates was observed. Results from the conventional oedometer tests and evidence during compaction tests suggest that the presence of soil aggregates may play a role in the mechanical response of the soil. The aggregates created upon mixing at different moisture contents and their influence on compacted structure was further investigated using Mercury Intrusion Porosimetry. Tests were then carried out on different specimens compacted of aggregates of a widely varying nature in order to assess their influence on the yielding and compressibility behaviour of the soil under constant water content and saturated conditions. The equipment used was designed and manufactured at UPC, Barcelona and is herein referred to as the UPC oedometer. Finally, a carefully designed series of tests were carried out under

suction controlled conditions in an attempt to isolate the effects of soil structure on volumetric behaviour.

7.2 Structured soils

The term soil structure as used herein refers to the definition given by Mitchell (1993), where structure is the combination of soil fabric and inter-particle forces, which are not purely frictional (e.g. cementation). In classical soil mechanics, soil is considered to be a homogeneous continuum (e.g. Houlsby, 1979) which can be described by considering the different fractions of solid and pore fluids present, quantified as values averaged over a representative volume (generally represented in phase diagrams). This approach assumes that soil structure at the particle scale does not have a significant influence on the macroscopic mechanical behaviour of the soil. However for some soils this is not the case, these soils are referred to here as structured soils. In general, the effects of structure on mechanical behaviour has been investigated for two main types of structured soils: (i) intact (or natural) bonded soils (Burland, 1990; Leroueil and Vaughan, 1990) and (ii) aggregated soils (Koliji, 2008).

7.2.1 Intact bonded soils

The mechanical response of intact (or natural) bonded soils differs from that of a reconstituted soil of the same mineralogy, where a reconstituted soil is defined as one which has been thoroughly mixed at a water content equal to or greater than the liquid limit (Burland, 1990). Essentially in a reconstituted soil, soil structure is considered to have been fully removed, and for this reason reconstituted soils are used as the reference state when investigating structured soils (Burland, 1990). The differing mechanical response exhibited by intact bonded soils is attributed to the bonding or cementation of particles (Leroueil and Vaughan, 1990), referred to here as inter-particle bonding.

Mitchell (1993) lists many different factors which may influence soil structure, with compositional and environmental factors contributing to initial soil structure with physical and chemical processes responsible for subsequent changes in structure. Leroueil and Vaughan (1990) detail

some of the specific causes of inter-particle bonding: (i) solution and deposition of silica at particle contacts in sands, (ii) cold welding at inter-particles under high pressure, (iii) deposition of carbonates, hydroxides and organic matter from solution, (iv) recrystallisation of minerals during weathering, (v) modification of adsorbed water layers and inter-particle attractive forces in clays. However despite the different origins of such inter-particle bonding, Leroueil and Vaughan (1990) suggest that the structural effects on engineering behaviour are similar.

The influence of bonded structures on mechanical behaviour has been investigated for a wide range of different soils including soft clays (e.g. Mesri et al., 1975; Smith et al., 1992), stiff clays (e.g. Burland et al., 1996; Amorosi and Rampello, 2007), granular soils (e.g. Coop and Atkinson, 1993) and residual soils (e.g. Wesley, 1974; Coop and Atkinson, 1993). Generally these studies have attributed structural effects to inter-particle bonding without an in-depth investigation of the soil fabric. On the whole these studies have been largely limited to testing intact samples under fully saturated conditions and comparing the behaviour with that of reconstituted samples.

Intact bonded soils typically exhibit stiff behaviour prior to yielding (Figure 7.1). This stiff behaviour has often been assumed to be recoverable, suggesting that such deformations are elastic and independent of structure (e.g. Gens and Nova, 1993). However although the pre-yield behaviour is stiff, Leroueil and Vaughan (1990) argue that the behaviour may not necessarily be elastic as structure may be damaged even at stresses lower than the primary yield.

The inter-particle bonds present in structured soils provide additional stability to the soil skeleton, increasing strength and increasing the stress domain within which the soil exhibits stiff behaviour (Leroueil and Vaughan, 1990). The position of yield (Y in Figure 7.1c) will depend on the strength of the bonded structure (Leroueil and Vaughan, 1990). The compression curves of intact bonded soils typically lie to the right of the normal compression curve of reconstituted soils (Figure 7.1a and b). It is the presence of the inter-particle bonds which enable the structured soil to exist at higher void ratios than are possible for the corresponding reconstituted soil at the same stress (Leroueil and Vaughan, 1990).

The bonded structure also influences the soil behaviour exhibited post-yield, as the structure is not removed immediately upon reaching the primary yield point (Y) (Leroueil and Vaughan,

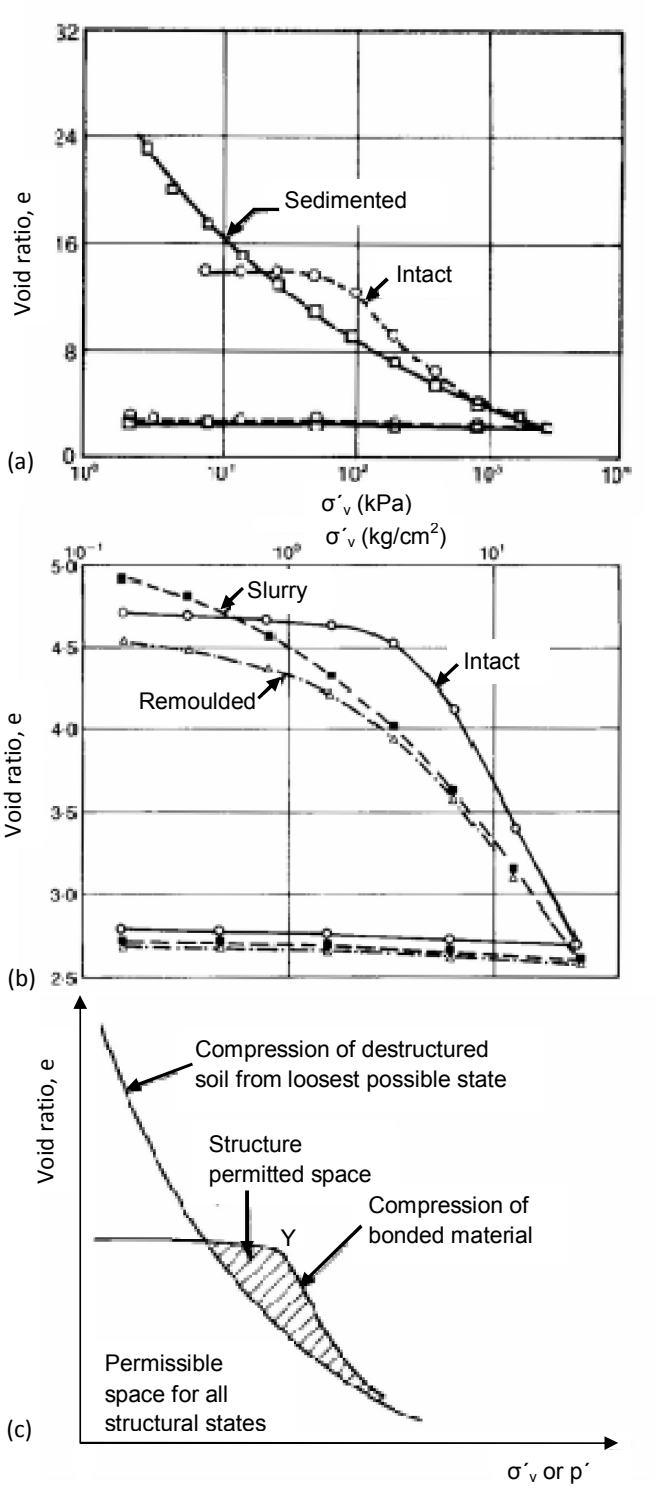

Figure 7.1: Comparison of the compression behaviour of structured and destructured specimens (a) intact samples of Mexico City clay (data from Mesri et al., 1975), (b) intact samples of residual soil from Java (data from Wesley, 1974) and (c) schematic of permissible space according to structural state (Leroueil and Vaughan, 1990)

1990). Typically bonded soils exhibit steeper post-yielding compression curves than for de-structured material, characterised by higher values of the compression index C_c (Burland, 1990; Leroueil and Vaughan, 1990). For structured soils C_c has been found to correlate with the initial void ratio and sensitivity of clays (Leroueil et al., 1983) rather than with plasticity (e.g. Skempton and Jones, 1944). It has commonly been observed that as the stress applied increases and the specimen has undergone sufficient strain, the compression curve exhibited by an initially bonded soil converges to that of the reconstituted material (e.g. Wesley, 1974; Mesri et al., 1975; Burland, 1990; Leroueil and Vaughan, 1990). This behaviour can be explained by considering that post-yield the material is undergoing a progressive loss of structure (destructuring) with increasing stress (Burland, 1990; Leroueil and Vaughan, 1990), such that the response of the material becomes similar to that of the reconstituted soil as the influence of structure reduces. However, Leroueil and Vaughan (1990) also argue that complete removal of structure does not necessarily imply that the state of the soil will lie upon the normal compression line of the reconstituted material, as further strains may be required to establish a similar fabric and packing arrangement.

7.2.2 Aggregated soils

The second group of soils for which structure may influence mechanical behaviour is aggregated soils. Such soils are characterised with aggregations of particles, which vary in terms of their size, shape, texture, stiffness and porosity. The arrangement of such aggregations may result in an open soil fabric with an often bi- or multi-modal pore size distribution. Aggregations are commonly found in compacted soils dry of optimum (e.g. Collins and McGown, 1974; Delage et al., 1996; Lloret et al., 2003) and in agricultural soils (e.g. Horn and Dexter, 1989; Horn, 2003; Carter, 2004). In agricultural soils, aggregations are desirable in that the resulting open structure eases the passage of water, light, nutrients and provides suitable spaces for biological activity (Charman and Murphy, 1998). Aggregated soils by definition have generally been investigated by considering their soil fabric, that is the arrangement (shape, size and distribution) of solid particles and pore space present (Collins and McGown, 1974). The classifications of soil fabric used today are still largely based on the hierarchy of solid particles and pore spaces outlined by Collins and McGown (1974). This classification was presented in detail in Section 5.3.3.

This chapter focuses on the influence of aggregated soil structures created by compaction, on mechanical behaviour.

The soil fabric created due to compaction has been an area of study for many years. Early concepts by Lambe (1958b) proposed that flocculated structures were created for clays compacted dry of optimum and that dispersed structures were created in clays at moisture contents wet of optimum, by considering the double water layer theory and colloidal chemistry. Lambe then attempted to relate these soil fabrics (dispersed and flocculated) to observed engineering behaviour (Lambe, 1958a).

Such early concepts have largely been replaced as a result of the development of microstructural investigation techniques including SEM, ESEM and MIP which have enabled direct observation and measurement of soil microfabric (e.g. Diamond, 1970; Barden et al., 1973; Collins and McGown, 1974; Prapaharan et al., 1991). More recently techniques such as neutron radiography and tomography have also been used to study soil fabric (e.g. Koliji, 2008). It is now generally accepted that a soil sample compacted dry of optimum is made up of an arrangement of aggregates whereas samples compacted wet of optimum consist of a matrix fabric of a more homogeneous texture. MIP results have indicated that soils compacted dry of optimum typically have a bi-modal or multi-modal pore size distribution whereas samples compacted wet of optimum demonstrate a mono-modal distribution (e.g. Diamond, 1970; Ahmed et al., 1974; Juang and Holtz, 1986a; Prapaharan et al., 1991; Delage et al., 1996), see Figure 3.16. Due to the compacted state of these soils, it is important to investigate the influence of an aggregated structure on mechanical behaviour under unsaturated conditions.

Compacted structure can influence water retention behaviour (e.g. Vanapalli et al., 1999), as discussed in Section 3.5.2. The influence of structure generated during compaction has also been linked with volumetric collapse behaviour. Typically specimens prepared dry of optimum at low dry density may exhibit collapse behaviour whereas specimens compacted wet of optimum may show no collapse or may even exhibit swelling behaviour. For the Bengawan Solo fill material such results were presented in Chapter 5 of this thesis. Studies carried out by Booth (1975; 1977) recognised the importance of considering soil structure when investigating volumetric collapse behaviour. In one of set of tests Booth (1975) compacted specimens at the same moisture content and then conditioned them to different moisture contents prior to loading by drying or

wetting. This was carried out for specimens at a number of different compactive efforts. Despite having the same initial fabric (compacted at same initial moisture content), the specimens conditioned to drier moisture contents exhibited higher collapse strains than those conditioned to higher moisture contents. This result indicates that initial fabric alone cannot account for the variations in volumetric collapse observed for many soils when compacted dry of optimum compared to samples compacted wet of optimum. Similarly in Chapter 5 of this thesis, Series COG illustrated that a specimen compacted wet of optimum may exhibit significant collapse after following a drying path. In another set of tests, Booth (1975) compacted specimens at different moisture contents to the same dry density and then conditioned the specimens to the same degree of saturation prior to loading. Of three different soils tested only one (sandy silt) exhibited some moderate difference in collapse strains attributed to differences in the initial compacted fabric. For the other two soils tested negligible differences in collapse behaviour were observed. Although Booth (1975) made attempts to control moisture content and dry density, these tests were carried out in conventional oedometer apparatus, without the benefit of suction control, and thus variations in suction may have also existed. With the significant developments in experimental techniques for suction measurement and suction control in the last fifty years, it is worthwhile to investigate now the influence of structure while also taking into account the effects of soil suction.

Gens et al. (1996) presented such a study on the influence of soil fabric on volumetric collapse. One set of tests presented, compares the behaviour of specimens (i) compacted under dry of optimum conditions (Series D) and (ii) prepared wet of optimum (Series W) and then brought to the same conditions of moisture content, dry density and suction of D prior to loading (see Figure 7.2a). In this way any differences in soil behaviour could be attributed to the soil fabric, as all conditions prior to loading were the same (w, ρ_d, s). Specimens in Series W and D both exhibited volumetric collapse on soaking at 600kPa, however that of Series D, compacted under dry of optimum conditions, exhibited significantly higher collapse (Figure 7.2b). This result indicates that the fabric created during compaction may have an important influence on the subsequent volumetric behaviour for some soils.

Despite these efforts to study the effect of structure on volumetric collapse behaviour, few studies have yet attempted to study the effect of aggregated structure solely on yielding and soil

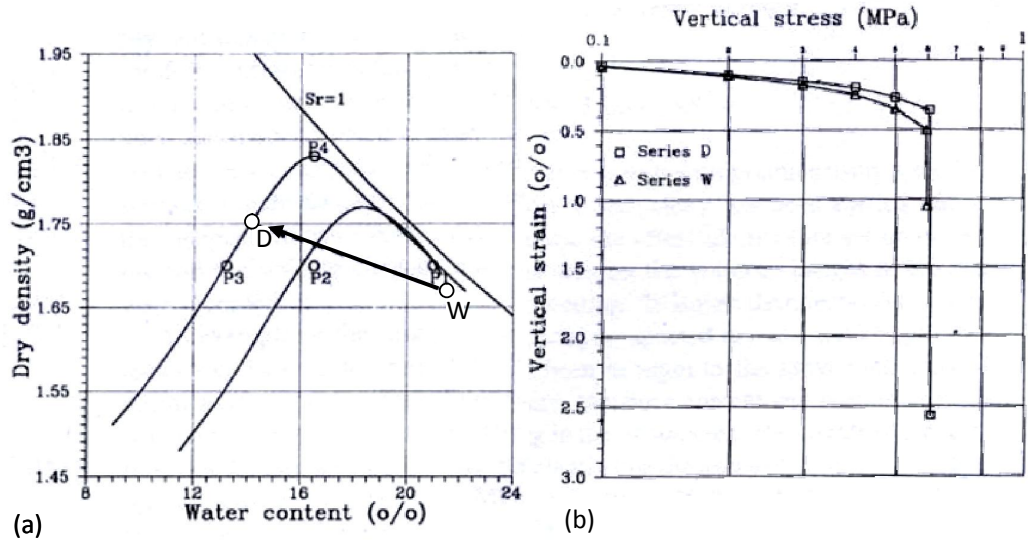

Figure 7.2: Influence of initial compacted structure on volumetric collapse behaviour (a) specimens compacted at dry of optimum (D), and wet of optimum (W) and brought to the same conditions of D, (b) volumetric collapse exhibited on loading at 600kPa (Gens et al., 1996)

compressibility. One such study is the work carried out by Koliji (2008), which compared the compression behaviour of aggregated and reconstituted specimens at different states of saturation. In this way the approach of the study was similar to those carried out for intact bonded soils using the reconstituted specimen as the reference state, but under different saturation conditions. As such specimens were not prepared at the same initial conditions of moisture content and dry density, all the reconstituted samples were prepared in an initially saturated state, although they were tested under the same applied suction in the oedometer. Comparison of the oedometer results (Figure 7.3) indicate that: (i) the compression curves for the aggregated and reconstituted specimens tend to converge at high effective vertical stresses, (ii) the aggregated specimens exhibit higher post-yielding compressibility (i.e. higher compression index C_c) and (iii) the aggregated specimens existed at higher void ratios than the reconstituted specimens at a given stress level (until very high stresses were reached). Essentially it appears that the influence of an aggregated structure on compression behaviour is very similar to that of an intact bonded soil, despite the different possible causes of the structure (as suggested by Leroueil and Vaughan, 1990).

Koliji (2008) also investigated the influence of suction on the mechanical response of these structured and destructured specimens (Figure 7.4). For both reconstituted and aggregated

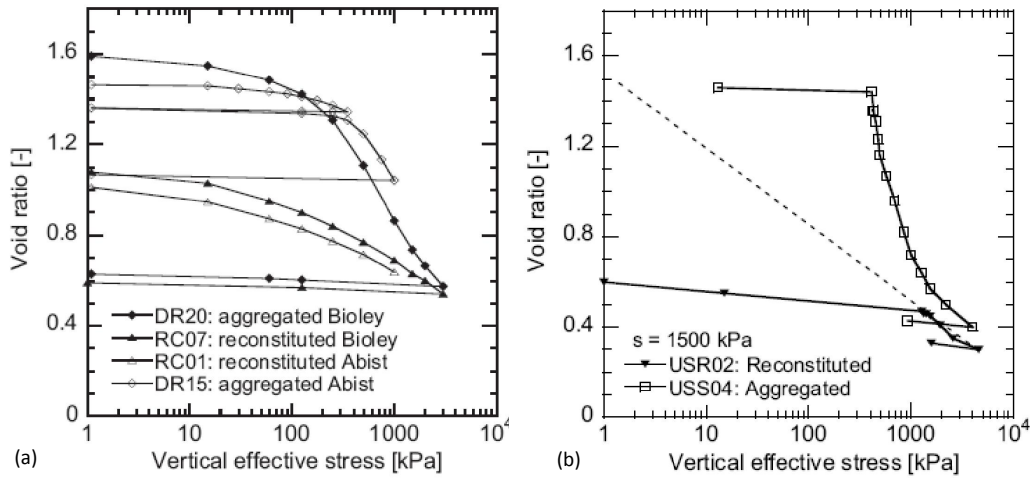

Figure 7.3: Comparison of compression behaviour of reconstituted and aggregated specimens under (a) dry conditions for Bioley silt and Abist silty clay and (b) suction controlled conditions at s = 1500kPa for Bioley silt (Koliji, 2008)

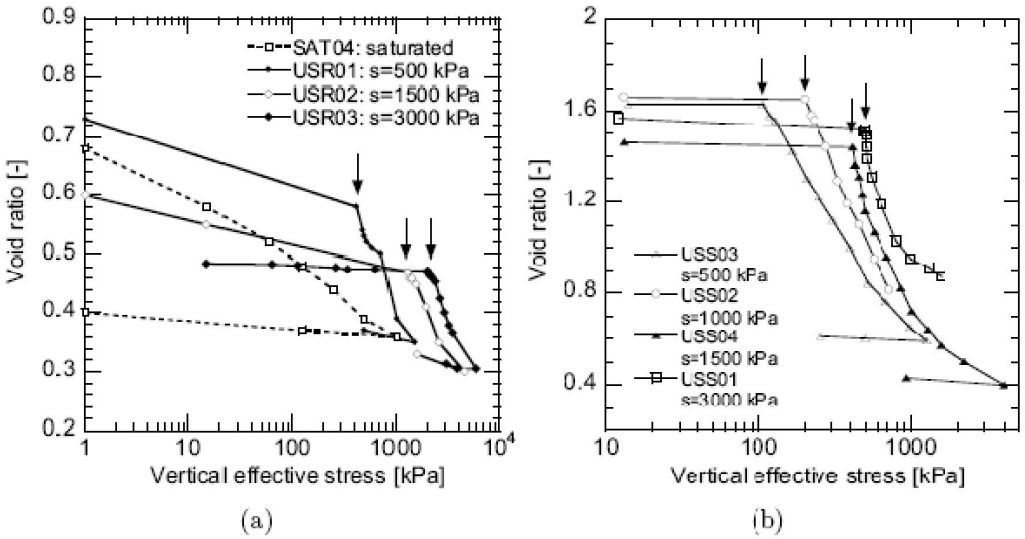

Figure 7.4: Comparison of unsaturated compression behaviour (a) reconstituted Bioley silt and (b) aggregated Bioley silt at different suction levels (Koliji, 2008)

specimens the yield stress was found to increase with increasing suction. The slope of the normal compression line of the reconstituted specimens increased moving from saturated to unsaturated specimens, but varied little thereafter with further increases in suction. Whereas the aggregated specimens exhibited a continuing increase in the slope of the post-yield compression curves with increasing suction. It is acknowledged here that the yield stress exhibited by structured specimens is a function of both stress state and stress history but also soil structure (Leroueil and Vaughan, 1990) and in unsaturated conditions suction. For this reason the term yield stress is adopted, rather than the term preconsolidation stress.

In this chapter the emphasis is on the influence of the aggregated soil structure of the Bengawan Solo fill created by compaction, on compression behaviour. Tests conducted using conventional oedometer apparatus presented in the next section investigate the influence of initial moisture content, dry density and soil fabric on yielding and compressibility of the Bengawan Solo fill. The types of aggregates created by mixing at different moisture contents and the corresponding compacted structure are then investigated. The second half of the chapter presents results from tests conducted in the UPC suction controlled oedometer, which have been specifically designed to investigate the influence of different soil structures on the yield stress and compressibility of the Bengawan Solo fill. Instead of only comparing aggregated structures with reconstituted (destructured) specimens, specimens with different fabrics have been created and brought to the same conditions of dry density, moisture content and suction prior to loading. In this way any difference in behaviour observed can be attributed solely to the effect of soil fabric.

7.3 Conventional oedometer tests

7.3.1 Testing programme & objectives

Initially conventional oedometer apparatus was used to investigate the influence of initial conditions (w_o, ρ_{d_o}) in compacted and reconstituted specimens, on the yielding behaviour and compressibility of the Bengawan Solo fill. Table 7.1 presents details of each series and the conditions of each test specimen prior to loading. The test references listed in Table 7.1 follow on from the naming convention used in Chapter 5 (e.g. COI1 refers to Conventional Oedometer

Table 7.1: Series details & initial conditions

Test Ref.	w_o (%)	ρ_{d_o} (Mg/m^3)	e_o	S_{r_o}	Loading Condition
COI1	16.2	1.17	1.324	33.3	CW
COI2	23.4	1.20	1.263	50.3	CW
COI3	27.2	1.22	1.226	60.3	CW
COJ1	22.3	1.34	1.030	59.0	SAT
COJ2	22.2	1.55	0.755	79.9	SAT
COK1	52.2	1.14	1.383	100.0	SAT
COK2	48.1	1.16	1.356	96.3	SAT
COK3	40.8	1.25	1.181	93.7	SAT
COK4	38.2	1.30	1.098	94.3	SAT
COB1*	24.0	1.18	1.298	50.3	SAT
COF2*	35.4	1.20	1.277	75.4	CW

*Tests from Chapter 5, presented here for comparison purposes

equipment, Series I, Test 1). In Series COI, specimens were compacted at a similar initial dry density (~1.2Mg/m^3) but at different moisture contents and tested under constant water (CW) conditions. In Series COJ specimens were compacted at a similar initial moisture content but to a different initial dry density and then tested under saturated conditions (SAT). In Series COK, specimens were all prepared from an initial reconstituted slurry sample, prepared at a moisture content close to the liquid limit ($w_L = 53\%$) and allowed to dry for durations of 1, 2 and 3 days respectively and were then tested under saturated conditions. During drying, shrinkage of the samples occurred and thus specimens achieved different moisture contents and dry densities but all originating from the same initial destructured fabric.

The objectives of these simple conventional tests are to investigate for the Bengawan Solo fill material: (i) the influence of moisture content and (ii) dry density on the yielding behaviour and compressibility of compacted and reconstituted specimens.

7.3.2 Experimental Methodology

The equipment used for these tests was the conventional oedometer apparatus, presented in Chapter 5, Section 5.2.4.

7.3.2.1 Specimen preparation

For Series COI and COJ specimens were prepared from 2mm sieved air dried, crushed material. Samples were mixed to the desired moisture content and left to homogenise for at least 24hrs before compaction. Samples were then prepared by compacting into the oedometer retaining ring (Ø = 60mm, h = 18mm) in three layers, using a tamping rod and light hammer. The mass required to reach a given density was weighed out in three batches and compacted in three separate layers to improve the homogeneity of the specimen.

In Series COK, each of the specimens were prepared from an initial slurry sample, prepared at a moisture content close to the liquid limit, in a much larger ring. The slurry sample itself was tested under saturated conditions alongside samples which were allowed to dry for 1, 2 and 3 days respectively. The slurry samples were prepared by lightly pressing the reconstituted material with a palette knife to ensure removal of air pockets and to give a smooth surface. A cutting ring with a sharp edge was used to sample specimens from the desiccated slurries. These specimens remained within the cutting rings during oedometer testing.

7.3.2.2 Test set-up

Specimens in Series COI were tested under constant water content conditions. No drainage was permitted from the bottom of the oedometer cell, and the top drainage outlet was open to the atmosphere. A small tube connected the top drainage outlet to a beaker of water, where the water surface was free to the atmosphere, in order to minimise moisture losses due to evaporation.

Specimens in Series COJ and COK were tested under saturated conditions; top and bottom drainage outlets remained open during loading. Water was added when the specimen was mounted and under a small contact load of 3kPa, any swelling observed was recorded.

7.3.2.3 Loading

Vertical stress was applied to the front loading oedometer by the addition of weights in 24hr intervals, up to a maximum of approximately 1MPa. Loading and unloading paths were followed.

7.3.3 Results

7.3.3.1 Series COI

Figure 7.5 presents the oedometer curves for Series COI, where specimens were tested under constant water content at similar initial dry density but varying moisture content, ranging from 16% to 35%. The saturated reconstituted slurry sample ($w = 52\%$, COK1) tested under saturated conditions is also presented here for comparison purposes. The constant water content results should be considered in terms of net vertical stress ($\sigma_v - u_a$) also denoted as $\overline{\sigma}_v$. The saturated test results should be considered in terms of effective stress $\sigma_v - u_a$ or σ'_v. In Series COI, u_a is atmospheric and in the saturated tests no back pressure was applied, thus all results are plotted against applied vertical stress (Figure 7.5). The yield stress $\overline{\sigma}_{vc}$ was determined for each curve using Casagrande's graphical method (Casagrande, 1936) and the compression index C_c and swell index C_s were also determined (Table 7.2). The swelling behaviour exhibited by soils due to unloading is typically well represented by a straight line in a semi-log plot of $v - \log \sigma'_v$ and it appears that this is also true of structured soils (e.g. Leroueil and Vaughan, 1990). On the other hand, it can be difficult to assign a single value of C_c to structured soils where the value of C_c may vary continuously after yielding. Terzaghi et al. (1996) suggest that a secant value of C_c (rather than tangential) be taken between σ'_{vc} and $2\sigma'_{vc}$, if such a parameter is required for settlement calculations. In this chapter values of C_c are presented in order to compare the post-yield compression behaviour of specimens of varying structure. The C_c values presented correspond to the steepest portion of the $v - \log \sigma_v$ plots, and is marked on each of the graphs for clarity. It is evident in Figure 7.5 that all of the compression curves of the compacted specimens lie to the right of the virgin compression line for the reconstituted material. As moisture content reduces the compacted compression curves lie further away from the reconstituted curve, withstanding higher void ratios under the same stress level.

Figure 7.6 illustrates more clearly how the compacted moisture content influences yield stress, soil compressibility and swelling behaviour. It is clear that $\overline{\sigma}_{vc}$ (or $\sigma'_{vc}$for COK1) increases as moisture content decreases from 20kPa at $w_o = 52\%$ to 200kPa at $w_o = 16\%$. Furthermore it is evident that C_c increases as the moisture content decreases, indicating that the compressibility of the soil increases as moisture content decreases, within the range of moisture contents tested.

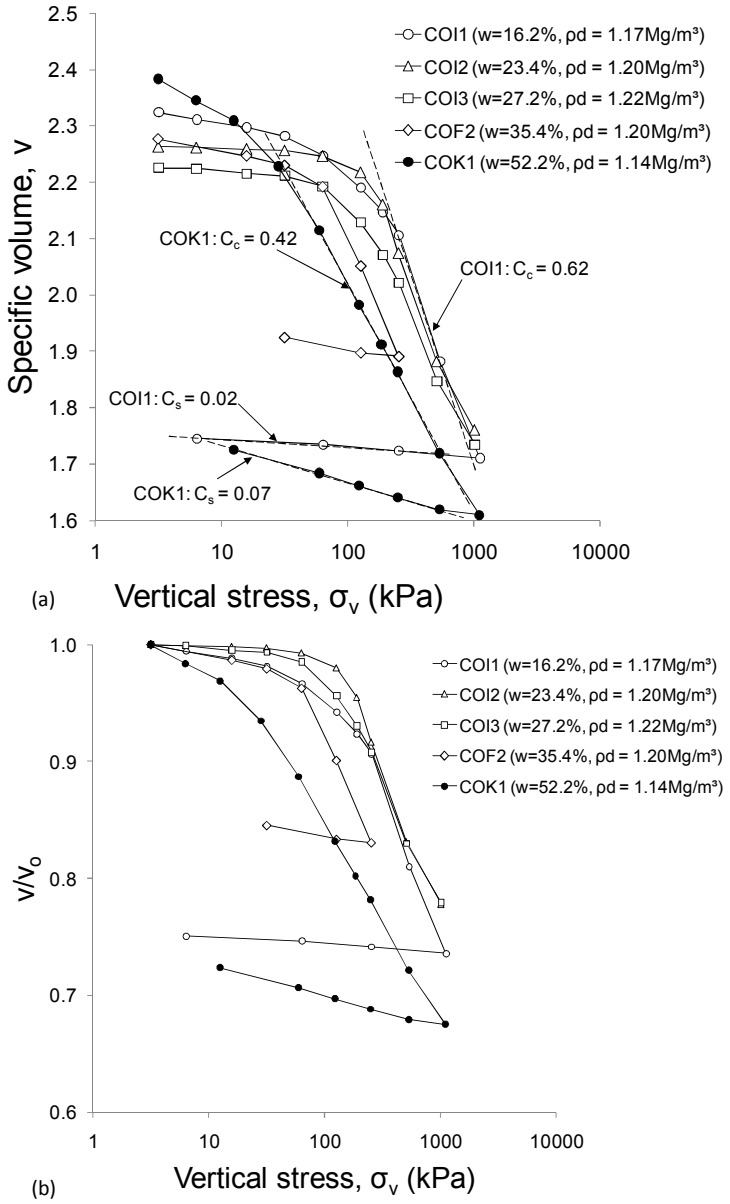

Figure 7.5: Series COI: Constant water content tests for specimens compacted at different initial moisture contents (a) specific volume and (b) normalised specific volume against effective vertical stress

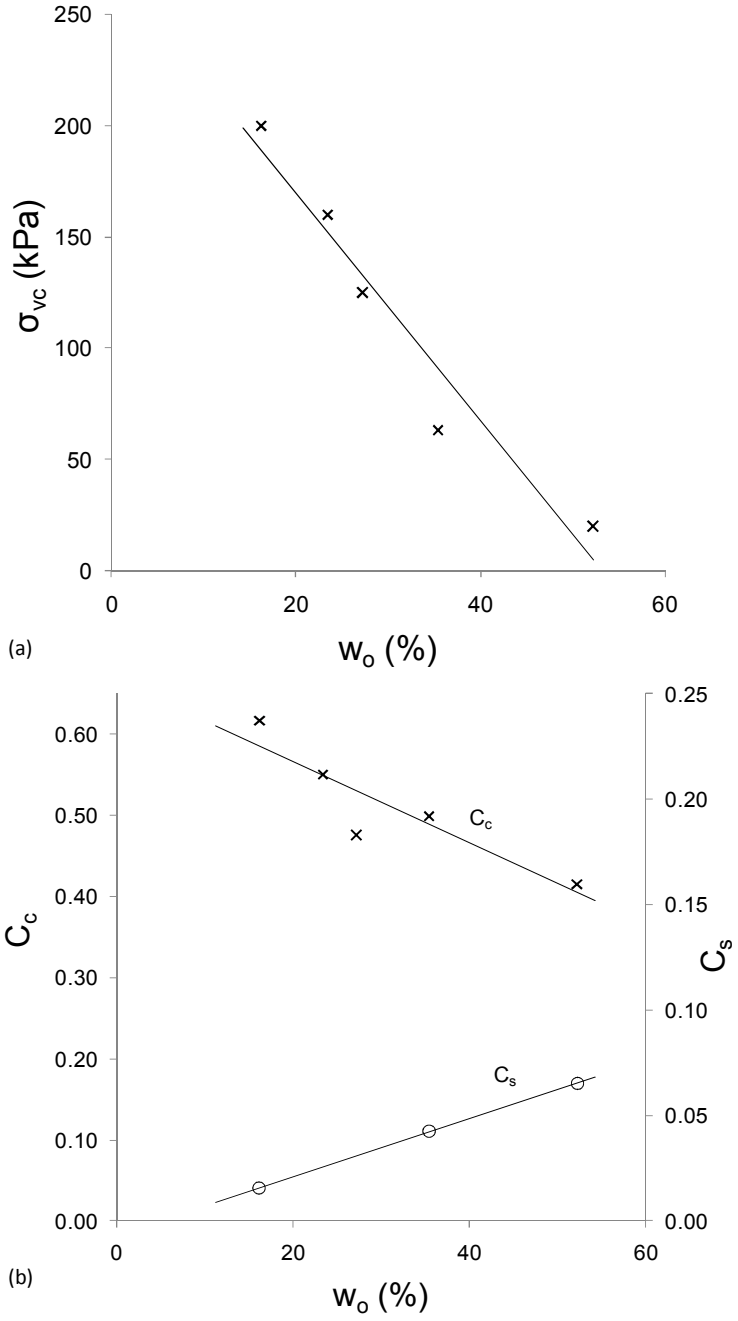

Figure 7.6: Influence of initial moisture content on (a) $\overline{\sigma}_{vc}$ and (b) C_c and C_s

The initial moisture content also appears to influence the swell index, with it increasing with increasing compacted moisture content. The influence of moisture content on $\overline{\sigma}_{vc}$, C_c and C_s observed in Series COI cannot be solely attributed to soil structure effects as the specimens compacted at different moisture contents will have different initial suctions which also influences yielding and compression behaviour. In order to investigate if compacted moisture content has an important influence on the soil structure of the Bengawan Solo fill, the aggregates created at different moisture contents and their corresponding compacted structure is investigated in further detail in Section 7.4.

7.3.3.2 Series COJ

Figure 7.7 presents the oedometer curves for three specimens compacted at similar initial moisture content but to different initial dry densities and loaded under saturated conditions. It is evident in these results that as the initial dry density increased, the yield stress exhibited increased, which we expect as for these specimens the yield stress is directly related to the compactive energy applied, with a higher compactive energy being required to prepare specimens at a higher density. Initially COB1 exhibits a markedly different post-yield compression behaviour with a much higher C_c value than COJ1. At higher stresses the post-yielding compression behaviour for the two specimens converges, this suggests that the initial steep curve of COB1 is due to destructuration of the soil fabric present in the lower density specimen. The compression curves of COB1 and COJ1 also converge towards that of COJ2 (high initial dry density). The swell index determined from the unloading curve was the same for all three tests (C_s=0.05) in Figure 7.7. Table 7.2 presents σ'_{vc}, C_c and C_s for the curves in Series COJ. The swelling potential observed on saturation increased as the initial dry density increased from 1.8% for COB1 to 3.0% for COJ2. It was not possible to determine C_c for COJ2, as it had not yet undergone much post-yield compression, even at 1MPa of effective vertical stress, indicating the stiffer nature of the high density specimen. These results indicate that initial dry density controls yield stress and that at low dry densities higher compressibility may be observed due to the more open fabric initially present.

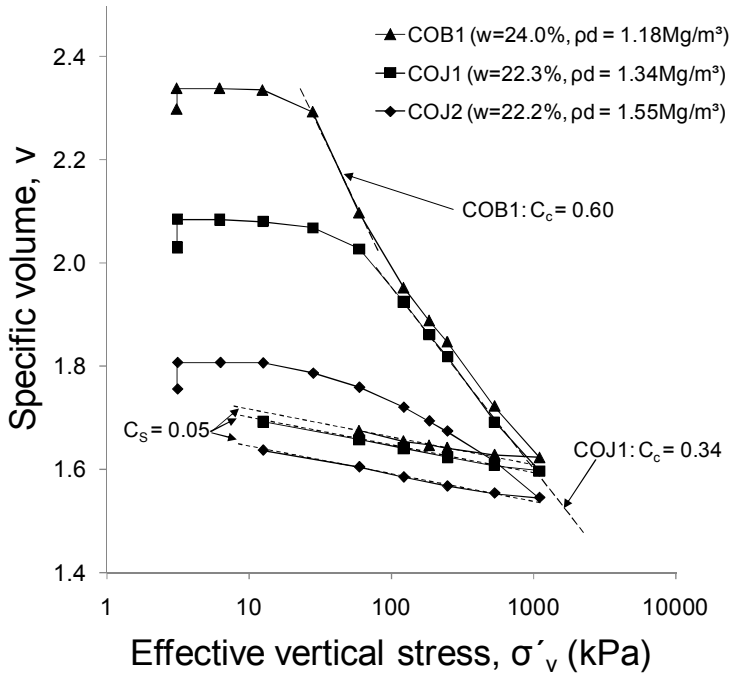

Figure 7.7: Series COJ: Saturated oedometer tests for specimens all prepared at different dry density but similar initial moisture content

7.3.3.3 Series COK

In Series COK slurry samples were prepared and then dried for 1 day, 2 days, and 3 days, and then loaded under saturated conditions. COK1 is the reconstituted specimen tested with no drying. As the samples were progressively dried from an initial slurry they underwent changes in moisture content and volume, as such these specimens all had different initial moisture contents and dry densities (Figure 7.8), but were all prepared from the same initial destructured fabric. In Figure 7.9 it is evident that all the specimens exhibit similar post-yield compression and swelling behaviour with values of C_c between 0.41 and 0.42 and values of C_s between 0.06 and 0.07 for all the specimens tested in Series COK. The main difference in the compression behaviour of specimens in Series COK is that as the dry density of the specimens increased, the yield stress increased. The increased dry density is a consequence of the shrinkage of the specimens during drying, resulting in a higher mass of solids per unit volume which corresponds to an increased domain in which stiff behaviour is exhibited. In Figure 7.10 σ'_{vc} is plotted against initial dry density, (initial referring here to the condition immediately prior to loading). Table 7.2 presents the values of σ'_{vc}, C_c and C_s determined for the curves presented in Figure 7.9. It should also be

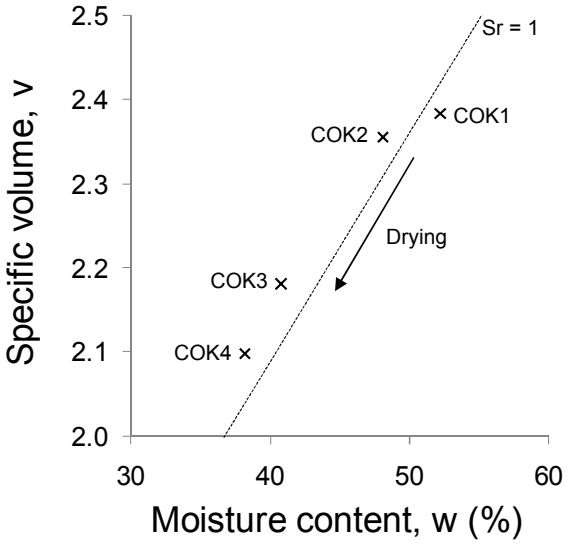

Figure 7.8: Shrinkage of slurry specimens

noted that despite the similarities in the values of C_c and C_s the specimens prepared by drying all lie to the right of the reconstituted line, perhaps this is an indication of some structural effects due to the drying process which have not been removed by hydration and subsequent loading. This difference is not thought to be due to an error associated with the experimental equipment as both COK1 and COK2 were carried out in the same experimental set-up (same oedometer cell, loading frame and linear displacement transducer).

Test COK1 will be used as a reference state for the comparison of compression curves of different specimens later in this chapter, following the approach adopted in the study of intact bonded soils. Burland (1990) proposed that the saturated compression curve of a soil reconstituted at a water content of between w_L and $1.5w_L$ be termed the intrinsic compression curve. The intrinsic properties associated with the reconstituted state are denoted with an asterisk (e.g. C_c^*,C_s^*). Figure 7.11 presents the intrinsic compression line of the Bengawan Solo fill and its associated intrinsic properties. The initial response of the reconstituted soil to loading is slightly stiffer than would be expected for such a sample and can be explained by the light pressing action undertaken when placing the material into the oedometer ring (to remove air pockets). Burland (1990) further proposed that the compression curves of natural (structured) and reconstituted (destructured) clays be compared using a normalised parameter of void ratio, defined as the

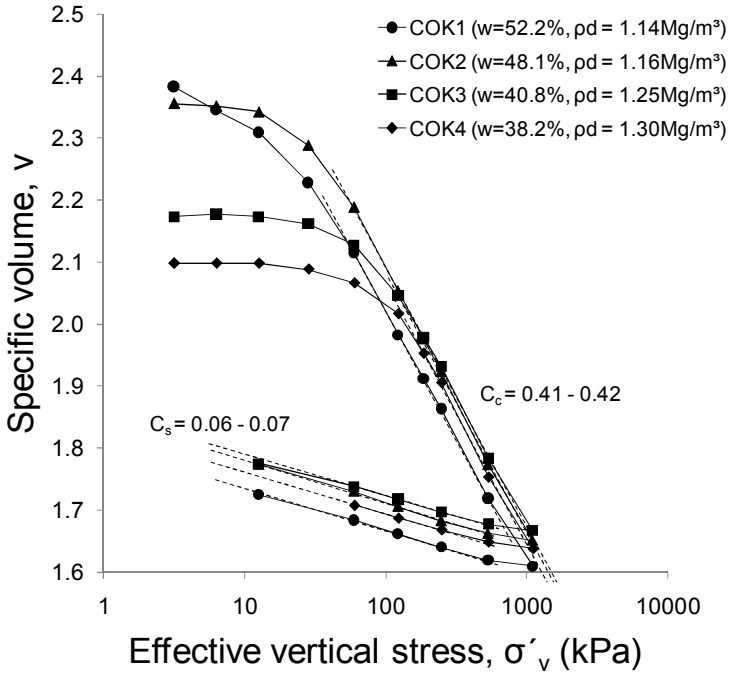

Figure 7.9: Series COK: Oedometer tests on saturated slurry specimen and specimens prepared at an initial slurry and dried for varying durations

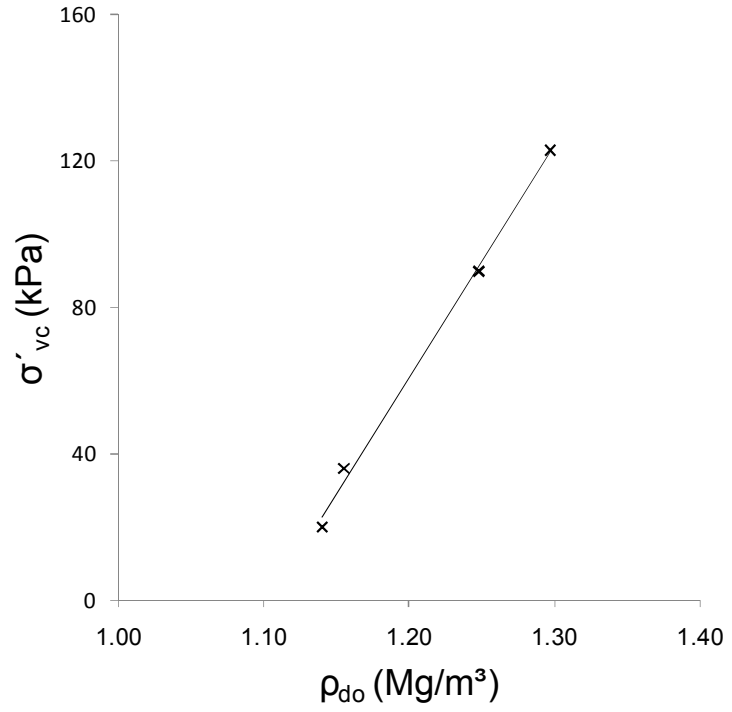

Figure 7.10: Variation of σ'_{vc} with initial dry density (i.e. density prior to loading) for Series COK

Table 7.2: Yielding and compressibility parameters of Series COI, COJ and COK

Test Ref.	w_o (%)	ρ_{d_o} (Mg/m³)	$\overline{\sigma}_{vc}$ or σ'_{vc} (kPa)	C_c	C_s
COI1	16.2	1.17	200	0.62	0.02
COI2	23.4	1.20	160	0.55	-
COI3	27.2	1.22	125	0.48	-
COF2*	35.4	1.20	63	0.50	0.04
COB1*	24.0	1.18	27	0.35	0.05
COJ1	22.3	1.34	60	0.34	0.05
COJ2	22.2	1.55	210	-	0.05
COK1	52.2	1.14	20	0.42	0.07
COK2	48.1	1.16	36	0.42	0.07
COK3	40.8	1.25	90	0.41	0.06
COK4	38.2	1.30	123	0.41	0.06

*Tests from Chapter 5, presented here for comparison purposes

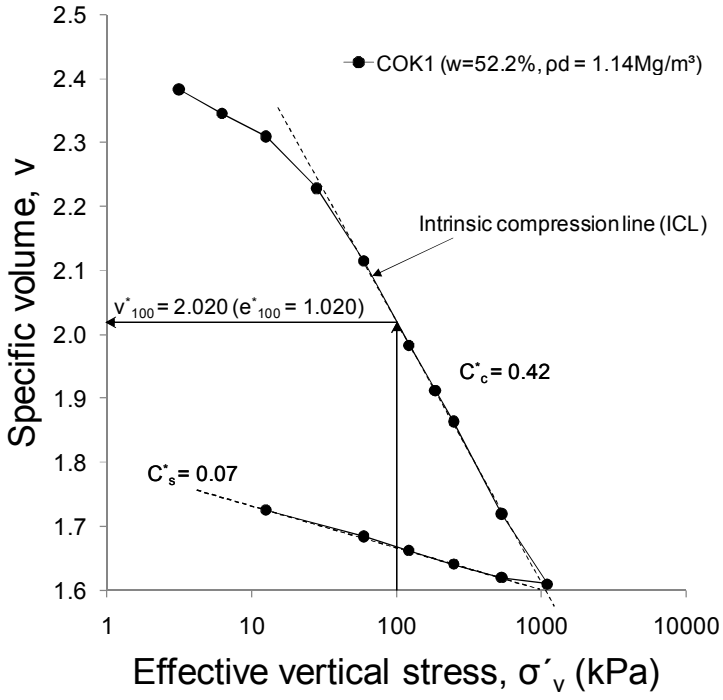

Figure 7.11: Intrinsic compression line and associated intrinsic properties of the Bengawan Solo fill

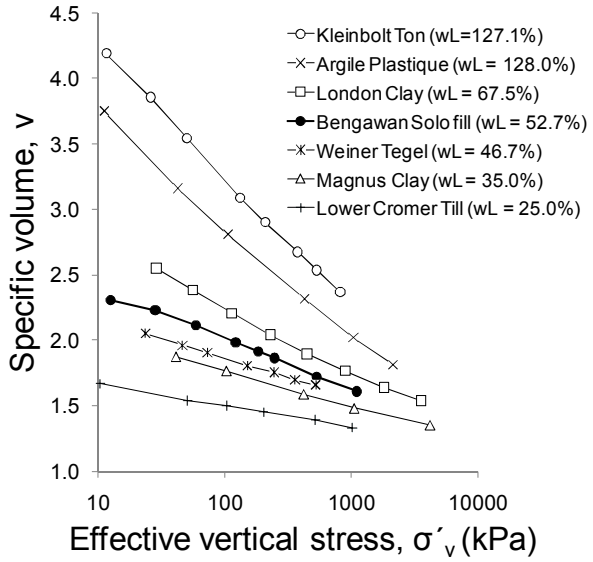

Figure 7.12: Comparison of intrinsic compression line of Bengawan Solo fill material with reconstituted clays. Plot after Burland (1990), data from Hvorslev (1937): Kleinbelt Ton, Wiener Tegel, Skempton (1944): Argile Plastique, Gens (1982): Lower Cromer Till, Jardine (1985): London Clay and Magnus Clay

void index, I_v:

$$I_v = \frac{e - e^*_{100}}{C^*_c} \tag{7.1}$$

where e^*_{100} is the void ratio of the saturated reconstituted soil under a vertical effective stress of 100kPa. For the Bengawan Solo fill e^*_{100}= 1.020 and C^*_c is the compression index of the reconstituted soil $C_c = 0.42$ (see Figure 7.11). Later in this chapter the void index (I_v) is used to compare the compression behaviour of specimens prepared with different soil fabrics.

The intrinsic compression line (ICL) for a number of different soils is presented in Figure 7.12, evidently there is a strong relationship between the ICL and the liquid limit (w_L). The void ratio at which a soil can exist in its reconstituted state at a given stress level decreases as the liquid limit reduces. Furthermore the gradient of the ICL also decreases with decreasing w_L. The ICL for the Bengawan Solo fill (w_L = 52.7%) plots between the data of soils with w_L of 46.7% and 67.5% respectively. Despite the fact that the Bengawan Solo fill plots below the A-line on the Casagrande's plasticity chart (see Figure 4.7), and all the other soils plotted on Figure 7.12 plot above the A-line (Burland, 1990), it appears in terms of the ICL to follow the same pattern closely related to the w_L.

7.3.4 Summary

These initial results carried out in the conventional apparatus have investigated the influence of moisture content, dry density and role of initial fabric on the yield stress and soil compressibility.

In Series COI, compacted specimens tested under CW conditions indicated that:

- the yield stress increased as the compacted moisture content decreased
- C_c increased as the compacted moisture content decreased
- C_s decreased as the compacted moisture content decreased

It is anticipated that such behaviour is due to a combination of structural and suction effects. As such in the next section the influence of moisture content on compacted soil fabric is investigated in detail.

In Series COJ, compacted specimens tested under saturated conditions indicated that:

- the yield stress increased as the compacted dry density increased
- specimens prepared at the same compacted moisture content exhibit similar post-yield compression and swell behaviour

In Series COK, reconstituted specimens tested under saturated conditions indicated that:

- as the duration of drying increased (up to 3 days), corresponding to decreases in the initial moisture content and increases in the initial dry density, the yield stress increased
- specimens prepared from the same initial fabric exhibit similar post-yield compression and swell behaviour.

7.4 Soil structure created by compaction

7.4.1 Soil aggregates

The first step in investigating the soil structure created by compaction was to identify the size and nature of the aggregates created at different moisture contents. All compacted specimens were prepared by spraying water onto the air dried material (passing the 2mm sieve) and hand-mixing. As the moisture content is increased the size of the aggregates also increases, see Figure 7.13. In order to determine the aggregate size distribution the aggregates created by mixing at 9%, 24% and 36% were then passed through a series of sieves with no addition of dispersant, water or mechanical force, i.e. the aggregate sizes were maintained. It is evident in Figure 7.13 that the aggregate size distribution changes with increasing moisture content, from a well-graded distribution for the 9% sample to a fairly uniform distribution for the 36% sample. The aggregates mixed at 9% range up to 4mm in size, the 24% sample contains aggregates up to 10mm, whereas the 36% sample contains aggregates up to 40mm. It is clear that the size of the aggregates produced is greatly influenced by the mixing moisture content, see Figures 7.13b, c and d. Tarantino and De Col (2009) presented similar evidence of increasing aggregate size with increasing moisture content for hand-mixed kaolin samples, although the sizes of the aggregates observed were much smaller overall, up to 1mm. The very large aggregates observed here at a high moisture content (36%) can be explained by considering that the clay fraction present in this material is montmorillonite and at high moisture contents, smaller aggregations easily attach themselves to each other to form larger overall aggregations (or assemblages).

Another important property of the aggregates is also influenced by moisture content: aggregate stiffness. The stiffness of individual aggregates reduces with increasing moisture content. At a moisture content of 9% the aggregates created are fine, dry and stiff. These aggregates cannot be broken between fingers easily, and are essentially granular in nature. In contrast however are the large, wet, soft aggregates created at 36% moisture content. These aggregates can easily be squeezed between fingers and are plastic in nature. At a moisture content of 24%, the aggregates have increased in size, but remain relatively firm.

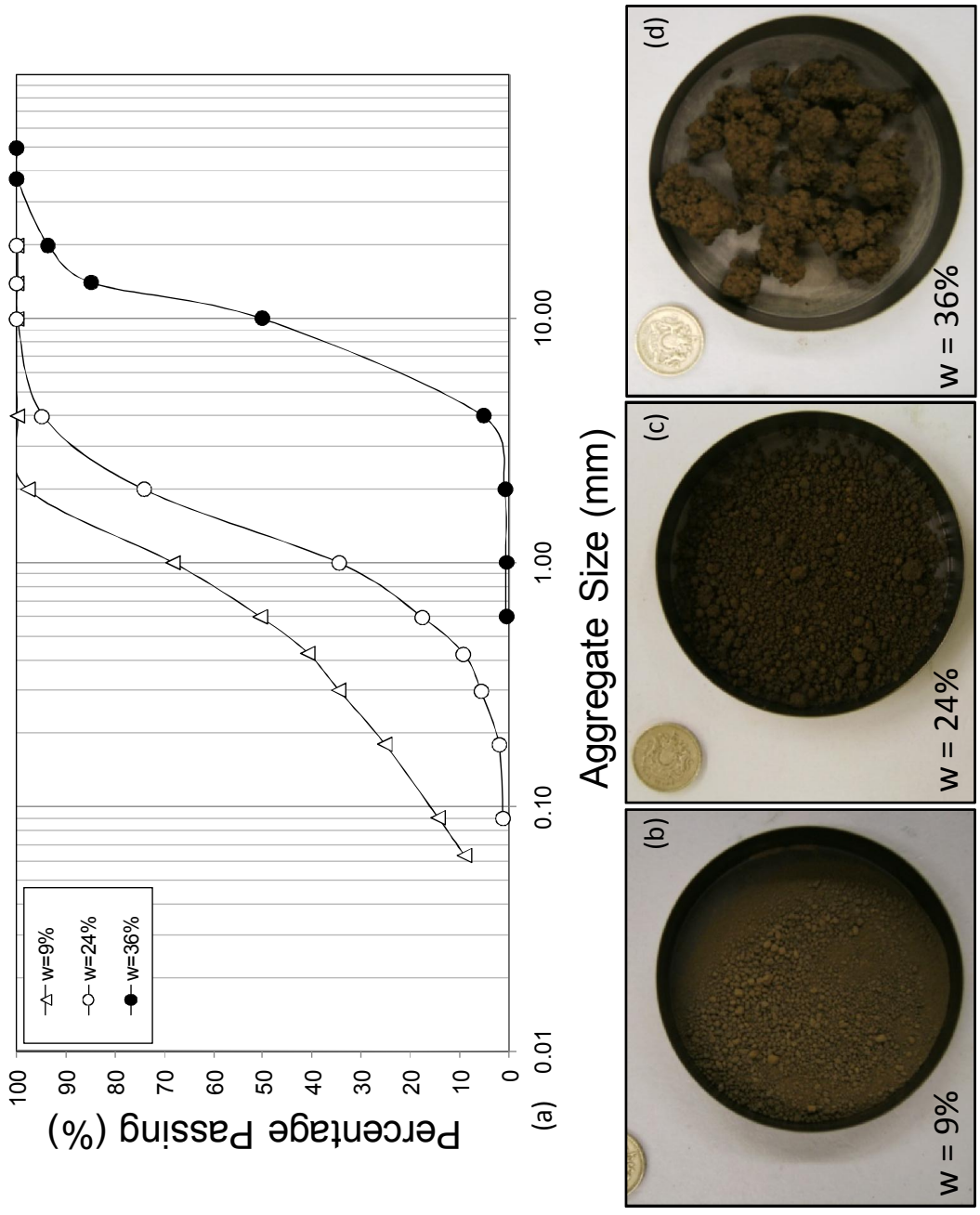

Figure 7.13: Influence of moisture content on aggregate size: (a) aggregate size distribution and (b, c, d) photographs of aggregates created

7.4.2 Irregular compaction curve

These changes in the nature of the aggregates is particularly important when considering the structure created by compaction. Essentially these changes can explain the irregular compaction curve obtained for the Bengawan Solo fill at low compactive efforts, introduced in Section 4.6. Figure 7.14 presents the double-peak compaction curve determined at a compactive effort of 132kJ/m^3 (Extreme Light compaction curve), alongside photographic evidence of the different structures created by compaction at different moisture contents. The first peak of the irregular compaction curve occurs at a moisture content of 9%, and can be explained by a dense packing of these very fine, dry (granular) aggregates. The second peak of the extreme light curve occurs at a moisture content of 36% and can be explained by its large soft aggregates, which easily fuse together under this compactive effort, creating a more homogeneous fabric. The trough (or valley) of the extreme light compaction curve occurs at a moisture content of 22-24% and is a result of the medium sized relatively firm aggregates created at this moisture content, which retain their aggregate form under this compactive effort, resulting in an open fabric being created. This aggregated open fabric is clearly visible in Figure 7.14 (w = 23.7%), its crumbly nature is also evident, illustrated by the difficulty in cutting slices of this compacted sample. The stiffness of these aggregates have provided sufficient resistance to the compactive effort, such that the form of the aggregates has been maintained.

On the basis of this information we can revisit the initial results presented from series COI, COJ and COK. In Series COJ and COK material was initially prepared at the same moisture content either in aggregated form (COJ) or reconstituted form (no aggregates, COK). For each of these series the post-yield compression behaviour of the specimens was similar, similar values of C_c and C_s. In Series COI however where specimens were compacted at different moisture contents and thus would have been formed of aggregates of varying size and stiffness, the compression behaviour exhibited was significantly different. However these tests were carried out under constant water content conditions and therefore suction alongside structure is likely to be influencing this behaviour. The tests carried out in the suction controlled oedometer have been designed to isolate the effects of structure from that of suction.

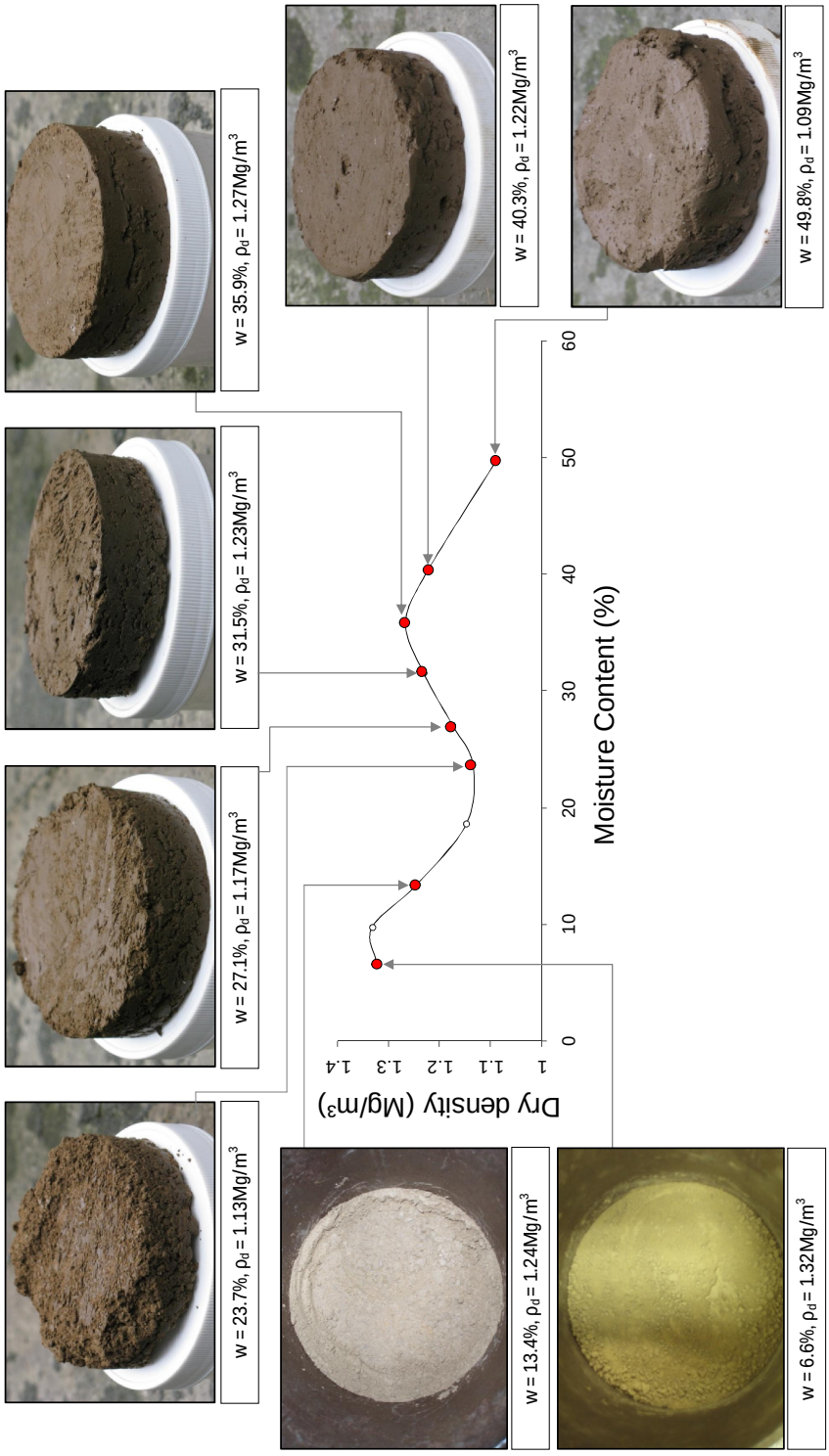

Figure 7.14: Irregular compaction curve & evidence of compacted structure

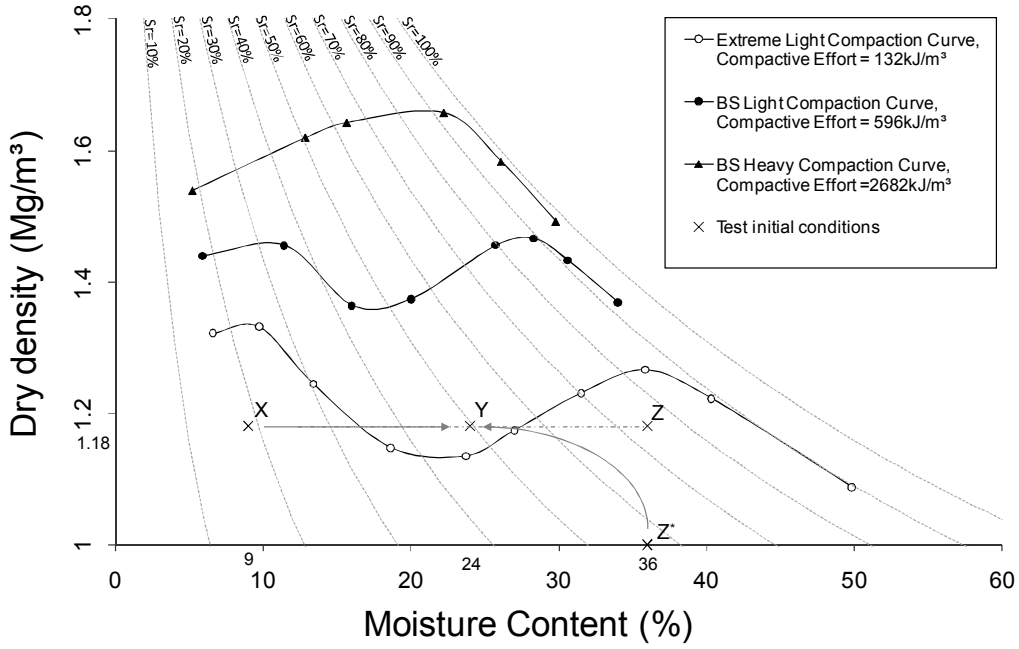

Figure 7.15: Initial conditions of microstructural study on compaction curve

7.4.3 Microstructural study

7.4.3.1 Objectives and methodology

Mercury intrusion porosimetry tests were carried out at UPC, Barcelona in order to determine how the aggregates created at different moisture contents influence the compacted structure obtained. Three specimens referred to as X, Y and Z were investigated, these were compacted at moisture contents of 9%, 24% and 36% respectively and compacted to an initial dry density of 1.18Mg/m^3 (see Figure 7.15). This low dry density was selected as it corresponds to 80% of the maximum BS Light dry density, is similar to in-situ low dry densities found, and has been used as a references state throughout this thesis. These compaction conditions correspond to the specimen conditions which were investigated further in the UPC oedometer.

Where possible the specimens were prepared and compacted at Strathclyde in the same way as for the UPC oedometer tests (Section 7.5.3.2) before being shipped to UPC for testing. In the case of the low moisture content specimens ($w \sim 9\%$), a sample of the material at the desired moisture content was shipped. Due to the granular powdery nature of these aggregates, Specimen X was compacted in the MIP penetrometer by light tamping. This is similar to the

Table 7.3: Initial conditions of specimens X, Y, Z

Specimen	$w_o(\%)$	$\rho_{d_o}(\mathrm{Mg/m^3})$	e_o	$S_{r_o}(\%)$	e_w
X	9.0	1.18	1.306	18.8	0.245
Y	24.0	1.18	1.304	50.2	0.653
Z	36.5	1.17	1.318	75.3	0.993

method used to prepare this loosely packed specimen in the oedometer retaining ring. The same porosimeter equipment was used for these tests as was presented in Section 5.3.6. Furthermore the results presented here were determined using the same values for the non-wetting contact angle (140°) and surface tension (0.484N/m) as presented in Section 5.3.6.

7.4.3.2 Comparison of specimens X, Y, Z

Specimens X, Y and Z were investigated using MIP in order to determine the influence of different types of aggregates on the resulting compacted structure of specimens with the same dry density. Initial conditions of the MIP specimens are presented in Table 7.3 and are also located on the compaction plot presented in Figure 7.15.

Figure 7.16 presents the cumulative void ratio intruded for the three specimens X, Y and Z. Even on this plot it is evident, that despite their similar initial dry density, there is a clear difference in the intrusion slopes of each specimen. The non-detected void ratio (e_{nd}) which corresponds to pores greater than 0.5mm was calculated as in Section 5.3.6.6 using the non-intruded void ratio (e_{ni}) which was determined for the high density desiccated slurry specimen (Figure 5.28), where e_{ni} is due to isolated pores and pores with an entrance diameter less than 7nm. For the Bengawan Solo fill e_{ni} is assumed to be a constant value for all soil specimens equal to 0.078. The water ratio e_w which is the volume of water per volume of solids ($e_w = w\frac{\rho_s}{\rho_w}$) is also noted in Figure 7.16. If we assume that water fills first the smallest pores in a soil then the e_w can be used to separate the pore sizes which correspond to the water filled pores and those pores which are air filled (Tarantino, 2010b). The water ratio is also listed in Table 7.3.

The differences in the three compacted structures are also more clearly identified in Figure 7.17. Considering that the specimens are all compacted to the same dry density, these results clearly indicate differences in pore size distribution due to the nature of the aggregates created at

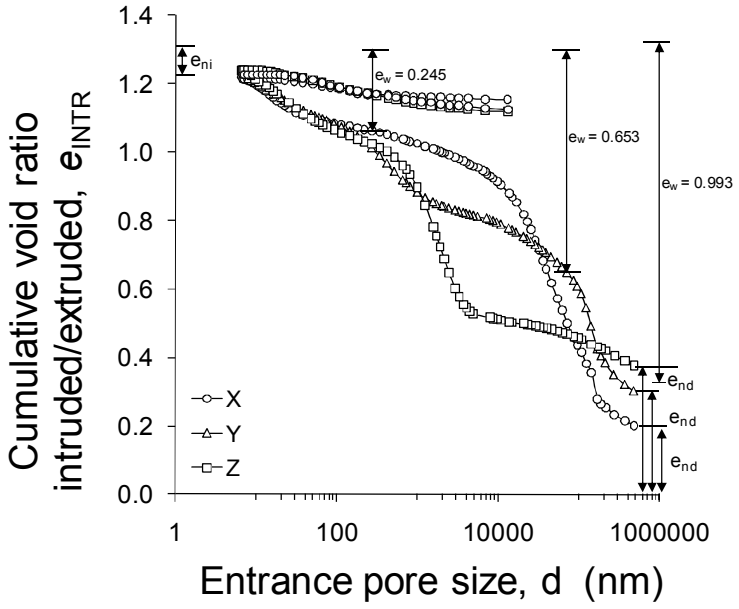

Figure 7.16: Cumulative void ratio intruded for Specimens X, Y and Z

different moisture contents and their subsequent arrangement when compacted. The three specimens (X, Y and Z) all exhibit multi-modal porosity within the range of pore sizes detected by the MIP (7nm to 0.5mm).

Specimen X exhibited a bi-modal distribution, with a dominant peak at an apparent pore diameter of 36µm, and a smaller peak at approx. 20nm (see Figure 7.17a). It is important to remember here that the specimens are prepared from air dried crushed material passing the 2mm sieve to which water is added. In the case of Specimen X ($w = 9\%$) only a small amount of water has been added (the hygroscopic water content is around 6% depending on relative humidity within the laboratory). Thus, if we consider that this specimen is made up of sand, silt and clay particles tightly bonded together to form dense soil packets at a high suction level (Tarantino and De Col, 2009), we can attribute the small pores (20nm) to pores within the clay packets (intra-clay aggregate porosity) and the larger pores (36µm) to the inter-aggregate porosity. Similar values for intra-clay aggregate porosity (8-20nm) have been reported for clays containing smectite (e.g. Lloret et al., 2003; Delage et al., 2006). The shaded area in Figure 7.17a corresponds to the water filled pores within Specimen X determined using e_w, which indicates that pores up to 268nm would be filled with water. This indicates that even at very low moisture contents the aggregates are themselves saturated when compacted, and it is the inter-aggregate

pores which are air filled. The fabric of Specimen X, based on this quantification of the pore size distribution, is illustrated in Figure 7.18a.

Specimen Y presents a tri-modal pore size distribution with a significant peak representing inter-aggregate pores at an apparent pore size of 140µm, a smaller peak at an apparent pore size of 0.4µm, representing the intra-aggregate pores and a third peak at an apparent pore size diameter of 20nm, as above this represents the intra-clay aggregate porosity (Figure 7.17b). Again, it is the intra-aggregate pores up to 68µm which are filled with water on compaction and the inter-aggregate pores are air filled. A possible schematic representation of the fabric of Specimen Y, with its tri-modal pore size distribution is presented in Figure 7.18b.

Specimen Z exhibited a bi-modal pore size distribution within the range detected by the MIP, with a dominant pore size at an apparent diameter of 1.9µm corresponding to the intra-aggregate porosity and a smaller peak corresponding to the intra-clay porosity (see Figure 7.17c and Figure 7.18c). It is expected that a porosity exists for this specimen at pore sizes greater than 450µm (outwith the range of the MIP) but it is not anticipated that this would be the dominant peak and it is more likely that it corresponds to an inter-assemblage porosity (see Figure 7.18). Furthermore it has commonly been reported that the frequency of inter-aggregate pores are reduced (and often absent) in specimens compacted wet of optimum compared to specimens compacted dry of optimum (e.g. Ahmed et al., 1974; Garcia-Bengochea et al., 1979; Delage et al., 1996).

Considering the soil aggregates prior to compaction, water is held within the intra-aggregate pores under tension (i.e. the pore water pressure is negative). Upon the application of a compactive effort in a compaction mould the aggregates will initially be subjected to undrained loading, which causes the pore water pressure within the aggregates to increase. If the pore water pressure increases to values above atmospheric pressure then water will be forced out of the intra-aggregate pores and begin to invade the inter-aggregate pore space (Tarantino, 2010b). This appears to be the case in Specimen Z (Figure 7.17c) where the shaded area representing the pore sizes filled with water extends beyond that of the intra-aggregate pores and in fact covers the entire range of pores detected by the MIP. This expulsion of water due to the loading of the aggregates also explains the distortion of the aggregates compacted at $w = 36\%$, which can easily be remoulded by hand, resulting in a fused fabric of homogeneous texture.

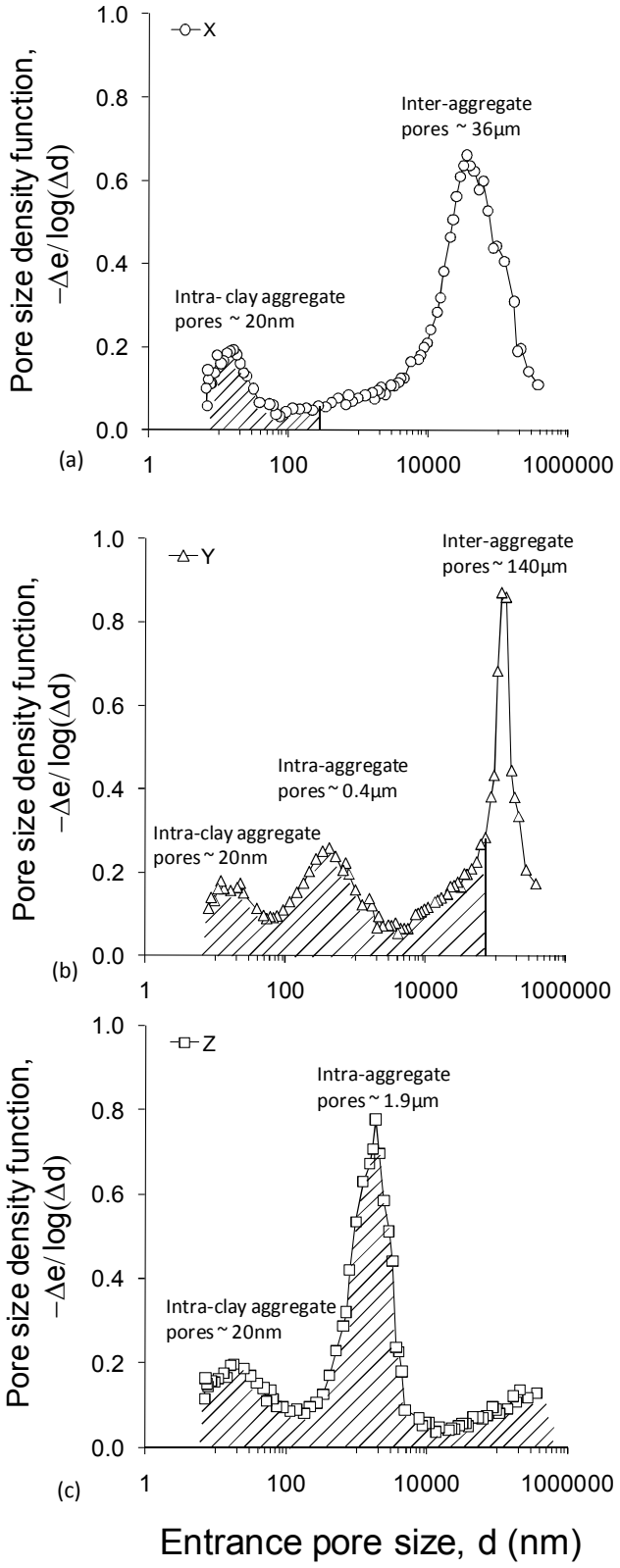

Figure 7.17: Pore size density function for Specimens (a) X, (b) Y and (c) Z

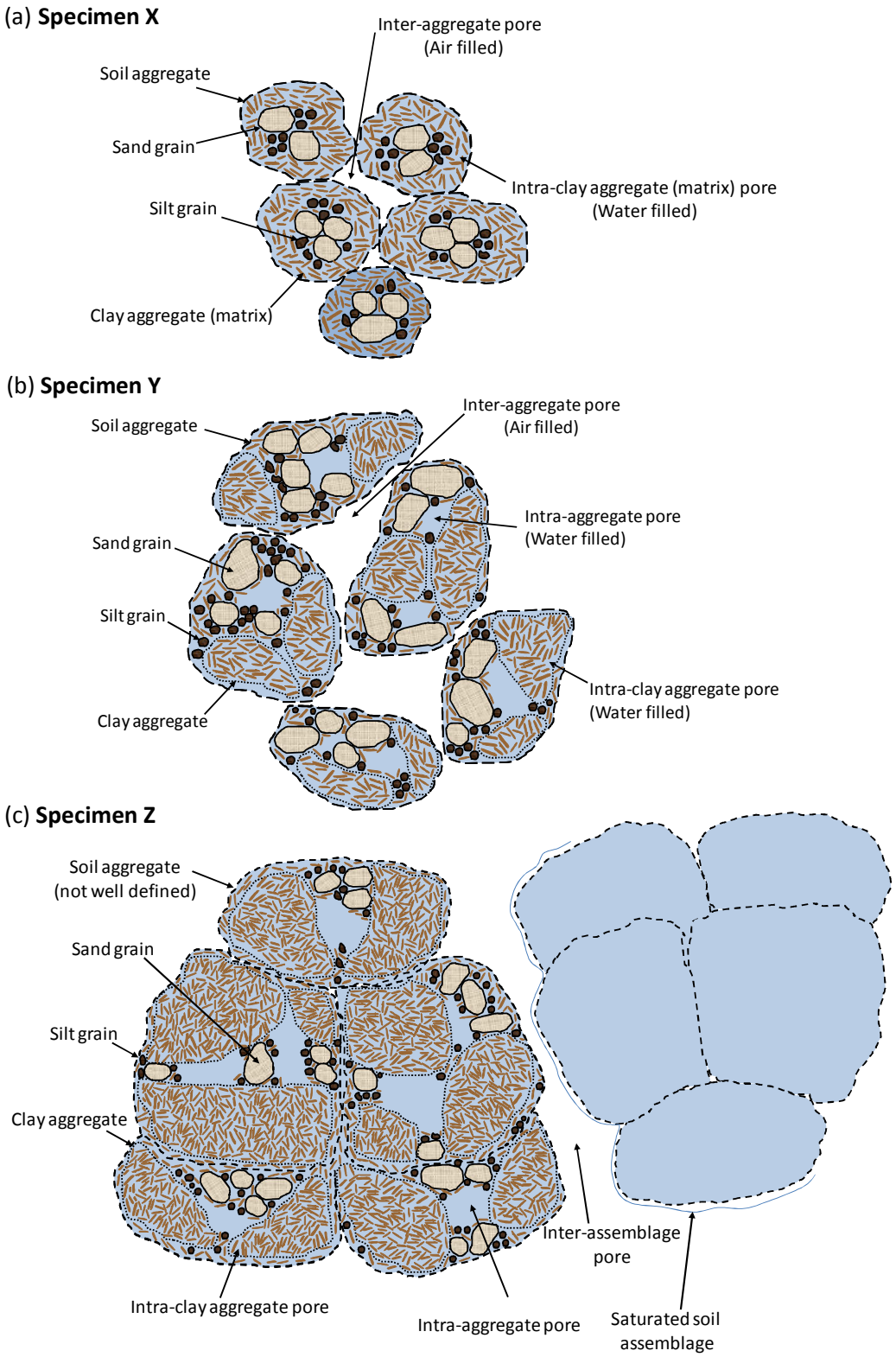

Figure 7.18: Simplified schematic of compacted soil fabric for Specimens (a) X, (b) Y and (c) Z of the Bengawan Solo fill

For all of the specimens the intra-clay aggregate porosity remains at approximately 20nm, indicating that this structural level is not affected by compactive effort as reported by Lloret et al. (2003). As moisture content was increased from X to Z it appears that the intra-aggregate porosity increases both in terms of pore size and frequency, with no intra-aggregate porosity found in X where the clay particles are tightly bonded together. Moving from Specimen Y to Z the intra-aggregate pore size increases in terms of pore size from 0.4µm to 1.9µm and frequency. It appears the size of the inter-aggregate pores increases from 36µm (X) to 140µm (Y). It is then expected that a larger inter-assemblage porosity exists for Specimen Z at a pore size >450µm. Such increases in pore sizes are related to the packing arrangement of the increasing size of the aggregates with moisture content as illustrated in Figure 7.18.

Although bi-modal pore size distributions have commonly been reported in the literature for clays compacted dry of optimum (Ahmed et al., 1974; Delage et al., 1996; Romero, 1999; Lloret et al., 2003; Tarantino and De Col, 2008 among others) it should not be surprising to find multi or tri-modal pore size distributions in soils with a mixture of sand, silt and clay particles, such as the Bengawan Solo fill. Futai and Almeida (2005) presented a tri-modal pore size distribution for an undisturbed residual gneiss soil, with two dominant peaks and a third much smaller peak at an intermediate pore size.

7.4.4 Water retention behaviour

It is possible to derive the relationship between soil moisture content and matric suction (water retention behaviour) from MIP data. In a normal soil drying path, e.g. as conducted in a pressure plate, water (the wetting fluid) recedes from the soil pores and it is air (the non-wetting fluid) which advances into the pores. A wetting fluid is one which at a solid surface makes a contact angle of less than 90° at the boundary with another fluid, whereas a non-wetting fluid makes a contact angle which is greater than 90° (see Figure 3.2). Thus the injection of mercury, which has a contact angle of 140° can also be considered as a soil drying path, with mercury, the non-wetting fluid advancing into the soil pores as air, in this case the wetting fluid recedes from the pores.

The relationship between the mercury pressure applied p and the equivalent matric suction

$(u_a - u_w)$ can be determined for the same pore diameter d (Romero, 1999):

$$(u_a - u_w) = \frac{4\sigma_w cos\theta_w}{d} \tag{7.2}$$

$$p = -\frac{4\sigma_{Hg} cos\theta_{nw}}{d} \tag{7.3}$$

$$(u_a - u_w) = -\frac{\sigma_w cos\theta_w}{\sigma_{Hg} cos\theta_{nw}} p \approx 0.196p \tag{7.4}$$

where σ_w is the surface tension of water which is equal to 0.0728N/m at a temperature of 20°C, $cos\theta_w$ is equal to 1 for the air-water interface. Thus with θ_{nw} equal to 140° and σ_{Hg} equal to 0.484N/m, suction is approximately equal to 0.196 times the applied mercury pressure.

The volume of pores not intruded by mercury should be used in the determination of the moisture content, which corresponds to the equivalent applied air pressure. The degree of saturation of the non-wetting fluid (mercury) Sr_{nw} plus the degree of saturation of the wetting fluid (air) Sr equals 1:

$$Sr_{nw} + Sr = 1 \tag{7.5}$$

Using the standard relationship between the degree of saturation of water Sr, void ratio e and particle density ρ_s, the moisture content w can be determined, but by using instead the degree of saturation not intruded $(1 - Sr_{nw})$ (Romero, 1999):

$$Sre = \rho_s w \tag{7.6}$$

$$w = \frac{e}{\rho_s}(1 - Sr_{nw}) \tag{7.7}$$

$$w = w_{sat}(1 - Sr_{nw}) \tag{7.8}$$

where w_{sat} is the moisture content at $Sr = 1$. However, a residual water content should be used to correctly evaluate the water content or degree of saturation corresponding to the equivalent applied matric suction which accounts for pores not intruded by the mercury and for the adsorption mechanism which occurs at higher suctions (Romero, 1999; Romero and Simms, 2008). In soils, water is generally held due to capillarity forces at the wetter range of the retention curve (usually at suctions below 1 MPa), and by adsorption forces on particle surfaces at higher suctions. Tuller and Or (2005) separate the water retention domain according to capillary and

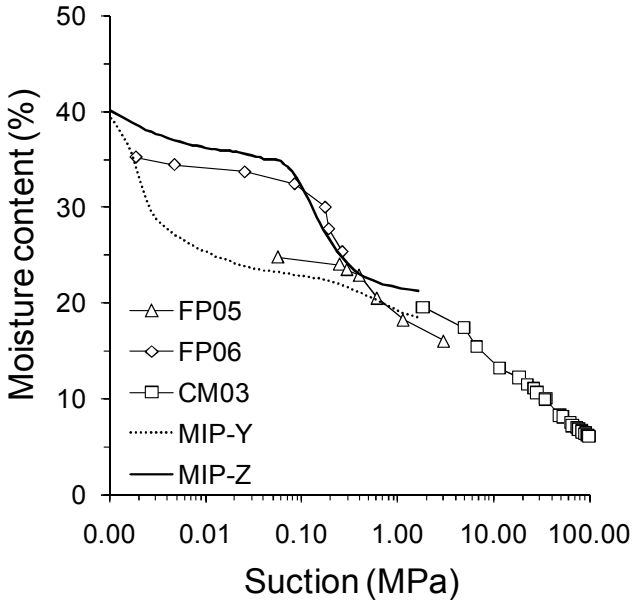

Figure 7.19: Experimental retention curve data compared with MIP derived retention curves: FP05: w_o = 24.8 %, ρ_{d_o} = 1.18 Mg/m^3, FP06: w_o = 35.7 %, ρ_{d_o} = 1.18 Mg/m^3, CM03: w_o = 23.6 %, ρ_{d_o} = 1.17 Mg/m^3, MIP-Y: w_o = 24.0 %, ρ_{d_o} = 1.18 Mg/m^3, MIP-Z: w_o = 36.5 %, ρ_{d_o} = 1.17 Mg/m^3 (FP - Filter paper data, CM - Chilled-mirror dew-point data, MIP - Mercury intrusion porosimetry data)

adsorptive contributions. In this case, the derivation of the water retention curve was limited to the low-suction range (suctions below 2 MPa), in which capillarity is assumed to dominate the water retention properties. In addition, a residual water content of 16% was considered to match MIP data with the psychrometer (chilled-mirror) and filter paper data at this transitional suction level.

Figure 7.19 presents the MIP derived water retention curves alongside some of the experimental data presented in Chapter 4 from filter paper (FP) and chilled-mirror dew-point tests (CM) on specimens compacted to similar initial conditions. The shape of the MIP curves for specimens Y and Z is similar to that obtained from the experimental data of FP05 (w_o = 24.8 %, ρ_{d_o} = 1.18 Mg/m^3) and FP06 (w_o = 35.7 %, ρ_{d_o} = 1.18 Mg/m^3) respectively. It is interesting to note that the MIP data for the higher moisture content specimen (MIP-Z) exhibits stiff behaviour at lower suctions followed by a change in slope as it approaches the main drying curve of the material at higher suctions and is similar in shape to the experimental data of series FP06 for an initial moisture content of 36%. This change in behaviour appears to be linked with the desaturation of

the intra-aggregate porosity (in this case sand, silt and clay aggregate arrangements). It follows then that the steep curve determined for MIP-Y at very low suctions (several kPa) can be attributed to inter-aggregate porosity, as it is the largest pores which desaturate first on drying (increasing suction). At high suctions (>1 MPa) the retention behaviour will be governed by the intra-clay aggregate porosity, but as mentioned other effects such as adsorption will tend to dominate over capillary effects within this range.

7.4.5 Summary

Mixing of the Bengawan Solo fill at different moisture contents results in the formation of aggregates which differ in terms of size and stiffness. Such aggregates appear to be responsible for the irregular double-peak compaction curve determined for this material. The microstructural investigation illustrated the differences in the pore size distribution of the fabrics created by compacting these different aggregates to the same dry density. Recollection of the water retention data here and comparison with MIP data has illustrated that the different fabrics owing to their different pore size distributions exhibit markedly different retention behaviour at low suctions (<1 MPa). In the next section, the response of the different compacted fabrics (X, Y and Z) to applied loading will be investigated under different saturation conditions.

If we consider that it can be difficult to accurately control moisture content and compactive effort during the construction of earthworks, these results can be important from a practical perspective. Small variations in the remoulding moisture content at the same compactive effort can result in significant differences in structure and dry density. Similarly variations in compactive effort will also influence dry density. In cases such as the construction of the Bengawan Solo fill embankments where traditional compaction methods are used, and where in the dry season soil broken down and spread out to dry, may become fully air dried in a matter of hours, it is difficult to have a good control over the compaction conditions. Ultimately this will lead to soil of varying moisture content, dry density and structure throughout the embankment.

7.5 UPC oedometer tests

7.5.1 Testing programme & objectives

The main objective of the testing campaign carried out using the UPC oedometer was to investigate the effect of structure on the volumetric behaviour of the Bengawan Solo fill material. Table 7.4 presents details of the different series, initial conditions and conditions prior to loading of the different specimens tested. Each test has been assigned a specific test reference, where for example UOA1 refers to UPC oedometer, Series A, Test 1. The location of the initial state of the specimens and paths followed were presented on the compaction curve in Figure 7.15. Series UOA investigates the volumetric behaviour of specimens X, Y and Z, compacted at three different moisture contents (9%, 24% and 36%) to the same initial dry density (1.18Mg/m^3) under constant water content conditions. In Series UOB, specimens X, Y, Z were loaded under saturated conditions. In Series UOC, three specimens of differing initial fabric were brought to similar conditions of dry density and moisture content prior to loading under constant water conditions. These specimens are referred to as X-Y, Y-Y and Z*-Y. Finally in Series UOD, these specimens of differing initial fabric were brought to similar conditions of dry density, moisture content and suction before loading under suction controlled conditions.

The main objectives of this experimental study was to:

- Investigate how the different structures created by compacting aggregates prepared at different moisture contents, influences yielding and compression behaviour exhibited during loading under constant water content (Series UOA) and saturated conditions (Series UOB)
- Investigate if initial compacted fabric influences volumetric behaviour even after similar conditions of moisture content, dry density (Series UOC) and suction have been reached prior to loading (Series UOD).

Table 7.4: Specimen conditions after compaction and prior to loading

Test	Specimen	Initial as-compacted conditions				Conditions prior to loading				Loading	CRL	Drainage
Ref.		w_o (%)	ρ_{d_o} (Mg/m^3)	e_o	S_{r_o} (%)	w (%)	ρ_d (Mg/m^3)	e	S_r (%)	Condition	(kPa/hr)	Length
UOA1	X	9.3	1.18	1.314	19.3	-	-	-	-	CW	100	H
UOA2	Y	24.4	1.18	1.313	50.5	-	-	-	-	CW	50	H
UOA3	Z	36.2	1.18	1.308	75.3	-	-	-	-	CW	5	H
UOB1	X	9.4	1.18	1.314	19.4	48.5	1.15	1.330	99.2	SAT	25	H/2
UOB2	Y	23.3	1.18	1.297	48.9	44.0	1.16	1.318	90.9	SAT	25	H/2
UOB3	Z	34.9	1.19	1.286	73.9	48.1	1.19	1.268	99.6	SAT	25	H/2
UOC1	X-Y	9.7	1.18	1.314	20.1	25.8	1.17	1.317	53.4	CW	50	H
UOC2	Z*-Y	35.3	1.00	1.733	55.4	24.1	1.16	1.356	48.4	CW	50	H
UOC3	Z*-Y	34.0	0.90	2.011	46.0	23.3	1.10	1.478	42.9	CW	50	H
UOD1	X-Y	10.6	1.17	1.323	21.9	23.8	1.19	1.292	50.1	SC	50	H
UOD2	Y-Y	23.3	1.19	1.285	49.3	23.5	1.20	1.267	50.4	SC	50	H
UOD3	Z*-Y	38.3	0.96	1.833	56.9	25.0	1.20	1.275	53.4	SC	50	H

7.5.2 Experimental Equipment

7.5.2.1 UPC oedometer cell

Figure 7.20 presents a schematic of the UPC oedometer cell used in this testing campaign and Figure 7.21 is a photograph of the cell and its accessories. Such equipment is used routinely at UPC, Barcelona, (e.g. Romero and Jommi, 2008). The stainless steel cell enables oedometer tests to be carried out on unsaturated soil specimens of maximum height 20mm and a diameter of 50mm. Unsaturated soils can be tested in this equipment by controlling either matric or total suctions. Matric suction is controlled through the axis translation technique by using base pedestals with a high air-entry value ceramic and by applying an air pressure inside the cell. A 1500kPa air entry ceramic discs was used in this testing campaign, see Figure 7.21. The cell has also been designed to enable application of total suctions by vapour transfer, where partially saturated salt solutions with varying quantities of salt solute can be used to achieve a predetermined relative humidity in the system. However in this testing campaign the vapour equilibrium technique was not used and where suction was controlled, the axis translation technique was used.

The cell has been primarily designed for pneumatic loading with the diaphragm pressure applied using compressed air, however in this campaign the diaphragm pressure was applied by hydraulic loading through the application of water pressure in the upper chamber, via a GDS pressure-volume controller. In order to use the cell as a hydraulic loading system it was important to ensure proper filling of the upper chamber, prior to the application of pressures. Thus, the cell had to be placed on its side during filling of the upper chamber in order to ensure the bleed valve was at the highest point during filling, so as to not to entrain any air bubbles in the upper chamber. The cell can be used with two different loading pistons, one which allows the application of a net vertical stress which is equal to the difference between the diaphragm pressure and the air pressure. The second piston enables a doubling of the net stress applied to be achieved for the same diaphragm pressure. In the following tests the 1:1 ratio loading piston was used (Figure 7.21). The upper chamber is separated from the specimen chamber by a 1mm thick rubber membrane (Figure 7.21) on which the diaphragm pressure acts, thus transferring a vertical stress onto the specimen.

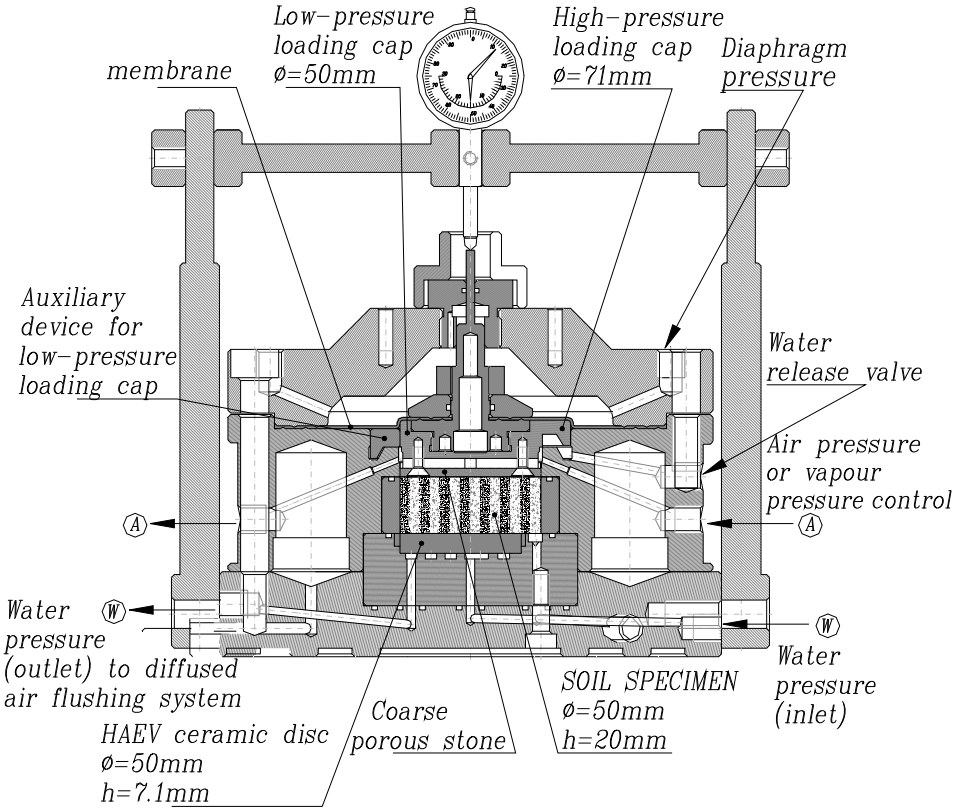

Figure 7.20: Schematic of UPC suction controlled oedometer

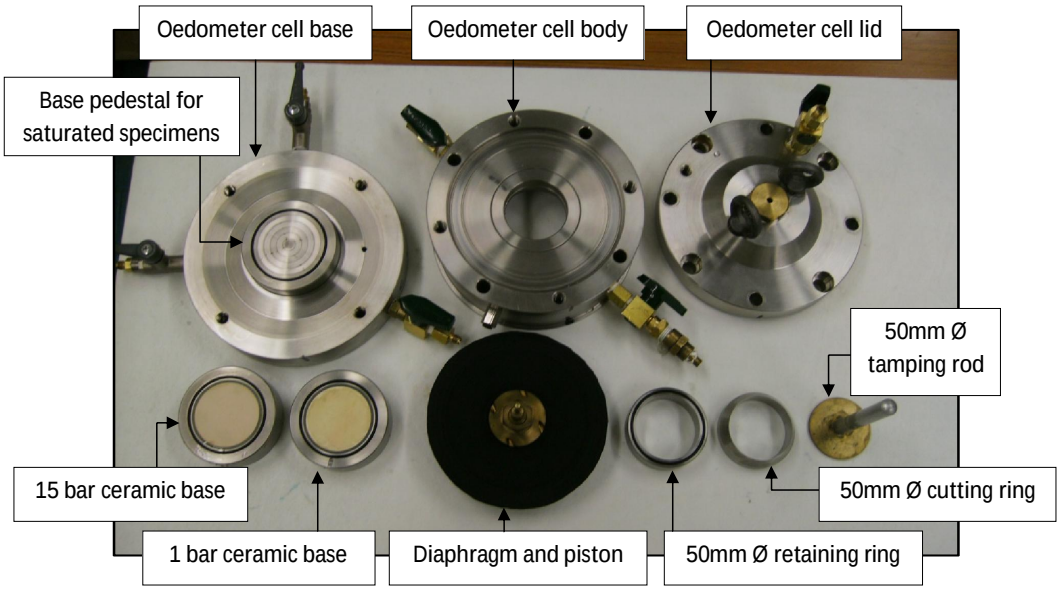

Figure 7.21: UPC oedometer cell and accessories

The UPC oedometer equipment used in this testing campaign benefited not only from the ability to control suction but also from the fact that continuous loading of the specimen was possible compared to the step-loading used with the conventional oedometer equipment. Cui and Delage (1996) presented evidence to suggest that continuous loading tests may be better suited for suction controlled tests than using a step loading procedure, particularly when higher suctions are to be applied. They proposed that in step loading tests the soil suction may not be controlled as desired, due to the sudden increase in load inducing undrained conditions and thus excess pore water pressures within the specimen. Depending on the permeability of the soil, this lower induced suction may exist for some time (48hrs for an oedometer specimen with a drainage path of 2cm, Cui and Delage, 1996).

7.5.2.2 System set-up

Figure 7.22 presents photographs of (a) the mounted oedometer cell and (b) the system set-up. Two GDS pressure-volume controllers were used in conjunction with the oedometer cell, one controlling the hydraulic loading, thus acting as the vertical pressure source. This controller was connected to the upper chamber of the oedometer cell. The other pressure-volume controller was used to control the pore water pressure under the base pedestal, as required. In the suction controlled tests, pore air pressure was applied via the specimen top cap (a series of concentric annular rings) by an air pressure compressor capable of reaching 1600kPa.

A 10mm ELE LVDT was used to measure the displacement of the soil specimen (Figure 7.22a) during testing. This transducer was calibrated against a dial gauge using a strain controlled loading frame. The calibration curve is presented in Appendix A (Figure A.14). The system included a GDS data acquisition pad in order to enable continuous displacement measurements to be recorded automatically. The GDS data acquisition pad was connected to the system PC using the standard RS232 serial connection. The two pressure-volume controllers were also connected to the PC, using a serial to USB converter connection. In this way aside from the pore air pressure which was controlled manually, the system was fully automated.

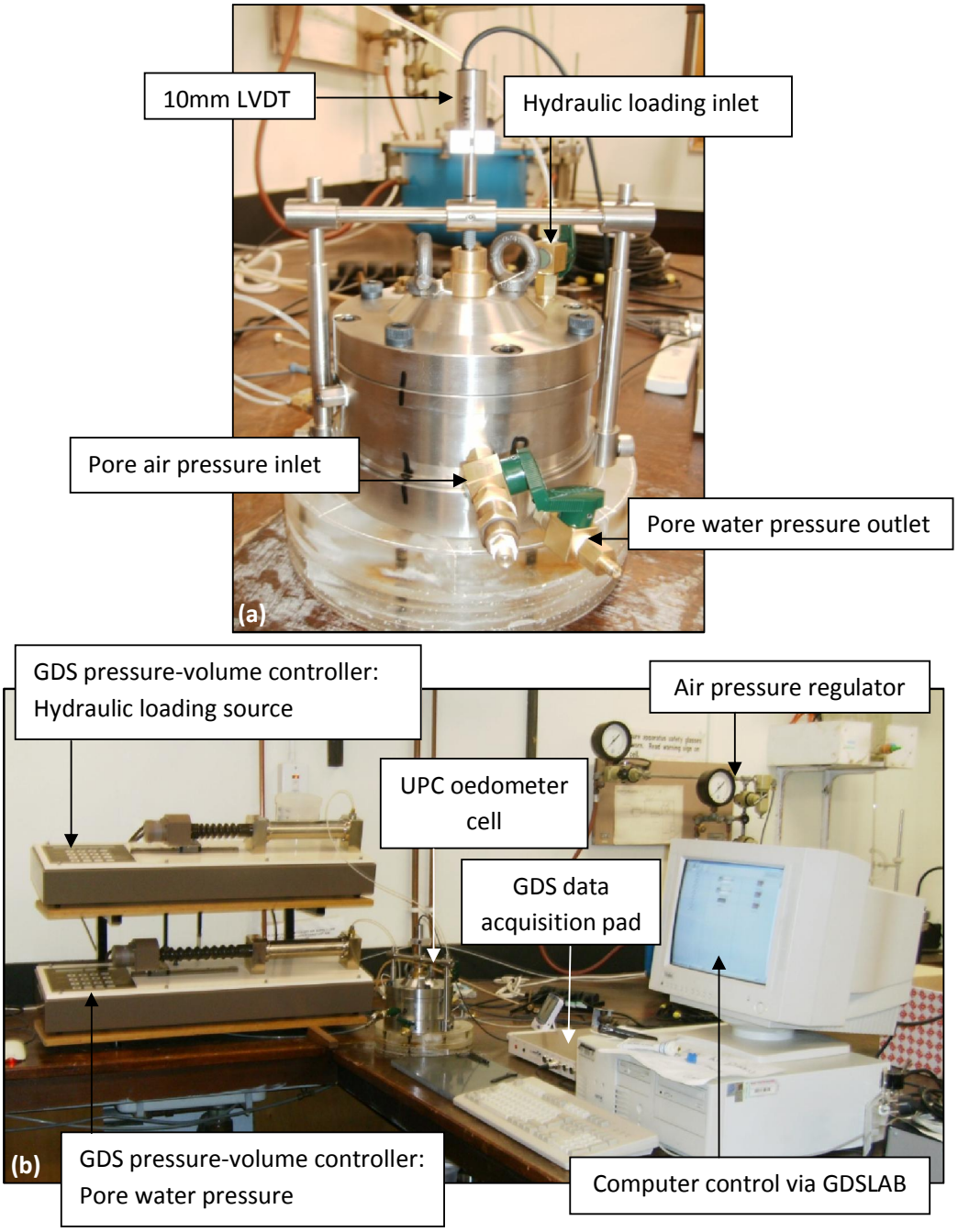

Figure 7.22: Photographs of (a) UPC suction controlled oedometer cell and (b) system set-up

7.5.3 Experimental Methodology

7.5.3.1 Sample Preparation

Samples of soil at moisture contents of 9%, 24% and 36% respectively were prepared from crushed air dried material passing the 2mm sieve. The water required to reach the desired moisture content was added using a fine spray bottle, and monitored by mass weighing until the addition of water required had been reached to within 1 decimal place. The added moisture was hand mixed in zip-lock bags after several sprays, ensuring water was evenly distributed. After mixing the bags were sealed (after removal of most of the air) and placed in sealable plastic containers. Samples were left for a minimum of 24hrs to ensure homogenisation of the moisture content, before compaction was carried out.

7.5.3.2 Specimen Preparation

In Series UOA (Constant water content tests) and UOB (Saturated tests) specimens were compacted in the retaining ring (50mm diameter, 20mm height) with samples prepared at the desired moisture contents of 9%, 24% and 36% respectively. As presented in Section 7.4, samples prepared at these moisture contents consist of very different aggregates, varying both in terms of size and stiffness of individual aggregates. Specimens were all compacted to an initial dry density of 1.18Mg/m^3. The preparation of these specimens at the same initial dry density required varying degrees of compactive effort, as can be deduced from Figure 7.15. Conditions X and Z both lie below the Extreme Light Compaction Curve, whereas condition Y lies above this curve, indicating that it requires more energy than the other two states to be produced. This was evident in the compaction process.

Specimen X was prepared by placing a mass of 50.5g in 3 layers, of the very fine, dry aggregates (w =9%) into the retaining ring; this specimen was loosely packed and required very little actual compactive effort, only light tamping was applied to ensure a level surface of each layer was obtained. For the preparation of Specimen Y, a mass of 57.5g was added in three layers, but due to the relatively firm aggregates present at this moisture content (w =24%) 8 blows of a light hammer were applied to the tamping rod for each layer. Between layers the soil was scarified

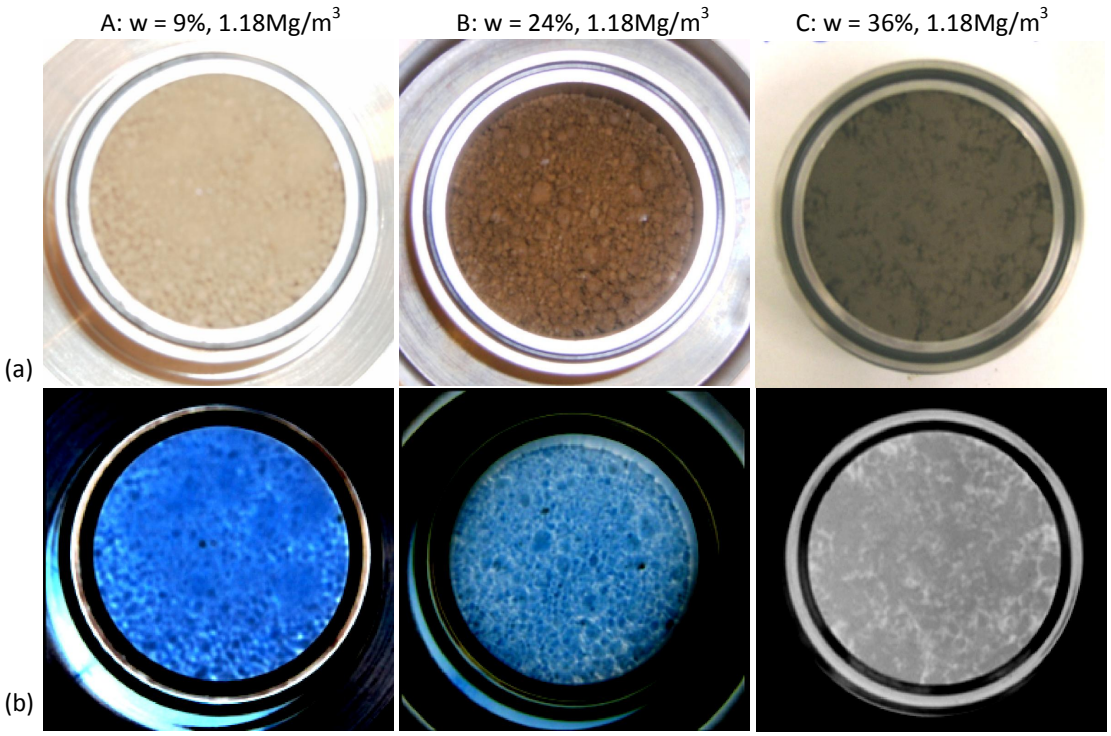

Figure 7.23: Photographs of compacted specimens X, Y & Z (a) in colour and (b) with the colours inverted

to ensure a good contact was created. A mass of 63g of soil was placed into the retaining ring in 3 layers for the preparation of Specimen Z. However a lower compactive effort was required to reach the desired initial dry density, due to the softness of the aggregates at this moisture content (w =36%), 2 blows of the light hammer were applied per layer. These procedures were determined by practice. Figure 7.23 illustrates the differences in the compacted specimens X, Y and Z. The photographs are presented both in colour and with their colours inverted in order to illustrate the differences in the compacted specimens produced; in particular highlighting the differences in the aggregates and associated porosity present within these specimens.

The range of moisture contents selected for investigation 9%, 24% and 36%, compacted at the same dry density of 1.18Mg/m^3 enabled a good range of the degree of saturation to be investigated, corresponding to specimens with S_r equal to approximately 20%, 50% and 75% respectively (Table 7.4).

The tests in Series UOC and Series UOD were dedicated to isolating the effects of structure on

volumetric behaviour. This was investigated by creating specimens with three different initial soil structures and bringing them to similar conditions of w (%), ρ_d (Mg/m^3) (24%, 1.18Mg/m^3) and thus also S_r (%) and e. The different initial structures were achieved by drying and wetting specimens prepared at different positions of the compaction curve (see Figure 7.15) and are referred to as Specimens X-Y (i.e. prepared at X and brought to the initial conditions of Y), Y-Y and Z*-Y. In Series UOC, these three specimens of differing initial structure were tested under constant water content conditions whereas in Series UOD, these three specimens were also brought to the same suction before loading under suction controlled conditions.

Specimen X-Y was prepared by compacting a sample at X (9%, 1.18Mg/m^3) and wetting under constant volume until a moisture content of 24% was reached (Figure 7.15). By maintaining a constant volume and changing only the amount of water present in the specimen, the dry density of 1.18Mg/m^3 could be maintained. The specimen X-Y was wetted by applying a negative suction of 15kPa (positive pore water pressure) while under a contact load of 20kPa. A volume of water of 6950mm^3 was required to achieve a moisture content of 24%. Using the 1500kPa high air entry ceramic stone this wetting could be achieved in approximately 33hrs. In order to ensure that swelling did not take place the vertical stress applied was ramped from an initial contact load of 20kPa to 25kPa over the first 5hrs of the wetting stage.

Specimen Z*-Y was prepared by compacting a sample at Z* (36%, 1.00Mg/m^3) and drying to 24%, 1.18Mg/m^3 (Figure 7.15). Samples were prepared at the lower dry density of 1.00Mg/m^3 to account for the increase in dry density due to shrinkage on drying. As a result this initial sample was prepared in a retaining ring of diameter 60mm and height 32mm. The change in moisture content of the sample on drying was monitored by weighing the sample until the desired moisture content of 24% had been reached. Typically this involved a loss of moisture of approximately 10.8g, which could be achieved by leaving the sample to air dry in the laboratory for approximately 43hrs. Once the desired moisture content had been reached the specimen was trimmed using a cutting ring (Figure 7.24) of diameter 50mm and height 20mm, and a wire saw. A moisture content check was carried out on the remaining trimmings, which was used for the calculation of the specimen conditions (conditions prior to loading). It was not possible to test the specimen within the cutting ring in the oedometer cell, as a flat surface was required at both the top and bottom of the retaining ring against which o-rings pressed to form a seal.

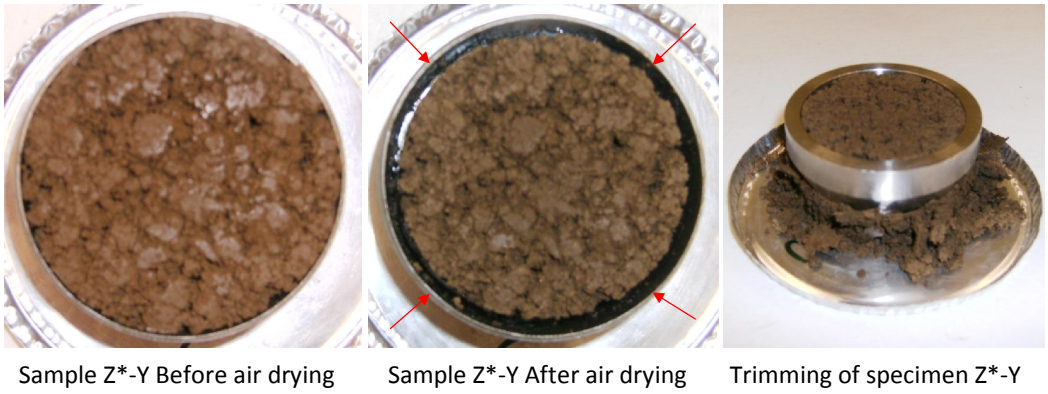

Figure 7.24: Preparation of specimen Z*-Y

The fine edge of the cutting ring, would not have enabled the system to be sealed. Thus, the specimen was then transferred from the cutting ring to the retaining ring of the oedometer cell prior to testing. Despite this not being an ideal situation, no visible disturbance of the specimen occurred during transfer.

7.5.3.3 Testing procedures

A number of different types of tests were carried out as part of this testing campaign including Constant Water content tests, Saturated tests and Suction controlled tests using the axis translation technique. Each type of test required slightly different test set ups and procedures to be followed.

In the saturated tests specimens were mounted on a base pedestal consisting of a series of concentric annular rings (see Figure 7.21). The specimens were wetted by applying a vertical pressure of 15kPa and a back pressure to the base pedestal of 8kPa with the port at the top of the specimen open, for a period of at least 15mins until no more air was observed exiting the specimen, and the rate of flow of water out was approximately equal to the inflow of water. After this, the vertical pressure was raised to 210kPa and the back pressure was raised to 200kPa to ensure full saturation. Any swelling occurring during the saturation stages was recorded. After the saturation stages, both the top and bottom of the specimen were connected to the back pressure source, enabling two way drainage of the specimen during loading and therefore a quicker rate of loading was permitted (25kPa/hr).

In constant water content tests, no pore water drainage was allowed, and only drainage of pore air was permitted. In these tests the specimens were mounted on top of a base pedestal which had a high air entry ceramic disc installed. The ceramic disc was fully air dried prior to testing in order to act as a barrier to flow. The valves to the base pedestal remained closed during these tests, ensuring no drainage of pore water was permitted. Only one valve connected to the top of the specimen remained open to the atmosphere during the test, in order to enable drainage of the pore air inside the specimen. To prevent drying occurring at the top of the specimen due to evaporation resulting from this open connection, the valve to the top of the specimen was connected to the atmosphere via tubing which was inserted into a beaker of water, with a free surface open to the laboratory atmosphere. This additional set-up was only used during loading stages, and was removed prior to unloading, as it would have led to the uptake of water.

Suction controlled tests were carried out using the axis-translation technique, thus the specimens were mounted on a base pedestal consisting of a 1500kPa high air entry value ceramic disc. As described in Section 6.5.2, the ceramic disc was saturated and the permeability checked prior to each test by applying a water pressure of 1600kPa above the stone while maintaining the back pressure under the stone at 0kPa. The 1500kPa ceramic stone used in these tests has a saturated water permeability of 5.3×10^{-11} m/s. Figure A.15 in Appendix A presents a typical curve of flow through the saturated ceramic stone. In order to minimise air diffusion through the ceramic stone the pore water pressure was maintained at a minimum of 200kPa during suction controlled tests and flushing underneath the stone was carried out regularly to remove air bubbles located below the ceramic. Finally the pore air coming from the compressor was first directed through a humidity chamber to minimise any drying effects. For further information on the adoption of these procedures see Section 6.5.2. For the suction controlled tests carried out in Series UOD, a suction of 470kPa was determined from the water retention behaviour of specimens at the initial conditions used in these tests (Figure 7.19) and was selected as it is close to the suction value corresponding to the initial compacted condition of Specimen Y (w_o = 24% and ρ_{d_o}=1.18Mg/m^3).

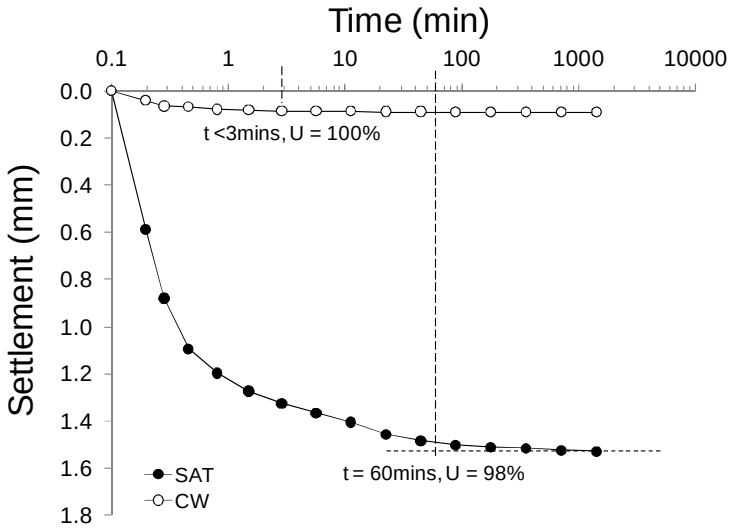

Figure 7.25: Time evolution of settlement for loading step (30kPa to 60kPa) in a Saturated and Constant Water Content oedometer test for specimens with w_o= 24% and ρ_{d_o}= 1.18Mg/m^3

7.5.3.4 Loading rates

In this experimental campaign loading was carried out in the suction controlled oedometer under constant loading rates by setting the water pressure in the upper chamber to increase to a certain pressure over a given time. In saturated tests, it is preferable to carry out tests at the same constant rate of loading in order to make the test results comparable, however in unsaturated tests this would make for very inefficient testing programmes with respect to time. In saturated tests only water is drained from the soil specimen, however in unsaturated tests, air is also drained from the specimen. It is important to note that the drainage of air can occur up to fifty times faster than the drainage of water (Romero, 1999), thus it is important in the selection of loading rates to consider if water or air drainage will be the dominant process, which is largely dependent on the degree of saturation of the specimens to be compressed. For this material it was considered that for specimens with $S_r > 85\%$, water drainage dominates, whereas for $S_r < 85\%$ air removal dominates. In suction controlled tests the presence of the ceramic disc directly below the specimen increases the drainage length and also has an impedance effect on water drainage.

When selecting the rates of loading to be applied, reference was made to the data available from the step loading oedometer tests carried out on specimens with $w = 24\%$ and $\rho_d = 1.18$Mg/m^3

(Series COB, Chapter 5). Figure 7.25 presents the evolution of settlement with time during a loading step from 30kPa to 60kPa carried out in the conventional oedometer equipment on a fully saturated specimen and one which was loaded under constant water content conditions (CW). For the saturated specimen, 98% of consolidation had occurred within approximately 60mins, whereas for the CW specimen 100% consolidation had been reached in less than 3mins. It appears that full consolidation of the saturated specimen is approached at t =177mins. This confirms that pore air drainage can occur up to fifty times faster than pore water drainage as found by Romero (1999). Considering these results, a constant rate of loading (CRL) of 25kPa/hr was selected for the saturated tests, providing double drainage was allowed (as was the case in the conventional oedometer apparatus), giving a drainage length of 10mm.

For Series UOA, the CW tests the constant rate of loading (CRL) selected for each test reflects the initial degree of saturation of the specimen. Specimen UOA1 with $S_r \approx 20\%$, a CRL of 100kPa/hr was selected, for Specimen UOA2 with $S_r \approx 50\%$, 50kPa/hr was selected and for Specimen UOA3 with $S_r \approx 75\%$, 5kPa/hr was selected. In Series UOC, where all specimens were brought to $S_r \approx 50\%$ prior to loading under constant water content conditions, a CRL of 50kPa/hr was selected. In Series UOD, all specimens were brought to $S_r \approx 50\%$ prior to loading under suction controlled conditions (s=470kPa), a CRL of 50kPa/hr was selected. These rates reflect the additional drainage length due to the ceramic disc and the single drainage, which gives a drainage length of 27mm, (specimen height is 20mm and ceramic thickness is 7mm).

7.5.4 Results & discussion

Figure 7.26 presents a comparison of results obtained for compacted Specimen Y, loaded under constant water content conditions in both the conventional step loading apparatus and in the UPC oedometer equipment. The change in volumetric behaviour (presented in terms of specific volume normalised with respect to initial specific volume) are in very good agreement with respect to the post-yield compression behaviour at high stresses and the swelling behaviour observed during unloading. The small differences observed in the compression curves close to the yield points are thought to be associated with the difference in the type of loading used within each apparatus. In the conventional apparatus, vertical stresses are applied in steps (corresponding to dead weights) whereas in the UPC oedometer continuously increasing

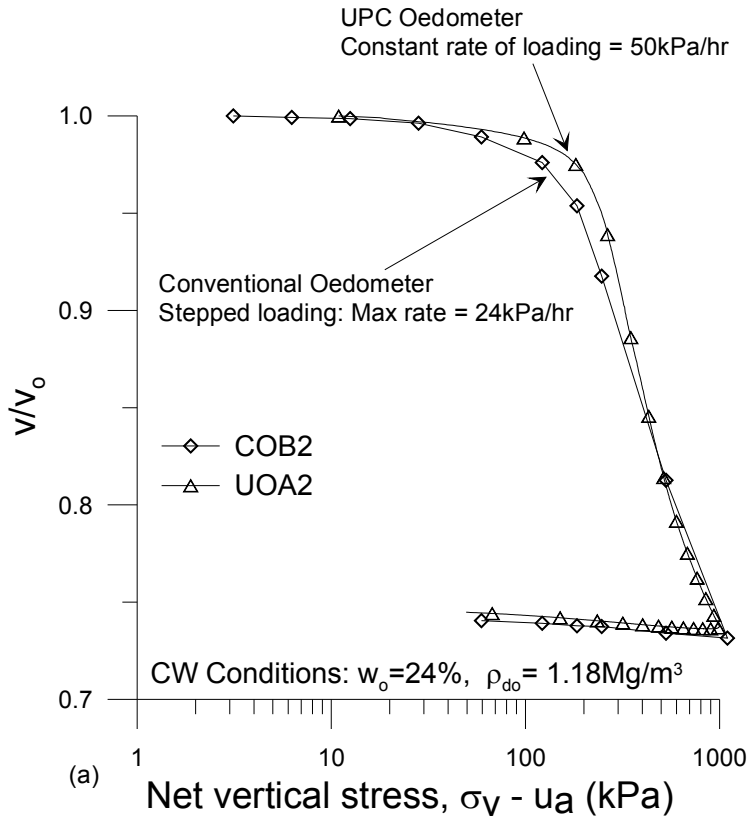

Figure 7.26: Comparison of constant water content tests at condition Y (w_o = 24%, ρ_{d_o} = 1.18Mg/m^3) carried out in the conventional oedometer equipment and UPC oedometer equipment

loading can be applied, (in this case hydraulically). It is likely that the much smaller increments of load applied with the UPC oedometer enabled the specimen to remain stiffer for longer, whereas the application of a much larger load increment at one time to achieve the same stress level corresponded to more compression. Nevertheless, these results on independent specimens validates the performance of the two types of oedometer equipment.

7.5.4.1 Influence of compacted fabric at different initial states

The behaviour of the Bengawan Solo fill material at compacted conditions corresponding to X, Y and Z are presented here first under constant water content conditions and then subsequently under saturated conditions in an attempt to investigate if the aggregated structure created during compaction influences the mechanical response upon one dimensional loading. Compaction

conditions responsible for compacted fabric are w_o, ρ_{do} and the method of compaction, whereas initial state conditions refer to the stress state and suction (σ_{vi}, s_i) of specimens prior to loading. In this section the specimens tested have been prepared at different compaction conditions thus generating different compacted fabrics. These specimens are then loaded from different initial states, (i.e. they have different initial suctions).

The volumetric behaviour of the specimens X, Y and Z compacted at w = 9%, 24% and 36%, each to an initial dry density of 1.18Mg/m^3 are compared in Figure 7.27a for loading under constant water content conditions (Series UOA). The results are presented in terms of specific volume against net vertical stress ($\overline{\sigma}_v$), where u_a is atmospheric. It is evident that there is no clear trend in yield stress ($\overline{\sigma}_{vc}$) or compressibility of the soil with respect to moisture content. In fact there is an increase in $\overline{\sigma}_{vc}$ from 150 to 220kPa when moving from UOA3 (w_o = 36%) to UOA2 (w_o = 24%) , but then $\overline{\sigma}_{vc}$ decreases to 96kPa when w_o is further reduced (UOA1). With respect to the post-yield compressibility of the soil, similar results are found, the value of C_c increases as w_o is reduced from 36% to 24% (UOA3 to UOA2), which was similarly observed in the results of Series COI presented at the beginning of this chapter. However by extending the range of moisture contents investigated here, it becomes clear that this is not the full story, as w_o is further reduced to 9%, soil compressibility post-yielding reduces. Thus it is Specimen UOA2 compacted at the intermediate water content of 24% which exhibits the greatest compressibility with a C_c value of 1.01. There appears to be less significant variation in the swell indexes determined. All the values corresponding to the yield stress, compression and swell indexes for all the curves listed in this experimental campaign are listed in the summary Table 7.5 at the end of the chapter.

If suction were the governing influence on the compression behaviour of these specimens, according to the Barcelona Basic Model (Alonso et al., 1990) it would be expected that a reduction in w and therefore an increase in suction would provide an additional bonding effect which would increase the domain in which stiff behaviour would be observed, and ultimately lead to an increase in yield stress. According to the water retention curves determined experimentally for the Bengawan Solo fill (Figure 7.19) the initial suction values for the compacted specimens are estimated to be 2kPa (Z: w_o = 36%), 470kPa (Y: w_o = 24%) and 40MPa (X: w_o = 9%) respectively. Despite this wide range in suctions covered, the yield stress did not appear to

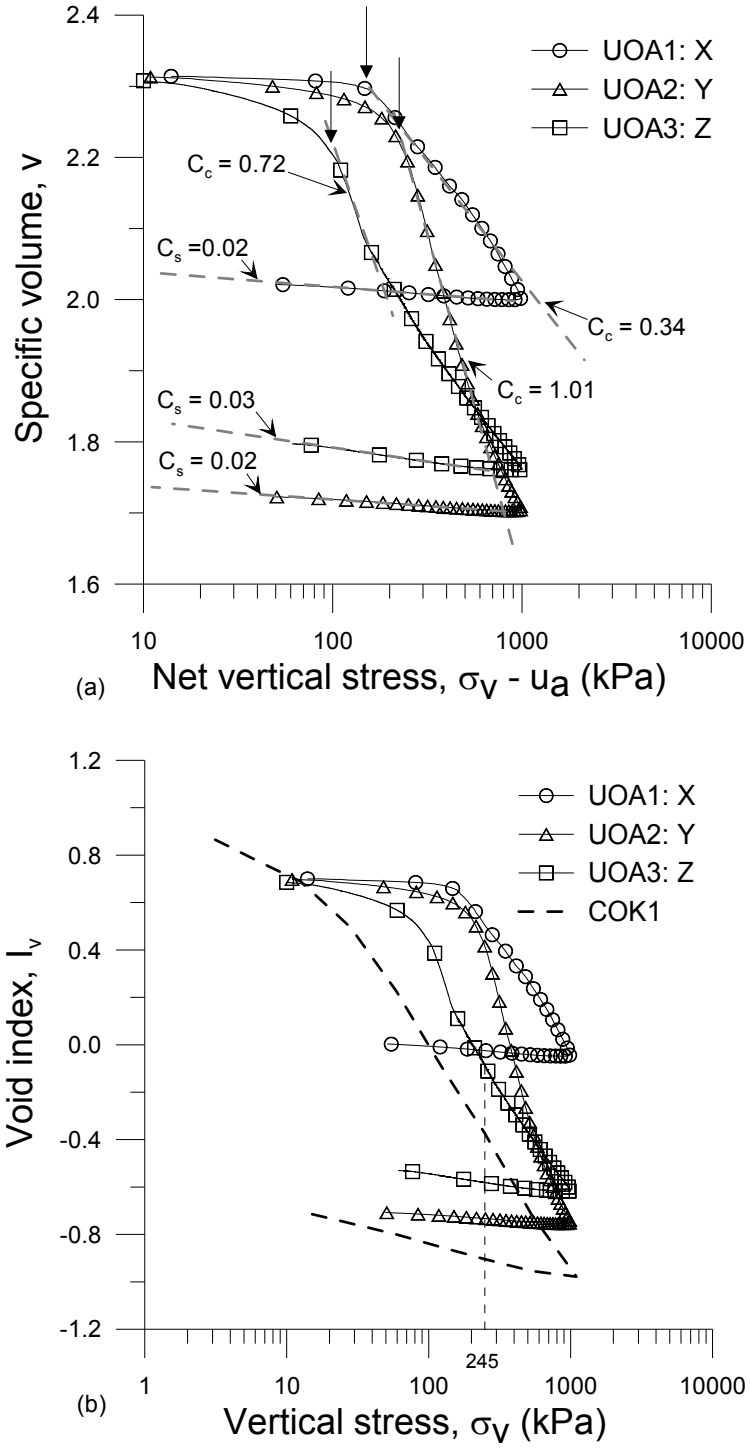

Figure 7.27: Series UOA : Constant water content, one-dimensional consolidation of samples prepared at three different initial moisture contents each compacted to the same initial dry density of 1.18Mg/m^3. UOA1: w_o = 9.3%, ρ_{d_o} = 1.18Mg/m^3, UOA2: w_o = 24.4%, ρ_{d_o}= 1.18Mg/m^3, UOA3: w_o = 36.2%, ρ_{d_o} = 1.18Mg/m^3, COK1: w_o = 52.2%, ρ_{d_o} = 1.14Mg/m^3. (a) specific volume vs net vertical stress and (b) comparison with reconstituted material in terms of void index.

increase continuously with increasing suction. In terms of compressibility behaviour governed by suction either an increase in the stiffening of the soil behaviour would be expected with increasing suction (e.g. Vicol, 1990; Romero, 1999) or a reduction in the stiffness (e.g. Futai and Almeida, 2005). However the BBM and other critical state models describing the influence of suction on the mechanical behaviour of unsaturated soils have generally been supported by the experimental testing of specimens which all have the same initial compacted conditions (prior to the application of different values of suction). This means that such specimens all have a common initial fabric. The microstructural investigation of the compacted specimens X, Y and Z clearly illustrated that these specimens each have a different initial fabric. It appears from Figure 7.27a that suction alone is not sufficient to describe the differences in the compression behaviour observed, and for this reason it may be concluded that the different compacted structures created also play a role in the mechanical response to loading.

In Figure 7.27b the compression curves for UOA1, UOA2 and UOA3 are plotted in terms of void index alongside the compression curve of the saturated reconstituted specimen (COK1), which is regarded here as defining the Intrinsic Compression Line (ICL). This is in line with the approach proposed by Burland (1990) for intact bonded soils. As for naturally bonded soils, the aggregated specimens lie to the right of the ICL. UOA2 appears to converge with the ICL at high stresses, which corresponds to a high degree of saturation (UOA2: S_r=94% at 1MPa). Test UOA3 was in fact not a truly constant water content test as it had a high initial degree of saturation (S_{r_o}= 75.3%) and on loading it remained under constant water content conditions until the volume change induced by loading resulted in full saturation of the specimen occurring, at which time water began to be expelled from the specimen. A degree of saturation of 100% was achieved at a vertical stress of 245kPa. Close to this stress level the slope of the post-compression curve of UOA3 follows approximately parallel to that of the ICL, however it is not clear the reason why it is shifted above the ICL even once the specimen has become fully saturated. This saturation of the specimen due to loading is the reason why it was important to select loading rates for the CW tests which reflected their initial degree of saturation.

In order to investigate solely the influence of the initial compacted fabric on the volumetric behaviour, the effect of suction was removed by testing under fully saturated conditions. Figure 7.28 presents the saturated compression curves carried out in Series UOB for specimens

at initial conditions X, Y and Z. Although structural effects are perhaps less apparent than for the partially saturated specimens tested in Series UOA, the curves do not all exhibit the same yielding and compression behaviour. In particular yielding does not occur at the same yield stress (σ'_{vc}); σ'_{vc} appears to increase as the initial compacted moisture content was reduced, from 18kPa (UOB3, $w_o = 36\%$) to 42kPa (UOB1, $w = 9\%$). The saturated compression curve of UOB3 follows closely the response exhibited by the reconstituted specimen (COK1), (Figure 7.28b). The curve of UOB2 ($w_o = 24\%$) lies below the ICL and then appears to cross over it again at higher stresses. Such an intersection of the ICL has previously been presented by Monroy (2006) when comparing the compression behaviour of compacted and reconstituted specimens of London clay under saturated conditions. It is more evident however that UOB1 (w_o= 9%) overall undergoes significantly less settlement under loading to the same effective vertical stress as specimens UOB2 and UOB3. Although it has a similar shape to the curve of UOB2, it does not appear to converge towards the ICL suggesting that there is some effect of fabric which is still influencing the mechanical response even at high stresses. These results are important because they indicate that the compacted fabric may still to an extent influence the volumetric behaviour, in this case the yield stress, even under saturated conditions.

In an attempt to separate the mechanical response which can be attributed to soil structure (fabric + bonding) and that which can be attributed to soil fabric only, the compression behaviour for each initial compacted state (X, Y and Z) are compared in Figure 7.29. In each plot (Figure 7.29a, b, and c), the specimens have the same initial fabric, the differences in the curves can be attributed to differences in suction: in the saturated tests suction is zero, whereas in the CW tests the suction is not controlled, but rather decreases with increasing load. It is evident that the corresponding partially saturated (CW) compression curves exhibit higher yield stresses and exist at higher specific volumes than their corresponding saturated specimens at the same effective stress. The CW compression curves appear to converge with the saturated compression curves at high degrees of saturation.

Considering the variation in yield stress observed in Series UOA and UOB, it is proposed that the initial stiff behaviour exhibited by the compacted specimens (X, Y and Z) is associated with the stiffness of the aggregates as also reported by Koliji et al. (2009). In the CW conditions the nature of the aggregates initially remain as reported after mixing (Section 7.4). In this way it

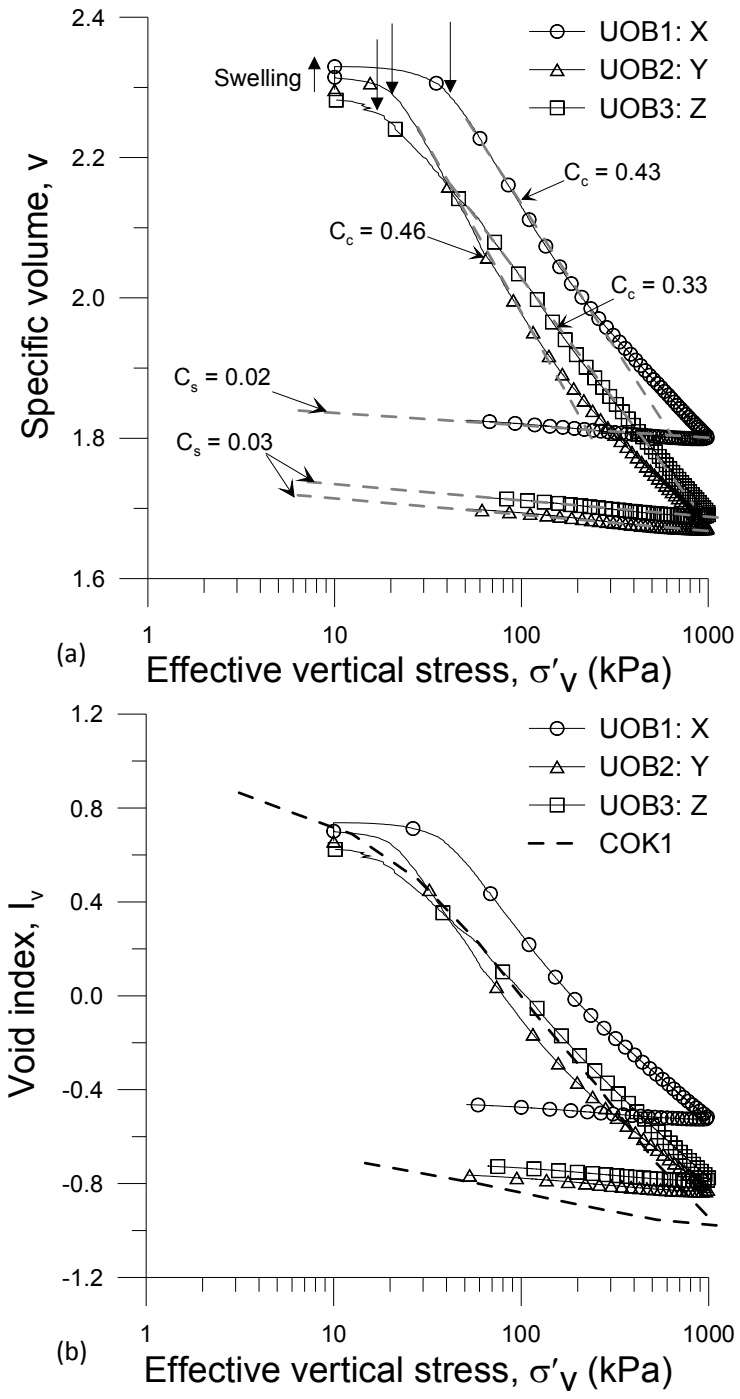

Figure 7.28: Series UOB: Saturated one-dimensional consolidation of samples prepared at three different initial moisture contents, compacted to the same an initial dry density. UOB1: w_o = 9.4%, ρ_{d_o} = 1.18Mg/m^3, UOB2: w_o = 23.3%, ρ_{d_o}= 1.18Mg/m^3, UOB3: w_o = 34.9%, ρ_{d_o} = 1.19Mg/m^3. (a) specific volume vs effective vertical stress and (b) comparison with reconstituted material in terms of void index.

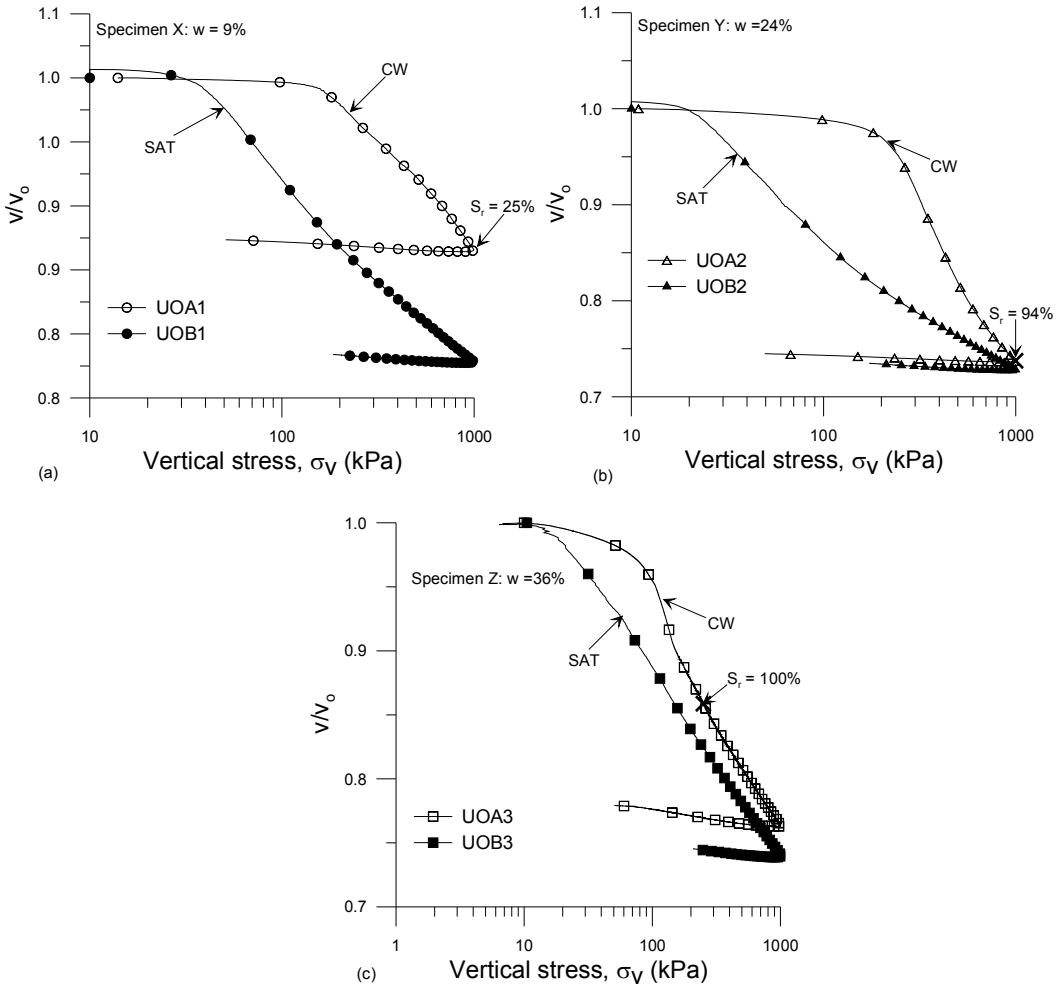

Figure 7.29: Comparison of constant water content and saturated results for Specimens (a) X, (b) Y and (c) Z in terms of normalised specific volume and vertical stress

becomes evident that Specimen Z (UOA3) with its soft wet aggregates would exhibit a smaller yield stress than that of Specimen Y, which has smaller firmer aggregates. Although the fine dry powdery aggregates of Specimen X were thought to be stiffer than those of Y, the lower $\overline{\sigma}_{vc}$ observed can be explained by considering the brittle nature of these aggregates in such a dry state ($w = 9\%$). In the case of Series UOB, despite all the specimens being saturated prior to loading, an aggregate stiffness appears to be retained from the initial compacted fabric. With σ'_{vc} increasing from Specimen Z to X.

It is important here to also remember that by compacting the specimens all at the same initial dry density, the specimens contain the same mass of solids in each specimen, and in particular have the same porosity ($n \sim 57\%$). The microstructural investigation highlighted however, that although the overall porosity may be the same for these compacted states, the distribution of that porosity differed significantly between Specimens X, Y and Z. Considering that compression essentially is the rearrangement of solids such that voids spaces are reduced, one can visualise how it may be easier for aggregated solids to move into a larger single pore space (e.g. an inter-assemblage or inter-aggregate pore space), than to occupy the same volume of voids by invading many pores of a much smaller entrance diameter. It has recently been argued that the aggregates within compacted soils are essentially similar to reconstituted soil of the same mineralogy and that the difference between compacted and reconstituted soils at a given suction is the presence or lack thereof of larger inter-aggregate porosity (Tarantino, 2010b). Thus, in order for an aggregated specimen to rejoin the ICL the large inter-aggregate (or inter-assemblage) pores must be closed.

The porosity of Specimen Z ($w = 36\%$) which was not detected by the MIP was attributed to much larger inter-assemblage pores (>450μm) as illustrated in Figure 7.18c. The removal of these large air filled pores (as determined by consideration of the water ratio of the specimen, Figure 7.17) is thought to correspond to the steep slope of the compression curve (UOA3) exhibited immediately after yielding (see Figure 7.29c). This steep slope is only observed over a small range of vertical stresses as this accounts for 25% porosity. The wet nature of the aggregates also ensures that the solids can deform easily into these large pore spaces at relatively lower applied stresses (compared to UOA1 and UOA2). It is evident in Figure 7.27a that the greatest post-yield compressibility was exhibited in curve UOA2 (Specimen Y), with a C_c value

of 1.01. This high compressibility can be explained by considering that the dominant pore size found for Specimen Y was an inter-aggregate porosity with an entrance diameter of 140µm. These air filled voids (see Figure 7.17b) account for 40% porosity of specimen Y and the relative stiffness of these aggregates requires a vertical stress of approximately 1MPa to force solid particles into almost all of these pore spaces (Figure 7.29b). As for Specimen X, the air filled voids correspond to over 50% porosity (total overall porosity for all specimens is approx. 60%), furthermore these pores are of a smaller entrance diameter (36µm) which makes it increasingly difficult for aggregated solids to intrude into. For this reason at a vertical stress of 1MPa UOA1 is not close to rejoining its corresponding saturated curve (UOB1), see Figure 7.29a.

7.5.4.2 Influence of compacted fabric on specimens brought to the same initial state conditions

It appears then that under partially saturated or fully saturated conditions compacted fabric may have an influence on the volumetric behaviour of the Bengawan Solo fill at different initial states. But an important question remains over whether the influence of compacted fabric on soil behaviour is in addition to the influence of initial states of stress and suction. Gens (1996) outlined two possible limits regarding the influence of initial compacted fabric. The first possibility is that initial compacted fabric is totally responsible for subsequent soil behaviour, in which case each compacted condition gives rise to essentially a different soil. Different initial states would result but furthermore different constitutive model parameters would be required to describe the behaviour of soil for each compaction condition. The second extreme limit is that initial compacted fabric has a negligible influence on soil behaviour and any differences in such behaviour may be explained by differences in initial states. This would suggest that for one soil, one set of constitutive model parameters would suffice for all compaction conditions and only the initial state conditions would vary. These two extremes regarding the influence of compacted fabric on soil behaviour, and how it may be accounted for in constitutive modelling are illustrated in Figure 7.30 (Gens, 1996).

In an attempt to provide some experimental evidence which may support one of the two possibilities presented above, two series of tests were carried out where the different initial compacted fabrics exhibited by specimens X, Y and Z were subsequently brought to similar conditions of

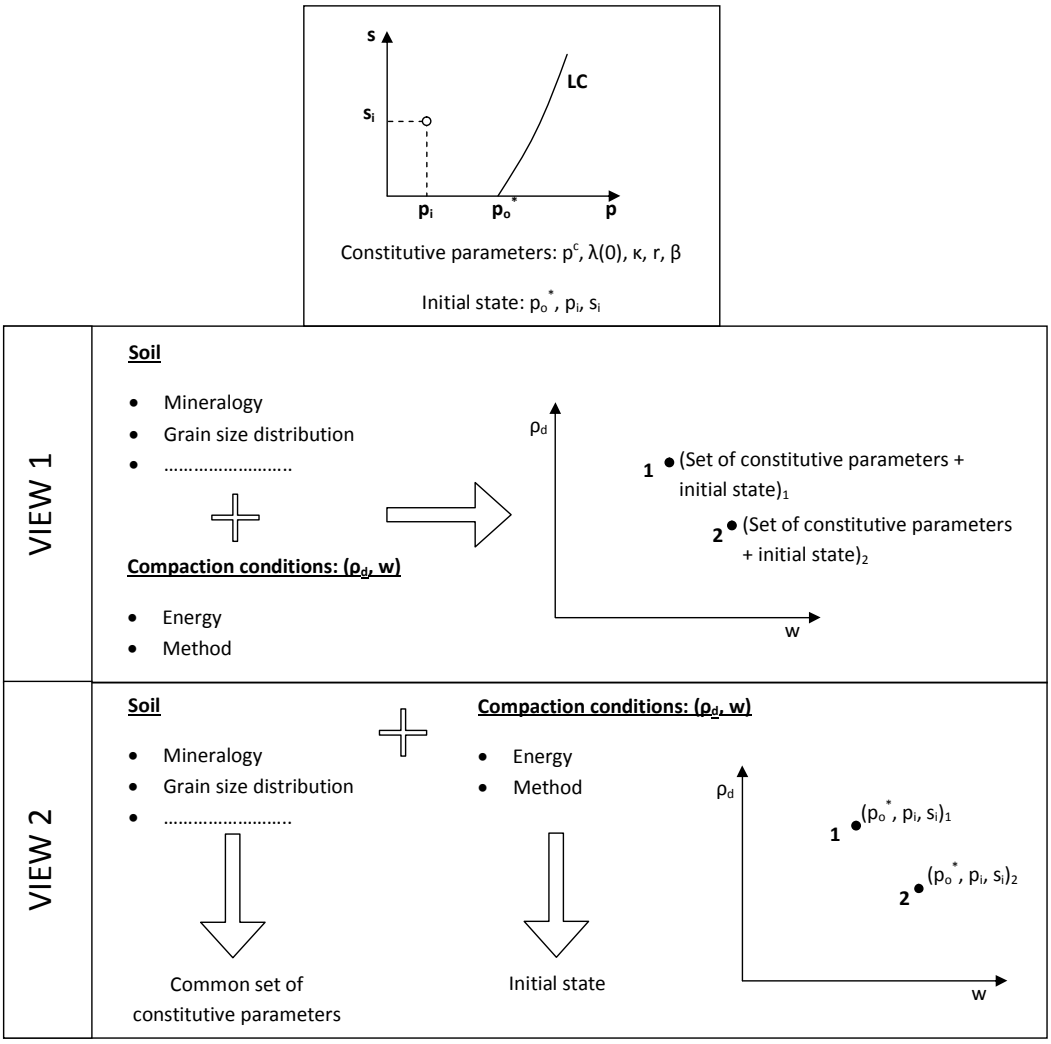

Figure 7.30: Extreme possible limits for considering influence of compacted fabric in constitutive modelling (After, Gens, 1996)

w and ρ_d prior to loading. In Series UOC, these specimens were loaded under CW conditions, whereas in Series UOD, the specimens were additionally brought to the same suction and then loaded under suction controlled conditions.

Figure 7.31 presents the results of the constant water content tests carried out on three specimens of differing initial fabric brought to similar conditions prior to loading (Series UOC). Specimen X-Y (UOC1), which was prepared at w_o = 9% and ρ_{d_o} = 1.18Mg/m^3 and then wetted under constant volume conditions (Figure 7.31b), shows markedly different behaviour to specimens Y (UOA2) and Z*-Y (UOC2). Specimen Z*-Y prepared at w_o = 35.3% and ρ_{d_o} = 1.00Mg/m^3 was dried to achieve similar conditions of w and ρ_d prior to loading. UOC1 (Specimen X-Y) exhibits a much lower yield stress ($\overline{\sigma}_{vc}$=55kPa) and a lower post-yield compressibility (C_c=0.57) compared to the specimens (Y and Z*-Y) (Table 7.5). The slightly higher w of X-Y prior to loading (w = 25.8%) is not thought to be solely responsible for these significant differences in behaviour. The swelling index values determined were different for each of the specimens. It appears that initial compacted fabric may have an important influence on subsequent soil behaviour.

Specimens Y (UOA2) and Z*-Y (UOC2) appear to have a very similar volumetric response to loading under CW conditions, which is evident despite the small difference in the dry density prior to loading (Figure 7.31a). Their yield stresses are of similar magnitude (Y: 250kPa, Z*-Y: 200kPa) and their post-yield compression curve is of similar shape and slope. The similarities in the behaviours of UOA2 (Y) and UOC2 (Z*-Y) can be explained by considering the nature of the aggregates present at the beginning of loading. In Specimen Z*-Y, the wetter softer aggregates created at Z* (w = 36%) have reduced in size on drying (aggregate shrinkage) and also as water has been removed from the aggregates they have become more rigid, essentially they have become aggregates similar to those presented in specimen Y, compacted at w = 24%.

On the other hand specimen X-Y does not have these medium sized aggregates (up to 10mm). Specimen X initially has much smaller aggregates (up to 4mm) and has an inter-aggregate porosity at a lower pore size (36µm). On wetting to position Y , the small aggregates have a tendency to swell as they absorb water (due to the montmorillonite present in the clay fraction). Carrying out this wetting path under constant volume conditions forces the aggregates to swell into the existing inter-aggregate porosity. It is proposed that this swelling forces the aggregates

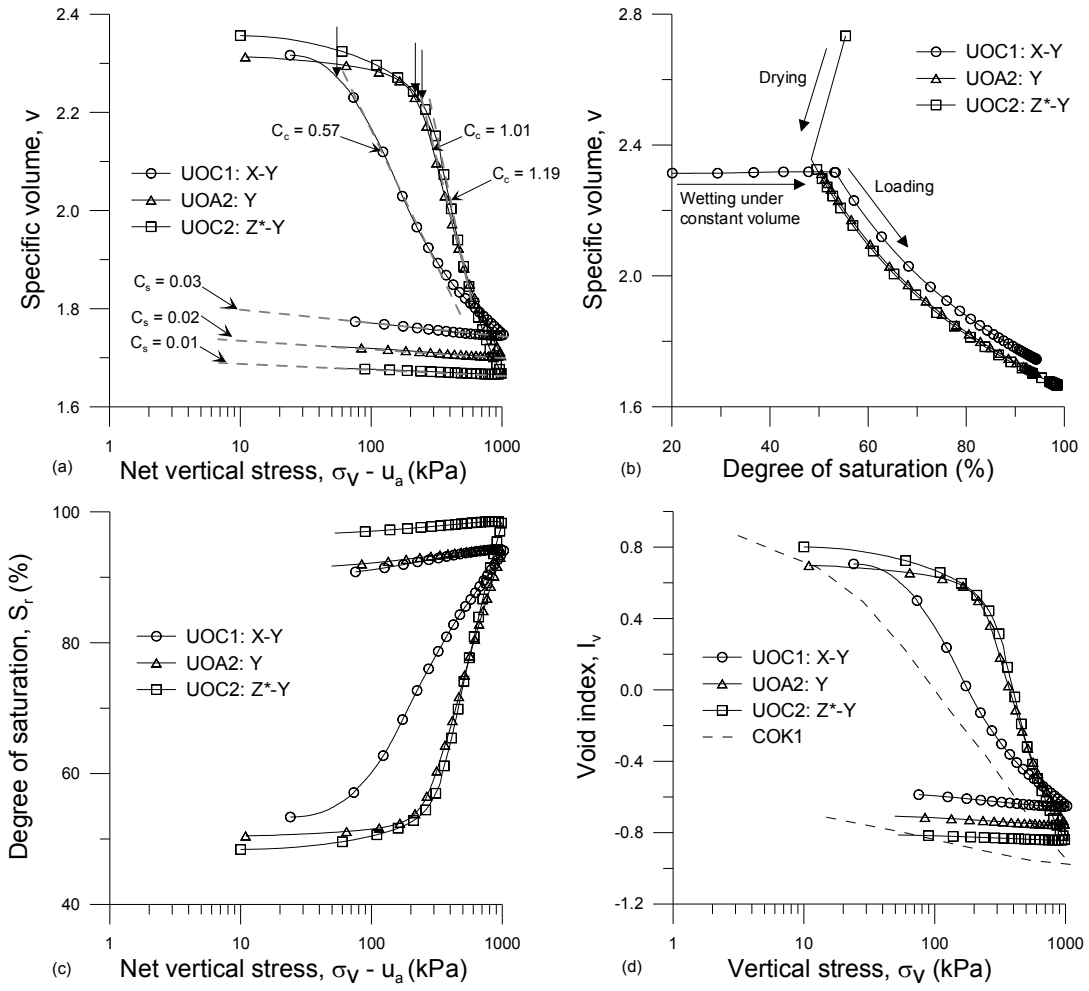

Figure 7.31: Series UOC: Constant water content one-dimensional consolidation tests, 3 samples of differing initial fabric brought to similar conditions prior to loading. UOC1: w = 25.8%, ρ_d = 1.17Mg/m^3, UOA2: w = 24.4%, ρ_d = 1.18Mg/m^3, UOC2: w = 24.1%, ρ_d = 1.16Mg/m^3. (a) specific volume vs net vertical stress, (b) specific volume vs degree of saturation, (c) degree of saturation vs net vertical stress and (d) comparison with reconstituted material in terms of void index

to thus fuse together creating a more homogeneous texture, which can no longer be characterised as an aggregated structure. Inter-aggregate porosity size has been further reduced and aggregate arrangements are no longer defined. The loss of the aggregated structure could explain the lower $\overline{\sigma}_{vc}$ observed in UOC1 and the reduction in inter-aggregate porosity would explain the stiffer post-yielding behaviour observed.

It had been planned that the specimens X-Y and Z*-Y would also be investigated using MIP. However due to difficulties with the freeze drying equipment, it was not possible to carry out these tests during the time frame of this thesis. With the recent acquisition of MIP equipment within the Faculty of Engineering at the University of Strathclyde, it is envisaged that these tests will be carried out in the near future, in order to support the results and discussion presented herein.

Figure 7.31b presents the variation in specific volume against the degree of saturation for the tests carried out under CW conditions. Loading and unloading follows along the same curve and the shape of this curve is very similar for all three tests, although it is slightly shifted for (UOC1) due to its slightly higher moisture content prior to loading. As expected in these CW tests the S_r increases as the vertical stress applied to the specimens increases, as the specimens are unloaded S_r reduces (Figure 7.31c). As for the results presented in Series UOA (CW), the compression curves of all the specimens lie to the right of the intrinsic compression line (COK1), (Figure 7.31d). In this Series the S_r was calculated by assuming that no pore water was removed or introduced into the specimens during loading. The actual variation in moisture content determined by measurement at the end of the tests indicates that UOC1 increased by 0.5%, UOA2 by 0.2% and UOC2 by 0.9% during the loading and unloading stages. These relatively small increases may be attributed to residual water remaining within the oedometer cell and accessories prior to mounting the specimens.

Figure 7.32 presents the compression curves of two different Z*-Y specimens (UOC2 and UOC3) dried from initial wet conditions, to different moisture contents and dry density and loaded under CW conditions. It is interesting to note that both specimens, compacted with the same wet aggregates w ~36% converge to exactly the same post-yielding compression line despite differences in compacted dry density and dry density prior to loading. The curve relating the variation in specific volume with degree of saturation is again very similar, showing that loading

and unloading steps follow along the same curve despite the differences in dry density between UOC2 and UOC3 (Figure 7.31b).

In order to investigate if the influence of compacted structure is in addition to the effect of the initial state, the specimens tested in Series UOC were brought to the same level of suction, using the axis-translation technique, prior to loading. Subsequently the specimens were loaded under suction controlled conditions (Series UOD). In this way any differences in volumetric behaviour upon one-dimensional loading and unloading may be attributed solely to the initial compacted fabric. A suction equal to 470kPa was selected for these tests in order to be as close as possible to the suction of Specimen Y at $w_o = 24\%$ and $\rho_{d_o} = 1.18\text{Mg/m}^3$, this was determined using the water retention data presented in Section 4.7.

Figure 7.33 presents the results of Series UOD, it is evident that the behaviour of UOD2 and UOD3 corresponding to specimens Y-Y and Z*-Y are more similar than that of UOD1, which corresponds to the X-Y specimen. As found in Series UOC (Figure 7.31a) the X-Y specimen exhibits a lower $\overline{\sigma}_{vc}$ than the other two specimens (143kPa) compared to 300kPa for UOD2 and 220kPa for UOD3. Specimen X-Y also exhibits lower post-yield compressibility ($C_c = 0.59$) than specimens Y-Y and Z*-Y. Although these effects are similar to those observed in Series UOC, the overall difference between the compression curves of the different specimens is much lower (Figure 7.33a). This suggests that although there may be some residual effects from the initial compacted fabric, the differences between specimens of different initial fabric are less significant when loaded from the same initial suction. This experimental evidence appears to support the second possibility proposed by Gens (1996) that the influence of initial compacted fabric is essentially negligible and that the soil behaviour can be adequately described by considering the initial state of stress and suction. This suggests that one set of model parameters would be sufficient to describe the behaviour of a given soil regardless of compaction conditions.

It is also interesting to note that the swell index determined for each curve under suction controlled conditions is the same ($C_s = 0.01$). Considering that in the Series UOC presented above, C_s varied for each of the different compacted fabrics, it appears that the swell index may be more related to suction and is independent of soil structure. This may be of consequence for constitutive modelling where often the recoverable (elastic) response of soil on unloading is considered to be independent of suction (e.g. BBM Alonso et al., 1990) and independent of soil

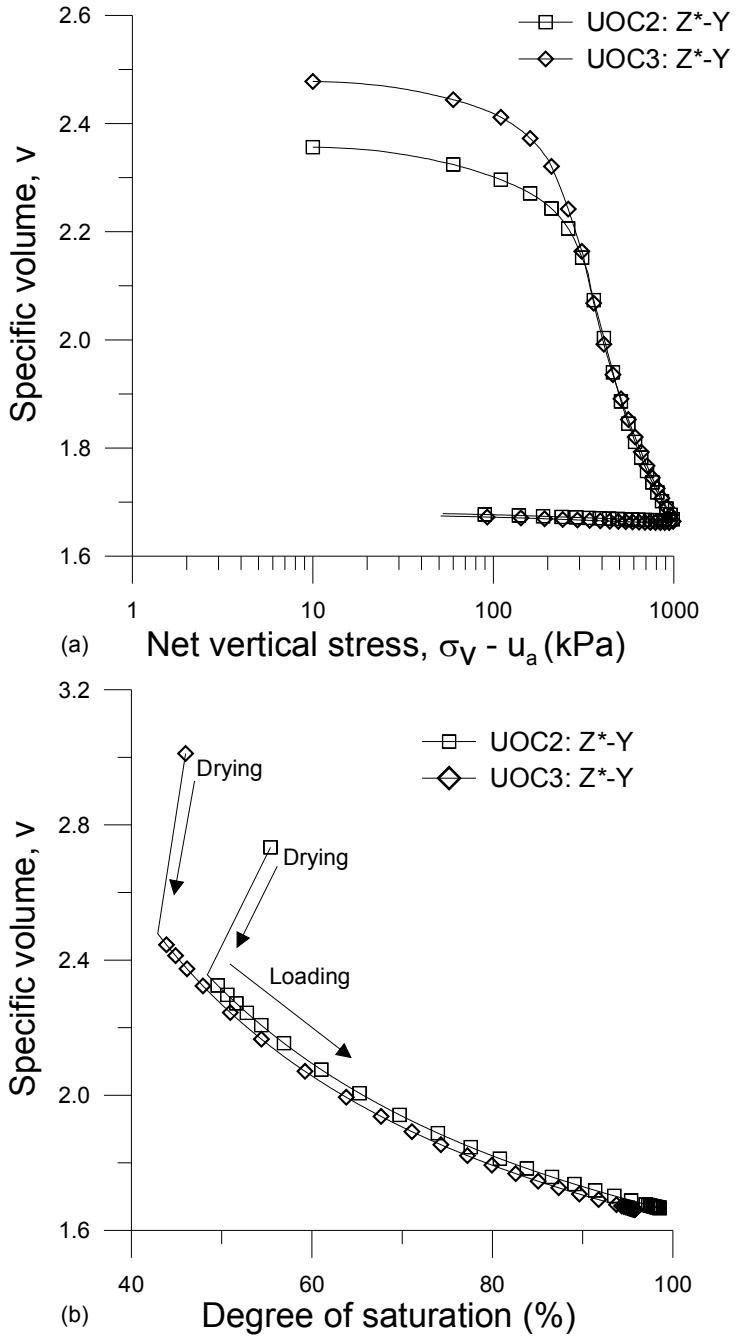

Figure 7.32: Two specimens dried from Z* to Y to different values of dry density and loaded under CW conditions. UOC2: $w = 24.1\%$, $\rho_d = 1.16\text{Mg/m}^3$, UOC3: $w = 23.3\%$, $\rho_d = 1.10\text{Mg/m}^3$, (a) specific volume vs net vertical stress and (b) specific volume vs degree of saturation.

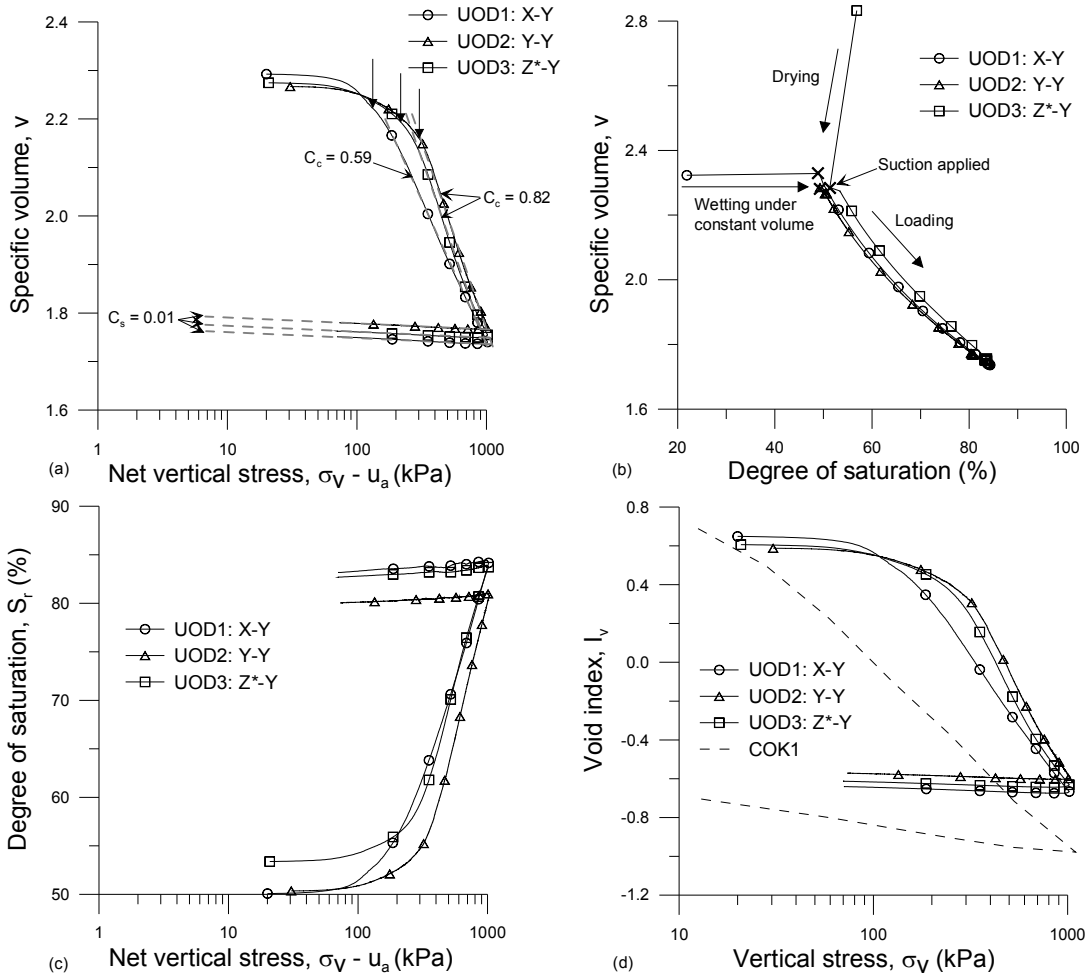

Figure 7.33: Series UOD: Suction controlled tests, 3 samples of differing initial fabric but with same conditions prior to loading of w, ρ_d, s and loaded under suction controlled conditions (s=470kPa). UOD1: w = 23.8%, ρ_d = 1.19Mg/m^3, UOD2: w = 23.5%, ρ_d = 1.20Mg/m^3, UOD3: w = 25.0%, ρ_d = 1.20Mg/m^3. (a) specific volume vs net vertical stress, (b) specific volume vs degree of saturation, (c) degree of saturation vs net vertical stress and (d) comparison with reconstituted material in terms of void index

Table 7.5: Yielding and compressibility parameters

Test Ref.	Specimen	Testing Condition	$\overline{\sigma}_{vc}$ or σ'_{vc} (kPa)	C_c	C_s
UOA1	X	CW	150	0.34	0.02
UOA2	Y	CW	220	1.01	0.02
UOA3	Z	CW	96	0.72	0.03
UOB1	X	SAT	42	0.43	0.02
UOB2	Y	SAT	20	0.46	0.03
UOB3	Z	SAT	18	0.33	0.03
UOC1	X-Y	CW	55	0.57	0.03
UOC2	Z*-Y	CW	250	1.19	0.01
UOC3	Z*-Y	CW	200	1.22	0.01
UOD1	X-Y	SC	143	0.59	0.01
UOD2	Y-Y	SC	300	0.82	0.01
UOD3	Z*-Y	SC	220	0.82	0.01

SAT - Saturated, CW- Constant water content, SC - Suction controlled

structure (e.g. Gens and Nova, 1993).

Figure 7.33b indicates that under suction controlled conditions the degree of saturation varies with void ratio, and again loading and unloading paths follows along the same curve. Such experimental evidence suggests that the degree of saturation is not only related to suction but also specific volume. This explains why specimens at the same suction may exist at different degrees of saturation if they have different specific volumes, as specific volume decreases (reduction in volume of voids) the retention curve becomes shifted, such that for a given suction, a lower v would retain a higher S_r than a specimen of higher v, see Figure 3.14.

The compression curves obtained during suction controlled conditions result in higher net yield stresses than for each of the same specimens tested in Series UOC (CW conditions), thus indicating that suction contributes an additional bonding effect which acts to resist against yielding under increased loading. See Table 7.5 for a summary of all yielding and compressibility parameters determined for the tests carried out in the UPC oedometer.

Again it had been anticipated that specimens X-Y, Y-Y and Z*-Y after the application of s = 470kPa would have been investigated using MIP; this was not possible at this time for the reason mentioned above, though is planned to be carried out in the future.

7.5.5 Summary

Investigation of specimens of varying initial compacted fabric at different initial states in the UPC oedometer has indicated that:

- In CW tests the effects of suction and aggregation were not separated and together they appeared to influence the partially saturated response of the Bengawan Solo fill to one dimensional loading (Series UOA)
- In partially saturated states the compression curves lie to the right of the intrinsic compression line (ICL), converging when the degree of saturation of the specimens tends towards unity. This is similar to the behaviour of intact bonded soils under saturated conditions (Series UOA).
- Even under saturated conditions, fabric effects due to aggregation appeared to not be completely removed with a specimen of smaller firmer aggregates undergoing overall less settlement (Test UOB1)
- The stress at which yielding occurs upon loading appears to be associated with the stiffness of the aggregates. Compacted specimens with firmer aggregates resulting in higher yield stresses (Series UOA and UOB).
- The variation in post-yield compressibility with different compacted fabrics is related to the pore size distribution, compressibility is higher where a large fraction of the porosity is characterised by pores with a large entrance diameter.

Comparing the volumetric response of specimens with different initial compacted fabric which were subsequently brought to similar initial conditions prior to loading illustrated that:

- On loading aggregated structures (defined by having a significant inter-aggregate porosity) exhibit a higher yield stress compared to specimens with a more homogeneous textured fabric (Series UOC and UOD)
- Aggregated structures exhibit a higher post-yielding compressibility compared to a more homogeneous textured fabric. It is anticipated that the compressibility is a function of the pore size distribution (Series UOC and UOD).

- Under CW conditions the specimens of varying initial compacted fabric but similar conditions of w and ρ_{d_o} prior to loading illustrated markedly different response from UOC1, which was a function of both structure and suction.
- Although similar effects were observed for different compacted specimens loaded at similar initial conditions of w and ρ_{d_o} and suction the differences between the compression curves were largely reduced (Series UOD).
- Comparing the results of Series UOC and UOD suggests that the swelling observed due to unloading may be more related to suction rather than structure, though further work would be necessary to confirm this.

7.6 Conclusions

This chapter presents an investigation into the compacted fabric created in the Bengawan Solo fill at low compactive efforts, typical of those found in-situ. At such a range the irregular double peak compaction curve was determined for this material. The type of aggregates created by mixing at different moisture contents of compacted soil fabric has been related to this irregular compaction curve, by considering aggregate size and stiffness. The microstructural study presented in Section 7.4 illustrated that such aggregates influenced the soil fabric created by compaction, (when compacting to low dry densities). The variation in the nature of the aggregates created with moisture content may be important when considering compaction in the field. As illustrated by the Extreme Light compaction curve, small variations in moisture content can result in important differences in dry density as a result of the aggregates formed.

Oedometer tests carried out on specimens with varying initial compacted fabric brought to the same initial conditions suggest that aggregated structures exhibit higher yielding stresses and higher post-yield compressibility than specimens of a more homogeneous texture (less aggregated). Under partially saturated conditions without suction control there appeared to be significant differences in volumetric behaviour related to initial compacted fabric. This is relevant for field conditions where suction is not controlled, and in particular for poorly compacted structures where the compaction conditions of moisture content or dry density are not rigorously maintained giving rise to significant variations in compacted fabric.

In carefully designed experiments taking into account the influence of suction (by also controlling w, ρ_d, e, S_r) it was observed however, that the residual effect on volumetric behaviour due to solely the influence of initial compacted fabric is small. This result illustrates the importance of considering soil structure for compacted specimens under suction controlled conditions. Furthermore these results support the view that for a given soil (of a certain mineralogy and grain size distribution) that the soil behaviour can be described through the use of one set of model parameters regardless of compaction conditions. At least this appears to be the case for the Bengawan Solo fill material, further experimental testing of a wide range of soils is required.

Chapter 8

Conclusions and recommendations

8.1 Introduction

The Bengawan Solo fill material investigated in this thesis was sampled from flood embankments located along the Bengawan Solo river in East Java, Indonesia. An underlying aim of this research was to investigate a *natural* soil from an engineering application in which unsaturated conditions may be relevant. In particular the main objectives of this research project were to:

1. Undertake a site and laboratory characterisation of the Bengawan Solo fill material, including detailed investigation of the soil mineralogy, compaction and water retention behaviour
2. Investigate the potential for volumetric collapse behaviour in this material, and to investigate the changes in soil fabric occurring due to loading and wetting
3. Investigate the isotropic compression and shearing behaviour of this material under different levels of suction
4. Investigate the soil structure of the Bengawan Solo fill created by compaction at different moisture contents and attempt to isolate the effect of compacted fabric on soil compression behaviour.

Throughout this thesis the findings of each chapter have been presented in the corresponding concluding section, and for this reason they are not repeated here in their entirety. In this final chapter only the main general conclusions are presented according to each of the objectives listed above. For clarity, the conclusions have been further divided into the following sections (where appropriate): (i) relevance to site conditions, (ii) contributions to existing knowledge and (iii) limitations and recommendations for future work.

8.2 Characterisation of the Bengawan Solo fill

8.2.1 Summary

Prior to investigation of the mechanical behaviour of the Bengawan Solo fill it was necessary to carry out an initial characterisation of the material. The important or interesting features of this material are listed below:

- The Bengawan Solo fill is an organic silt of high plasticity (MHO) according to BS5930:1999.
- X-ray diffraction indicated that the clay fraction is mostly made up of montmorillonite (88%), which explains why despite the small clay fraction present in this fill material, it plays an important role in the overall mechanical behaviour of this material.
- An irregular double-peak compaction curve was obtained for this material at low compactive efforts (similar to those used in the field) and was related to the varying nature of soil aggregates (in terms of size and stiffness) created on mixing with water.
- Investigation of the water retention behaviour using a combination of different techniques including the pressure plate filter paper and chilled mirror psychrometer, indicated that at high moisture contents (>35%), suction was in the range of several kPa whereas in air dried compacted specimens at low moisture contents (~6%), suctions of up to 100MPa were recorded.

8.2.2 Limitations & recommendations for future work

The main shortcoming with regards to the characterisation of the Bengawan Solo fill material was the limited field study conducted. A more in depth analysis of the performance of the embankments would require information on the variation of the dry density and moisture content of the embankment fill with seasonal changes. This would have required at least several more visits to the site, at a distance of more than 7,500 miles from the University of Strathclyde, for which additional funding would have had to be sourced. Furthermore the distance to the site and limited collaboration led to difficulties in obtaining detailed information on the construction of the Bengawan Solo embankments. The majority of the work conducted as part of this PhD was carried out on disturbed material sampled from the embankments and remoulded in the laboratory. Further work on this material could be carried out on the undisturbed block and cylindrical specimens sampled to investigate further the in-situ soil structure and its evolution when following drying and wetting paths.

8.3 Volumetric collapse behaviour

8.3.1 Relevance to site conditions

Load and soak oedometer tests carried out in conventional oedometer apparatus illustrated that the Bengawan Solo fill material is collapsible under dry of optimum and low density conditions, at compaction conditions close to the as-constructed conditions of the man-made embankments. Significant volumetric collapse was also observed in specimens compacted wet of optimum at low dry density and then subsequently dried prior to loading (and then soaking), despite an overall reduction in dry density. This highlights the importance of achieving a sufficiently high dry density during construction, regardless of compaction moisture content, in order to minimise subsequent volumetric collapse. ESEM and MIP results indicate a strong similarity between the microstructure of undisturbed specimens and specimens which have been remoulded in the laboratory and undergone subsequent volumetric collapse. This appears to suggest that the undisturbed material in the embankment has already undergone the process of volumetric collapse in-situ.

8.3.2 Contributions to existing knowledge

The use of both MIP and ESEM techniques enabled the changes occurring in the microstructure due to loading and wetting to be identified. For the Bengawan Solo fill, soaking after loading resulted in a reduction in the inter-aggregate porosity, which was readily visible in the ESEM micrographs. The MIP study confirmed this indicating that soaking alone was responsible for a shift in the dominant pore mode from 170µm to 2.4µm. Furthermore the ESEM micrographs indicated that the soaking process resulted in the softening of aggregations, the loss of the stabilisation due to suction and the loss of strength of bridging material and contacts, all of which contributed to the formation of a fused uniform fabric with very few inter-aggregate pores present.

Three different failure pathways were proposed which illustrate how volumetric collapse on wetting could possibly play a role in triggering failure modes in flood embankments, where fill material has been compacted to low dry densities. This work highlights how collapsible fill layers in flood embankments may reduce the overall integrity of such embankments and could possibly lead to the local or global failure of an embankment, despite the fact that this phenomenon is rarely cited in the literature as a possible failure mode of flood embankments. The behaviour of such collapsible fill layers is of particular importance where remediation measures are to be installed which will introduce additional loading to low density fill material, as in the case of the Bengawan Solo embankments.

The investigation into the volumetric collapse behaviour of the Bengawan Solo fill has demonstrated how simple load and soak oedometer tests using conventional oedometer apparatus can provide an important indication of the collapsible behaviour of fill material under planned construction conditions (or conditions present in the field). It is recommended that these simple tests should be carried out as standard practice before selecting compaction conditions for new flood embankments or particularly as a check in cases where additional loading is to be introduced to existing embankments.

8.3.3 Limitations & recommendations for future work

The large inter-aggregate pores (>450μm) present in the compacted specimen could not be detected using MIP, such larger pores found in low density open structures require a combination of techniques to detect the wide range of pore sizes present. Neutron tomography could be used to detect pore sizes in the larger range (up to 10mm) as used by Koliji (2008). Work is currently being carried out at the University of Strathclyde on the development of a laser for non-destructive volume measurements which could be used in the quantification of larger pore sizes.

Additional research should be carried out to investigate how heterogeneities in the compaction of fill material can influence the variation in the potential for volumetric collapse throughout a flood embankment. This kind of research should be carried out ideally on a test embankment at the field scale using different compaction methods.

8.4 Isotropic & shearing behaviour

8.4.1 Relevance to site conditions

The shear strength of the Bengawan Solo fill material was investigated under four different suction levels and three different net confining stresses. Using shear strength data obtained from the triaxial tests, a routine slope stability analysis indicated that the reduction in shear strength due to saturation did not influence negatively the stability of the embankments. A simple analysis investigating rapid drawdown illustrated that embankments constructed of this fill material are likely to be susceptible to failure as a result of this process. Given though that there is no record of closure of the Babat Barrage close to when the failure of the gabion reinforced embankment occurred, it is likely that a combination of other mechanisms have been responsible for this global failure including erosion and volumetric collapse, among others.

8.4.2 Contributions to existing knowledge

The isotropic and triaxial tests carried out on the Bengawan Solo fill provide a set of data regarding the compression behaviour and shear strength for a compacted soil under a number of different suction levels. The isotropic compression tests indicated that as suction increased the yield stress increased, and the post-yield compressibility also increased. Both the angle of friction (ϕ') and the cohesion intercept (c') appeared to increase with increasing suction. At suctions less than 500kPa it appears that suction influences more strongly ϕ' than c'. Significantly higher shear strength parameters were obtained under air dried conditions (s ~ 100MPa), which may be attributed not only to the level of suction but also the bonded aggregated structure of such air dried specimens.

8.4.3 Limitations & recommendations for future work

A major limitation of this work is the lack of reliable volume change data during shearing. This is attributed to shortcomings in the experimental set-up resulting from adaptation of existing equipment for unsaturated soils testing. Prior to use of this equipment in any future experimental campaigns, the issue of volume change will be fully addressed and rectified.

The permeability of the Bengawan Solo fill material was not investigated in detail as part of this research and it is recommended that an experimental campaign be carried out to characterise the variation of permeability with dry density and suction in order to account for seepage through the embankment and thus enable an improved understanding of the performance of the Bengawan Solo embankments. It is hoped that the experimental data presented herein can be used to inform future detailed investigations into factors influencing the stability of the Bengawan Solo embankments.

8.5 Influence of compacted fabric on volumetric behaviour

8.5.1 Relevance to site conditions

The differences in the nature of the aggregates formed at different moisture contents may be relevant for field compaction. Such aggregations appear to strongly influence the compacted fabric and as such attempts should be made at the Bengawan Solo embankments to better control the moisture content of the fill material during construction. Furthermore in future projects using this fill material the compactive effort applied should be more rigorously controlled to minimise variation in the dry density throughout the embankment.

8.5.2 Contributions to existing knowledge

The irregular double peak compaction curve observed at low compactive efforts for the Bengawan Solo fill has been attributed to the type of aggregates created by mixing at different moisture contents. A microstructural investigation illustrates that aggregates prepared at different moisture contents lead to very different compacted fabrics, even at the same dry density.

Specimens of varying initial fabric brought to the same conditions of w, ρ_d prior to loading under CW conditions illustrated that more aggregated fabrics exhibit a higher yield stress and a higher post-yield compressibility than specimens of a more homogeneous texture. Under CW conditions, initial compacted fabric appeared to influence volumetric behaviour but taking suction also into account, the differences in behaviour due to initial compacted fabric greatly reduced. This is an important result in terms of constitutive modelling as it supports the argument that for a given soil, one set of model parameters could be sufficient to describe its behaviour, regardless of initial compaction conditions. At least this appears to be the case for the Bengawan Solo fill material.

8.5.3 Limitations & recommendations for future work

It was not possible during the time frame of the thesis to conduct MIP tests on specimens X-Y, Y-Y and Z*-Y once brought to the same level of suction (s = 470kPa). It was originally

envisaged that these tests would be carried out as part of the PhD to support the experimental campaign presented in Chapter 7, however due to difficulties with the freeze drying equipment at UPC, this was not possible. In light of the recent acquisition of a mercury intrusion porosimeter by the Engineering Faculty at Strathclyde, it is anticipated that these tests will be carried out in the near future to complete this study presented into the influence of compacted structure on subsequent volumetric behaviour.

As a continuation of this study, it would be interesting to investigate if these same specimens X-Y, Y-Y and Z*Y, prepared using different compaction conditions (w, ρ_d) and then brought to the same initial state (σ_v, s) exhibit significant differences in volumetric collapse behaviour. Such additional information is required for a range of different soils in order to investigate further the influence of initial compacted fabric on subsequent volumetric behaviour and should be considered alongside the results presented by Booth (1975) and Gens et al. (1996).

In order to provide further understanding to the role of soil structure, it is recommended here that additional experimental information is required comparing the volumetric and shearing behaviour exhibited by reconstituted and compacted material of the same soil under saturated and suction controlled conditions. Testing should be carried out for a wide range of different soils and be supplemented with detailed information of the soil structure. Such research would provide additional insight into the influence of suction on post-yield compressibility (due to loading) and swelling behaviour (due to unloading), an area which remains to be fully understood.

References

Agus, S. S., Schanz, T., and Fredlund, D. G. (2010). "Measurements of suction versus water content for bentonite-sand mixtures.." *Can Geotech J*, 47, 583–594.

Ahmed, S., Lovell, C., W. J., and Diamond, S. (1974). "Pore size and strength of compacted clay." *Journal of the Geotechnical Engineering Division, ASCE*, 100(4), 407–425.

Airò Farulla, C. and Ferrari, A. (2005). "Suction controlled oedometric tests: some technical aspects." *Proc. Int. Symp. On Advanced Experimental Unsaturated Soil Mechanics*, Experus, 2005, Trento, Italy. Balkema, 43–48.

Aitchison, G. D. (1965). "Moisture equilibria and moisture changes in soils beneath covered areas." *A Symposium in Print*, 278pp.

Alonso, E. E. (1993). "Unsaturated soils: Recent developments and applications." *Constitutive Modelling of Unsaturated Soils*, Civil Engineering European Courses Programme of Continuing Education 1993, Barcelona, Spain.

Alonso, E. E., Gens, A., and Gehling, W. Y. Y. (1994). "Elastoplastic model for unsaturated expansive soils." *Proc 3rd Eur Conf Num Methods Geotech Eng, Manchester, UK*, 11–18.

Alonso, E. E., Gens, A., and Hight, D. W. (1987). "Groundwater effects in geotechnical engineering." *Proceedings of the 9th European Conference on Soil Mechanics and Foundation Engineering*, E. T. Hanrahan, T. . L. L. Orr, and T. F. Widdis, eds., Vol. 3, Dublin, Ireland. A. A. Balkema / Rotterdam / Brookfield.

Alonso, E. E., Gens, A., and Josa, A. (1990). "A constitutive model for partially saturated soils." *Géotechnique*, 40(3), 405–430.

Alonso, E. E., Lloret, A., Gens, A., and Yang, D. Q. (1995). "Experimental behaviour of highly expansive double-structure clay." *Proc 1st Int Conf on Unsaturated Soils, Paris, France*, 1, 11–16.

Alonso, E. E., Romero, E., Hoffman, C., and García-Escudero, E. (2005). "Expansive bentonite - sand mixtures in cyclic controlled - suction drying and wetting." *Engineering Geology*, 81(3), 213–226.

Alonso, E. E., Vaunat, J., and Gens, A. (1999). "Modelling the mechanical behaviour of expansive clays." *Eng Geol*, 54, 173–183.

Amorosi, A. and Rampello, S. (2007). "An experimental investigation into the mechanical behaviour of a structured stiff clay." *Géotechnique*, 57(2), 153–166.

Baker, R. and Frydman, S. (2009). "Unsaturated soil mechanics. critical review of physical foundations." *Eng Geol*, 106, 26–39.

Balmaceda, A. (1991). "Compacted soils: A theoretical and experimental study," PhD thesis, Universitat Politécnica de Catalunya, Barcelona.

Barbour, S. L. (1998). "Nineteenth canadian geotechnical colloquium: The soil-water characteristic curve: a historical perspective." *Can Geotech J*, 35, 873–894.

Barden, L., McGown, A., and Collins, K. (1973). "The collapse mechanism in partly saturated soil." *Eng Geol*, 7, 49–60.

Barden, L. and Sides, G. R. (1970). "Engineering behaviour of structured compacted clay." *J Soil Mech Found Div ASCE*, 96 SM4, 1171–1201.

Basham, D. L., Blanton Jr., W. R., Dorman, J., Garcia, D. F., Gilson, S., Halpin, E., Harder Jr, L. F., Jacoby, K. M., Kennedy, C., Matsuda, E., Mayer, R. G., Perri IV, P. P., Medlock, S. R., Sanders, C. A., Spagna, S., Stankiewicz, M. R., Stockton, S. L., Sweeney, J., Thomas, M., Turner Jr., R. A., Verigin, S. W., Williams, W. D., and Zien, T. R. (2009). "Draft: recommendations for a national levee safety programme. a report to congress from the national committee on levee safety. an involved public and reliable levee systems.

Bassett, D., Pettit, A., Anderton, C., and Grace, P. (2007). "Scottish flood defence asset database, final report.

Baudin, C. M. H., Moes, C. J. B., and van Baalen, M. (1989). "The influence of uplift water pressures on the deformations and stability of flood embankment." *Proc. 12th International Conf. Soil Mechanics Foundation Engineering*, Vol. 3, Rio de Janerio, Brazil. Balkema, Lisse, 1713–1716.

Bear, J. (1972). *Dynamics of fluids in porous media.* American Elsevier Publishing Company Inc.

Becker, D. E., Crooks, J. H. A., Been, K., and Jefferies, M. G. (1987). "Work as a criterion for determining in situ and yield stresses in clays." *Can Geotech J*, 24, 549–564.

Bezuijen, A., Kruse, G. A. M., and Van, M. A. (2005). "Failure of peat dikes in the netherlands." *Proceedings of the 16th Int. Conf. Soil Mech. Geotech. Eng.*, Osaka, Japan. 1857–1860.

Bishop, A. (1959). "The principle of effective stress." *Teknisk Ukeblad*, 106 (39), 859–863.

Bishop, A. and Blight, G. (1963). "Some aspects of effective stress in saturated and partially saturated soils." *Géotechnique*, 13 (3), 177–197.

Bishop, A. W. and Donald, I. B. (1961). "The experimental study of partly saturated soils in the triaxial apparatus." *Proc 5th Int Conf Soil Mech Found Engng, Paris*, 1, 13–21.

Blatz, J. A., Cui, Y.-J., and Oldecop, L. (2008). "Vapour equilibrium and osmotic technique for suction control." *Geotech Geol Eng*, 26(6), 661–673.

Blatz, J. A. and Graham, J. (2000). "A system for controlled suctions in triaxial tests." *Géotechnique*, 50(4), 465–469.

Booth, A. R. (1975). "The factors influencing collapse settlement in compacted soils." *Proceedings of 6th Regional Conference for Africa on Soil Mechanics & Foundation Engineering*, Vol. 1, Durban, South Africa. A. A. Balkema, 57–63.

Booth, A. R. (1977). "Collapse settlement in compacted soils." *CSIR Research Report 324 Bulletin 13*, National Institute for Transport and Road Research.

BPS (2006). "Sosialisasi hasil sensus ekonomi." *Report no.*, Badan Pusat Statistik.

Brooks, R. H. and Corey, A. T. (1964). "Hydraulic properties of porous media." *Hydrology Paper*, 3, 22–27.

Brown, R. L. (1999). "Vientiane plain flood protection: urgent phase.." *Flood Management and Mitigation in the Mekong River Basin, Proceedings of the regional workshop*, number 1999/14., Vientiane, LAO PDR,. RAP Publication.

BS1377-2:1990 (1990). "Methods of test for soils for civil engineering purposes - part 2: Classification tests.

BS1377-3:1990 (1990). "Methods of tests for soils for civil engineering purposes - part 3: Chemical and electro-chemical tests.

BS1377-4:1990 (1990). "Methods of test for soils for civil engineering purposes - part 4: Compaction - related tests.

BS1377-8:1990 (1990). "Methods of test for soils for civil engineering purposes - part 8: Shear strength tests (effective stress).

BS1377-9:1990 (1990). "Methods of test for soils for civil engineering purposes - part 9: In-situ tests.

BS5930:1999 (1999). "Code of practice for site investigations.

BS6031 (1981). "Code of practice for earthworks.

BS8004:1986 (1986). "Code of practice for foundations.

Buckingham, E. (1907). "Studies of the movement of soil moisture." *Report no.*, United States. Bureau of Soils. Bulletin 38.

Bulut, R. and Leong, E. C. (2008). "Indirect measurement of suction." *Geotech Geol Eng*, 26(6), 633–644.

Bulut, R., Lytton, R. L., and Wray, W. K. (2001). "Soil suction measurements by filter paper." *Expansive Clay Soils and Vegetative Influence on Shallow Foundations (GSP 115)*, Proceedings of the Geo-Institute Shallow Foundation and Soil Properties, 243–261.

Burland, J. B. (1990). "On the compressibility and shear strength of natural clays." *Géotechnique*, 40(3), 329–378.

Burland, J. B., Rampello, S., Georgiannou, V. N., and Calabresi, G. (1996). "A laboratory study of the strength of four stiff clays." *Géotechnique*, 46(3), 491–514.

Cardoso, R., Romero, E., Lima, A., and Ferrari, A. (2007). "A comparative study of soil suction measurement using two different high-range psychrometers." *Experimental Unsaturated Soil Mechanics*, Vol. 112. 79–93.

Carter, M. R. (2004). "Researching structural complexity in agricultural soils." *Soil and Tillage Research*, 79, 1–6.

Casagrande, A. (1936). "Determination of the preconsolidation load and its practical significance.." *Proc 1st Int Conf Soil Mech Found Eng, Cambridge, Mass., USA*, 3, 60–64.

Chandler, R. J., Crilly, M. S., and Montgomery-Smith, G. (1992). "A low-cost method of assessing clay desiccation for low-rise buildings." *Proc Inst Civ Eng Civ Eng*, 92, 82–89.

Chandler, R. J. and Gutierrez, C. I. (1986). "The filter-paper method of suction measurement." *Géotechnique*, 36(2), 265–268.

Chandler, R. J., Harwood, A. H., and Skinner, P. J. (1992). "Sample disturbance in london clay." *Géotechnique*, 42(4), 577–585.

Charman, P. E. V. and Murphy, B. W. (1998). *Soils: Their Properties and Management*. Oxford University Press, 5th edition.

Childs, E. C. and Collis-George, N. (1948). "The permeability of porous materials." *Proceedings of the Royal Society of London*, A (201), 392–405.

Christensen, J. H., Hewitson, B., Busuioc, A., Chen, A., Gao, X., Held, I., Jones, R., Kolli, R. K., Kwon, W.-T., Laprise, R., Magaña Rueda, V., Mearns, L., Menéndez, C. G., Räisänen, J., Rinke, A., A., S., and Whetton, P. (2007). "Regional climate projections. climate change 2007: The physical science basis." *Contribution of Working Group I to the Fourth Assessment Report of the Intergovernmental Panel on Climate Change*, S. Solomon, D. Qin, M. Manning, Z. Chen, M. Marquis, K. B. Averyt, M. Tignor, and H. L. Miller, eds. Cambridge University Press, Cambridge, United Kingdom and New York, NY, USA.

Chu, T. Y. and Mou, C. H. (1973). "Volume change characteristics of expansive soils determined by controlled suction tests." *Proc 3rd Int Conf Expansive Soils, Haifa*, 177–185.

Collins, K. and McGown, A. (1974). "The form and function of microfabric features in a variety of natural soils." *Géotechnique*, 24(2), 223–254.

Cooling, L. and Marsland, A. (1954). "Soil mechanics studies of failures in the sea defence banks of essex and kent." *Conference on the North Sea Floods of 31st January / 1st February, 1953*.

Coop, M. R. and Atkinson, J. H. (1993). "The mechanics of cemented carbonate sands." *Géotechnique*, 43(1), 53–67.

Croney, D. and Coleman, J. D. (1948). "Soil thermodynamics applied to the movement of moisture in road foundations." *Proc 7th Int Cong Appl Mech*, 3, 163–177.

Croney, D., Coleman, J. D., and Black, W. P. (1958). "Movement and distribution of water in soil in relation to highway design and performance. highway research board special report. issue: 40, pp. 226-252." *Report no.*, Transport Research Board.

Croney, P. and Croney, D. (1998). *The design and performance of road pavements*. McGraw-Hill Professional, 3rd edition edition.

Cruz, R. V., Harasawa, H., Lal, M., Wu, S., Anokhin, Y., Punsalmaa, B., Honda, Y., Jafari, M., C., L., and Huu Ninh, N. (2007). "Asia. climate change 2007: Impacts, adaptation and vulnerability." *Contribution of Working Group II to the Fourth Assessment Report of the Intergovernmental Panel on Climate Change*, M. L. Parry, O. F. Canziani, J. P. Palutikof, P. J. van derLinden, and C. E. Hanson, eds. Cambridge University Press, Cambridge, UK, 469–506.

Cui, Y. J. and Delage, P. (1996). "Yielding and plastic behaviour of an unsaturated compacted silt." *Géotechnique*, 46(2), 291–311.

Cunningham, M. R. (2000). "The mechanical behaviour of a reconstituted, unsaturated soil," PhD thesis, Imperial College of Science, Technology and Medicine, University of London.

Cunningham, M. R., Ridley, A. M., Dineen, K., and Burland, J. B. (2003). "The mechanical behaviour of a reconstituted unsaturated silty clay." *Géotechnique*, 53(2), 183–194.

Cusinier, O. and Masrouri, F. (2005). "Hydromechanical behaviour of a compacted swelling soil over a wide suction range." *Eng Geol*, 81(3), 201–212.

D6386-02, A. (2003). "Standard test methods for determination of the soil water characteristic curve for desorption using a hanging column, pressure extractor, chilled mirror hygrometer, and/or centrifuge.

Danilatos, G. D. (1993). "Introduction to the esem instrument." *Microsc Res Tech*, 25, 354–361.

Decagon Devices, I. (2003). *WP4 Water Dewpoint Potentiometer. Operator Manual, Version 2.2.* Pullman, USA.

Defra (2008). "The government's response to sir michael pitt's review of the summer 2007 floods." *Report no.*, Department for Environment, Food and Rural Affairs.

Delage, P. (2002). "Experimental unsaturated soil mechanics." *Proc. 3rd Int. Conf. on Unsaturated Soils, Recife, Brazil*, 3, 973–996, Balkema.

Delage, P., Audiguier, M., Cui, Y., and D., H. M. (1996). "Microstructure of a compacted silt." *Can Geotech J*, 33, 150–158.

Delage, P. and Graham, J. (1996). "Mechanical behaviour of unsaturated soils." *Proc. 1st Int. Conf on Unsaturated Soils, Paris*, 3, 1223–1256.

Delage, P., Howat, M. D., and Cui, Y. J. (1998). "The relationship between suction and swelling properties in a hevaily compacted unsaturated clay." *Eng Geol*, 50, 31–48.

Delage, P. and Lefebvre, G. (1984). "Study of the structure of a sensitive champlain clay and of its evolution during consolidation." *Can Geotech J*, 21, 21–35.

Delage, P., Marcial, D., Cui, Y. J., and Ruiz, X. (2006). "Ageing effects in a compacted bentonite: a microstructure approach." *Géotechnique*, 56(5), 291–304.

Delage, P., Romero, E., and Tarantino, A. (2008). "Recent developments in the techniques of controlling and measuring suction." *Proceedings of the 1st European Conference on Unsaturated Soils, Unsaturated Soils. Advances in Geo-Engineering*, D. G. Toll, C. E. Augarde, D. Gallipoli, and S. J. Wheeler, eds., Durham, UK. Taylor and Francis Group, London, 33–52.

Delage, P., Suraj de Silva, G. P. R., and De Laure, E. (1987). "Un nouvel appareil triaxial pour les sols non saturés." *Proc 9th European Conf Soil Mech Found Engng, Dublin*, 1, 26–28.

Delage, P., Tessier, D., and Marcel-Audiguier, M. (1982). "Use of the cryoscan apparatus for observation of freeze-fractured planes of a sensitive quebec clay in scanning electron microscopy.." *Can Geotech J*, 19(1), 111–114.

Diamond, S. (1970). "Pore size distribution in clays." *Clays Clay Miner*, 18, 7–23.

Dineen, K. (1997). "The influence of suction on compressibility and swelling," PhD thesis, Imperial College of Science, Technology and Medicine, University of London.

Dineen, K., Colmenares, J. E., Ridley, A. M., and Burland, J. B. (1999). "Suction and volume changes of a bentonite-enriched sand." *Proc. Instn. Civ. Engrs. Geotech. Engng.*, 137, 197–201.

Dudley, J. H. (1970). "Review of collapsing soils." *J Soil Mech Found Div ASCE*, 96 SM3, 925–947.

Dunbar, J. B., Torrey III, V. H., and Wakeley, L. D. (1999). "A case history of embankment failure : geological and geotechnical aspects of the celotex levee failure, new orleans, louisiana." *Technical report GL-99-11*, prepared for U.S. Army Engineer Division, Mississippi Valley and U.S. Army Corps of Engineers Civil Works Research and Development Program, Risk Analyses for Dam Safety.

Dyer, M. (2004). "Performance of flood embankments in england and wales." *Proc Inst Civ Eng Water Manage*, December 2004, Issue WM4, 177–186.

Dyer, M., Utili, S., and Zielinski, M. (2009). "Field survey of desiccation fissuring of flood embankments." *Proc Inst Civ Eng Water Manage*, June 2009, Issue WM3, 221–232.

EA (2009). "Investing for the future flood and coastal risk management in england: A long-term investment strategy.

Ellis, C. I. (1980). "Soil compaction at low moisture content - field trials in sudan.." *Proceedings of the 7th Regional Conference for Africa on Soil Mechanics and Foundation Engineering, Accra, Ghana.*

Escario, V. (1980). "Suction controlled penetration and shear tests." *Proc 4th Int Conf Expansive Soils*, 2, 781–797.

Escario, V. and Juca, J. (1989). "Strength and deformation of partly saturated soils." *Proc 12th Int Conf Soil Mech Found Eng, Rio de Janeiro*, 3, 43–46.

Escario, V. and Sáez, J. (1986). "The shear strength of partly saturated soils." *Géotechnique*, 36(3), 453–456.

Escario, V. and Sáez, J. (1987). "Shear strength of soils under high suction values. written discussion. session 5.." *Proc 9th European Conf Soil Mech Found Engng, Dublin*, 3, 1157.

Esteban, F. (1990). "Caracterizacion experimental de la expansividad de una roca evaporitica," PhD thesis, Universidad de Cantabria, Santander, Spain [In Spanish].

Esteban, V. and Saez, J. (1988). "A device to measure the swelling characteristics of rock samples with control of the suction up to very high values." *ISRM Symposium on Rock Mechanics and Power Plants*, 2.

FAO/RAP (1999). "Summary report. in: Flood management and mitigation in the mekong river basin, proceedings of the regional workshop.." *Report No. RAP Publication 1999/14.*, Food and Agriculture Organization of the United Nations, Regional Office for Asia and the Pacific, Vientiane, LAO PDR,.

Fisher, R. A. (1926). "On the capillary forces in an ideal soil; correction of formulas by w.b. haines." *J Agric Sci*, 16, 492–505.

Fookes, P. G. (1990). "Tropical residual soils, report of the geological society engineering group working party." *Q J Eng Geol Hydrogeol*, 23(1), 4–101.

Franklin, A. F., Orozco, L. F., and Semrau, R. (1973). "Compaction of slightly organic soils." *J Soil Mech Found Div ASCE*, Vol. 99, No. SM7, 541–557.

Fredlund, D., N.R., M., and Widger, R. (1978). "The shear strength of unsaturated soils." *Can Geotech J*, 15 (3), 313–321.

Fredlund, D. and Rahardjo, H. (1993). *Soil mechanics for unsaturated soils.* John Wiley & Sons Inc., New York.

Fredlund, D., Xing, A., Fredlund, M. D., and Barbour, S. L. (1996). "The relationship of the unsaturated soil shear strength to the soil-water characteristic curve." *Can Geotech J*, 33, 440–448.

Fredlund, D. G. (1979). "Appropriate concepts and technology for unsaturated soils." *Can Geotech J*, 16(1), 121–139.

Fredlund, D. G. and Morgenstern, N. R. (1977). "Stress state variables for unsaturated soils." *J Geotech Eng Div ASCE*, 103, 447–466.

Fredlund, D. G. and Xing, A. Q. (1994). "Equations for the soil-water characteristic curve." *Can Geotech J*, 31(4), 521–532.

Fredlund, G. (2006). "Unsaturated soil mechanics in engineering practice." *J Geotech Geoenviron Eng ASCE*, 132(3), 286–321.

Frydman, S. and Baker, R. (2009). "Theoretical soil-water characteristic curves based on adsorption, cavitation, and a double porosity model." *Int J Geomech ASCE*, 9(6), 250–257.

Futai, M. M. and Almeida, M. S. S. (2005). "An experimental investigation of the mechanical behaviour of an unsaturated gneiss residual soil." *Géotechnique*, 55(3), 201–213.

Gallipoli, D., Gens, A., Sharma, R., and Vaunat, J. (2003). "An elasto-plastic model for unsaturated soil incorporating the effects of suction and degree of saturation on mechanical behaviour." *Géotechnique*, 53(1), 123–135.

Gallipoli, D., Wheeler, S. J., and Karstunen, M. (2003). "Modelling the variation of degree of saturation in a deformable unsaturated soil." *Géotechnique*, 53, 105–112.

Gan, J. K. M., Fredlund, D. G., and Rahardjo, H. (1988). "Determination of the shear strength parameters of an unsaturated soil using the direct shear test." *Can Geotech J*, 25, 500–510.

Garcia-Bengochea, I., Lovell, C. W., and Altschaeffl, A. G. (1979). "Pore distribution and permeability of silty clays." *J Geotech Eng Div ASCE*, 105, NO. GT7, 839–856.

Gardner, W. (1956). "Mathematics of isothermal water condition in unsaturated soils.." *International symposium on physio-chemical phenomenon in soils*, Highway Research Board Special Report 40, Washington DC. 78–87.

GDS (2005a). *Advanced Pressure/Volume Controller (ADVDPC)*. GDS.

GDS (2005b). *Standard Pressure/Volume Controller (STDDPC)*. GDS.

Geiser, F., Laloui, L., and Vuillet, L. (2000). "Modelling the behaviour of unsaturated silt." *Experimental evidence and theoretical approaches in unsaturated soils*, A. Tarantino and C. Mancuso, eds., Vol. 1. 155–175.

Geiser, F., Laloui, L., and Vulliet, L. (2000). "On the volume measurement in unsaturated triaxial test." *Unsaturated soils for Asia*, H. Rahardjo, D. G. Toll, and E. C. Leong, eds. A. A. Balkema, Rotterdam, The Netherlands, 669–674.

Gens, A. (1982). "Stress-strain and straength characteristics of a low plasticity clay," PhD thesis, Imperial College, University of London.

Gens, A. (1996). "Constitutive modelling: Application to compacted soils." *Unsaturated Soils/Sols Non Saturés*, E. E. Alonso and P. Delage, eds. 1179–1200.

Gens, A. (2010). "Soil-environment interactions in geotechnical engineering." *Géotechnique*, 60(1), 3–74.

Gens, A. and Alonso, E. E. (1992). "A framework for the behaviour of unsaturated expansive clays." *Can Geotech J*, 29, 1013–1032.

Gens, A., Alonso, E. E., Suriol, J., and Lloret, A. (1996). "Effect of structure on the volumetric behaviour of a compacted soil." *Unsaturated Soils/Sols Non Saturés*, E. E. Alonso and P. Delage, eds. 83–88.

Gens, A., Guimaraes, L. d. N., Sánchez, M., and Sheng, D. (2008). "Developments in modelling the generalised behaviour of unsaturated soils." *Unsaturated Soils: Advances in Geo-Engineering*, 1, 53–61.

Gens, A., Guimarães, L., and Olivella, S. (2002). "Coupled chemomechanical analysis for saturated and unsaturated soils." *Environmental Geomechanics*, L. Vulliet, L. Lalui, and B. Schrefler, eds. Lausanne: EPFL Press, 109–123.

Gens, A. and Nova, R. (1993). "Conceptual bases for a constitutive model for bonded soils and weak rocks." *Geotechnical Engineering of Hard Soils - Soft Rocks*, 485–494.

Gens, A., Sánchez, M., Guimarães, L., Alonso, E. E., Lloret, A., Olivella, S., and Villar, M. V.and Huertas, F. (2009). "A full-scale in situ heating test for high-level nuclear waste disposal: observations, analysis and interpretation." *Géotechnique*, 59(4), 377–399.

Gens, A., Sánchez, M., and Sheng, D. (2006). "On constitutive modelling of unsaturated soils." *Acta Geotechnica*, 1, 137–147.

Ghataora, G. S., Burns, B., Hassan, M., and Morris, M. (2007). "Soil piping tests on thorngumbald flood embankment." *Science Report FD2411/TR3*, Joint Defra / EA Flood and Coastal Erosion Risk Management R&D Programme.

Griffiths, F. J. and Joshi, R. C. (1989). "Changes in pore size distribution due to consolidation of clays." *Géotechnique*, 1, 159–167.

Grim, R. E. (1953). *Clay Mineralogy*. McGraw-Hill, New York.

Grozic, J. L. H., Lunne, T., and Pande, S. (2003). "An oedometer test study on the preconsolidation stress of glaciomarine clays." *Can Geotech J*, 40, 857–872.

Gulhati, S. K. and Satija, D. J. (1981). "Shear strength of partially saturated soils." *Proc. 10th Int. Conf. Soil Mech. Found. Eng.*, 609–612.

Haines, W. B. (1930). "Studies in the physical properties of soil. v. the hysteresis effect in capillary properties, and the modes of moisture distribution associated therewith." *J Agric Sci*, 20, 97–116.

Head, K. H. (1982). *Manual of Soil Laboratory Testing, Volume 2: Permeability, Shear Strength and Compressibility Tests*. Pentech Press, London.

Head, K. H. (1992). *Manual of Soil Laboratory Testing, Volume 1: Soil Classification and Compaction Tests (2nd Edition)*. Pentech Press, London, 2nd edition.

Head, K. H. (1998). *Manual of Soil Laboratory Testing, Volume 3: Effective Stress Tests*. John Wiley & Sons, 2nd edition.

Hidayat, F., Sungguh, H. M., and Harianto (2008). "Impact of climate change on floods in bengawan solo and brantas river basins, indonesia." *11th International Riversymposium in Brisbane, Australia, 1 - 4 September 2008, published online at www.riversymposium.com.*

Hilf, J. W. (1956). "An investigation of pore-water pressure in compacted cohesive soils, technical memo. 654." *Report no.*, U.S. Bureau of reclamation, Design and construction division, Denver, USA.

Hird, C. C., Marsland, S., and Schofield, A. N. (1978). "The development of centrifuge models to study the influence of uplift pressures on stability of a flood bank." *Géotechnique*, 28 (1), 85–106.

Ho, D. and Fredlund, D. (1982). "Strain rates for unsaturated soil shear strength testing." *7th Southeast Asian Geotechnical Conference, Hong Kong.*

Hoffman, C., Romero, E., and Alonso, E. E. (2005). "Combining different controlled-suction techniques to study expansive clays." *Proceedings of International symposium on advanced experimental unsaturated soil mechanics, Trento, Italy*, 1, 61–68.

Hoffmann, C. and Tarantino, A. (2008). "Loading-collapse tests for investigating compressibility and potential collapsibility of embankment coarse well graded material." *Unsaturated Soils: Advances in Geo-Engineering*, D. G. Toll, C. E. Augarde, D. Gallipoli, and S. J. Wheeler, eds., Durham, UK. 967–972.

Holtz, W. G. and Hilf, J. W. (1961). "Settlement of soil foundations due to saturation." *Proceedings of the 5th International Conference on Soil Mechanics and Foundation Engineering*, Vol. 1. 673–679.

Horn, R. (2003). "Stress - strain effects in structured unsaturated soils on coupled mechanical and hydraulic processes." *Geoderma*, 116, 77–78.

Horn, R. and Dexter, A. (1989). "Dynamics of soil aggregation in an irrigated desert loess." *Soil and Tillage Research*, 13, 253–266.

Houlsby, G. T. (1979). "The work input to a granular material." *Géotechnique*, 29(3), 354–358.

Houlsby, G. T. (1997). "The work input to an unsaturated granular material." *Géotechnique*, 47(1), 193–196.

Houston, S. L., Houston, W. N., Zapata, C. E., and Lawrence, C. (2001). "Geotechnical engineering practice for collapsible soils." *Geotech Geol Eng*, 19, 333–355.

Huang, S. Y. (1994). "Evaluation and laboratory measurement of the coefficient of permeability in deformable, unsaturated soils," PhD thesis, Department of Civil Engineering, University of Saskatchewan, Saskatoon.

Huang, S. Y., Barbour, S. L., and Fredlund, D. G. (1998). "Development and verification of a coefficient of permeability function for a deformable, unsaturated soil." *Can Geotech J*, 35, 411–425.

Hvorslev, M. J. (1937). "Uber die festigkeitseigenschaften gestorter bindiger boden. danmarks naturvidenskabelige samfund." *Ingeniorvidenskabelige Skrifter*, A(5).

Jacobsen, H. (1992). "Bestemmelse af forbelastningstryk i laboratoriet.." *11. Nordiske Geoteck-nikermøde NGM-92, Aalborg*, 2, 455–460.

Janbu, N. (1969). "The resistance concept applied to deformation of soils." *Proc of the 7th Int Soil Mech and Found Eng Conf, Mexico City, Mexico*, 1, 191–196.

Jardine, R. J. (1985). "Investigation of pile-soil behaviour with special reference to the foundations of offshore structures," PhD thesis, Immperial College, University of London.

Jennings, J. E. and Burland, J. B. (1962). "Limitations to the use of effective stresses in partly saturated soils." *Géotechnique*, 12(2), 125–144.

Jennings, J. E. B. and Knight, K. (1957). "The additional settlement of foundations due to collapse of structure of sandy subsoil on wetting." *Proceedings of the Fourth International Conference on Soil Mechanics and Foundation Engineering*, Vol. 1. 316–319.

Jommi, C. and Della Vecchia, G. (2010). *Mechanics of Unsaturated Geomaterials*, chapter Chapter 15, Geomechanical analysis of river embankments. ISTE - John Wiley & Sons.

Jommi, C. and Sciotti, A. (2003). "A study of the microstructure to assess the reliability of laboratory compacted soils as reference material for earth constructions." *System-based vision for strategic and creative design*, F. Botempi, ed., Vol. 3. A.A. Balkema, Lisse, 2409–2415.

Josa, A., Alonso, E. E., Lloret, A., and Gens, A. (1987). "Stress-strain behavoiur of partially saturated soils." *Proc 9th European Conf Soil Mech Found Engng, Dublin*, 2, 561–564.

Josa, A., Balmaceda, A., Gens, A., and Alonso, E. E. (1992). "An elasto-plastic model for partially saturated soil exhibiting a maximum of collapse." *Proc 3rd Int Conf on Computational Plasticity, Barcelona*, 1, 815–826.

Jotisankasa, A. (2005). "Collapse behaviour of a compacted silty clay," PhD thesis, Univeristy of London (Imperial College).

Jotisankasa, A., Coop, M., and Ridley, A. (2007). "The development of a suction control system for a triaxial apparatus." *Geotechnical Testing Journal*, 30(1), 1–7.

Jotisankasa, A., Coop, M., and Ridley, A. (2009). "The mechanical behaviour of an unsaturated compacted silty clay." *Géotechnique*, 59(5), 415–428.

JP (2009). "Bojonegoro levee section collapses, affected residents flee." *The Jakarta Post*, The Jakarta Post, Saturday 28th February 2009, 9:31am, http://www.thejakartapost.com/news/2009/02/28/bojonegoro–levee–section–collapses–affected–residents–flee.html.

Juang, C. H. and Holtz, R. D. (1986a). "Fabric, pore size distribution and permeability of sandy soils." *J Geotech Eng ASCE*, 112, No. 9, 855–868.

Juang, C. H. and Holtz, R. D. (1986b). "A probabilistic permeability model and the pore size density function." *Int J Numer Anal Meth Geomech*, 10, 543–553.

Karstunen, M. and Pande, G. N. (1994). "On the mechanical response of gassy clays: some theoretical considerations." *Numerical Methods in Geotechnical Engineering, Manchester*, 75–80.

Karube, D. and Kawai, K. (2001). "The role of pore water in the mechanical behavior of unsaturated soils." *Geotech Geol Eng*, 19, 211–241.

Kassif, G. and Ben Shalom, A. (1971). "Experimental relationship between swell pressure and suction." *Géotechnique*, 21(3), 245–255.

Khalili, N. and Khabbaz, M. H. (1998). "A unique relationship for the determination of the shear strength of unsaturated soils." *Géotechnique*, 48(5), 681–687.

Kim, J., Jeong, S., Park, S., and Sharma, J. (2004). "Influence of rainfall induced wetting on the stability of slopes in weathered soils." *Eng Geol*, 75, 251–262.

Koliji, A. (2008). "Mechanical behaviour of unsaturated aggregated soils," PhD thesis, École Polytechnique Fédérale de Lausanne, Switzerland.

Koliji, A., Laloui, L., and Vulliet, L. (2009). "Behaviour of unsaturated aggregated soil in oedometric condition." *Soils and Foundations*, 49(3), 369–380.

Krahn, J. and Fredlund, D. G. (1972). "On total, matric and osmotic suction." *J Soil Sci*, 114(5), 339–348.

Krahn, J., Fredlund, D. G., and Klassen, M. J. (1989). "Effect of soil suction on slope stability at notch hill." *Can Geotech J*, 26, 269–278.

Kruse, G. A. M. (1998). *Dikes and Revetments: Design, Maintenance and Safety Assessment*, chapter 6, Impact of weathering on erosion resistance of cohesive soil, 113–124. Taylor & Francis.

Lambe, T. W. (1958a). "The engineering behavior of compacted clay." *J Soil Mech Found Div ASCE*, 1655(SM2), 1–35.

Lambe, T. W. (1958b). "The structure of compacted clay." *J Soil Mech Found Div ASCE*, 1654(SM2), 1–34.

Lawrence, G. P. (1978). "Stability of soil pores during mercury intrusion porosimetry." *J Soil Sci*, 29, 299–304.

Lawton, E. C. (1986). "Wetting-induced collapse in compacted soil," PhD thesis, Washington State University.

Lawton, E. C., Fragaszy, R. J., and Hardcastle, J. H. (1989). "Collapse of compacted clayey soils." *J Geotech Eng ASCE*, 115, 1252–1267.

Lawton, E. C., Fragaszy, R. J., and Hetherington, M. D. (1992). "Review of wetting induced collapse in compacted soil." *J Geotech Eng ASCE*, 118, 1376–1394.

Lee, P. Y. (1976). "Study of irregular compaction curves." *Soil Specimen Preparation for Laboratory Testing*, ASTM STP 599, 278–288.

Lee, P. Y. and Suedkamp, R. J. (1972). "Characteristics of irregularly shaped compaction curves." *Highway Research Record*, 381, 1–9.

Leonards, G. A. and Narain, J. (1963). "Flexibility of clay and cracking of earth dams." *J Soil Mech Found Div ASCE*, 89(2), 47–98.

Leong, E. C., Tripathy, S., and Rahardjo, H. (2003). "Total suction measurement of unsaturated soils with a device using the chilled-mirror dew-point technique." *Géotechnique*, 53(2), 173–182.

Leong, E. C., Widiastuti, S., Lee, C. C., and Rahardjo, H. (2007). "Accuracy of suction measurement. technical note." *Géotechnique*, 57 (6), 547–556.

Leroueil, S., Magnan, J.-P., and Tavenas, F. (1990). *Embankments on soft clay.* Ellis Horwood, London.

Leroueil, S., Tavenas, F., and Le Bihan, J. P. (1983). "Propriétés caractéristiques des argiles de l'est du canada." *Can Geotech J*, 20(4), 681–705.

Leroueil, S. and Vaughan, P. R. (1990). "The general and congruent effects of structure in natural soils and weak rocks." *Géotechnique*, 40(3), 467–488.

Lim, P. C. (1995). "Characterization and prediction for the coefficients of diffusion and adsorption for inorganic chemicals in unsaturated soils," PhD thesis, Department of Civil Engineering, University of Saskatchewan, Saskatoon.

Lim, P. C., Barbour, S. L., and Fredlund, D. G. (1998). "The influence of the degree of saturation on the coefficient of aqueous diffusion.." *Can Geotech J*, 35, 811–827.

Lindenberg, J. and de Groot, M. (1998). *Dikes and Revetments: Design, Maintenance and Safety Assessment*, chapter 4, Geotechnical Boundary Conditions and Soil Investigation, 75–100. Taylor & Francis.

Linford, T., Jones, Y., Barrett, J., and Agency, B. G. E. (2002). "National flood and coastal defence database." *37th DEFRA Flood and Coastal Management Conference, Keele, September 2002.*, 1–5.

Lloret, A. and Alonso, E. E. (1985). "State surfaces for partially saturated soils." *Proc 11th Int Conf Soil Mech Found Eng, San Fransisco*, 2, 557–562.

Lloret, A., Villar, M. V., Sánchez, M., Gens, A., Pintado, X., and Alonso, E. E. (2003). "Mechanical behaviour of heavily compacted bentonite under high suction changes." *Géotechnique*, 53(1), 27–40.

Loret, B. and Khalili, N. (2002). "An effective stress elasticplastic model for unsaturated porous media." *Mechanics of Materials*, 34, 97–116.

Lourenço, S. (2008). "Suction measurements and water retention in unsaturated soils," PhD thesis, Durham University.

Macari, E. J., Parker, J. K., and Costes, N. C. (1997). "Measurement of volume changes in triaxial tests using digital imaging techniques." *Geotechnical Testing Journal*, 20(1), 103–109.

Marinho, F. A. M., Take, W. A., and Tarantino, A. (2008). "Measurement of matric suction using tensiometric and axis translation technique." *Geotech Geol Eng*, 26(6), 615–631.

Marsland, A. (1957). "The design and construction of earthen flood banks." *Journal of Institution of Water Engineers*, 11 (3), 236–258.

Marsland, A. (1961). "A study of a breach in an earthen embankment caused by uplift pressures." *Proc 5th Int Conf Soil Mech Found Engng, Paris*, 2, 663–668.

Marsland, A. (1968). "The shrinkage and fissuring of clay in flood banks. internal report no. 39/68." *Report no.*, Building Research Station.

Marsland, A. and Cooling, L. (1958). "Tests on full scale clay flood bank to study seepage and the effects of overtopping. internal report no. c562." *Report no.*, Building Research Station.

Marsland, A. and Randolph, M. (1978). "A study of the variations and effects of pore water pressures in the pervious strata at crayford marshes." *Géotechnique*, 28 (4), 435–464.

Masrouri, F., Bicalho, K. V., and Kawai, K. (2008). "Laboratory hydraulic testing in unsaturated soils." *Geotech Geol Eng*, 26(6), 691–704.

Maâtouk, A., Leroueil, S., and La Rochelle, P. (1995). "Yielding and critical state of a collapsible unsaturated silty soil." *Géotechnique*, 45(3), 465–477.

Matyas, E. L. and Radhakrishna, H. S. (1968). "Volume change characteristics of partially saturated soils." *Géotechnique*, 18, 432–448.

Mesri, G., Rokhsar, A., and Bohor, B. F. (1975). "Composition and compressibility of typical samples of mexico city clay." *Géotechnique*, 25(3), 527–554.

MGS, M. G. S. (2004). "Gabion walls design guide. revision 11/04. Design Guide.

Miller, S. P. (1990). "Embankment overtopping." *Notes for design and safety surveillance of embankment dams*, U.S. Army Enginner Waterways Experiment Station, Vicksburg, MS.

Miranda, A. N. (1988). "Behavior of small earth dams during initial filling," PhD thesis, Colorado State Univeristy, Colorado, USA.

Mitchell, J. K. (1993). *Fundamentals of soil behavior*. John Wiley and Sons.

Mitchell, J. K. and Soga, K. (2005). *Fundamentals of soil behavior*. Wiley, 3rd edition edition.

Möller, J., Weißmann, R., Schüttrummpf, H., Grüne, J., Oumeraci, H., Richwien, W., and Kudella, M. (2002). "Interaction of wave overtopping and clay properties for seadikes." *Proceedings of the 28th International Conference on Coastal Engineering*, Vol. 2, ASCE, Cardiff, U.K. 2105–2115.

Moisture, S. (2008). *Porous ceramics catalog*. Soil Moisture Equipment Corporation.

Monroy, R. (2006). "The influence of load and suction changes on the volumetric behaviour of compacted london clay," PhD thesis, University of London (Imperial College).

Monroy, R., Ridley, A., Dineen, K., and Zdrakovic, L. (2007). "The suitability of osmotic technique for the long term testing of partly saturated soils." *Geotech Testing J*, 47(4), 220–226.

Morgenstern, N. R. and Price, V. E. (1965). "The analysis of the stability of general slip surfaces." *Géotechnique*, 15(1), 79–93.

Morris, M., Dyer, M., and Smith, P. (2007). "Management of flood embankments, a good practice review." *R&D Technical Report FD2411/TR1*, Defra.

Mualem, Y. (1986). *Methods of soil analysis*, chapter Hydraulic conductivity of unsaturated soils: prediction and formulas, 799–823. American Society of Agronomy, Madison, Wisconsin.

Nam, S., Gutierrez, M., Diplas, P., Petrie, J., Wayllace, A., Lu, N., and Muñoz, J. J. (2009). "Comparison of testing tech-niques and models for establishing the swcc of riverbank soils." *Eng Geol*, 110, 1–10.

Navaneethan, T., Sivakumar, V., Wheeler, S. J., and Doran, I. G. (2005). "Assessment of suction measurements in saturated clays." *Proc Inst Civ Eng Geotech Eng*, 158, 15–24.

Nawari, O. and Schetelig, K. (1991). "Geotechnical study on kordofan tropical black soils (sudan republic)." *Eng Geol*, 31, 1–26.

Ng, C. W. W. and Chiu, A. C. F. (2001). "Behavior of a loosely compacted unsaturated volcanic soil." *J Geotech Geoenviron Eng ASCE*, 127(12), 1027–1036.

Ng, C. W. W. and Chiu, A. C. F. (2003). "Laboratory study of loose saturated and unsaturated decomposed granitic soil." *J Geotech Geoenviron Eng ASCE*, 129(6), 550–559.

Ng, C. W. W., Zhan, L. T., and Cui, Y. J. (2002). "A new simple system for measuring volume changes in unsaturated soils." *Can Geotech J*, 39(2), 757–764.

Nitao, J. J. and Bear, J. (1996). "Potentials and their role in transport in porous media." *Water Resour Res*, 32, 225–250.

Nova, R., Castellanza, R., and Tamagini, C. (2003). "A constitutive model for bonded geomaterials subject to mechanical and/or chemical degradation." *Int J Numer Anal Method Geomech*, 27(9), 705–732.

Nuth, M. and Laloui, L. (2008a). "Advances in modelling hysteretic water retention curve in deformable soils." *Computers and Geotechnics*, 35, 835–844.

Nuth, M. and Laloui, L. (2008b). "Effective stress concept in unsaturated soils: Clarification and validation of a unified framework." *Int. J. Numer. Anal. Meth. Geomech*, 32, 771–801.

Olson, R. E. (1963). "Effective stress theory of soil compaction." *J Soil Mech Found Div ASCE*, Vol. 89, No. SM2, 27–45.

Onitsuka, K., Hong, Z., Hara, Y., and Yoshitake, S. (1995). "Interpretation of oedometer test data for natural clays." *Soils and Foundations*, 35, 61–70.

Pacheco Silva, F. (1970). "A new graphical construction for determination of the preconsolidation stress of a soil sample." *Proc of the 4th Brazilian Conf on Soil Mechanics and Found Eng, Rio de Janeiro, Brazil*, 2(1), 225–232.

Padfield, C. and Schofield, A. (1983). "Development of centrifugal models to study the influence of uplift pressures on stability of a flood bank." *Géotechnique*, 33 (4), 57–66.

Pereira, J. H. F. and Fredlund, D. G. (2000). "Volume change behaviour of collapsible compacted gneiss soil." *J Geotech Geoenviron Eng ASCE*, 126, 907–916.

Pereira, J. H. F., Fredlund, D. G., Cordão Neto, M. P., and Gitirana Jr., G. G. . (2005). "Hydraulic behaviour of collapsible compacted gneiss soil." *J Geotech Geoenviron Eng ASCE*, 131, 1264–1273.

Perry, E. B. (1998). "Innovative methods for levee rehabilitation." *Technical report REMR-GT-26*, prepared for U.S. Army Corps of Engineers.

Peterson, R. and Iverson, N. L. (1953). "Study of several low earth dam failures." *Proc 3rd Int Conf Soil Mech Found Eng, Zurich*, 2, 273–276.

Pilarczyk, K. W. (1998). *Dikes and Revetments: Design, Maintenance and Safety Assessment*, chapter 1, Introduction. Taylor & Francis.

Pintado, X., Lloret, A., and Romero, E. (2009). "Assessment of the use of the vapour equilibrium technique in controlled-suction tests." *Can Geotech J*, 46, 411–423.

Pinyol, N. M., Alonso, E. E., and Olivella, S. (2008). "Rapid drawdown in slopes and embankments." *Water Resour Res*, 44, 1–5.

Poppe, L. J., Paskevich, V. F., and Hathaway, J. C. (2001). "A laboratory manual for x-ray powder diffraction." *Report no.*, US Geological Survey Open-File Report 01-041.

Prapaharan, S., White, D. M., and Altschaef, A. G. (1991). "Fabric of field- and laboratory-compacted clay." *J Geotech Eng ASCE*, 117(12), 1934–1940.

Péron, H., Hueckel, T., and Laloui, L. (2007). "An improved volume measurement for determining soil water retention curves." *Geotechnical Testing Journal, ASTM*, 30(1), 1–8.

Rahardjo, H., Lim, T. T., Chang, M. F., and Fredlund, D. G. (1995). "Shear strength characteristic of residual soils." *Can Geotech J*, 32, 60–77.

Rampino, C., Mancuso, C., and Vinale, F. (1999). "Laboratory testing on an unsaturated soil : equipment, procedures, and first experimental results.." *Can Geotech J*, 36(1), 1–12.

Rao, S. M. and Revanasiddappa, K. (2006). "The influence of cyclic wetting drying on collapse behaviour of compacted residual soil." *Geotech Geol Eng*, 24, 725–734.

Raveendiraraj, A. (2009). "Coupling of mechanical behaviour and water retention behvaiour in unsaturated soils," PhD thesis, University of Glasgow, UK.

Reed, M. A., Lovell, C. W., Altschaeffl, A. G., and Wood, L. E. (1980). "Reply: Frost heaving rate predicted from pore size distribution." *Can Geotech J*, 17, 639–640.

Richards, L. A. and Ogata, G. (1958). "A thermocouple for vapour pressure measurement in biological and soil systems at high humidity." *Science*, 128, 1089–1090.

Ridley, A. M. and Burland, J. B. (1993). "A new instrument for the measurement of soil moisture suction." *Géotechnique*, 43(2), 321–324.

Ridley, A. M. and Burland, J. B. (1999). "Use of the tensile strength of water for the direct measurement of high soil suction. discussion." *Can Geotech J*, 34, 604–614.

Ridley, A. M., Dineen, K., Burland, J., and Vaughan, P. (2003). "Soil matrix suction: some examples of its measurement and application in geotechnical engineering." *Géotechnique*, 53 (2), 241–253.

Ridley, A. M. and Wray, W. K. (1996). "Suction measurement: A review of current theory and practices.." *Proc. 1st Int. Conf on Unsaturated Soils, Paris, France*, 3, 1293–1322, Balkema, Rotterdam.

Romero, E. (1999). "Characterisation and thermo-hydro-mechanical behaviour of unsaturated boom-clay: An experimental study," PhD thesis, Universitat Politècnica de Catalunya, Barcelona, Spain.

Romero, E., Facio, J. J. A., Lloret, A., Gens, A., and Alonso, E. E. (1997). "A new suction and temperature controlled triaxial apparatus." *Proc 14th Int Conf Soil Mech Found Eng, Hamburg, Germany*, 1, 185–188.

Romero, E., Gens, A., and Lloret, A. (2003). "Suction effects on a compacted clay under non-isothermal conditions." *Géotechnique*, 53(1), 65–81.

Romero, E. and Jommi, C. (2008). "An insight into the role of hydraulic history on the volume changes of anisotropic clayey soils." *Water Resour. Res*, 44, W12412.

Romero, E. and Simms, P. (2008). "Microstructure investigation in unsaturated soils: A review with special attention to contribution of mercury intrusion porosimetry and environmental scanning electron microscopy." *Geotech Geol Eng*, 26, 705–727.

Romero, E. and Vaunat, J. (2000). "Retention curves of deformable clays." *Experimental evidence and theoretical approaches in unsaturated soils*, A. Tarantino and C. Mancuso, eds. Rotterdam, Balkema, 91–106.

Roscoe, K. H. and Burland, J. B. (1968). *On the generalized stress-strain behaviour of wet clay*, 535–609. Cambridge University Press.

Roscoe, K. H., Schofield, A. N., and Wroth, C. R. (1958). "On yielding of soils." *Géotechnique*, 8, (1) 22–53.

Saiyouri, N., Hicher, P., Y., and Tessier, D. (2000). "Microstructural approach and transfer water modelling in highly compacted unsaturated swelling clays." *Mechanics of cohesive-frictional materials*, 5, 41–60.

Seed, R. B., Bea, R. G., Abdelmalak, R. I., Athanasopoulos-Zekkos, A., Boutwell, G. P., Briaud, J.-L., Cheung, C., Cobos-Roa, D., Ehrensing, L., Govindasamy, A., Harder Jr., L., Inkabi, K. S., Nicks, J., Pestana, J. M., Porter, J., Rhee, K., Riemer, M. F., Rodgers, J. D., Storesund, R., Vera-Grunauer, X., and Wartman, J. (2008). "New orleans and hurricane katrina. i: Introduction, overview, and the east flank." *J Geotech Geoenviron Eng ASCE*, 134, 701–717.

Sentenac, P. and Zielinski, M. (2009). "Clay fine fissuring monitoring using miniature geo-electrical resistivity arrays." *Environ Geol*, published online, 1–10.

Sharma, R. S. (1998). "Mechanical behaviour of unsaturated highly expansive clays," PhD thesis, University of Oxford, UK.

Sheng, D., Sloan, S. W., and A., G. (2004). "A constitutive model for unsaturated soils: thermomechanical and computational aspects." *Computational Mechanics*, 33, 453–465.

Sillers, W. S., Fredlund, D. G., and Zakerzadeh, N. (2001). "Mathematical attributes of some soil-water characteristic curve models." *Geotech Geol Eng*, 19, 243–283.

Simms, P. H. and Yanful, E. K. (2002). "Predicting soil-water characteristic curves of compacted plastic soils from measured pore-size distributions." *Géotechnique*, 52(4), 269–278.

Simms, P. H. and Yanful, E. K. (2005). "A pore-network model for hydromechanical coupling in unsaturated compacted clayey soils." *Can Geotech J*, 42, 499–514.

Simon, A., Langendoen, E. J., Collison, A., and Layzell, A. (2003). "Incorporating bank-toe erosion by hydraulic shear into a bank-stability model: Missouri river, eastern montana." *Proceedings, EWRI-ASCE. World Water & Environmental Resources Congress*. 11p.

Simon, A., Thomas, R. E., Curini, A., and Shields Jr, F. D. (2002). "Case study: Channel stability of the missouri river, eastern montana." *J Hydraul Eng ASCE*, 28(10), 880–890.

Sivakumar, V. (1993). "A critical state framework for unsaturated soil," PhD thesis, University of Sheffield, UK.

Sivakumar, V., Sivakumar, R., Murray, E. J., P., M., and Boyd, J. (2010). "Mechanical behaviour of unsaturated kaolin (with isotropic and anisotropic stress history). part 1: wetting and compression behaviour." *Géotechnique*, 60(8), 581–594.

Skempton, A. (1960). "Effective stress in soils, concrete and rock." *Pore Pressures and Suction in Soils*.

Skempton, A. W. (1944). "Notes on the compressibility of clays." *Quarterly Journal of the Geological Society of London*, 100, 11–135.

Skempton, A. W. (1953). "The colloidal activity of clays." *Proc 3rd Int Conf Soil Mech Found Eng, Zurich*, Vol. 1, 57–61.

Skempton, A. W. (1954). "The pore water coefficients a and b." *Géotechnique*, 4, 143–147.

Skempton, A. W. and Jones, O. T. (1944). "Notes on the compressibility of clays." *Quarterly Journal of the Geological Society of London*, 100, 11–135.

Smith, P. R., Jardine, R. J., and Hight, D. W. (1992). "The yielding of bothkennar clay." *Géotechnique*, 42(2), 257–274.

Sánchez, M. and Gens, A. a. (2005). "A double structure generalized plasticity model for expansive materials." *Int J Numer Anal Meth Geomech*, 29, 751–787.

Sánchez, M., Villar, M., Gens, A., Olivella, S., and L., G. (2007). "Modelling the effect of temperature on unsaturated swelling clays." *Numerical Models in Geomechanics NUMOG X*, 1, 57–62.

Soemitro, R. A. A. (2005). "Performance and reliability evaluation research, case study : River solo (indonesian)." *Report no.*, Report to East Java, Ministry of Public Works, Institut Teknologi Sepuluh Nopember.

Stroud, M. A. and Butler, F. G. (1975). "The standard penetration test and the engineering properties of glacial materials." *Proc. Symp. Engng. Behaviour of Glacial Materials, Birmingham*, 124–135.

Sudarsono (2009). "The bengawan solo water council - providing insight and directions." *Report no.*, CRBOM Small Publications Series No. 5, Centre for River Basin Organizations and Management, Solo, Central Java, Indonesia, Available at: http://crbom.org/SPS/Docs/SPS05-TKPSDA-0.pdf.

Susandi, A. (2007). "Perubahan iklim indonesia dan implikasinya, program studi meteorologi." *Report no.*, ITB, Bandung.

Takeuchi, K., Jayawardena, A. W., and Takahasi, Y. (1995). "Catalogue of rivers for southeast asia and the pacific - volume 1." *Report no.*, UNESCO-IHP Regional Steering Committee for Southeast Asia and the Pacific.

Tang, A. M. and Cui, Y. J. (2005). "Controlling suction by the vapour equilibrium technique at different temperatures and its application in determining the water retention properties of mx80 clay." *Can Geotech J*, 42, 287–296.

Tarantino, A. (2004). "Panel lecture: Direct measurement of soil water tension." *Proc 3rd Int Conf on Unsaturated Soils, Recife, Brazil*, 3, 1005–1017.

Tarantino, A. (2009). "A water retention model for deformable soils." *Géotechnique*, 59(9), 751–762.

Tarantino, A. (2010a). *Mechanics of Unsaturated Geomaterials*, chapter Chapter1: Basic concepts in the mechanics and hudraulics of unsaturated geomaterials. ISTE - John Wiley & Sons.

Tarantino, A. (2010b). "Unsaturated soils: compacted versus reconstituted states." *Proceedings of the fifth international conference on unsaturated soils, Barcelona, Spain*, 1, 113–136.

Tarantino, A. and De Col, E. (2008). "Compaction behaviour of clay." *Géotechnique*, 58(3), 199–213.

Tarantino, A. and De Col, E. (2009). "Discussion: Compaction behaviour of clay." *Géotechnique*, 59(1), 75–77.

Tarantino, A., Gallipoli, D., Augarde, C., De Gennaro, V., El Mountassir, G., Gomez, R., Laloui, L., Mancuso, C., Munoz, J., Pereira, J.-M., Peron, H., Pisoni, G., Romero, E., Raveendiraraj, A., Rojas, J. C., Toll, D., Tombolato, S., and Wheeler, S. (2011). "Benchmark of experimental techniques for measuring and controlling suction, in: Partial saturation in compacted soils." *Géotechnique*, (submitted).

Tarantino, A. and Mongovì, L. (2001). "Experimental procedures and cavitation mechanisms in tensiometer measurements." *Geotech Geol Eng*, 19, 189–210.

Tarantino, A. and Mongovì, L. (2003). "Calibration of tensiometer for direct measurement of matric suction." *Géotechnique*, 53 (1), 137–141.

Tarantino, A., Romero, E., and Cui, Y.-J. (2008). "Special issue on laboratory and field testing of unsaturated soils." *Geotech Geol Eng*, 26(6), 613–826.

Tarantino, A. and Tombolato, S. (2005). "Coupling of hydraulic and mechanical behaviour in unsaturated compacted clay." *Géotechnique*, 55(4), 307–317.

Terzaghi, K. (1936). "The shearing resistance of saturated soils and the angle between the planes of shear." *Proc 1st Int Conf Soil Mech Found Eng, Cambridge, Mass., USA*, 1, 54–56.

Terzaghi, K., Peck, R. B., and Mesri, G. (1996). *Soil mechanics in engineering practice*. Wiley, 3rd edition.

Thom, R., Sivakumar, R., Sivakumar, V., Murray, E. J., and Mackinnon, P. (2007). "Pore size distribution of unsaturated compacted kaolin: the initial states and final states following saturation." *Géotechnique*, 57(5), 469–474.

Toll, D. G. (1990). "A framework for unsaturated soil behaviour." *Géotechnique*, 49(1), 31–44.

Toll, D. G. (2000). "The influence of fabric on the shear behaviour of unsaturated compacted soils." *Advances in Unsaturated Geotechnics*, C. D. Shackleford, S. L. Houston, and N.-Y. Chang, eds., Geotechnical Special Publication No. 99. ASCE, 222–234.

Toll, D. G. and Ong, B. H. (2003). "Critical-state parameters for an unsaturated residual sandy clay." *Géotechnique*, 53(1), 93–103.

Tuller, M. and Or, D. (2005). "Water films and scaling of soil characteristic curves at low water contents." *Water Resour Res*, 41, W09403, doi:10.1029/2005WR004142.

Tuller, M., Or, D., and Dudley, L. M. (1999). "Adsorption and capillary condensation in porous media: Liquid retention and interfacial configurations in angular pores." *Water Resour Res*, 35(7), 1949–1964.

UN (2004). "Indonesia factfile." *United Nations Public Administration Network*.

Van, M., Koelewijn, A., and Barends, F. (2005). "Uplift phenomenon: Model, validation, and design." *Int J Geomech ASCE*, 5 (2), 98–106.

van Baars, S. (2005). "The horizontal failure mechanism of the wilnis peat dyke." *Géotechnique*, 55(4), 319–323.

van Genuchten, M. T. (1980). "A closed-form equation for predicting the hydraulic conductitivty of unsaturated soil." *Soil Sci Soc Am J*, 44, 892–898.

Vanapalli, S. K. (1994). "Simple test procedures and their interpretation in evaluating the shear strength of unsaturated soils," PhD thesis, Department of Civil Engineering, University of Saskatchewan, Saskatoon, Sask.

Vanapalli, S. K., Fredlund, D. G., and Pufahl, D. E. (1999). "The influence of soil structure and stress history on the soil-water characteristics of a compacted till." *Géotechnique*, 49(2), 143–159.

Vanapalli, S. K., Fredlund, D. G., Pufahl, D. E., and Clifton, A. W. (1996). "Model for the prediction of shear strength with respect to soil suction." *Can Geotech J*, 33, 379–392.

Vanapalli, S. K., Nicotera, M. V., and Sharma, R. S. (2008). "Axis-translation and negative water column techniques for suction control." *Geotech Geol Eng*, 26(6), 645–660.

Vaunat, J., Romero, E., and Jommi, C. (2000). "An elastoplastic hydro-mechanical model for unsaturated soils." *Proc. International Workshop on Unsaturated Soils: Experimental evidence and theoretical approaches*, 1, 121–138.

Vaunat, J., Romero, E., Marchi, C., and Jommi, C. (2002). "Modelling the shear strength of unsaturated soils." *Proc. 3rd Int. Conf. on Unsaturated Soils, Recife, Brazil*, 1, 245–251.

Vicol, T. (1990). "Comportement hydraulique et mécanique d'un sol fin non saturé. application a la modélisation," PhD thesis, CERMES, Ecole Polytechnique, Ecole National des Ponts et Chaussées, Paris, France.

Villar, M. V. and Lloret, A. (2001). "Variation of the intrinsic permeability of expansive clays upon saturation." *Clay Science for Engineering*, K. A. M. Fukue, ed. A.A. Balkema, Rotterdam, 259–266.

Ward, W. H. (1948). "A slip in a flood defence bank constructed on a peat bog." *Proc. 2nd Int. Conf. Soil Mech. Found. Engng.*, Vol. 2, Rotterdam, The Netherlands. 19–23.

Ward, W. H., Penman, A., and Gibson, R. E. (1955). "Stability of a bank on a thin peat layer." *Géotechnique*, 5(2), 154–163.

Warnana, D. D. (2008). "Identifikasi scouring sebagai potensi kelongsoran tanggul sungai bengawan solo berdasarkan survei gpr (studi kasus desa widang, kabupaten 'fuban) [in indoneisan]." *Journal Fisikadan Aplikasinya*, 4, 080207–1 – 080207–6.

Washburn, E. W. (1921). "Note on a method of determining the distribution of pore sizes in a porous material." *Proceedings of the National Academy of Sciences*, 7, 115–116.

Wesley, L. D. (1974). "Discussion: Structural behaviour of residual soils of the continually wet highlands of papua new guinea." *Géotechnique*, 24(1), 101–106.

Wheeler, S. (1988a). "The undrained shear strength of soils containing large gas bubbles." *Géotechnique*, 38(3), 399–413.

Wheeler, S. J. (1986). "The stress-strain behaviour of soils containing gas bubbles," PhD thesis, Univeristy of Oxford.

Wheeler, S. J. (1988b). "A conceptual model for soils containing large gas bubbles." *Géotechnique*, 38(3), 389–397.

Wheeler, S. J., Gallipoli, D., and Karstunen, M. (2002). "Comments on use of the barcelona basic model for unsaturated soils." *Int J Numer Anal Meth Geomech*, 26, 1561–1571.

Wheeler, S. J. and Karube, D. (1996). "State of the art report: Constitutive modelling." *Proc 1st Int Conf Unsat Soils, Paris*, 3, 1323–1356.

Wheeler, S. J., Sharma, R. S., and Buisson, M. S. R. (2003). "Coupling of hydraulic hysteresis and stress-strain behaviour in unsaturated soils." *Géotechnique*, 53(1), 41–54.

Wheeler, S. J. and Sivakumar, V. (1995). "An elasto-plastic critical state framework for unsaturated soil." *Géotechnique*, 45(1), 35–53.

Yong, R. N., Japp, R. D., and How, G. (1971). "Shear strength of partially saturated clays." *Proc 4th Asian Reg Conf Soil Mech Found Eng, Bangkok*, 2(12), 183–187.

Zhang, G., Germaine, J. T., and Whittle, A. J. (2005). "Drying induced alteration to the microstructure of a tropical soil." *Proceedings of International Symposium on advanced experimental unsaturated soil mechanics*, A. Tarantino, E. Romero, and Y. J. Cui, eds., Trento, Italy. Taylor & Francis Group, London, 443–449.

Zur, B. (1966). "Osmotic control of the matric soil water potential." *Soil Sci*, 102, 394–398.

Appendix A

Equipment calibration

A.1 Conventional oedometer equipment

A.1.1 Calibration of conventional loading frames & cells

Following the procedure outlined in Head (1982) the conventional oedometer loading frames and cells were calibrated as a single unit for each set-up. The cells were assembled as for a standard test but with a stainless steel disc in the place of the soil specimen, loads were applied to the specimen and any deformation in the loading frame and cells recorded. Three loading and unloading cycles were applied up to a maximum of 1000kPa (as used in the oedometer tests) and the mean deformation loading curve for each set-up obtained. This is presented in Figure A.1. Incremental deformations of the loading frame were then subtracted from the settlement readings at the end of a loading step for tests on soil specimens.

A.1.2 Calibration of linear displacement transducers

The linear displacement transducers used in the conventional oedometer tests were calibrated prior to use, against a dial gauge using a strain controlled loading frame where the base platen was displaced at a constant rate of 0.165mm/s. As is evident in Figure A.2 the displacement

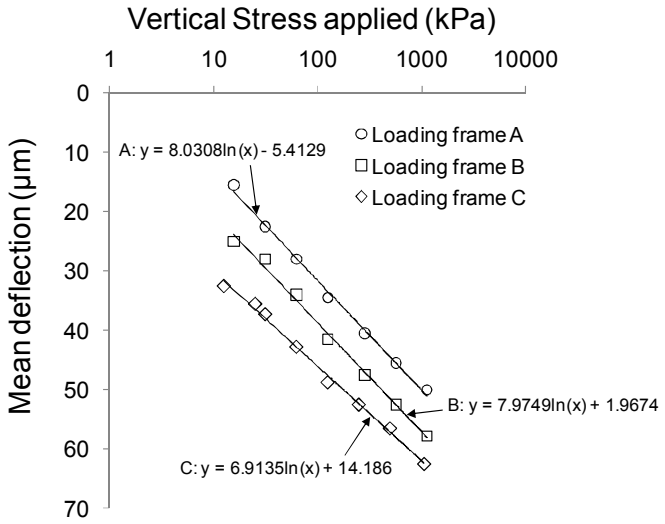

Figure A.1: Calibration of loading frames used in conventional oedometer tests

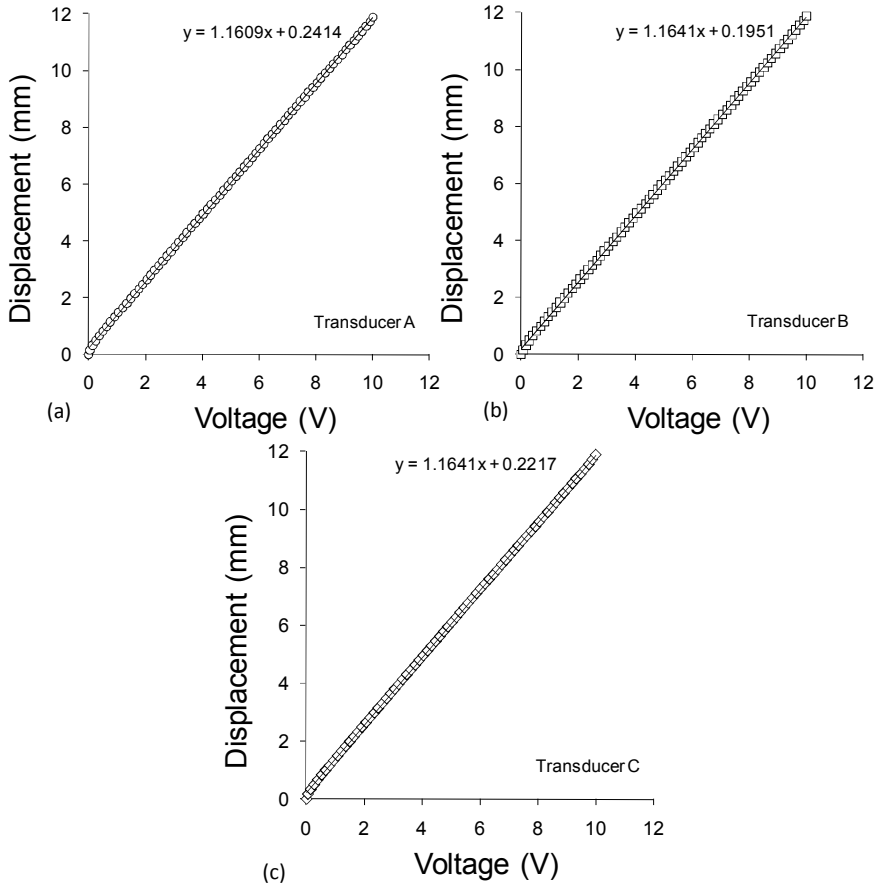

Figure A.2: Calibration of linear displacement transducers used in conventional oedometer tests

transducers do not respond in a very linearly manner at the extreme limits of use (as is typical of many transducers), the transducers were always positioned such that they were located well within their working range at the beginning of a test, and were capable of recording any potential swelling or compression behaviour. For each transducer used a linear calibration with an accuracy of $\pm$ 0.03mm was obtained within the range of 2 - 8 mm.

A.2 Isotropic compression equipment

A.2.1 Isotropic cell

In order to measure the change in volume of a specimen by measuring global volume changes occurring within the cell, changes in volume due to immediate expansion and creep had to be taken into account. Immediate volume changes due to expansion of the cell walls as cell pressure is applied was determined by following the procedure outlined by Head (1998) (Section 17.3.1). Immediate volume changes were recorded using a GDS pressure-volume controller up to the maximum cell pressure used in the isotropic tests. The immediate volume changes exhibited are presented in Figure A.3. During calibration and in all of the tests, filling of the cell was carried out very slowly to minimise the volume of air trapped within the cell. Membranes were folded over the o-rings at the top and bottom of soil specimens, to avoid air bubbles becoming trapped between the o-rings. Two separate linear calibrations were used to account for immediate cell volume changes, those occurring up to 140kPa and for cell pressures applied beyond 140kPa.

In the isotropic tests the effect of creep was deemed to be less important than immediate cell volume changes as the pressure was not held constant but rather increased continuously during loading and decreased continuously during unloading. However in order to ensure there were no discrepancies due to creep volume changes, the volume change due to expansion of the cell walls over time was investigated at several pressures: 500kPa, 1000kPa and 1500kPa covering the range of cell pressures to be tested in the isotropic cell. Figure A.8 presents the changes in cell volume over time for up to 4 days at a cell pressure of 1000kPa.

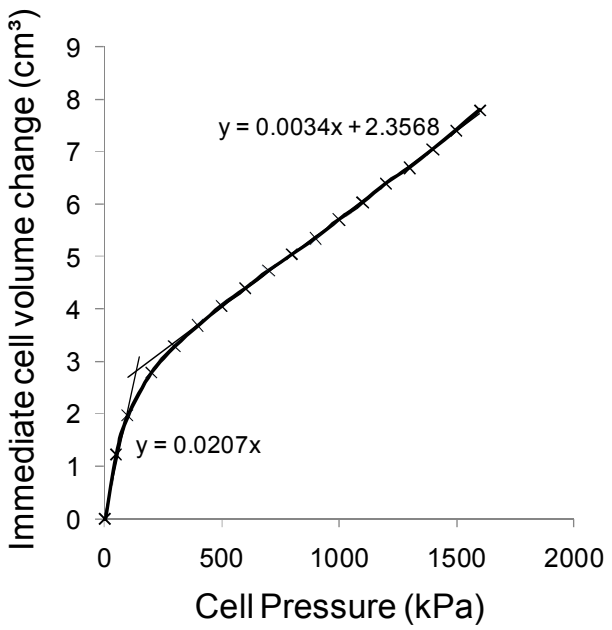

Figure A.3: Variation in immediate cell volume change in isotropic cell with cell pressure

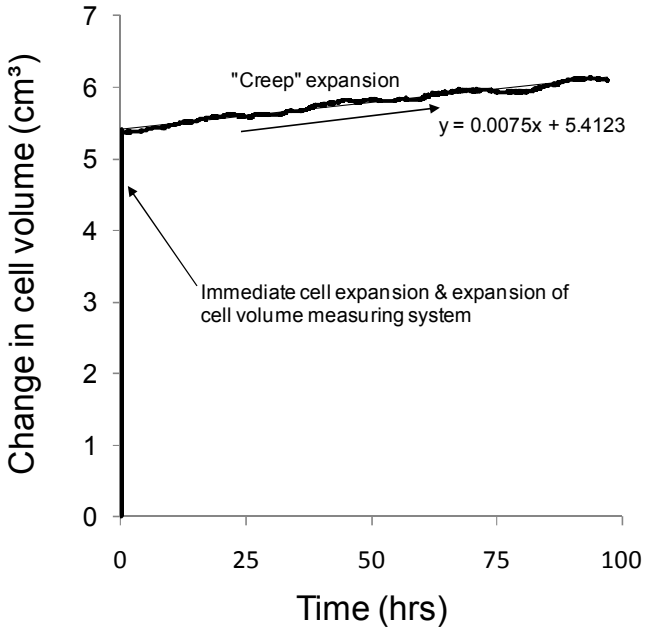

Figure A.4: Cell volume changes due to creep at a cell pressure of 1000kPa

A.2.2 GDS pressure-volume controllers

In the isotropic system an advanced GDS pressure - volume controller (ADVDPC) was used to control the cell pressure and monitor cell volume changes. A standard GDS pressure-volume controller (STDDPC) was used to control the pore water pressure and record the volume of water flowing into or draining out of the specimen. Details of the operating capacity, resolution and accuracy of these controllers is given in Table A.1. In all of the other test set-ups described in this thesis, only ADVDPC pressure-volume controllers have been used.

Table A.1: Comparison of GDS pressure - volume controllers GDS (2005a,b)

Controller	STDDPC	ADVDPC
Pressure range (MPa)	3	2
Volume capacity (cm^3)	200	200
Pressure resolution (kPa)	1	0.5
Volume resolution (mm^3)	1	0.5
Pressure measurement accuracy (kPa)	4.5	2
Volume measurement accuracy (% of measured value)	< 0.25	< 0.1
Volume measurement accuracy (backlash mm^3)	± 30	± 12

A.2.3 Instrumentation

Figure A.5 presents the calibration of the pore water pressure transducer used in the saturated isotropic compression tests. The pressure transducer was calibrated while mounted in the cell, against the ADVDPC pressure-volume controller, by applying increasing cell pressure to the cell. Prior to the start of any test, the pressure-volume controllers and pressure transducer if used, were all set to zero pressure at the same position, The bleed valve at the top of the cell was used as the zero datum point, due to ease of checking and resetting if necessary. A linear calibration was obtained with an accuracy of $\pm$ 1.2kPa.

The manual air pressure gauge used to regulate the pore air pressure applied in the suction controlled tests was calibrated against the ADVDPC pressure-volume controller via an air-water bladder interface. Figure A.6 presents the calibration of the manual air pressure gauge. During the isotropic tests presented herein the pressure was maintained constant and therefore the air pressure was maintained at a constant value during loading. This calibration was therefore only

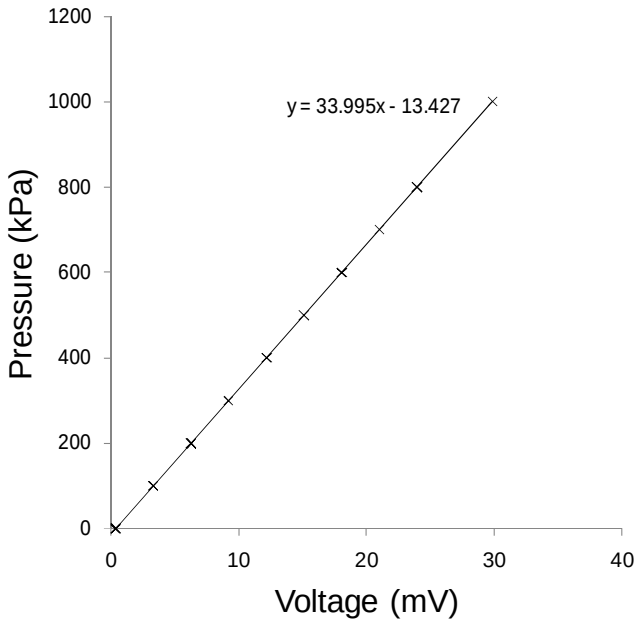

Figure A.5: Calibration of pore water pressure transducer used in the saturated isotropic tests

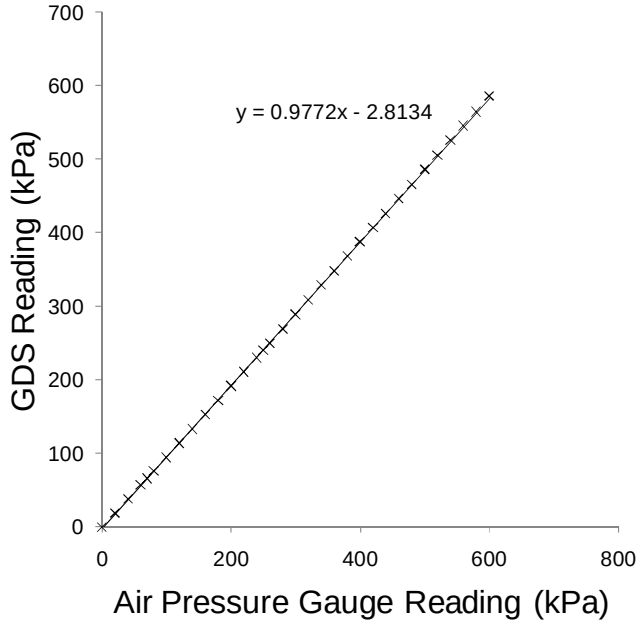

Figure A.6: Calibration of air pressure gauge used in isotropic set-up

used to determine the value at which the air pressure gauge should be positioned during the tests.

A.3 Triaxial testing equipment

A.3.1 Triaxial cell

As for the isotropic cell, the triaxial cell was calibrated for immediate cell volume changes related to cell pressure variation, (Figure A.7). Similar to the isotropic cell the immediate cell volume changes were accounted for by considering two linear correlations, one for pressure up to 70kPa and another for pressures above 70kPa. In the triaxial tests cell pressure was maintained constant during shearing. Thus it was important to determine the relevant changes in volume due to time dependent effects (creep) at different pressures (Figure A.8). The rate of change of volume with time did not appear to be highly dependent on pressure level and were within a range of 0.03cm^3/day to 0.05cm^3/day. Considering a test which runs for one month, creep alone could contribute to 1.5% volume change of a specimen of 38mm diameter. The creep effects may also have contributed to the unreliable volume change measurements obtained in these tests. Furthermore there appeared to be a significant variation in the data obtained which may be related to temperature effects in the laboratory. All the triaxial tests were conducted in a temperature controlled laboratory but independent measurement of the actual temperature at the triaxial test location was not measured during the tests.

A.3.2 Instrumentation

The 5kN ELE load cell used in the triaxial tests was calibrated using a proving ring, which had been calibrated directly against dead weights. The proving ring was mounted onto the load frame and the load cell was lined up directly onto the proving ring. The base platen of the load frame was raised at a constant rate, divisions of the proving ring were recorded and converted to kN, and the output voltage of the load cell was recorded. Figure A.9 presents the linear calibration of the load cell which within the range used for the triaxial tests ($<$ 2kN) has an

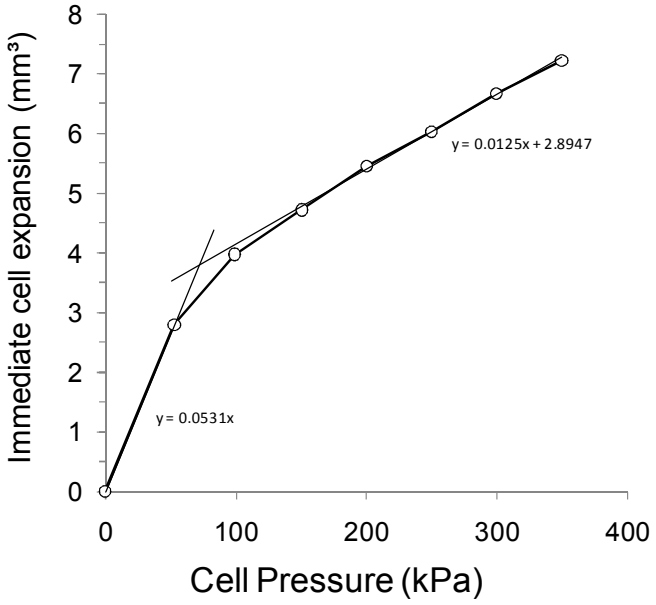

Figure A.7: Immediate cell volume changes in triaxial cell

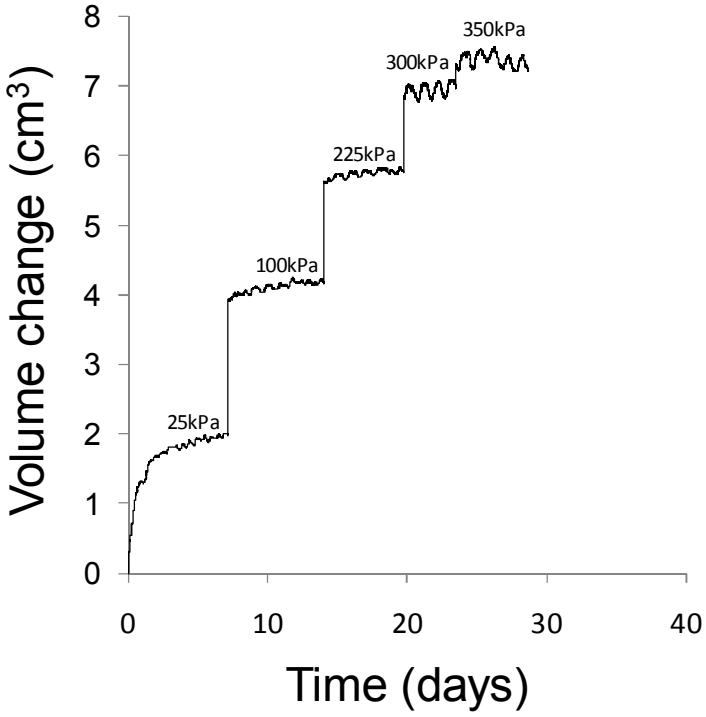

Figure A.8: Cell volume changes due to creep at different pressure levels in triaxial cell

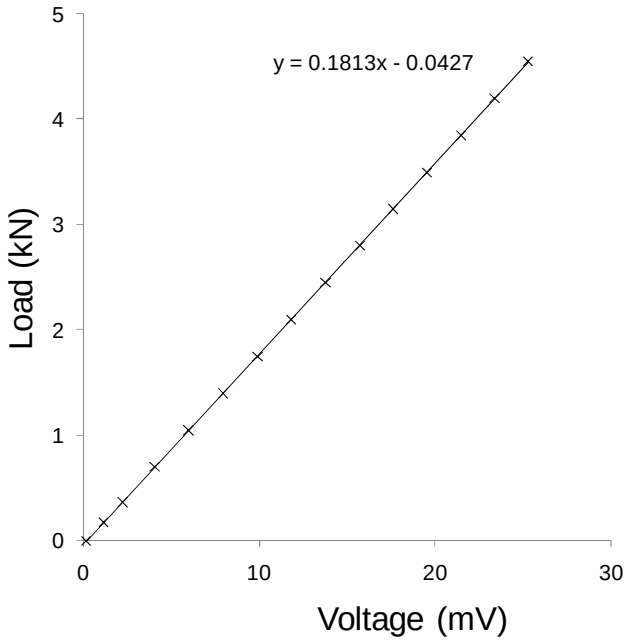

Figure A.9: Calibration of 5kN Load cell

accuracy of ± 0.005kN, which corresponds to an accuracy of the deviator stress of ± 4.4kPa for a 38mm diameter soil sample.

It was not possible to use an internal submersible load cell due to the small size of the triaxial cell used in these tests, because of this it was necessary to take into account the uplift force acting on the load cell due to the cell pressure applied within the cell. Theoretically the uplift force should be equal to the area of the piston ram multiplied by the cell pressure applied. Piston diameter is 18.95mm and the area of the piston ram (A_{ram}) is 282mm^2 . In order to check for friction effects in the piston ram, this relationship was checked by reading the uplift force recorded by the load cell with increasing pressure (see Figure A.10). It is evident that the friction effects for this piston are not significant and thus uplift force was accounted for in the triaxial results using the aforementioned relationship ($A_{ram} * \sigma_3$).

The linear displacement transducer used in the triaxial tests was calibrated against a dial gauge, both were mounted onto the strain controlled load frame, and the base platen was raised at a constant rate. Figure A.11 presents the calibration relationship for the linear displacement transducer, which had an accuracy of ± 0.04mm in the range of 0.5 mm to 25mm, again non-linearity is evident close to zero displacement. The volume change associated with the movement

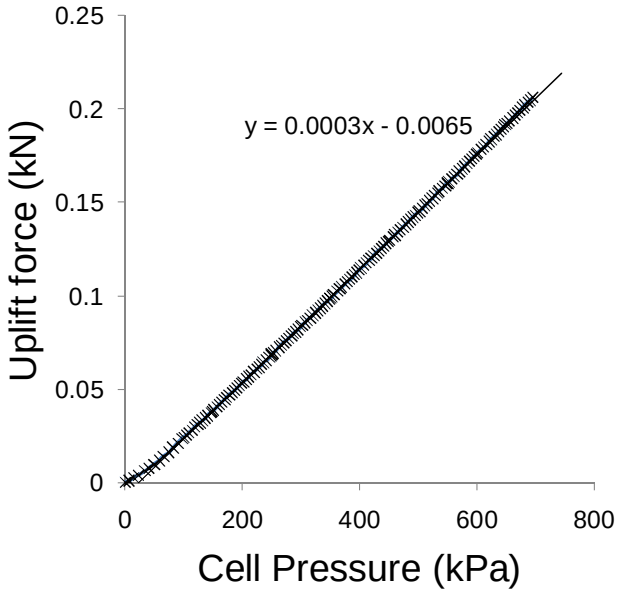

Figure A.10: Load cell readings due to uplift pressure

of the piston ram into the cell (V_{ram}) during shearing was calculated as:

$$V_{ram} = A_{ram} * \triangle H \tag{A.1}$$

The pore pressure transducer used, in the saturated tests was calibrated while mounted in position connected to a port on the standard base pedestal, by filling the cell with water only and applying increasing cell pressures. Figure A.12 presents the calibration of the pore pressure transducer. A linear calibration was obtained between 0 and 1000 kPa with an accuracy of $\pm$ 1.3kPa.

In order to ensure there were no differences in pressures between the different devices used in the tests, the pressure-volume controllers were reset to a zero pressure datum prior to the start of each test. This was carried out while setting up the cell for the saturation of the porous stone. The bleed valve at the top of the cell was used as the zero pressure datum, simply because it facilitated checking of the pressures easily. When the pore water pressure transducer was used, its pressure was also set to zero at the same datum. At the same time, the load cell reading was set to zero when raising the base platen (with a water only filled cell) caused water to emerge from

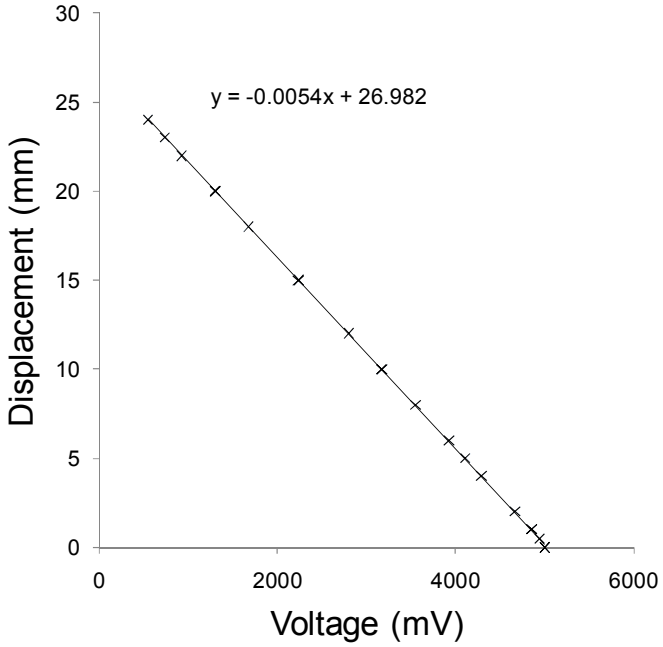

Figure A.11: Calibration of 25mm Linear displacement transducer

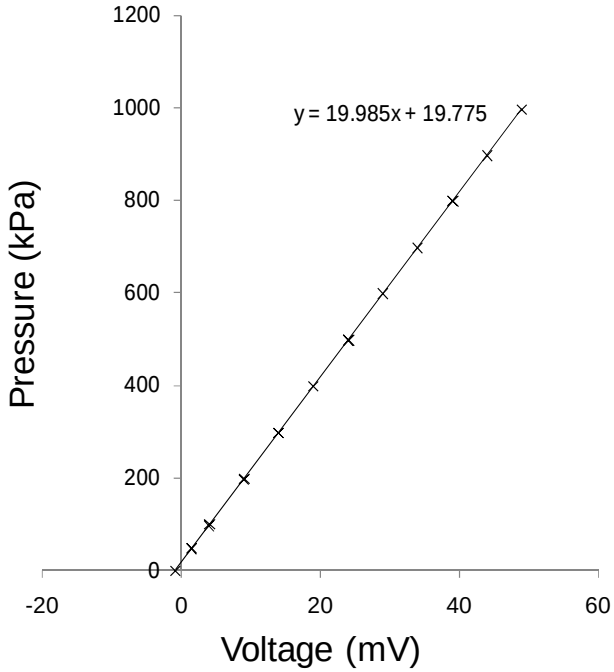

Figure A.12: Calibration of pore pressure transducer

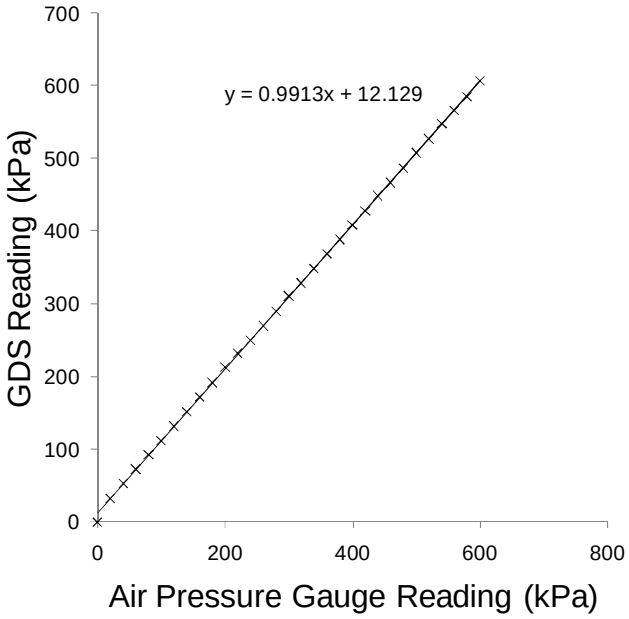

Figure A.13: Calibration of air pressure gauge

the bleed valve. The gauge used to control the pore air pressure manually was also calibrated against a GDS pressure-volume controller, where the pressure had been set to zero at the bleed valve position. The gauge was calibrated by connecting it to an air-water pressure cylinder, where the pressure is transferred between the two phases across a bladder. Figure A.13 presents the calibration of the air pressure gauge against a pressure volume controller. This calibration was used to regulate the pore air pressure applied in the suction controlled tests.

A.4 UPC Oedometer equipment

A.4.1 Instrumentation

Figure A.14 presents the calibration curve for the ELE 10mm linear displacement transducer used in the UPC oedometer set-up. The ELE displacement transducer was found to have a good accuracy in its working range of $\pm$ 0.008mm.

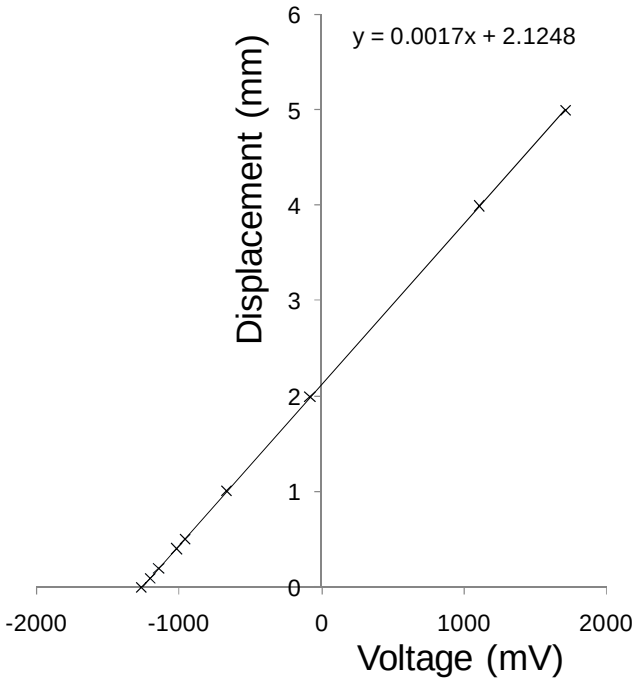

Figure A.14: LVDT Calibration curve

A.4.2 Saturation of ceramic disc

Figure A.15 presents a typical curve of the flow through the ceramic disc used in the UPC oedometer set-up once saturation had been achieved. The ceramic disc was saturated by applying a constant pressure above the ceramic disc of 1600kPa and zero water pressure below the disc, these pressures were maintained using the GDS pressure-volume controllers. This pressure differential was maintained for approximately 30mins prior to each test. The saturated permeability of the disc was then calculated and compared with previously obtained values in the laboratory to ensure that no cracking of the disc had occurred. The disc had a saturated permeability of 5.3×10^{-11} m/s.

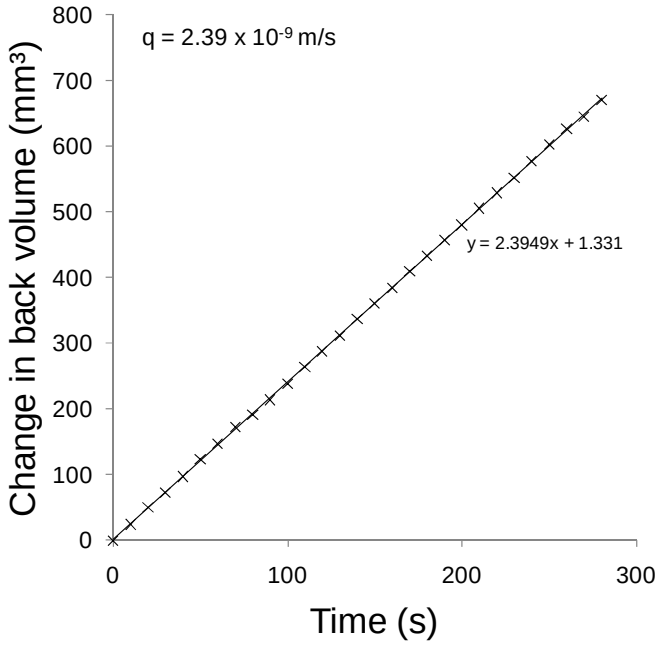

Figure A.15: Saturation of the 1500kPa air entry ceramic disc